Volume n° 2 - from B16 to B33

Field Trip Guide Book - B16

32nd INTERNATIONAL GEOLOGICAL CONGRESS

WESTERN PYRENEES FOLD-AND-THRUST-BELT: GEODYNAMICS, SEDIMENTATION AND PLATE BOUNDARY RECONSTRUCTION FROM RIFTING TO INVERSION

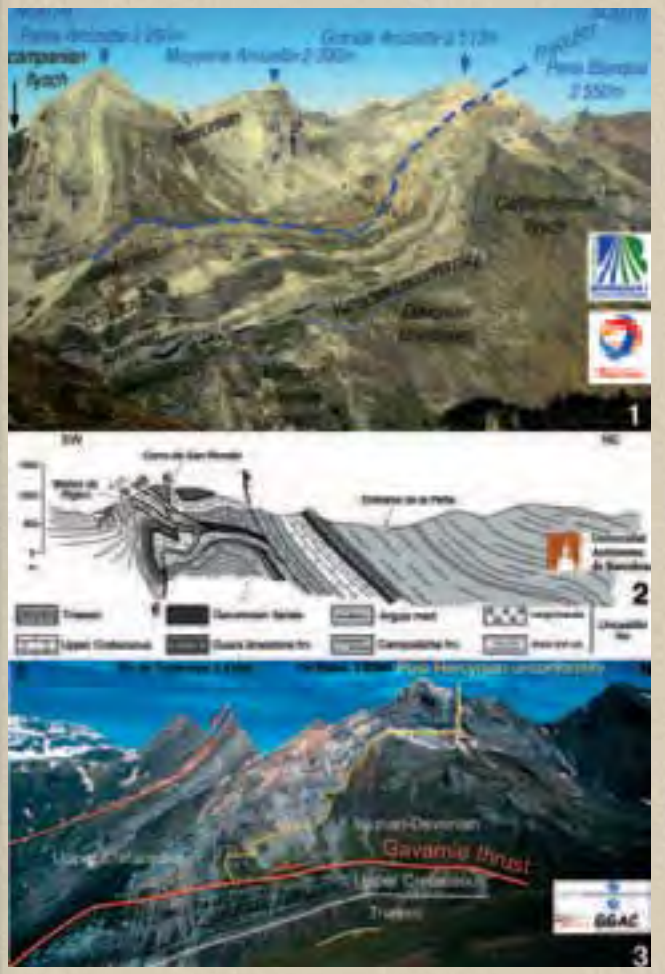

Leaders:
R. Bourrouilh, L. Moen-Maurel,
J. Muñoz, A. Teixell

Florence - Italy
August 20-28, 2004

Pre-Congress **B16**

The scientific content of this guide is under the total responsibility of the Authors

Published by:
APAT – Italian Agency for the Environmental Protection and Technical Services - Via Vitaliano Brancati, 48 - 00144 Roma - Italy

Series Editors:
Luca Guerrieri, Irene Rischia and Leonello Serva (APAT, Roma)

English Desk-copy Editors:
Paul Mazza (Università di Firenze), Jessica Ann Thonn (Università di Firenze), Nathalie Marléne Adams (Università di Firenze), Miriam Friedman (Università di Firenze), Kate Eadie (Freelance indipendent professional)

Field Trip Committee:
Leonello Serva (APAT, Roma), Alessandro Michetti (Università dell'Insubria, Como), Giulio Pavia (Università di Torino), Raffaele Pignone (Servizio Geologico Regione Emilia-Romagna, Bologna) and Riccardo Polino (CNR, Torino)

Acknowledgments:
The 32nd IGC Organizing Committee is grateful to Roberto Pompili and Elisa Brustia (APAT, Roma) for their collaboration in editing.

Graphic project:
Full snc - Firenze

Layout and press:
Lito Terrazzi srl - Firenze

Volume n° 2 - from B16 to B33

32nd INTERNATIONAL GEOLOGICAL CONGRESS

WESTERN PYRENEES FOLD-AND-THRUST-BELT: GEODYNAMICS, SEDIMENTATION AND PLATE BOUNDARY RECONSTRUCTION FROM RIFTING TO INVERSION

AUTHORS:

R. Bourrouilh[1], L. Moen-Maurel[2], J. Muñoz[3], A. Teixell[4]

[1] Laboratoire CIBAMAR, Université Bordeaux 1, Talence Cedex - France
[2] TOTAL, Pau Cedex - France
[3] Departament de Geodinamica i Geofisica, Facultat de Geologia, Universitat de Barcelona - Spain
[4] Departament de Geologia, Universitat Autònoma de Barcelona, Bellaterra - Spain

Florence - Italy
August 20-28, 2004

Pre-Congress

B16

Front Cover:
1. Thrusts and Folds structures of Les Eaux Chaudes in the Ossau Valley, France. DAY 2, Stop 2.5b.
2. Thrusts and Folds structures of the External Sierras, Spain. DAY 5, Stop 5.3.
3. Thrusts and Folds of Gavarnie at La Estiba, Spain. DAY 6, Stop 6.2.

Leaders: R. Bourrouilh, L. Moen-Maurel, J. Muñoz, A. Teixell

Introduction

This field trip along a geotraverse through the north-western and south-western Pyrenees area has three main purposes:

1. To analyse the present-day structures in the fold and thrust belt and to reconstruct their structural evolution in order to better understand the subsurface foreland structures (some of them being oil/gas traps or prospects).
2. To describe the stratigraphic evolution of the Mesozoic and Tertiary formations (with respect to plate tectonics and to the Iberian plate drift) on several transects: along the Ossau Valley, the Aspe Valley, the Mendibelza and Orhy Massifs for the northern side, and from the Orhy Massif to Jaca and Aïnsa for the southern side.
3. To give petroleum geoscientists the recent concepts and keys for the Pyrenean foreland and foothills hydrocarbon exploration.

The scenic landscapes of the Pyrenees mountain range provide an exceptional laboratory for examining the orogenic processes, from rifting to collision, both in the crustal lithosphere as well as in the foreland basins.

A comparison to more classical fold-and-thrust belts will be proposed along the way and in the wrap-up conclusion of the field trip.

Field References:

Topographic and Road maps : for example:

Michelin n°234 Aquitaine 1/ 200,000

Michelin n°573, Regional 1/400,000:
Pais Vasco/Euskadi, Navarra, La Rioja.

Michelin n°574, Regional:1/400,000:
Aragon, Cataluña/Catalunya

Geological maps :

S.N.P.A. (Société Nationale des Pétroles d'Aquitaine) (1972). Carte géologique des Pyrénées, scale 1:250,000, P. Soler ed. 4 plates.

B.R.G.M. (1980). Carte Tectonique de la France, scale 1:1,000,000, B.R.G.M. Ed.

B.R.G.M.: 1/50,000 geological Maps: n° XIII-46, St Jean Pied de Port; XIV-46, Tardets-Sorholus; XIV-47, Larrau ; XV-45, Pau; XV-46, Oloron Sainte Marie; XV-47, Laruns (under press).

Instituto Geologico y Minero de Espana, Geological Maps at 1/ 250,000 and at 1/50,000: n°118 Zuriza, n° 144 Anso, n°145 Sallent.

General geological setting (Plate 1, fig.1 and 2).

Introduction

Situated between the European plate and the Iberian plate, the Pyrenean orogenic belt extends from the NW part of Spain or Galicia, to the Southern part of the Alps and the Gulf of Genoa, in the Mediterranean. It is thus a belt almost 2,000 km long, of which only the central part, or the Pyrenees, is a visible collisional orogen, whereas both the Western part or the Bay of Biscay and the Eastern part or the Gulf of Lion and Gulf of Genoa remain at subsea.

The Pyrenees resulted from an orogeny which developed over a previously thinned continental crust, but without an intervening oceanic crust between the two diverging plates. Underplating of the Iberian plate underneath the European plate led to the sinking of a deep crustal root along a north-dipping plane while coeval delamination of the upper crust led to the propagation of a major fold-and-thrust belt to the south as well as of a conjugate north-verging back-thrust system. Thus the range is characterized by a doubly-verging asymmetric thrust stack wedge:

- the southern fold-and-thrust belt (FTB) represents a south-verging imbricate fan affecting cover formations (Mesozoic and Cenozoic in age) rooting into an antiformal stack of basement rocks (Precambrian to Paleozoic variscan folded series) in the axial zone. The piggy-back thrust sheets indicate a crustal shortening which reaches over 100 km along, i.e. 90% of the total orogen collision;
- the northern fold-and-thrust belt is confined over a narrower zone north of the axial zone or the High Chain, in a conjugate position to the underplating process (Moen-Maurel *et al*., 1999).

The relatively minor inversion in the Northern FTB protected the rifting series and structures from uplift and erosion, thus permitting the examination of the initial processes of the orogenesis.

The genesis of the Pyrenean belt is the result of:

- 1. the break-up of the 250 Ma old Wegener's Pangea and reactivation of its structural inherited fabrics,
- 2. the correlative propagation of the Atlantic Mid-Oceanic Ridge from Central Atlantic to the North, with an Atlantic RRR triple junction along its Eastward opening branch entering Bay of Biscay,
- 3. the Late Jurassic - Late Cretaceous diachronous Eastward opening of the Bay of Biscay which

Volume n° 2 - from B16 to B33

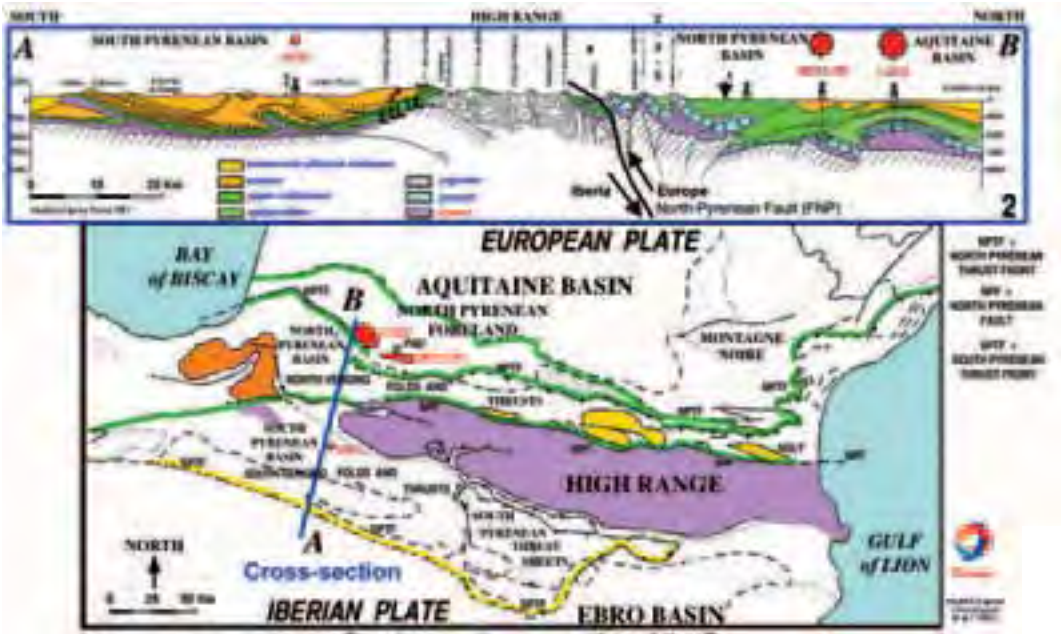

Plate 1 - 1. Structural Map of the Pyrenees with location of cross section AB. 2. Transversal cross section AB of the Pyrenees, from the Ebro Basin (South) to the Aquitaine Basin (North).

resulted in the drift and progressive rotation of the Iberian plate and in the birth of rifted interplate basins, such as the N- Pyrenean basin at the tip of the Bay of Biscay. In Turonian the Eastward Atlantic R junction point aborted (R-->r), the North-Pyrenean rift never produced oceanic crust: it can thus be called "aulacogen",

- 4. the northward push by the large African plate Stopping the free drift of the Iberian plate toward the south-east. This drift is due to the Cretaceous oceanic opening of both the South Atlantic and Indian Oceans, as well as by the closure of the Tethys, which provoked

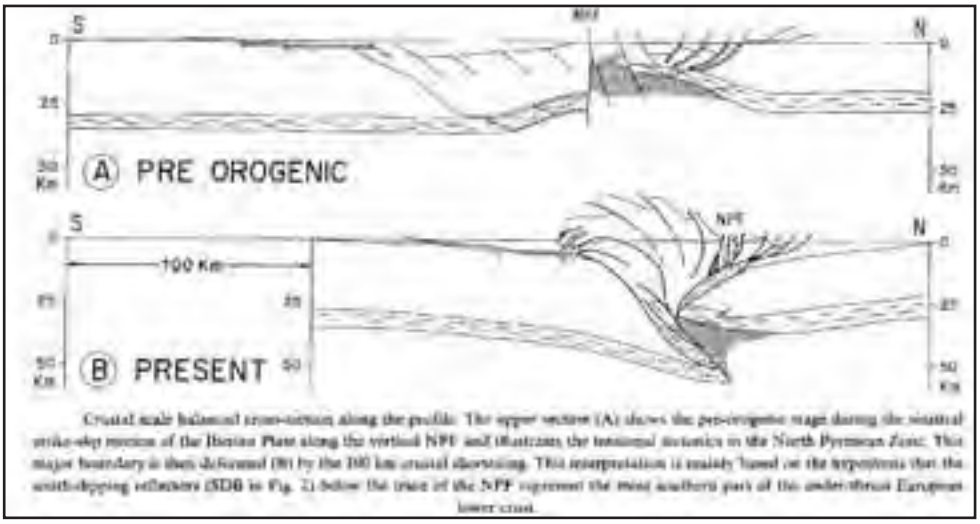

Figure 1 - Crustal scale balanced cross section, ECORS seismic profile, from Choukroune et al. , 1989.

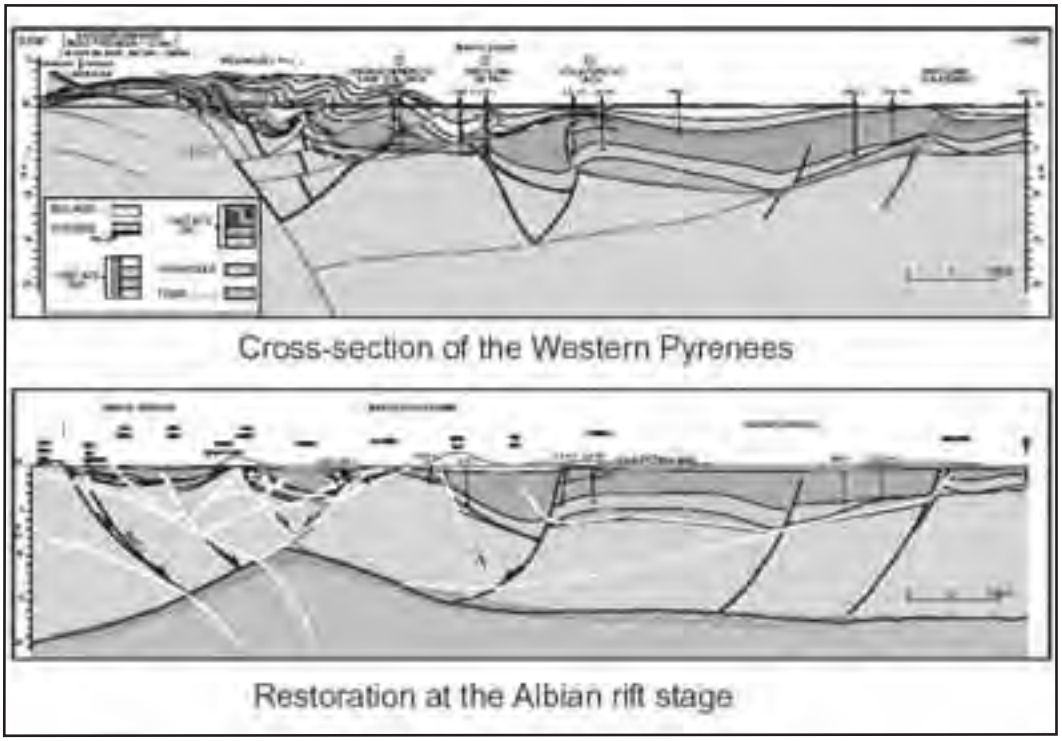

Figure 2 - Cross-section passing through the Lacq and Meillon gas fields (Moen-Maurel et al.1999).

the migration of the African plate towards the NE and then towards the N. This plate motion crushed the open space between Europe and Africa and formed the Pyrenean-Alpine orogenic belt in a diachronous compression which proceeded westwards along the northern margin of the Iberian plate.

As a result of the collision between the Iberian and European plates, which began during the Turonian and continued:

- 1. the rifted N-Pyrenean basin became a foredeep basin
- 2. a lithospheric compensation responded to the collision and the associated crustal thickening, creating a large intraplate foreland over the Iberian plate, (the South-Pyrenean basin), and a retro-foreland basin on the Northern edge of the Iberian plate and over the

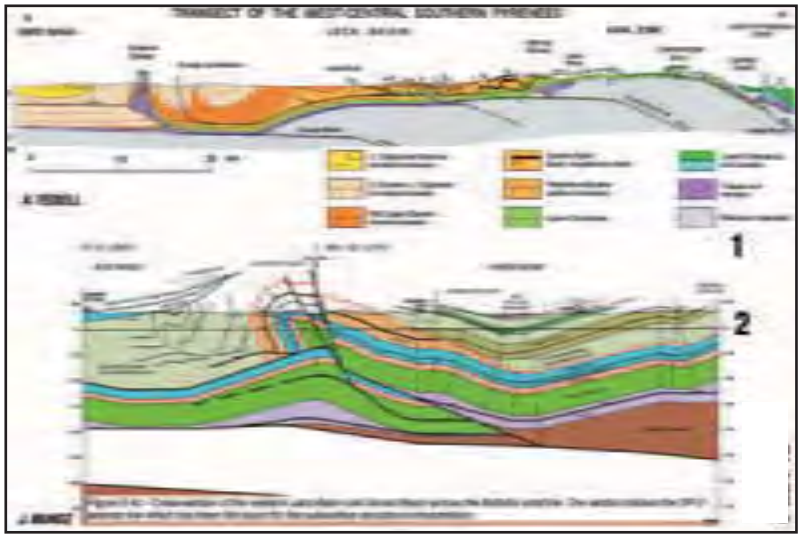

Plate 2 - 1. Transect Of The West-central Southern Pyrenees, from A. Teixell. 2. Cross-section of the Western Jaca basin and Ainsa basin across the Boltaña anticline, from J. Muñoz.

European plate (the Aquitaine basin).
- 3. the Pyrenean orogenic belt displays a fan-shaped cross-section, resulting from the crustal ductile underthrusting or underplating of the Pre-Pangean basement (Precambrian-Paleozoic) of the Iberian plate underneath the European plate. Since the initial stages of the Pyrenean collision at Late Santonian-Campanian times two foreland basins developed, one on each side of the double-wedge (Figs. 1 and 2).
- 4. The post-Pangean sedimentary infill of the interplate (north) and the intraplate (south) basins thrusted toward either the north (Aquitaine basin) and south (Ebro basin) forelands, in successive shallow fold-and-thrust piggy-back sheets.

Deformation of the Pyrenean double-wedge migrated outwards in a piggy-back manner, although synchronous hindward internal deformation has also been documented. The forward propagation of the deformation in the southern Pyrenees was modified, in the last stage of the evolution of the thrust-belt, by a break-back reactivation of the older thrusts and by the development of new, minor out-of sequence thrusts affecting syntectonic deposits (Martínez *et al*., 1988, Vergés and Muñoz, 1990). Thrust transport direction was constantly N-S to NNE-SSW through most of the tectonic evolution as deduced by the map pattern of the structures, kinematic criteria along thrust planes and the absence of significant rotation around a vertical axis along the analyzed cross-section (Dinares *et al*., 1992). This implies a near normal convergence through the main orogenic phase. The strike slip convergence vector between the two plates must be found at depth, decoupled from the cover deformation. A partitioning of the deformation must occur both in map view and with depth in favour of the activation of detachment horizons.
Although an isostatic balance occured all along the Pyrenean orogeny, between compression - erosion -sedimentation, the main apparent mountain uplift has occurred since the Pleistocene, following mainly the glaciations. It mostly affects the Iberian plate, as a result of the isostatic rebound of the crustal Pyrenean subducted root.

Structure of the Pyrenees

The Pyrenees can be considered an immature, incomplete orogen resulting from plate drift rotations which leads to varying deformations along strike. To the west, the space between the European and Iberian plates still remains open in the Bay of Biscay, the northern margin of Spain showing an incipient north-verging subduction. To the east, the Pyrenean orogenic belt extends in the Alps of Provence, exhibiting minor inversion thrusts and folds (Debelmas, 1974). More to the south, the Neogene Mediterranean extension, consecutive to the Betico-Rifean compressional events (Bourrouilh and Gorsline, 1979) overprints the Pyrenean belt.
Between these belt-tip areas, where the European and Iberian plates are in full contact, i.e. in the Pyrenees *sensu stricto*, the collision directly affected the continental lithosphere, since no oceanic floor was present. Using an inherited Precambrian (?) - Variscan fault network, the collision provoked an inversion of the deep fault network in the crustal basement, and the building of a deep-rooted fan-shaped mountain range (Fig.1 and 2, and Plate 1). In the Central Pyrenees the associated strike-slip motion that is well visible along one of the faults of the southern rift margin (North-Pyrenean Fault) marks the plate boundary. Along our geotraverse the NPF is concealed underneath a south-verging thrust (Plate 1). The North-Pyrenean rift structures were little inverted north of the rift axis, and remained north of the North-Pyrenean Thrust Front. South of its axis the tilted blocks of the rifting stage were affected by inversion and uplifted, either towards the south or the north, depending on the original dip sense of the rift faults, either sheared by wrenching, or thrust along the detachments in the Triassic evaporites and the Upper Cretaceous flysch.
The south-verging thrusting along successive shallow basal and internal plastic décollements also affected the cover of the High Chain, as well as the sedimentary infill of the South-Pyrenean intraplate basin. The plate collision resulted in the piggy-back stacking of south-verging folds and thrusts involving the basement as well as its cover.

The crustal and cover structuration is clearly observable in the field, in the Pyrenean mountain belt and foothills. It can be subdivided from north to south into different structural units (fig. 2 and Plate 1, fig.1 and 2) (Castéras, 1974):
The northern foreland basin, in the southern part of the Aquitaine basin, consists of a thick (few km) succession of Upper Cretaceous turbidites overlain by an up to 4 km thick Paleogene series. Most of the latter are represented by continental deposits as only marine platform sediments of Lower Ypresian age are observed (Buy and Rey, 1975). The Aquitaine basin mainly developed in the footwall of the North-Pyrenean Frontal Thrust and was not greatly involved

in the North-Pyrenean thrust system.
The southern part of the Aquitaine Basin is affected by folds with large curvature radii related to the Pyrenean Tertiary tectonic phase. In this area the Pyrenean compression is mainly Eocene in age. This phase enhanced salt tectonics.
The Sub-Pyrenean Zone or northern folded foreland (which lies beneath and north of the North Pyrenean Thrust Front (or NPTF) is characterized by north-verging blind thrusts and asymmetric folds often cored by a salt ridge or an inverted rift graben.
The NPTF is composed of a series of en-echelon N-verging thrust faults running from the Bay of Biscay up to the South-Western Alps.
The North Pyrenean Zone or NPZ, lies to the south of the NPTF and is characterized by north-verging thrusts and folds verging either north or south depending on the dip sense of the inverted normal faults. The southern part of this zone has been deformed by schistose deformation and low-grade Pyrenean-age metamorphism, at the contact with the NPF.
Precambrian to Paleozoic basement outcrops in the NPZ, constituting the N-Pyrenean massifs.
The North Pyrenean Fault or NPF lies to the south of these units, and appears in various ways throughout the belt. Its variable aspects take on the status of the orogenic axis of the range (Iberian-European plate boundary), the change-over zone from northern to southern vergence (Central Pyrenees), the zone of intense deformation (various schistosities), a metamorphic zone, and a lherzolite (mantle-derived ultrabasic granulitic rock) injection zone (fig. 2 and Plate 1, fig. 2).
The fault evolved from an initial Albo-Cenomanian transtensional regime with the formation of pull-apart basins and the development of a thermal metamorphism (Debroas, 1990; Goldberg and Maluski, 1988) to a later transpressional regime during the onset of convergence in Early Senonian time (Puigdefàbregas and Souquet, 1986; Debroas, 1990). Lower crustal granulitic rocks as well as ultrabasic upper mantle rocks (lherzolites) are observed embedded between the Lower Mesozoic metamorphic rocks along a narrow strip parallel to the North Pyrenean Fault (Choukroune, 1976; Vielzeuf and Kornprobst, 1984). These rocks were carried to upper crustal levels during the strike-slip faulting. Apart from this narrow strip parallel to the North Pyrenean fault neither post-Hercynian metamorphic rocks nor lower crustal rocks are observed at the surface in the Pyrenees.
The Axial Zone or High Chain (Plate 1, fig. 2 and Plate 2, fig. 1) is the highest part of the range, and represents the present-day orographic axis. It is composed of Precambrian series, possibly folded (?) during the Late Proterozoïc, and of thick Paleozoic series that were folded during the Variscan (Hercynian) orogeny and redeformed during the Upper Cretaceous to Tertiary Pyrenean tectonic phases. The High Chain basement is overlain by discontinuous Permo-Triassic deposits and by a thick Upper Cretaceous shelf carbonate series; this shelf is overlain by the edge of an Upper Cretaceous to Tertiary synorogenic flysch basin, which developed synchronously with the compression and with the tectonic subsidence and deepening of the South and North Pyrenean foredeep basins.
The basement rocks of the Axial Zone constitute an antiformal stack. This antiformal stack only involves upper crustal rocks, its floor thrust being located 15 km below the top of the basement. In the Central Pyrenees it is constituted by three main structural units: Nogueres, Orri and Rialp thrust sheets (Muñoz, 1992). The regional westward plunge of the basement antiformal stack leaves only the Nogueres – equivalent thrust sheet at outcrop level; it is then called Gavarnie - Eaux Chaudes in the Western Pyrenees. The Nogueres-Gavarnie thrust sheet is the uppermost of the antiformal stack and its southern tip is the basement of the lower cover thrust sheets. In the central Pyrenees, the contact between the cover Upper Thrust sheets and the basement antiformal stack corresponds to a passive-roof backthrust (Morreres backthrust). During the development and southward displacement of the basement antiformal stack the cover units have been wedged by delamination, and on the top of the basement, as described in other orogenic belts (Price, 1986). A mirror image of this delamination of the cover by the basement thrust sheets also exist in the North-Pyrenean foreland at the edge of the Paleozoic Basque Massifs, which make a cartographic salient and a splinter wedge into the northern foreland (Figure 1).
The South Pyrenean Zone (Plate 2, fig. 2) is characterized by South-verging thrusts and folds. The stratigraphy is essentially represented by Permo-Triassic deposits, locally overlain by Jurassic, but mostly covered by Upper Cretaceous shelf carbonates passing to Eocene turbidites (in the western part) and Oligocene molasses conglomerates
In the southern Pyrenees the cover Upper Thrust Sheets (Muñoz *et al*., 1986) consist of Mesozoic and

Volume n° 2 - from B16 to B33

syntectonic Paleogene rocks which were initially detached from the basement over the Upper Triassic evaporites. These thrust sheets were later thrusted on top of autochthonous Paleogene rocks in continuation with the Ebro foreland basin (Fig. 2). They are the Central-South Pyrenean thrust sheets (Cotiella, Boixols, Montsec and Sierras Marginales) in the central Pyrenees and the Pedraforca thrust sheets in the eastern Pyrenees (Figs. 1 and 2). The Mesozoic series is only tens of meters thick in the southernmost units and progressively thickens northwards up to 7km. This sedimentary wedge is the result of the progressive southwards thinning and pinch out of the Cretaceous stratigraphic units coupled with the geometry imposed by Cretaceous (mainly Lower Cretaceous) extensional faults. The Upper Thrust Sheets show numerous oblique and lateral structures, probably related to the original Mesozoic basin configuration. From these structures an approximately N-S transport direction can be deduced. Location of thrusts is strongly controlled by previous extensional faults, mainly Lower Cretaceous in age. Inversion tectonics is a structural feature of the Upper Thrust Sheets.

The South-Pyrenean Thrust Front or SPFT extends from the east to the north-west (Plate 1, Fig. 2) and represents the Frontal thrust of the ramps and duplexes system which affects both the High Chain and the sedimentary infill of the South-Pyrenean foreland basin.

The Ebro Basin represents the autochthonous external foreland south of the Southern Pyrenees Frontal Thrust. It is mainly filled by the last stage continental sediments of the foreland basin after the Lower Priabonian evaporites. These evaporites represent the paleogeographical closing of the Ebro basin. Upper Eocene-Lower Miocene continental clastics filled the enclosed basin and progressively backfilled and buried the south-Pyrenean thrust system during its late development stages (Coney, *et al*., 1996).

Geophysical data and crustal structure

The crustal and lithospheric structure of the Pyrenees has been investigated by different geophysical techniques (deep reflection and refraction seismic profiles, gravity, magnetotellurics, magnetic anomalies, tomography, heat flow). The data that best constrain the Pyrenean crustal structure are from the deep seismic reflection profiles, mainly the ECORS-Pyrenees profiles (Choukroune et el., 1989, Roure 1989). These profiles have been interpreted to show the subduction of the Iberian plate below the European one and has been the basis for the construction of crustal balanced cross-sections (Roure *et al*., 1989, Muñoz, 1992).

Several different interpretations of the crustal structure of the Pyrenees have been given on the basis of the combined geological and geophysical data (Roure *et al*., 1989, Mattauer, 1990, Muñoz, 1992). We believe that an explanation in which the orogenic double-wedge involves only upper crustal rocks provides the best geometry in which to integrate all these data (Fig. 4). Apparently, the crust was decoupled and the lower crust, below the upper crustal double-wedge, was subducted together with the lithospheric mantle into the mantle. This inferred crustal subduction is compatible with other geophysical data such as tomographic analyses (Souriau and Granet, 1995) and by a magnetotelluric profile across the central Pyrenees (Pous *et al*.,1995).

Balanced and restored cross-sections

Balanced and restored cross-sections were constructed not only to integrate geophysical and geological data but also to estimate the amount of orogenic contraction (Fig. 1). A geometrical solution of a crustal cross-section of the central Pyrenees along the ECORS profile gave a total shortening of 147 km (Muñoz, 1992). However, this value increases up to 160 km if the internal deformation of the crust below the sole thrust of the Pyrenean thrust system is restored. Other cross-section restorations of the central Pyrenees have estimated shortening values over 100 km (Deramond *et al*., 1985; Roure *et al*., 1989). A shortening calculation for a crustal cross-section in the eastern Pyrenees yielded a shortening estimate of about 125 km (Vergés *et al*., 1995). No more than 15 km of shortening can be accounted by the north-verging structures north of the North Pyrenean Fault (Moen-Maurel *et al*., 1995). Therefore about 90% of the collision shortening is produced by the south-verging thrusts and antiformal stacks, south of the North Pyrenean Fault.

These shortening calculations are compatible with the estimated separation of the Iberian and European plates as deduced by reconstruction of the past motion of Iberia after paleomagnetic data (Roest and Srivastava, 1991). These paleomagnetic data, as well as cross-sections west of the ECORS one, show that shortening decreases westwards. Shortening values on the order of 80 km are reached westwards from

the ECORS cross-section (Grandjean, 1992, Teixell, 1996, 1998).

The estimated duration of convergence in the central Pyrenees is about 60 Ma, which gives a mean shortening rate of 2.5 mm/yr. A similar shortening rate has also been deduced in the eastern Pyrenees during a shorter period of convergence (Vergés *et al*., 1995). The latest deformation migrated westwards. It Stopped during Middle Oligocene time in the eastern Pyrenees and continued to the Middle Miocene in the westernmost Pyrenees (Vergés, 1993). In the central Pyrenees, along the ECORS cross-section, deformation ended by Early Miocene times.

Stratigraphic and geodynamic evolution

(Fig. 3) (See further on the contribution of A. Teixell and of J. Muñoz for a more detailed study of the Southern Pyrenean side).

According to Bourrouilh, Richert and Zolnaï, 1995, Richert *et al*., 1995, the stratigraphic and structural evolution of the Pyrenees can be summarized as follows:

Precambrian to Paleozoic

The evolution of the Precambrian and Paleozoic domain related to the geodynamics of the Pyrenees, Montagne Noire and Western Mediterranean has

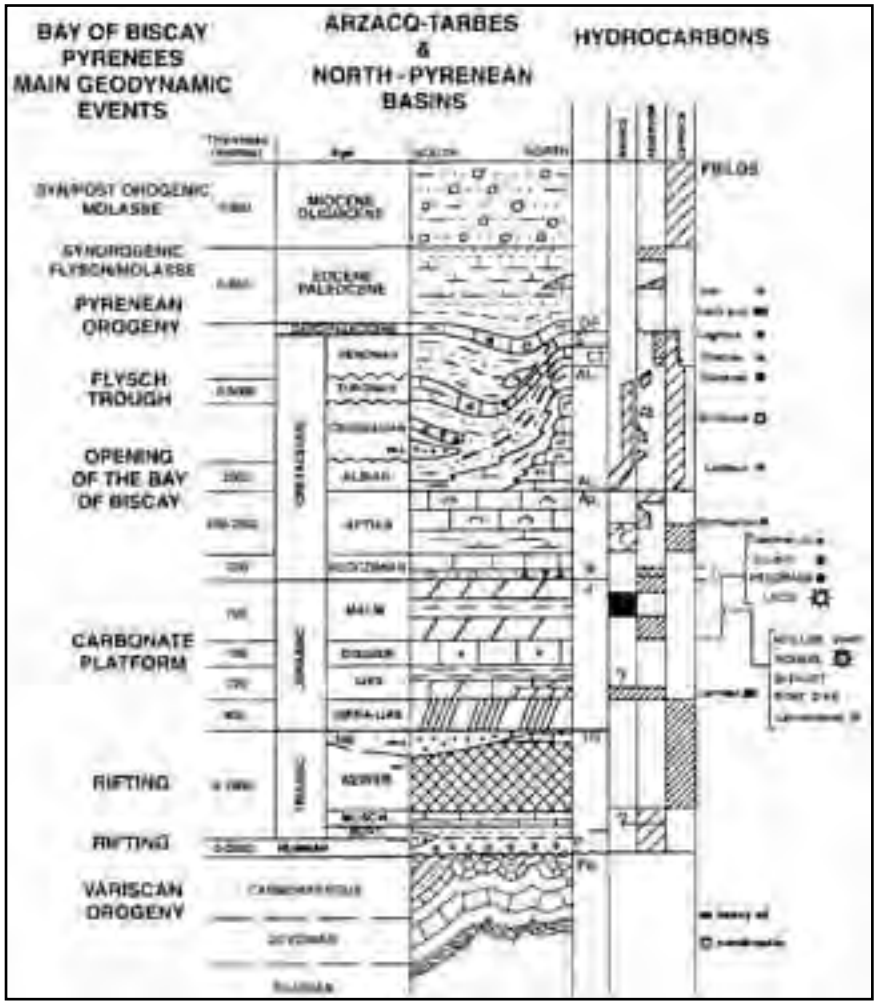

Figure 3 - Geodynamic evolution of Bay of Biscay-Pyrenees and North-Pyrenean basins, from Bourrouilh et al., 1995, modified.

Volume n° 2 - from B16 to B33

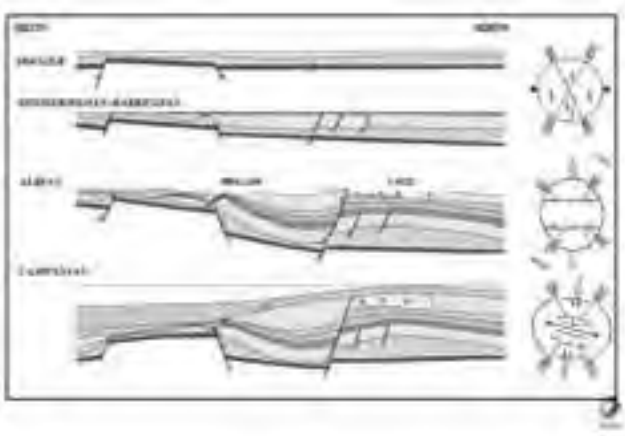

Figure 4 - Tectono-stratigraphic evolution of the Lacq-Meilllon area (Total).

been synthetized by Bourrouilh and al. (1980). The Paleozoic has been studied in the Aquitaine area by Winnock (1971), Autran and Cogné (1980), Bourrouilh and Mirouse, (1984) and others.

The structural framework of the Precambrian basement was acquired during the Late Proterozoïc (Cadomian). Generally, Precambrian series are metamorphosed (Agly massif) and radiochronologically dated (Ursuya-Baigoura massif). The Paleozoic contains six main members: a post-orogenic conglomeratic and then locally stromatolithic Cambrian (Bouquet *et al*., 1985), a thick fine-grained silici-clastic Ordovician (Gapillou, 1981), a black-shaly Silurian interval, a limy Devonian, a sandy-shaly carboniferous section and the red Permian member. Precambrian and Paleozoic basement were then successively affected by Caledonian and Variscan (or Hercynian) orogenies. The Variscan orogeny was accompanied by large thrusts and folds and metamorphism. Upper Variscan granites locally intruded the series.

The **Permian** lies unconformably on the previously deformed series. It is composed of continental red beds, in which locally an andesitic volcanism provides volcanic debris (Lucas 1985) but also basaltic flows, as witnesses of oceanic expansion.

Triassic to Early Liassic (Fig.3)

The Triassic series are of a typical Germano-type i.e. a three-fold stratigraphy: from base to top: post orogenic red conglomerates and sandstones, marine carbonates and red shales with evaporites and volcanics. The thickest volcanic wedge showing crustal distension, has been emplaced along the southernmost rifted basin edge (over several hundreds of metres), while they taper off to zero towards the Aquitaine present-day basin center.

Jurassic

The Lower Liassic anhydrites grade upwards into a shallow-marine dolomitic, then mainly limestone platform sequence (Dogger-Malm). The Oxfordian through Early Kimmeridgian time period can be associated to a more active extensional phase leading to structural and paleogeographical differentiation on the platform (Canérot, 1987). The local Pangean platform is subdivided into two major provinces: an inner part with dolomites and limestones of the Meillon and Bayseres Formations to the east versus a more open marine environment to the west : Oxfordian Ammonite marls and Lower Kimmeridgian shaly limestones of the lower Cagnotte Formation. Following this phase of differentiation, the Middle to Late Kimmeridgian period represents a stable environment of deposition, affected only by local condensed sedimentary deposits, related to synsedimentary salt tectonics along basement faults. At the end of the Jurassic, the Neo-Kimmerian tectonic phase leads to a general regression. The dolomitic facies of the Mano Dolomite (200 m thick in average) are associated to this regressive cycle. In the Late Portlandian to Berriasian, the platform is again separated into two domains, along the

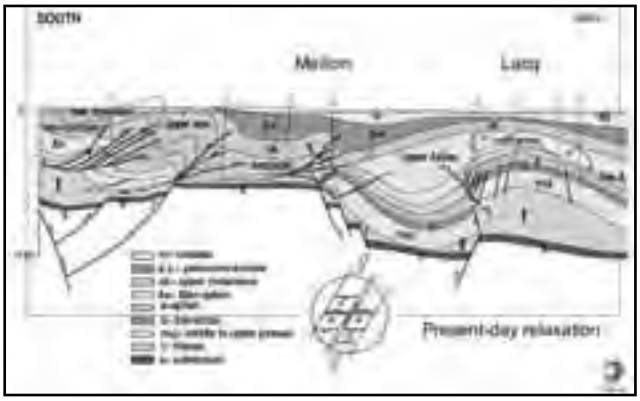

Figure 5 - Cross-section of the Lacq-Meillon area (Total).

submeridian trend defined here above. At the Jurassic-Cretaceous boundary large areas became emergent as demonstrated by the presence of anhydrite, some coal, red shale, clastics (sand), sand-rich carbonates and intra-formational (desiccation) breccias. The first salt-movements (gentle swells and salt-cushions) seem to have started as early as in the Portlandian (Winnock and Pontalier 1970). Massive sand-bodies were deposited in the Parentis Basin during the Purbeckian-Wealdian period. The equivalent series of the southern Aquitaine sub-basins are carbonates, intraformational breccias and shales (Lacq). The sedimentation over the south-western part of the basin indicates a deeper environment of deposition and a more continuous sedimentation during the Late Jurassic – Early Cretaceous transition (Hauterivian – Berriasian). Montagné's thesis (1986) evidenced rifting during Late Jurassic, south of Bayonne. Later, ODP Leg 103 (1988) found turbidites in the off-shore Hauterivian sequences in the westernmost part of the basin near Bilbao, indicating yet another opening (rifting) attempt of the Bay of Biscay.

Early Cretaceous

From Late Jurassic onward, a new paleogeography developed, provoking the formation of en-echelon diamond-shaped grabens in relation with the activation of inherited structural fabrics.

Within these basins three major phases of subsidence associated to extensional phases can be distinguished:

Barremian to Early Aptian.

The depocenters are associated to very thick black shale deposits, while the surrounding carbonate platforms show a very low rate of sedimentation. One of the main salt diapiric event also occurs during this time along the border faults of the newly formed basins by migration of the Triassic evaporites from the subsiding depocenters towards the edges.

Latest Aptian to Early Albian.

The shelf-basin configuration is acquired during this period. The basins are yet characterized by a very high rate of subsidence and sedimentation of black shales. Halokinesis is still going on, such as at the edges of the Aptian-Albian pull-apart basins and rhomb-grabens, e.g. the huge Audignon anticline to the north of the Arzacq Basin. The shelf-basin transition is marked by a system of limy patch reefs while the platforms surrounding the shelves show a low rate of sedimentation.

Late Albian.

The paleogeography changes completely, and is entirely controlled by the important tectonic movements taking place along the plate boundaries (Peybernès and Souquet, 1984). As a result, the subsiding zones shift to the south towards this very mobile zone, while a massive transgression develops over the entire area. The Late Albian sedimentation overlaps the earlier paleogeographies, demonstrating the change of structural stress at this time. Locally salt tectonics enhanced erosion and subsidence, producing the main hydrocarbon traps as they are known today.

Late Cretaceous

An important inversion occurred diachronously all along the Europe-Iberia plate boundary. While the western part remains extensive in a rift mode, the eastern part of the domain progressively became in compression and in a foredeep mode. Correlatively, two extensive carbonate platforms developed, covering to the north the major part of the Aquitaine Basin, and to the south the persistently high Iberian plate, both carbonate and separated by the N-Pyrenean flysch-furrow in between. Thus, the Late Cretaceous paleogeography shows three major domains from North to South:

On the Aquitaine platform, to the north, the syntectonic sedimentation of the foredeep evolves laterally to a carbonate shelf (Dubois and Seguin, 1980) of Cenomanian to Maastrichtian ages. This domain is located in a more distal and more stable environment within the Late Cretaceous paleogeography. It is important to point out that, along the southern limit of the shelf (South Aquitaine margin), the Cenomanian carbonates unconformably rest over the Upper Albian sediments. This unconformity fades out northwards into the platform. ***Salt-lineaments*** of varied orientations as well as circular diapirs were also enhanced in this apparently stable platform and in the Parentis Basin. They are located mostly along major faults and fault-intersections, such as the diapirs near the city of Dax, and along the oil-bearing structures of the Arzacq Basin, (Fig. 6).

The N-Pyrenean basin progressively becomes equivalent to a Cenomanian to Maastrichtian foredeep located immediately to the north of North-Pyrenean Fault (NPF), thus bordering the European-Iberian plate boundary. The entire fast-subsiding, turbidite-filled, mobile belt becomes progressively the North Pyrenean Zone, where the major part of the orogenic thin-skinned deformation of the North-Pyrenees will take place (Zolnai 1971). During the

Figure 6 - Structural framework and Petroleum Provinces of the South Aquitaine and N-Pyrenean basins (Total).

Cenomanian, the en-echelon rift basins merged into a single N-Pyrenean basin, which corresponds to an E-W asymmetric and narrow trough or furrow (Moen-Maurel *et al*., 1999).

As compression between the two plates became prominent, the axis of the foredeep migrated northwards, from Turonian to Lower Maastrichtian. The flysch sedimentation in the deep North Pyrenean furrow by now became fine-grained, dominated by marls and ended with a thick mudstone series during the Maastrichtian. Transpression provoked wrenching and salt tectonics. Olistostromes composed of Triassic material (salt, shale) are also emplaced, mainly into the mobile domains of the foredeep (Stevaux and Zolnai 1975). Within the North Pyrenean furrow the salt-structures acted as paleogeographic barriers and influenced the distribution of the turbiditic systems.

To the South, on the Iberian plate, an Upper Cretaceous carbonate platform developed. The massive, thick (about 500m) Iberian Upper Cretaceous carbonate series of the "calcaires des Eaux Chaudes" or "calcaires des cañons" overlay the earlier sediments and/or the basement, with a sharp angular unconformity.

However, as a result of the ongoing north-westward Pyrenean compression and of the formation of the intraplate retro-foreland basin, the Southern Upper Senonian flysch domain progressed over the former Iberian carbonate platform along the area of the High Chain in the present-day central and western Pyrenees. Its connection with or independence from the North Pyrenean equivalent flysch basin is under study.

In conclusion, the two Upper Cretaceous carbonate p7latforms to the north (Aquitaine) and to the south (Iberian plate) are separated by a flysch foredeep then a retro-foreland basin. No transitional facies are known between the platforms and the North Pyrenean Trough sediments, as a result of the progressive cannibalisation of the platform edges.

Tertiary

The Paleocene was a time with relatively low plate convergence between Europe and Africa (Roest and Srivastava, 1991). After a Dano-Paleocene period of relatively reduced tectonic activity, the Tertiary paleogeography and its basin evolution are under the control of the ongoing compression, which is diachronous and oblique, progressing from east to west again.

The eastern and central parts of the foreland basins

changed from marine to continental as topography developed and the amount of eroded material was sufficient to fill the basins. In the western Pyrenees the crust would have recovered its initial thickness later than in the central and eastern Pyrenees as a result of a greater extension of the Pyrenean crust during Early Cretaceous times coupled with a younger and lesser amount of convergence. In this area Paleocene rocks are represented by deep-water carbonate and siliciclastic sediments deposited in continuity with the Upper Cretaceous turbidites (Pujalte *et al*., 1989).
Two main events will arise :
1. the N-Pyrenean foredeep basin will retreat from east to west, and thus the related sedimentary facies synchronously will do the same, recording the orogenic evolution, horizontally and vertically. From east to west and from bottom to top, facies will pass from syntectonic flysch facies to tidal deposits and then to syn- and post-orogenic fanglomerates.
In detail: the Late Cretaceous-Paleocene time period is still marked by margin instability, with large submarine collapses of carbonates mass-flows (see here below, Stop 1.2 at Le Tucq).
In Late Paleocene-Eocene (Ypresian) rhythmic sedimentation continued in the N-Pyrenean basin, constituting a new thick flysch sequence.
During the Early-Middle Eocene thrusting rate increased. Both foreland basins experienced a deepening which resulted into the widest extension of marine deposits in the Pyrenean foreland basins (Puigdefàbregas *et al*., 1992, Burbank *et al*., 1992a). The thrust front in the southern side of the central Pyrenees strongly advanced because deformation of the Mesozoic wedge on top of a weak detachment level (Triassic evaporites). Shallow marine deposits were deposited in the foreland as well as in the piggy-back basins which demonstrate a subhorizontal mean topography over the southern frontal wedge. Strongly subsident troughs filled by turbiditic sequences were developed south of the uplifted basement in the footwall of the upper thrust sheets. Some relief existed hindwards as evidenced by the N-S river systems supplying basement clastics and by the geometry and location of proximal alluvial fans. A maximum topography of 1-2 km has been calculated based on paleotopographic reconstructions and flexural modelling (Vergés *et al*., 1995, Millán *et al*., 1995).
In Oligocene along the future Pyrenean foothills i.e. the orogenic foreland, sedimentation became progressively more terrigenous from east to west, with large masses of coarse continental fanconglomerates ("poudingues") deposited in successive sequences, in a suite of fans.
The Ebro basin became closed and separated from the Atlantic because the tectonic relief growth during the inversion of the Lower Cretaceous basins in the western Pyrenees. Erosional debris of the Pyrenees and other surrounding chains of the Ebro basin (Iberian and Catalan Coastal Ranges) progressively filled the basin and then backfilled, to bury the flanking thrust belts on its margins (Coney *et al*., 1996). This progressive backfilling forced deformation to migrate hindwards and as a consequence reactivation of previously developed thrust structures and break-back thrust sequences occurred (Vergés and Muñoz, 1990, Burbank *et al*., 1992b). The southern Pyrenees were almost completely buried by Early-Middle Miocene times.
The greatest part of the Aquitaine Basin, to the north of the orogenic foreland, nevertheless, remained shallow marine, until the general filling of the basin caused the sea to progressively retreat to the west.
The abrupt and subsequent Miocene-Pliocene re-excavation of the southern Pyrenees and the Ebro basin to develop the present fluvial system was some combination of the Miocene rifting of the western Mediterranean and the Messinian desiccation crisis.

Structural history of the Pyrenees

Inherited structures of Precambrian to Paleozoic age affected the tectonic basement of the Pyrenean orogeny, and had a fundamental influence on the geometry of the Upper Jurassic to Upper Cretaceous extensional (grabens and rift margins) and on the Upper Cretaceous to Tertiary compressive structures (frontal and lateral ramps). This combination of pre-rifting events produced three trends:
- ***N 20°E to 40°E:*** corresponding to the Garonne - Villefranche fault zone crossing through Toulouse city. It is active in Late Variscan times as a left-lateral strike slip fault.
- ***N 90°E to N 120°E:*** its corresponds to the Celt-Aquitaine hinge-line and to the North Pyrenean fault zone which acts as a left-lateral strike-slip fault in Late Variscan times.
- ***N 160°E*** represented in the Axial Zone by kilometer-high folds and incipient cleavage of Variscan age.
A succession of events affected the N-Pyrenean domain (fig. 4 and 5), after the Variscan orogeny.

The **first post-Variscan rifting** attempt took place

as soon as the **EARLY PERMIAN**, i.e. during the late stages of the post-variscan peneplanation. The Permian lies unconformably on the previously deformed series. Roughly N-S and E-W oriented, grabens are known in the Pyrenees as well as under the basin itself; they are filled with red continental clastics and volcanic flows, with thicknesses up to 1,000 m. One of these grabens is the transverse (NE-SW-oriented) Elizondo trough in Basque country (Gapillou 1981) near St Jean Pied de Port.

Triassic - Jurassic

The **Triassic** was widely deposited in a flat-lying basin in the centre of the area, while **a second rifting event** prevailed in both the Parentis Basin, and along the southern basin edge, (near the North Pyrenean Fault Zone). High emerging blocks (e.g. Arbailles, Grand Rieu) were formed along the southern basin-edge, which alternated with deep corridors already during the Late Triassic. Submarine (ophitic) volcanic flows and intrusions took place at the Triassic-Jurassic transition (approximately between the Keuper salts and the Liassic anhydrites), near the Iberian-European plate boundary, but also to the north.

The thick Keuper evaporitic and shaly potential detachment horizon, which locally can be more than 1 km thick, allowed diapirism, folding and thrusting, as well as gravity tectonics (Zolnaï, 1975).

Jurassic- Early to Mid-Cretaceous rifting

This period is characterized by the beginning of the opening of the Central Atlantic Ocean and the propagation to the North of the Mid-Atlantic Ridge. The Bay of Biscay rifting corresponds to the extensive phase of the Late Jurassic (Montagné, 1986) - Early Cretaceous "revolution" or **third rifting episode** which creates E-W striking normal faults connected by N 20°E right-lateral and N 160°E left-lateral transtensional faults. A regional sinistral wrenching between the two plates is related to that deformation phase. In Aquitaine, the Jurassic paleogeography is characterized by diffuse W-NW/E-SE extension. As a result, the Jurassic sedimentation appears to be controlled primarily by the inherited basement faults (essentially the N 20°E, N 50°E-70°E and N 160°E sets of faults).

Transtension and pull-apart basins :

The Early Cretaceous geological evolution is marked by the paroxysm of the general north-south extension and anticlockwise rotation of the Iberian Plate, which resulted in the opening of the Bay of Biscay. Although the major transcurrent motion takes place along the European-Iberian plate boundary in a Baja-California style (Miranda Avilès, 2002), the entire region from the Parentis basin (north of the Aquitaine Basin) to the Ebro platform is affected by diffuse strike-slip movements. The high rate of sedimentation is controlled by the activation of N 110°E inherited faults while the N 40°E and N 160°E directions are used as minor relay faults. The Jurassic platform is dislocated along these main fault zones (Canérot, 1989), allowing for the development of a set of NW-SE rapidly subsiding, diamond-shaped basins or potentially pull-apart basins (Bourrouilh, Richert and Zolnaï, 1995, R. Miranda Avilès, 2002) and uplifts (with E-W and NNW-SSE trending edges. The W-E to WNW-ESE oriented **North Pyrenean Fault** was initially a braided fault-system. It stretches over 500 km in successive segments, between the easternmost Pyrenees to Basque country, where it splits into several E-W oriented branches, separating the different elements of the Basque Massifs. Its trace is lost beyond the transverse NE-SW Pamplona- fault array.

North-Iberian margin and oceanisation:

During Late Jurassic and Early Cretaceous, as the opening of the Bay of Biscay progressed eastward, faulted tilted blocks (of ten-km width), calved from the Iberian margin and landmass. Large areas of the present-day High Chain became emergent e.g. to the south of the Mendibelza massif in Basque country (Boirie and Souquet 1982), or in the Central Pyrenees, offering source areas for coarse clastics, which deposited into the deep sea-arm ("aulacogen", Souquet and Debroas 1981) to the north. Above the basal wildflyschs, the first thick sandy-shaly turbidite (flysch) sequence was deposited (Albian-Cenomanian).

In the meantime tholeitic basalt masses (pillows and lava flows as well as sheeted dykes and sills) were emplaced within the flysch furrow, between Bilbao and the area south of Tarbes. Correlative to the Bay of Biscay sea-floor spreading, the strike-slip tectonics and the differential drift movements of the Iberian and European plates (Plate 1, figs. 1 and 2), provoked the remobilization of lherzolites and a peculiar shear metamorphism all along the N-Pyrenean fault zone, known as "N-Pyrenean metamorphism".

Late Cretaceous – Tertiary diachronous extension/collision

Compression comes from the East...

Since at least the beginning of Late Cretaceous, the Iberian plate became in compressional contact with

the NW moving African plate. Iberia progressively crushed the space between its northern margin and the European plate. Compression was diffuse during Late Albian to Cenomanian; it became effective as early as in the mid ***Late Cretaceous*** (Turonian-Senonian) in the eastern part of the Pyrenees (Henry and Mattauer 1972, Souquet and Deramond 1989), and propagated progressively to the west during the Senonian. Compression provoked gigantic linear gravity slope sequences or "Evolutionary-mass flow-megaturbidites" (Bourrouilh *et al*. 1983), which can reach 90 km in length and a thickness of about 60 m. Similarly, in the southern Pyrenean Basin, but during the Eocene, compression is accompanied by the emergence of a syntectonic cycle of gigantic mass-flow-megaturbidites extending over 140 km in map view, and more than 200 m thick (Soler *et al*., 1970, Johns *et al*., 1981).

The main north-south compressional event of the Pyrenees began nevertheless from **MIDDLE EOCENE** onward. The main ductile deformation occurred at the plate boundary, within the North Pyrenean Fault Zone, which represents the most strongly compressed, schistosed, crushed part of the belt (Choukroune, 1974), and along the northern edge of the Iberian block. Former normal faults and hingelines were inverted into overthrusts, the northern limit of the highly compressed zone corresponding to the earlier boundary between the flysch furrow and the northern carbonate plaform. This long-lived tectonic edge has thus become the North Pyrenean Thrust Front.

The main structural events created or re-activated in this period from Late Cretaceous (Maastrichtian) to Oligocene are:

N 110°E folds, cleavage, stylolites, reverse faults and thrust planes either to the north or to the south.

N 20°E to 40°E, left-lateral lateral ramps.

N 160°E, right-lateral lateral ramps.

Normal faults are also present: in some areas they are striking N-S; some minor sub-E-W faults are also created in close relation to major thrusts trending E-W and salt ridge keystone collapse.

During the orogeny, several compressional episodes followed each other, the younger, more external faults (sole-faults of allochthonous units or rafts) deforming the earlier, more internal ones in a piggy-back fashion. The deformation and structural styles appear controlled by the rheology of the material involved: (a) the already fractured deep basement complex was involved in the compression, setting the sites for the major dislocations, and (b) major formations of the sedimentary column (e. g. Keuper salt, Lower Cretaceous marls, Albian to Tertiary flysch and molasse series) were still extremely incompetent during the period of compression. Large, open synclines and anticlines were first formed; the synclines later became overthrusted, overturned and/or thinned, sheared by the overriding anticlines. Specific structures or " nappes " were thus generated, which would seem uncommon in areas of greater crustal rigidity and with more competent sedimentary sequences (there are very few true flat-and-ramp thrusts and "duplexes" in the northern Pyrenees, Moen-Maurel *et al*., 1999).

The North and South Pyrenean Thrust Fronts are actually tectonic envelopes, and not continuous, unique, sole faults. They are composed by segments which relay each other, sometimes with important offsets. On the Northern Pyrenean side, several structural arcs exist: the Basque Arc, along the north-western Pyrenees, the Lannemezan Arc in the central northern Pyrenees etc., but also on the southern side, such as the Graus-Tremp Arc in the southern Pyrenees; their tips all lay in lateral or oblique ramps which were inherited from the rift basin edges. Two well-explored surface anticlines are centered in the northern arcs : the Ste. Suzanne structure to the west, and the "Petites Pyrénées" in the Central Zone. Thrust sheets do not exceed 12 km.

The Southern thrust sheets are therefore the most spectacular ones:

From Early Eocene to Oligocene, the Upper Thrust Sheets (Muñoz *et al*. 1986) or the South Pyrenean Central Unit (Seguret, 1972), composed of Mesozoic to syntectonic Tertiary formations, were successively transported along a sole of Keuper evaporites, argilites and marls (Bresson, 1903, Seguret, 1972, Muñoz *et al*. 1986). They are, from East to West, the Pedraforca, Boixols, Montsec, Cotiella Thrust sheets; the front of all outlines the South-Pyrenean Front Thrust, which produced the Sierras Marginales (plate 1).

In the High Chain, these cover thrust sheets root into the Upper Paleozoic basement, along with the deeper thrusts which are the Nogueras and the Gavarnie-Mont Perdu Units.

The total shortening of the Pyrenees is evaluated, depending on the authors, between 100 to 160 km.

Pyrenean orogeny and inversion continued during the **MIOCENE.**

Partitioning of the deformation (see Miranda Avilès, 2002) as well as rotational constrains induced along the basement faults produced "N-40°E" dip-slip (mostly left-lateral due to S-compression) and "N-160°E" (right- and left-lateral).

Neotectonic relaxation and uplift

The very latest, **PLIOCENE to HOLOCENE** episode of the Pyrenean orogeny seems to have been an important **relief development**, which uplifted the former southern (Iberian) margin to form the present-day High "axial" mountain Chain (+ 2,000 to +3,500 m MSL.), where Paleozoic outcrops were exhumed by erosion. This uplift movement, possibly a late- or post-orogenic isostatic adjustment, also deformed the former overthrust sheets, back-steepening those of southern vergence to near vertical.

Petroleum exploration framework

History

The Aquitaine area represents the largest oil and gas province of France. Although seeps have been known since Roman times, petroleum exploration of the South Aquitaine basins (foreland and foothills) started in the 1930's and resulted in the discovery of the St-Marcet Gas Field in 1939 (8 Gm3 of gas – 290 BCF) (Comminges Basin). The discovery well was drilled on a surface anticline. The area's positive potential was then confirmed by the discoveries of the upper Lacq oil field in 1949, the deep giant Lacq gas field in 1951 (260 Gm3 gas – 9.2 TCF) (discovery wells were drilled on gravimetric anomalies) and the Meillon gas field in 1965 (65 Gm3 gas – 2.3 TCF) (this discovery was made using 2D seismic data showing a surface anticline). In the same Arzacq basin, several smaller sized fields (Ucha/Lacommande, Rousse, Cassourat …) with accumulations ranging from 3 to 7 Gm3 gas (110 to 250 BCF) were also discovered during the same period. In the 1970's, exploration interest moved northward towards the basin edges, resulting in the discoveries of five sizable oil fields (Pecorade, Vic Bilh, Lagrave, Castera Lou and Bonrepos-Montastruc, fig. 6). Two hydrocarbon trends are clearly identified: a gas trend to the south along the leading edge and the proximal foreland of the Pyrenees Fold and Thrust Belt (the "Lacq-Meillon" domain), and an oil trend to the north along the edges of the foreland basin (the "salt ridges province") (fig. 6 and 7).

Reservoirs (Fig. 7).

Jurassic dolomites and Barremian limestones

They represent the main petroleum objectives; their occurrence is closely linked to the Jurassic and Earliest Cretaceous paleogeographic setting. Two domains can be distinguished in accordance with the paleogeographic provinces described earlier.

On the Jurassic eastern shelf the reservoirs are represented by the Lower Kimmeridgian Meillon dolomites (200 m thick in average), the Portlandian Mano dolomites (150 to 200 m thick) and Garlin breccias. These reservoirs are totally or partially gas-bearing on the Meillon gas-field trend as well as along the Ucha, Lacommande and Rousse trend of structures. For these two reservoirs the petrophysical characteristics are rather poor (2 to 4% matrix porosity for the Mano dolomites and 4 to 8% for the Meillon dolomite). For these formations, effective permeability is primarily due to joint fractures and vugs (due to secondary diagenesis), allowing for good well productivity.

In the Jurassic outer shelf to the west (Lacq, Pecorade and Vic Bilh fields), only the Mano dolomites are preserved as reservoirs within the Jurassic sequence. Even though the petrophysical characteristics are better, they remain poor (2 to 10%). Production is again primarily associated with intense fracturing and intervals characterized by a high energy of deposition. Within this same area the reservoirs also include the Upper Barremian limestones, which display porosities ranging from 10 to 15%. Permeability is again relatively poor but enhanced by the intense fracturing.

The Lower Barremian is also one of the reservoirs of the Lacq giant field. Its low porosities (2-11%) and permeability are also enhanced by intense fracturation.

The Upper Cretaceous reservoirs

They correspond to the Lower Senonian limestones (200 m to 250 metres thick) of the Upper Cretaceous platform. The good reservoir characteristics of these limestones (15 to 20% matrix porosity) are closely linked to the high energy facies distribution and to a secondary dolomitization in the vicinity of the main Pyrenean faults. It is demonstrated by the example of the Lagrave Field where dolomitization and therefore reservoir capacity decrease significantly away from the immediate setting of the Tertiary Seron transcurrent fault system.

Seals (Fig. 7).

Barremian and Jurassic plays

Hauterivian to Valanginian shales, Barremian shales and anhydrites and Lower Aptian shales represent the most efficient seals for the oil and gas fields in the

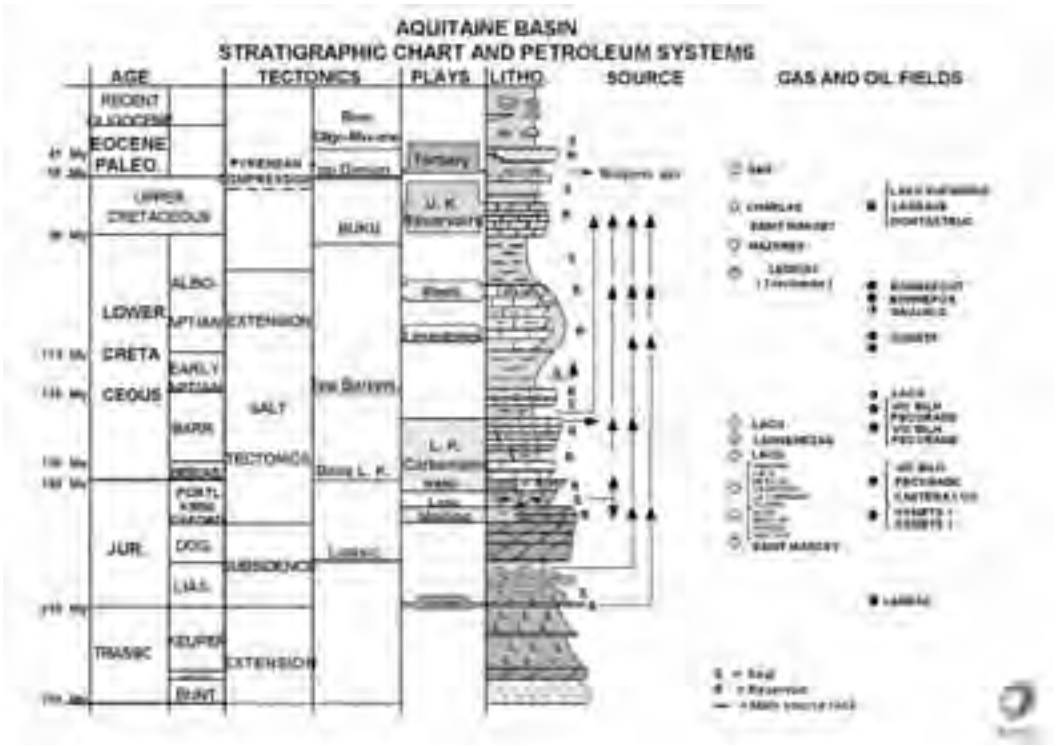

Figure 7 - Aquitaine basin : stratigraphic chart and Petroleum Systems (Total).

Arzacq basin.

Upper Cretaceous plays

Seals are composed of the Upper Senonian shaly or marly intervals and by the Lower Tertiary slope shales.

Source rocks (Fig. 7).

Important reserves of oil and gas have been discovered in the Aquitaine Basin, implying that sources with a regional extension and good petroleum potential are present in order to expel significant quantities of oil and gas. Although some source potential has been recognized in the Tertiary, Albian and Liassic shales, these formations are low-quality source rocks.

The main source rocks are clearly associated to the Barremian and Kimmeridgian formations (Lons Fm) as shown by the source-to-oil condensate and source-to-gas correlations.

The Barremian organic matter is primarily of marine origin including woody material (type II-III). Across the basin the oil window is reached at – 3,000 metres on average, while the gas window is reached at – 4,000 metres (fig. 8). It is noteworthy that expulsion of hydrocarbons started during the Late Albian at the level of the Lower Cretaceous depocenters of the Arzacq Basin and occurred during the Tertiary on both sides of the basin (fig. 8).

The Kimmeridgian source rocks appear to have the best potential. The organic matter is again primarily of marine origin (type II-III).

Trap types and hydrocarbon charge (Fig. 8).

The traps for the different fields are clearly related to structures which are inherited from the Early Cretaceous extension (platform to basin transition) and its associated salt tectonics along the limits of the basins (erosional pinch-out of the Jurassic and Barremian reservoirs). These traps have been enhanced by the Pyrenean orogeny. Some of them are located in the Pyrenean fold and thrust belt (Saucede and Ledeuix); but most occur within the proximal (Lacq, Meillon, Ucha, Lacommande, Rousse fields) and distal forelands (Vic Bilh, Castera Lou, Lagrave). Exceptional productive traps can be even found in episyenites (Moen-Maurel *et al*., 1996).

Volume n° 2 - from B16 to B33

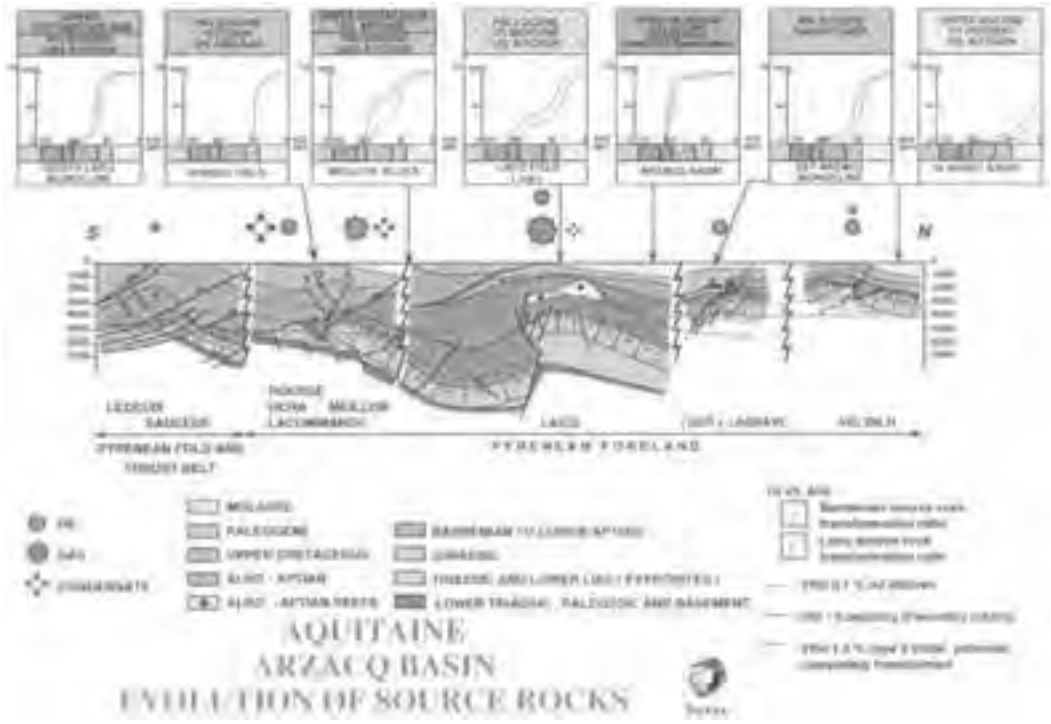

Figure 8 - Aquitaine-Arzacq Basin : Evolution of Source Rocks (Total).

Comparison with other Fold-and-Thrusts Belts

In comparison to others FTB, the following striking characteristics should be pointed out :

1) Crustal characteristics :

The continental crust here underwent diffuse stages of rifting from Triassic to Albian at the western tip of the tethyan domain over a broad area (400 km N-S wide) extending from the Parentis basin to the north to the Ebro basin and Cantabrian domain to the South. At the paroxysm of the Albian rifting, many rifts that can be investigated in the subsurface today, were en-echelon, as a result of the control of previous oblique basement fabrics that were acquired in Paleozoic times. However extension was never sufficient east of the Bay of Biscay to produce an oceanic floor and two differentiated passive margins.

Pyrenean (Late Cretaceous to Eocene) inversion mainly affected the Iberian plate, leaving the rift basins of the European plate in a little deformed retro-arc position (and preserving its petroleum systems, Moen-Maurel *et al*., 1999).

2) Plate motion vector evolution :

The anticlockwise rotation of the Iberian plate with respect to the European plate from Early Cretaceous to Cenomanian led to variations in trend, magnitude and sense of the displacement vectors, producing at the same time extension in the west and compression or strike-slip in the east.

The oblique extension between the Iberian and the European plates from Early Cretaceous to Cenomanian led to the partitioning of the deformation between strike-slip which focused on specific shear fault zones (supposedly reaching tens of km in strike-slip), and diffuse extension which produced en-echelon grabens with minor horizontal displacements along faults (no more than 5% horizontal stretching, Moen-Maurel *et al*., 1999).

During collision the use of potential detachments in the Triassic evaporites and in the Upper Cretaceous flysch led to varying structural styles making it difficult to measure the amount of strike-slip in the shortening phases from Turonian to Miocene. Nevertheless most thrust tips still exist at the outcrop or in the subsurface, therefore the cover deformation cannot accommodate any major oblique collision.

3) Salt tectonics

The existence of Triassic evaporites led to halotectonics

from Late Jurassic onward. Salt pillows and ridges were re-activated as anticlines during compression while evaporite-rich widespread units acted as detachments and thrust soles. The salt mobility triggered enhanced amplitude and curvature in fold axes, non-cylindricity and virgation, as well as a diachronous record of the tectonic stress events. When salt is involved onset and end ages of tectonic events may vary through time and space making it difficult to tie deformation to stress and/or plate tectonics.

4) Fold-and-Thrust belt structural style:

Thick-skinned thrusting affected the Iberian plate margin along the underthrusting plane, resulting in antiformal stacks of basement (Paleozoic) producing the axial zone of the mountain range. The steep dips of the basement ramps may have been facilitated by the oblique component of the collision initial vector and the existence of steep and weak shear zones from the Early Cretaceous drift stage (such as the North-Pyrenean Faut system).

Thin-skinned thrusting was possible when cover detachments could be activated over large distances: for the southern FTB it resulted in transferring the uplift and the 100 km range shortening in piggy-back fashion over a few large thrust sheets towards the external sierras, and for the northern FTB it resulted in producing a retroarc and in accommodating the axial overload with thrusts and nappes mostly affecting the Upper Cretaceous to Eocene flysch basins.

The shape and magnitude of the thrust sheets was strongly influenced by the attitude and potential friction of the detachment stratigraphic horizons: salt ridges in the north favoured large amplitude (up to 5 km) upright and overturned when they slid over flysch units. Rift grabens and flysch basins morphology influenced the location of both frontal and lateral ramps. This stratigraphic control leads to structural styles that are common along the alpine (tethyan) orogen, unlike craton margin orogens where isopach formations rather, led to flat-and-ramp thrust propagation such as in the Appalachians and the Rocky Mountains.

5) Petroleum evaluation

The North-Pyrenean retro-arc basin was a prolific oil and gas province with giant fields (Perrodon, 1980) because:

- the petroleum system trilogy (source rock, reservoir and seal) belonged to pre- and syn-rift series which are usually characterized by extensive and stable marine sedimentation making hydrocarbon migration easy and exploration more predictable even in areas of poorly imaged seismic prospecting (Moen-Maurel *et al*, 1995).
- the petroleum system trilogy series were protected from uplift and erosion over the Parentis and North-Pyrenean basins since they remain situated in the outer rim of the collision, in a little affected retroarc position. After rifting subsidence, the additional burial which was achieved with the foredeep deposition led to reaching the gas window and to the development of large gas traps.
- salt tectonics eventually enhanced the amplitude of traps and their closure. Such providence makes the Aquitaine oil and gas structures quite similar to North Sea oil and gas fields.

To conclude, it should finally be emphasized that first of all, the structural history of the whole area is controlled by a N110°E plate boundary crustal anomaly, running from West Greenland to the Tethys and then to the modern Mediterranean (R. Bourrouilh, 1970, 1973). This lineament is evidenced by the N-Pyrenean Fault and its peculiar metamorphism, the thinning of the crust, the Biscay rifting, the injection of the mantle lherzolites. The plate boundary crustal anomaly seems to be Pre-Triassic, putting in contact an Iberian deeply structured (with pre-existing crustal detachment faults) and thick continental lithosphere to the south, and a thin, less structured European one to the north. The Late Cretaceous to Tertiary tectonic shortening is asymmetric, being estimated, depending on the authors and the area, at 100 to 160 km over the Iberian plate, and at 5 to 12 km over the European one.

In its western part (Bay of Biscay), the Pyrenean orogen is incomplete. To the east, it interferes with the Betico-Kabylo-Alpine orogen and is overprinted by the extensive Neogene Mediterranean structures.

The result of the collision in the Pyrenees produces an asymmetric fan-shaped orogen, resulting from the crustal ductile underthrusting or underplating of the Iberian Precambrian-Paleozoic basement underneath the European plate.

The Pyrenean orogenic complex of the Pyrenees is devoid of granitic intrusions and syn-orogenic volcanism, there are no ophiolitic masses and the known metamorphism is restricted to the trace of the North Pyrenean Fault Complex (Choukroune 1974). This indicates that the major orogenic event in the area was the variscan one (tectonics with major crustal shortening, penetrative metamorphism and granitization). Parts of this structural crustal heritage (or regional fabrics) were activated during the Mesozoic extensions, re-utilized by the Late Cretaceous to Tertiary Pyrenean orogenic convergence.

Field Itinerary

DAY 1

Pau

Welcome to the field trip and the Pyrenees

By R. Bourrouilh, L. Moen-Maurel, J. Muñoz And A. Teixell.

Briefing and introduction to the Field Trip.

Stop 1.1:

Panorama of the Pyrenees : figure 1.1.

I. A transect of the northern pyrenees

By R. Bourrouilh* and L. Moen-Maurel**,

*Laboratoire CIBAMAR, Université de Bordeaux 1, Avenue des Facultés, 33405 Talence Cedex, France, e-mail : **r.bourrouilh@cibamar.u-bordeaux1.fr**

** TOTAL, 64018 Pau Cedex, France, e-mail : **laure.moen-maurel@total.com**

DAY 2

from Pau to Oloron Sainte Marie

Stop 2.1:

Le Tucq : the North-Pyrenean margin and the Upper Cretaceous flysch :

figures 2.1 a, 2.1 b, 2.1 c, 2.1d

Introduction: the South Aquitaine margin developed as a passive rifted margin during the opening of the Bay of Biscay. The N-Pyrenean rifted basins were created and filled by syn-rift Lower Cretaceous black shales. During Cenomanian (-96 Ma), rifted basins merged in a long and narrow furrow or the N-Pyrenean basin or trough, which was rapidly filled up by synrift and drift calcareous Cretaceous Flysch. However, the area underwent compressional tectonics as recently as 80 Ma ago, during the Late Cretaceous and the furrow rapidly retreated westwards, from 80 Ma to today, forming, up to now, the modern Bay of Biscay. The North-Pyrenean flysch sedimentation, can reach 7 km in thickness.

The section studied in this Stop pertains to Upper Cretaceous-Paleocene sedimentation (but the KT limit is now covered by road work) which is coeval with the closure of the basin, and the westward progradation of the silici-clastic Paleocene sedimentation.

Access: the Stop is on the D 934, on the right side of the road, just at the locality "Le Tucq". The outcrop section is located in the curve of the road (figure 1.1a) and the measured section (figure 2.1b, Tucq section and 2.1c, Guillampeau section) along the side of the adjacent car track.

Structural and sedimentological landscape: the D

Figure 1.1 - Geological view of the Pyrenees, from the Boulevard des Pyrenees, Pau.

Figure 2.1a - Flysch section at Guillampeau, top is on the right.

934 crosscuts the Upper Cretaceous flysch. The curve of the river, as well as that of the road are provoked by the top of the Upper Cretaceous flysch, containing large white mudstone mudflows, as well as reworked Triassic (first diapiric) gravity slabs mass-flows, silici-clastic mass flows etc. In the landscape, the curve is marked by an old chalk oven, and prolonged by a smooth wooded cliff.

Along the western side of the road two field sections have been measured in the gently north-dipping turbiditic and mass-flow sequences with internal slumps (Bourrouilh, Montagné and Doyle, 1993, unpublished data).

The first one, or the Tucq section is just on the curve of the road, in front of the Tucq restaurant, but is now covered by road work (figure 2.1b):

The Upper-Cretaceous to Paleocene section is 27 m thick and represents a mixed silici-clastic-carbonate sedimentation. Five sedimentary units can be distinguished. On the four basal units, the sedimentation is mainly constituted by successive silici-clastic mass-flow deposits, reworked mudstones

Figure 2.1b - measured section at Le Tucq, from R.Bourrouilh et al., 1993, unpub. data.

and anoxic mud clasts, and by silici-clastic Bouma-type turbidites. Measured sedimentary fold axes are, successively, from bottom to top : N 60°, dip 35°E (unit 2, lower part), N 83°, dip 10° SE (small slump, unit 3), N 175° (large slump, unit 3), N 90° to 110° (clast, base of unit 4), N 115°, dip 25°N, (base of unit 5), N 115°, dip 22° N-NE.

However, carbonate gravity sedimentation comes back again and forms unit 5, considered the base of a large carbonate mud-flow.

Figure 2.1ca - measured section 1 at Guillampeau, from R.Bourrouilh et al., 1993, unpub. data.

Figure 2.1cb - measured section 2 at Guillampeau, from R. Bourrouilh et al. 1993, unpub. data.

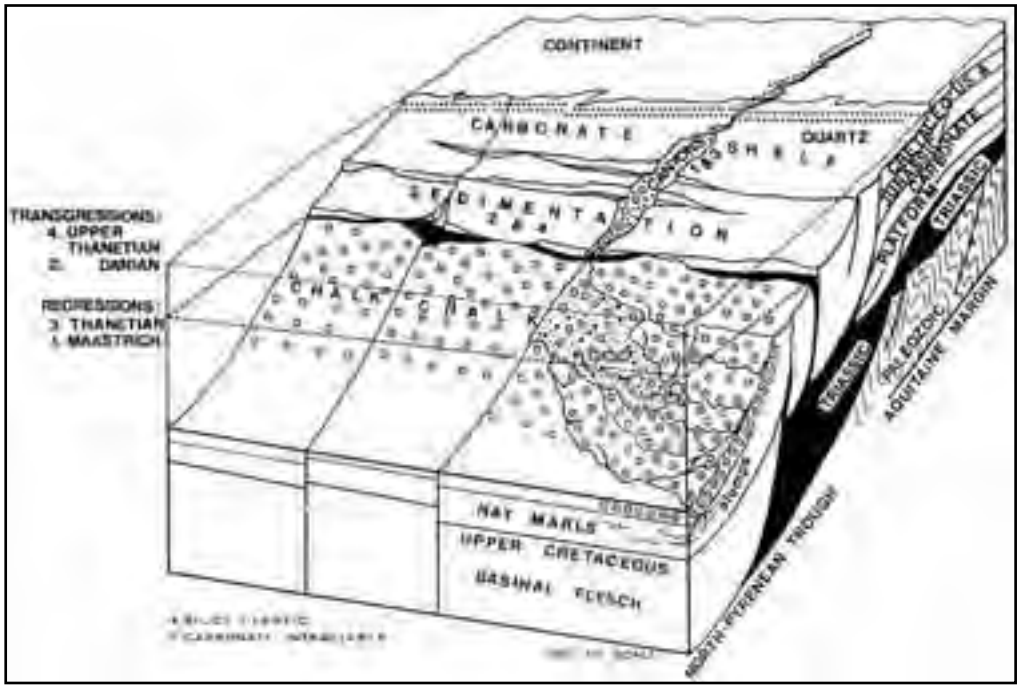

Figure 2.1d - Schematic reconstruction of the Dano-Paleocene Aquitaine margin at Le Tucq, from R.Bourrouilh et al. 1993, unpub. data.

The second one or the Guillampeau section is measured along the side of the road (fig. 2.1ca and 2.1cb)

Conclusions: figure 2.1d : the margins of the N-Pyrenean basin appear to be instable during the late Late Cretaceous to the Early Paleocene even though thicknesses across the North-Pyrenean domain do not vary as much as below in the Campanian and above in the Ypresian. This relative instability is due to a high amount of carbonates deposited on the edge of the shelf and to the progressive closure of the N-Pyrenean basin-Bay of Biscay, due to the progressive westward migration of the interplate compression.

For further information: Stevaux and Zolnaï, 1975, G. Montagné, 1986, Seyve, 1984.

Stop 2.2:

the Ossau Valley: uplifting, glaciers and neotectonics: Sévignacq (figure 2.2)

The small village of Sevignacq is built on the morainic frontal vallum of the glacier, which went down from the High Range and the Pic du Midi d'Ossau, flowing northward through the Ossau Valley (in Béarnais, which is the local language: Aüssaü = high valley).

Access: leaving the main road D 934 from Pau to Laruns, at Sevignacq, on the right take the small road

Figure 2.2 - Panoramic view of the Mailh Arrouy and Ossau Valley (Total).

D 232, from Sevignacq to Bescat. The Stop is located after leaving Sevignacq and a few hundred metres down, after the cemetery, in the plain.

Structural landscape: the panorama shows, from left to right: the Mesozoic high mountain of Mont du Rey, the glacial U-shaped valley of Ossau, with the high chain and the faulted caldera of Pic du Midi d'Ossau in the background, and on the right, the Mesozoic Lazerque (1,368m) and Mailh Arrouy (1,251m) mountain range.

Interpretation: the Ossau glacier was one of the most important Würmian Pyrenean glaciers, which flowed south to north, from the High Chain to Sevignacq. At its front, it produced a large moraine, which surrounds us as a morainic vallum. Deglaciation began some 11,000 years ago and the glacier was about 1,000 m thick here. Melting of the ice provoked a reduction of the ice weight on the crustal lithosphere, which began an upward isostatic buoyancy and slowly rose up. The mountain range is still being uplifted under relaxation at present. Rising of the mountain all around provoked in turn the Ossau river to change its course from north to west, cutting the moraine and the Urgonian limestone to the West.

The Ossau river now flows towards the west after cutting the frontal moraine and the cretaceous bedrock in a narrow deep neo-tectonic canyon, located in the western outskirts of Arudy village.

But an underground northward paleocirculation of the Ossau waters still exists and flows to the north, under the frontal moraine and producing a resurgent spring in the karstified limestone north of Rébénacq. There, the river is called "Luy du Néez".

Stop 2.3:

Arudy: opening of the rift as recorded by mud mound markers (fig. 2.3a and 2.3b)

Introduction: at the village of Arudy, several Aptian-Albian mud-mounds are or were worked for marble. Geological studies (Bouroullec *et al*., 1979), generally

Figure 2.3a - Stratigraphy and geodynamic evolution of the Arudy basin, from R. Bourrouilh, 2000.

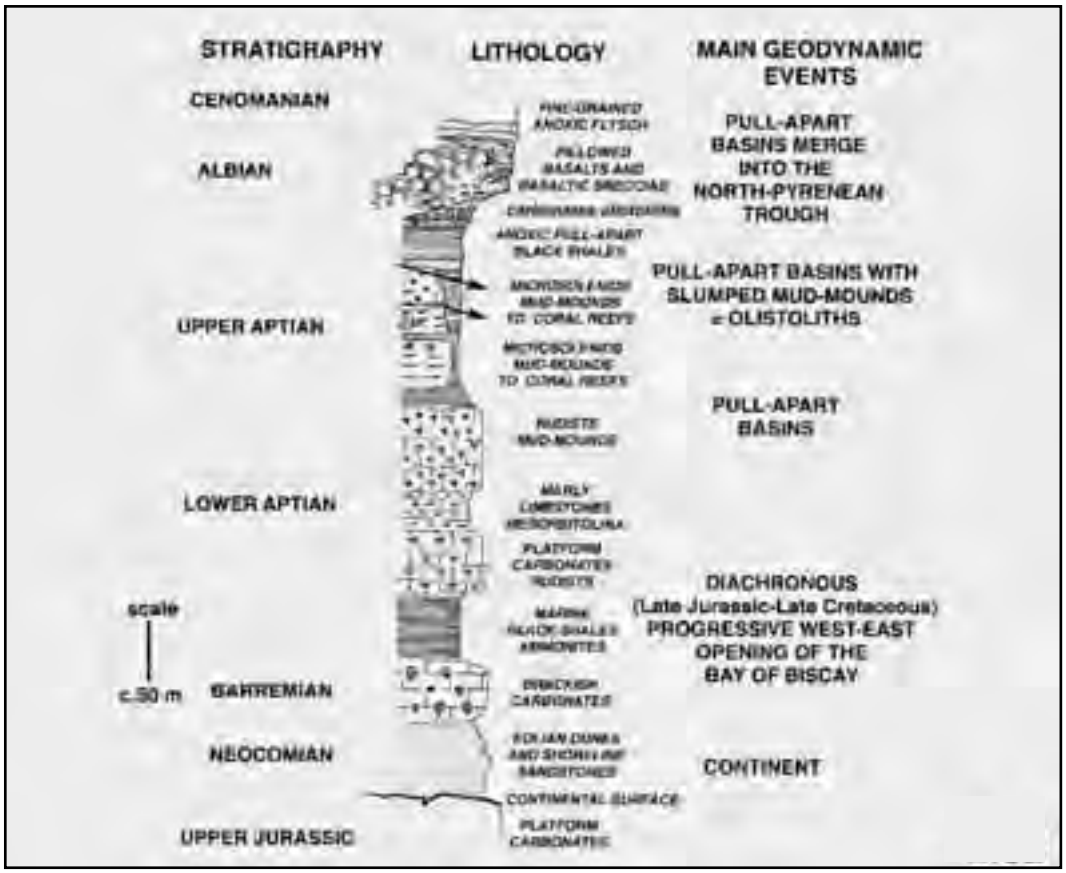

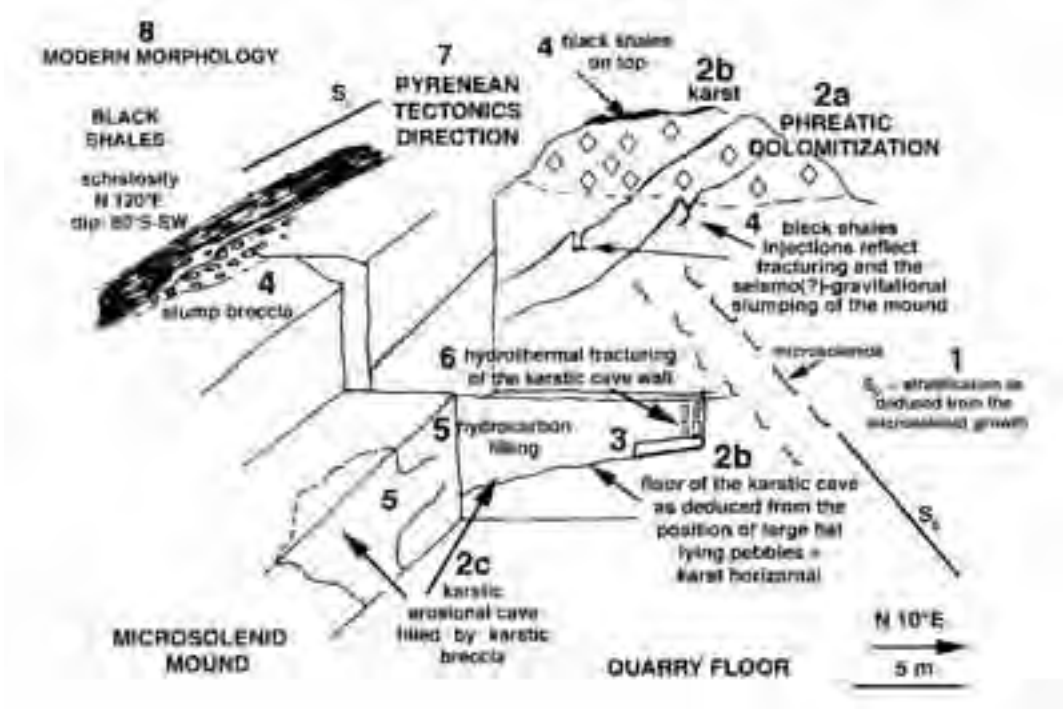

Figure 2.3b - Sketch of the Bois du Bager quarry, as visible in 1997, from R. Bourrouilh, 2000.

dealt with stratigraphy and micropaleontology. Digbehi (1987) was the first to present consistent sedimentological data on the area and to suggest that some reefs and mud-mounds of Arudy were in fact large blocks that have slumped into the black shale basin. Lenoble et Canérot (1993) and Canérot (1996), studied the relationship of the buildups to sea levels changes but they did not consider that some of these buildups could be not in their original position or that they could have been gravitationally displaced from their original environment.

Here we will only visit the Bois du Bager quarry, which represent an uppermost Aptian mud-mound slid into the black shale basin of Arudy during the latest development stage of the mud-mound complex.

Access: only the Bois du Bager quarry (or Borde Dela quarry) and mud mound, will be visited in this excursion. Access to the quarry is restricted. Ask Mr Laplace for access authorization well before visiting at the Paloma quarry along the Arudy to Lurbe road. Visiting the quarry, even when authorized, is at your own risk. North of Arudy, follow D 918 towards the West (Lurbe-St-Christau direction). After 1 km, turn left on a gravel road crossing the forest and leading up to the quarry, past a metal gate.

Structural landscape (R. Bourrouilh, 2000): on the southern edge of the N-Pyrenean rift, the stratigraphic sequence (Fig. 2.3a) shows a typical extensional and transgressive sequence: an Upper Jurassic to Lower Cretaceous disconformity is overlain by continental sandstones (Grès de Lacq), then by Lower Barremian lagoonal carbonates. From the Bay of Biscay, the sea invaded the area south of Pau during the Barremian and Ammonitic black shales were deposited. Then an Aptian-Albian carbonate platform developed: near the small village of Arudy, south of the city of Pau, this platform was marked by the growth of Aptian-Albian reefs and mud-mounds (Fig. 2.3a and 2.3b). These build-ups grew in a context of anoxic pull-apart basins. These pull-apart basins were progressively intruded by basic volcanism with floods of basalts, indicating the eastward progression of sea floor spreading of the Bay of Biscay onto the European continent (Plate 1, fig. 1 and 2).

We will focus here on the Bois du Bager mud-mound, situated 2 km south-west of Arudy. It consists of massive grey mudstones containing flat microsolenidae corals. According to L. Beauvais (pers. comm. 1995), microsolenids can develop in quite deep water and can tolerate a certain amount of turbidity in the water.

Those corals have umbrella-shaped morphologies, indicating a low energy environment; they grow in successive layers, indicating the stratification and the upper part of the mound.

The base of the mound shows a locally deformed contact with the underlying black shales (Fig. 2.3b). Along the basal contact, the lower part of the mound shows a slump breccia, with large mud-mound elongated clasts, some of them with microsolenidae, embedded in a black shale matrix. The mound also exhibits two layers of black shale, locally contorted and with load pockets. These layers of black shales can be interpreted as recurrence of mud sedimentation, or they reflect shale intrusions into the mound which slid downwards with the mound itself. Observation of the orientation of the microsolenids show that these two black shales are obliquely oriented, and clearly indicate that the mud-mound has tilted over to an angle of about 90° from its normal position, considering that the concave side of the umbrella-shaped microsolenids faces upwards. The body of the mound consist of massive grey microsolenidae mudstones but it also shows a large karstic erosional cavity which reflects emergence (Canérot, 1996). The cave is filled with a karstic breccia, partly originating from the mound itself. (Fig. 2.3b). The breccia is partly dolomitized and locally impregnated by bitumen.

In order to determine the diagenesis of the mound and the quality of the marmoreal limestone, a new geophysical tool, the electrostatic quadripole was used (Benderitter *et al*, 1997). A precise resistivity map of the diagenesis and of the fracturing was obtained, showing the mud-mound build-up, the karstic cave and its brecciated karstic infill.

This side of the mound is karstified and the karstic cavities are filled with black shales (Fig. 2.3b). This area presents a white to light grey colour and it is largely dolomitized. Study of the dolomitization shows that this reflects the contact of the mound with the phreatic lens (Bourrouilh-Le Jan, 1973, 1975), related to emergence.

Geodynamic interpretation: a provisional scenario for this mound development is proposed hereafter based on geometry, stratification, geopetal structures, karst, filling of the karst, diagenesis (Fig. 2.3b) The following numbers refer to the numbers on Fig. 2.3b:

1. The Bois du Bager mud-mound began to develop as soon as turbiditic black shale deposition input decreased significantly (microsolenids can tolerate a certain amount of turbidity). The mound probably grew near the aphotic-subphotic zone transition, and certainly below storm wave base (no evidence of wave action). Stratigraphy and original position of the mound is shown by the layering of microsolenids (So on Fig. 2.3b).

2. Due both to growth and to the opening of the Arudy Basin, the mound slid and rotated 65° clockwise towards the NE (N 30°E). This rotation produced emergence of the SW flank of the mound; this emergence does not seem to reflect a sea level fall, as proposed by Canérot (1996). Emergence was accompanied by aerial and karstic erosion of the mound. The flank of the mound is eroded by karstic cavities. Karstic erosion penetrated deep into the dead mound, resulting in the formation of a large karstic cavity, which was then filled by a breccia (Fig. 2 .3b). A large part of the breccia is autochtonous, but blocks of overlying shallow water units, some as long as 2 metres, also fell down in the cavity.

3. These clasts are interpreted here as reworked parts of coarse graded supratidal to intertidal storm deposits (Fig. 2.3b). The original deposits, where they originate, are not observable in place, laterally or directly overlying the mound, but the presence of such clasts among the karstic breccia testify that near the emerged mound, supratidal to intertidal storm sediments were deposited. These flat-lying clasts indicate horizontal bedding during the karstification period, which is in agreement with the geometry of the karstification. We can suppose that the storm deposits have been eroded, broken and taken away as clasts, which fell down in the karstic cavity.

4. Renewed tectonic activity led to an anticlockwise 125° rotation of the mound towards the SW (N 210°E). As a result, the mud-mound collapsed and slid down into the deep black shale basin, where it was buried, forming a large olistolith (the mound is covered up by, and embedded into the black shales). The slumping resulted in the formation of a slump breccia (on the base of the mound, 4, Fig. 2.3b), and of the two intrusive black shale layers, parallel to the basal surface of the mound (4, Fig. 2.3b). These black shale layers are deformed and contorted.

5. The dead mound was then buried in the black shales and later in the basin evolution, oil migrated into the karstic cave (5, Fig. 2.3b).

6. The thermal development which matured the oil also seems to have been responsible for exfoliation of the karstic cave wall, above the reworked "pebbles" (6, Fig. 2.3b). Fragments of exfoliated cave wall are observed lying perpendicularly to the

basal clasts. White calcitic cements filling the pores between exfoliated wall fragments may also be of hydrothermal origin.

7. The Pyrenean orogeny folded the whole area, producing a N 120°E subvertical schistosity in the black shales and fracturation of the mound

Hydrocarbons: the Aptian karsts that affect the mud-mounds produced dissolutions which enhanced the permeability (and thus the productivity) of subsurface analogs (Bonnefond field). The Clansayesian reef intervals also represent one of the plays of the Aquitaine basin (Gaujacq diapiric oil shows in the Arzacq Basin, Mimizan North oil field in the Parentis Basin).

The hydrocarbon filling of the Bois du Bager mud-mounds karstic cavities is a good example of how HCs migrate and how they can concentrate into mud-mounds or intrabasinal high-porosity anomalies.

For further information: Canérot and Lenoble (1991), Canérot (1996), Bourrouilh (2000)

Stop 2.4:

Cezy unconformity and stratigraphy of the Iberian Upper Cretaceous limestones or "calcaires des cañons" or "calcaires des Eaux Chaudes" (fig. 2.4a and 2.4b).

Introduction: crossing the North Pyrenean Fault at Laruns, we now drive along D934 through the Paleozoic basement of the high chain and the Iberian plate. Passing the crossroad with D 918 to Les Eaux Bonnes and Aubisque pass, to the left the road cuts metamorphosed Devonian limestones; to the right, a scenic view shows the ice-age Ossau Valley. When the road begins to turn left, and before entering a tunnel, it is possible to observe, on the right side, the deep sub-glacier valley of the Ossau river, which cuts the Devonian limestones in a deep canyon; meanwhile the base of the glacier is clearly observable above, with its characteristic U-shaped profile.

The road will cross in the forest several south-verging thrusts near Les Eaux Chaudes.

Access: crossing the village of " Les Eaux-Chaudes ", so called for its warm thermal waters related to the North Pyrenean Fault, we will Stop on D 934 to observe the Cezy Upper Cretaceous unconformity (figure 2.4a).

Figure 2.4a - Southverging Thrusts and Folds of Les Eaux Chaudes and panorama of Cézy. Pal= Paleozoic, T= Triassic, C=Cenomanian, T=Turonian, Co=Coniacian, Sa= Santonian

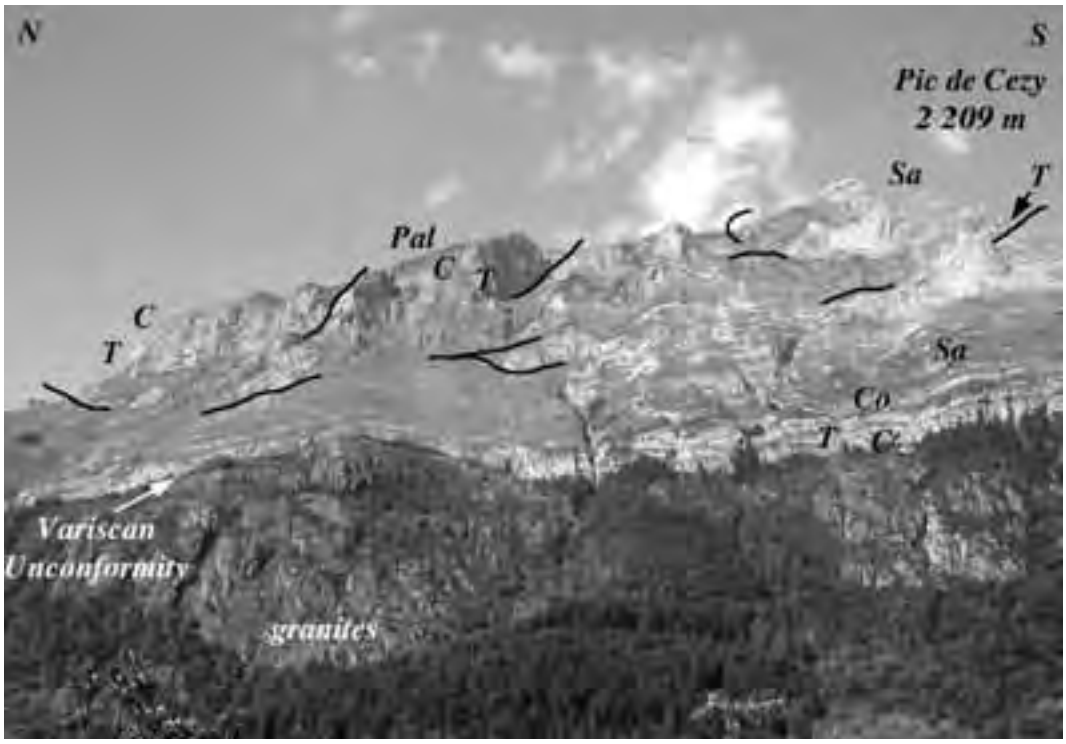

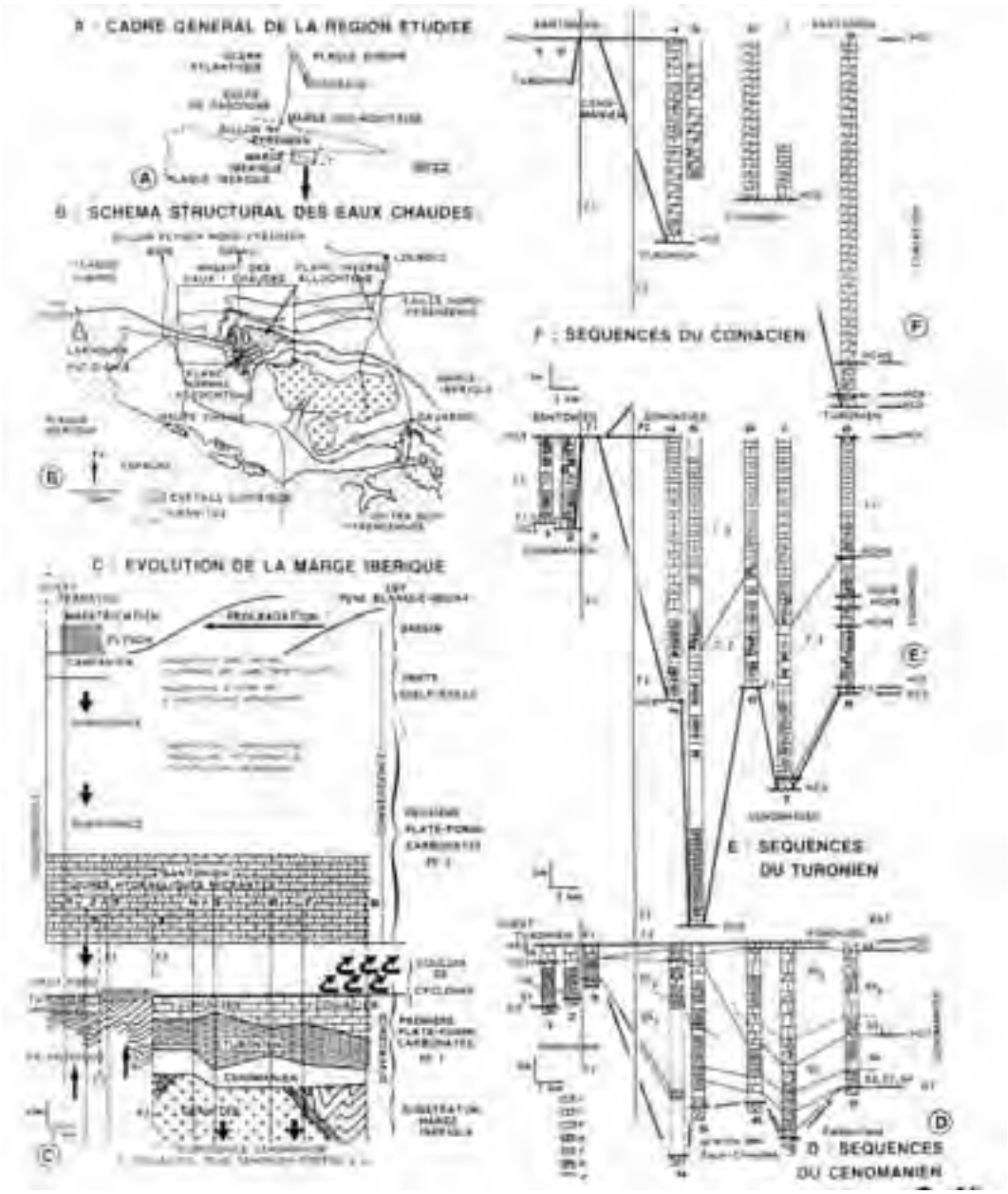

Figure 2.4b - Stratigraphy and geodynamic interpretation of the Iberian margin and of the " Canyon Limestones " or "Calcaires des Eaux Chaudes", at locus typicus. A, B = location and structural sketch ; C= Iberian Margin evolution ; D= Cenomanian ; E= Turonian ; F= Coniacian. From R. Bourrouilh and M. Alhamawi, 1993.

Structural landscape (figure 2.4a): the High Chain is there composed by a huge Paleozoic series, intruded by the Variscan granites of Les Eaux-Chaudes, which metamorphosed the surrounding rocks. Observing the panorama, we see the granites, abruptly eroded and overlain by the transgressive Cenomanian shallow water limestones, followed by Turonian and Santonian (yellow) limestones. This autochthonous

Volume n° 2 - from B16 to B33

Upper Cretaceous series is overlain by a thrust, composed by a slab of evaporitic Triassic at the base, followed upwards by a thick series of Upper Cretaceous limestones. A second Upper Cretaceous series, still resting on evaporitic Triassic, is thrusted again over the underlying thrust, forming an inverted flank of a south-verging recumbent fold. The inverted Paleozoic basement form the pic de Goupey (2,209m) just above the parking area.

Interpretation: when the Jurassic Aquitaine platform broke up in response to the opening of the Bay of Biscay, the Iberian plate remained emerged in this area up to the Cenomanian (-96 Ma). In large areas such as the Cezy Mountain, the emerged Iberian basement was eroded. Huge erosion accompanied by fluvial transportation led to deposition of thick fluvial and deltaic conglomerates (1 km thick) called the Mendibelza conglomerates. Such fanglomerates deposited on the northern margin of the Iberian plate, from here westwards to the Bay of Biscay. During the Cenomanian, the sea came again in a general transgression. In this period, the Iberian plate was located south of its actual position, in an intertropical latitude. Upper Cretaceous shallow water limestones deposited directly on the Iberian plate basement, from Cenomanian to Santonian, sealing the pre-Cenomanian erosional continental surface of the Iberian plate or resting above the Eaux-Chaudes granites. During the deposition of these Upper Cretaceous shallow water limestones, the Iberian northern margin was also the margin of the deep (-3,000 m deep ?) North-Pyrenean basin which developed north, along a N 110° axis.

Sedimentation of the Upper Cretaceous limestone occurred in a shallow sea (figure 2.4b), in an environment quite similar to the modern Bahamas and, like in the Bahamas, the Eaux Chaudes limestone or " limestone of the cañons " exibits sedimentation features from hurricane trails (Bourrouilh and Alhamawi, 1985). However, as the tectonic compression between Iberian and European plates progressed during the Late Cretaceous, the South Pyrenean and North-Pyrenean foredeep basins developed while the Iberian plate differentially sunk westwards. As a consequence, deep calcareous flysch facies appear here during the Late Santonian-Campanian announcing compression in the West (Bourrouilh and Alhamawi, 1985).

For further information: Ternet (1965), Bourrouilh and Alhamawi (1993).

Stop 2.5:

Artouste: the South-verging Folds and Thrusts of Les Eaux-Chaudes: figure 1.5 and Plate 1, fig.1

Introduction: the Paleozoic basement of the Iberian plate was folded during the Variscan orogeny and then intruded by granites. Directly on this continental basement the Cenomanian transgressive sea deposited shallow marine limestones and this sedimentation continued during a major part of the Late Cretaceous. An incipient compression began here during the Senonian: the future High Chain downwarped, the shallow water limestone facies deepened and was overlain by deep water flysch facies. Tectonic compression migrated westwards and provoked the tectonic inversion of the northern margin of the South Pyrenean basin, and a series of successive basement + cover south-verging thrusts.

Access: from the bank of the Fabrèges dam reservoir we will take the telepherique (cable-car) up to the Artouste ski resort. A short walk will bring us to the top of a Paleozoic crest.

Stop 2-5a:

in this panorama to the south (Fig. 2.5a), the highest peak of Pic du Midi d'Ossau (2,884m), springing out of the landscape to the West, is constituted by a ring dyke surrounding a large caldera (about 7 km in diameter) of an Upper Carboniferous-Permian volcano. Later, the caldera was truncated by Upper Variscan faults and then, during the Pyrenean orogeny, the northern half of the caldera and of the ring dyke were thrusted to the south; post-glacial erosion as well as recent uplifting of the Chain produced the Pic du Midi d'Ossau (F. Bixel *et al*., 1985).

The high part of the Ossau Valley clearly shows a glacial morphology, created by the Quaternary Ossau glacier, now occupied by the Fabrèges reservoir.

Stop 2-5b:

crossing the crest, we now go downhill and have a northward panorama on the Eaux Chaudes massif: see front cover, figure 1: over the Paleozoic basement of the High Chain (right), intruded by Upper Variscan granites, the Upper Cretaceous limestones rest unconformably and are overlain by the large south-verging thrust sheet of Les Arcizettes. Further to the north, this thrust sheet is also overlain by another south-verging thrust sheet of Gourzy, which is an overturned fold (Ternet, 1965, Alhamawi, 1985).

For futher information: Ossau peak: F. Bixel *et al*., 1985, Eaux Chaudes massif: Y. Ternet, 1965, M. Alhamawi, 1985, R.Bourrouilh and M. Alhamawi, 1993.

Figure 2.5a - Southverging Thrusting of the Late Paleozoic Ring Dyke of the caldeira of the Pic du Midi d'Ossau.

Stop 2.6:

the Benou Plateau : thrusts and folds in the Ossau Valley: figure 2.6a and 2.6b.

This Stop represents a panoramic view of the Ossau Valley in the North Pyrenean Zone. It is the domain of the Béarn Ranges dominated by E-W structures (Mailh Arrouy, Barescou syncline, Moulle de Jaout anticline …). Nevertheless, the Ossau Valley marks the occurrence of transverse structures (lateral ramp),

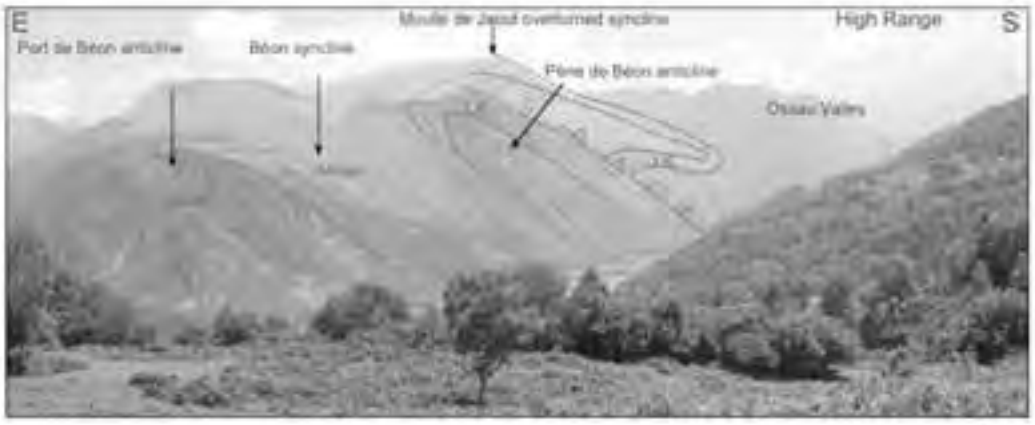

Figure 2.6a - The Benou Plateau : thrusts and folds in the Ossau Valley.

Volume n° 2 - from B16 to B33

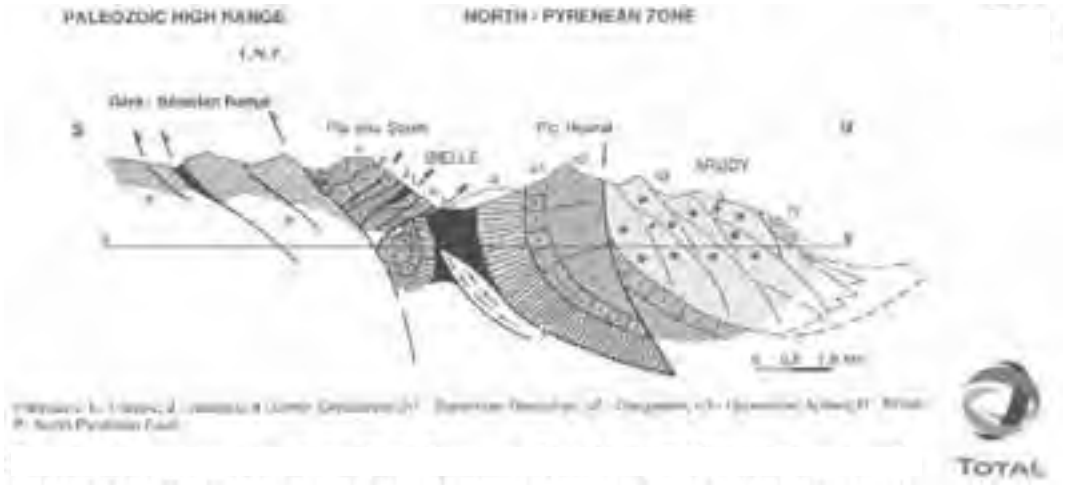

Figure 2.6b - Structural cross-section of the N-Pyrenean Zone in the Bielle area, Ossau Valley, (Lenoble and Canérot, 1992).

related to inherited Cretaceous normal faults.

Access: head towards the eastern end of the Benou plateau above Bielle. Take the trail that heads north, up to the vulture feeding grounds. Park around the high-voltage electric post.

Structural landscape: the glacial topography of the middle Ossau Valley can be observed here from the plateau on the Benou lateral moraine. The view of the southern slope of the valley shows the following, from south to north (Fig. 2.6a and 2.6b):

The Pyrenean High Chain, with its unconformable Upper Cretaceous cover deformed in the complex of the "Eaux Chaudes" recumbent folds (Pic de Ger, especially, see Stop 2.5b).

The North Pyrenean Fault (NPF), striking east-west, which is subvertical and outcrops in the Aste-Béon Triassic strip and in the Louvie pass.

Finally, ***the North Pyrenean Zone,*** detailed by the Jaout Albian-Aptian folded series (Jaout syncline, the Pène de Béon faulted anticline) and the reverse monocline series (Lias to Albian) dipping 70° towards the south, in Rey Mountain. This series is faulted against the Port de Béon Aptian units (Port de Castet fault). This fault zone consists of Triassic ophite horses mixed with Paleozoic horses.

To the east, the Rey Mountain series outcrop again on the crest of the Izeste Woods. The twisted series dips towards the north. The extension of the folded Jaout complex can be found in the five imbricate slices of Pla dou Soum. The latter constitute the detached cover of the Paleozoic sheet of Gère-Bélesten. The entire group is thrust to the northwest over the folded WE, sub-vertical structures of Bergoueits Woods. The flexured thrust fault, called the Ossau transverse thrust, strikes N30°E (Lenoble and Canérot, 1992).

Interpretation: the Ossau thrust clearly cuts the south-verging Benou thrust front (and that of the Mailh Arrouy). Its late activity has a W-E right-lateral strike-slip component. It has been established that the fault re-used an ancient N30° normal fault, active during the Liassic, the Early Kimmeridgian and the Albian. That fault bordered the western edge of the Ossau Horst. Lenoble and Canérot (1992) have also demonstrated that the Pic de Lauriolle diapir (second generation ridge), marked by breccia infill (collapse breccias) to the south of the Lassourde basin, is located exactly at the intersection of that N30° Albian Ossau fault and the Ibech fault (a W-E fault running along the Haute Soule first generation diapir ridge). This again demonstrates the fundamental role that is played by extension-related (transtension) Mesozoic paleogeographic structures in the subsequent development of compressional structures (transpression).

For further information: Lenoble and Canérot, 1992; Casteras, 1974; Henry, 1987.

Stop 2.7:

Mailh Arrouy view from Barescou syncline (Jurassic reservoir and source rocks) : figure 2.7a and 2.7b.

Access: at Escot, take the road that leads along the Barescou Valley to the Ossau Valley through the Marie Blanque pass. Park near the bridge which

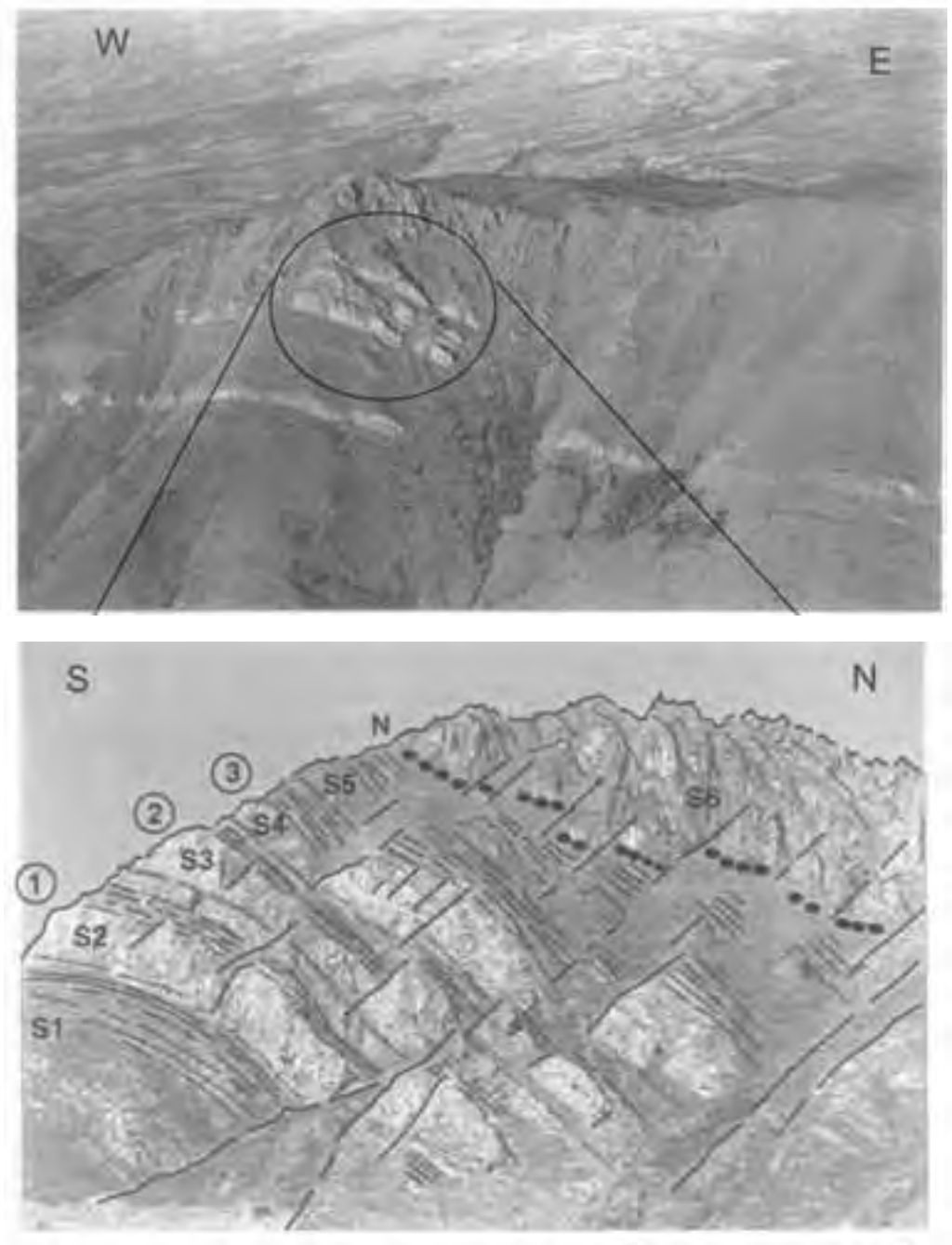

Figure 2.7a and b - Sequence Stratigraphy of the Middle Jurassic of the Mailh Arrouy (Total).

crosses over the Barescou stream.

Structural landscape: The topography of the Mail Arrouy reveals good outcrops of the Jurassic series that are thrusted southwards with a sole of Triassic evaporites and shales onto the Albian flysch of the Barescou syncline (Fig. 2.7a and 2.7b). This series shows, from base to top, the Lower and Middle Liassic limestones, the Upper Liassic marls, the

Volume n° 2 - from B16 to B33

grey "filament limestones" of the Aalenian, lower dolomites called the "Mailh Arrouy dolomites" made of recrystallized oolitic shoals and lagoonal facies.
The thrust fault dips 20° to 30° northward, at the base of the Lower Liassic limestones, and laterally at the base of the Triassic.
Sequence stratigraphy: the Bathonian limestones were divided into 3 third-order sequences (S2, S3 and S4, shown on Fig. 16 a and 16 b). Observe the sequence limits in the grey scarps of the landscape. Each sequence limit begins with a coarsening upward series (highstand system tract, followed by lowstand system tract) and then a fining upward series (transgressive system tract). The grassy slopes separating the limestone cliffs comprise the maximum flooding surfaces of the sequences. The overlying black dolomites were cut into two complete series (S5 and S6). Note the rapid development of the highstand system tract in S6 (pinnacle of the Mailh Arrouy).
Hydrocarbons: the Mailh Arrouy dolomites are thick and porous (especially the oolitic shoals), and constitute good hydrocarbon reservoirs. They can be compared to the dolomitic levels of the Meillon field. The Liassic marls constitute one of the source rocks in the Aquitaine basin, especially in the eastern sector (Comminges basin – Saint Marcel field).
The geometry of the monocline (and particularly the southern edge of the block) is also similar to the structure of the Meillon gas field.
For further information: Henry, 1987.

Stop 2.8:

Herrere : Pillow-lavas of the Albian rift stage: figure 2.8 (Moen-Maurel *et al*., 1996).
Access: south of Herrère (D 920) between Oloron and Arudy), park at the Courrèges Farm just north of the railroad crossing. Pillow-lava flows are located in the cliff beside the corn crib. A pedestrian path is located to the left of the farm gate.
Stratigraphy : the pillow-lava flows are interbedded within the Albian black marls (Fig. 2.8). They are part of a suite of volcanic textures also displaying basaltic columns and pyroclastic breccias, visible in other parts of the Ogeu Basin. The epivolcanic to mesovolcanic magmatic rocks include episyenites and teschenites (under-saturated syenites) that are exposed a few km to the west, and that are prevalent in the subsurface to the west. Here the submarine volcanic lava tubes dip 20-30 to the south and end in larger round tips to the southwest. Smaller pillows are intercalated between the tubes.

Figure 2.8 - Pillow-lavas flows of the Albian rift stage at Herrer (20 cm long pencil for scale).

Structural setting and hydrocarbons: part of the dip of the tubes was acquired during folding of the Belair Anticline whose N110 axis is located a few hundred metres to the north of the pillow-lava outcrop. The axis of the anticline plunges gently to the west beneath the Gave d'Oloron Thrust. In the 3D seismic, one can see at - 1200 m/SS a similar antiform made of low frequency markers that were drilled at Ledeuix and which produced gas (Moen-Maurel *et al*., 1996). The reservoir consisted of chilled margins of episyenite sills. The source rocks were the Albian black marls that were affected by magmatism. These marls acted as source rock and seal. The Albian marls can be over a km thick, and thus provide the best seal over most of the Aquitaine fields (Lacq, Meillon ...).
Tectonic significance: the southward flow of the tubes indicates that the normal (extensional) fault that favoured the uplift was located to the north of the outcrop. Volcanics and episyenites represent the magmatic expression of the mid-Cretaceous rifting between Iberia and Europe. However there is no sign of oceanic crust development, nor of margin separation. In the North-Pyrenean domain the rift was limited to half-grabens en-echelon basins, and basins controlled by diamond-shaped fault patterns. Rift axes that are located over the Pyrenean axial zone (eroded down to the basement, or likely beneath the thrust

sheets, such as for the North-Pyrenean Fault) would be better candidates for the hundred-km long, left-lateral strike-slip displacement that occurred between Iberia and Europe through the Mid-Cretaceous.

DAY 3

from Oloron Ste Marie to Saint Jean Pied de Port

Leaving Oloron by the southern road N 134 to Col du Somport and the Spanish border, we enter the Aspe Valley, along which runs the Gave (river) d'Aspe. Along the valley, there also exists a railway linking Oloron and the Spanish railway station of Canfranc. This railway was cut a long time ago and discussions between Spain and France are still taking place, to restore it and the railway link. Entering the valley and the mountain, railway bridges, tunnels are visible on both sides of the N 134.

Stop 3.1:

Pont d'Escot - Ste Suzanne Formation (seal) : figure 3.1a, 3.1b, 3.1c

Access: 15 km south of Oloron, on the N 134, we will Stop in the parking lot, just after passing one of these railway bridges, the Pont d'Escot.

Stratigraphy, structural geology: from south to north, the road cut reveals the Aptian sedimentary evolution of the Sarrance anticline's sub-vertical northern limb. The rapid transition from Bedoulian Ste-Suzanne marls, to Gargasian (Urgonian) limestones (with Toucasia) is nevertheless progressive within a highstand environment. Further up-section, the Urgonian facies is prevalent within the lowstand of the next sequence (Fig. 3.1). The sequence limit probably corresponds to a sedimentary hiatus, which can be observed at the base of the thick beds with abundant Rudistids. The schistosity is particularly well marked within the marly beds. Further south, and upslope, the marls are interbedded with limestones, indicating that the marly series comprises two distinct groups (Fig. 3.1b). This intermediate limestone and dolostone is a regional seismic marker in the foothills and foreland sub-surface.

Hydrocarbons: the Sainte Suzanne marl formation forms the upper or direct seal of many hydrocarbon fields in Aquitaine (Vic-Bilh, Pecorade, Lacq), and Meillon gas field, located 30 km SE.

For further information: Canérot, 1964; Castéras, 1974.

Stop 3.2:

Sarrance roadcut - Jurassic dolomites (reservoir formation).

Access: again driving south on the N 134 the Stop concerns the road-cut, three kilometres north of Sarrance. Park at the picnic grounds. Park on the side of the road-cut, please, put on the warning lights.

Sequence stratigraphy: the road cuts across the Jurassic rocks of the sub-vertical northern limb of the Sarrance anticline (fig. 3.1c). The road-cut reveals some sedimentary key points which have given rise to a proposed sequence stratigraphy (Canérot *et al*., 1990) for the North Pyrenees dolomite series. This study concerns the stratigraphic interval from the Bathonian to the Upper Callovian in the Bearn Ranges. The set was divided into five third-order sequences, termed DSI to DSV (Lenoble, 1992). Only part of sequences DS III to DS V can be observed here (Fig. 3.2).

Sequence DS III (30 m): finely bedded dolomites (outer shelf), grading into oolitic (offshore bars) and finally reef deposits (colonial corals, fig 3.2b). The series in this first unit represents the highstand system tract. The contact with sequence DS IV is not distinct.

Sequence DS IV (40 m): bioclastic dolomites, thick and then finely bedded (offshore bars), characterizing the lowstand system tract. They are overlain by a striking ferruginous discontinuity, overlain by bioclastic horizon, interpreted as a transgressive surface. The oolitic bars (shoreface) and the overlying striped dolomites (inner lagoon) probably correspond to a highstand system tract. The maximum flooding surface has not been identified.

Sequence DS V (15 m): thick dolomites (shoreface bars) overlain by striped dolomites (inner lagoon) correspond to lowstand and highstand system tract, respectively. The transgressive interval and the maximum flooding surface have not been clearly observed.

Because of intense fracturing, it was not possible to make a precise reconstitution of the described sequence. Stratigraphic determinations (Bathonian for DS III, Callovian for DS IV and DS V) are based on the correlation scheme between the Béarn dolomite series and the Basque series with abundant Ammonites, which was not subjected to epigenetic processes.

Hydrocarbons: the dolomite complex represented in the area was designated as the Mailh Arrouy formation, and considered as the equivalent of the

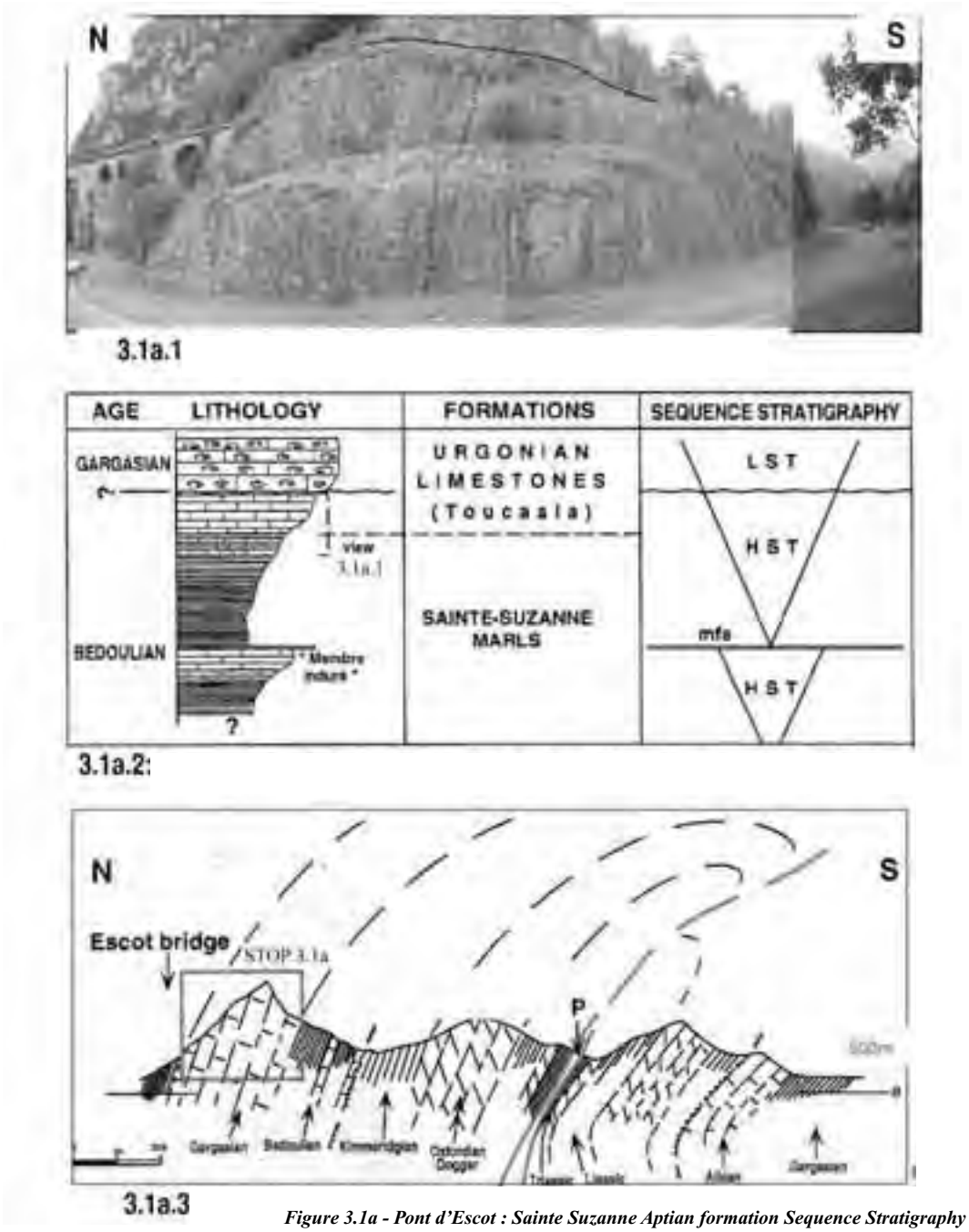

Figure 3.1a - Pont d'Escot : Sainte Suzanne Aptian formation Sequence Stratigraphy .

Meillon gas-bearing dolomitic formation. Further research has revealed that the Meillon formation is probably much younger (Upper Oxfordian to Lower Kimmeridgian) than the Sarrance sequence (or than the Mailh Arrouy sequence).

For further information: Canérot *et al*., 1990; Lenoble, 1992.

Stop 3.3:

Bedous : the southern margin of

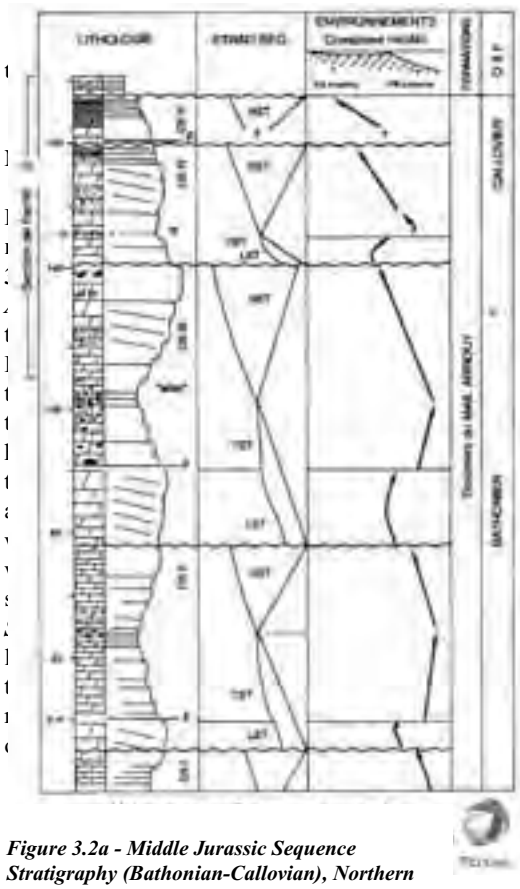

Figure 3.2a - Middle Jurassic Sequence Stratigraphy (Bathonian-Callovian), Northern side of Sarrance anticline, (Canérot and Lenoble, 1993).

(Fig. 3.3). In the Bedous Valley, the Triassic includes Muschelkalk limestones, Keuper shales and ophites in slivers of duplexes that were thrust to the south (visible along the halpin road). These rocks were thrust onto the flysch of the Upper Cretaceous cover in the High Range, around the village of Lées (Fig. 3.3). Further north, the crest of the Layens Mtn shows a thick sub-horizontal Jurassic and Lower Cretaceous series belonging to the normal limb of a recumbent anticline verging to the north. To the east of the viewpoint the Bergon Mtn shows a hanging recumbent syncline with a top-to-the-north vergence.

Geodynamic interpretation: the Bedous area marks the mid-point of the double vergence that

Figure 3.2b - Colonial corals in Sequence DIII.

Figure 3.3 - Structure of the High Range at Bedous, Aspe Valley, (Total). Fl= Upper Cretaceous Navarella flysch (Senonian), UK= Upper Cretaceous Canyon Limestones (Cenomanian- Lower Senonian), Tr= Triassic ophites.

Volume n° 2 - from B16 to B33

Figure 3.4a - Megaturbidite at Osquich Pass.

Figure 3.4b - The folded Megaturbidite in the landscape.

characterizes the Pyrenean mountain range. Some authors traditionally set the North-Pyrenean Fault at this location but this hundred-km long strike-slip fault is likely concealed beneath the south-verging thrust sheets, and would occur further north in depth, probably where some earthquakes still originate nowadays.

To the South, subduction of Iberia beneath Europe was so large in magnitude that only south-verging thrusts and nappes can be observed. To the north, depending on the original dip of the rift faults, inversion produced either north-verging or south-verging folds. The rift structures are located in a retro-arc setting, which limited its inversion and its uplift (and erosion), thus permitting the petroleum system to exist till today.

Stop 3.4:

Osquich Pass: Upper Cretaceous Megaturbidites: figure 3.4a, 3.4b, 3.4c and 3.4d.

Access: from Stop 3.3, drive back to Accous and now drive N 134 back to Oloron. At the entrance to Oloron, drive on D 936 to Navarrenx and Sauveterre de Béarn. 11 km from Oloron, take on the left the D 25 to l'Hôpital St Blaise and Mauléon-Licharre and then the D 918 to Col d'Osquich.

The Stop is located on the road from Mauléon to Larceveau, D 918, about 1km after the Osquich pass, at the first curves in the road, just before the village of St Jean Ibarre.

The Megaturbidite concept was first established by Soler and Puigdefàbregas, 1970; Rupke, 1976, for huge gravity deposits occurring among Eocene deposits of the Southern Pyrenean basin. Later, Johnson and al (1981) studied the South-Pyrenean basin and Labaume *et al*. (1983) studied these deposits in detail. Megaturbidites were later identified among the Cretaceous North Pyrenean sediments and were studied in detail by Bourrouilh, Coumes and Offroy (1984) and Offroy (1984) who interpreted the infilling of the North-Pyrenean cretaceous flysch basin, demonstrating that:

- two large megaturbidites occurred in the basin. One of them extends over more than 90 km, and varies from 60m in thickness, near Pau, to 20m in its western part, near the Atlantic Ocean.
- Megaturbidites originate as evolutionary mass-flow-megaturbidites (figure 3.4d)

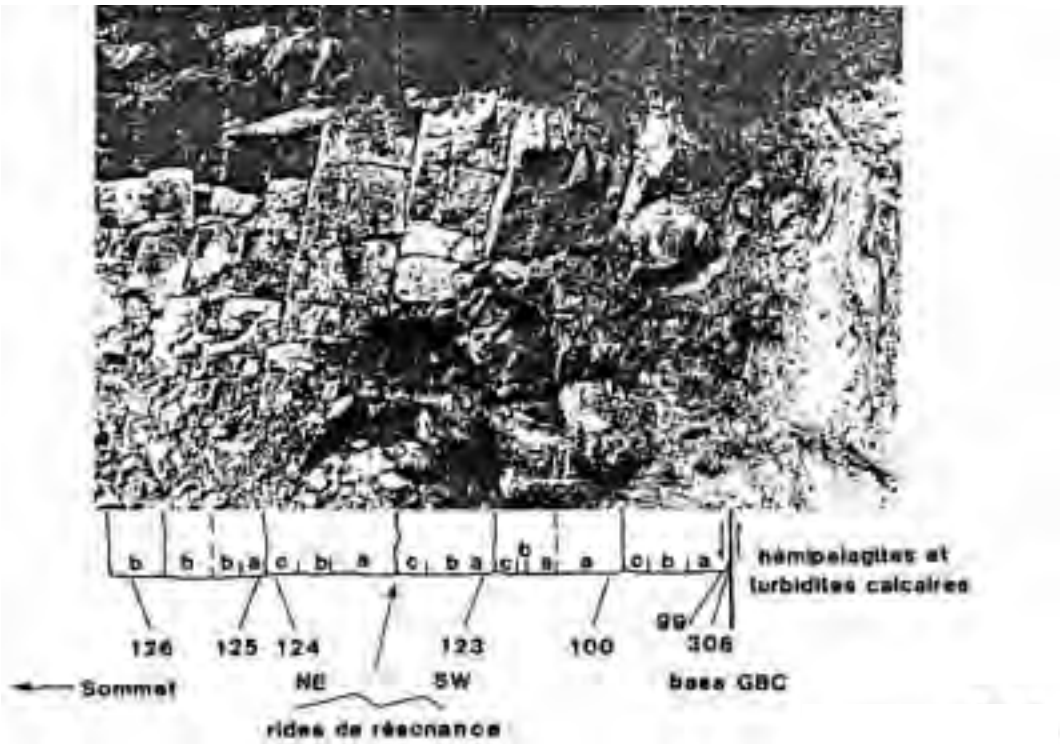

Figure 3.4c - Sedimentological interpretation of the Megaturbidite, from Offroy, 1984.

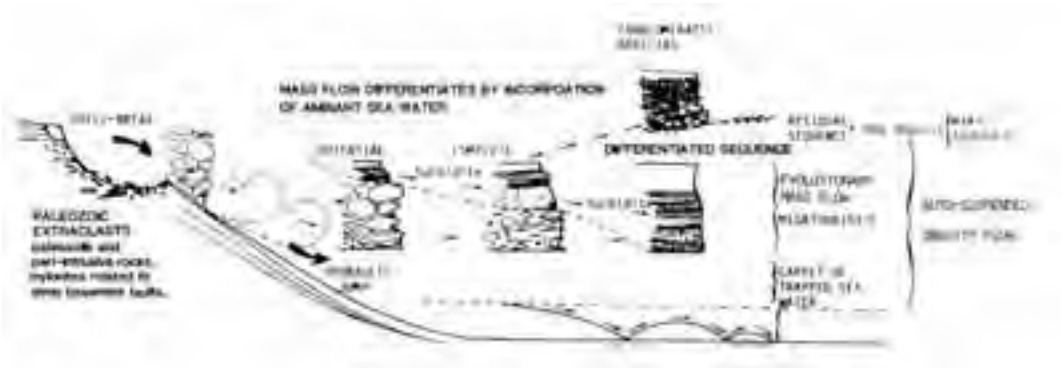

Figure 3.4d - The Evolutionnary-Mass-Flow-Megaturbidite concept, R. Bourrouilh et al., 1984, R. Bourrouilh, 1987.

Structural landscape: the panorama shows a massive turbidite, 40 m thick, which outcrops on the right side of the road, but also in the landscape, on the left side of the road.

Interpretation: studied by Bourrouilh and Offroy (1983), Offroy (1984), this megaturbidite is constituted by successive but amalgamated Bouma's intervals, which demonstrate that the turbiditic flow was internally stratified, each strata having a specific kinetic energy. Vibratory ripples can be also observed in interval surfaces (figure 3.4c).

On the left side of the road, and if the light is oblique enough, we can observe large Pyrenean kink-folds affecting the flysch and particularly the Megaturbidite (figure 3.4b).

For further information:

Bourrouilh and Offroy, 1983, Bourrouilh, Coumes and Offroy (1984), Offroy (1984),.

Stop 3.5:

Ahusquy Pass: Structure of the tilted blocks and of the Iberian margin : (figure 3.5).

We drive back to Mauléon by the D 918 road.

Introduction: from Mauléon to the small village of Aussurucq, the road cuts the Upper Cretaceous flysch of the N-Pyrenean trough. From Aussurucq to the Ahusquy pass, the road will cross a little-deformed tilted Mesozoic block of the Iberian margin (Arbailles block), whose northern edge is deformed in a NE verging thrusted anticline. This N110°E anticline shows a complete series, from the Upper Carboniferous, unconformably overlain by a typical German type Triassic, followed by a calcareo-dolomitic Jurassic. The tilted block was part of the southern margin of the N-Pyrenean Lower Cretaceous rift which extended the Bay of Biscay. This history is clearly registered in the erosional surface affecting the Upper Jurassic limestone, locally showing bauxitic remnants. The progressive rotation of the tilted block is demonstrated by the unconformable fan-like dips of the Neocomian continental sands, the Hauterivian-Barremian shallow water limestones and finally by the first large transgressive marine deposits of "the marnes de Ste Suzanne". Then, the shallow marine partly reefal limestones of the Urgonian were deposited. These competent limestones form the frame of the tilted block or the " Arbailles " block.

The Arbailles anticline is followed to the south by a

Figure 3.5 - Panorama from Ahusquy Pass.

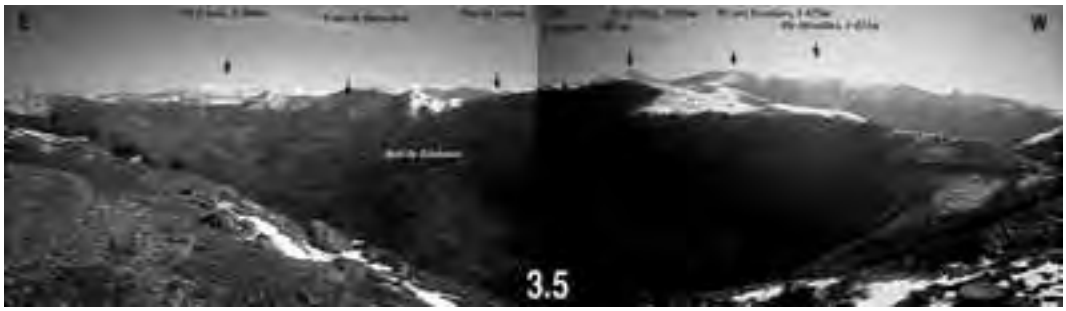

large syncline, formed by the Upper Aptian-Albian black shales, in what was the downthrown part of the Arbailles block.

Access: on the way to Mauléon by road D 918, we will take the small road D 147 on the left to Mendy and to Aussurucq and then through the Forêt des Arbailles massif, up to the Ahusquy pass.

Structural landscape and Interpretation: Ahusquy pass is situated on the Upper Aptian-Albian black shales, which form the core of the Apanicé-Bois de Zouhoure syncline.

The southern flank of this syncline is verticalized. The underlying Urgonian limestones, which form the frame of the Arbailles anticline to the north, crops out here again, forming a continuous rocky ridge, reaching an elevation of 1,265 m at the Pic de Behorleguy. The Jurassic and the evaporitic Triassic outcrop on the southern side of the syncline, in a narrow ridge separating it from the Mendibelza conglomerates; this N 110°E zone is generally interpreted as a major Pyrenean Fault, extending to the West Souquet's "Faille de Bigorre" (Souquet et Debroas, 1980). However, this hypothesis does not fit with structural and drill-hole data and could be discussed during the field trip. Immediately south of this fault zone, the thick black Albian-Vraconian conglomerates of the Mendibelza (this name means: black mountain in Basque) range are directly discordant on the Paleozoics. In the background of the panorama, the Upper Cretaceous "calcaires des cañons" or "calcaires des Eaux Chaudes" present a sheared unconformable contact with the Paleozoics of the High Chain (see Stop 2.4a and 2.4b, here above), which culminates at the Pic d'Anie (2,504 m high, to the left) and in front of us, at the Pic d'Orhy, at an elevation of 2,017m.

For further information: see the geological map at 1/50 000 n° XIV-46, Tardets -Sorholus

Stop 3.6:

Lutogagné: Structure of the Lower Cretaceous tilted blocks: figure 3.6.

Introduction: this is a general panorama along the strike of the southern flank of the Arbailles, or the Apanicé-Bois de Zouhoure syncline.

Access: leaving the Ahusquy pass, we drive to the Iraty pass and we will progressively cross the Albian black shales of the syncline to reach the Triassic outcrops and the panorama.

Structural landscape: we Stop near the Cayolar (mountain barn) of Arhansus. Looking to the north, we now examine the southern limb of the Arbailles syncline culminating locally in front of us at the Lutogagné peak (1,097m). This southern flank is rotated vertically with the folding of the syncline, and deeply fractured in this area.

Interpretation: according to Canérot and Lenoble (1991), the Jurassic (Lower Lias to Bajocian) is covered by diapiric breccias (Etchebar collapse breccias) of Lower Cretaceous age, and unconformably overlain by an uppermost Gargasian-Clansayesian limestone containing typical Foraminifera. (Peybernès and Garot, 1984). Therefore most of the Jurassic and Barremian carbonates are absent; a reconstruction with subcrop maps indicates the presence in the Barremian to Albian of a diapiric ridge which developed along the downfaulted side of the Arhansus Fault. This ridge was then squashed by the subsequent compression between the upthrown

Figure 3.6 - Lower Cretaceous tilted blocks.

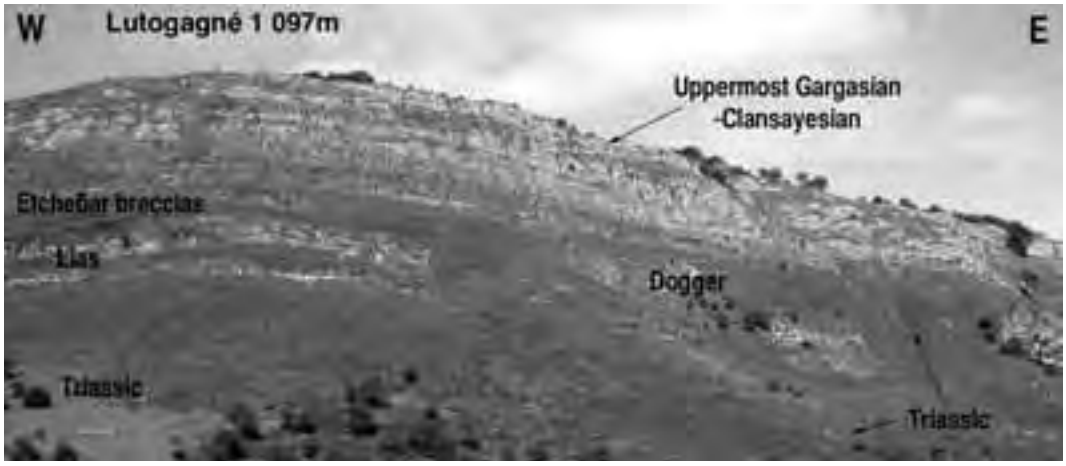

block of the Iberian margin of the North-Pyrenean rift and the Albian syncline which occupied the downfaulted half-graben of the Arbailles Block.

Hydrocarbons: the Clansayesian series regionally marks the vertical transition from the Urgonian platform (Aptian) to the Albian marl basin. This sequence has been observed in the Arzacq and Tarbes basins, where it contains reef structures which have been drilled, and are locally HC bearing and productive (Gaujacq).

For further information: Peybernès and Garot, 1984, Canérot and Lenoble, 1991

Stop 3.7:

Mendibelza mass flow conglomerates:
figure 3.7.

Introduction: directly resting unconformably on the Paleozoics, the Mendibelza Albian conglomerates result from the erosion of the Iberian plate. They rework all the Paleozoic series, from at least the Ordovician to the Permian, and also, Triassic evaporites (bipyramidal quartz), Triassic ophites, Jurassic limestones (Digbehi, 1987), as well as subcontemporaneous Lower Cretaceous shallow water and reefal limestones and black shales. They also contain layers with remnants of leaves, broken branches and debris, of the coeval forests which grew up along the coast and the delta bayous. The conglomerates are interpreted as resulting from margin uplift of the North Iberian margin, as the opening of the Bay of Biscay rapidly progressed eastwards. Thus, these fanglomerates mark the passage between the rift and the early plate drift stage. They are a thick accumulation of fluvial to canyon and slope fanglomerates, rapidly slurried down on the growing divergent Iberian margin.

Access: on the road to Iraty pass

Structural landscape: several mass-flow sequences are observable, top on the left.

Interpretation: these slurried beds were emplaced by immature, i.e. proximal mass-flows, probably resulting from fluvial (deltaic) overfloods. Frequently, the top of mass-flow sequences is abruptly washed out by a high energy water current, which took off a part of the former deposited sequences, leaving isolated pebbles outcropping on the sea floor.

For further information: Boirie, 1981, Bourrouilh, Coumes and Offroy, 1984; Digbehi, 1987; Miranda Avilès, 2002.

Figure 3.7a - General view of the Mendibelza massif.

Figure 3.7b - Sedimentology of Mendibelza conglomerates (Total).

Stop 3.8:

Mendibelza conglomerates on Iraty road,
figure 3.8.

Introduction: this Stop allows us to observe large olistostromes, with olistolithes of Paleozoic blocks, Lower Cretaceous shallow water limestones, including reefal limestones, and reworking pebbles and gravels of quartz, Ordovician quartzites, Devonian limestones, carboniferous radiolarites and muscovite-rich greywackes, as well as Triassic ophites and bipyramidal quartz.

Access: down Iraty pass, driving to Lecumberry on road D 18, leaving the Saint Sauveur Chapel on the right, the

Figure 3.8 - Olistostromes and olistolithes in Mendibelza conglomerates.

Stop begins about 1 km down from the Chapel crossroad, on the first road curve (Fig. 3.8).

Structural landscape: the large olistostrome crops out all along the right side of the road, over several tens of metres, gently resting on channelized mass-flow. Large pebbles and Paleozoic and Lower Cretaceous calcareous fossiliferous olistolithes are clearly observable on the side of the road.

The other side of the road shows the Mendibelza massif and, far in the background the Atlantic coast and the Bay of Biscay.

Interpretation: the on-going growth of transtensional basins provoked inversion of the morphology of their southern margin, revealed both by the infilling of the basins by large amounts of fluvial conglomerates (Mendibelza ones) and by large olistostromes, reworking olistolithes of former deposits but also of the subcontemporaneous reefal carbonates (Boirie, 1981, Souquet and Boirie, 1985, Digbehi, 1987). These transtensional basins are similar to the modern Baja Californian divergent basins of the Gulf of California (Miranda Avilès, 2002).

For further information: Boirie, 1981, Souquet et Boirie, 1985, Digbehi, 1987, Miranda Avilès, 2002.

Stop 3.9:

tilted blocks and European-Iberian margin, 2 km NW of Lecumberry : figure 3.9.

Introduction : this Stop allows us to observe the Arbailles tilted block and the European-Iberian margin.

Access: on road D 18, about 2 km NW from Lecumberry, on the small slope of the road.

Structural landscape and Interpretation:

1. The post-rifting, syn-drifting " European " plate is represented here by the western structure of the Arbailles tilted-block, showing the southern limb of the Arbailles (Apanicé) syncline, culminating here at Behorleguy peak (1,265 m).

The Urgonian ridge of the Behorleguy peak is verticalized. The shallow water Urgonian carbonates rest unconformably on bauxitic deposits filling up a previous karst and were mined. This diachronous bauxite extends unevenly from here to Provence, over 800 km away, testifying to complex and polyphased emersions/submersions of the "Durancian isthmus". The slope down the Behorleguy peak is formed by an incomplete Jurassic series, the pre-Urgonian erosion reaching irregularly the Callovo-Oxfordian, the Dogger or even the Liassic.

The Lecumberry valley strikes through the soft evaporitic to calcareous, and arenitic Triassic.

The possible fault previously discussed at Lutogagné, must run on the right side of the valley

2. the Iberian plate is constituted here by the large amount of Albian to Vraconian Mendibelza conglomerates, unconformably resting on the Paleozoics. Far in the background, the Mendibelza conglomerates are locally covered by the Upper Cretaceous "calcaires des Cañons".

For further information: see the geological map at 1/50 000, n° XIII-46, St Jean Pied de Port.

Figure 3.9 - Tilted blocks and European-Iberian margin.

DAY 4

from St Jean Pied de Port to Jaca

The road to Larrau and to the Port de Larrau will drive us through the Mendibelza conglomerates.

Morning:

Stop 4.1a:

Pic d'Orhy South-verging Thrust and Fold structures

Introduction : resting on the Mendibelza conglomerates, a huge series of Upper Cretaceous shallow water carbonates form the main frame of the Pyrenean High Chain. We already observed these limestones the first day, in the Ossau Valley, forming the high peaks of the Eaux Chaudes Massif. These "calcaires des cañons " or "canyon limestones" develop from Cenomanian to Lower Campanian. Then, a carbonate flysch facies up to the Lower Lutetian progressively appears.

Access: from Larrau, road D 26 climbs up to the Port de Larrau, 1,575 m high. We will Stop at 1,400 m elevation, near the thrust surface (fig.4.1a1).

Structural landscape and interpretation: looking westwards we can observe the S-shaped south-verging folds of the Orhy peak, 2,017m high, forming a souththrusted anticline, involving the Upper Cretaceous flysch, followed by an south-verging overturned syncline, formed by the Paleocene-Lower Eocene flysch (fig.4.1a2).

Here we can see one of the highest fold-and-thrust tectonic units.

For further information: see the geological map at 1/50 000, n° XIV-47, Larrau.

Stop 4.1b:

Port de Larrau: Structural Panorama

Access: drive on D 26 up to the Port de Larrau, 1,573 m high.

We are now in the heart of the Pyrenean High Chain, just below Orhy Peak and with the ample panorama of the Iberian plate in front of us.

Structural landscape and Interpretation: the High

Figure 4.1a1 - Geological map of the Pic d'Orhy area, from BRGM Map, n° XIV-47, Larrau.

Chain now develops west and eastwards, the Upper Cretaceous to Lower Eocene "Calcaires des Cañons" forming the mountain range.
To the south, the large south Pyrenean basin develops, filled with Eocene flysch of the Hecho Group.

Stop 4.2a:

Igountze Thrust and St-Engrace Thrust sheet.

Access: take the D 26 back to Larrau and then along the Gave de Larrau to take road D113 on the right along the northern slope of the Ste-Engrace valley. Stop 500m east of the Kakoueta canyon road access.

Stratigraphy, structural geology: the Igountze unit consists of the Devonian – Carboniferous basement and of its unconformable Albian cover comprising the Mendibelza conglomerates. This unit is southward thrusted, almost horizontally, over the Ste Engrace thrust sheet (fig.4.2a1 and 4.2a2). The latter is also thrusted (fig.4.2a3) over the so called canyon limestones (Cenomanian to Campanian) and the Navarella flysch (Campanian and Maastrichtian). This flysch joins the unconformable cover overlying the Paleozoic basement, in the High Range further to the south.
Flattened and sheared (boudinage-affected)

Figure 4.1a2 - Aerial view of the Pic d'Orhy, courtesy of Vivien De Feraudy (Total).

Figure 4.2a1 - Geological map of the Saint-Engrâce area, from BRGM map n°XIV-47, Larrau.

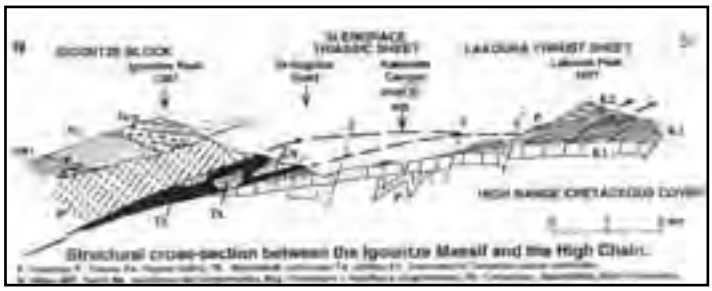

Figure 4.2a2 - Structural cross-section between the Igountze Massif and the High Chain (Total).

sedimentary breccias occur at the base of the flysch. Laterally the internal shearing of the Senonian series beneath the Igountze thrust is characterized by a north-dipping duplex shear belt, located at the limestone-flysch contact. To the south, Lakoura Peak is made of a klippe with a complex structure (Paleozoic covered by the Mendibelza conglomerates, the Canyon limestones and the flysch) which is disconnected in front of the main thrust sheet.

Structural interpretation: the Igountze Thrust reactivated an ancient north-dipping normal fault. In the Early Cretaceous this fault separated the Igountze block from the High Range basement. The diversity of the marine facies in the Mendibelza conglomerates (enormous fanglomerates with Paleozoic fragments from the south, and then puddingstones that reworked the basement and the Permian-Triassic sandstones and siltstones) as well as their sedimentary organization (onlap deposition, gradual thickening towards the south), suggest that these are canyon-cone deposits on a tilted block with increasing drowning to the south (Boirie, 1981). This organization is similar to, but younger than the one in the Arbailles (see former Stops). The Igountze Block therefore corresponds to a slab of the Pyrenean Iberian margin that collapsed during the Albian. The conglomerates that reworked the basement belong to the southernmost block (which was still high) of the High Range. The block collapsed in the Senonian, demonstrating the progressive widening of the Pyrenean sedimentary basin towards the South, during the Late Cretaceous (Souquet *et al*., 1985).

For further information: Ribis,

Figure 4.2a3 - Larrau-Lakhoura Thrust sheet (Total).

1965; Ducasse and Velasque 1988, Boirie 1981.

Stop 4.2b:

Intra-Senonian duplex underneath the Igountze and Lakhoura Thrusts.

Access: 500m east of the previous Stop. Park on the south side of the road.

Stratigraphy and structural geology: the Navarella turbiditic flysch (Campanian to Maastrichtian) is mainly composed of alternating marly limestones and marly sandstones. The beds are intensely sheared (fig.4.2b). Intraformational duplexes result from the development of reversed parallel south-verging ramps accompanying the motion of the Ste Engrace-Igountze Thrust sheet above, as well as that of the Larra Thrust further to the south.. At this Stop we can observe an antiformal duplex, with a subhorizontal floor shear plane and a roof shear plane folded along a N 120 axis. The sub-NS hinges of gravity slumps are preserved in the internal layers of the duplex.

This intense shear deformation occurred for at least 7 km southward, along a bedding plane slip zone at the top of the Canyon Limestones and underneath the Igountze and Lakhoura Thrusts, to the south of the modern Kakoueta canyon. The intraformational duplexing contributed to the southward allochthonous transport of the Igountze-Ste-Engrace Thrust and the Lakoura Thrust over a minimum of 7 km. The whole sheared Navarella flysch acts as a detachment thrust with a thick sole.

Figure 4.2b - Larrau-Saint Engrâce-Lakhoura Thrust Sheet.

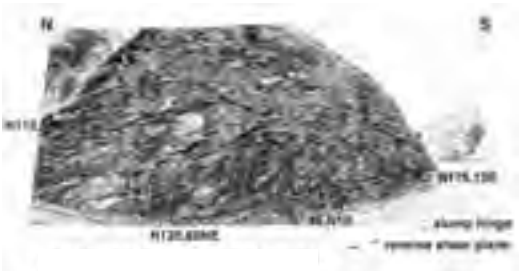

Figure 4.2b2 - Intra-formational antiformal duplex Navarella Flysch; St. Engrâce road

II. A transect of the Southern Pyrenees and Jaca basin

by Antonio Teixell

Departament de Geologia, Universitat Autònoma de Barcelona, 08193 Bellaterra, Spain

e-mail : **antonio.teixell@uab.es**

Aim of the field trip

The aim of this itinerary is to examine thrust tectonics and interaction with sedimentary systems in the Southern Pyrenees. The Southern Pyrenees consist of south-vergent folds and thrusts and contain a very well-preserved record of synorogenic sedimentation. Synorogenic sediments are of uppermost Cretaceous to Lower Miocene age, and constitute the Jaca and Ebro basins (Plate 2, fig.1).

The field itinerary will proceed from north to south from the Axial Zone -a large thrust culmination that forms the orographic axis of the Pyrenees- to the Jaca basin -a Paleogene foredeep now incorporated in the the orogen showing a typical turbidite to molasse succession-, and finally to the southern mountain front of the External Sierras –where the Pyrenees overthrust the present foreland of the Ebro basin. Synthetic geological descriptions of the transect visited can be found in Teixell (1996, 1998).

During the trip we will have the opportunity to study features as 1) detailed kinematics and mechanics of thrusting, 2) interactions between growing thrust faults and folds and proximal alluvial fans, and 3) episodic evolution and progressive deformation of foreland basin deposits.

Afternoon: Axial zone and Northern Jaca basin

Stop 4.3:

Pierre-Saint-Martin. The Larra thrust system.

Access: follow the main road NA 1370 to the SW to cross the Spain/France border and park some 100 m after the signal, beside a road bend.

Structural landscape: the Upper Cretaceous rocks

Volume n° 2 - from B16 to B33

that form the Axial Zone cover consist of basal platform limestones ("Calcaires des Cañons", Cenomanian to Santonian) that rest directly on the Paleozoic. Overlying the limestones are open marine shales, and a sandstone/shale turbiditic unit, visible in the landscape (Ribis, 1965). The latter formations are of Campanian-Maastrichtian age, and represent a drowning of the Santonian platform that can be attributed to flexure at the initial stages of the Pyrenean thrust loading.

One special interest of the Cretaceous rocks of the visited region lies in that post-Hercynian rocks have been eroded away in more eastern parts of the Pyrenean Axial Zone (Plate 2, fig. 1), and thus the area provides an unique opportunity to constrain the Alpine deformation in this basement massif.

In this Stop we can observe details of the Larra thrust system, characteristic of the Upper Cretaceous rocks of this northern part of the Axial Zone. The Larra system is a thin duplex composed of numerous south-vergent ramps that root in a bedding-parallel floor thrust (Larra thrust) (Fig. 4.3a). In the study area, the Larra thrust is located within the Calcaires des Cañons, at the boundary between a lower massive limestone member and a upper, well-bedded and chert-bearing limestone member (Teixell, 1990; Teixell *et al*., 2000). The ramps above cut the chert limestones and the Zuriza shales.

From the parking area we can walk westwards for some metres to get a panoramic view of thrust imbrications on a hillside in the landscape.

Back to the road, the cuts located just north of the parking place show a good outcrop of a thrust ramp, with a set of associated minor structures that provide inferences for the kinematics of the thrust system. The thrust ramp, brings the middle part of the chert-bearing limestone member and the shaly upper part of this stratigraphic unit in contact (Fig. 4.3a). Bedding is truncated in a ramp-over-ramp geometry. The fault zone is characterized by two main subparallel fracture surfaces, which enclose an intervening rock slice that is strongly deformed and displays an internal oblique foliation coherent with ramp shear. Within the wall rocks, there are contractional, conjugate en-echelon arrays of calcite veins. As the shortening axes of the arrays have been tilted together with bedding, they indicate an early episode of layer-parallel shortening prior to folding. An incipient foliation, oblique to bedding, is also present. Transport directions (contraction or shear) that can be deduced from the orientation of minor structures range from N-S to NE-SW (fig. 4.3b).

Stop 4.4:

Pierre-Saint-Martin. Fault zone structure of the Larra floor thrust.

Access: walk down the road back to the roadside outcrops by the signal post of the Spain/France border.

Structural landscape: the Larra thrust fits the definition of a décollement: a bedding-parallel slip plane without repetition of stratigraphy. The Larra thrust dips parallel to footwall bedding, at gentle angles to the N, due to post-thrust tilting and normal faulting during the development of the Axial Zone antiform (Gavarnie thrust stage).

The Larra thrust appears in outcrop as a meter-thick band of strongly foliated rock that, at first sight, resembles a mylonitic marble. However, closer inspection shows that its foliated aspect is due to a densely packed stack of bedding-parallel calcite veins. A detailed profile of the fault zone at this locality is presented in figure 4.4. Bedding-parallel veins are

Figure 4.3a - Detailed geological map and cross-section of a segment of the Larra thrust system in the northern Axial Zone (Pierre-Saint-Martin area) (after Teixell, 1990). The Refugio de Belagua is located some 5 km to the SW.

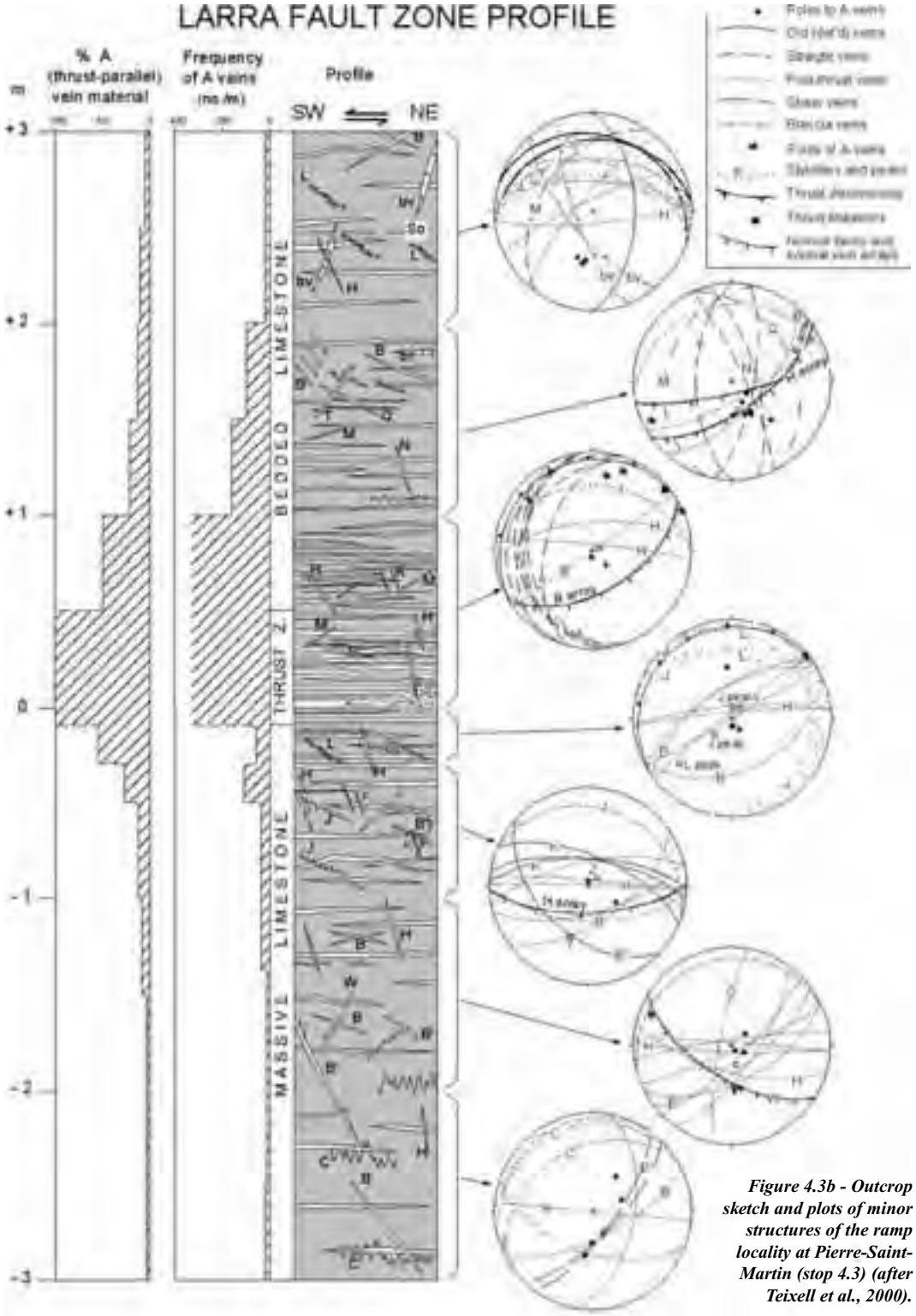

Figure 4.3b - Outcrop sketch and plots of minor structures of the ramp locality at Pierre-Saint-Martin (stop 4.3) (after Teixell et al., 2000).

Figure 4.4 - Structural profile of the fault zone of the Larra floor thrust at Pierre-Saint-Martin (stop 4.3). Positions and observed cross-cutting relations of chief structures are shown. Thrust-parallel veins are labelled 'A'. Other letters refer to different sets of veins, stylolites and other minor structures, as indicated in the legend. Orientations are on the right; percentage and frequency of A veins on the left (after Teixell et al., 2000).

abundant for at least 3 m in both hangingwall and footwall, and their frequency increases towards the fault zone center, where the rock appears formed by almost 100% vein material. From a microstructural point of view, veins are filled with blocky calcite crystals with variable internal deformation by twinning and recrystallization. No fibers have been observed. Cross-veins oblique to bedding are also present, although less abundant. In fact, there is a complex assemblage of diverse mesostructures that, apart from the veins include vein breccias, stylolites, folds and minor faults. On the basis of aspect, orientation and relationships to one another, the mesostructures have been correlated across the profile and grouped in sets (Fig. 4.4).

The Larra thrust has the singularity of being located within a mechanically strong limestone unit. Hence rheological weakness and water-generating capacity of the host rock were not primary causes for detachment. Teixell *et al*. (2000) proposed that the weakening was induced by stress and fluid channeling. Fluid channeling at a slight lithologic change within the limestone caused episodic brittle weakening and localized yield. Yield initially took the form of bedding-parallel extensional fractures.

Being constituted by interfaces between solid and fluid, the open extensional fractures ("water sills") were surfaces of zero shear strength that could accommodate appreciable increments of slip during short time spans. Even though twinning and recrystallization are conspicuous at the thin section scale, these were not key mechanisms in movement of the Larra thrust, which can be regionally estimated to be in the order of 5 km. Displacement was mostly accommodated by slip on the water sills, leaving little signature.

A remaining problem lies in that bedding-parallel veins are compatible with subhorizontal maximum stress in a thrust regime, but as major floor thrust displacement was parallel to bedding, there must have been some sort of stress reorientation to impart a shear stress on the fracture. This may have occurred by differential elastic contraction (Teixell *et al*., 2000). Hence, we infer that movement on the Larra thrust was achieved by a cyclic repetition of episodes of 1) bedding-parallel stress and crack dilation, and 2) stress reorientation and bedding-parallel shear (leading to décollement slip).

Stop 4.5:

Refugio de Belagua. General view and stratigraphy of the Cretaceous cover of the Axial Zone, figure 4.5.

Access: driving south on NA 1370 up to the mountain hut of the Refugio de Belagua (signal).

Structural landscape: from the Refugio there is a good overview of the Axial Zone and the overlying Lakora klippe. A cross-section of the area is shown in figure 4.5. Upper Cretaceous limestones that are close to the Refugio contain shallow-water forams.

Figure 4.5 - Geological cross-section of the Belagua-Lakora area, located in the northern Axial Zone. Indicated as «hut» is the position of the Refugio de Belagua (stop 4.5).

Overlying the limestones are strongly cleaved shales, outcropping along the road to the Refugio.

The large-scale structure that can be deduced in the landscape is a broad antiform. Minor, south-directed thrust faults deforming the Cretaceous formations in the vicinity of the Refugio belong to the Larra thrust system, formed earlier (Teixell, 1990). Thrusts cause numerous limestone-shale repetitions, and show

fault-related anticlines that bear an associated north-dipping slaty cleavage, especially in shaly rocks.

Stop 4.6:

Roncal valley. The Eocene flysch of the Southern Pyrenees (Hecho group).

Access: drive down the Roncal valley and stop along the main road some 2 km south of the village of Roncal.

The roadcuts at this stop provide a good outcrop of the Eocene turbidites of the Hecho group. Turbidites consist of silici-clastic sandstone/shale decimetric-scale cycles, in which the pelitic component is largely dominant. They represent relatively distal, basin plain facies within the Hecho group, and they have been dated as Lutetian in age (Mutti, 1984; Labaume *et al*., 1985).

Structural landscape: the turbiditic beds describe a synclinal fold at the outcrop scale, to which an axial planar cleavage is associated. This fold illustrates the characteristic deformation style of the Hecho group, which originally accumulated in a foredeep in front of the growing orogen, and was later deformed and incorporated in the mountain chain (e.g. Plate 2, fig. 1).

Above this outcrop, in the landscape, we can see a carbonate megabreccia bed, also characteristic of the Hecho group. Clasts within the megabreccia derive from carbonate platforms that flanked laterally the turbiditic trough. The position of these platforms and the geodynamic significance of the megabreccias have been the subject of diverse interpretations. Some authors have proposed a northern provenance of the resedimented material, from hypothetical platforms lying on top of the active thrust margin of the basin (Séguret *et al*., 1984; Labaume *et al*., 1985), wheras other authors have proposed a southern source area, from platforms existing in the distal (foreland) margin of the basin (Barnolas and Teixell, 1994).

The megabreccia bed that we observe is numbered 5 in the sequence of 8 main units like this in the northern Jaca basin. It shows a large mushroom-like feature interpreted to be a giant water-escape structure by Labaume *et al*. (1983).

DAY 5

from Jaca to Labuerda.

Morning

Southern Jaca basin and External Sierras

Stop 5.1:

San Juan de la Peña. Oligocene conglomerates of the Jaca basin.

Access: drive from Jaca to the west along C134 and then take the road to the left that drives to the San Juan de la Peña monastery. On the way to the External Sierras, we stop at San Juan de la Peña for an overview of the Campodarbe formation that forms the youngest infill of the Jaca basin (Puigdefàbregas, 1975).

Structural landscape: the Campodarbe beds describe the Guarga synclinorium (the present-day axis of the Jaca basin), whose position in the general cross-section can be observed in Plate 2, fig. 1. Fluvial sandstone channels and shales grade upwards to layered and massive alluvial fan conglomerates, which constitute the San Juan de la Peña massif. The age of these rocks is Upper Eocene to Lower Oligocene. The conglomerates show growth strata (progressive unconformities) within synclinal folds. The San Juan de la Peña massif is best known by its monastery of the X-XII centuries, picturesquely sheltered by the conglomeratic cliffs.

Stop 5.2:

Embalse de la Peña. Stratigraphy of the External Sierras

Access: follow N240 to the south to stop in the proximity of the reservoir Embalse de la Peña. Proceed along the roadcuts to the south of the reservoir and the bridge.

Structural landscape: the External Sierras are the foothills that constitute the South Pyrenean thrust front (Plate 2, fig. 1). Emergent thrusts bring Mesozoic rocks to the surface, starting with Triassic shales and evaporites (Keuper facies) that, when present, form the regional décollement level of the Pyrenean cover thrusts (Séguret, 1972).

The stratigraphic succession of the External Sierras is sketched in Fig. 5.2. We can recognize the diverse units in the gorge of the río Gállego, which provides one of the best and most visited sections across the Sierras.

Figure 5.2 - Stratigraphic log of the Mesozoic and Tertiary of the External Sierras (taken from Millán et al., 1995).

Above the Keuper, we find rudist-bearing of Upper Cretaceous age. Although there may be hiatuses of poorly constrained extent, the overlying red beds and lacustrine limestones (Garumnian facies) are of uppermost Cretaceous to lowest Tertiary age. The few hundred m of platform limestone of the Guara formation (middle Eocene) are the basin-margin counterparts of the Hecho turbidites. The Arguís and Campodarbe beds are similar to those within the Jaca basin, but much reduced in thickness.

Stop 5.3:

Riglos. Thrust front and proximal alluvial fan interactions.

Access: continue down the N240 and take the road to Riglos on the left (HU 310). Cross the village and park just below the conglomerate pillars of the Mallos. From the parking place walk up along the trail between the two prominent Mallos up to the Cerro Leonar.

The Mallos is the local name of a group of picturesque stacks that form a well-known touristic attraction of the area. They are built by Upper Oligocene-Lower Miocene conglomerates attached to the southern face of External Sierras.

The conglomerates are composed of clasts derived from the Mesozoic and Tertiary of the Sierras, and formed within small alluvial cones that towards the south pass rapidly to fluvial sandstones and shales (Puigdefàbregas, 1975; Hirst and Nichols, 1986). They accumulated synchronically with the main emergence of the External Sierras, and they represent the last synorogenic foreland basin deposits of this segment of the Pyrenees (see front cover, fig.2 and Fig. 5.3, A and B).

The Mallos show beautiful signs of syntectonic sedimentation. As we will clearly see by the itinerary up the Cerro Leonar, the conglomerates onlap a pronounced paleorelief, sealing some of the older thrust faults, but are in turn overridden by higher-level thrust sheets. This kind of relationship is common in the area, providing evidence for thrust sequences (Millán *et al*., 1995).

From the top of the itinerary we have a good panoramic view of the entire External Sierras overlooking the Gállego gorge. The structure of the Sierras is certainly very complex, with refolded thrusts and large overturned successions (see front cover, fig. 2). It puzzled geologists for decades, and was not resolved until the work by Puigdefàbregas and Soler (1973). They showed the existence of a large south-vergent thrust fault rising from the axial plane of a tight anticline, a thrust that is itself folded in an antiformal arch (see front cover, fig. 2, Plate 2, fig.1, and fig. 5.3, A and B), so its leading edge, isolated by later erosion, appears unrooted and completely overturned.

The antiform that arches the thrust has a strong easterly plunge, so it develops a fold closure located beneath our feet, just above the Gállego river. The leading edge of the thrust is sealed by the conglomerates of the Mallos, that in turn show progressive unconformities (growth strata) associated to the later antiform (Teixell and García Sansegundo, 1995). Minor out-of-sequence thrusts, as those observed along the way up, also show syntectonic relationships with the conglomerates.

Afternoon

III. The Ainsa Basin

By Josep Anton Muñoz,
Departament de Geodinamica i Geofisica, Facultat de Geologia, Universitat de Barcelona, Pedralbes, 08028 Barcelona, Spain, e-mail: **josep@geo.ub.es**

Introduction

The Ainsa basin is located in the footwall of the Cotiella-Montsec thrust sheet (Seguret, 1972) (Figs. 5.4b, 5.5a). This cover thrust sheet consists of Mesozoic and syntectonic Paleogene rocks that have been detached from the Variscan basement on Lower Triassic evaporites. During the Early Eocene southward displacement of the Cotiella-Montsec, the Tremp piggy-back basin developed on its hangingwall (Fig. 5.5a). The basin contains platformal and continental terrigenous facies that grade westward across an oblique lateral ramp of the Cotiella-Montsec thrust sheet (in the region of the La Foradada fault, Fig. 5.5a) into the marine Ainsa turbidite basin (Nijman and Nio, 1975, Mutti *et al*., 1988).

The Ainsa basin is deformed by the Peña Montañesa thrust system in the northeast, by the north-trending Mediano anticline in the south, and by the Boltaña anticline to the west (Fig. 5.4b). The structure of the eastern part of the Ainsa basin is dominated by a northwest-trending imbricate thrust system and related folds. Two main thrusts in the footwall of the Cotiella thrust sheet, the Atiart and Los Molinos thrusts, detach the Ainsa turbiditic basin from underlying Paleocene and Lower Eocene carbonate platform rocks. The Ainsa basin evolved to a piggy-back condition as thrusting propagating forelandwards and the detachment Mediano anticline and the fault-propagation Boltaña fold developed. These folds developed during the filling of the Ainsa basin synchronously with their dextral rotation in the footwall of the Cotiella thrust sheet.

The basin originated as a foredeep ahead of the innermost of these thrusts in the Early Eocene (Fig. 5.5a) and evolved into a piggy-back setting as the thrust front propagated towards the foreland. The

Figure 5.3 - Cross-sections through the External Sierras (after J. García Sansegundo, in Teixell & García Sansegundo, 1995).

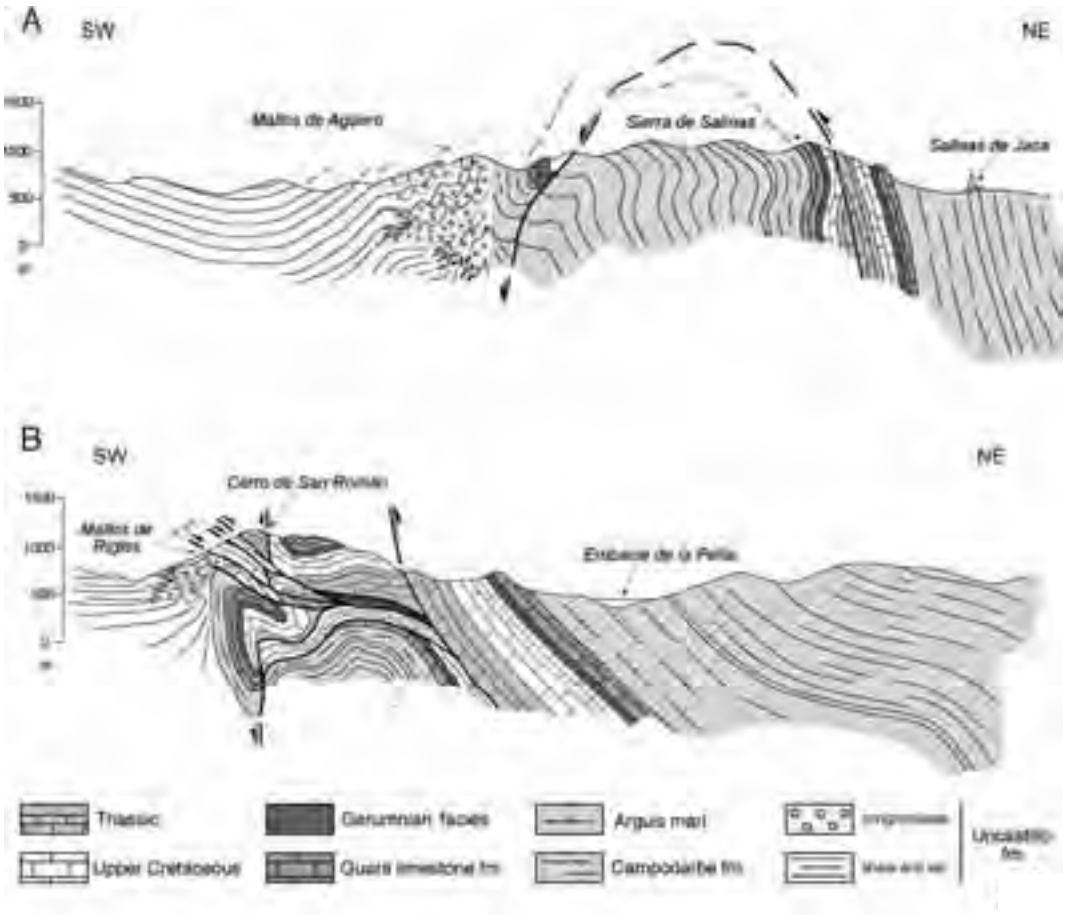

Volume n° 2 - from B16 to B33

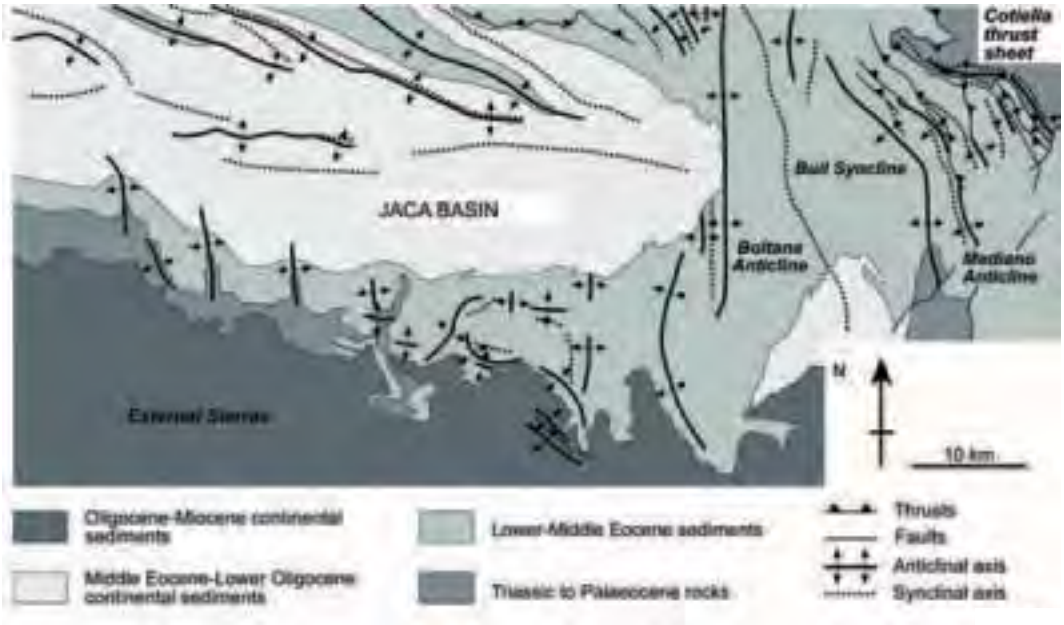

Figure 5.4a - Geological sketch map of the External Sierras, Jaca Basin and the Ainsa Basin.

foredeep filled mostly with a slope complex which is up to 4,000 m thick, 40 km long and 30 km wide. The slope complex had a fluviodeltaic source in the southwest and evolved to the NW into a basin-floor complex (Figs. 5.5a and 5.5b). The basin-floor complex in the Jaca basin consists of the classically termed "outer-fan" sandstone lobes, which are replaced downcurrent by basinal sandstone and mudstone interbeddings. The individual sandstone-dominated lobe elements are several tens of metres thick, more than 15 km wide and up to 80 km long.

The Ainsa Slope Complex consists primarily of mudstones where coarser-grained lithosomes are embedded. The latter correspond to turbidite systems with outcrops allowing the reconstruction of their 3D anatomy. The turbidite systems are generally thinner than 300 m, few kilometres wide, with a preserved length reaching up to 20 km, and mostly formed by channels and associated overbank elements. The outcrops allow insights on channel to overbank transitions and one system preserved significant changes downslope. Most of the facies involved indicate deposition from a broad variety of turbidity currents; however, in particular positions of turbidite systems, packages of turbidites are faulted and

Figure 5.4b - Geological sketch map of the Eastern part of the Ainsa Basin and of the Boltaña Anticline.

deformed by slumping at diverse scales or transformed into debris flow deposits. The resedimentation process interacted with turbidite deposition and introduced a degree of architectural complexity.

The interplay between tectonics and sedimentation in the Ainsa basin had different scales. Below is a summary of these relationships, ordered from basin scale to the scale of individual turbidite channel elements.

The propagation of the thrust front caused the Ainsa basin fill to be segmented as four major depositional cycles which are delineated by widespread angular unconformities and are stepped towards the foreland (Fig. 5.5b). These unconformities are submarine truncations, up to several hundreds of meters deep, which laid parallel to the elongation of the basin and were carved by mass wasting. The potential for mass wasting was created by forelimb rotation along the active basin margin and by flexural downwarping in the outer basin margin. These "cañons" acted as containers for further slope deposition.

Within a single depositional cycle, an overall decreasing rate of tectonic deformation caused an overall decrease in slope gradient, in turn responsible for contrasts on facies, architectural style and external geometry among stratigraphically consecutive turbidite systems (Fig. 5.5b).

Pulses of increased deformation caused angular unconfomities at the base of turbidite systems. These evolved overall towards abandonment, trough cycles of channel-complex development and abandonment. However, their internal architecture and external geometry varies between end-members: 1) vertically-stacked and symmetrical in cross-section and 2) complexly juxtaposed and markedly asymmetrical. The more complex patterns arose in zones left piggy-back between growing anticlines. The overall straight downslope platform of individual turbidite channels was in some cases modified by anticline-related topographies.

Objectives: to examine the tectono-sedimentation relationships of the Ainsa basin, growthg folds and the surrounding thrust systems.

Figure 5.5a - Palaeogeography of the South Pyrenean foreland basin at Early Lutetian. Turbiditic systems of the Ainsa basin had feeder fluvial systems in the Tremp basin. Clast composition is dominated by limestone clasts derived from Paleocene and Mesozoic rocks, but it also includes granites, volcanic rocks and others, which correlates to the exposed rocks in the hinterland, as it is also indicated by alluvial fans fringing the Northeastern Tremp Basin. From Arbués et al. 1998.

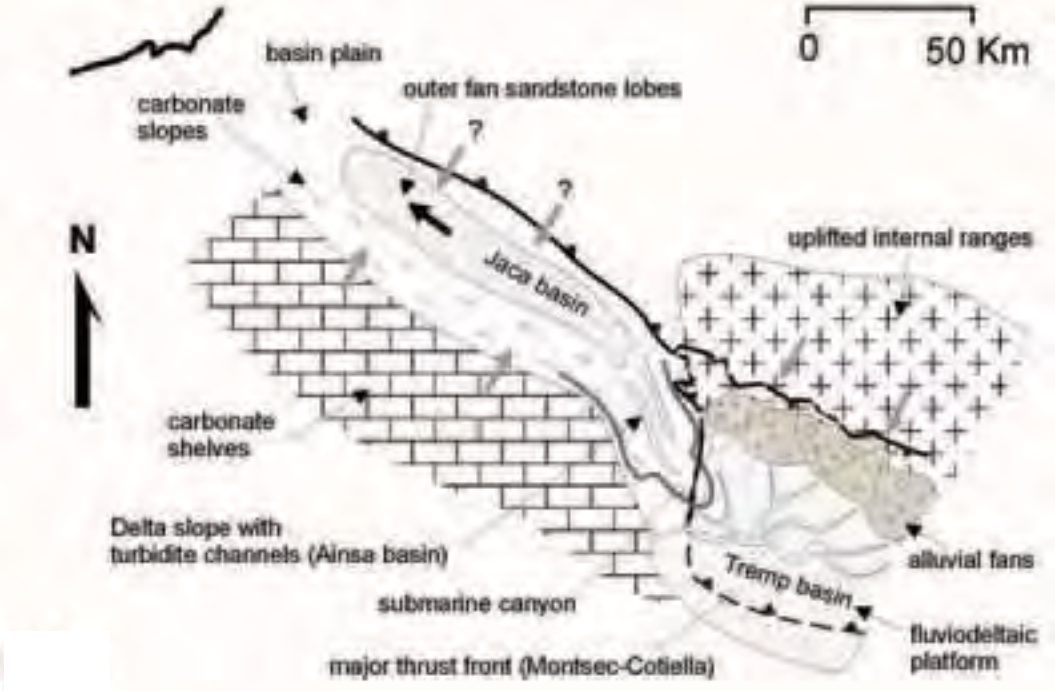

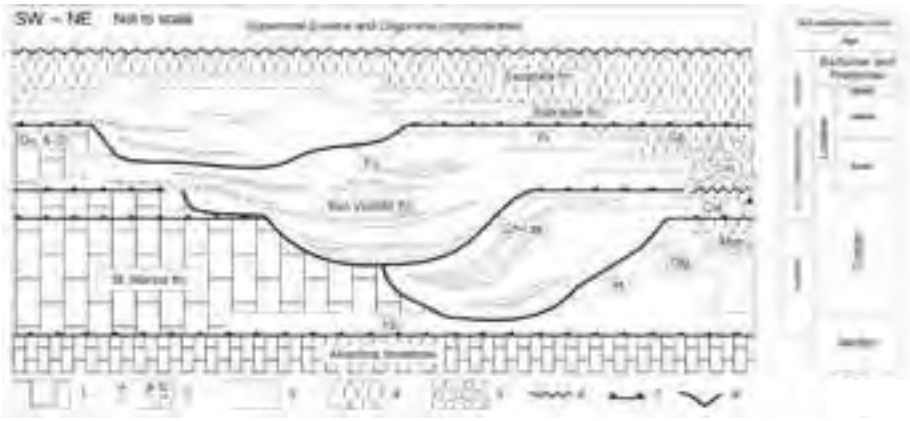

Figure 5.5b - Synthetic stratigraphy of the Ainsa Basin.
Main depositional facies :1 : carbonate shelf ; 2 : delta and carbonate slope ; 2A : mudstones, 2B : silici-clastic turbidites ; 2C : resedimented carbonates ; 3 : delta ;4 : alluvial plain ; 5 : alluvial plain. Discontinuities : 6 : subaerial unconformity ; 7 : condensed section ; 8 : surface of submarine gravitational erosion. Code for local names of stratigraphic units : Yb : Yerba marls (^) ; Gu & Gr :Guara limestones (+) and Grustan mb (*) ; Cgl : Castilgaleu fm ; Mon : Montilobat fm. ; Cst : Castissent fm. ; Cm : Campanué conglomerates (*) ; Cp : Capella fm. ; Pr : Perarrua fm. . Code for surfaces of subamrine gravitational erosion : At : Atiart ; Ch-Lsz : Charo-Lascorz ; Fo : Formigales. Other codes : Fu : Fuendecampo tectosedimentary unit. From Arbués et al. 1988.

Figure 5.6a - Geological map of the Mediano anticline, Ainsa basin (after Poblet et al. 1988).

Stop 5.4:

Boltaña anticline

Access:

From Broto, drive east to Ainsa. Stop in the intersection leading to the village of Janovas.

The Boltaña anticline is considered the western boundary of the Ainsa basin, however it grew during the latest stages of the turbidite filling of the Ainsa basin and mostly during the Middle to Late Eocene and 5.4c). Most of the turbidite systems of the Ainsa basin continued basinward into the Jaca basin without a topographic barrier at the present location of the Boltaña anticline (Fig 5.5a).

This Stop shows the steep, west-dipping limb of Eocene limestones of the Boltaña anticline.

Stop 5.5:

Tozal de Guaso. Panoramic view of the Ainsa basin.

Access :

From Boltaña drive east to Ainsa. Take the road to Guaso and the Guara park after crossing the Ara river. Follow this road to an intersection, turn right and follow the road to the village of Guaso. Take the road to the church at the top of the hill.

Structural landscape

From this viewpoint the Ainsa basin and the surrounding structures are visible: the Boltaña

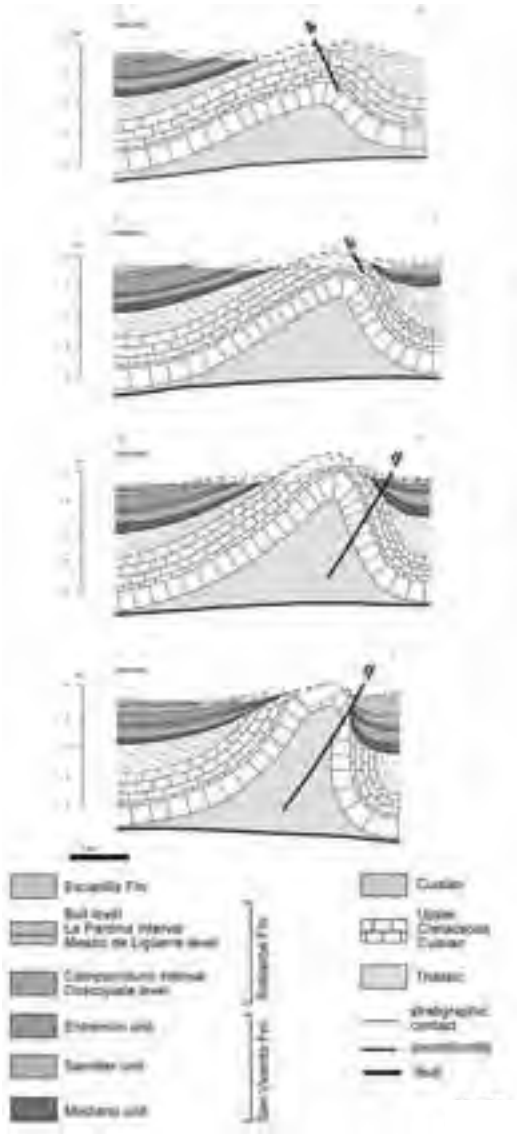

Figure 5.6b - Mediano anticline evolution.

anticline to the west, the Mediano anticline to the east and the Monte Perdido-Gavarnie, Peña Montañesa and Cotiella thrust sheets to the north-northeast.
This viewpoint is an excellent spot to discuss the main geological features of the area, summarize the structures observed these two days.

Stop 5.6:

Ermita de San Emiterio and San Celedonio.

Access: drive to Ainsa and take the C-138 towards Barbastro. Continue southwards past the now submerged village of Mediano. Turn left onto a small side road that leads to the village of Samitier and park the vehicles near the small square and fountain in the centre of the village.
From the parking spot in the village take the farm track that leads off to the left and up the hill to the Ermita de San Emiterio and San Celedonio. Several good view Stops can be found along the way overlooking Mediano lake and the western limb of the Mediano anticline.
Climb to the old church at the Ermita de San Emiterio and San Celedonio. From here there are excellent views of the Mediano anticline, the onlapping Ainsa turbidites, and the Buil syncline to the left. In the distance (if the weather is clear) the main ranges of the Pyrenean axial zone can be seen.

Structural landscape

The Mediano anticline is a north-plunging, north-trending detachment anticline developed above the Triassic evaporites (Fig. 5.6a). It is cored by massive to thick-bedded Eocene limestones (Fig. 5.6b). Eocene (Lutetian) turbidites onlap the anticline in a syn-folding growth sequence (Figs. 5.6a, 5.6b and 5.6c). The geometry, facies distribution (from alluvial to deep-water silici-clastics and carbonate rocks) plus the available magnetostratigraphy and biostratigraphy pose restrictions to the kinematic evolution of the anticline (Fig. 5.6c).

Stop 5.7:

Cotiella and Peña Montañesa thrust sheets.

Access: drive back to Ainsa and Labuerda and continue north along the main road (N-138) until the village of Escalona. At this locality turn left to the Añisclo valley and immediately take the small road to the right to the village of Puertolas. Continue up the mountain and Stop just past the small village of Santa Maria before the village of Puertolas.

Structural landscape

From this viewpoint the large klippes at Peña Montañesa and the Cotiella thrust sheets can be viewed. The flat-lying floor thrusts of these thrust sheets bring Mesozoic and Paleocene limestones on top of the Lower Eocene turbidites and marls of the Ainsa basin. The Atiart thrust (floor of the Peña Montañesa thrust sheet) merges hindwards with the Cotiella thrust.

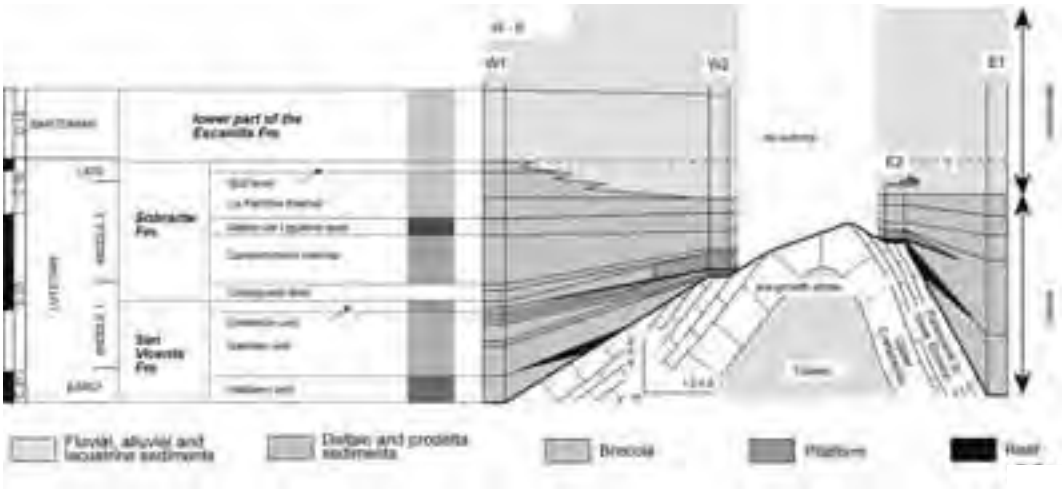

Figure 5.6c - Synsedimentary growth and kinematics of the Mediano anticline.

DAY 6

from Labuerda to Pau.

IV. The Alpine structure of the Basement of the Axial Zone and the Monte-Perdido-Gavarnie and Cotiella Thrust Sheets

By Josep Anton Muñoz

Introduction

The Cotiella thrust sheet (Fig.6.1a) is the northeastern part of the Montsec thrust sheet, the most extended unit of the South Pyrenean Central Unit (Seguret, 1972) or the so-called Mesozoic Upper Thrust Sheets (Muñoz *et al*., 1986). It consists of several structural units characterized by a very thick Mesozoic succession (mostly Upper Cretaceous), detached above the Triassic evaporites (Fig.6.1b). The floor thrust of the Cotiella thrust sheet is folded by the emplacement of the lower structural units (Monte Perdido-Gavarnie and basement thrust sheets). It dips subhorizontaly for most of its cartographic extension and dips southwards in the north above the lower thrust sheets. The Cotiella floor thrust climbs up southwards in the footwall from the Paleocene limestones into the Lower Eocene turbidites of the Ainsa basin. The Cotiella thrust sheet was displaced southwards a minimum of 20 km during the Early Eocene.

Below the Cotiella, the Monte Perdido-Gavarnie thrust sheet shows a distinct stratigraphy. It involves the Hercynian basement and the Mesozoic succession is more reduced and much thinner than the Cotiella. The basement consists of Silurian, Devonian and Carboniferous slightly to non-metamorphosed shales and limestones affected by Hercynian thrusts and folds. The Upper Cretaceous limestones, marls and sandstones rest unconformably on top of the Hercynian basement. They form a succession several hundred meters thick (800m aprox.) in contrast with the several km thick Upper Cretaceous series of the overlying Cotiella thrust sheet. The Paleocene consists of limestones and dolomites and is overlain by the Lower Eocene marls and turbidites.

The Monte Perdido-Gavarnie thrust sheet is structurally in continuation with the Ainsa basin (i.e underneath). The thrusts related with the Boltaña and Mediano anticlines are the southern continuation of the Gavarnie thrust which clims up section southwards into the hangingwall from the Silurian-Devonian rocks to the bottom of the Mesozoic succession. Above the basement, this thrust sheet shows a pile of small thrust imbricates repeating the Upper Cretaceous and Paleocene formations. These units show an increasing displacement westwards and have been described as the Monte Perdido thrust sheet (Seguret, 1972). The Monte Perdido thrusts merge upwards into the lower part of the Lower Eocene turbiditc succession of the Ainsa basin.

Below the Gavarnie thrust, basement thrust sheets with a different stratigraphy are exposed. They consist of metamorphic Lower and Upper Paleozoic rocks intruded by Upper-Hercynian granitoids.The cover of these lowermost thrust sheets only consists of Triassic red beds, unconformably overlying the

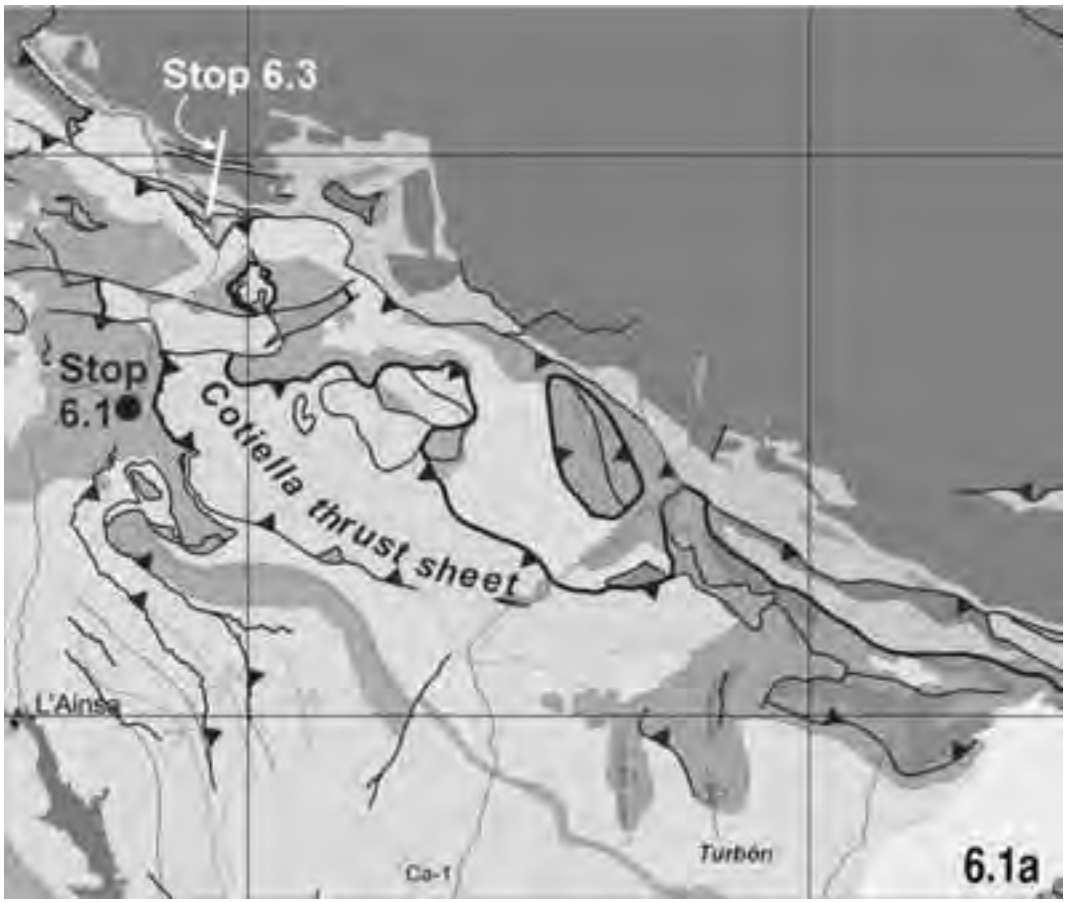

Figure 6.1a - Geological sketch map of the Cotiella thrust sheet and location of stops.

basement, Keuper above, and a thin bed (few tens of meters) of Upper Cretaceous limestones on top. The basement and the cover are both tightly folded and affected by thrusts.

Objectives: to examine the Alpine thrust structure of the basement units of the Pyrenean Axial Zone as well as the structure of the main cover thrust sheets above the basement.

Stop 6.1:

Cotiella thrust and structure of its footwall.

Access: from Labuerda drive north to Bielsa (N-138) until the village of La Fortunada. Pass the village for 1 km before the road tunnel of Las Devotas.

Structural landscape

The purpose of this Stop is to continue a general cross section of the area as well as to observe some structural features of the Cotiella thrust sheet and its footwall (Fig.6.1a, 6.1b, 6.1c, 6.1d). On the other side of the valley the Cotiella thrust is visible at the bottom of the Upper Cretaceous limestone cliffs (1,200 meters high). It lies subhorizontaly above the lowermost Eocene marls. Northwards of this locality the thrust as well as the Upper Cretaceous-Eocene beds in the footwall (Monte Perdido-Gavarnie thrust sheet) are tilted to the south 25-30º and truncated by a pair of E-W trending conjugate extensional faults (Fig. 6.1c, 6.1d).

The Eocene marls are folded and affected by a prominent N-S, NNW-SSE trending cleavage at a high angle with the general E-W, ESE-WNW general trend of the beds. This geometry is the result of a late tilting of the deformed marls and the Cotiella thrust sheet by thrusting of underlying basement thrust sheets.

Volume n° 2 - from B16 to B33

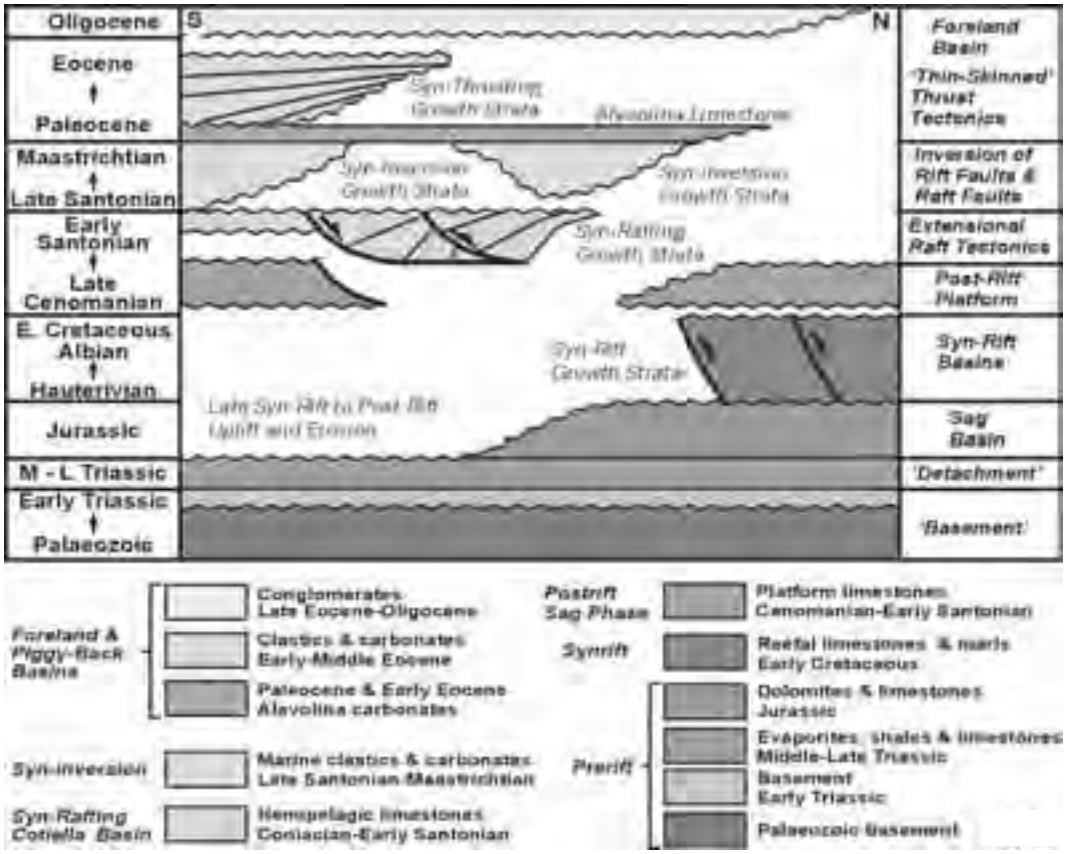

Figure 6.1b - The Syn-Rafting Cotiella basin replaced in the tectono-stratigraphic evolution of the South-Pyrenean basin.

Stop 6.2:

Cross-section of the Monte Perdido and Gavarnie thrust sheets. La Larri tectonic window.

Access

Continue north to Bielsa (N-138) and turn left to Pineta-Parador Nacional Monte Perdido. Take the track immediately before the Parador and park once the river is crossed. Walk for 1 hour.

Structural landscape

This is one of the most spectacular geological scenes of the Pyrenees and a key locality for

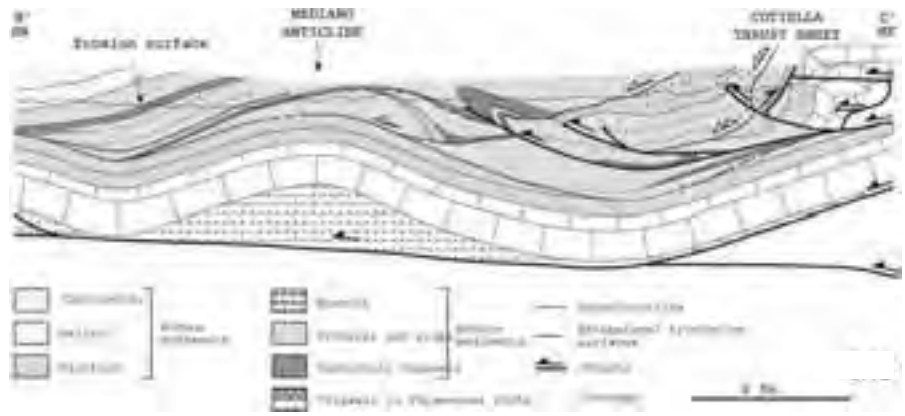

Figure 6.1c - Structure of the Cotiella Thrust Sheet and of its footwall.

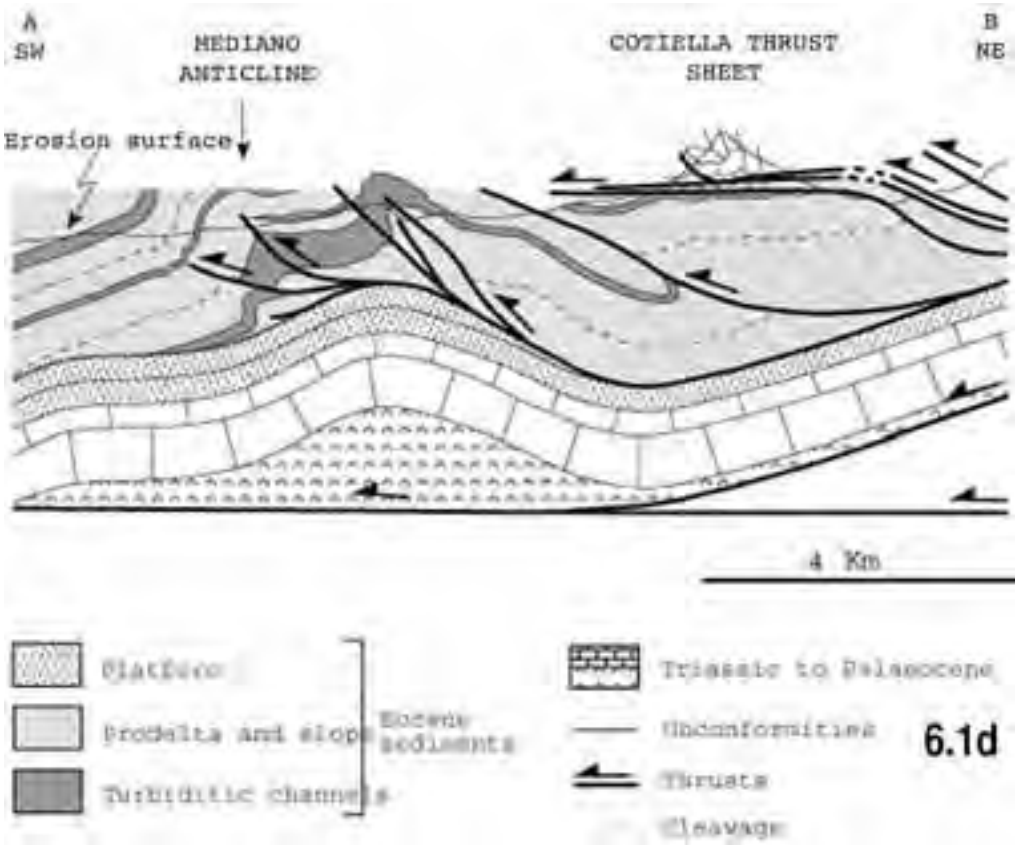

Figure 6.1d - Kinematics of the Cotiella Thrust sheet and the Mediano anticline.

understanding the basement involvement into the Alpine thrust structure and the structural relationships between the cover and the basement thrust sheets.

The course will follow the Pineta glacier cirque across the lower part of the Upper Cretaceous succession of the Gavarnie thrust sheet. The trail climbs up into the lateral glacier valley of La Larri where the Triassic red beds in the footwall of the Gavarnie thrust outcrop.

Climb the grassy slopes southwards of that valley towards La Estiba in order to get a view of the

Figure 6.2a - The Gavarnie Thrust at La Estiba.

Volume n° 2 - from B16 to B33

northern ridge. From this viewpoint, the Devonian basement of the Gavarnie thrust sheet below the Upper Cretaceous rocks is visible. It rests on top of the Upper Cretaceous limestones-Triassic red beds and the metamorphic basement outcropping at the bottom of the valley. This fault contact corresponds with the Gavarnie thrust. Note its antiformal attitude, the folded unconformity above the Hercynian basement in its hangingwall and the stratigraphic differences between the hangingwall and the footwall (Fig. 6.2a, and Front cover, fig.3).

Stop 6.3:

Structure of the granite basement in the footwall of the Gavarnie thrust. Bielsa-Parzán cross-section.

Access

Drive back to Bielsa and reach main road N-138 leading to the French border.

Structural landscape

Several observations will be made along the roadcuts between the villages of Bielsa and Parzan in order to characterize the fold and thrust structure of the Upper Cretaceous, Triassic red beds and granitic basement of the outcropping lower thrust sheets.

DAY 7

End of the field trip and return of the participants to Florence

Acknowledgements

This work is a contribution to the knowledge of the Pyrenean Mountain belt. It has benefited from the Research programs of the Université de Bordeaux 1 (R. Bourrouilh), of the Universitat Autonoma de Barcelona, Bellaterra (A. Teixell) , of the Universitat de Barcelona, Pedralbès (J. Muñoz), and of Total (L. Moen-Maurel). We thank TOTAL for permission to publish special in-house work and for material support. Fieldtrip guidebook was edited at Laboratoire CIBAMAR, Université de Bordeaux 1.

References

Alhamawi. M. (1992). Sédimentologie, Pétrtographie sédimentaire et Diagenèse des calcaires du Crétacé supérieur de la Marge Ibérique: Vallée d'Ossau-Vallée d'Aspe, Haute Chaîne, Pyrénées Atlantiques, *Thèse Université de Bordeaux 1*, 320 pages

Arbués P., Muñoz J.A., Poblet J.; Puigdefàbregas C. and McClay, K.. (1998). Significance of submarine truncation surfaces in the sedimentary infill of the Ainsa basin (Eocene of South-Central Pyrenees, Spain. *In*: J.C. Cañaveras, M.A. García del Cura and J.Soria (eds.), Abstracts of the *15th International Sedimentological congress*, IAS, Alicante, Spain p.145-146.

Barnolas, A. and Teixell, A. (1994). Platform sedimentation and collapse in a carbonate-dominated margin of a turbiditic foreland basin (Eocene, Jaca basin, southern Pyrenees). *Geology*, 12, 1107-1110.

Benderitter Y., Bourrouilh R. and Bourrouilh-Le Jan F.G. (1997). Application du quadripôle électrostatique à l'évaluation des carrières de marbres : exemple d'Arudy, Pyrénées-Atlantiques, France. *C. R. Acad. Sci. Paris*, 325, 545-552.

Biteau J.J., Le Marrec A., Moen-Maurel L. and Noual G. 1995b. Evolution géodynamique et pétrolière de l'avant-pays nord-pyrénéen. *Soc. Géol. France Spec. Meeting on Pyrenees*, Toulouse, Fieldtrip guidebook.

Bixel F., Clin M., Lucas Cl., Majeste-Menjoulas Cl., Mirouse R. and Roger P. (1985). Pyrénées : 500 millions d'années, itinéraires géologiques dans le parc national. *BRGM ed*, 101p.

Boirie J.M. (1981). Etude sédimentologique des poudingues de Mendibelza (Pyrénées Atlantiques). *Thèse 3ème cycle, Université de Toulouse*, 115 p.

Boirie J.M. and Souquet P. (1982). Les Poudingues de Mendibelza : dépôts de cônes sous-marins du rift albien des Pyrénées. *Bull. C.R.P. Elf-Aquitaine*, vol . 6, n° 2 p. 405-435.

Bouquet C., Bourrouilh R., Guérangé B. et Vaché E. (1990). Le Cambro-Ordovicien de l'Hospice de France, Haute Chaîne, Pyrénées Centrales, Sédimentologie et premières corrélations *in* Sassi and Bourrouilh, Eds., IGCP n° 5, *Newsletter 7*, p.131-133, 1 fig.

Bouroullec J., Delfaud J. and Deloffre R. (1979). Organisations sédimentaires et paléoécologiques de l'Aptien supérieur à faciès urgonien dans les Pyrénées occidentales et l'Aquitaine méridionale. *Géobios, Mémoire spécial* n° 3, 25-43, 12 fig. 1 pl.

Bourrouilh R. (1970). Le problème de Minorque et des Sierras de Levante de Majorque. *Ann. Soc. géol. Nord,* t. XC, fasc 4, p.363-380, 13 fig.

Bourrouilh R (1973). Stratigraphie, Sédimentologie et Tectonique de l'île de Minorque et du NE de Majorque (Baléares). La terminaison nord-orientale des Cordillères bétiques en Méditerranée occidentale. *Thèse d'Etat. Université de Paris V*I, 2 tomes, 822 p., 196 fig. et 95 planches dans le texte, 6 hors texte : 2 cartes géologiques au 1/50.000 et fonds topographiques, 2 planches de coupes géologiques.

Bourrouilh R. (1983). Estratigrafia, Sedimentologia y Tectonica de la Isla de Menorca y del Noreste de Mallorca (Baleares). La Terminacion Nororiental de Las Cordilleras beticas en el Mediterraneo occidental. *Mem. Inst. Geol. Min. de Espana*, t. 99, 1 vol. 692 p., 1 vol. 95 pl. et hors-textes, 2 cartes géol. 1/50.000e.

Bourrouilh R. (1987). Evolutionary Mass-Flow-Megaturbidites in an Interplate basin: example of the North Pyrenean Basin. *GeoMarine Letters*, volume 7, n° 2, p.69-81. Springer Verlag.

Bourrouilh R. (2000). Mud-mounds on divergent and extensional transform margins: Devonian and Lower Cretaceous examples of Southern France. *The Geological*

Exploration in Murzuq Basin, M. A. Sola and D. Worsley, Ed. *Elsevier*, ch.23, p. 463-483.

Bourrouilh R. and Alhamawi M. (1993). Données nouvelles sur l'évolution de la marge ibérique dans les unités tectoniques des Eaux Chaudes, Vallée d'Aspe-Vallée d'Ossau. *C. R. Acad. Sci. Paris.* t. 317, série II, p.979-985.

Bourrouilh R. and Doyle L. J. (1985). Petroleum Geology, Tectonics and Sediments of the French Pyrenees and Associated Aquitaine Basin. *A.A.P.G. Field Seminar*, 103 p.

Bourrouilh R. and Mirouse R. (1984). Le Paléozoïque supérieur des bordures du Bassin d'Aquitaine : analyse de données bibliographiques inédites. *Géologie profonde de la France*, *Thème 7, Bassins paléozoïques cachés sous l'Aquitaine.* Doc. BRGM n° 81-7, 10 p.

Bourrouilh R. and Gorsline D. S. (1979). Pre-Triassic fit and alpine tectonics of continental blocks in the Western Mediterranean. *Geol. Soc. Am. Bull*. v. 90, 1074-1083.

Bourrouilh R. et Offroy B. (1983). Séquences de mass-flow évolutif - mégaturbidites du flysch Sénonien Nord-Pyrénéen. Traitement informatique et Anatomie du bassin Sénonien. Colloque sur le Sénonien. Marseille, septembre 1983. *Géol. Méd.* X, 345-359.

Bourrouilh R., Cocozza T., Demange M., Durand Delga M., Gueirard S., Guitard G., Julivert M., Martinez F.J., Massa D., Mirouse R. et Orsini J.B. (1980). Essai sur l'évolution paléogéographique, structurale et métamorphique du Paléozoïque du Sud de la France et de l'Ouest de la Méditerranée. *26ème Congrès géol. Intern. Colloque C 6,* 159-188, 11 fig. Paris.

Bourrouilh R., Coumes F. et Offroy B. (1984). Mécanismes séquentiels et événements exceptionnels du Flysch Sénonien Nord-Pyrénéen. Corrélations par les dépôts gravitaires profonds. *Bull. Soc. géol. Fr*. 7, XXVI, 1223-1234.

Bourrouilh R., Doyle L.J., Gapillou Cl., Offroy B. et Perlet J. (1984). Les massifs paléozoïques basques et leur couverture récente. Mécanismes de sédimentation du flysch du Crétacé supérieur. *Livret guide de l'Excursion AGSO*, 19, 20 et 21 septembre 1984, 84 p., nbses fig. *BRGM-AGSO*.

Bourrouilh R., Richert J.P. and Zolnai G. (1995). The North Pyrenean Aquitain Basin, France : Evolution and Hydrocarbons. *AAPG Bulletin*, V 79, N° 6 (June 1995), 831-853.

Bourrouilh-Le Jan F. G. (1973). Dolomitisation actuelle dans le monde. Une revue. *Sciences de la Terre*, XVIII, 3, 279-298. Nancy.

Bourrouilh-Le Jan F. G. (1975). Géochimie et isotopie des calcaires et dolomies de Lifou, sondage et subsurface : diagenèse et évolution d'une plate-forme carbonatée du SW Pacifique. *11è Cong. Intern. Sédim*. Thème 7, 25-32, Nice.

Bourrouilh-Le Jan F. G. (1996). Plate-formes carbonatées et atolls du Centre et Sud Pacifique. Stratigraphie, sédimentologie, minéralogie et géochimie. Diagenèses et émersions : aragonite, calcite, dolomite, bauxite et phosphate. *Doc. BRGM*, 249, 365p.

B.R.G.M., ELF-Rap, ESSO-REP and SNPA (1974). Géologie du bassin d'Aquitaine .*B.R.G.M. Ed.*

Brunet M.F. (1984). Subsidence history of the Aquitaine Basin determined from subsidence curves. *Géol. Mag*, 121, 421-428.

Burbank, D., Puigdefàbregas, C. and Muñoz, J.A. (1992a). The chronology of the Eocene tectonic and stratigraphic development of the eastern Pyrenean foreland basin, northeast Spain. *Geol. Soc. Am. Bull*. 104, 1101-1120.

Burbank, D., Verges, J., Muñoz, J.A. and Bentham, P. (1992b). Coeval hindward- and forward-imbricating thrusting in the central southern Pyrenees, Spain: timing and rates of shortening. *Geol. Soc. Am. Bull*. 104:3-17

Canérot J. and Lenoble J.L. (1991). Diapirisme sur une marge en distension, puis en décrochement. (Exemple des Pyrénées occidentales françaises). *Public. Sp. N° 13 de l'Association des Sédimentologistes Français*, 125 p.

Canérot J. and Lenoble J.L. (1993). Diapirisme crétacé sur la marge ibérique des Pyrénées occidentales : exemple du Pic de Lauriolle ; comparaison avec l'Aquitaine, les Pyrénées centrales et orientales. *Bull. Soc. Géol. Fr*., 164, 5, 719-726.

Canérot J. and F. Delavaux, 1986. Tectonique et sédimentation sur la marge nord ibérique des chaînons béarnais, Pyrénées basco-béarnaises. *C. R. Acad. Sci. Paris.* v. 302, sér. II, n° 15, p. 951-956.

Casteras M. (1974). Les Pyrénées, in J. Debelmas ed.“ *Géologie de la France* ”, tome 2, p. 296-345, Masson, Paris

Choukroune P. and ECORS Team (1989). The ECORS Pyrenean deep seismic profile: Reflection data and the overall structure of an orogenic belt. *Tectonics*, Washington, 8, 1, pp. 23-39.

Choukroune P. and Mattauer M. (1978). Tectonique des plaques et Pyrénées: sur le fonctionnement de la faille transformante nord-pyrénéenne; comparaison avec des modèles actuels. *Bull. Soc. Géol. Fr*., Paris (7), XX, p. 689-700.

Choukroune P. (1974). Structure et évolution tectonique de la zone Nord-Pyrénéenne. Analyse de la déformation dans une portion de chaîne à schistosité subverticale. *Mém. Soc. Géol. Fr*., nlle série, t. V, n° 127, p. 1-116.

Choukroune P., Le Pichon X., Seguret M. and Sibuet J.C. (1973) ΦBay of Biscay and Pyrenees. *Earth and Planet Sc. Lett*. 18, p. 109-118.

Choukroune P., Seguret M. and Galdeano A. (1973) Φ Caractéristiques et evolution structurale des Pyrénées : un modèle de relations entre zone orogénique et mouvement des plaques. *Bull. Soc. Géol. Fr.* (7), XV, n° 5-6, 600-611.

Combes P.J. (1969). Recherches sur la genèse des bauxites dans le Nord-Est de l'Espagne, le Languedoc et l'Ariège (France). *Mém. C.E.R.G.H.,* Montpellier, t. III-IV, 1 vol. 275 p.

Coney, P.; Muñoz, J.A., McClay, K. and Evenchick, C. 1996. Syntectonic burial and post-tectonic exhumation of the southern Pyrenees foreland fold-thrust belt. *Journal of the Geological Society*, London, 153, 9-16.

Curnelle R. (1983). Evolution structuro-sédimentaire du Trias à l'Infralias d'Aquitaine. *Bull. Centres Rech. Explor. Prod. Elf Aquitaine,* 7, 1, 69-99, 16 fig.

Curnelle R., Dubois P. and Seguin J.C. (1982) Φ The

Mesozoic-Tertiary evolution of Aquitaine basin, Phil. *Trans. R. Soc. Lond*. A 305, p. 63-84.

Curnelle R., J. Dubois and Seguin J.C. (1980). Le bassin d'Aquitaine, substratum anté-Tertiaire et bordures mésozoiques. *Bulletin des Centres de Recherches Exploration-Production d'ELF-Aquitaine*, Mém. 3, p. 47-58.

Curnelle R. and Dubois P. (1986). Evolution mésozoïque des grands bassins sédimentaires français (Bassin de Paris, d'Aquitaine et du Sud-Est). *Bull. Soc. Géol. France* (8), 529-546.

Daignieres M., Canérot J., Damotte B., Debroas E.J., Desegaulx P., Estival J., Grandjean G., Hirn A., Levot M., Marthelot J.M., Seguret M., Spaecht M. and Villien A. (1991). The Arzacq-western Pyrenean Ecors Profile: a seismic section from the Pyrenean mountains to the deep Aquitaine Foreland Basin. *EUG VI, Strasbourg,* 6, p. 9 Fig.

Daignieres M., Gallart M., Banda E. and Hirn A. (1982). Implications of the seismic structure for the orogenic evolution of the Pyrenean Range. *Earth Planet Sci. Lett*. 88-100.

Dardel R.A. and Rosset R. (1971). Histoire géologique et structurale du bassin de Parentis et de son prolongement en mer. *In* : *Histoire structurale du Golfe de Gascogne*. IV.2.1-IV.2.28, Technip, Paris.

Debroas E.J. and Souquet P. (1976). Sédimentogenèse et position structurale des flyschs crétacés sur le versant nord des Pyrénées centrales. *Bull. B.R.G.M*., sect. 1, n° 4, 305-320.

Debroas E.J. (1987). Modèle de bassin triangulaire à l'intersection de décrochements divergents pour le fossé albo-cénomanien de la Ballongue (zone nord-pyrénéenne, France). *Bull. Soc. Géol., France* (8), 3, 887-898.

Debroas E.J. (1990). Le Flysch noir albo-cénomanien témoin de la structuration albienne à sénonienne de la zone nord-pyrénéenne en Bigorre (Hautes-Pyrénées, France). *Bull. Soc. Géol., France* (8), VI, n° 2, pp. 273-285.

Debroas E.J. (1991). Le diapir d'Arbas (Haute-Garonne, France) nouvel élément turono-sénonien inférieur de la zone transformante nord-pyrénéenne. Table ronde sur le diapirisme, *in* : Canérot J. and Lenoble J.L. (1991). *Public. Sp. n° 13 de l'Association des sédimentologistes français*, 125 p.

Debroas E.J., Sagon J.P. and Azambre B. (1991). Diapirisme, sédimentation et métamorphisme dans le flysch turono-sénonien inférieur d'Arbas (zone nord-pyrénéenne, France). *Soc. Géol., Fr., réunion spécialisée sur l'halocinèse*, 14 Octobre 1991, Paris, France.

Digbehi B.Z. (1987). Etude comparée de la sédimentation des premiers stades d'ouverture Atlantique : Golfe de Guinée-Golfe de Gascogne. (Sédimentologie-Biostratigraphie). *Thèse Université de Pau*, 318 p, 41 pl.

Deramond J., Graham R.H., Hossack J.R., Baby P. and Crouzet G. (1985). Nouveau modèle de la chaîne des Pyrénées. *C.R. Acad. Sci., Paris*, (II), 301, 1213-1216.

Dinares, J., McClelland, E. and Santanach, P. (1992). Contrasting rotations within thrust sheets and kinematics of thrust-tectonics as derived from palaeomagnetic data: an example from the southern Pyrenees *in*: *Thrust Tectonics* (ed. by K.McClay). Chapman and Hall Ed. 265-275.

Ducasse L., Muller J. and Velasque P. Ch. (1986). La chaîne pyrénéo-cantabrique : subduction hercynienne, rotation crétacée de l'Ibérie et subductions alpines différentielles. *C.R. Acad. Sci., Paris,* t. 303, série II, n° 5, p. 419-424, 1 Pl.

Ducasse P.Ch., Velasque L. and Muller J. (1986). Glissements de couverture et panneaux basculés dans la région des Arbailles (Pyrénées occidentales) : un modèle évolutif crétacé de la marge nord-ibérique à l'Est de la transformante de Pamplona. *C.R. Acad. Sci., Paris* (II), 303, 1477-1482.

Dupouy-Camet J. (1952). Recherches structurales sur les accidents triasiques du Sud-Ouest de l'Aquitaine. *Bull. Carte géol. Fr.* n° 233, t. XLIX, 287 p.

Espitalie J. and Drouet S. (1992). Petroleum Generation and Accumulation in the Aquitaine Basin (France; Generation, Accumulation and Production of Europe Hydrocarbons II, AM. Spencer Ed., *Special publication of the European Association of Petroleum Geoscientists* N° 2, Springer Verlag, pp. 127-149.

Esquevin J., Fournie D. and De Lestang J. (1971). Les séries de l'Aptien et de l'Albien des régions nord-pyrénéennes et du sud-aquitain. *Bull. Cent. Rech. Pau* (5), 1, pp. 87-151.

Galdeano A., Minvelle M., Merino Del Rio J., Rossignol J.C. and Tessier C. (1989). Sur l'existence d'accidents transversaux à la chaîne pyrénéenne : apports des sondages géomagnétiques profonds dans les Pays basques. *C.R. Acad. Sci Paris*, t. 290, série B, pp. 227-229.

Gapillou C., (1981). Vers une approche métallogénique d'une région presque oubliée. Les minéralisations à Cu, Ag, Pb, Zn et les sidérites du Paléozoïque et du Trias du Pays Basque Français entre Aïnhoa et Banca. *Thèse 3ème cycle, Université de Paris VI.*

Garcia-Mondejar J. (1990). The Aptian – Albian carbonate episode of the Basque – Cantabrian Basin (northern Spain) : general characteristics, controls and evolution. *Spec. Publs int. Ass. Sediment*. 9, 257-290.

Grandjean, G. (1994). Etude des structures crustales dans une portion de chaîne et de leur relation avec les bassins sédimentaires. Application aux Pyrénées occidentales. *Bull. Centre Rech. Explor.-Prod. ElfAquitaine*, 18, 2, 391-420.

Henry J. and Zolnai G. (1971). Trias resédimenté dans le Sud-Ouest du Bassin Aquitain. *Bull. Centre Rech. Pau, SNPA*, vol. 5, n° 2, p. 389-398.

Henry J. (1987). Enquête géologique sur les Pyrénées "Mes cinq dernières minutes" – Special issue n° 37. *Bull. Techn. Exploration-Production.*

Henry J. and Mattauer M. (1972). Pyrénées, in A.M. Spencer ed., Mesozoic-Cenozoic orogenic belts; data for orogenic studies. *The Geological Society of London.*

Hirst J.P.P. and Nichols G.J. (1986). Thrust tectonic controls on Miocene alluvial distribution patterns, southern Pyrenees in: P. A. Allen and P. Homewood (eds.), *Foreland Basins. Spec. Publ. Int. Assoc. Sedimentologists*, 8, 247-258.

Johns D.R., Mutti E., Rosell J. and Séguret M. (1981). Origin

of a thick, redeposited carbonate bed in Eocene turbidites of the Hecho Group, South Central Pyrenees, Spain. *Geology,* 9, 161-164.

Labaume P., Mutti E., Seguret M. and Rosell J. (1983). Mégaturbidites carbonatées du bassin turbiditique de l'Eocène inférieur et moyen sud-pyrénéen. *Bull. Soc. géol. France,* (6), 25, 927-941.

Labaume P., Seguret M. and Seyve C. (1985). Evolution of a turbiditic foreland basin and analogy with an accretionary prism: Example of the Eocene South-Pyrenean basin. *Tectonics*, 4, 661-685.

Lenoble J.L. and Canérot J. (1992). Halocinèse associée à l'extension de la Marge Ibérique des Pyrénées : exemple du diapir du Lauriolle (Pyrénées Occidentales). *Réunion des Sciences de la Terre,* Toulouse, 13-15 Avril 1992.

Lenoble, J.L., (1992). Les plate-formes carbonatées Ouest-pyrénéennes du Dogger à l'Albien – Stratigraphie séquentielle et évolution géodynamique. *Thèse, Université de Toulouse,* 413p.

Majesté Menjoulas C. (1979). Evolution alpine d'un segment de chaîne varisque (Pyrénées centrales et occidentales). *Thèse d'Etat, Université de Toulouse,* 343p.

Martinez, A., Verges, J. and Muñoz, J.A. (1988). Secuencias de propagación del sistema de cabalgamientos de la terminación oriental del manto del Pedraforca y relación con los conglomerados sinorogénicos. *Acta Geol. Hisp.,* 23, 119-127.

Mattauer, M. (1990). Une autre interprétation du profil ECORS Pyrénées. *Bull. Soc. géol. France*, VI(2), 307-311.

Millan, H., Pocovi, A. and Casas, A. (1995). El frente de cabalgamiento surpirenaico en el extremo occidental de las Sierras Exteriores. *Rev. Soc. Geol. España,* 8, 73-90.

Miranda Avilès R. (2002). Etude géologique comparée des bassins de Santa Rosalia (Basse Californie du Sud, Mexique) et de Mendibelza (Pyrénées, France). *Thèse, Université de Bordeaux 1 and IPN, Mexico,* 235 p.

Moen-Maurel L., Flament J. M., Richert, J. P., and Schnitzler J. J., (1999). Rifting to thrusting in a ductile regime : a different type of inversion, North-Pyrenean Foothills. *Thrust Tectonics Conference abstract volume,* Royal Holloway, London.

Moen-Maurel L., Noual G. and Biteau J.J. (1995). Petroleum exploration in the Pyrenean Thrust belt. *AAPG International Annual Meeting, abstracts*, Nice, France.

Moen-Maurel L, Noual G., Chemin F., Leyrit H. and Ott d'Estevou Ph. (1996). Géodynamique du gisement de gaz d'épisynénites albiennes de la région d'Oloron-Ste-Marie ; apport de la sismique 3D. *Réunion Annuelle des Sciences de la Terre*, abstracts.

Montagné G. (1986). Les anomalies du flysch Nord-pyrénéen de Pau à Ascain (Pyrénées-Atlantiques). *Thèse Université de Pau,* 328 p.

Muñoz, J.A. (1992). Evolution of a continental collision belt: ECORS-Pyrenees crustal balanced cross-section *in: Thrust Tectonics* (ed. by K.McClay). Editorial Chapman and Hall. 235-246.

Muñoz, J.A., Coney, P.; McClay, K. and Eevenchick, C. (1997). Discussion on syntectonic burial and post-tectonic exhumation of the southern Pyrenees foreland fold-thrust belt. *Journal of the Geological Society, London*, 154, 361-365.

Muñoz, J.A., Martínez, A. and Vergés, J. (1986). Thrust sequences in the eastern Spanish Pyrenees. J. Struct. Geol., 8 (3/4), 399-405.

Mutti, E. (1984). The Hecho Eocene Submarine Fan System, South-Central Pyrenees, Spain. *Geo-Marine Letters,* 3, 199-202.

Noual G., Moen-Maurel L. and Biteau J.J. (1995). Hydrocarbon exploration in the Pyrenean Thrust Belt. Abstract *in: AAPG Conference Abstract Volume*, Nice.

ODP Leg 103. Boillot G. and Scientific Party, Proceedings of the Ocean Drilling Project, (1987), *Part A : Initial Reports, 1988, Part B : Scientific Results :* College Station, v.103.

Offroy B. (1984). Approche des mécanismes de sédimentation gravitaire : exemple des dépôts carbonatés des flyschs Crétacé supérieur des Pyrénées Atlantiques. *Thèse 3 ème cycle, Université Paris VII,* 230 p,

Perrodon A. (1980). Géodynamique pétrolière. *ELF-Aquitaine and Masson ed*. Paris.

Peybernès B. and Garot B. (1984). Les brèches d'écroulement aptiennes, témoins de la paléomarge Nord-ibérique du domaine pyrénéen dans la zone des Chaînons Béarnais. *Bull. Soc. Hist. Nat.,* Toulouse, t. 120, p. 51-60.

Peybernès B. and Souquet P. (1984). Basement blocks and tectosedimentary evolution of the Pyrenees during Mesozoic times. *Geol. Mag*. 121, 397-405.

Pous J., Muñoz J.A., Ledo J., Liesa M. (1995). Partial melting of the subducted continental lower crust in the Pyrenees. *J. Geol. Soc., London,* 152: 217-220.

Price R.A., 1986. The southeastern Canadian Cordillera, thrust faulting, tectonic wedging, and delamination of the lithosphere. *Journal of Structural Geology,* 8, 239-245.

Puigdefàbregas C. and Soler M. (1973). Estructura de las Sierras Exteriores Pirenaicas en el corte del Rio Gállego (prov. de Huesca). *Pirineos*, 109, 5-15

Puigdefàbregas C. (1975). La sedimentación molásica en la cuenca de Jaca. *Pirineos*, 104, 188 p.

Puigdefàbregas C. and Souquet P. (1986). Tectonostratigraphic cycles and depositional sequences of the Mesozoic and Tertiary from the Pyrenees. *Tectonophysics,* 129, 173-203.

Puigdefàbregas, C.; Muñoz, J.A. and Verges, J. (1992). Thrusting and foreland basin evolution in the Southern Pyrenees. *In: Thrust Tectonics* (ed. by K.McClay). Editorial Chapman and Hall. 247-254.

Pujalte, V., Robles, S., Zapata, M., Orue-Etxebarria, X. and Garcia Portero, J. (1989). Sistemas sedimentarios, secuencias deposicionales y fenómenos tectono-estratigráficos del Maastrichtiense superior-Eoceno inferior de la cuenca Vasca (Guipúzcua y Vizcaya). *XII Congreso Español de Sedimentología,* Bilbao, Guia de Excursiones, 47-88.

Ribis, R. (1965). Contribution à l'étude géologique du Crétacé supérieur de la Haute-Chaîne dans la région de la Pierre-Saint-Martin (Basses-Pyrénées). *Thèse 3ème Cycle, Université de Paris,* 200 p.

Volume n° 2 - from B16 to B33

Richert J.P., Moen-Maurel L., Canérot J. and Biteau J.J., (1995). The Northern Pyrenees Thrust Belt and Foreland in the vicinity of the Lacq and Meillon gas fields. *AAPG Nice Conference Field Trip Guidebook*. 68p.

Richert, J.P., Moen-Maurel, L., Biteau J.J., Canérot J., (1995). Evolution géodynamique et pétrolière de l'avant-pays Nord-Pyrénéen, *Soc. Géol. France Annual Meeting, Fieldtrip* guidebook, 62 p.

Roest, W.R. and Srivastava, S.P.(1991). Kinematics of the plate boundaries between Eurasia, Iberia and Africa in the North Atlantic from the Late Cretaceous to the present. *Geology*, 19: 613-616.

Roure F., Choukroune P., Berastegui X., Muñoz J.A., Villien A., Matheron P., Bareyt M., Seguret M., Camara P. and Deramond J. (1989). ECORS Deep Seismic data and balanced cross-sections, geometric constraints to trace the evolution of the Pyrenees. *Tectonics*, 8 (1), 41-50.

Rupke (1976). Larger scale slumping in aflysch basin, Southwestern Pyrenees, *Jour geol. Soc. London*, 132, 121-130.

Séguret M. (1972). Etude tectonique des nappes et séries décollées de la partie centrale du versant sud des Pyrénées. *Publication de Ustela, Université de Montpellier,* série Géologie Structurale, n° 21.

Seguret M., Labaume P. and Madariaga R. (1984). Eocene seismicity in the Pyrenees from megaturbidites in the South-Pyrenean Basin (North Spain). *Mar. Geol.,* 55, 117-131.

Seyve C. (1984). Etude micropaléontologique du passage Crétacé/Tertiaire, du Paléocène et de l'Yprésien au Sud de Pau. Thèse *3ème cycle, Université Pierre-et-Marie-Curie.* Tome 1 :129p, t.2 : annexes : 34 pl, XVIII p. Bibliographie.

Soler M. and Puigdefàbregas C. (1970). Lineas generales de la geologia del Alto Aragon Occidental. *Pirineos*, v. 96, p. 5-20.

Souquet P. and Debroas E.J. (1981). Tectonogenèse et évolution des bassins de sédimentation dans le cycle alpin des Pyrénées *in* Colloque C7, 26ème Congrès Géologique International, Paris, *Mémoire B.R.G.M*. n° 107 p. 213-233.

Souquet P. and Deramond J., (1989). Séquence de chevauchements et séquences de dépôts dans un bassin d'avant-fosse. Exemple du sillon crétacé du versant Sud des Pyrénées (Espagne). *C. R. Acad. Sc. Paris,* 309, 137-144.

Souquet P., Debroas E.J., Pons Ph., Fixari G., Roux J.C., Dol J., Thieuloy J.P., Bonnemaison M., Manivit H. and Peybernès B. (1985). Le Groupe du Flysch Noir (Albo-Cénomanien) dans les Pyrénées. *Bull. CREP Elf Aquitaine,* 9, 1, 183-252.

Souquet P., Peybernès B., Billotte M. and Debroas E.J. (1977). La chaîne alpine des Pyrénées *in Géologie Alpine* t. 53, fascicule 2, p. 149-192, Université de Grenoble ed..

Souriau A. and Granet M. (1995). A tomographic study of the lithosphere beneath the Pyrenees from local and teleseismic data. *Journal of Geophysical Research*, 100 (B9): 18117-18134.

Taberner C. (1983). Evolución ambiental y diagenética de los depositos del Terciario inferior (Paleoceno y Eoceno) de la Cuenca de Vic. *Tesis Doctoral, Univ. de Barcelona,* 1-1400.

Teixell, A. (1990). Alpine thrusts at the western termination of the pyrenean Axial Zone. *Bull. Soc. géol. France.* (8), 6, 241-249.

Teixell, A. (1996). The Ansó transect of the southern Pyrenees: basement and cover thrust geometries. *Jour. geol. Soc. London*, 153, 301-310.

Teixell, A. (1998). Crustal structure and orogenic material budget in the west central Pyrenees. *Tectonics,* 17, 395-406.

Teixell, A., Durney, D.W. and Arboleya, M.L. (2000). Stress and fluid control on decollement within competent limestone. *Journ. Struct. Geol.,* 22, 349-371.

Teixell A. and Garcia-Sansegundo J. (1995). Estructura del sector central de la Cuenca de Jaca (Pirineo central). *Rev. Soc. Geol. España,* 8, 207-220.

Vail P.R., Colin J.P., Jan Du Chene R., Kuchly J., Mediavilla F. and Trifilieff V. (1987). La stratigraphie séquentielle et son application aux corrélations chronostratigraphiques dans le Jurassique du Bassin de Paris. *Bull. Soc. Géol. France*, 8, III, p. 1301-1321.

Verges, J., and Muñoz, J.A. (1990). Thrust sequences in the Southern Central Pyrenees. *Bull. Soc. Géol. France,* 8, VI(2), 265-271.

Verges, J., Millan, H., Roca, E., Muñoz, J.A., Marzo, M., Cires, J., Den Bezemer, T., Zoetemeijer, R. and Cloetingh, S. (1995). Eastern Pyrenees and related foreland basins: pre-, syn- and post-collisional crustal-scale cross-sections. *Marine and Petroleum Geology*. 12(8): 893-915.

Verges, J., Muñoz, J.A. and Martinez, A. (1992). South Pyrenean fold-and-thrust belt: role of foreland evaporitic levels in thrust geometry *in: Thrust tectonics*, McClay, K.R. (ed.). Chapman and Hall, London, 255-264.

Vielzeuf, D. and Kornprobst, J. (1984). Crustal spliting and the emplacement of Pyrenean lherzolites and granulites. *Earth and Planetary Science Letters,* 67: 383-386.

Viennot P. (1927). Recherches structurales dans les Pyrénées Occidentales françaises. *Bull. Serv. Carte Géol. France*, n° 155, 267 p.

Villien A. and Matheron P. (1989). Géodynamique de la zone nord pyrénéenne : conséquences sur l'exploration pétrolière. *Bulletin Technique Exploration-Production Elf Aquitaine,* 131, 3-19.

Winnock E. (1971). Géologie succincte du bassin d'Aquitaine (contribution à l'histoire du Golfe de Gascogne), *in Histoire structurale du Golfe de Gascogne,* p. IV 1.1 – IV 1.30, Technip, Paris.

Zolnai G. (1971). Le front nord des Pyrénées Occidentales, *in Histoire structurale du Golfe de Gascogne*, Technip, Paris.

Zolnai G. (1975). Sur l'existence d'un réseau de failles de décrochement dans l'avant-pays nord des Pyrénées Occidentales. *Rev. Géog. Phys. Géol. Dyn.,* XVII, 3, 219-238

Back Cover:
Itinerary of the field trip B16

32nd INTERNATIONAL GEOLOGICAL CONGRESS

Edited by APAT

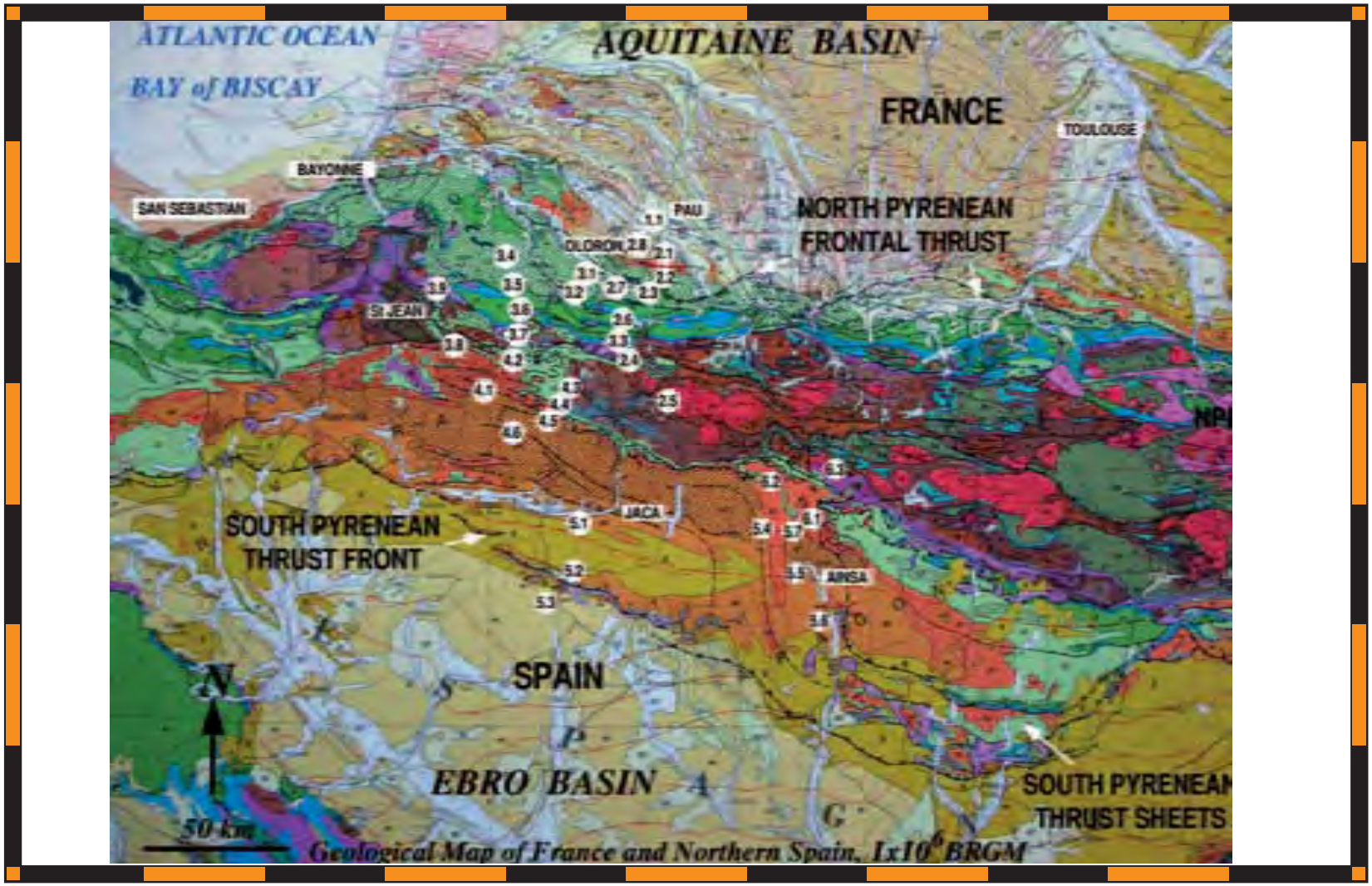

FIELD TRIP MAP

Volume n° 2 - from B16 to B33

32nd INTERNATIONAL GEOLOGICAL CONGRESS

THE PERIADRIATIC INTRUSION OF VEDRETTE DI RIES - RIESERFERNER (EASTERN ALPS): PETROLOGY, EMPLACEMENT MECHANISMS AND CONTACT AUREOLE

Leaders: B. Cesare, A.M. Fioretti, C. Rosenberg

Field Trip Guide Book - B17

Florence - Italy
August 20-28, 2004

Pre-Congress

B17

The scientific content of this guide is under the total responsibility of the Authors

Published by:
APAT – Italian Agency for the Environmental Protection and Technical Services - Via Vitaliano Brancati, 48 - 00144 Roma - Italy

Series Editors:
Luca Guerrieri, Irene Rischia and Leonello Serva (APAT, Roma)

English Desk-copy Editors:
Paul Mazza (Università di Firenze), Jessica Ann Thonn (Università di Firenze), Nathalie Marléne Adams (Università di Firenze), Miriam Friedman (Università di Firenze), Kate Eadie (Freelance indipendent professional)

Field Trip Committee:
Leonello Serva (APAT, Roma), Alessandro Michetti (Università dell'Insubria, Como), Giulio Pavia (Università di Torino), Raffaele Pignone (Servizio Geologico Regione Emilia-Romagna, Bologna) and Riccardo Polino (CNR, Torino)

Acknowledgments:
The 32nd IGC Organizing Committee is grateful to Roberto Pompili and Elisa Brustia (APAT, Roma) for their collaboration in editing.

Graphic project:
Full snc - Firenze

Layout and press:
Lito Terrazzi srl - Firenze

Volume n° 2 - from B16 to B33

32nd INTERNATIONAL GEOLOGICAL CONGRESS

THE PERIADRIATIC INTRUSION OF VEDRETTE DI RIES - RIESERFERNER (EASTERN ALPS): PETROLOGY, EMPLACEMENT MECHANISMS AND CONTACT AUREOLE

AUTHORS:
B. Cesare[1,2], A.M. Fioretti[2], C. Rosenberg[3]

[1]Dipartimento di Mineralogia e Petrologia, Università di Padova - Italy
[2]C.N.R. Istituto di Geoscienze e Georisorse, Sezione di Padova - Italy
[3]Department of Geology, Freie Universität, Berlin - Germany

Florence - Italy
August 20-28, 2004

Pre-Congress

B17

Front Cover:
The Collalto - Hochgall (3436 m a.s.l.)
is the highest peak of the Vedrette di Ries massif.
It is composed of fine-grained tonalite.

Leaders: B. Cesare, A.M. Fioretti, C. Rosenberg

Introduction

During the Oligocene the Alpine chain was the centre of an extensive magmatism, mainly represented by calc-alkaline, which resulted in a series of plutons situated along and adjacent to the Periadriatic Lineament. These intrusives are hence referred to as "Periadriatic plutons".

With an outcrop length of approximately 40 km, and a vertical exposure of 2500 m from base to roof, Vedrette di Ries (Rieserferner) represents one of the best exposed plutons worldwide (Figure 1).

The intrusion of the pluton is characterised by three major pulses of tonalitic to granodioritic composition, with distinct petrographic and geochemical signatures. The ascent of these magmas was controlled by the Defereggen-Anterselva-Valles (DAV) line, which strikes along large parts of the southern margin of the pluton. The contact aureole of the intrusion developed in the metapelitic country rocks, and is characterised by a complete zoneography from andalusite-staurolite to sillimanite-K-feldspar. The presence of synmetamorphic andalusite-bearing veins, related to the dehydration of metapelites, is a unique feature of this contact aureole.

During the field trip we will show the key outcrops of the pluton, discussing both the results and the new ideas arising from detailed structural, petrologic and geochemical investigations performed over the past twenty years.

Geologic and topographic maps

1:25.000 topographic map, sheet n. 035 "Valle Aurina - Vedrette di Ries", Ed. Tabacco.

Cammelli F. (1994) Alpi pusteresi. Guida escursionistico-alpinistica. Available also in German, Ed. Athesia.

Carta Geologica d'Italia 1:100.000, sheet n. 4b "Dobbiaco".

Geologic Map of Italy 1:50.000, sheet n. 009 "Anterselva" (in print).

Hammerschmidt K. 1981 Isotopengeologische Untersuchungen am Augengneis vom Typ Campo Tures bei Rain in Taufers, Südtirol. Mem.Sci.Geol., 34, 273-300, with geologic map.

Mager D. 1985 Geologische Karte des Rieserfernergruppe zwischen Magerstein und Windschar (Südtirol). 'Der Schlern', 6, Bozen.

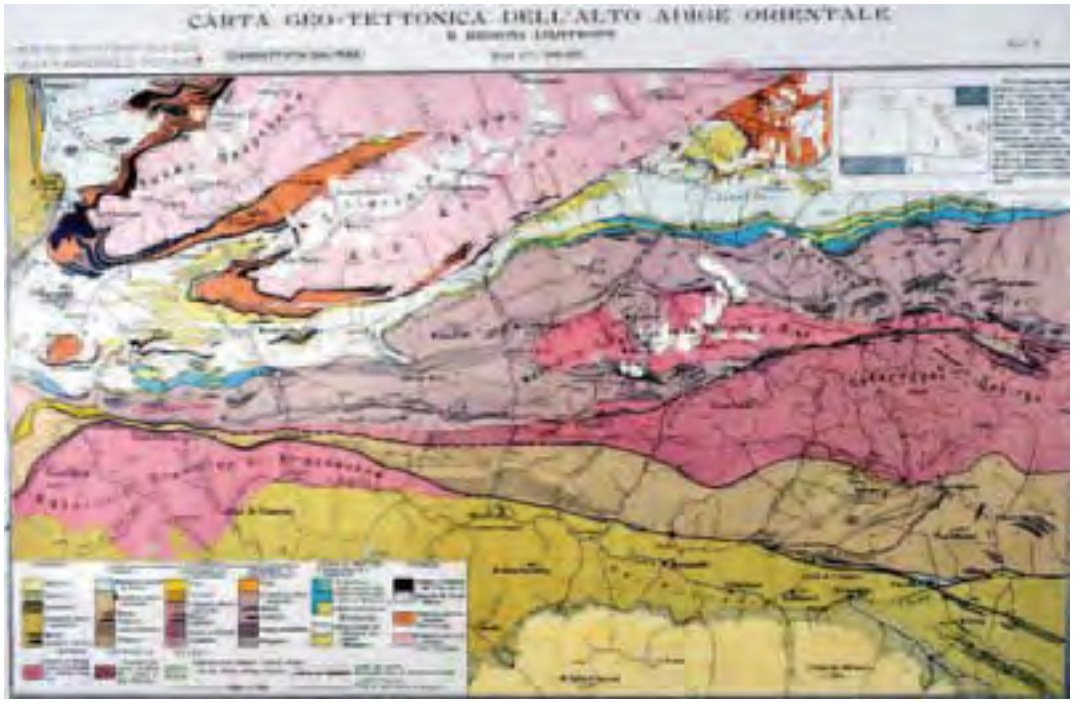

Figure 1 - Geologic map of the Eastern Alto Adige (South Tyrol) from Dal Piaz (1934)

Volume n° 2 - from B16 to B33

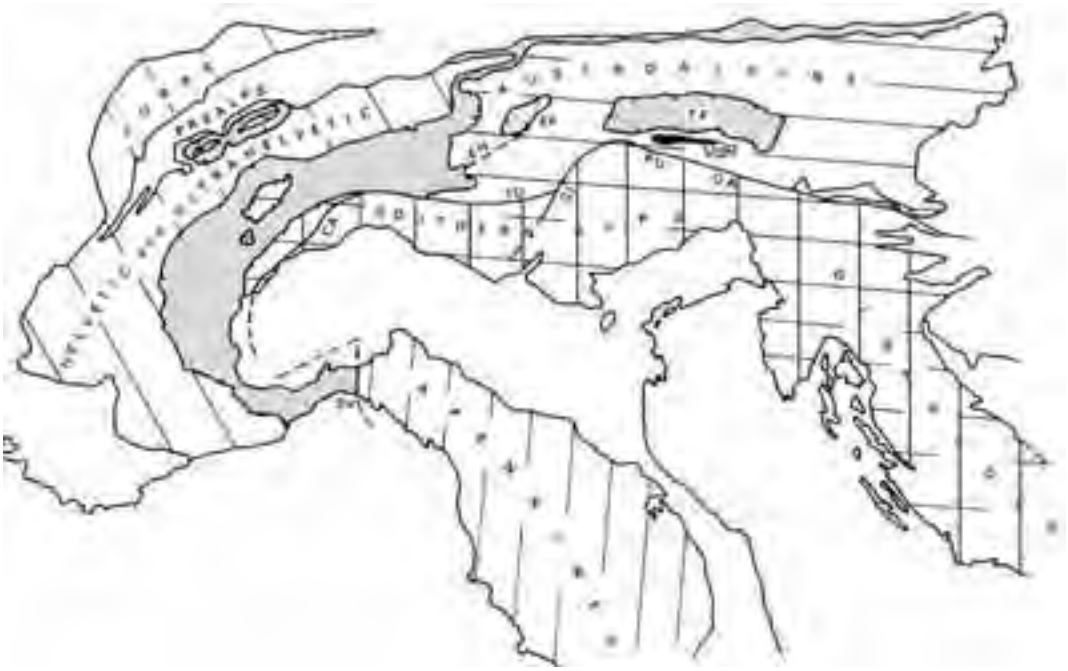

Figure 2 - Main Structural and paleogeographical domains of the Alps (from Dal Piaz et al., 1975).

Schulz B. (1994) Geologische Karte des Altkristallin östlich des Tauferer Tals. Erlanger Geol. Abh., 124; 1-28.

Senarclens-Grancy W. (1972) Geologische Karte der westlichen Deferegger Alpen, Ostirol, 1:25.000. Geol. B. A., Wien.

Regional geologic setting

The Alpine chain (Figure 2) may be subdivided into the following paleogeographic domains (e.g. Froitzheim et al., 1996): (1) The European margin, represented by the Helvetic cover nappes, the external massifs, and the lowermost penninic nappes; (2) the Adriatic (Apulian and Insubric) margin, found in the Austroalpine basement and cover nappes north of the Periadriatic Line and by the unmetamorphosed Southalpine nappes south of the Periadriatic Line; (3) the remnants of two oceanic domains (the Valais ocean and the Piedmont-Ligurian ocean), represented by ophiolites and «Buendnerschiefer», located along the contact between the European and Adriatic units; (4) the Briançonnais, a microcontinent separating the two oceanic domains, found in the uppermost Penninic Units and the cover nappes of the «Préalpes Romandes» in Switzerland.

Most of these units are outcropping in the area of the Vedrette di Ries pluton. The Dolomites, south of the pluton, belong to the Southalpine domain; the Austroalpine basement makes the country rock of the intrusion. The latter unit(=the basement? the Brianconnais?) are thrusted over the oceanic and European units, as can be seen in a large tectonic window (the Tauern window) north of Vedrette di Ries. The oceanic units form the border of the Tauern window (Schieferhuelle), whilst its core exposes basement rocks (Zentral Gneiss) from the European margin.

Eclogites of Cretaceous as well as Tertiary age occur in the Alps. The former ones are found in the Austroalpine domains, whereas the latter ones are part of the Penninic and ophiolitic units of the Valais and Piedmont-Ligurian oceans. These two ages of eclogitization correspond to different tectonic events which occurred in different parts of the Alpine region (Froitzheim et al., 1996). Cretaceous eclogite metamorphism results from the closure of the Meliata-Halstatt ocean (Neubauer, 1994), a Triassic ocean whose remnants are found from the Carpathians to the eastern Alps (Kozur, 1991). In contrast, Tertiary eclogites reflect the subduction of the Jurassic Piedmont-Ligurian ocean (early Paleocene), followed by that of the Valais ocean (early Eocene), below the Adriatic plate. Parts of the European continental margin were also subducted, as

shown by the occurrence of high-pressure and ultra-high pressure rocks in the Dora Maira massif of the western Alps (Chopin et al., 1991).

During the Oligo-Miocene the eastern Alps and the area of Vedrette di Ries were affected by intense N-S shortening, contemporaneous with orogen-parallel extension, resulting in eastward extrusion. This tectonic regime formed large pop-up structures (the Tauern Window), delimited by syn-convergence, low angle normal faults at its eastern (the Brenner Fault) and western margins (the Katschberg Fault). Lateral extrusion, was accommodated by sets of conjugate dextral (e.g., the Periadriatic Line) and sinistral (e.g., the SEMP Line) strike-slip faults. The widespread occurrence of subhorizontal E-W striking stretching lineations and fold axes in the country rocks of Vedrette di Ries records this phase of orogen-parallel extension.

Ongoing shortening and thickening of the orogen caused a propagation of the deformation front towards the more external zones of the chain in the middle- to late Miocene. Hence, the Jura Mountains and thrusting in the Molasse basin were initiated to the north of the Alps, whilst thrusting in the Southern Alps and in the Po Plain affected the southern part of the chain.

The Periadriatic Magmatism and Vedrette di Ries.

The Periadriatic magmatism took place along the entire Alpine chain during the Oligocene, (Exner, 1976; Laubscher, 1985) i.e., long after the continental collision between the African (Insubric) and European plates, which occurred starting from the Eocene. Based on their andesitic, calc-alkaline characters and geological setting these magmas were interpreted as products of a subduction process (Sassi et al., 1980, Bellieni et al., 1981, Kagami, 1991). Dal Piaz & Venturelli (1983) and Laubscher (1985) questioned this interpretation, and proposed that the magmatism, postdating the main tectono-metamorphic event related to the collision, developed during a short extensional phase following the continental collision. According to these authors this extensional phase triggered the ascent and emplacement of the Periadriatic plutons along a belt extending for ca. 700 km from the western Traversella body, in the Piemonte region, to the eastern Pohorje pluton in

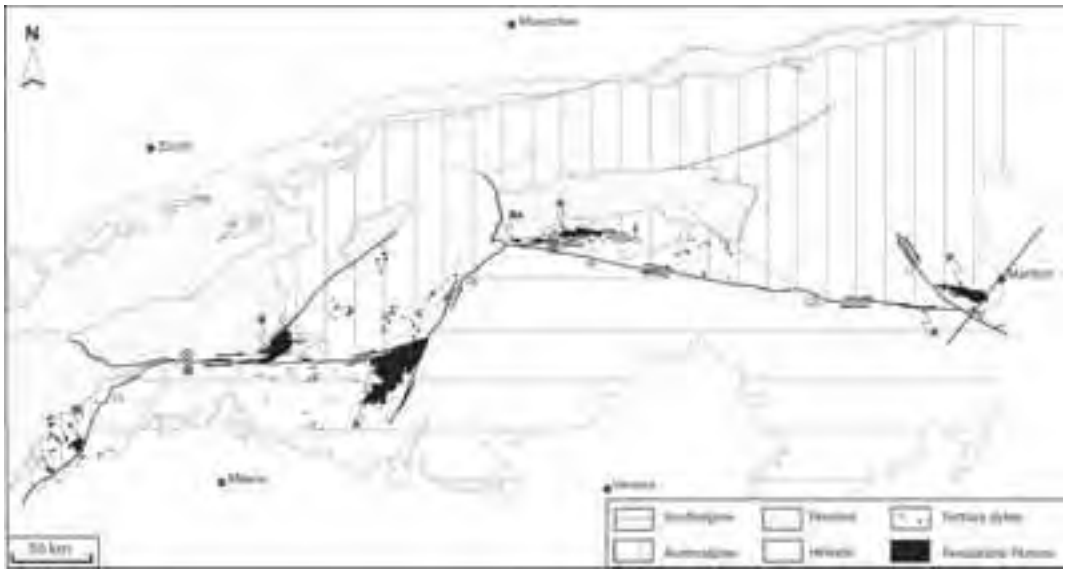

Figure 3 - Simplified tectonic map of the Alps, with enlargements of some segments of the PFS showing the spatial distribution of the Oligo-Miocene dikes and of the Periadriatic plutons. Only the major faults of Tertiary age are shown. Redrawn after Bigi et al. (1990). Faults: CL: Canavese Line; DAV: DAV Line; GL: Giudicarie Line; GTL: Gailtal Line; IL: Insubric Line; LT: Lavantal Line; PL: Pustertal Line. Plutons: A: Adamello; An: Andesites of the Canavese Line; B: Bergell; Bi: Biella; K: Karawanken; L: Lesachtal body; M: Miagliano pluton; P: Pohorje; R: Rieserferner; Re: Rensen; T: Traversella; TL: Tonalitic Lamellae. Full circles: dikes. Note that only part of the dikes are dated. Most of them are inferred to be Oligocene on the basis both of petrographic analogy with the dated ones and of crosscutting relationships with their country rocks. The size of the dikes is exaggerated by several orders of magnitude.

Volume n° 2 - from B16 to B33

Slovenia (Figure 3).

However, structural investigations of some of these plutons showed that ascent and emplacement occurred in a transpressive tectonic setting (Rosenberg et al., 1995; Steenken, 2000; Rosenberg, in press). The latter interpretation is consistent with the generation of the Periadriatic magmas by slab break-off, as suggested by the distribution of the magmatic bodies and their geochemical signature (Von Blankenburg and Davis, 1995).

The Periadriatic magmatism includes plutonic and volcanic rocks of calc-alkaline orogenic series, as well as dikes ranging from andesitic to shoshonitic and ultrapotassic lamprophiric compositions. The whole Periadriatic magmatism can be subdivided into three main sectors. In the western sector, with a NE-SW orientation, plutons intrude mainly the Southern Alps and extend up to the limit with the overthrusted Austroalpine continental crust. Magmatism is represented by small plutons, volcanic covers and high-K andesitic dikes (Dal Piaz and Venturelli, 1983). In the central sector the Periadriatic magmatism reaches its widest extension and is represented by the Adamello batholith, which intruded the South Alpine basement and its Permo-Mesozoic sedimentary cover, and by the Bregaglia-Iorio pluton intruding five nappes of the Alpine pile, including Penninic crystalline, ophiolites and Austroalpine crust (Trommsdorff and Nievergelt, 1983).

In the eastern Alps the Periadriatic magmatism is concentrated in the Austroalpine domain. Only minor occurrences are reported in the northern part of the Southern Alps (Dal Piaz and Venturelli, 1983). In this sector of the chain most plutons (Rensen, Monte Alto –Altberg, Cima di Vila – Zinsnock, Vedrette di Ries) have an overall E-W elongated shape, reflecting their emplacement along the active Periadriatic lineaments. Vedrette di Ries constitutes the main plutonic body of the eastern Periadriatic magmatism. The smaller Cima di Vila pluton, once considered part of the Vedrette di Ries plutonic complex, is now recognized as a geochemically distinct magmatic body (Bellieni, 1980; Bellieni et al., 1982).

Geometry and emplacement of the pluton

Post-intrusive tilting of the pluton (Borsi et al., 1978; Steenken et al., 2002) and 2000 m of relief provide an exceptional exposure of the intrusive body, allowing us to reconstruct its 3D geometry (Figure 4). The roof of the pluton crops out over several tens of square kilometers in the central and northern parts of the intrusion, and the base is exposed at its westernmost end. The main body of the pluton is ~2 km thick, relatively flat-lying and becomes steeply south-dipping, as it gets closer to the DAV (Figure 5). The contact between the fine-grained and the coarse-grained tonalites is subhorizontal in the gently-dipping main body of the pluton (Figure 5)

The foliation pattern in the main body of the intrusion (Figure 6) and a contour map of the contact (Figure 4) show that the roof of the pluton consists of two domal structures separated by a synform. The north-south striking axial plane of the synform is perpendicular to all regional structures of the country rocks away from the pluton, suggesting that this fold and the associated domes result from forceful emplacement of the tonalite rather than from regional deformation (Wagner et al., in review).

Large parts of the roof are discordant to the foliation in the country rocks, but there is no field evidence for stoping. Stoped blocks are lacking (Steenken et al., 2000) and rare xenoliths, generally < 50 cm long, only occur in the immediate vicinity of the contact. Hence, instead of stoping, the discordant contacts are inferred as resulting from extensional fracturing along a gently inclined plane (Figure 7; Wagner et al., in review).

The southern margin of the intrusion is steeply dipping to the south, parallel to the foliation of the country rocks and to the DAV (Figure 5). Locally preserved magmatic fabrics, oriented parallel to the solid-state mylonites of the DAV, suggest a syn-tectonic intrusion.

Within parts of this steep zone, concentric foliation patterns with steeply plunging magmatic lineations (Steenken et al. 2000; Wagner et al., in review) are found from the outcrop scale to that of several hundreds of meters (Figure 6). Such structures do not occur in other parts of the pluton, nor in the enclosing rocks.

The spatial coincidence of these structures with the steeply oriented part of the pluton suggests that this zone acted as the feeder for the intrusion (Figure 7). Therefore, ascent of the tonalitic magmas occurred in the southern part of the pluton, adjacent to the DAV mylonites. As a result of tilting, the easternmost continuation of the steep zone (the eastern tail of the pluton in map view) represents a higher crustal level than the main body and is therefore inferred as representing the upper continuation of the Vedrette feeder (Figure 7), which may have fed other plutons at higher crustal levels.

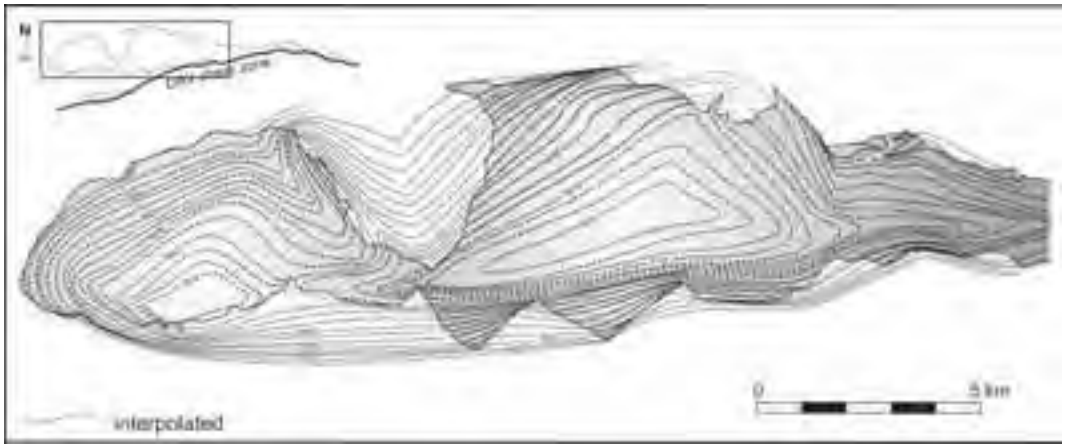

Figure 4 - Contour map of the pluton contact. Modified after Wagner et al., in review.

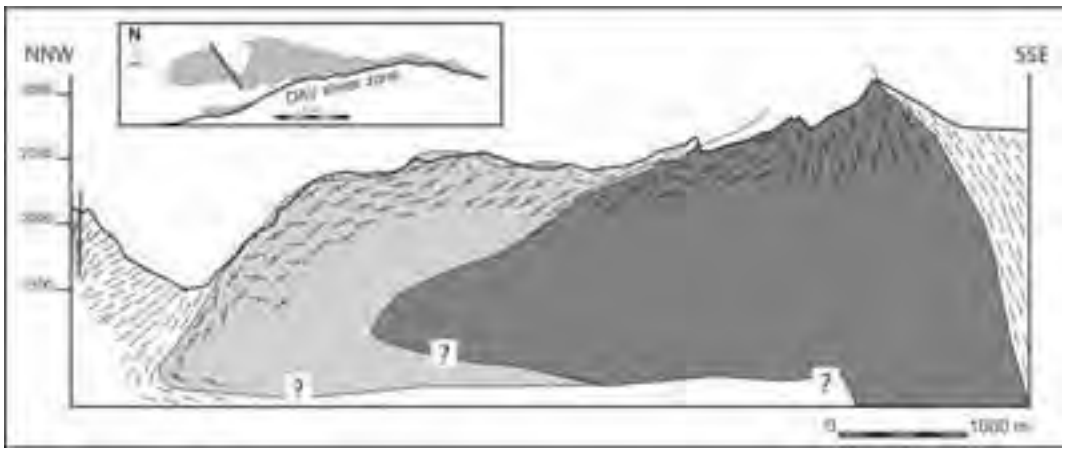

Figure 5 - N-S cross-section of the pluton. From Rosenberg, in press.

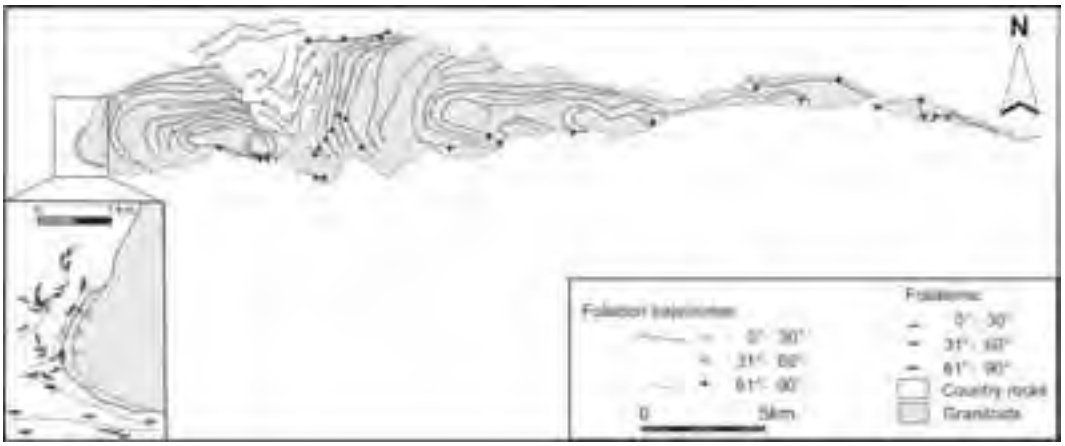

Figure 6 - Foliation trajectories in the Vedrette di Ries.

Volume n° 2 - from B16 to B33

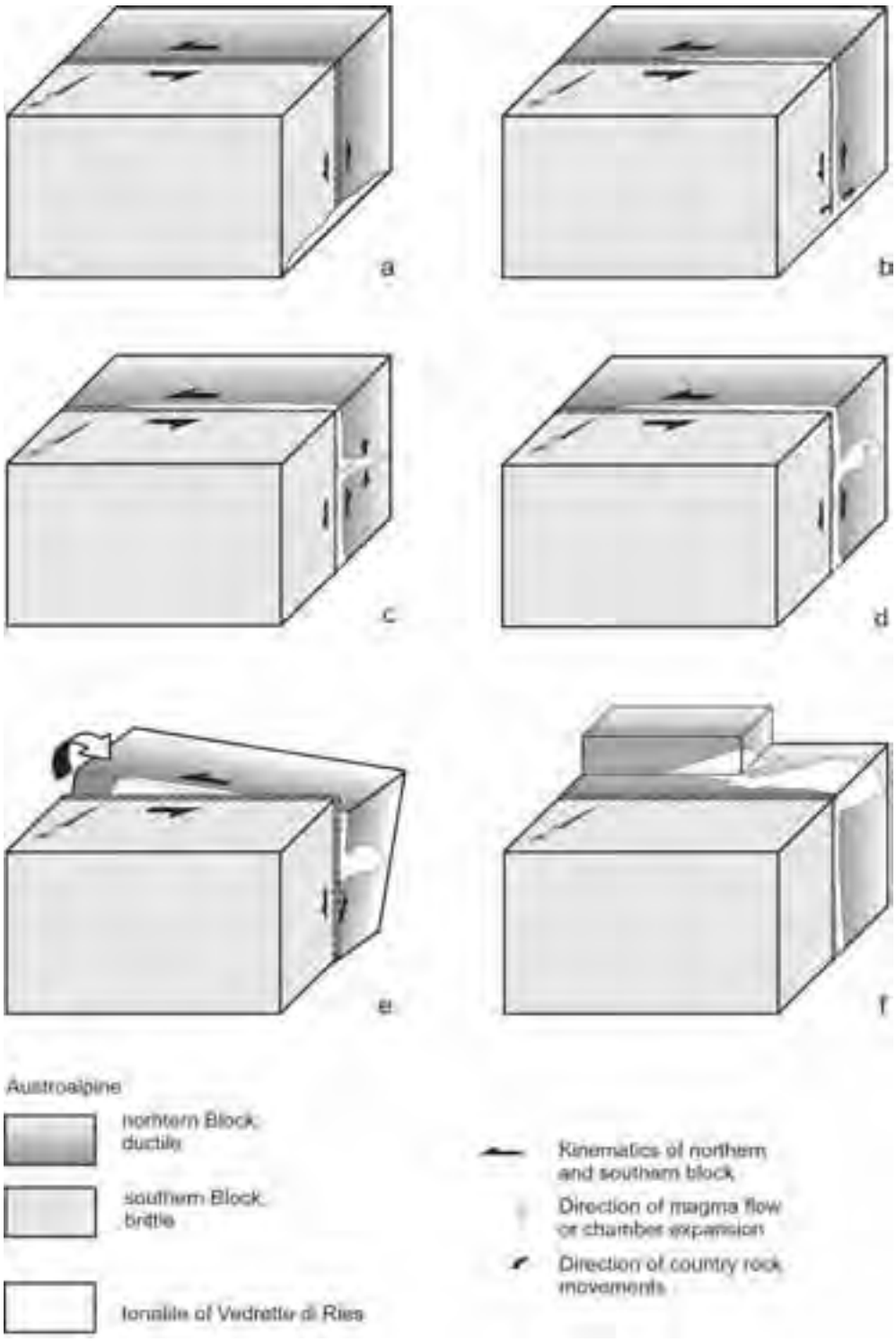

Figure 7 - Ascent and emplacement model for the Vedrette di Ries pluton, from Wagner et al., (2003).

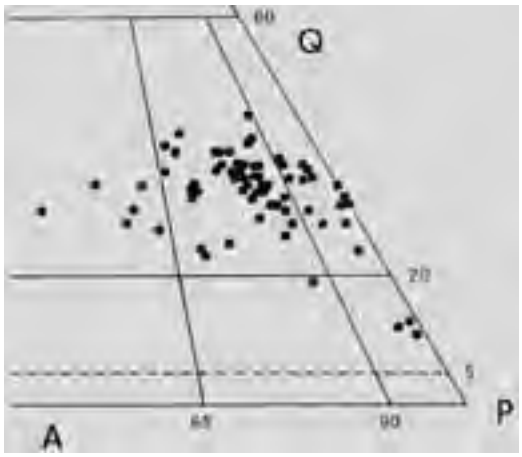

Figure 8 - Distribution of Vedrette di Ries rocks on the QAP classification diagram (taken from Bellieni et al., 1976).

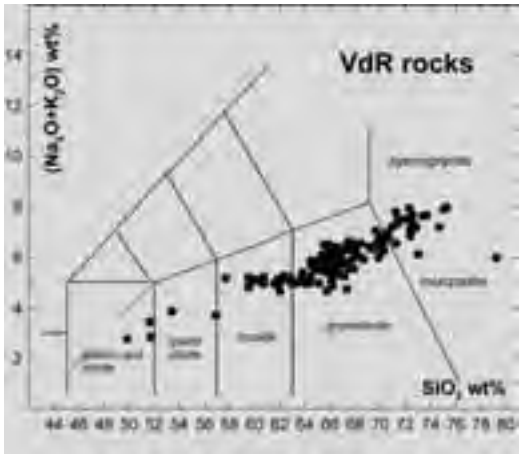

Figure 9 - TAS (Total Alkali Silica, Bellieni et al., 1995) classification diagram for rocks from the Vedrette di Ries pluton.

Igneous lithologies and field relationships.
Vedrette di Ries is a composite pluton, consisting mainly of granodiorite and tonalite, with minor amounts of granite and diorite (Figure 8 and Figure 9).

Three main suites of rocks can be distinguished both in the field and from their geochemical characteristics (Bellieni et al. 1976, Bellieni et al., 1981, Steenken et al., 2000).
Following their emplacement order we distinguish a **first, coarse-grained suite** (Figure 10), characterized by the presence of "book biotite" in piles up to 0.5 cm thick, stubby amphibole, and up to centimetric magmatic garnet (Bellieni et al., 1979, Bassani et al., 1997).

Rocks of this suite are mainly located in the western part of the body and discontinuously decorate its northern and, to a lesser extent, southern borders

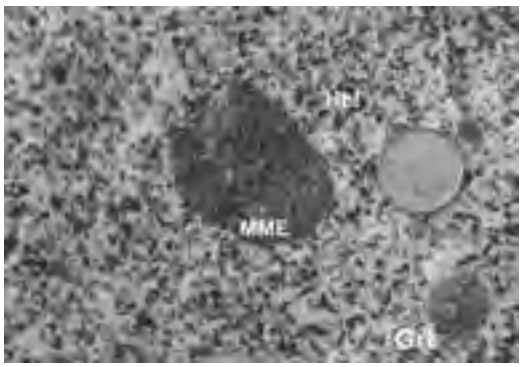

Figure 10 - Coarse-grained tonalite with up to centimetric garnet (Grt), stubby amphibole (Hbl), and frequent Mafic Microgranular Enclaves (MME)

Figure 11 - Distribution of the various magmatic suites in the Vedrette di Ries Pluton (from Steenken et al. 2000).

Volume n° 2 - from B16 to B33

Figure 12 - Sharp contact between coarse-grained garnet tonalite from suite 1 (right) and medium-grained granodiorite from suite 2 (left). Transitional contacts were observed in other places. As a rule, mafic microgranular enclaves are more aboundant in tonalite than in granodiorite (2 km E of Ponte Tobel, a small quarry on the right side of the Reintal).

(Figure 11). This suite ranges in composition from diorite to granodiorite, with dominant tonalite. Small dioritic bodies are located along the south-eastern

Figure 13 - Initial stage of mingling between granodiorite and tonalite of the second, medium- to fine-grained suite (Western Geltal, area N of Rauchkofel, 2500m asl).

side of the pluton. Granite is rare and its affiliation to the suite is evidenced by the presence of rare garnet. The contacts among different lithologies are generally transitional with local evidence of mixing, although sharp contacts are also observed (Figure 12).

The second suite, displaying a sharp to transitional contact with the coarse-grained suite, is medium- to fine-grained and is characterized by the relative abundance of biotite and the presence of rare amphibole, sometimes in coarse crystals. Biotite is generally present in small "flakes", although some

Figure 14 - Mingling (lower part of the picture) and layering (upper left) between tonalite and granodiorite from the second suite (Western Geltal, area N of Rauchkofel, 2500m asl).

Figure 15 - Interlayering of medium-to finegrained granodiorite and tonalite.

"book" crystals can be observed in the contact zones. Rocks of this suite range in composition from tonalite to granite and do not any contain garnet. The contact between tonalitic and granodioritic rocks is mainly transitional, with evidence of mingling (Figs. 13, 14) and interlayering (Figs. 14, 15).

Figure 16 - Sharp contacts between granodiorite and tonalite from the second suite. Dikes of evolved granodiorite magma cut and disrupt the (partially) crystallized tonalite (South of Riesernock, along the Hartdegenweg, 2320m asl).

Sharp contacts and dikes of granodiorite intruding and dismembering the tonalite are also observed (Figure16).

The third suite, located in the central-eastern part of the pluton and mostly surrounded by rocks of the second suite, is medium- to fine-grained and displays a rather homogeneous leuco-granodioritic composition. Biotite, in accessory quantities, is the only mafic mineral, and K-feldspar appears in centimetric individuals. Contacts with rocks of the previous suite are sharp (Steenken et al., 2000).

Chemical characters of the Vedrette di Ries rocks and genetic hypothesis

The intrusive rocks of Vedrette di Ries show a calcalkaline character. They have invariably low TiO_2 content (<0.8 wt%), high Al_2O_3 and low FeO/MgO ratio.

From the geochemical point of view the three suites (Figure 17) can be distinguished based on their Ca, Sr, Rb (Figure 18) contents and trends (Bellieni et al., 1978).

Further investigations pointed out that, based on their REE contents, rocks of Vedrette di Ries can be subdivided into two main groups characterized by low (<1.1) Tb_N/Yb_N and high Tb_N/Yb_N values (Figure 19).

According to Bellieni et al. (1981) the rock series represents the product of a two-stage crystal/liquid fractionation starting from one and the same parent magma. During a first stage, at high pressure, separation of hornblende + garnet lead to magmas with high Tb_N/Yb_N, representing the ancestor of each suite. These magmas, during their rise at lower pressure, underwent a second stage of fractional crystallization with separation of hornblende + plagioclase, and then evolved towards Sr-poor compositions. Processes of contamination with crustal material and separation of accessory phases had an important role in determining the high $^{87}Sr/^{86}Sr$ values and the uneven distribution of some trace elements (Bellieni et al., 1981).

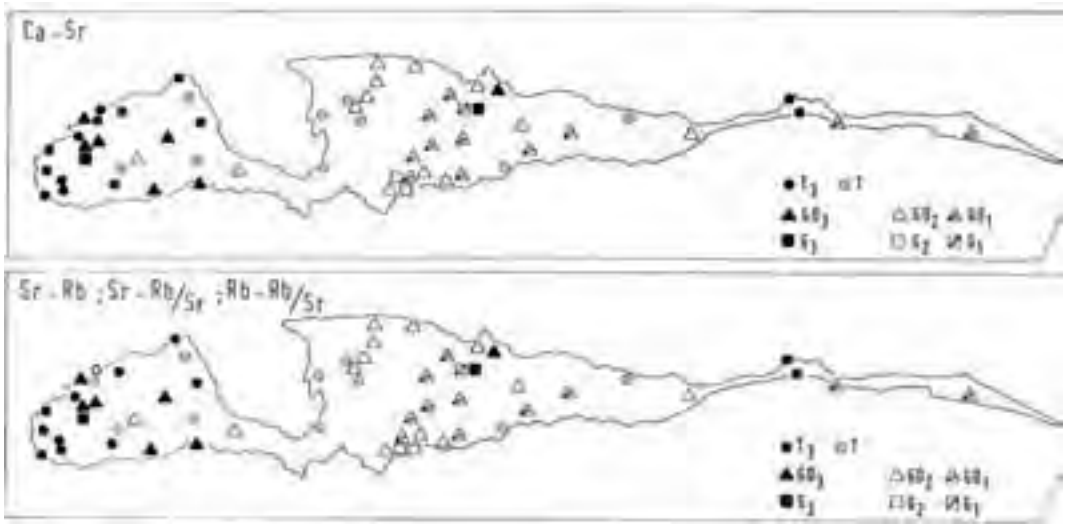

Figure 17 - Areal distribution of the three different suites of rocks in Vedrette di Ries as identified by the Ca-Sr and Rb-Sr variation diagrams (taken from Bellieni, 1978).

Volume n° 2 - from B16 to B33

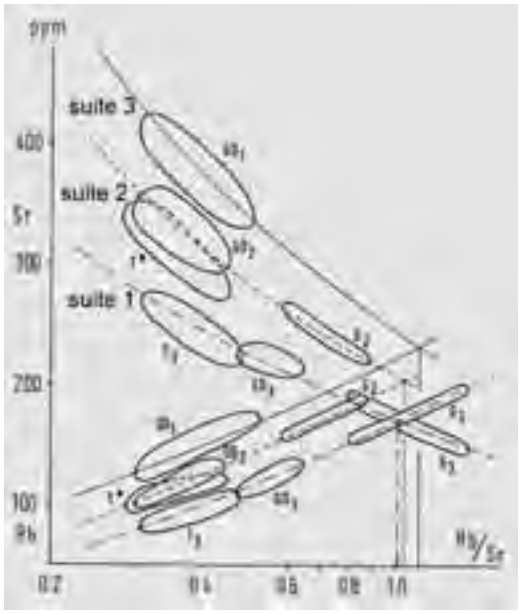

Figure 18 - Cumulative diagram of Rb and Sr vs Rb/Sr taken as a differentiation index. The three suites of rocks define different trends. The intersection of Rb and Sr curves for each suite takes place at different Rb/Sr values. Suite T3-GD3-G3 corresponds to the first, coarse-grained, garnet bearing suite. Suite T-GD2-G2 corresponds to the second, fine-to medium-grained suite. GD1 represents the third, central, homogeneous leuco-granodiorite. (Taken from Bellieni, 1978).*

Mafic microgranular enclaves (MME) are common. They are abundant in the first, coarse-grained suite and occasional in the third granodioritic suite. Their abundance decreases with the increasing SiO_2 of the host and their composition reflects that of the host, the most mafic enclaves being observed in most mafic hosts. Garnet is restricted to MME sampled within the garnet-bearing suite. Based on their petrographic, geochemical and isotopic characters, Bellieni et al. (1989) argued that MME represent blobs of mafic magma whose original composition was modified by interaction with the host magma (Figure 20). MME are therefore good strain markers (Figure 21).

Metamorphic xenoliths are locally abundant not only close to the country rocks, but also in some central areas of the magmatic body. Small metamorphic "surmicaceous" xenoliths are particularly abundant in rocks from the second suite. Assimilation of country rocks actually played an important role in the evolution of these magmas, as indicated by their high initial $^{87}Sr/^{86}Sr$ isotopic composition and by its wide

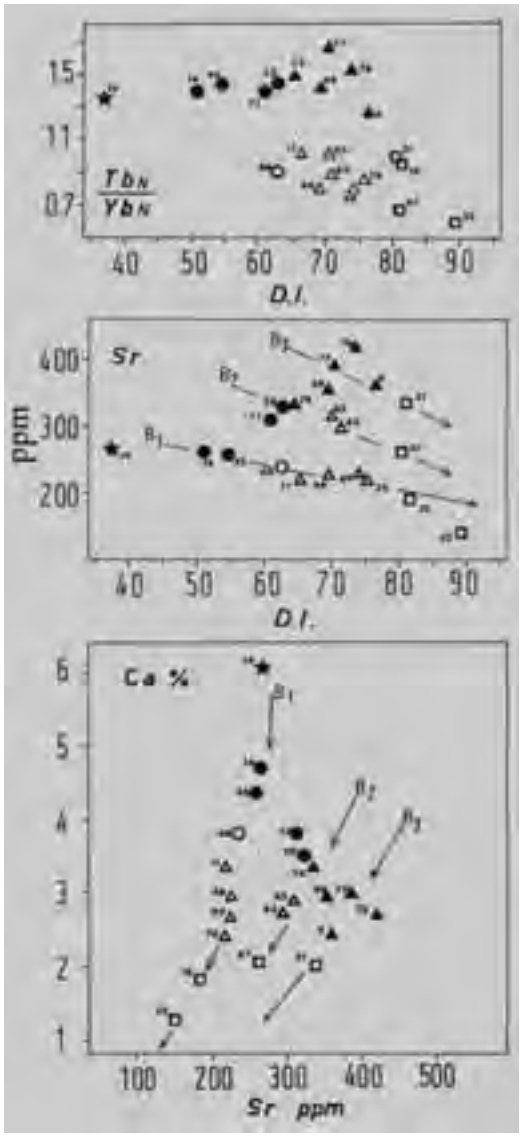

Figure 19 - Two main groups of rocks can be identified in Vedrette di Ries based on their Tb_N/Yb: rocks with low (<1.1) Tb_N/Yb_N values (empty symbols), and rocks with high Tb_N/Yb_N (filled symbols). In the Sr versus D.I. (Differentiation Index) and Ca vs Sr diagrams, rocks with high Tb_N/Yb_N plot at the origin of each of the three distinct geochemical trends of Vedrette di Ries (reported as B1, B2, B3). Stars: diorite; circles: tonalite; triangles: granodiorites; squares: granite.

variational range (Borsi et al., 1979).

All suites are cut by late acidic and mafic dikes and veins (Figure 22). Acidic dikes range from centimetric to metric, have an overall E-W orientation, and often

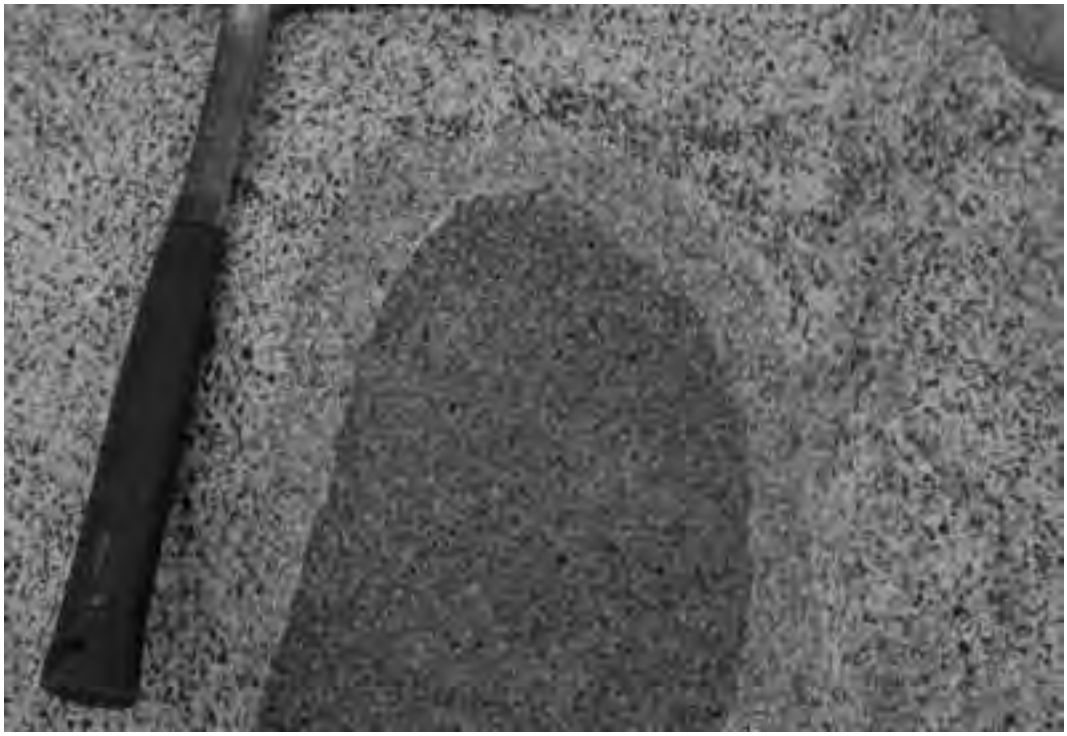

Figure 20 - Mafic microgranular enclave surrounded by a centimetric reaction halo.

Figure 21 - Example of late flattening on a mafic microgranular enclave and an aplitic dike.

Volume n° 2 - from B16 to B33

Figure 22 - TAS classification diagram for acidic and mafic dikes within Vedrette di Ries Pluton (Fioretti et al., unpublished).

constitute swarms of subparallel individuals that only seldom intrude the metamorphic country rock. Aplitic dikes are more common than pegmatitic ones and may contain spessartine garnet. They represent the latest magmatic activity linked to the emplacement and evolution of Vedrette di Ries.

Lamprophyric dikes with a dominant N-S orientation, show sharp contacts with the intruded host (Figure 23).

Mafic dikes are not part of the Vedrette di Ries magmatic cycle. They cut both the plutonic rocks, including aplite and pegmatite dikes, and the metamorphic country rocks. They are centimetric to decametric and range in composition from trachy-basalt to basaltic andesite (Figure 21). Both calcalkaline and shoshonitic products are present, sometimes even within the same dike (Schiavon, unpublished degree thesis), where pristine shoshonitic magma is intruded and disrupted by younger calcalkaline magma (Figs. 24 and 25)

Mafic dikes are commonly found also in the surrounding basement. They belong to a widespread "andesitic" l.s. dike activity that interested not only the Austroalpine, but also the Southern Alpine and Pennidic units (Gatto et al., 1976). K-Ar age determinations on a lamprophyric dike within Vedrette di Ries yields an age of 26.3±3 Ma (Steenken et al., 2000).

Figure 23 - Mafic dike with magmatic lineation along the wall (S-SE of Rifugio Roma).

Geochronology

Borsi et al., (1979) reported a whole rock Rb/Sr age for Vedrette di Ries of 30±3 Ma and $^{87}Sr/^{86}Sr$ with an initial ratio of 0.709. Higher values of the initial $^{87}Sr/^{86}Sr$ (up to ca. 0.720) were obtained from other batches of magmas and from some granite (Borsi et al., 1979, Cavazzini et al., unpublished data). Field evidence indicates that Vedrette di Ries is younger

Figure 24 - Veining of a mafic dike by more evolved magma. The horizontal lines are glacial stripes.

Figure 25 - Pristine magma disrupted by younger calcalkaline magma within the same dike.

than the acidic porphyritic dikes outcropping in the surrounding basement (Cescutti et al., 2003). These dikes have been correlated (Cescutti et al., 2003) with those outcropping at the Austroalpine-Penninic limit north of Rensen (Figure 3), dated at 30.9±0.2 Ma by Müller et al. (2000). The late lamprophyric dikes cross-cutting Vedrette di Ries are 26.3±3 Ma (Steenken et al., 2000).

Metamorphism

In the region between the Tauern Window and the Periadriatic Lineament, the Austroalpine basement of the Eastern Aps forms an E-W trending belt, divided into three blocks by two major tectonic lines: the Defereggen-Anterselva-Valles (DAV) line and the Kalkstein-Vallarga (KV) line (Borsi et al. 1978).

Unlike the other two blocks, which display an essentially pre-Alpine tectono-metamorphic history, the block north of the DAV line was involved in the Alpine metamorphic cycle (Borsi et al., 1978): its polymetamorphic history can be summarized as follows:

1 - "Caledonian" metamorphism of undetermined P-T conditions (Borsi et al., 1973; Hammerschmidt, 1981)

2 - Variscan high grade metamorphism and anatexis at P = 6±1 kbar and T = 650 °C (Stöckhert, 1985, 1987; Schulz, 1997);

3 - Eo-Alpine metamorphism under relatively high-P/low-T conditions (7.5 ± 1.5 kbar and 450 ± 50 °C, Stöckhert, 1984, 1987; Prochaska, 1981);

4 - "Main-Alpine" ("Tauern") metamorphism under lower greenschist facies conditions (Sassi et al., 1980);

5 - Oligocene contact metamorphism in the aureole of the Vedrette di Ries pluton (Bianchi, 1934; Prochaska, 1981; Schulz, 1989; Cesare, 1994a, 1999a): the last metamorphic event recorded in the area.

Metamorphism was accompanied by intense deformation during both the eo-Alpine (Stöckhert, 1987) and the late-Alpine events (Kleinschrodt, 1987). Oligo-Miocene dextral and sinistral mylonites are widespread throughout the area, pointing to an intense coaxial component of deformation in front of the Dolomite indenter (e.g. Müller et al., 2001). Discrete mylonite zones of considerable thickness and lateral continuity occur far from (and north of) the DAV line, in addition to numerous smaller and discontinuous ones (Mancktelow et al., 2001).

However, parts of the block escaped the Alpine structural reworking (not the metamorphic overprint) preserving pre-Alpine structures and metamorphic relict assemblages (Borsi et al., 1978). One of these areas is located south of the Vedrette di Ries tonalitic

Volume n° 2 - from B16 to B33

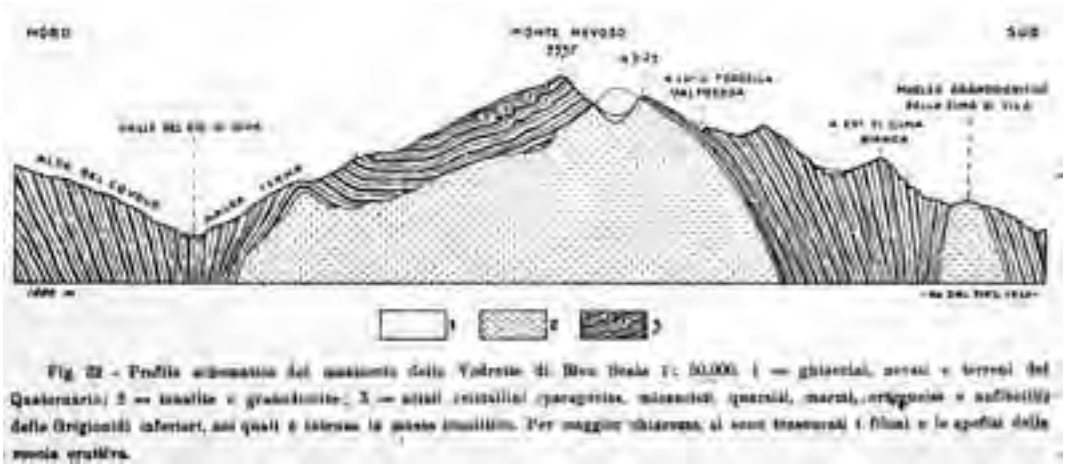

Figure 26 - North-south cross-section across the Vedrette di Ries pluton (from Dal Piaz, 1934) showing the antiformal structure in the country rocks.

pluton; here metapelitic schists and migmatitic paragneisses are dominant, with minor interbedded layers of pegmatite gneiss, marble, quartzite and amphibolite. The well-developed Variscan metamorphic layering, isoclinally folded, strikes E-W and dips south 30° to 60°; the overall structure represents the southern flank of a kilometer-sized antiform quasi-concordant with the pluton margin (Figure 26).

The contact aureole of the Vedrette di Ries tonalite is approximately 1.5 kilometres wide and has been divided by Cesare (1992) into five mineralogic zones, which correspond to type 2bii of Pattison & Tracy's (1991) facies series scheme. The pressure of contact metamorphism is estimated at 2.5-3.75 kbar (Cesare, 1994a, using the Holdaway's (1971) Al_2SiO_5 triple point of, with maximum temperatures of 600-620°C. A weak deformation, occurring as a reactivation of the earlier main foliation, accompanied the contact metamorphism and is localized in the zones of highest metamorphic grade, close to the pluton contact.

Field trip itinerary

The area we are going to visit is completely enclosed in the "Naturpark Rieserferner-Ahrn".

The Park is the largest one in Southern Tyrol and was founded 13 years ago. It constitutes a successfull example of protecting a wide area not by imposing restrictions that eventually prevent the native population from using it, but by pursuing a considerate policy of integration and sustainable development. The Park is not only accepted by the population but also protected and actively maintained.

Figure 27 - "May the Lord be praised": carved block of tonalite, Franziskusweg, Naturpark Rieserferner-Ahrn.

The mountains, woods, water, and grazing areas are home for the people living here. Cultural traditions are proudly cultivated and transmitted. The beauty of these places testifies to the care and love of the local population for their homeland, and for which God is also gratefully acknowledged (Figure 27).Please, be considerate. Whereas you are certainly allowed to take some samples with you, we kindly request you not to leave any major trace of your passage.

DAY 1

Brunico (Bruneck) - Campo Tures (Sand in Taufers) - Riva di Tures (Rein in Taufers) - Sorgiva (Ursprung) valley – Rifugio Roma (Kasseler Hütte).

a) Riva di Tures valley (Reintal): a visit to the tonalite quarries and introduction to the petrology and

geochemistry of the composite pluton of Vedrette di Ries. b) Sorgiva-Ursprung valley: walk to the northern contact of the pluton. Outcrops of mylonites at the contact and intensely deformed tonalite. Discussion of the structural and chronological relationships between emplacement and ductile deformation, and of the role of the northern mylonite zone. c) A walk along the Hartdegenweg to the Rifugio Roma (2275 m a.s.l.): outcrops of various facies of the tonalite. Strain gradient in the tonalite, mingling and injection relationships between fine-grained and coarse-grained facies, aplitic, granitic and lamprophyric dikes cutting the main body.

Stop 1:

Road between Campo Tures - Riva di Tures (c. 1150m a.s.l.). Quarries of tonalite along the Rio di Riva Valley. Coarse-grained, Grt-bearing tonalite and granodiorite. Contact with the medium- to fine-grained granodiorite without garnet. Granite and aplitic dikes. Petrogenetic implications of the presence of garnet will be discussed.

Garnet is one of the main features of the coarse-grained suite (Figure 10). In calc-alkaline magmas garnet is rare, but not unusual; experimental work by Green (1972) and Green & Ringwood (1972) have demonstrated that it forms at pressure conditions > 10 Kbar. However, the observations that magmatic garnet-bearing rocks in Vedrette di Ries represent a sort of belt around the pluton close to the contact with the metamorphic country rocks, and that all along the contacts magmatic rocks contain metamorphic xenoliths with abundant garnet, suggested that garnet in the Vedrette di Ries plutonic rocks might exclusively be linked to the assimilation of country rocks. This problem was addressed by Bellieni et al. (1979) and recently reconsidered by Bassani (unpublished degree thesis, 1996).

Garnet in Vedrette di Ries tonalite and granodiorite is up to 2 cm wide and is generally idiomorphic. It is typically surrounded, and sometimes totally replaced, by a reaction rim made up of fine-grained plagioclase ± biotite ± quartz (± amphibole) (Figure 28). Preserved individuals show concentric shells of Pl ± Qtz ± Bt ± Hbl inclusions, likely representing samples of the coexistent crystallizing magma. Garnet is zoned with a wide, rather homogeneous, nucleus of almandine composition (Alm 50-70%, Sps 2-10%) and a narrow more spessartine-rich rim (Alm 35-40%, Sps 12-15%). The core composition of garnet is independent from the rock, i.e. core composition of garnet in diorite, tonalite and granodiorite is the same

Figure 28 - Subhedral garnet with atoll inclusions (amphibole ± plagioclase ± biotite ± opaque minerals), surrounded by a thin reaction rim.

(Fig 29).

The compositional range of rims is more scattered, possibly due to different degrees of interaction with distinct magmas.

The composition of included minerals shows some systematic differences compared to that of the same phases occurring in the rock. While plagioclase in the rock shows a marked zoning with bytownite core and up to oligoclase rim, plagioclase within garnet lacks the An-poor external rim, and its intermediate zones are very thin. Amphibole in garnet is Fe-hornblende and is Al-richer than the Mg-hornblende of the rock. On the other hand, the composition of biotite inside garnet and within the rock is almost the same. Petrographic and minero-chemical characters fit the hypothesis that minerals in inclusions formed by crystallization of portions of the magmatic liquid trapped in garnet during its crystallization (Figure 30). The composition of minerals in the reaction rim is rather homogeneous. Plagioclase is oligoclase, and amphibole composition straddles the

Figure 30 - Inclusion in garnet. The shape of the inclusion, a negative garnet crystal, and the composition of the mineral phases suggest that included minerals crystallized from a portion of trapped magmatic liquid.

Volume n° 2 - from B16 to B33

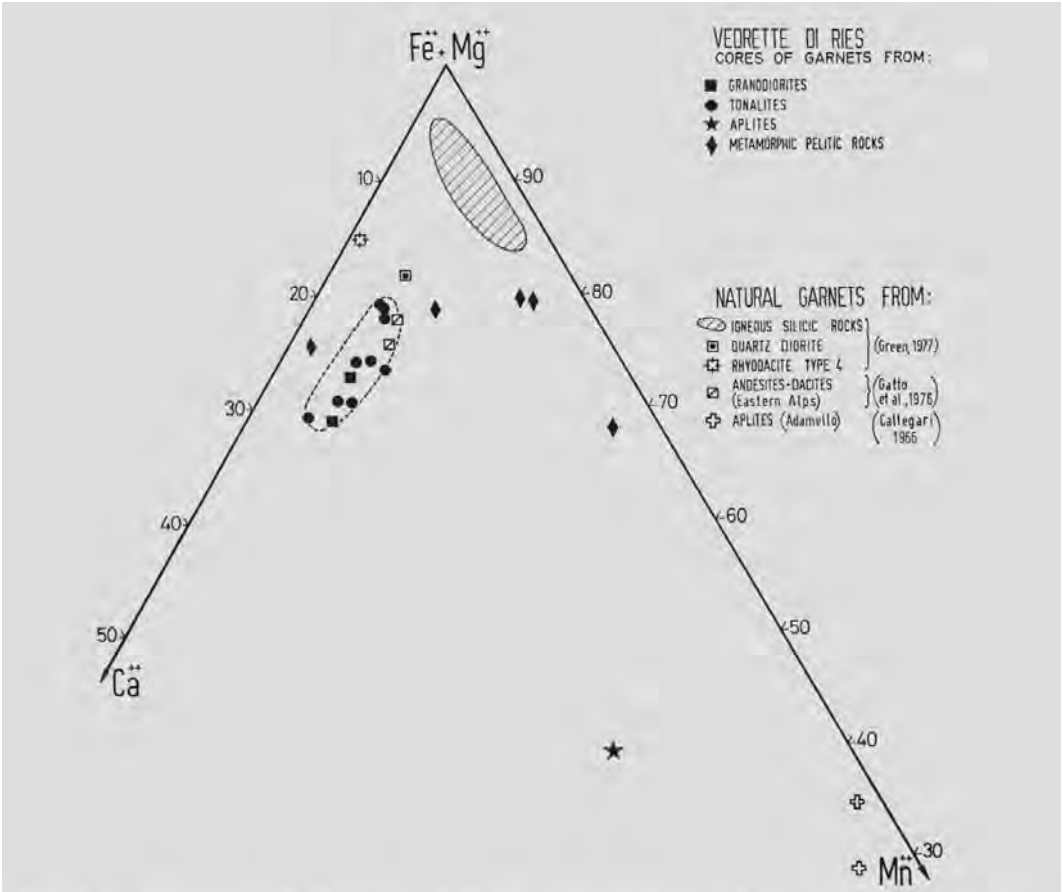

Fig. 8. Composition of the cores of the garnets studied and of some garnets known in the literature (GREEN, 1977).

Figure 29 - Composition of garnet core from tonalite and granodiorite (full squares and circles), from the country metamorphic rock (diamonds) and from aplite (star). Magmatic cores define an elliptical coherent field with rather constant spessartine contents.

Figure 31 - Reaction border around garnet. The width of the reaction border ranges from a thin rim to the complete substitution of the original garnet.

fields of Fe-hornblende and Mg-Hornblende.

Taking into consideration the garnet cores, Bellieni et al. (1979) estimated that garnet was in equilibrium with liquidus at P>10 Kb, T<950°C and water content of approximately 5%. Garnet either formed or grew on relics during magmatic crystallization, and reached instability conditions only during a later stage, as suggested by the presence of a reaction border (Figure 31).

The instability of the garnet, accompained by a marked plagioclase zoning (Bellieni et al., 1976), is presumably linked to a relatively rapid uprising of the magma towards shallower crustal levels (ca.

2 Kb), where the magma eventually emplaced. An identical conclusion was independently reached by studying the crystallization of the cotectic minimum of the granitic rocks (Bellieni, 1977). Contact mineral assemblage of the country rocks (Bellieni, 1977; Cesare, 1992) further confirms the final emplacement level of the Vedrette di Ries magma.

Stop 2:

Path 8c, 1735m a.s.l.. Foliated, coarse-grained tonalite just before the bridge over Rio di Riva. Foliations dip to the N-NW of 50-60°.

Stop 3:

Path 8c from Riva di Tures (Loc. Säge) to Ursprungalm, along the river, 1850m a.s.l.. Strongly foliated country rocks at the northern intrusive contact.

The mylonitic paragneisses contain both layer-parallel and discordant dikes and apophyses of coarse-grained tonalite. These relationships suggest that mylonitic deformation was active in this area during the initial stages of pluton emplacement, and that it stopped before the final stages of emplacement.

Along path 8c to Ursprungalm several aspects and phenomena deserve consideration:

4) at 1900m a.s.l: paragneisses with transposed tonalite injections along mylonitic foliation;
5) from 1900m to 2100m a.s.l: the path climbs up to the north of a hill mostly made of amphibolites;
6) at 2290m a.s.l: the amphibolites and paragneisses are crosscut by a porphyritic dike (Cescutti et al., 2003). The dike is c. 3 m thick, and is strongly sheared within the dominant mylonitic foliation. This kind of dikes, of granitic composition, never crosscuts the Vedrette di Ries plutonic rocks, and is therefore older. Similar rocks, named "porphyritic tonalites" have been dated at 30.9±0.2 Ma by Müller et al. (2000).

The mineral assemblage of this kind of dikes is plagioclase, quartz, K-feldspar, muscovite, and biotite. Garnet, allanite, apatite, opaque minerals and zircon are present in accessory quantities. Based on petrographic evidence (garnet composition and zoning, its presence inside the core of zoned plagioclase, overgrowth of new garnet around individuals not included in plagioclase, partial resorption and subsequent crystallization of new plagioclase), and their chemical signature, a genesis by partial melting of deep crustal material and an emplacement at shallow levels following a polybaric crystallization was proposed for these dikes (Cescutti et al., 2003).

Stop 4:

Path 8a to Rifugio Roma, 2320m a.s.l. The well-exposed northern contact of the pluton.

Mylonitic paragneisses with transposed tonalitic dikes. The country rocks in this area are largely made of mylonitic paragneisses, containing numerous veins and apophyses of coarse-grained tonalite, transposed and boudinaged within the foliation (Figure 32, see also Steenken, 2002). In the paragneisses, biotite and fibrolitic sillimanite occur in the synkinematic assemblage. As sillimanite occurs in this area only as a product of contact metamorphism, we can conclude

Figure 32 - Small tonalitic dike transposed in the foliation of country rock paragneisses. In the paragneiss, the foliation is outlined by synkinematic sillimanite (fibrolite).

Figure 33 - Boudinage of a dm-thick amphibolite layer at the northern intrusive contact of the Vedrette di Ries tonalite, in the upper Val Sorgiva.

that the mylonitic foliation developed during contact metamorphism, i.e., that it was synchronous with pluton emplacement.

Amphibolites, metacarbonates and calc-silicate rocks at the immediate contact. As also observed in the

Volume n° 2 - from B16 to B33

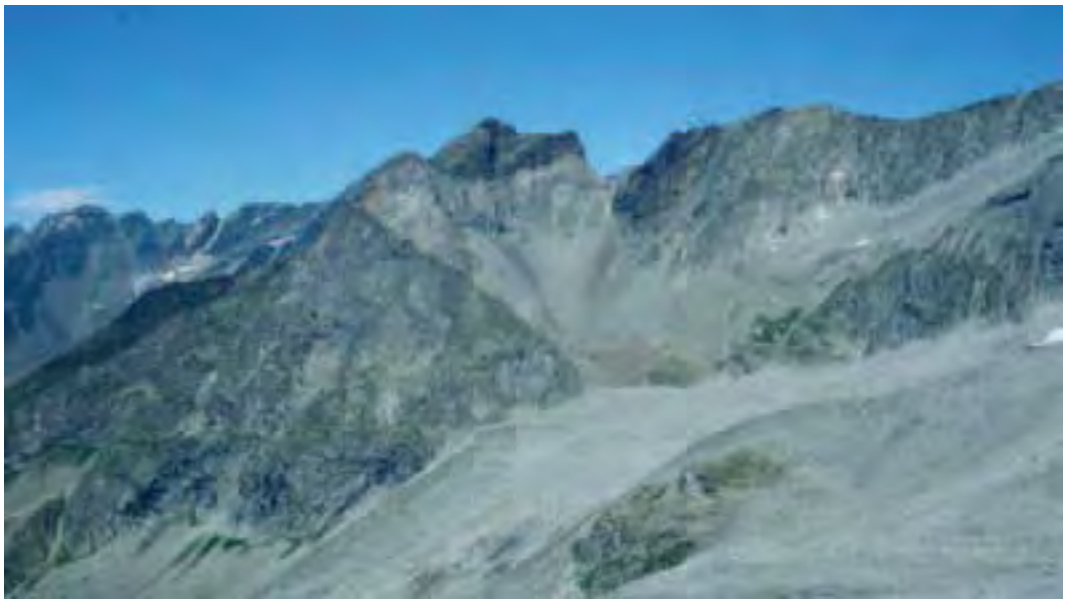

Figure 34 - Remnants of the pluton's roof (darker colour) on top of the Sprone delle Vedrette Giganti.

lower Val Sorgiva, country rocks at the immediate contact of the tonalite are often composed of fine-grained, biotite-bearing amphibolites, marbles and calc-silicate rocks. The latter contain garnet, epidote and clinopyroxene, and may develop a very coarse grain-size. As in the metapelitic mylonites, a strong deformation can be observed also in these rocks, with beautiful examples of boudinage in the amphibolite layers (Figure 33).

Boudinage of tonalite within the enclosing paragneisses points to a more competent behaviour of the tonalite, and hence to deformation in the solid state. This area records the largest strain of the entire pluton and it is characterised by sinistral shearing along a steep, E-W striking zone, displaying subhorizontal stretching lineations. Magmatic fabrics are entirely overprinted by greenschist facies deformation. However, melt-bearing shear bands are found locally, suggesting a continuous deformation from the magmatic to the solid state. Aspect ratios of enclaves of ~ 10:1 rapidly decrease to ~ 3:1 towards the pluton's interior (Wagner et al., in review).

Stop 5:

Path 8 to Rifugio Roma, c. 2400m a.s.l. A ten-metre-sized zone of mingling of coarse- and fine-grained tonalite at the northern contact.

Again, the country rocks at the contact are characterized by the presence of marbles and calc-silicate rocks. The coarse-grained tonalite contains some garnet here.

Stop 6:

Path 8 to Rifugio Roma, c. 2320 m asl. Sharp contacts between medium- to fine-grained tonalite and granodiorite.

Dikes of evolved granodiorite magma cut and disrupt the already crystallized tonalite (see Figure 16). The foliation is discordant to the wall of the dikes.

From the Rifugio, a panoramic view towards the eastern sector of the massif, with large remnants of the pluton's roof (Figure 34) on top of Sprone delle Vedrette Giganti (Riesernock). That is the only location where the divariant KNASH contact metamorphic assemblage Ms-Kfs-Qtz-Sil (or "second sillimanite" zone) has been observed in paragneisses, helping constrain the P-T conditions of contact metamorphism (Cesare, 1992, 1994a).

DAY 2

Rifugio Roma and surroundings.

Aplitic and lamprophyric dikes post-dating the main intrusion of Vedrette di Ries. Ice-polished outcrops at the front of the Monte Nevoso Glacier: intrusive contact between the tonalite and the metapelites of the Austroalpine basement; synintrusive deformation

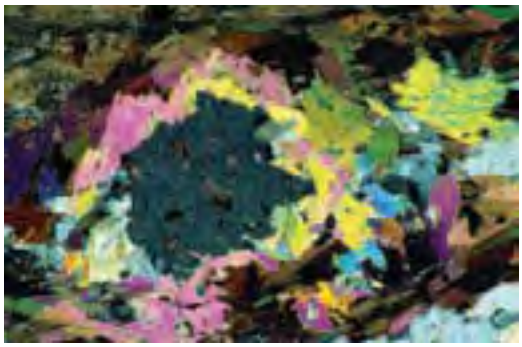

Figure 35 - Replacement of andalusite by coarse-grained, prograde muscovite. Sillimanite (fibrolite) is the stable Al_2SiO_5 polymorph, and occurs in the matrix around the nodular pseudomorph.

Figure 36 - The reaction of staurolite to hercynite accompanies the topotactic replacement of andalusite by sillimanite in the metapelites at Stop 2. Taken from Cesare (1994a).

and contact metamorphism of the country rocks; oligocene Grt-Ms-Tur-Ber-bearing pegmatites.

Stop 1:

Swarm of mafic, lamprophyric dikes with a general N-S direction. Sharp, brittle contacts, intrusion of thin lamprophyre apophyses along fracture zones, and presence of angular granodioritic xenoliths within the dikes testify for their late emplacement. Chilled margin and magmatic foliation are well developed in wider dikes (Figure 23). Subsequent intrusions along the same feeder are testified by network of less mafic veins (Figure 24) that eventually lead to the disruption of the already solidified mafic magma (Figure 25). Spherical to ameboid geodes of acicular amphibole in a medium grained matrix within the mafic dikes suggest a crystallization at high P_{H2O}.

Stop 2:

Ice-polished rocks at the base of the Tristenferner glacier, c. 1800 m south of Rifugio Roma, 2550 m a.s.l.. Here is one of the best exposures of the intrusive contact between underlying fine-grained tonalite and overlying metapelitic country rocks, thoroughly affected by contact metamorphism and synintrusive deformation. Rather than a sharp surface, the contact is an intrusion/interaction zone of some tens of metres in thickness, where several layer-parallel tonalite injections are observed. Overall, the contact is generally concordant with the country rocks' foliation, and dips c. 30° to the north. This area can be considered a part of the pluton's roof.

The country rocks are mostly migmatitic paragneisses (Hofmann et al., 1983) characterized by a Qtz-Pl-Ms-Bt-And-Sil-St-Spl-graphite assemblage. Although easily recognized in the hand specimen, staurolite and andalusite are metastable relicts of lower-grade contact metamorphism, and are transformed into

Figure 37 - Contact metamorphic prismatic sillimanite bent and wrapped by fibrolite-bearing foliation.

Figure 38 - Tourmaline and garnet in the pegmatites of likely Oligocene age.

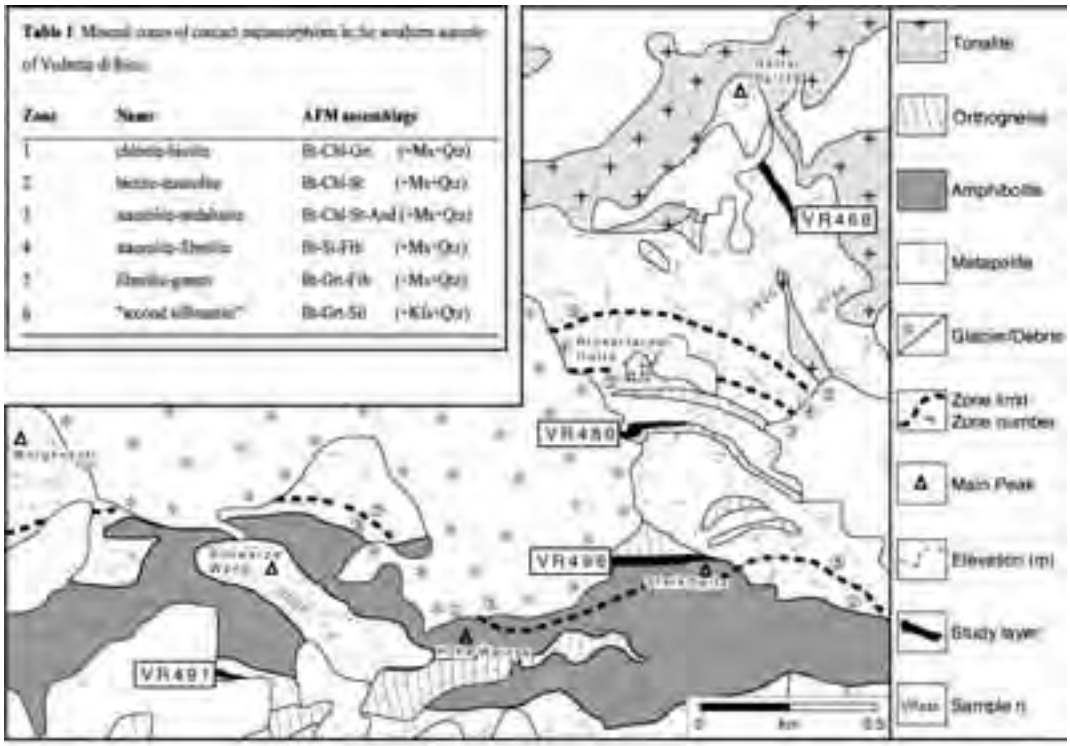

Figure 39 - Simplified geological map (after Mager, 1985) of the southern aureole of Vedrette di Ries, with location of the rock layers studied and respective sample numbers. Mineral zones as in Table 1 (inset).

nodular pseudomorphs consisting of coarse-grained muscovite (Figure 35), topotactic prismatic sillimanite and hercynite (Figure 36).

In the above microstructures, Cesare (1994a) has formulated the decomposition of staurolite to hercynitic spinel as:

$$Fe\text{-}St = 3.85Her + 5.1Sil + 2.55Qtz + 2H_2O$$

and has constrained the P-T conditions of contact metamorphism at 2.5-3.75 kbar and 585-655 °C.

Like in the upper Val Sorgiva, the well-developed foliation of the paragneisses is outlined by fibrolitic sillimanite. In addition, prismatic sillimanite appears to have been bent and wrapped by the foliation (Figure 37). Therefore, the foliation of the country rocks developed, or was reactivated, during the contact metamorphism.

The Vedrette di Ries pluton is typically poor inpegmatitic rocks. Among the few pegmatites which are likely to be related to the Vedrette di Ries intrusion are some meter-thick discordant dikes which occur in this outcrop. Although in this location one cannot observe the pegmatites which intrude the tonalites, the structural features suggest that these rocks post-date contact metamorphism. In fact, the pegmatites form a set of parallel injections at a high angle compared to the foliation of the host paragneisses. Along with quartz and feldspars, these pegmatites contain biotite, muscovite, garnet and tourmaline (Figure 38). Light green beryl has also been discovered here.

The fine-grained underlying tonalite is strongly oriented, with elongated microgranular enclaves. It also shows widespread cataclastic deformation and low-temperature alteration, with development of abundant chlorite and epidote.

This area is also particularly interesting for the observation of the geomorphological effects of the little ice age (1450-1850), such as huge lateral and terminal morains, ice-polished rocks and small glacial lakes. The glaciers of the Vedrette di Ries massif are undergoing a dramatic retreat (Santilli et al., 2002).

Afternoon: descent to Riva di Tures and trip to Anterselva.

Figure 40 - Hand specimen of a graphitic schist from lower Zone 3, with abundant coarse-grained andalusite porphyroblasts.

Figure 41 - Metapelitic schist from upper Zone 3. The light brown to orange nodules are polycrystalline aggregates of staurolite. See Figure 42 for a microscopic view of an aggregate from this rock.

DAY 3

Rifugio Forcella Valfredda (Rieserfernerhütte) and surroundings.

Contact metamorphism and related phenomena in the southern aureole of Vedrette di Ries. Profile of the outer, regionally metamorphosed (Variscan and Alpine) metapelites up to the intrusive contact; observation of the well-developed St-And-Sil zoneography; discussion of thermobarometric constraints to depth of emplacement. The Andalusite-bearing veins and their fluid inclusions: a marker of fluid-rock interactions during contact metamorphism.

Participants will walk along a S-N oriented profile covering the whole contact aureole up to the intrusive contact with the fine-grained tonalite. We are not dividing the day into stops, as there would be too many. However, we will refer to the maps provided herewith. Here follow the detailed descriptions of the two main objects of this part of the field trip: the contact metamorphism and its zoneography and the andalusite-bearing veins.

Contact Metamorphism at Vedrette di Ries

The area of Rifugio Forcella Valfredda is the ideal place to observe the effects of contact metamorphism induced by the tonalite of Vedrette di Ries. The southern aureole is mainly composed of metapelites, but orthogneisses, quartzites, amphibolites and marbles also occur. As previously stated, these rocks belong to the Austroalpine basement to the north of the DAV line, and have undergone a complex and polyphase metamorphic evolution before being affected by the Oligocene contact metamorphism. We will focus our attention on the effects of contact metamorphism on metapelitic lithologies.

The southern contact aureole of Vedrete di Ries has been divided into five mineralogical zones (Table 1, Figure 39, Cesare 1992) which developed at c. 3 kbar. In the metapelites, the most evident minerals of contact metamorphic origin are the abundant and very coarse andalusite (up to 10 cm in length, Figure 40), and the unusually fine-grained staurolite, which often occurs in polycrystalline nodules (Figure 41).

Another peculiarity of this area is that layers of a distinctive rock type crop out in at least four localities, at variable distance from the intrusive contact (Figure 39). These rocks allow for reconstruction of the multi-stage pseudomorphic replacement of a primary garnet: here follows a summary of the microstructural study and of the main conclusions outlined by Cesare (1999a, b), where further details and an updated reference list can be found. The layers have a thickness of < 20 m, and consist of fine-grained mica-schists with a marked millimetric compositional layering, with abundant quartz-rich ribbons, probably the result of mylonitic deformation. The foliation wraps around lensoid domains in which garnet, kyanite, staurolite, andalusite and muscovite are dominant in turns. The systematic distribution of Al_2SiO_5 polymorphs in the aureole, and the resulting isograd pattern (Figure 39), indicate that during the contact metamorphic event only the layer closest to the contact (i.e. sample VR466) reached temperatures sufficient for the crystallization of sillimanite. It follows that in all the other layers any occurrence of sillimanite is attributed

Volume n° 2 - from B16 to B33

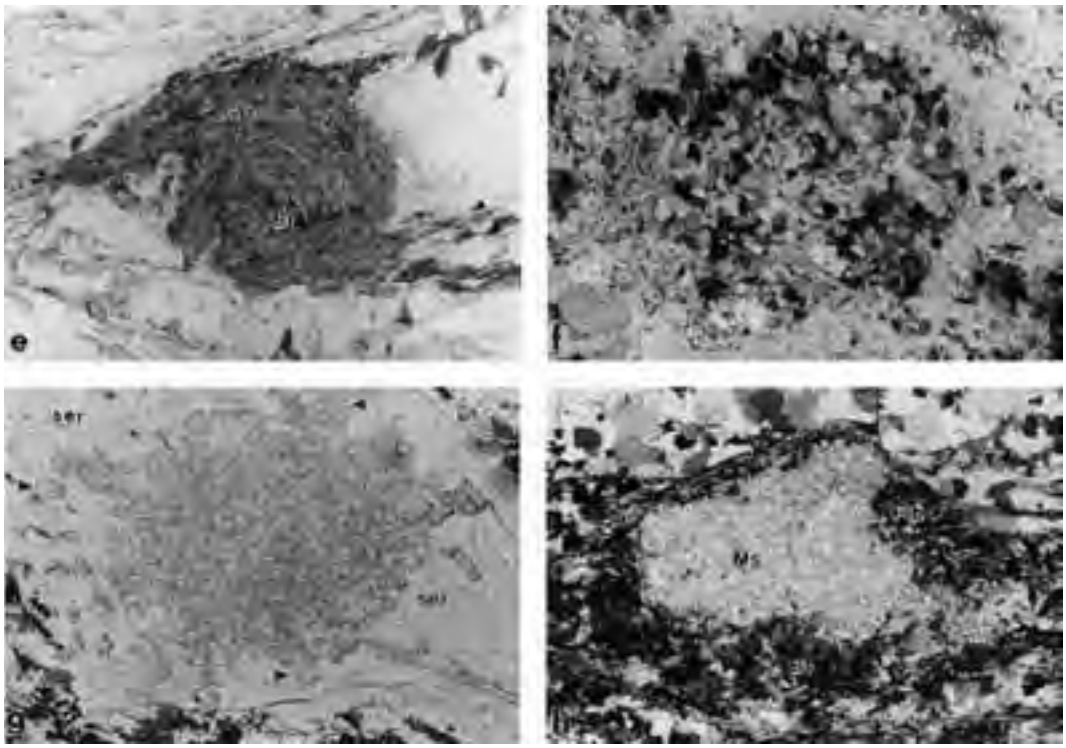

Figure 42 - Close-up views of nodules from each sample. e: VR491. Round aggregate of microgranular kyanite with minor biotite, ilmenite and garnet. Two kyanite-rich asymmetric tails (arrows) extend in the subhorizontal main foliation. Plane-polarized light (PL), width of view (wv)= 6.5 mm. f: VR496. Nodule of kyanite and staurolite. Kyanite occurs at the core of most staurolite crystals (stars). Crossed polars (CP), wv = 6.5 mm. g: VR480. Monomineralic nodule of staurolite in a sericite aggregate (ser). Note (arrows) the coarser grain-size of staurolite on the periphery of the aggregate, or isolated in the sericite matrix. Sericite around nodule (lower right) shows preferred orientation with incipient shear band cleavage. This suggests reactivation of the main foliation during contact metamorphism. PL, wv = 6.5 mm. h: VR466. Decussate monomineralic aggregate of muscovite wrapped by folia of biotite and fibrolite. PL, wv = 6.5 mm.

to earlier metamorphism. Both field appearance and microstructural characteristics suggest that these rocks, although showing different mineralogical composition at each locality, may represent the same primary rock type (the same folded layer?), variably transformed during the complex metamorphic evolution of this area.

Sample description

Four samples have been chosen as representative of the rock type at each location, and used for microstructural, bulk chemical, and mineral chemical analysis. See Figure 39 for their locations.

VR491: from Zone 1 (chlorite-biotite) of contact metamorphism. The sample furthest from the intrusive contact. It is a silvery, muscovite-rich schist, with abundant nodular aggregates of kyanite, typically <5mm in diametre. Garnet is present, either as isolated porphyroblasts, or associated with kyanite in the aggregates.

VR496: from the outer Zone 2 (andalusite-staurolite). Light gray, strongly layered but massive schist, rich in garnet porphyroblasts and nodules of fine-grained, brown sturolite. Staurolite often forms coronas around garnet. Andalusite crystals, up to 3 cm in length, occur in the muscovite-rich layers of the matrix.

VR480: from the inner Zone 2. A dark-brown rock, with orange-brown nodules composed of microgranular staurolite up to 1 cm in diametre. Coarse porphyroblasts of andalusite occur in the mica-rich layers that contain biotite, muscovite and staurolite. Quartz ribbons and rods may reach one cm in thickness.

VR466: from Zone 4 (sillimanite-garnet). The sample location is very close (approx 50 m) to the pluton. This massive rock is almost black, owing to the biotite-rich matrix that forms layers alternating with

quartz ribbons and fibrolite-rich folia. Pink andalusite porphyroblasts are abundant, whereas the scarce muscovite is mainly concentrated within mm-sized nodules.
Figure 42 compares the general textural appearance of the four samples at the thin section scale. The most striking similarities are the presence of nodular aggregates of comparable size, wrapped around by the matrix, and the occurrence of quartz-rich ribbons. In addition, all rock samples are graphitic, and contain tourmaline crystals with similar, complex zoning. A progressive grain-size coarsening of matrix phases (e.g. biotite and muscovite), aggregate phases (e.g. staurolite), as well as nodular aggregates themselves, can be observed, even in hand specimens, in the transition from sample VR491 to sample VR 466. This is consistent with the higher temperatures and the longer duration of contact metamorphism in the samples closer to the pluton.

A model for the evolution of a primary garnet site

The above microstructural information allow for reconstruction of the complex textural evolution of a primary garnet site, now represented by the nodules. Preservation of the subspherical shape of garnet was favoured by the very low strain experienced by these rocks after garnet crystallization, which resulted in the static growth of minerals in all the subsequent metamorphic events. The textural sequence can be divided into five (or six) stages:
The Garnet Stage (VR491, VR496) - This is the earliest microstructural stage, with garnet porphyroblasts of < 1 cm diameter wrapped by the micaceous layers. Inclusions in garnet consist of quartz, biotite, ilmenite and muscovite, and provide no information regarding the metamorphic history of the metapelite prior its crystallization.
The Fibrolite Stage (VR491, VR496) - Although there is no direct evidence for a stage where nodules were composed of fibrolite, several indications point to this occurrence. They include: i) the presence of fibrolite in close association with the nodules, formerly occupied by garnet; ii) the radiating arrangement of needles, diverging from the nodule; iii) the presence of biotite with exsolution of ilmenite and iv) the proposed crystallization sequence, in which fibrolite predates kyanite. These data are suggestive of the high-T reaction of garnet to fibrolite + Ti-rich biotite. Thermodynamic modelling of this reaction predicts a complex behaviour for garnet, which then may dissolve, grow or not react at all depending on the local configuration of the matrix. This is in agreement with the presence, in sample VR491, of untransformed garnet crystals adjacent to partially or completely pseudomorphed ones.
The Kyanite Stage (VR491, VR496) - This is represented by the nodules of microgranular kyanite which maintain their primary shape of garnet, but are not thought to have replaced it directly. The very fine grain-size of kyanite in the nodules is an anomalous feature for metapelites; this peculiarity, and its possible cause, is discussed below.
As it is not clear whether sericite pre-dates kyanite or is coeval with it, the possibility of a further stage pre-dating the Kyanite stage, and represented by sericite crystallization (the Sericite stage), has to be considered. Sericite would form "shimmer aggregates" upon replacing fibrolite, and leave relict needles within quartz and muscovite adjacent to nodules.
The Staurolite Stage (VR491, VR496, VR480) - This stage, initiated in sample VR491 and completed in sample VR480, produces the nodules of microgranular staurolite. Microstructures indicate that staurolite crystallization is coeval with that of andalusite, or that it commenced slightly before, and continued during, andalusite growth. As a consequence, the staurolite stage is related to the contact metamorphism.
The Muscovite Stage (VR466) - This is the final stage, in which decussate aggregates of muscovite replace staurolite. Although this kind of pseudomorph is common during retrograde metamorphism, even in this area, in this sample it has been shown to represent a prograde feature. Similar prograde pseudomorphs of muscovite after staurolite were first described by Guidotti (1968) in a regional metamorphic context.
The inferred age of the stages can be summarized as follows:

Stage	Age	Setting
Grt	Variscan	Regional
Fib	Variscan	Regional
Ser	Variscan? Eo-Alpine?	Regional
Ky	Eo-Alpine	Regional
St	Oligocene	Contact
Ms	Oligocene	Contact

Andalusite-bearing veins at Vedrette di Ries

Schists outcropping in the southern aureole of the Vedrette di Ries pluton contain several vein generations distinguished by their mineralogical composition. The following discussion considers only those veins which are discordant compared to the pervasive regional foliation, indicating that they

Volume n° 2 - from B16 to B33

Figure 43 - Andalusite-quartz vein at Site 1. The vein is very thin and discontinuous.

are younger than (or contemporaneous with) Alpine deformation. Among these are some andalusite-bearing veins, which occur up to 1 km from the tonalite. The veins are thin, parallel-sided, filled fractures, generally straight and in parallel sets (Figure 43). They are oriented at a high angle to the

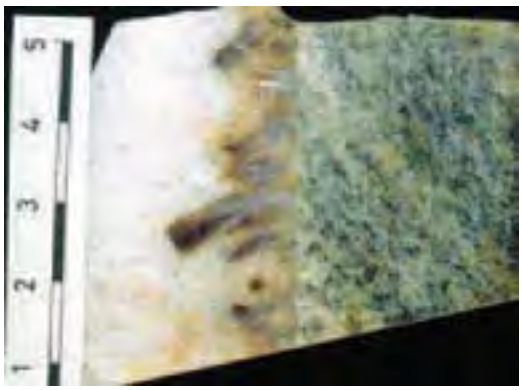

Figure 44 - Polished surface of an andalusite-quartz vein from Site 2, showing euhedral andalusite crystals which cluster at the straight vein wall; they exhibit concentric zoning with Fe-enriched darker areas. Base of photo: 5cm. From Cesare (1994b).

south-dipping foliation, and are not folded, implying that major ductile deformation did not affect the area during or after the vein formation.
The fine-grained pegmatitic structure and the euhedral shape of andalusite crystals (Figure 44) indicate crystallization within fluid-filled fissures.

Two sites with abundant veins in the area of Forcella Valfredda were chosen for further investigation (Figure 45). Site 1 is in the staurolite-andalusite zone, 800 m from the intrusion; Site 2, in the garnet-fibrolite

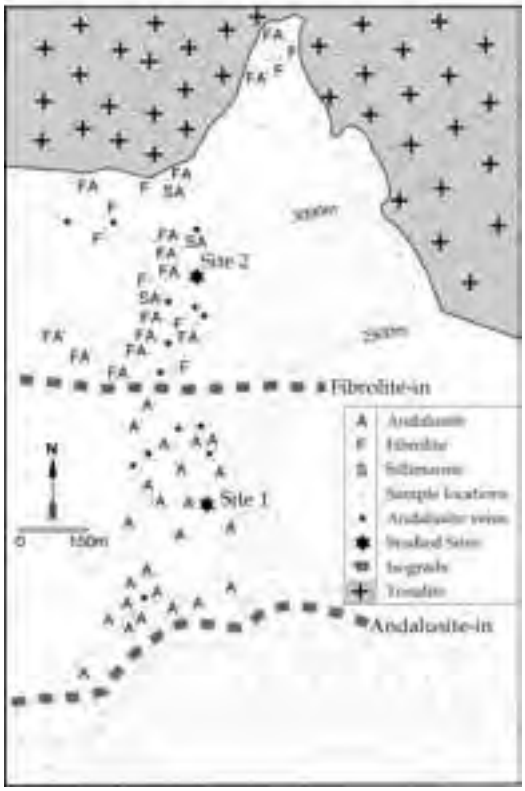

Figure 45 - Occurrences of andalusite-bearing veins and distribution of the Al_2SiO_5 polymorphs in the southern Vedrette di Ries aureole. After Cesare (1994b).

zone, is closer to the pluton. Figure 45 shows the distribution of the different Al_2SiO_5 polymorphs in the area, and the relationship between vein occurrence and andalusite presence within schists. Most of the vein occurrences reported in Figure 45 consist of single, thin veinlets. Therefore, the vein/host-rock volumetric ratio is extremely low.

At Site 1, host-rocks are pelitic hornfelses and schists containing quartz, plagioclase, andalusite, staurolite, biotite, ilmenite and graphite (± garnet ± chlorite). They preserve the older penetrative planar foliation dipping south and a well-developed E-W subhorizontal stretching lineation.
Andalusite veins are very thin, usually < 1cm and no longer than 1 metre. They contain quartz and andalusite in equal amounts, with variable biotite, and rare plagioclase and/or white mica. Biotite, which may reach up to 30%, is directly correlated to the abundance of garnet in the immediately adjacent host-rocks.

At Site 2, the country-rocks are pelitic hornfelses, composed of quartz, plagioclase, biotite, muscovite, acicular and prismatic sillimanite, garnet, ilmenite and graphite, with abundant relicts of andalusite.
Veins are larger and more abundant, and may in some cases reach a few metres in length and up to five cm in thickness.
Veins are discordant, their direction being quite random, but always very steep. There are two end-member types of andalusite-bearing pegmatitic veins at outcrop 2: biotite-absent, quartz-rich veins (the larger ones, Figure 44), and biotite-rich, quartz-poor veins. In the first type, euhedral andalusite crystals generally project from the vein walls into the quartz-rich inner zone as isolated prisms (up to 3 cm in length) or rosette aggregates. The second type occurs within garnet-bearing host-rocks; coarse-grained biotite is located at the vein walls, but also occurs in the central portion of the veins, alone or associated with andalusite.
The veins show a mineralogical zoning with andalusite and biotite abundant at the vein borders, whereas quartz is dominant at the centre.
All of the andalusite-bearing veins occur within those parts of the aureole in which andalusite crystallized during contact metamorphism (cf. Figure 45), and are always hosted by andalusite-bearing rocks. Where veins occur in non-pelitic lithologies (e.g., pegmatitic gneiss or quartzite), they do not contain andalusite or biotite. In the few cases where veins crosscut different lithologes, there is a different mineral assemblage in each part. The general relationships between the mineralogy of veins and that of host-rocks are outlined in Figure 46.

The orientation of veins can be consistently related

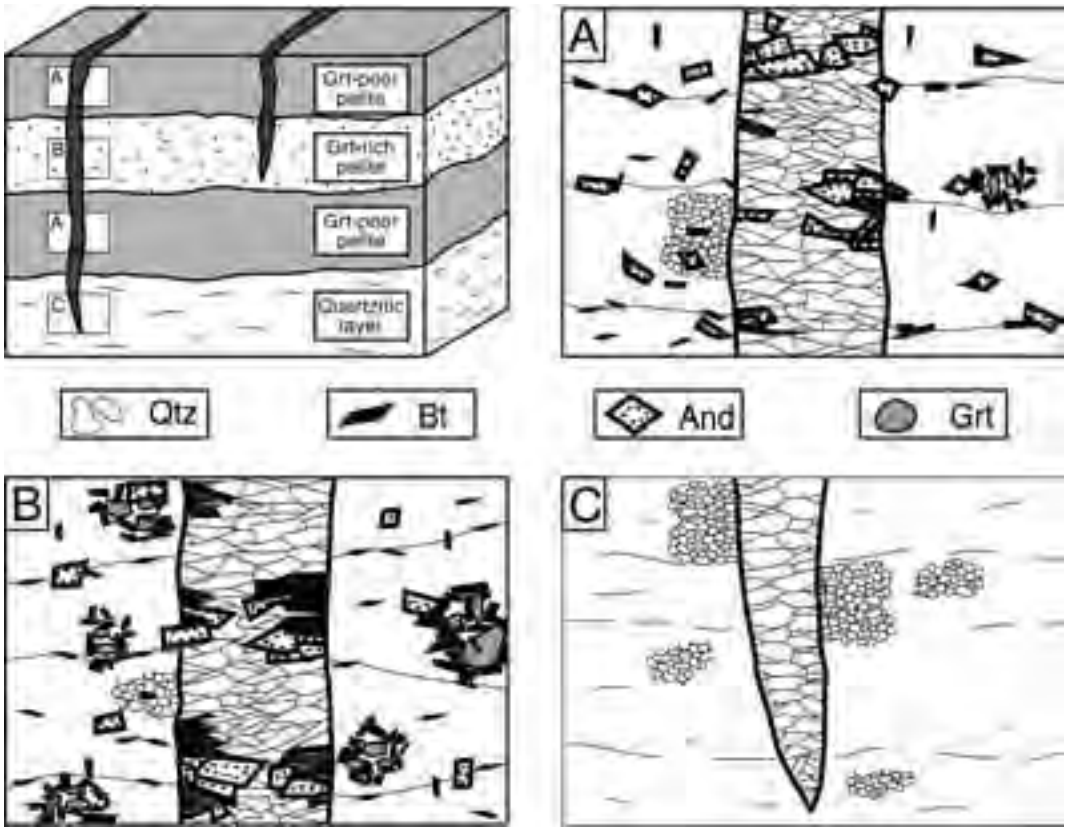

Figure 46 - Schematic diagram summarizing meso- and microstructural observations on the andalusite-bearing veins of the Vedrette di Ries aureole. Veins that formed in a layered rock (upper left) comprising metapelites and quartzite display a variable mineralogy, depending on the composition of the adjacent host-rock. A, B and C represent observed mineral composition and texture of veins in three end-member host-rock lithologies, respectively garnet-poor pelite, garnet-rich pelite, and quartzite. From Cesare (1994b).

Volume n° 2 - from B16 to B33

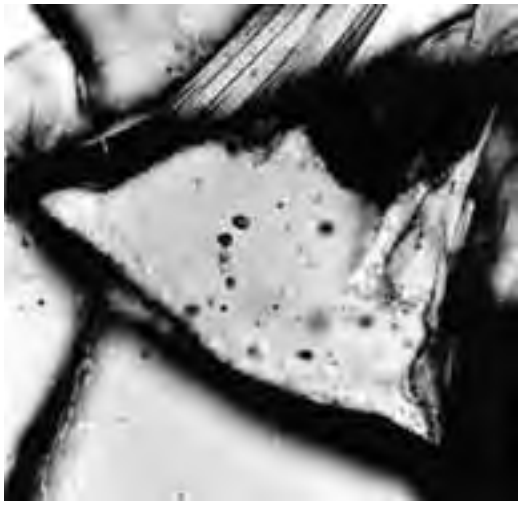

Figure 47 - Primary fluid inclusions in quartz crystals from within Andalusite-bearing veins.

to the stress field generated by the emplacement of the underlying tonalite, which gives a subvertical $\Uparrow_1$. In particular, the N-S vein directions at outcrop 1 are concordant with the marked elongation of the pluton, which defines the E-W direction of minimum principal stress in the schists.

The fluid inclusions within quartz of Andalusite-bearing veins (Figure 47) have been studied by Cesare and Hollister (1995).

Their results suggest that the fluids present during vein formation are those occurring in the isolated fluid inclusions defined as Type A. These are water-rich H_2O-CO_2-CH_4-NaCl mixtures, with low salinity and high CO_2/CH_4 ratio. The composition and density of these "primary" inclusions are consistent with a C-O-H fluid in equilibrium with graphite at the estimated P-T conditions of veining, and with a regime of lithostatic fluid pressure during crystallization of vein minerals. The low salinity of the aqueous fraction indicates that increased solubility in 'aggressive' fluids (e.g. Kerrick, 1990) is not required for effective aluminum transport. In the inclusions, density changes are variously recorded in each sample as a function of the degree of strain and of the relative abundance of quartz and andalusite.

Based on field, microstructural and fluid inclusion data, a mechanism of synmetamorphic veining (Cesare, 1994b; Cesare et al., 2001) is here summarized. It accounts for the processes of fracture opening, migration of matter, and precipitation of minerals during the formation of the Andalusite-bearing veins.

Vein Opening: Timing, Mechanisms, and Fluid Behaviour

Veins formed during the contact metamorphic event, before the crystallization of sillimanite. At that time the P-T conditions were within the stability field of andalusite (T = 500 ± 50 °C, Cesare, 1992), and schists were undergoing further heating. Furthermore, growth of andalusite in veins and host-rocks was coeval. Hence, mineral precipitation in veins was synmetamorphic: it was synchronous with metamorphic reactions taking place in the host-rock at the time of vein formation.

Hydraulic extension fracturing (hydrofracturing) requires elevated fluid pressures and low deviatoric stress, and generates fractures perpendicular to $\Uparrow_3$. It occurs when the fluid pressure (P_f), exceeds the sum of minimum stress ($\Uparrow_3$) and tensile strength of the rock ($\Downarrow_0$), according to the failure condition:

$$P_f \, B \Uparrow_3 + \Downarrow_0.$$

In the example studied, the hydrofracturing model is consistent with the orientation of veins compared to the stress field induced by the underlying tonalite. Since the typical features of shear fracturing are minimal, it can be concluded that the main mechanism of vein opening was hydrofracturing, caused by fluid release during devolatilization reactions. Decrease in modal chlorite and white mica, which is recorded proceeding upgrade within the andalusite zone of the aureole, is clear evidence that host-rock metapelites were undergoing dehydration during andalusite formation. Combining the above data with the textural observation of biotite pseudomorping garnet, the reaction

$$Grt + Chl + Ms = And + Bt + Qtz + H_2O \qquad (1)$$

can be proposed as one plausible dehydration reaction in the hornfelses capable of producing the vein mineral assemblage.

Opening of fissures in the rock generates a sudden increase in the volume available for the fluid phase, and a consequent drop in pore pressure. Fractures become a source for local pressure gradients which immediately drive fluids into the open cavities, filling them. However, to keep a vein open, fluid pressure in the vein must be equal to $\Uparrow_3$: after a rapid initial fluid flow toward the cavity, a condition of mechanical stability between fracture and host-rock will be attained and will inhibit pressure gradients and permanent flow. Frequent occurrences of isolated, thin, andalusite-bearing veins in the studied aureole, and the lack of interconnected vein networks are

additional observations against large-scale fluid circulation.

Mass transfer and mineral deposition

After the initial, transient flow, fluid can be considered as virtually stagnant, acting as a passive medium, in thermal and mechanical equilibrium with the surrounding rocks. Moreover, chemical equilibrium can also be assumed, given present theoretical models and the equal parageneses and mineral chemistry in vein and host-rock. It follows that crystallization of vein minerals was simply controlled by heterogeneous mineral reactions in the host-rock (e.g. reaction 1).

Nucleation of product phases (andalusite, biotite and quartz) is favoured on the strained minerals at vein walls; once nuclei form, concentration and chemical potential gradients between reactants and products are established, and the transfer of chemical components, continuously provided by dissolving reactants, is activated. This implies synchronous growth of andalusite in vein and host-rock. Mass transfer from adjacent host-rock to the vein occurs via intercrystalline diffusion, which can be very effective, and dominant during metamorphism. Since the fracture is filled with fluid that allows for faster diffusion, the growth of vein minerals is also faster and grain-size coarser; this explains the pegmatitic vein texture.

Because intergranular diffusion is the mass-transfer process during synmetamorphic veining, diffusion halos around veins can be expected. The plagioclase-rich border zones that sometimes occur at vein margins can be interpreted as diffusion halos. Conversely, such an explanation is not applicable to the biotite-rich zones, which are located within the veins, and cannot be interpreted as residual portions of metasomatically-depleted country rocks.

DAY 4

Anterselva (Antholz) valley - Passo Stalle (Staller Sattel) - Brunico (Bruneck).

Morning: descent to Anterselva. Outcrops of tonalite at Cima di Vila (Zinsnock): discussion of its geochemical and petrologic features (Bellieni, 1980; Bellieni et al. 1982) and of the genetic relationships with the Vedrette di Ries Pluton.

Afternoon: Drive to Passo Stalle (Staller Sattel) (2000 m asl): cross sections along the cataclasites and mylonites of the Defereggen-Anterselva-Valles (DAV) line from the pass to the Vedrette di Ries tonalite. Shear bands in greenschist facies rocks, indicating the sinistral kinematics of the DAV. High- and low-temperature deformation of the tonalite, and its relationships to the DAV mylonites. In this area the southern contact of the pluton dips steeply to the south, concordantly to the mylonites of the DAV. No kinematic indicators have been found within the tonalite, but preserved magmatic foliations parallel to the mylonitic foliation of the DAV call for syntectonic intrusion. This part of the pluton is inferred to be the feeder of the main body located further to the north. This conclusion is based on the occurrence of a steep magmatic foliation associated with steep lineations (Steenken et al., 2000; Wagner et al., in review). The location of the feeders of the intrusive bodies along segments of the Periadriatic Lineament is a common feature of the Periadriatic plutons.

Discussion of the emplacement mechanisms within the framework of the Oligocene tectonics of the Eastern Alps.

DAY 5

Return to Florence - End of Field Trip.

Acknowledgments

Financial support was received from CARG-PAB, the Province of Bolzano, from CNR-IGG, from the University of Padova and from DFG (Project Ha 2403/3-2). We wish to thank Gottfried Leitgeb (Rif. Forcella Valfredda), Arnold Seeber (Rif. Roma) and Maria Mair (Geltalalm) for their assistance during field work. The critical reading of Giuliano Bellieni is gratefully acknowledged.

References

Bassani S., Fioretti A.M., Bellieni G. (1997). Il granato nelle masse intrusive di Rensen, Vedrette di Ries e Polland (Alpi Orientali). *Plinius n.18*; 43-44.

Bellieni G. (1977). Caratteri geobarometrici delle intrusioni granitiche del plutone delle Vedrette di Ries (Rieserferner)(Alto Adige Orientale) alla luce dei sistemi sperimentali Q-Or-Ab-An-H2O. *Rend. Soc. It. Miner. Petr.*, 33, 631-645.

Bellieni G. (1978) Caratteri geochimici del massiccio granodioritico-tonalitico delle Vedrette di Ries (Rieserferner)-Alto Adige Orientale. *Rend. Soc. It. Miner. Petr.*, 34, 527-548.

Bellieni G. (1980) The Cima di Vila (Zinsnock) Massif: Geochemical features and comparisons with the Vedrette di Ries (Rieserferner) pluton (Eastern Alps-Italy). *Neu. Jb. Mineral. Abh.*,

138, 244-258.

Bellieni G., Comin Chiaramonti P., Visonà D. (1976). Contributo alla conoscenza del plutone delle Vedrette di Ries (Alpi Orientali). *Boll. Soc. Geol. It.*, 95, 351-370.

Bellieni G., Molin G.M., Visonà D. (1979) The petrogenetic significance of the garnets in the intrusive massifs of Bressanone and Vedrette di Ries (Eastern Alps-Italy). *Neu. Jb. Mineral. Abh.*, 136, 238-253.

Bellieni G., Peccerillo A., Poli G. (1981). The Vedrette di Ries (Rieserferner) Plutonic Complex: Petrological and Geochemical Data Bearing on Its Genesis. *Contrib. Mineral. Petrol.*, 78, 145-156.

Bellieni G., Peccerillo A., Poli G. (1982) REE distribution in the Cima di Vila (Zinsnock) granodioritic complex and its petrogenetic significance (Eastern Alps, Italy). *Neu. Jb. Mineral. Abh.*, 145, 50-65.

Bellieni G., Cavazzini G., Fioretti A.M., Peccerillo A., Poli G., Zantedeschi P. (1989). Petrology and geochemistry of microgranular mafic enclaves from the Vedrette di Ries plutonic complex (Eastern Alps). *Per. Mineral.*, 58, 1-3, 45-65.

Bellieni G., Justin Visentin E., Zanettin B. (1995). Use of the chemical TAS diagram (Totali Alkali Silica) for classification of plutonic rocks: problems and suggestions. Soc. It. Mineral. Petrol. *Plinius,* 14, 49-52.

Bianchi A. (1934). Studi petrografici sull'Alto Adige orientale e regioni limitrofe. Mem. Ist. Geol. R. Univ. Padova, 10; 243pp.

Bigi, G., A. Castellarin, M. Coli, G. V. Dal Piaz, M. Sartori, P. Scandone, and G. B. Vai (1990) Structural model of Italy, S.E.L.C.A., Florence (Italy).

Borsi S., Del Moro A., Sassi F.P., Zanferrari A., Zirpoli G. (1978). New geopetrologic and radiometric data on the alpine history of the austridic continental margin South of the Tauern Window (Eastern Alps). *Mem. Sci. Geol.*, 32, 17pp.

Borsi S., Del Moro A., Sassi F.P., Zirpoli G. (1973). Metamorphic evolution of the Austridic rocks to the south of the Tauern Window (Eastern Alps): radiometric and geopetrologic data. *Mem. Soc. Geol. It.*, 12, 549-571.

Borsi S., Del Moro A., Sassi F.P., Zirpoli G. (1979). On the age of the Vedrette di Ries (Rieserferner) massif and its geodynamic significance. *Geol. Rdsch*., 68, 41-60.

Cesare B. (1992). Metamorfismo di contatto di rocce pelitiche nell'aureola di Vedrette di Ries (Alpi Orientali, Italia). *Unp. PhD Thesis, Univ. Padova*, 106 pp.

Cesare B. (1994a). Hercynite as the product of staurolite decomposition in the contact aureole of Vedrette di Ries, eastern Alps, Italy. *Contributions to Mineralogy and Petrology*, 116, 239-246.

Cesare B. (1994b). Synmetamorphic veining: origin of andalusite-bearing veins in the Vedrette di Ries contact aureole, Eastern Alps, Italy. *Journal of Metamorphic Geology*, 12, 643-653.

Cesare B. (1999). Multi-Stage pseudomorphic replacement of garnet during polymetamorphism: Microstructures and their interpretation. *Journal of Metamorphic Geology*, 17, 723–73*4*

Cesare B. (1999). Multi-Stage pseudomorphic replacement of garnet during polymetamorphism: 2. algebraic analysis of mineral assemblages. *Journal of Metamorphic Geology*, 17, 735–746

Cesare B. and Hollister L.S. (1995). Andalusite-bearing veins at Vedrette di Ries (Eastern Alps - Italy): fluid phase composition based on fluid inclusions. *Journal of Metamorphic Geology*, 13, 687-700.

Cesare B., Poletti E., Boiron M-C. & Cathelineau M. (2001). Alpine metamorphism and veining in the Zentralgneis Complex of the SW Tauern Window: a model of fluid-rock interactions based on fluid inclusions. *Tectonophysics*, 336, 121-136

Cescutti C., Fioretti A.M., Bellieni G. & Cesare B. (2003). Studio petrografico e geochimico dei filoni porfirici acidi affioranti nel basamento austroalpino nei dintorni di Vedrette di Ries (Alto Adige Orientale). *GeoItalia 2003 Congress, Abstract* pg. 201

Chopin, C., Henry, C., and Michard, A. (1991) Geology and petrology of the coesite-bearing terrain, Dora-Maira Massif, western Alps. *Eur. J. Mineral*., 3, 263-291.

Dal Piaz, Gb., (1934). Studi geologici sull'Alto Adige orientale e regioni limitrofe. *Memorie Istituto di Geologia Regia Università di Padova*, 10, 242 pp.

Dal Piaz G.V., Von Raumer J., Sassi F.P., Zanettin B., Zanferrari A. (1975). Geological outline of the Italian Alps. Reprinted from "Geology of Italy" Coy Squyres Ed. The Earth Sciences Society of

the Libyan Arab Republic. Tripoli.

Dal Piaz G.V., Venturelli G., 1983. Brevi riflessioni sul magmatismo post-ofiolitico nel quadro dell'evoluzione spazio-temporale delle Alpi. *Memorie Società Geologica Italiana*, 26, 5-19.

Exner C.H., (1976). Die Geologische Position der Magmatite des periadriatischen Lineaments. *Verh. Geol.,* B 4:3-64.

Froitzheim, N., Schmid, S.M., and Fey, M. (1996) Mesozoic paleogeography and the timing of eclogite-facies metamorphism in the Alps : A working hypothesis. *Eclogae geol. Helv*., 89, 81-110.

Gatto G.O., Gregnanin A., Molin G.M., Piccirillo E.M., and Scolari A. (1976). Le manifestazioni Andesitiche polifasiche dell'Alto Adige occidentale nel quadro geodinamico alpino. *St. Trentin. Sc. Nat.,* 53, 21-47.

Guidotti C.V., (1968). Prograde muscovite pseudomorphs after staurolite in the Rangeley-Oquossoc areas, Maine. *American Mineralogist*, 53, 1368-1376.

Green T.H. (1972). Crystallization of calc-alkaline andesite under controlled high-pressure hydrous conditions. *Contrib. Mineral. Petrol*. 34, 150-166.

Green T.H., and Ringwood A.E. (1972). Crystallization of garnet-bearing rhyodacite under high-pressure hydrous conditions. *J. Geol. Soc. Aust.* 19, 203-212.

Hammerschmidt K. (1981). Isotopengeologische Untersuchungen am Augengneis vom Typ Campo Tures bei Rain in Taufers, Südtirol. *Mem. Sci. Geol*., 34, 273-300.

Hofmann K.H., Kleinschrodt R., Lippert R., Mager D. und Stöchkert B. (1983). Geologische Karte des Altkristallin südlich des Tauernfensters zwischen Pfunderer Tal und Tauferer Tal (Südtirol). *Der Schlern*, 57; 572-590.

Holdaway M.J. (1971). Stability of andalusite and the aluminum silicate phase diagram: *American Journal of Science*, 271, 97–131

Kagami H., Ulmer P., Hansmann W., Dietrich V., and Steiger R.H. (1991). Nd-Sr isotopic and geochemical characteristics of the Southern Adamello (northern Italy) intrusives: implication for crustal versus mantle origin. *J. Geophys. Res.* 96, 14331-14346.

Kerrick D.M. (1990). The Al_2SiO_5 polymorphs. *Reviews in Mineralogy*, **22**.

Kleinschrodt R. (1987). Quarzkorngefügeanalyse im Altkristallin südlich des westlichen Tauernfensters (Südtirol/Italien). *Erlanger Geol. Abh.*, 114, 1-82.

Kozur, H. (1991) The evolution of the Meliata-Halstatt ocean and its significance for the early evolution of the Eastern Alps and Western Carpathians. P*aleogeogr. Paleoclimatol. Paleoecol.* 87, 109-135.

Laubscher H.P. (1985). The late Alpine (Periadriatic) intrusions and the Insubric Line. *Mem. Soc. Geol. It.*, 26, 21-30.

Mager D. (1985). Geologische Karte des Rieserfernergruppe zwischen Magerstein und Windschar (Südtirol). *Der Schlern*, 6, Bozen

Mancktelow N.S., Stöckli D.F., Grollimund B., Müller W., Fügenschuh B., Viola G., Seward D. and Villa I.M. (2001). The DAV and Periadriatic fault systems in the eastern Alps south of the tauern Window. *Int. J. Earth Sci*., 90, 593-622.

Mann A. and Scheuvens D. (1998). Structural investigation of the northern contact of the Rieserferner Plutonic Complex (Eastern Alps) - first results. *Terra Nostra*, 98, 62.

Müller W., Mancktelow N.S. and Meier M. (2000). Rb-Sr microchrons of synkinematic mica in mylonites: an example from the DAV fault of the Eastern Alps. *Earth and Planetary Science Letters,* 180, 385-397

Müller W., Prosser G., Mancktelow N.S., Villa I.M., Kelley S.P., Viola G., and Oberli F. (2001). Geochronological constraints on the evolution of the Periadriatic fault system (Alps). *Int. J. Earth Sci.*, 90, 623-653.

Neubauer, F. (1994) Kontinentkollision in den Ostalpen. *Geowissenschaften* 12, 136-140.

Pattison, D.R.M. & Tracy, R.J., 1991: Phase equilibria and thermobarometry of metapelites. In: Kerrick, D.M. (ed.): *Contact metamorphism*. Reviews in Mineralogy, **26**; 43-104

Prochaska W. (1981). Einige Gangesteine der Rieserfernerintrusion mit neuen radiometrischen Altersdaten. *Mitteilungen der Gesellschaft der geologie und Berbaustudent, Wien*, 27, 161-171.

Rosenberg, C.L., A. Berger, and S. M. Schmid (1995) Observations from the floor of a granitoid pluton; inferences on the driving force of final emplacement, *Geology,* 23, 443-446.

Rosenberg, C. L., in press, Shear zones and magma ascent: A model based on a review of the Tertiary magmatism in the Alps. *Tectonics.*

Sassi, F.P. & Zanettin, B. (1980) Schema degli eventi

Volume n° 2 - from B16 to B33

metamorfici e magmatici nelle Alpi Orientali. *Rendiconti Società Italiana di Mineralogia e Petrologia*, 36; 3-7.

Santilli M., Orombelli G. and Pelfini M. (2002). Variations of Italian glaciers between 1980 and 1999 inferred by the data supplied by the Italian Glaciological Committee. *Geogr. Fis. Dinam. Quat.* 25, 61-76.

Schulz B. (1989). Jungalpidische Gefügeentwicklung entlang der Defereggen-Antholz-Vals-Linie (Osttirol, Österreich). *Jahrbuch. Geol. Bundesanst.*, 132; 775-789.

Schulz B. (1997). Pre-Alpine tectonometamorphic evolution in the Austroalpine basement to the south of the central Tauern Window. *Schweizerische Mineralogische Petrographische Mitteilungen*, 77, 281-297.

Steenken A., Siegesmund, S. and Heinrichs, T. (2000). The emplacement of the Rieserferner Pluton: Constraints from from field observations, magnetic fabrics and microstructures. *Journal of Structural Geology*, 22, 1855-1873

Steenken A. (2002). The emplacement of the Rieserferner Pluton and its relation to the DAV-Line as well as to the kinematic and thermal history of the Austroalpine basement (Eastern Alps, Tyrol) *Geotektonische Forschungen*, 94, 120 pp.

Steenken A, Siegesmund S, Heinrichs T, Fugenschuh B (2002). Cooling and exhumation of the Rieserferner Pluton (Eastern Alps, Italy/ Austria). *Int. J. Earth Sci*., 91, 799-817.

Stöckhert B. (1984). K-Ar determinations on muscovites and phengites from deformed pegmatites, and the minimum age of the Old Alpine deformation in the Austridic basement to the south of the western Tauern Window (Ahrn valley, Southern Tyrol, Eastern Alps). *Neu. Jb. Mineral. Abh*., 150, 103-120.

Stöckhert B. (1985). Pre-Alpine history of the Austridic basement to the south of the western Tauern Window (Southern Tyrol, Italy). Caledonian versus Hercynian event. *Neu. Jb. Geol. Paläont. Mh.,* 618-642.

Stöckhert B. (1987). Das Uttenheimer Pegmatit-Feld (Ostalpines Altkristallin, Südtirol) Genese und alpine Überprägung. *Erlanger Geol.Abh*., 114, 83-106.

Trommsdorff V. and Nievergelt P., (1983) The Bregaglia (Bergell) Iorio Intrusive and its field relations. *Mem. Soc. Geol. It.,* 26, 55-68.

Von Blankenburg F. and Davis J.H. (1995). Slab breakoff: A model for syncollisional magmatism and tectonics in the Alps. *Tectonics* 14, 120-131.

Wagner R., C. L. Rosenberg, M.R. Handy, C. (2003). *Memorie di Scienze Geologiche (Padova), 54,*

Wagner R., C. Rosenberg L., Handy M.R., Möbus C., and Albertz M. in review, Buoyancy-driven inflation of a mid-crustal sill fed by a transpressive shear zone: The Rieserferner Pluton, Eastern Alps. *Geol. Soc. Am. Bull.*

Back Cover:

Road map of the area NE of Brunico. Numbers in yellow dots indicate the localities of each field trip's day as in the Guide.

32nd INTERNATIONAL GEOLOGICAL CONGRESS

FIELD TRIP MAP

Edited by APAT

Volume n° 2 - from B16 to B33

32nd INTERNATIONAL GEOLOGICAL CONGRESS

SKARN DEPOSITS IN SOUTHERNTUSCANY AND ELBA ISLAND (CENTRAL ITALY)

Leader: M. Benvenuti

Associate Leaders: M. Boni, L. Meinert

Pre-Congress **B18**

Field Trip Guide Book - B18

Florence - Italy
August 20-28, 2004

The scientific content of this guide is under the total responsibility of the Authors

Published by:
APAT – Italian Agency for the Environmental Protection and Technical Services - Via Vitaliano Brancati, 48 - 00144 Roma - Italy

Series Editors:
Luca Guerrieri, Irene Rischia and Leonello Serva (APAT, Roma)

English Desk-copy Editors:
Paul Mazza (Università di Firenze), Jessica Ann Thonn (Università di Firenze), Nathalie Marléne Adams (Università di Firenze), Miriam Friedman (Università di Firenze), Kate Eadie (Freelance indipendent professional)

Field Trip Committee:
Leonello Serva (APAT, Roma), Alessandro Michetti (Università dell'Insubria, Como), Giulio Pavia (Università di Torino), Raffaele Pignone (Servizio Geologico Regione Emilia-Romagna, Bologna) and Riccardo Polino (CNR, Torino)

Acknowledgments:
The 32nd IGC Organizing Committee is grateful to Roberto Pompili and Elisa Brustia (APAT, Roma) for their collaboration in editing.

Graphic project:
Full snc - Firenze

Layout and press:
Lito Terrazzi srl - Firenze

Volume n° 2 - from B16 to B33

32nd INTERNATIONAL GEOLOGICAL CONGRESS

SKARN DEPOSITS IN SOUTHERN TUSCANY AND ELBA ISLAND (CENTRAL ITALY)

AUTHORS:
***M. Benvenuti** (Università di Firenze - Italy)*
***M. Boni** (Università "Federico II" di Napoli - Italy),*
***L. Meinert** (Washington State University - USA)*

Florence - Italy
August 20-28, 2004

Pre-Congress

B18

Front Cover:
Historic site of Rocca San Silvestro in the Campiglia Marittima mining district

Leader: M. Benvenuti
Associate Leader: M. Boni, L. Meinert

Introduction

Aim and Localities of the Field Trip

IGC field trip B18 will investigate the classic skarn localities of Tuscany and the Island of Elba. Tuscany includes several different skarn types but the most famous, and the ones that we will visit on this field trip, are the Fe and Zn skarns at Isola d'Elba and in the Campiglia Marittima district. These are of historical, mineralogical, and economic importance. The field trip will start with a general overview at the historic site of the Etruscan town of Populonia. Following this, we will travel by ferry to the Island of Elba to examine the Fe-skarns at several localities. The second day we will focus on the classically zoned Zn-skarn system around Campiglia. The trip will conclude with a visit to the archeometallurgically interesting beach slags at the Baratti Gulf.

Figure 1 - Itinerary of the field trip.

Volume n° 2 - from B16 to B33

Regional setting

Geology and geodynamics

The two areas which will be visited during our field trip (i.e., Elba Island and the Campiglia Marittima district: **Fig. 1**) belong to the Northern Apennines chain (**Fig. 2**). The Northern Apennines chain is mainly composed of a pile of NE-verging tectonic units, accompanied by second-order back-thrusts (Finetti et al., 2001). As schematically shown in **Fig. 3**, the uppermost are the Ligurian Units (or Ligurides), originally deposited in an oceanic realm (i.e. the Ligurian–Piedmontese sector of the Alpine Tethyan ocean). The Ligurian units, consisting of ophiolites with their Jurassic to Eocene sedimentary cover, tectonically overlie the Tuscan and Umbria–Marche units, originally deposited on the passive margin of the Adria Plate since the middle Triassic. The Tuscan and Umbria–Marche units consist of an upper 2000–3000 m-thick succession of Oligocene–Miocene age, formed by siliciclastic foredeep sediments, and a lower succession of Mesozoic–Cenozoic age, mainly composed of carbonate rocks. Both successions rest on about 1000–1500 m-thick Triassic evaporites (Burano Fm.), grading to dolomites in the Adriatic Sea area. The base of the thick evaporitic layer is a very important detachment plane for thrusting and gravity sliding. Due to time–space outward migration of the thrust front, Oligocene–Miocene tectonostratigraphic units deposited in the foredeep system, become progressively younger eastward.

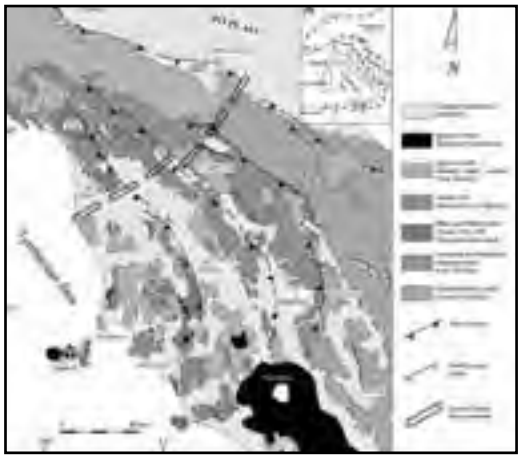

Figure 2 - Geological sketch-map of the northern Apennines (modified from Bonini et al., 2001).

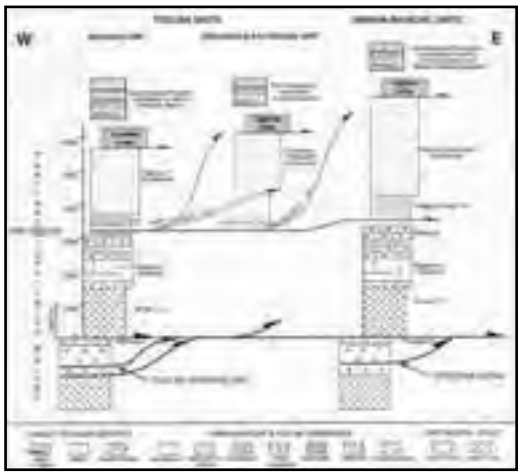

Figure 3 - Schematic stratigraphic columns of the Tuscan and Umbria-Marche units (from Finetti et al., 2001)

Neogene-Quaternary Magmatism

During the post-collisional phase of the Apenninic orogeny (from Late Miocene to Pleistocene), a large variety of magmatic bodies were emplaced at different crustal levels in the Northern Apennines hinterland (mainly in southern Tuscany). Volcanic to intrusive bodies were emplaced in the time span of 8 to 0.2 Ma, showing a trend of decreasing ages from west to east (Civetta et al., 1978; Ferrara and Tonarini, 1985; Peccerillo et al., 1987). They include crustal anatectic acid peraluminous rhyolites and granites, and a wide range of mafic to intermediate rocks such as lam-

Figure 4 - Location and age of magmatic rocks of the Tuscany Magmatic Province (Peccerillo et al., 2001)

proites, high-potassium calcalkaline and shoshonitic rocks (**Fig. 4**). Rock compositions straddle the I and S fields of Chappel and White (1974), the most basic rocks being mainly I-type and the high-silica ones S-type (Peccerillo et al., 2001, and references therein). Most of the acid rocks appear to have undergone mixing and mingling with various types of mantle-derived calcalkaline to potassic melts (Poli, 1992). Mafic rocks, in fact, are commonly found as micro-granular enclaves and veins in most acid extrusive and intrusive bodies of the Tuscan Province. Several geochemical and petrological features, further suggest a heterogeneous mantle source for the mafic melts (Peccerillo, 1999). According to Peccerillo et al. (2001) the overall petrogenetic history for the Tuscan Province can be described in three main steps: 1) subduction-related metasomatism of upper mantle (both asthenospheric and lithospheric) by interaction with upper crustal material; 2) variable degrees of partial melting of heterogeneous mantle due to asthenospheric uprise, and formation of various types of magmas; 3) injection of mafic magmas into the continental crust, uprise of isotherms, onset of crustal anatexis, and acid-mafic magma mingling.

Ore Geology

For about 30 centuries, Tuscany has been one of the most important mining regions of Italy producing a large variety of resources, including pyrite, iron, base metals, geothermal steam and several industrial minerals and rocks (Lattanzi et al. 1994, and references therein). Today the mining industry in Tuscany is limited to industrial minerals (feldspars, halite), ornamental stones, and building materials. The Tuscan metallogenic province includes (**Figs. 5 and 6**): the Fe oxides deposits of Elba Island, the pyrite (± barite ± Fe oxides) deposits of southern Tuscany and Apuane Alps, the base-and precious-metals deposits of the "Colline Metallifere" district (southern Tuscany), the Hg deposits of the Monte Amiata area, the Sb deposits of the Capalbio-Monti Romani belt (cf. Cipriani, Tanelli, 1983; Tanelli, 1983). The newest addition to the metallogenic framework of Tuscany, is the discovery in the mid '80s of "Carlin-type" epithermal gold mineralization. Most of the Au prospects, of limited economic importance, are closely related to Sb deposits (Tanelli et al., 1991; Lattanzi, 1999).

A number of different skarn deposits occur in the southwestern portion of the Tuscan metallogenic province (**Fig. 7**): they include calcic iron skarns (Capo Calamita, Ginevro, Sassi Neri and Ortano at Elba Island; Niccioleta in the Colline Metallifere district) and lead-zinc(-copper) skarns (Temperino mine in the Campiglia M.ma district; Serrabottini near Massa Marittima). These deposits have been studied by Bartholomé, Evrard, 1970; Corsini et al., 1980; Dimanche, 1971; Tanelli, 1977; Lattanzi, Tanelli, 1985; Del Tredici (1990), Torrini (1990) and Dünkel (2002). According to Tanelli (1977) the Tuscan skarn deposits formed by replacement of Triassic

Figure 5 - The main mining districts of Tuscany (modified after Tanelli, 1983)

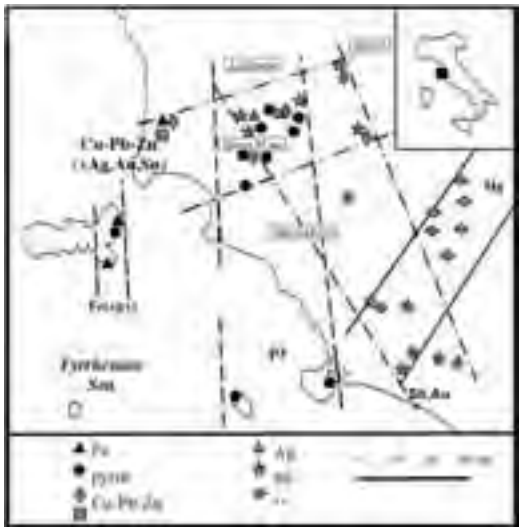

Figure 6 - Distribution of main ore types of southern Tuscany

Figure 7 - Location of Tuscan skarn deposits (after Tanelli, 1977)

carbonate rocks of the Tuscan Unit by metasomatic processes triggered by the emplacement at shallow crustal levels of the Neogene magmatic rocks of the Tuscan Province. Skarn bodies may be in contact with magmatic rocks (e.g., at Temperino mine), or at various distances (Niccioleta, Ortano). The presence of magmatic rocks in close proximity to skarn bodies does not necessarily imply a genetic link: at Ginevro, for instance aplitic dikes appear to predate skarn formation (*cf.* Dimanche, 1971). Source(s) of elements for Tuscan skarn deposits are still poorly constrained. Corsini et al. (1980) maintain that isotopic composition of sulfur from the Temperino skarn deposit is compatible with a local, non magmatic source (i.e., sulfides/sulfates from Permo-Triassic country rocks). On the other hand, the uniform lead isotope composition of pyrite and galena from the Campiglia Marittima and Niccioleta deposits may reflect contribution of lead (and other metals?) from Neogene-Quaternary magmatic rocks (Lattanzi et al., 1991).

Elba Island

The geologic framework

Due to its location midway between Corsica and the Northern Apennines, Elba Island is a key element for the reconstruction of the tectono-stratigraphic evolution of the Apenninic chain after the opening of the Tyrrhenian basin. Other elements of interest are the presence of an extensive Mio-Pliocene magmatism, with attendant swarms of aplitic and pegmatitic dikes, as well as the occurrence of the world-famous iron ore deposits. Elba Island's long-living geologic history starts in the Palaeozoic, but its Alpine tectonic evolution begins in the Late Cretaceous - Early Tertiary with the consumption of the western Tethyan ocean (Ligurian-Piedmontese Basin). After the Upper Eocene-Lower Miocene collision and polyphase deformation of the European (Corsica) and Adriatic (Tuscany Domain) margins, in the Late Miocene-Pliocene/? Quaternary syn- and post-magmatic extensional events took place (Bortolotti et al., 2001).

The tectonic frame of central and eastern Elba Island is made up by the following nine major tectonic units (from the geometrically lowermost upwards):

(1) Porto Azzurro Unit; (2) Ortano Unit and (3) Acquadolce Unit; (4) Monticiano-Roccastrada Unit, (5) Tuscan Nappe Unit and (6) Gràssera Unit; (7) Ophiolitic Unit with seven subunits; (8) Paleogene Flysch Unit and (9) Cretaceous Flysch Unit (Bortolotti et al., 2001 and references therein).

In eastern Elba the units of this tectonic pile are characterised by a general top to east vergence, and are separated each other by roughly NS verging overthrust surfaces. The various units, originally deposited in quite different palaeogeographic domains, were deformed and piled up into their present position during the compressional stage of the Apenninic orogeny, and later affected by an important extensional phase. This stage was also accompanied by the emplacement of several magmatic intrusions at shallow crustal levels (cf. Dini et al. 2002; Maineri et al., 2003, and references therein): the Monte Capanne pluton (6.9 Ma), the monzogranitic stock of Porto Azzurro (6.2-5.0 Ma), several swarms of aplitic and pegmatitic dikes (the latter almost exclusively found associated with the Monte Capanne pluton), and a laccolith complex made of subvolcanic porphyritic rocks (>8.5-6.85 Ma). Dini et al. (2002) suggest that the emplacement of the Monte Capanne pluton triggered the movement of an important extensional detachment fault (Elba Central Fault), which controlled the eastward translation of about 10 km of upper plate rocks (including Complex V with intruded laccolith complex) from their original position on the top of Monte Capanne pluton.

The Elba Central Fault caused intense fluid circulation and resulting pervasive hydrothermal alteration of porphyritic aplites and formation of the "eurites" (sericite replacing primary albite and K-feldspars) exploited at La Crocetta and Marciana mines (Maineri et al., 2003). At 6.2-5.0 Ma, the emplacement of the Porto Azzurro stock caused deactivation of the

Elba Central Fault, although additional eastwards tectonic translations took place along another major low-angle fault, the Zuccale fault (Pertusati et al., 1993). The emplacement of the Porto Azzurro pluton caused also a strong thermometamorphic imprint on the geometrically lowermost Units of the Elba structural edifice (namely, the Porto Azzurro, Ortano and Acquadolce Units). Crosscutting relationships between the Zuccale fault and aplitic dikes indicate that the detachment postdated, at least partially, the emplacement of the magmatic dikes. The last tectonic stage at Elba Island is mainly represented by N-S trending high-angle extensional faults, affecting the entire N-Tyrrhenian basin. This last episode ended before about 3.5 Ma (Keller and Pialli, 1990).

Geology, mineralogy and textures of Elba iron deposits

Iron ores from Elba Island have been mined without interruption for almost three millennia, since the early Etruscan mine workings (early 1st Millennium BC: Corretti and Benvenuti, 2001) up to about twenty years ago (1981, closure of the Ginevro mine). At least 60 million tons of Fe ore have been extracted from Elba deposits from ancient times to the present (data from Fabri, 1887; Pullè, 1921). To preserve this long mining tradition a "Mining and Mineralogical Park" has been recently established in eastern Elba (cf. Tanelli and Benvenuti, 1999).

As shown in **Figure 8**, the Fe deposits of Elba Island are restricted to a relatively narrow belt extending NS along the eastern coast of Elba Island, from Monte Calendozio (Rio Albano mine) to the Calamita promontory. The ore bodies range from stratiform to pod-like or vein-type, although the first appears to be dominant (Zuffardi, 1990). Stratiform Fe bodies are predominantly hosted by Palaeozoic-Triassic formations belonging to the Tuscan domain. Many Fe ores are associated with faults (Debenedetti, 1952; Gillieron, 1959): a first set of thrust faults, striking NS and dipping 30°-45° W, corresponding to the thrust surfaces among the various tectonic units, and two sets of normal, high-angle faults, one striking NS and dipping 30°-60° E, the other one with strike NE-SW and dips of 45°-70° to NW or SE.

As reviewed by Tanelli and Lattanzi (1986) there is disagreement in the literature about whether all of the Fe deposits are genetically associated with late-Apenninic granitic stocks or whether in some cases the intrusions simply metamorphosed and partly

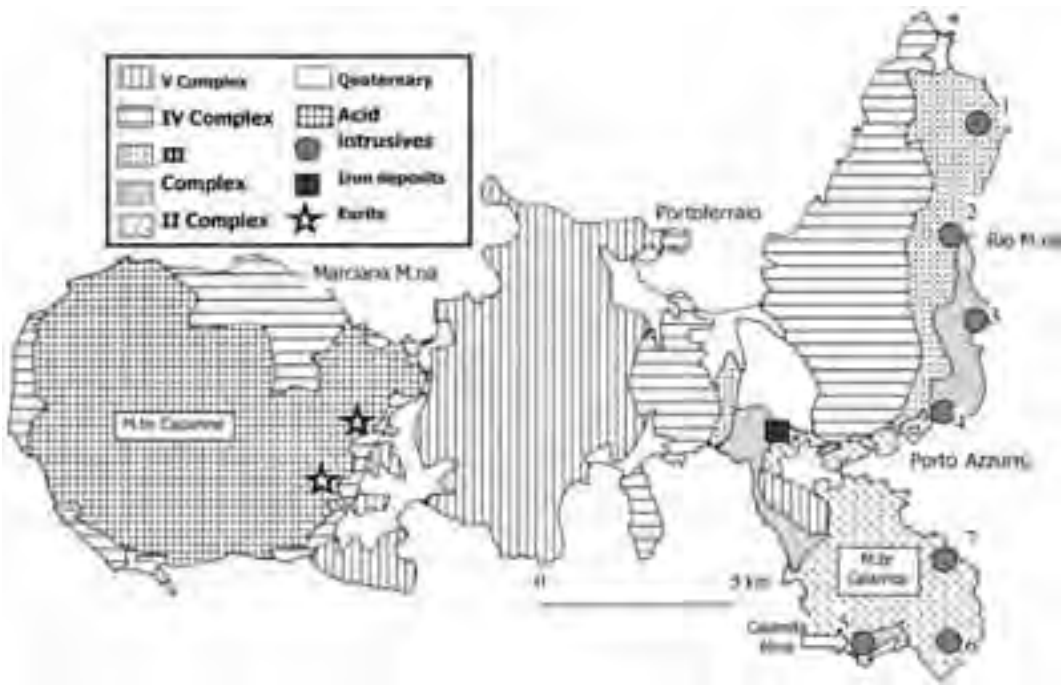

Figure 8 - Location of main iron deposits of Elba Island. Legend: 1) Rio Albano; 2) Rio Marina; 3) Ortano; 4) Terranera; 5) Calamita; 6) Ginevro; 7) Sassi Neri.

remobilised the iron ores that were formed, or at least pre-concentrated, in sedimentary and/or hydrothermal sedimentary environments of Triassic and/or Palaeozoic age (stage *ii* of Lattanzi et al., 1994).

Moving from Rio Marina towards the Calamita Peninsula, the association of iron ores with skarn bodies and/or aplitic dikes becomes more and more distinct. Even at Rio Marina skarn bodies were encountered at depth. Drilling and limited underground workings in the 1950s revealed the existence of hematite-pyrite skarn bodies replacing wedge-shaped carbonatic masses (the Vigneria limestones of Gillieron, 1959), which are now interpreted as tectonic slices of the overlying Jurassic to Oligocene carbonatic formation of the Monticiano-Roccastrada Unit (Bortolotti et al., 2001). Immediately south of Rio Marina town, very large skarn bodies with hedenbergite-ilvaite-epidote ± quartz, chlorite, magnetite, pyrite and pyrrhotite extend along the coast (Torre di Rio skarns, **Fig. 9**). Skarn minerals occur along schistosity planes of the Acquadolce calc-schists, as reported in detail by Lotti (1886, pp. 205-206). Moving southwards, other skarn bodies occur at Ortano, Porticciolo, Tignitoio and Capo d'Arco. The Ortano deposit shows a different ore mineralogy (pyrite, pyrrhotite ± hematite, magnetite), associated with pyroxene-epidote-ilvaite skarn bodies, which replace marbles and calcareous phyllites along a cataclastic horizon separating the Acquadolce Unit from the overlying Ortano Unit. Lenses of hematite + pyrite ± magnetite occur at Terranera within the Monticiano – Roccastrada Unit, and are in close proximity to skarn bodies cropping out at the nearby Punta delle Cannelle. The iron mineralization appears to be coeval and cogenetic with skarn development, based upon a 7.3 ± 0.4 Ma radiometric age of one hematite sample (Lippolt et al., 1995).

Fe ores and skarns of southeastern Elba Island are associated with aplitic dikes linked to the Porto Azzurro pluton. This association is particularly evident in the Calamita Peninsula (see **Fig. 8**), where several skarn-bearing iron deposits (Capo Calamita, Ginevro **(Fig. 9a)**, Sassi Neri, Stagnone) are hosted by the Porto Azzurro Unit. At Capo Calamita stratiform garnet (andradite)-rich skarn and lesser ilvaite-hedenbergite skarn (Torrini, 1990) developed mostly at the contact between the Mt. Calamita Formation and the overlying carbonatic formation ("crystalline dolostones and dolomitic limestones" of Bortolotti et al., 2001). The exploited ores were spatially associated with both types of skarn, and consisted of lenses and massive bodies of magnetite ± hematite, goethite and trace amounts of base metal sulfides. The Ginevro and Sassi Neri deposits appear to be higher temperature and more reduced than the other deposits. At Ginevro, for instance, skarn mineralization totally replaced the carbonate rocks and there is a great abundance of aplitic dikes (Dimanche, 1971; Del Tredici, 1990). The skarns contain ferropargasite, associated with grossular-almandine garnet and only minor amounts of hedenbergite, ilvaite and epidote. Finally, the Stagnone deposit was recognized through a drilling project, but was never exploited; no detailed information is thus available.

Primary ore mineralogy of Elba's iron deposits is relatively simple, being made up of Fe oxides. As a general rule, hematite is dominant in the northern deposits, whereas magnetite (±pyrite±Cu,Pb,Zn,As,Bi sulfides) is enriched in the skarn-associated deposits of the Calamita peninsula. Typically, magnetite occurs as pseudomorphs after primary hematite (mushketovite), as first suggested by Vom Rath (1870) and confirmed by Cocco and Garavelli (1954), Tanelli (1977), Torrini (190) and Dünkel (2002). Del Tredici (1990) has observed the same texture at Sassi Neri. Elba is especially famous worldwide for its beautiful crystals of hematite (variety "oligisto" = glaze iron) ± pyrite, most coming from the Rio Marina stopes. Deschamps et al. (1983) suggested that the hematite ±pyrite (±quartz) assemblage is paragenetically late, being derived from oxidation and remobilisation of primary pyrite. The final alteration products of primary Fe minerals are limonitic aggregates of variable types and morphologies (earthy, massive, concretionary, sometimes stalactitic), which were actively exploited in the past, especially at Rio Albano, Capo Bianco and Capo Calamita mines (cfr. Calanchi et al., 1976).

Figure 10 shows the two paragenetic sequences proposed for the Calamita iron deposit by Dünkel (2002) and Torrini (1990). The former author describes an early cassiterite+pyrite assemblage, which was not observed by Torrini (1990).

Sulfides, which are very rare or absent in the Rio Marina – Rio Albano deposits, are significantly more abundant in the magnetite-type deposits, where they normally form in a late paragenetic stage. Masses of Fe-Cu sulfides (pyrrhotite, pyrite, chalcopyrite ± malachite, azurite, chalcantite, etc.) were locally exploited at Capo Calamita at the contact between the garnet skarn and the magnetite lenses. (Torrini, 1990).

As mentioned previously, the genesis of iron deposits of Elba Island and other Tuscan districts (namely, Colline Metallifere and Alpi Apuane) is not well

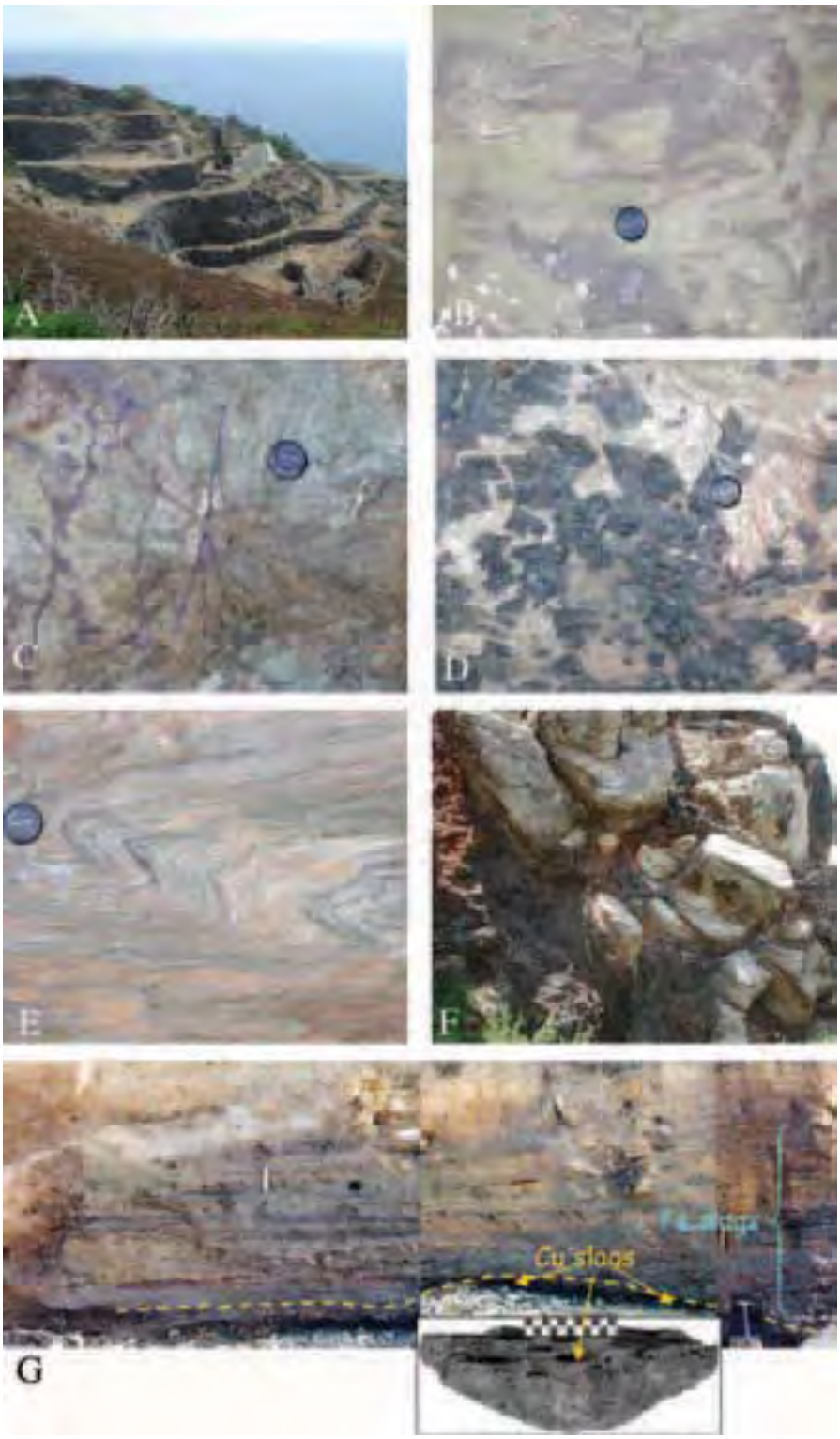

Fig. 9 - Photographs of Elba Fe skarn features: a) Open Fe Ginevro mine along the Elba coast b) Interlayered brown garnet and green pyroxene at Rio Marina c) Coarse-grained radiating crystals of hedenbergitic pyroxene cut by black ilvaite veins at Capo Calamita d) Euhedral black ilvaite crystals intergrown with hedenbergitic pyroxene at Rio Marina e) Isoclinally folded metasedimentary host rocks at Rio Marina f) Distal pyroxene-magnetite veins cutting marble at Capo Calamita g) Beach slag deposit from early mining activities along the Baratti Gulf.

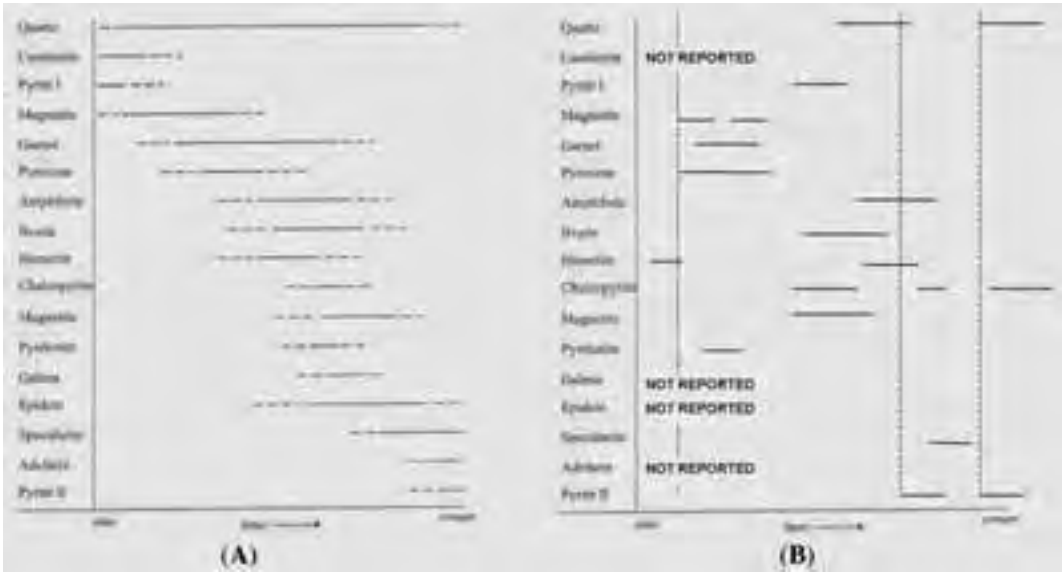

Figure 10 - Paragenetic sequences of the Capo Calamita iron skarn deposit. (A): Dünkel (2002); (B): Torrini (1990). The vertical dashed lines indicate deformation episodes.

understood. Descriptive models for the individual deposits are mostly incomplete and results of some research on specific deposits (Capo Calamita: Torrini, 1990; Sassi Neri: Del Tredici, 1990; Terranera: Seeck, 1998) are still largely unpublished. Radiometric age estimates of the hematite+adularia assemblages from Terranera and Rio Marina deposit fall between 6.4 ± 0.4 and 5.32 ± 0.11 Ma (U+Th vs He age of hematite and K/Ar age of associated adularia, respectively), i.e., the same time span as the Porto Azzurro stock (Lippolt et al., 1995). However, taking into account the regional framework, for which much more quantitative data are available (cf. Lattanzi et al., 1994), and the results obtained for the Calamita Peninsula deposits (Del Tredici, 1990; Torrini, 1990), Tanelli et al. (2001) suggest that the primary stage of iron concentration could have preceded (at least in part) the emplacement of the Porto Azzurro intrusion and related aplitic dikes (6.2-5.0 Ma), as well as the formation of skarn bodies.

Campiglia Marittima

Geologic framework

The ore deposits of Valle del Temperino, are located 2 km north of Campiglia Marittima (Livorno) village (**Fig. 11**). Several formations of the Tuscan Unit sequence crop out in this area, which can be described as a N-S trending wedge-shaped horst ("Campiglia Ridge") bordered by high angle N-S and NW-SE trending faults on the western and eastern margins, respectively (Acocella et al., 2000). The Campiglia Ridge is made up of several formations, which belong to the Tuscan Unit, ranging from Liassic massive limestone ("Calcare Massiccio") to Oligocene turbiditic sandstone ("Macigno"). The Tuscan Unit formations are tectonically overthrust by the allochthonous "Ligurian" and "Subligurians" Units, consisting of calcareous, marly and shaly turbidites of Upper Jurassic to Eocene age. The latter sequences are then unconformably overlain by Quaternary sediments, consisting of alluvium, fluvial and beach deposits (Giannini 1955; Giannini and Lazzarotto, 1967; Costantini et al., 1993; Bossio et al., 1993).

Magmatic activity strongly affected the Campiglia Marittima area in the Late Miocene-Lower Pliocene. Several kinds of both plutonic and volcanic bodies were emplaced, mostly with an overall acid to intermediate composition. The earliest emplaced magmatic body, cropping out in the Campiglia Maritima area is the "Granito di Botro ai Marmi", dated at 5.7 Ma by Borsi et al. (1967). Most chemical data for the Botro ai Marmi stock plot in the syenogranite field; some rocks encountered in drill holes have granodioritic compositions (Lattanzi et al., 2001). The contact with the host rocks (mainly represented by the "Calcare Massiccio" formation) is marked by a N-S trending thermometamorphic aureole, approximately 5 km long, 1, 5 km wide and 300 m thick (Rodolico, 1945;

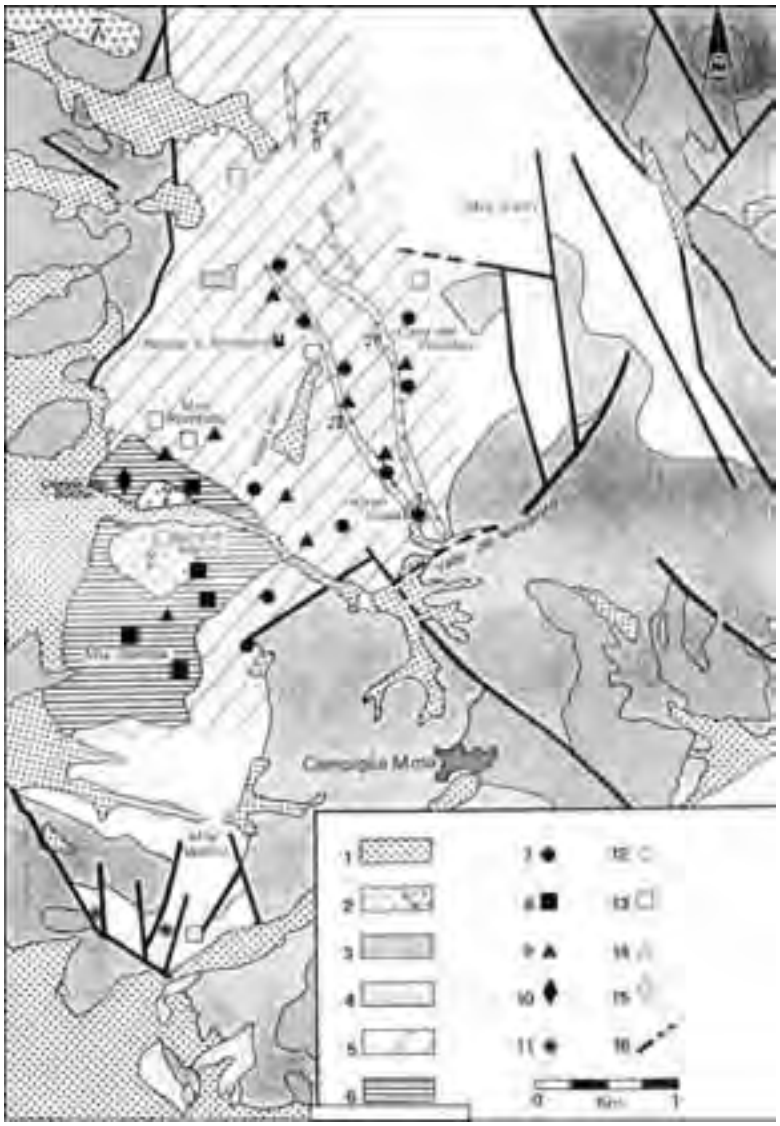

Fig. 11 - Geological map of the Campiglia Marittima district (modified after Tanelli et al., 1993). Key to symbols: (1) Neoautochtonous (Quaternary); (2) Magmatic rocks: quartzmonzonites (), quartzlatites (), porphyries (); (3) Ligurian and Subligurian Units; (4) Tuscan Unit (Middle Jurassic-Oligocene): Posidonomya Marls, Radiolarites, Polichromous Schists, Macigno Sandstone; (5) Tuscan Unit (Lower Jurassic): "Calcare Massiccio" (Massive Limestone) partially metamorphosed to marbles (shaded areas), Reddish Limestone with Ammonites, Cherty Limestones; (6) Tuscan Unit (Lower-Middle? Trias) stratified dolomitic limestomes metamorphosed to grey marbles; (7) ilvaite-hedenbergite skarns (Cu,Pb,Zn±Sn) ; (8) diopside skarns (Cu,Fe±Sn); (9) Fe gossans; (10) supergene (?) Fe oxyhydoxide deposits; (11) Fe oxyhydroxide±cassiterite (supergene/placer) deposits;

Costantini et al., 1993). The dominant calcite-tremolite-diopside skarn assemblage suggests emplacement conditions characterized by temperatures A500°C and pressures Al kb (Barberi et al., 1967).

Between 5 and 4 Ma, several swarms of porphyry dikes intruded the eastern part of the Campiglia area (Peccerillo et al., 1987). According to Rodolico (1931) and Barberi et al. (1967), three types of dikes can be distinguished: quartz-monzonite, monzonitic (also called "Green Porphyry") and potassic alkaline porphyries ("Yellow Porphyry"). The "Green Porphyry" ("Porfido Verde"), also known as "augitic porphyry", represents a diopside-bearing mafic differentiate, with intermediate silica contents, high Mg-V (64-71), Ni and Cr, and relatively low Al_2O_3 and Na_2O contents (Peccerillo et al., 1987). All the fertile skarn bodies exploited in the Campiglia Marittima district are closely related to the "Green Porphyry". The "Yellow Porphyry" and the quartz-monzonitic porphyry are acidic in composition (i.e., very similar to the the "Botro ai Marmi" intrusion), and display a strong potassic alteration. The extensive degree of alteration of the Campiglia porphyry dikes makes it difficult to establish whether the quartz-monzonite and "yellow" porphyries are both evolved products from the "Green Porphyry" or represent independ-

ent magmas (Peccerillo at al., 1987). For the same reason, the age of 4.3 Ma, obtained by Borsi et al. (1967) from the Yellow Porphyry, should be viewed with caution.

To the north of the Botro ai Marmi intrusion, the San Vincenzo rhyolites (actually quartz-latites according to Pinarelli et al., 1989) were erupted at about 4.4 Ma (Ar^{40}/Ar^{39} radiometric age: Feldstein et al., 1994). They probably resulted from mixing between a crustal "anatectic" melt and minor but significant amounts of subcrustal, mafic-internediate melt of possible calcalkaline affinity (Pinarelli et al., 1989; Ferrara et al., 1989).

According to Acocella et al. (2000) a releasing bend formed during right-lateral strike-slip faulting on the western margin of the Campiglia Ridge favoured the emplacement of the Botro ai Marmi intrusion. Pliocene extensional tectonics reactivated the strike-slip lineaments and probably controlled the Campiglia dikes as well as extrusion of the San Vincenzo rhyolites.

Ore geology and mineralogy

The Campiglia Marittima area has long been known for Cu-Pb-Zn(±Fe,Ag,Sn) skarn deposits (Corsini et al. 1980), which have been exploited since pre-Etruscan times up to a few decades ago. In the "Relazione Generale Mineraria" of 1975, the reserves in the district were estimated to be in the order of 250,000 tons at 4% Zn, 2% Pb, 0.8-1% Cu, and 20-70 g/t Ag, (with inferred reserves of about 700,000 tons: data from Cipriani and Tanelli, 1983). These deposits lie 1-2 km E and NE of the Botro ai Marmi stock, in strict spatial association with (4-5 Ma?) porphyry dikes; only minor skarn occurs in the immediate proximity of the intrusion (**Fig. 11**). A number of industrial minerals and rocks are also mined in the district.

The skarn-sulfide deposits of Campiglia Marittima can be subdivided between those outcropping in the area of Valle dei Lanzi (predominant Pb-Zn, mostly with galena>sphalerite: e.g., Cava del Piombo) and the Cu (Pb-Zn) orebodies from Valle del Temperino (**Fig. 11**). Both skarn complexes are completely enclosed in white marbles, derived from contact metamorphism of the Liassic "Calcare Massiccio" by the Botro ai Marmi and/or related intrusions. However, the skarn ores of the Campiglia area are not related to the Botro ai Marmi granite stock, but instead to the more extensive, though not outcropping, parent intrusion of the already mentioned network of Yellow and Green porphyry dikes.

The Valle del Temperino deposits occur in an area of about 0.4 Km^2 where they have been mined, even if on a small scale, from the surface at 250 m down to 50 m a.s.l. According to Corsini & Tanelli (1974) and Corsini et al. (1980), the skarn complex of Valle del Temperino consists of two west-northwest-east-southeast elongated masses, which appear to be strictly associated with the "Green Porphyry" (**Fig. 12**). The latter seems to be completely embedded in the orebodies, and is crossed by small mineralized

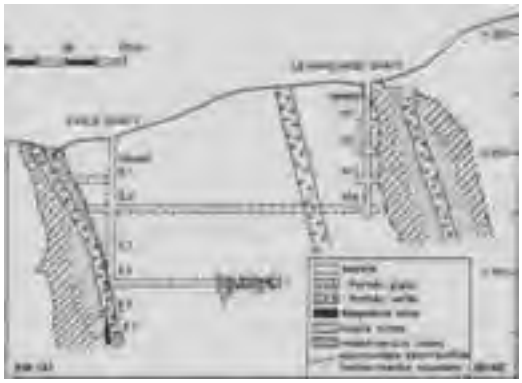

Figure 12 - Schematic cross section of the Valle del Temperino deposit (after Corsini et al., 1980)

veinlets bearing the calcite-epidote-quartz, K-mica and K-feldspar association (**Fig. 13a**).

The skarn complex consists of manganoan ilvaite (Table 1; up to 9.5 wt % MnO, after Rodolico 1931), hedenbergite-johannsenite pyroxene, quartz, calcite, epidote, and traces of andradite, rhodonite, fluorite and ferroactinolite (Bartholomé & Evrard, 1970). End member johannsenite of the solid solution hedenbergite-johannsenite series occurs near Rocca San Silvestro (**Fig. 13d; Table 1**). Epidote is particularly abundant in association with the Yellow Porphyry. Most common ore minerals include chalcopyrite, pyrrhotite, sphalerite, galena, pyrite, magnetite, hematite (traces), arsenopyrite, bismuthinite, mackinawite and galenobismutinite (Tanelli, 1977). Supergene minerals are only present in the upper levels of the mines and in small gossans.

According to Corsini et al. (1980), three zones of mineralization, namely with prevailing magnetite, ilvaite and hedenbergite occur between the Green Porphyry and the metamorphosed Liassic limestone (**Fig. 12**). The magnetite zone occurs only in the deepest levels of the skarn-sulfide deposit; it consists of a 1m thick, massive aggregate of coarse subhedral crystals of magnetite with quartz and traces of pyrite,

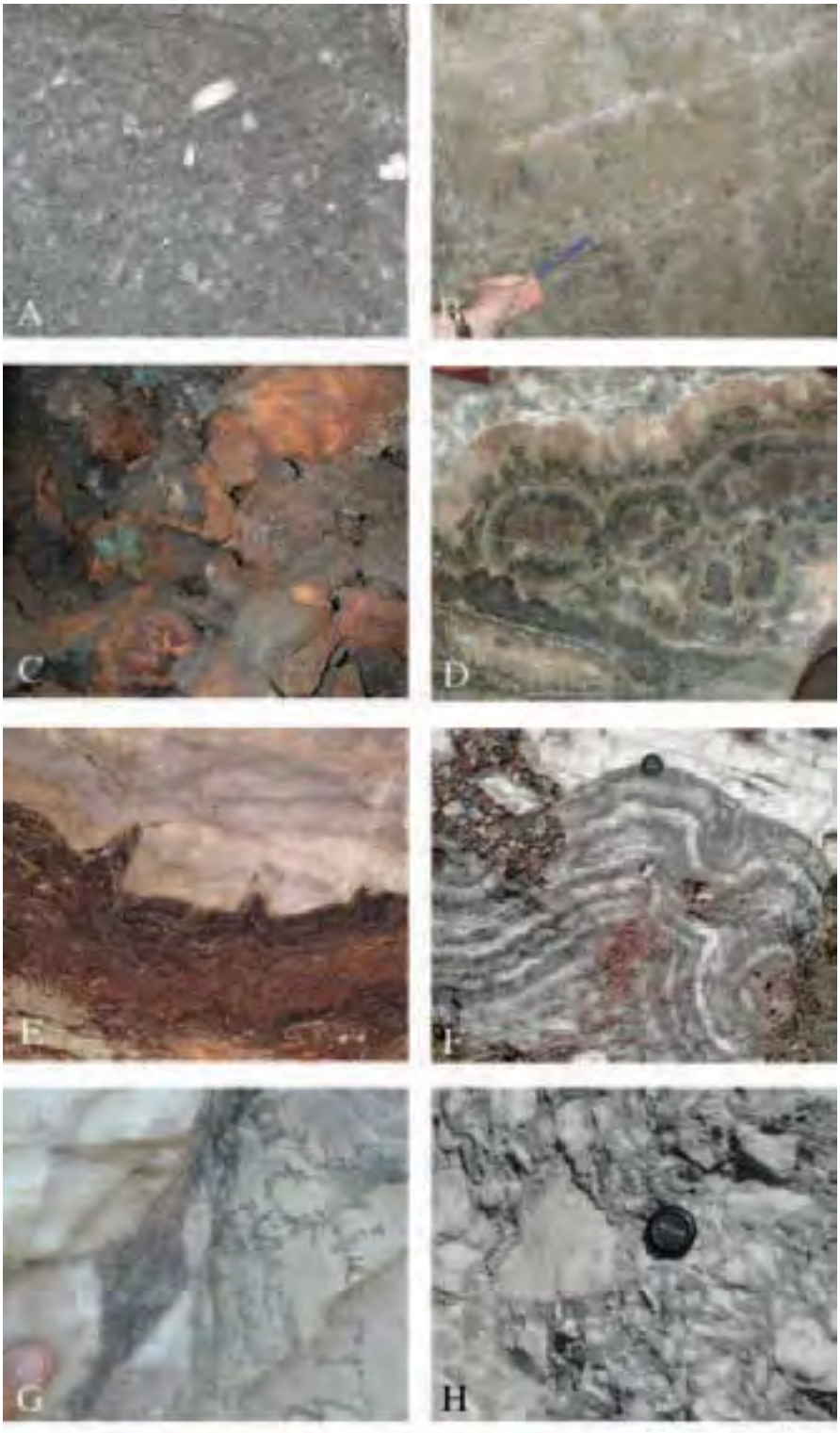

Fig. 13 - Photographs of Campiglia Marittima skarn features:
a) The "green porphyry" dike (underground mine gallery, V. Temperino)
b) Coarse-grained columnar hedenbergitic pyroxene (underground mine gallery, V. Temperino)
c) Sphalerite-rich stope fill from historic mining when Zn was not an economic commodity (underground mine gallery, V. Temperino)
d) Johannsenite from Grotta Johannsenite
e) Contact between banded johannsenite skarn and marble from Grotta Johannsenite
f) Metasomatic banding of Fe-Mn oxyhydroxides and carbonate from Campo alle Buche
g) Distal johannsenitic pyroxene vein and dendritic Mn oxide veinlets in marble near Rocca San Silvestro
h) Distal hydrothermal breccia with near Rocca San Silvestro

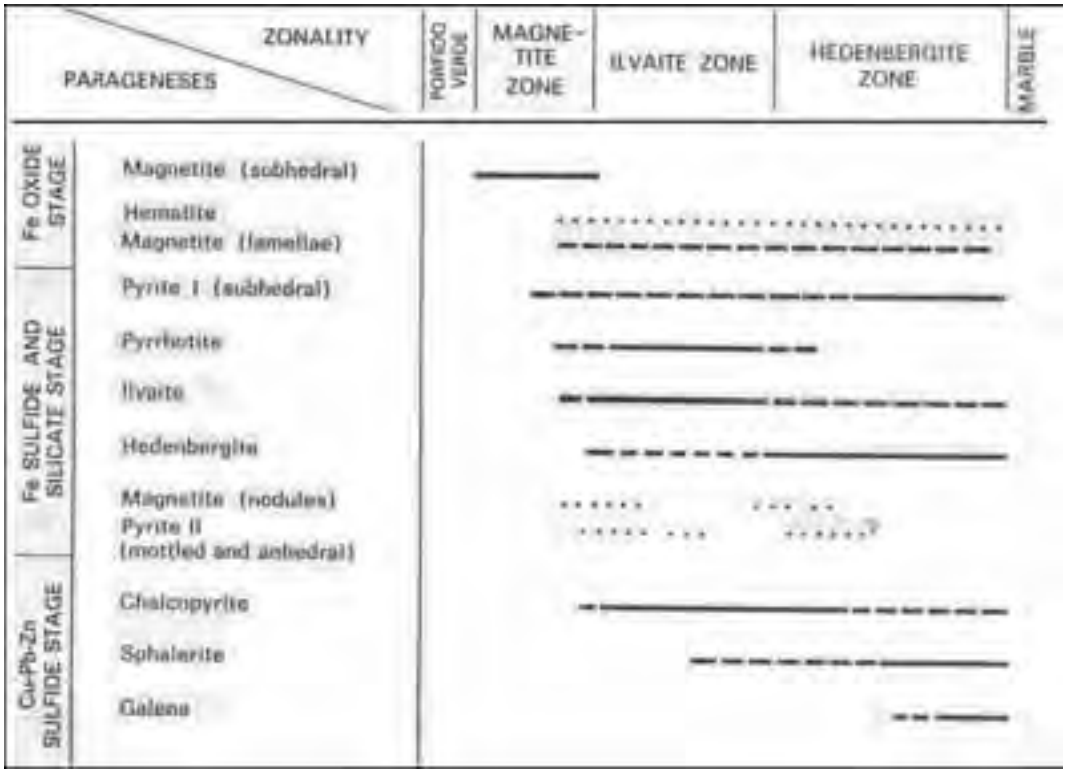

Figure 14 - Summary diagram of the space-time relationships as shown by the main minerals of the Valle del Temperino skarn-sulphide (after Corsini et al. 1980, Fig. 4)

pyrrhotite and chalcopyrite. The ilvaite zone occurs directly at the contact with the Green Porphyry: the typical ore assemblage consists of chalcopyrite and pyrrhotite, with minor magnetite, pyrite and Fe-rich sphalerite. Magnetite occurs here generally only as pseudomorphs after lamellar hematite. Pyrrhotite seems to be one of the earliest mineral phases, and is replaced by the other sulfides, as well as by magnetite. Sphalerite is quite late in the sulfide paragenesis and has an iron content ranging from 17.2 to 21.3 moles% FeS (Corsini and Tanelli, 1974). The hedenbergite zone is characterized both by well-developed, radiating and concentric aggregates of clinopyroxene with long fibers (**Fig. 13b**), and by marbles corroded and enclosed within the skarn bodies, showing that the skarn minerals were growing toward the limestone side of the complex (**Fig. 13e**). An increase in the Mn content of the clinopyroxene has been recorded, from manganoan hedenbergite (2.6 wt % MnO) in the core of the skarn body, to quite pure johannsenite (27.6 wt% MnO) at the contact with the marbles. The ore assemblage consists of chalcopyrite, pyrite, iron-poor sphalerite and finally of galena, with only minor lamellar magnetite and hematite remnants. Gangue minerals are quartz, calcite, epidote, minor ilvaite and andradite.

The ore mineral deposition at Valle del Temperino (Corsini et al., 1980) appears to have been a multi-stage process, which can be divided into three main stages (**Fig. 14**). The first corresponds to the deposition of iron oxides, mainly magnetite. Temporary changes of physicochemical parameters allowed hematite to form at first in the outer zones, and to be quickly reduced again to magnetite before the second stage took place. In the second stage, a first pyrite generation (I) was formed, then pyrrhotite, and then a second generation of pyrite (II). During this second stage, crystallization of ilvaite and hedenbergite took place. The third stage brought to the deposition of Cu-Pb-Zn sulfides, chalcopyrite being the first to precipitate, followed by sphalerite and finally by galena. The banded rocks contain ilvaite, hedenbergite, chalcopyrite and pyrrhotite. The replacement of ilvaite by hedenbergite and vice versa, indicates that these two

minerals overlap.

As mentioned above, absolute age measurements and the geological reconstruction of the Campiglia area, indicate a Pliocene age for the formation of the Valle del Temperino skarn-sulfide complex. Regional stratigraphy indicates that the maximum thickness of the sediments over the "Calcare Massiccio" during the Pliocene was about 1500 to 2000 m (Bartholomé & Evrard, 1970). Based on mineralogy and S-isotope data Corsini et al. (1980) estimated that sulfide deposition at Valle del Temperino occurred during decreasing temperatures from about 400 °C to 250 °C. They also sugget that sources of sulfur for these deposits, may have been sulfate ($\delta^{34}S$ = 12÷14.6 ‰) and/or sulfide ($\delta^{34}S$ = 5÷12 ‰) associated with the Paleozoic/Mesozoic basement formations (namely, the "Filladi di Boccheggiano" and/or "Calcare Cavernoso"), both of them containing evaporites.

A different type of mineralization, consisting of layered iron minerals (mainly goethite, hematite, siderite ± marcasite, chlorite) and sparry calcite crystals, with apparently karstic features, occurs in the old mining locality of Campo alle Buche (**Fig. 13f**). This deposit has been exploited by both underground and open pit mine workings in the XIX-XX centuries, although there are evidences of older (Etruscan?) mining activity. According to Bertolani (1958) skarn sulfide mineralization occurs at some depth below the calcite-iron oxyhydroxides mineralization. The Campo alle Buche deposit has been regarded as a gossan-type ore by early authors (e.g. Ciampi, 1910); alternatively, it can be considered the product of late-stage, low-temperature hydrothermal fluids still related to the Pliocene magmatism which was responsible of the emplacement of the Cu-Pb-Zn(Ag,Sn) skarn bodies of the Campiglia Marittima district (*cf.* Tanelli, 1977; Tanelli et al., 1992).

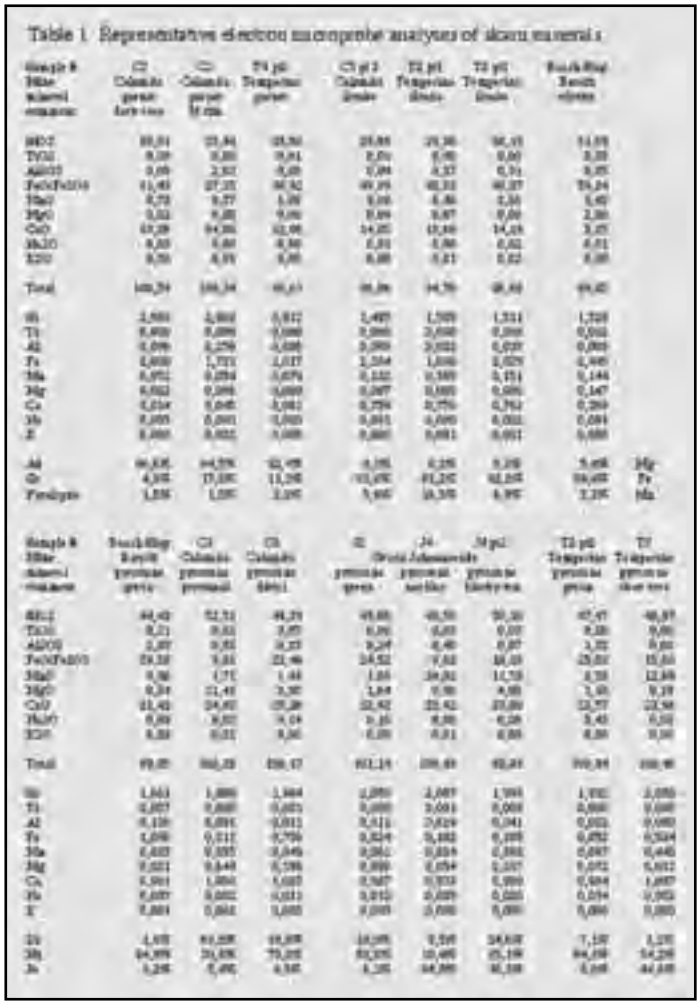

Table 1 Representative electron microprobe analyses of skarn minerals

Table 1 Representative electron microprobe analyses of skarn minerals

A brief review of mining and metallurgy in Etruria Mineraria

Mineral resources of Tuscany have long been exploited, at least since Chalcolithic times, and were very important in the development of Etruscan and Roman civilizations; in medieval times, numerous city-states derived important revenues from mining exploitation and metal production. The same applies, on a larger scale, after the unification of Tuscany under the Medici government in the 16th century. Even in more recent times some mineral resources, such as the Elba iron ore, were successfully exploited.

However, despite their economic importance, the archaeology and history of the Tuscan mines has not been well studied. Recently, a joint project carried out by the Dipartimento di Scienze della Terra of Firenze and the Dipartimento di Storia Medievale of Siena with

Volume n° 2 - from B16 to B33

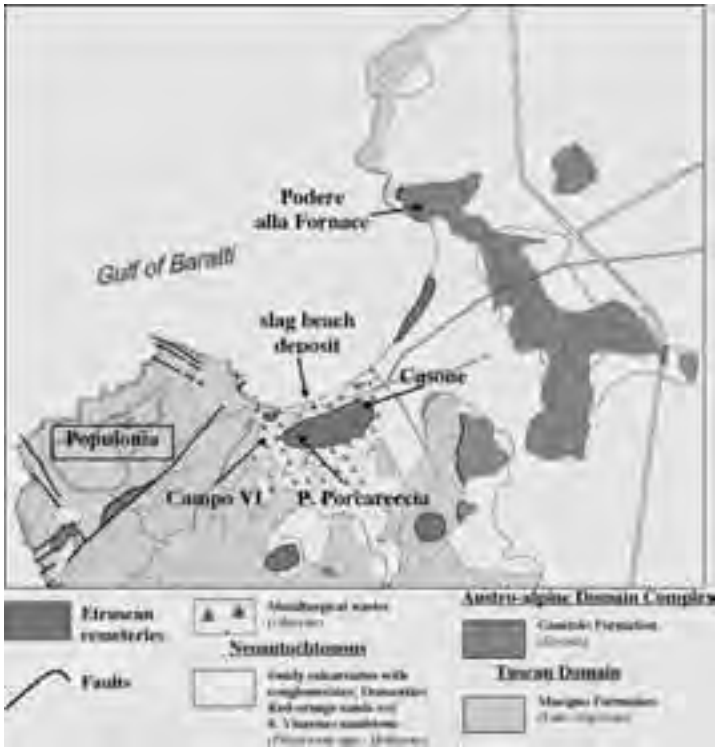

Figure 15 - Sketch map of the archaeometallurgical site of Populonia-Baratti (modified after Benvenuti et al., 2000)

the financial support of Regione Toscana (Tuscany Regional Government), has provided an exhaustive review of the mineral resources in Tuscany as a whole (Mascaro et al., 1991) with particular attention to the *Colline Metallifere* district (Cutero and Mascaro, 1995), from the double perspective of their geo-mineralogical and historical-archaeological background. These studies provide a detailed overview of all known mineral resources, from major deposits to minor occurrences, which could have been exploited by ancient miners.

A key role in the production and trade of metals (especially, but not exclusively, iron) in the Mediterranean area during the 1st Millennium BC, was played by the Etruscan town of Populonia. Populonia was an important metal production centre during Etruscan (7th-3rd century BC) and Roman (2nd century BC – 1st century AD) times. Such a prominent role was mainly due to its strategic location, midway between the large iron deposits of eastern Elba Island and the polymetallic Cu-Pb-Zn-Fe-Ag-Sn ores of the Campiglia Marittima area. The huge heaps of slags (probably in excess of 40,000m^3), discharged along the foreshore of the Gulf of Baratti could document a total iron production of some thousands tonnes of iron bloom (up to half a million tonnes according to Voss 1988). In the last ten years, a detailed research program on four main excavation sites in the Populonia-Baratti industrial zone (Poggio della Porcareccia, Casone, Campo VI and the Baratti beach deposit: **Fig. 15**) has been undertaken, with the aim of establishing the types and extent of metallurgical activities for iron and non-ferrous metals (mainly copper and tin), as well as on the provenance of smelted ores in the Etruscan and Roman periods. The main results so far obtained have been published elsewhere (Benvenuti et al., 2000, 2003a, 2003b, with references), and will be briefly summarized here.

From the analysis of stratigraphic relationships, morphological, mineralogical, textural, and chemical features of metallurgical materials the following can be concluded:

- although most archeometallurgical deposits at Baratti-Populonia can be ascribed to iron production, the existence of an earlier (and partly coeval) copper metallurgy can also be documented in the area, particularly from the slag beach deposits (**Fig. 9g**),
- two different types of copper slags, which could be related to different metallurgical steps, have been distinguished,
- the mineralogical and compositional features of some metallurgical scraps (Campo VI), dating to the 3rd century BC or earlier, provide evidence of local bronze production. In agreement with archaeological data, bronze was probably obtained by cementation, i.e., by adding unsmelted cassiterite to refined copper,
- trace element geochemistry (e.g., tin anomalous content of some iron slags: **Fig. 16a**) and Pb-isotope analyses indicate that iron ores came mainly from Elba and, to a lesser extent, from the Campiglia Marittima district (where Fe-Sn ores are common, e.g. at Monte Valerio); the latter district appears to be the most likely source area for smelted copper and,

possibly, for tin.

Field Itinerary

Elba Island (August 18, 2004)

Stop 1.1:

The ilvaite-hedenbergite skarn bodies of Torre di Rio

The area is characterized by a NW-plunging sequence of marbles and calc-schists (**Fig. 9e**) of variable size with minor grey/greenish quartzitic phyllites. They belong to the Acquadolce Unit of Bortolotti et al. (2001). Syn-metamorphic tight to isoclinal folds with a pervasive axial plane schistosity are well exposed. Deino et al. (1992) obtained a $^{40}Ar/^{39}Ar$ radiometric age of 19-20 Ma for this schistosity. A 1-metre thick, grey/whitish calc-schist level is well exposed along the road. Moving southwards from the Appiani Clock-Tower and along the coast, we can easily observe the gradational passage from calc-schists to the hedenbergite-ilvaite-epidote skarn bodies. Skarn bodies consist of almost monomineralic masses of garnet-epidote, hedenbergitic pyroxene and ilvaite (**Fig. 9b**), with associated quartz, chlorite and minor amounts of iron minerals (magnetite, pyrite and pyrrhotite), which justified limited exploitation activity in the past. Mesoscale textures clearly indicate that the replacement of minerals in the calc-schists by skarn minerals, occurred preferentially along the schistosity planes of the original rock, as pointed out by Lotti (1886,pp. 205-206). Ilvaite is here exceptionally abundant (**Fig. 9d**): it occurs in beautiful, centimetric black, prismatic crystals, with typical vertical striae and submetallic lustre. This is the type locality where ilvaite (so called after the Latin name of Elba Island: "Ilva") was first discovered and described in 1802 (Franchini et al., 2002).

Stop 1.2:

The Rio Marina mining area (seen from Torre di Rio)

Looking from the Appiani clock-tower to the NW, the landscape is dominated by the Rio Marina mines (from the left: Bacino, Zuccoletto, Valle Giove and Vigneria mines) and by the Torre del Giove hill (351 m), with the ruins of a castle of the XVIth century.

The Rio Marina ores are hosted in the Permo-Carboniferous (Rio Marina Fm.) and in the Triassic Verrucano Auctt.) metasiliciclastics of the Monticiano-Roccastrada Unit. The iron deposits of Rio Marina (as well as Rio Albano, to the north) consist of stratiform, massive or vein-like bodies, hosted by Trevisan (1950)'s Complex III rocks, preferentially at the contact between the Rio Marina Formation, or the Verrucano, and the overlying calcareous levels ("Calcare Cavernoso" Auctt.). According to some authors (cfr. Gillieron, 1959) at Rio Albano the setting of the orebodies is structurally controlled. Nevertheless, at least in the Valle Giove area, Deschamps et al. (1983) discovered a pyrite-bearing horizon within Verrucano Fm. ("Schistes verts minéralisés"), which they interpreted as a relic (syngenetic) of an iron protore. In the Rio Marina and Rio Albano deposits hematite ("specularite") is the main ore mineral which may show either a typical lamellar-micaceous habits or flattened, rhombohedral crystals, often covered by iridescent films of iron hydroxides. Pyrite is also common, predominantly as pyritohedra, although octahedra or cubes have been observed as well. Exogenous limonites, in massive or concretionary (sometimes stalactitic) forms may locally constitute the main ore minerals, especially at Rio Albano and other mineral showings to the north. It should be noted that in the 1950's-60's underground mine workings partly exploited a hematite+pyrite orebody associated with skarn silicates, known in the literature as "Rio Marina profondo" (= Rio Marina deep body").

Stop 1.3:

Along the Calamita mine road

After leaving Capoliveri, we pass by the tectonic contact between the Flysch Unit and the Porto Azzurro Unit, constituted by Mt. Calamita Fm. (Palaeozoic grey to brown micaschists, phyllites and quartzites locally intruded by aplitic dikes) and the Barabarca Fm. quartzites (Middle-Late Triassic). Just above the sea-village of Pareti (down the cliff) we can observe along the road some lenticular dark green bodies of amphibolites (tremolite + andesinic plagioclase + chlorite ± sphene, apatite) which Puxeddu et al. (1984) referred to WPB metabasites. We finally reach the former Calamita Mine Headquarters ("Palazzo"), which is one of several open pit and underground Fe mines along the coast (**Fig. 9a**).

Stop 1.4:

The Calamita mine: northern stopes

In this area thermometamorphic carbonate rocks occur. They consist mainly of stratified dolostones and dolomitic limestones, grey-whitish in colour, with rare phyllitic intercalations (Late Triassic?). To the east, along the road, there are outcrops of whitish saccharoid marbles (Hettangian?), massive or poorly stratified, with local grey dolomitic levels. These car-

bonate rocks may represent part of the original Mesozoic cover of the Mt. Calamita Fm.: more to the west, the quartzites of the Barabarca Fm. occur between the Mt. Calamita Fm. and the carbonate rocks. The latter have been affected by extensive metasomatism, which led to the development of two main types of skarn: a garnet (andradite)- skarn, quantitatively the most abundant, and an ilvaite-hedenbergite skarn (Torrini, 1990). Skarn bodies mainly occur at the contact between metacarbonates and the underlying Mt. Calamita Fm. The skarn is zoned from garnet-rich in the proximal southwest to pyroxene-ilvaite in distal zones (**Fig. 9c,f**), as is typical of most skarn systems (Meinert 1992, 1995, 1997).

Mining activity at Calamita probably dates back to Etruscan?-Roman times; according to Pullé (1921) at least 2 million tonnes of iron ore had been exploited in the period 1860-1920 by open pit mining, with iron reserves of approximately the same order of magnitude. The northern sector of the Calamita Mine is subdivided into several mine-working areas: Civetta, Albaroccia, Macei, Polveraio, Coti Nere. The exploited ores were associated with both types of skarns described above, and consisted of lenses and massive bodies of magnetite (±kenomagnetite, hematite). Additional phases include goethite and trace amounts of sphalerite, chalcocite, arsenopyrite, bornite and pyrite. Moreover, masses of Fe-Cu sulfides (pyrrhotite, pyrite, chalcopyrite ± malachite, azurrite, chalcantite, etc.) were locally exploited at the contact between the garnet skarn and the magnetite lenses (Torrini, 1990).

In the southern stopes of the Calamita Mine (not to be visited during this field trip) the exploitation activity focussed on several magnetite lenses associated with hedenbergite-ilvaite skarn bodies, beautiful examples of which can be observed just on the seaward cliffs (Punta della Calamita). A U-shaped trench (altitude: 112 m. a.s.l.), excavated in the metacarbonates and easily visible from the mine road separates the two main stopes (Vallone Basso and Vallone Alto). At the beginning of the past century the production mainly involved the limonitic gossan of iron ores, which were subsequently exploited almost exclusively for magnetite. At the so-called "Grotta Rame" (= Copper Cave) site, just below the U-shaped trench, veinlets of malachite, azurite, atacamite, paratacamite, etc. have been reported. At Vallone Alto, moreover, rare "organic" minerals like minguzzite ($K_3Fe(C_2O_4)_3 \cdot 3\ H_2O$) and oxalite ($FeC_2O_4 \cdot 2\ H_2O$) have been reported by Cocco, Garavelli (1954).

Campiglia Marittima district (August 19, 2004)

Stop 2.1:

Valle dei Lanzi. View from the Rocca San Silvestro; "Yellow Dike" with skarn envelope and nearby hydrothermal breccia

We will start the ascent to Rocca San Silvestro, an old medieval village built around the mining of base metals from shallow skarns and gossans. Here have been found also some remnants and slags with copper, lead and silver, derived from the early metallurgical works in this area. From the top of Rocca San Silvestro one can enjoy the panorama of Valle de Lanzi (Lanzi= from the german *Landsknechte*, who were at times working in the local mines), with the Botro ai Marmi granite in the background.

At the base of Rocca San Silvestro, along an internal road to the limestone quarries, it is possible to observe an outcrop of the "Yellow Porphyry", with thin skarn envelopes (**Fig. 13g**), as well as distal alteration features like a hydrothermal breccia and small Mn-oxide veins. (**Fig. 13h**) Around the "Yellow Porphyry", abundant concentrations of epidote also occur.

Stop 2.2:

Grotta Johannsenite (Gallerione)

From the upper part of the Valle dei Lanzi, we drive (walk) to the classical locality of Grotta Johannsenite (**Fig. 11**). Here we can observe the occurrence of very fine specimens (do not hammer the outcrop!!!) of Johannsenite occurring as pinkish rosettes and bands, replacing the marbles derived from "Calcare Massiccio" contact metamorphism (**Fig. 13d,e**). This Mn-pyroxene is a typical component of the Zn-skarn assemblage and represents here one of the end-members of of the hedenbergite-johannsenite solid solution.

Stop 2.3:

Mineral Museum of Valle del Temperino

We will visit the small, but very interesting Museum, set up in one of the old mine buildings at Valle del Temperino. The Museum is dedicated to the geology, mineralogy and mining history of this area and contains some spectacular mineralogical samples taken from the Cu- and Zn-Pb mines. Old maps of the mining districts are also among the exhibits and in a small, but well organized shop are sold several books on this theme and on the fauna and flora of the whole area.

Stop 2.4:

Underground Mine Valle del Temperino: Green Dike and Hedenbergite skarn

This Stop will take us underground in one mine gallery of the copper mine of Valle del Temperino. The mine is not active anymore, having been converted into a popular tourist attraction, and it's walls show the characteristic green patina of supergene copper minerals.. Nevertheless, there are still many interesting sites in the mine where geologists can observe the geological occurrence of the "Green Porphyry Dike" (**Fig. 13a**) thought to be genetically associated with mineralization, the marble host rocks, and hedenbergite skarns (**Fig. 13b**) with sphalerite and chalcopyrite. It is interesting to note that many of the old workings were backfilled with high grade Zn-ore, also occurring in the skarn, which was not economic in pre-industrial times (**Fig. 13c**).

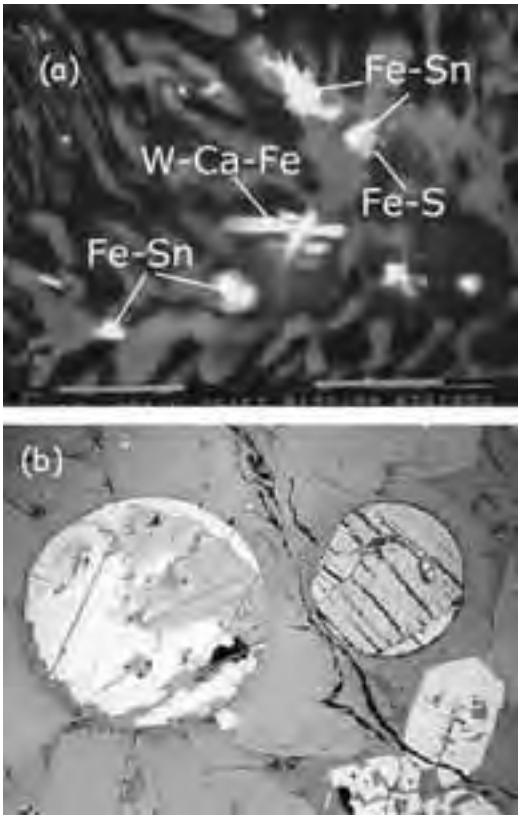

Figure 16 - Photomicrographs of archaeometallurgical samples from Populonia-Baratti: a) Backscattered electron image of partially smelted mineral charge showing micrometric globules of Fe-Sn phases (white), sometimes surrounded by Fe-S phases. The groundmass is composed of a glassy matrix and acicular crystals of hedenbergitic composition. Bar = 10 µm. b) Reflected light image of sulphidic droplets in (type-A) copper slags. Abbreviations: cc = chalcosite-djurleite; cv = covellite. Width of field: about 500 µm.

Figure 17 - Location of the principal mine workings at Calamita Mine (after Calanchi et al., 1976). Legend: 1. Civetta; 2. Albaroccia; 3. Nuova Zona; 4. Macei Alto; 5. Polverio; 6. Coti Nere; 7. Le Piane; 8. Punta Rossa; 9. Macei Basso; 10. Vallone Alto; 11. Vallone Basso.

Stop 2.5:

Mn-vein outcrops near mine exit along road to the "Gran Cava" pyroxene locality

Out of the underground adit, we walk up a small mine road characterized by interesting exposures of distal Mn-oxide veins and internal sediment-filled fractures, as well by hydrothermal breccias that directly overlie the underground ores. Such distal alteration features are common in the periphery of most skarn districts in the world. The road will bring us to the "Gran Cava", a small open pit also known as "Cava Etrusca", so called because it is thought to have been exploited already in Etruscan times. There we will observe coarse-grained hedenbergite pyroxenes and a well-exposed skarn-marble contact.

Stop 2.6:

Fe-Oxides at Campo alle Buche

Our last outcrop is situated at the westernmost

Figure 18 - Schematic geologic map of the Valle del Temperino deposit area (modified after Corsini and Tanelli, 1974)

extremity of the Campiglia area, in close proximity with a NNE-SSW trending fault. The old mining area of "Campo alle Buche" = literally "field with holes" was exploited for iron ore until the early decades of the twentieth century. The mineralized lithotype consists here of alternating bands of laminated Fe minerals (mainly goethite, hematite, siderite ± marcasite, chlorite) with calcite crystals (**Fig. 13f**). Interpreted as gossan-like deposits by early authors (e.g. Ciampi,. 1910). The Campo alle Buche mineralization probably represents the distal product, in a more oxidizing environment, of the same hydrothermal fluids that were associated with skarn formation.

The archaeometallurgical site of Populonia-Baratti (August 19, 2004)

Stop 2.7:

The beach slag deposit at Baratti

At the end of our visit to the Campiglia Marittima district, we move back towards Piombino, and take the road to Populonia. We enter the Parco Archeologico di Baratti. We leave the bus and reach the beach in order to observe the remains of the slag deposit, a poorly cemented heap of Etruscan and Roman slags discharged over an erosional terrace (**Fig. 9g**). The bottom portion of the deposit mostly consists of copper slags, clearly identifiable by the greenish spots (due to exogenous alteration of copper sulfides) on their surfaces. Preliminary analyses of the Baratti beach slag deposit led to the recognition of two main types of copper slags: type-A and type-B slags (Benvenuti et al., 2000). Type-A copper slags are characterized by a groundmass of dominant olivine, pyroxene, magnetite, and minor glass, with abundant metallic droplets, mostly fine aggregates of metallic copper, copper oxides (cuprite) and sulphides (covellite, chalcocite/dijenite) (see **Fig. 16b**). In type-B copper

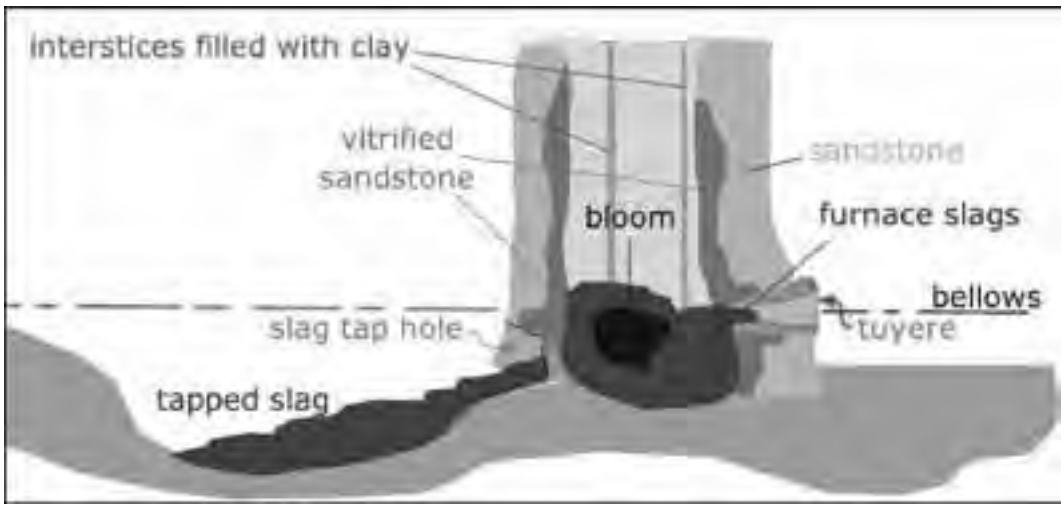

Figure 19 - Proposed reconstruction of Etruscan iron furnaces from Baratti (after Benvenuti et al., 2003b).

slags magnetite and cuprite are much less abundant, metallic copper is consistently absent, and the metallic globules (100-150μm in size) are mainly copper-iron-sulphur phases (matte) showing fine exsolution textures. These features could indicate a multi-stage copper smelting process, with type-B slags belonging to an earlier (matte production) stage than type-A slags.

The largest portion of the slag deposit consists of iron slags of different kinds (furnace slags, tapped slags, furnace conglomerates). The iron slags are mainly a silicate groundmass of fayalitic olivine (with up to 1.45% CaO) in an iron-rich interstitial glassy matrix (up to *c*25 wt.% FeO), which in itself is normally a eutectic of anorthite and fayalite. Wüstite, magnetite, hercynite and partially smelted, relic phases like quartz, hematite and scheelite (?), occur in variable amounts, and are especially abundant in furnace slags. Fayalite crystals in tapped slags occur as small laths associated with micrometric dendrites of wüstite, while in furnace slags both minerals show a significant increase in size. Unlike tapped and furnace slags, furnace conglomerates show abundant relics of hematite and quartz and a more silica-rich (and FeO-poor) glassy groundmass. Iron slags almost invariably contain droplets of metallic iron. Some iron slags are enriched in tin and may contain micrometric globules of iron-tin alloys, approximating FeSn and $FeSn_2$ in composition (**Fig. 16a**).

Fragments of smelting furnaces are also commonly present in the Baratti beach deposit. They are made up of local Macigno sandstone and baked clay, possibly derived from the terrigenous Canetolo formation (see **Fig. 18**). The baked clays show characteristic colour zoning from red to black, corresponding to increasing reducing atmosphere and temperatures in the furnaces. The reconstruction of Etruscan (and/or Roman?) iron furnaces proposed by Benvenuti et al. (2003*b*) is shown in **Fig. 19**.

If time permits, we will visit some of the Etruscan tombs located in the nearby archeological site.

Bibliography

ABBATE E., BORTOLOTTI V., PRINCIPI G. (1980) – Apennine ophiolites: a peculiar oceanic crust. *In*: Rocci, G. (ed), Tethyan Ophiolites, Western Area, Ofioliti, Spec. Issue, vol.1, 5-96.

BARBERI F., INNOCENTI F., MAZZUOLI R. (1967) – Contributo alla conoscenza chimico-petrografica e magmatologica delle rocce intrusive, vulcaniche e filoniane del Campigliese (Toscana). Mem. Soc. Geol. It., 6, 643-681.

BARTHOLOMÈ P., EVRARD P. (1970) – On the genesis of the zoned skarn complex at Temperino, Tuscany. *In*: *Problems of hydrothermal ore deposition; the origin, evolution, and control of ore-forming fluids*. I.U.G.S., Series A(2), Stuttgart, 53-57.

BENVENUTI M., CHIARANTINI L., NORFINI L., CASINI A., GUIDERI S., TANELLI G. (2003*a*) - The "Etruscan tin": a preliminary contribution from researches at Monte Valerio and Baratti-Populonia (southern Tuscany, Italy). Colloqium on «Archéométallurgie: le problème de l'étain à l'origine de la métallurgie », XIV Congr. U.I.S.S.P., Liège, 2-8 septembre 2001, Archeopress, BAR [in press].

BENVENUTI M., MASCARO I., COSTAGLIOLA P., TANELLI G., ROMUALDI A. (2000) – Iron, copper and tin at Baratti (Populonia): smelting processes and metal provenances. Historical Metallurgy, Historical Metallurgy Soc. Ed., London, England, 34 (2), 67-76.

BENVENUTI M., MORELLI F., CORSINI F., MASOTTI A., LATTANZI P., TANELLI G. (1994) - New isotopic data on the pyrite (±Cu-Pb-Zn) deposit of Campiano (southern Tuscany). Mem. Soc. Geol. It., 48, 691-697.

BENVENUTI M., PECCHIONI E., CHIARANTINI L., CHIAVERINI J., MARIANI A., MASCARO I. (2003*b*) - An investigation on iron smelting furnaces from the Etruscan site of Baratti-Populonia (Tuscany). Proceedings Volume of the 6th Int. Congress on Ancient Ceramics (EMAC '01), Fribourg (Svizzera), 3-6 Ottobre 2001 (in press).

BOCCALETTI M., GUAZZONE G. (1974) – Remnant arcs and marginal basins in the Cainozoic development of the Mediterranean. Nature, 252, 18-21.

BONINI M., BOCCALETTI M., MORATTI G., SANI F. (2001) – Neogene crustal shortening and basin evolution in Tuscany (Northern Apennines). *Ofioliti* 26 (2a), 275-286.

BORSI S., FERRARA G. & TONGIORGI E. (1967) – Determinazioni con il metodo K/Ar dell' età delle rocce magmatiche della Toscana. Boll. Soc. Geol.

Italiana, 86, 403-410.
BORTOLOTTI V., FAZZUOLI M., PANDELI E., PRINCIPI G. BABBINI A., CORTI S. (2001) - The geology of the Central and Eastern Elba Island, Italy. *Ofioliti* 26 (2a), 97-150.
BOSSIO A., COSTANTINI A., FORESI L.M., LAZZAROTTO A., LIOTTA D., MAZZANTI R., MAZZEI R., SALVATORINI G., SANDRELLI F. (1993) – Rassegna delle conoscenze sulla stratigrafia del Neoautoctono Toscano. Mem. Soc. Geol. It., 49, 17-98.
CALANCHI N., DAL RIO G., PRATI A. (1976) – Miniere e minerali dell'Elba orientale. Bologna, 102 pp.
CIAMPI A. (1910) – Alcune recenti osservazioni sulle limoniti del Campigliese. Boll. Soc. Geol. It., 29 (1), 156-164.
CIPRIANI C., TANELLI G. (1983) - Le risorse minerarie della Toscana: note storiche ed economiche. Acc. Tosc. Sc. Lett. "La Colombaria", 48: 241-283, Firenze.
CIVETTA L., ORSI G., SCANDONE P., PECE R. (1978) - Eastward migrations of the Tuscan anatectic magmatism due to anticlockwise rotation of the Appennine. Nature, 276: 604-605.
COCCO G., GARAVELLI C. (1954) - Studio di alcuni problemi geochimici relativi al giacimento di ferro di Capo Calamita (Elba). Rend. Soc. Miner. It., 10: 269-350.
CORRETTI A., BENVENUTI M. (2001) - The beginning of iron metallurgy in Tuscany; with special reference to *Etruria Mineraria*. Proceedings of the First International Colloquium on The Archaeology of Africa and the Mediterranean Basin, The Museum of Natural History in Geneva, 4-7 June, 1999, Mediterranean Archaeology, vol. 14., 127-145.
CORSINI F. & TANELLI G. (1974) – Analisi alla microsonda elettronica delle blende del giacimento della Valle del Temperino (Campiglia Marittima, Toscana). Rend. Soc. Italiana Mineralogia Petrologia, 30, 205-221.
CORSINI F., CORTECCI G., LEONE G., TANELLI G. (1980) - Sulfur isotope study of the skarn-(Cu-Pb-Zn) sulfide deposit of Valle del Temperino, Campiglia Marittima, Tuscany, Italy. Econ. Geol., 75, 83-96.
CORTECCI G., LATTANZI P., TANELLI G. (1985) - Barite-iron oxides-pyrite deposits from Apuane Alps (northern Tuscany, Italy). Mem. Soc. Geol. It., 30: 337-345.
COSTANTINI A., LAZZAROTTO A., MACCANTELLI M., MAZZANTI R., SANDRELLI F., TAVARNELLI E., ELTER F.M. (1993) – Geologia della provincia di Livorno a Sud del fiume Cecina. Quaderni Museo Storia Naturale Livorno, Vol. 13, Suppl. n.2, 1-164.
CUTERO F., MASCARO I. (1995) - Colline Metallifere. Inventario del patrimonio minerario e mineralogico: aspetti naturalistici e storico-archeologici, Firenze.
DEBENEDETTI A. (1952) - Osservazioni geologiche nelle zone minerarie dell'isola d'Elba. Boll. Serv. Geol. It., 74: 53-85.
DEINO A., KELLER J.V.A., MINELLI G., PIALLI G. (1992) - Datazioni $^{40}Ar/^{39}Ar$ del metamorfismo dell'Unità di Ortano-Rio Marina (Isola d' Elba): risultati preliminari. Studi Geol. Camerti, CROP 1-1A, Vol. Spec. 1992/2: 187-192.
DEL TREDICI F. (1990) - Studio del giacimento a skarn di Sassi Neri (Isola d'Elba). Unpublished Thesis, Università di Firenze, 200 pp.
DESCHAMPS Y., DAGALLIER G., MACAUDIER J, MARIGNAC C., MAINE B., SAUPÉ F. (1983) - Le gisement de pyrite-hématite de Valle Giove (Rio Marina, Ile d' Elbe, Italie). Contribution à la connaissance des gisements de Toscane- I. Partie 1. Schweiz. Mineral. Petr. Mitt., 63: 149-165.
DIMANCHE F. (1971) - Les minerais de magnetite et les skarns du Ginevro (Ile d'Elbe – Italie). Mineral. Dep., 6, 356-379.
DINI A., INNOCENTI F., ROCCHI S., TONARINI S., WESTERMAN D.S. (2002) - The magmatic evolution of the late Miocene laccolith-pluton-dike granitic complex of Elba Island, Italy. Geol. Mag., 139(3), 257-279.
DÜNKEL, I. (2002) - The genesis of East Elba iron ore deposits and their interrelation with Messinian tectonics. Tübinger Geowissenschaftliche Arbeiten (TGA), A, 65, S.276.
EINAUDI M., MEINERT L.D., NEWBBERRY R.J. (1981) - Skarn deposits. In: Econ. Geol. 75° Anniv. Volume: 317-391.
FABRI A. (1887) - Relazione sulle miniere di ferro dell'Isola d'Elba. Mem. Descr. Carta Geol. It., 11, 162 pp.
FELDSTEIN S.N., HALLIDAY A.N., DAVIES G.R., HALL C.M. (1994) – Isotope and chemical microsampling constraints on the history of a S-type rhyolite, San Vincenzo, Tuscany (Italy). Geochim. Cosmochim. Acta, 58, 943-958.
FERRARA G., PETRINI R., SERRI G., TONARINI S. (1989) – Petrology and isotope geochemistry of San Vincenzo rhyolites (Tuscany, Italy). Bull. Volcanol., 51, 379-388.
FERRARA G., TONARINI S. (1985) - Radiometric

geochronology in Tuscany: results and problems. Rend. Soc. It. Mineral, Petrol., 40, 111-124.

Franchini, M.B., Meinert, L. D., and Vallés, J.M., 2002, First occurrence of ilvaite in a Au skarn deposit: Economic Geology, v. 97, p. 1119-1126.

GIANNINI E. (1955) – Geologia dei Monti di Campiglia Marittima (Livorno). Boll. Soc. Geol. It., 84, 1-77.

GIANNINI E., LAZZAROTTO A. (1967) – Studi geologici di una sezione tra i monti di Campiglia Marittima e la parte centromeridionale dei Monti del Chianti. Atti Soc. Tosc. Sc. Nat. Mem., Ser. A, 78-101.

GILLIERON F. (1959) - Osservazioni sulla geologia dei giacimenti di ferro dell'Elba orientale. L'Ind. Miner., X (1), 1-10.

JUTEAU M., MICHARD A., ALBAREDE F. (1986) - The Pb-Sr-Nd isotope geochemistry of some recent circum-Mediterranean granites. Contrib. Mineral. Petrol., 92: 331-340.

KELLER J.V.A., PIALLI G. (1990) - Tectonics of the Island of Elba: a reappraisal. Boll. Soc. Geol. It., 109: 413-425.

LATTANZI P. (1999) - Epithermal precious metal deposits of Italy: an overview. Mineralium Deposita, 34, 630-638.

LATTANZI P., BENVENUTI M., COSTAGLIOLA P., MAINERI C., MASCARO I., TANELLI G., DINI A., RUGGIERI G. (2001) - Magmatic versus hydrothermal processes in the formation of raw ceramic material deposits in southern Tuscany. Proceedings 10th Int. Symposium on Water-Rock Interaction, Villasinius (Italy), 10-15 June 2001, 725-728.

LATTANZI P., BENVENUTI M., COSTAGLIOLA P., TANELLI G. (1994) - An overview on recent research on the metallogeny of Tuscany, with special reference to the Apuane Alps. Mem. Soc. Geol. It., 48 (1992): 613-625, 6 figg., 2 tavv., Roma.

LATTANZI P., BENVENUTI M., GALE N.H., HANSMANN W., KOEPPEL V., STOS-GALE Z. (1997) - Pb-isotope data on ore deposits of Southern Tuscany. Plinius, 18: 123-124.

LATTANZI P., TANELLI G. (1985) - Le mineralizzazioni a pirite, ossidi di Fe e Pb-Zn(Ag) della zona di Niccioleta (Grosseto). Rend. S.I.M.P., 40: 385-408.

LATTANZI P.F., HANSMANN W., KOEPPEL V., COSTAGLIOLA P. (1992) - Source of metals in metamorphic ore-forming processes in the Apuane Alps (NW Tuscany, Italy): constraints by Pb-isotope data. Mineral. and Petrol., 45: 217-229.

LATTANZI, P., HANSMANN, W., KOEPPEL, V. (1991) - Preliminary data on the Pb-isotope composition of mineral deposits in southern Tuscany, Italy. In: M. Pagel and J.L. Leroy (Eds), Source, Transport and deposition of metals. Proceedings of the 25 years SGA Anniversary Meeeting, Balkema, Rotterdam: 317-320

LIPPOLT, H.J., WERNICKE, R.S., BÄHR, R. (1995) - Paragenetic specularite and adularia, Elba Island, Italy: Concordant, U+Th-He and K-Ar ages. Earth Planet.Sci.Lett., 132: 43 – 51.

LOTTI B. (1886) - Descrizione geologica dell'isola d'Elba. Mem. Descr. Carta Geol. d' Italia, 2, 254 pp.

MAINERI C., BENVENUTI M., COSTAGLIOLA P., DINI A., LATTANZI P., RUGGIERI G., VILLA I. (2003) - Alkali-metasomatic processes at La Crocetta raw ceramic material mine (Elba Island, Italy): interplay between magmatism, tectonics and mineralization. *Mineral. Deposita*, Springer-Verlag, Berlin-Heidelberg, 38, 67-86.

MARINELLI G. (1975) - Magma evolution in Italy. In: C.H. Squyres (Ed.), Geology of Italy. Earth Sci. Soc. Libyan Arab Republic, Tripoli, p. 165-219.

MASCARO I., GUIDERI S., BENVENUTI M. (1991) – Inventario del patrimonio minerario e mineralogico in Toscana. Aspetti naturalistici e storico-archeologici, Firenze, Ed. Regione Toscana, 2 vv.

Meinert, L.D., 1992, Skarns and skarn deposits: Geoscience Canada, v. 19, p. 145-162.

Meinert, L.D., 1995, Compositional variation of igneous rocks associated with skarn deposits - Chemical evidence for a genetic connection between petrogenesis and mineralization: in Thompson, J.F.H., ed., Magmas, fluids, and ore deposits, Min. Assoc. Can. Short Course Series, v. 23, p. 401-418.

Meinert, L.D., 1997, Application of skarn deposit zonation models to mineral exploration: Exploration and Mining Geology, v. 6, p. 185-208.

PECCERILLO A. (1999) - Multiple mantle metasomatism in central-southern Italy: geochemical effects, timing and geodynamic interpretations. Geology, 27: 315-318.

PECCERILLO A., CONTICELLI S., MANETTI P. (1987) - Petrological characteristics and the genesis of the recent magmatism of Southern Tuscany and Northern Latium. Period. Mineral., 56, 157-172.

PECCERILLO A., POLI G., DONATI C. (2001) - The Plio-Quaternary magmatism of southern Tuscany and northern Latium: compositional characteristics, genesis and geodynamic significance. Ofioliti, 26 (2a), 229-238.

PERTUSATI P.C., RAGGI G., RICCI C.A., DURANTI S., PALMERI R. (1993) - Evoluzione post-collisionale dell'Elba centro-orientale. Mem. Soc. Geol.

It., 49: 223-312.
PINARELLI L., POLI G., SANTO A. (1989) – Geochemical characterization of recent volcanism from the Tuscan magmatic province (Central Italy): the Roccastrada and San Vincenzo centers. Periodico di Mineralogia, 58, 67-96.
POLI G. (1992) - Geochemistry of Tuscan Archypelago Granitoids, Central Italy: the role of hybridisation and accessory phases crystallisation in their genesis. J. Geol., 100, 41-56.
PRINCIPI G., TREVES B. (1984) - Il sistema Corso-Appenninico come prisma di accrezione. Riflessi sul problema generale del limite Alpi-Appennini. Mem. Soc. Geol. It., 28, 549-576.
PULLÈ G. (1921) - Le miniere dell'Elba. In: A. Stella (Ed.), Le miniere di ferro dell'Italia, Lattes, Torino, p. 181-259.
PUXEDDU M., SAUPÉ F., DECHOMETS R., GIANELLI G., MOINE B. (1984) - Geochemistry and stratigraphic correlations. Application to the investigation of geothermal and mineral resources of Tuscany, Italy (contribution to the knowledge of the ore deposits of Tuscany, II). Chem. Geol., 43, 77-113.
RODOLICO F. (1931) – Osservazioni cristallografiche sull'ilvaite. Periodico di Mineralogia, 2, 122-132.
RODOLICO F. (1945) – Ragguagli sul granito del Campigliese. Atti Soc. Tosc. Sc. Nat., 52, 125-132.
RUGGIERI G., LATTANZI P., TANELLI G. (1993) – Carbonate-hosted epithermal gold mineralization in southern Tuscany: the examples of Frassine and La Campigliola. In: P. Fenoll Hach-Ali, J. Torres-Ruiz and F. Gervilla (Eds.), Current Research in geology applied to ore deposits, Balkema, Granada, p. 551-554.
SAUPÉ F., MARIGNAC C., MOINE B., SONET J., ZIMMERMAN J.L. (1982) - Datation par les methodes K/Ar et Rb/Sr de quelques roches de la partie orientale de l' ile d'Elbe (Province de Livourne, Italie). Bull. Mineral., 105, 236-245.
SEECK I. (1998) - Die Genese der Eisenerzlagerstätte Laghetto di Terra Nera auf Ostelba und deren geologischer Rahmen. Diplomarbeit und Diplomkartierung, Eberhard-Karls-Universität Tübingen.
TANELLI G, LATTANZI P. (1986) - Metallogeny and mineral exploration in Tuscany: state of the art. Mem. Soc. Geol. It., 31: 299-304.
TANELLI G. (1977) - I giacimenti a skarn della Toscana. Rend. Soc. It. Mineral. Petrol., 33(2), 875-903.
TANELLI G. (1983) - Mineralizzazioni metallifere e minerogenesi in Toscana. Mem. Soc. Geol. It., 25: 91-109.
TANELLI G., BENVENUTI M. (1999) - Minerals and mines from Elba Island (Italy): conservation of an outstanding heritage and its use as an educational tool towards the growth of a "geologic culture". Memorie Descrittive del Servizio Geologico d'Italia, Vol. LIV, *Atti IInd Int. Symp. ProGEO*, Rome, 20-22 May 1996, 465-470.
TANELLI G., BENVENUTI M., COSTAGLIOLA P., DINI A., MAINERI C., MASCARO I., LATTANZI P., RUGGIERI G. (2001) - The iron mineral deposits of Elba Island: state of the art. Ofioliti 26 (2a), 239-248.
TANELLI G., LATTANZI P., RUGGIERI G., CORSINI F. (1991) - Metallogeny of gold in Tuscany, Italy. In: E.A. Ladeira (Ed.). Brazil Gold '91, Balkema, Rotterdam, p. 109-114.
TANELLI G., MORELLI F. & BENVENUTI M. (1993). I minerali del Campigliese: "Beni ambientali, culturali e industriali". Boll. Soc. Geol. It., 112, 715-728.
TANELLI G., SCARSELLA A. (1990) – Tipologia e modellizzazione genetica delle mineralizzazioni aurifere della Toscana meridionale. L'Industria mineraria, 3rd Series, 11(2): 1-9.
TORRINI G. (1990) - Studio del giacimento a skarn e magnetite di Capo Calamita, Isola d'Elba (cantieri settentrionali). Unpublished Thesis, Università di Firenze, 163 pp.
TREVISAN L. (1950) - L'Elba orientale e la sua tettonica di scivolamento per gravità. Mem. Ist. Geol.. Univ. Padova., 16: 5-39.
VOLLMER R. (1977) - Isotopic evidence for genetic relations between acid and alkaline rocks in Italy. Contrib. Mineral. Petrol., 60: 109-118.
VOM RATH G. (1870) - Die Insel Elba. Geognostisch-mineralogische Fragmente aus Italien. III Theil. Zeitschrift der Deutschen geologischen Gesellschaft., B, 22: 591-732.
ZUFFARDI P. (1990) - The iron deposits of the Elba Island (Italy): remarks for a metallogenic discussion. Mem. Lincei Sc.Fis. Nat., Serie IX, 1 (4): 97-128.

Back Cover:
field trip itinerary

32nd INTERNATIONAL GEOLOGICAL CONGRESS

FIELD TRIP MAP

Edited by APAT

Volume n° 2 - from B16 to B33

32nd INTERNATIONAL GEOLOGICAL CONGRESS

THE RECORD OF MESSINIAN EVENTS IN THE NORTHERN APENNINES FOREDEEP BASINS

Leaders: M. Roveri

Associate Leader: A. Landuzzi

Field Trip Guide Book - B19

Florence - Italy
August 20-28, 2004

Pre-Congress **B19**

The scientific content of this guide is under the total responsibility of the Authors

Published by:
APAT – Italian Agency for the Environmental Protection and Technical Services - Via Vitaliano Brancati, 48 - 00144 Roma - Italy

Series Editors:
Luca Guerrieri, Irene Rischia and Leonello Serva (APAT, Roma)

English Desk-copy Editors:
Paul Mazza (Università di Firenze), Jessica Ann Thonn (Università di Firenze), Nathalie Marléne Adams (Università di Firenze), Miriam Friedman (Università di Firenze), Kate Eadie (Freelance indipendent professional)

Field Trip Committee:
Leonello Serva (APAT, Roma), Alessandro Michetti (Università dell'Insubria, Como), Giulio Pavia (Università di Torino), Raffaele Pignone (Servizio Geologico Regione Emilia-Romagna, Bologna) and Riccardo Polino (CNR, Torino)

Acknowledgments:
The 32nd IGC Organizing Committee is grateful to Roberto Pompili and Elisa Brustia (APAT, Roma) for their collaboration in editing.

Graphic project:
Full snc - Firenze

Layout and press:
Lito Terrazzi srl - Firenze

Volume n° 2 - from B16 to B33

32nd INTERNATIONAL GEOLOGICAL CONGRESS

THE RECORD OF MESSINIAN EVENTS IN THE NORTHERN APENNINES FOREDEEP BASINS

AUTHORS:
M. Roveri[1], A. Landuzzi [2], M.A. Bassetti [4], S. Lugli [3], V. Manzi [1], F. Ricci Lucchi [5], G.B. Vai [5]

[1]Dipartimento di Scienze della Terra, Università degli Studi di Parma - Italy
[2]DISTART, Università degli Studi di Bologna - Italy
[3]Dipartimento di Scienze della Terra, Università di Modena e Reggio Emilia, Modena - Italy
[4]Departamento de Geologia y Paleontologia, Facultad de Ciencias, Salamanca - Spain
[5]Dipartimento di Scienze della Terra, Università degli Studi di Bologna -Italy

Florence - Italy
August 20-28, 2004

Pre-Congress

B19

Front Cover:
Panoramic view of the Vena del Gesso (Gessoso-Solfiera Formation) along the west side of the Santerno valley at Borgo Tossignano

Leader: M. Roveri
Associate Leader: A. Landuzzi

Introduction

Why a field trip on the Messinian salinity crisis in the Romagna Apennines? We believe there are many good reasons indeed. We are going to introduce in these brief notes only some of the most relevant arguments, hoping the participants at the end of the field trip will have completed their own list with many others.

Firstly, although not adequately recognized by the scientific community, the Northern Apennines holds the most complete, and probably the best, record of the large amplitude paleoenvironmental changes that affected the Mediterranean area during the Messinian age (i.e. the time interval lasting about 2 million years between 7.2 and 5.33 My), and usually referred to as the "Messinian salinity crisis" (**MSC**).

Moreover, in no places of the Mediterranean area has the fascinating history of the Messinian salinity crisis left so many indelible signs on both the physical and cultural landscape as in the Northern Apennines area, which extends from Bologna to Rimini.

Figure 1 - Remnants of the IV-VIII century AD selenite walls, preserved and recycled in the Ghisilardi Fava Palace at Bologna .

Gypsum rocks formed during Messinian events constitute an almost continuous and prominent belt (the so called *Vena del Gesso*) along the Apennines foothills. This rocky belt is characterized by peculiar morphology and ecosystems, and has been attractive to man for various uses since antiquity, providing the base for an important social, artistic, and economic development. The large-size, twinned crystal variety of gypsum, known as *selenite*, has been used as building stone since Roman times, and maybe even before. A short walk downtown in Bologna may quickly substantiate this; the basement of many Middle Age buildings, included the famous towers, as well as the ancient walls (IV-VIII century AD) are made up of squared selenite blocks (Fig. 1), many of which were recycled from the Roman theatre. Selenite derived from quarries located in the foothills of Bologna, and more to the east, in the Santerno and Lamone valleys (western Romagna). Also from Messinian gypsum-bearing successions, but dominated by the microcrystalline, thin-laminated variety of gypsum known as *balatino*, derives the sulphur extensively exploited till the early 60s in many small quarries and mines in eastern Romagna, i.e. from the Rabbi to the Marecchia valleys.

The great economic value of gypsum rocks stimulated early geological studies, at least since the beginning of the 18th century. As recently pointed out by Marabini and Vai (2003), Luigi Ferdinando Marsili, an outstanding scientist of the *Istituto delle Scienze* of Bologna, carried out, around 1717, what can well be considered the first modern stratigraphic study at a regional scale. In an, unpublished manuscript, partially reproduced in Marabini and Vai (2003), he describes in great detail the vertical superposition of gypsum and shale beds in the sulphur mines of eastern Romagna, suggesting correlations and recognizing their close relationships with the selenite rocks occurring to the west, and pointing out the occurrence of a continuous gypsum belt from Bologna to Ancona. Enclosed with Marsili's manuscript, is what can be regarded to as the first geologic map in the world (Fig. 2): an accurate representation of outcropping gypsum bodies connecting and accounting for a series of aligned sulphur mines in the Forlì and Cesena foothills. During the third and fourth day of this field trip, we will run over Marsili's outcrops again, which shows how geologic interest in this area has

Volume n° 2 - from B16 to B33

Figure 2 - The 1717 geological map by L.F. Marsili (from Marabini and Vai, 2003).

stood the test of time. The distinct spatial distribution of selenite and sulphur mines, as already recognized by Marsili, mirrors two different stratigraphic and geologic settings developed during the Messinian in the Romagna Apennines. Roughly speaking, selenite was formed through the primary precipitation of gypsum from dense brines in shallow-water settings, while extensive sulphur mineralization is related to the diagenetic transformation of clastic gypsum deposits– accumulated in somewhat deeper waters – into limestones. In the field trip area, these depositional settings are separated by a tectonic feature oblique to the main Apennine structural trend.

Three centuries after the pioneering work of Marsili, the Messinian outcrops of this area still offer a unique opportunity to observe a complete sedimentary succession developed in both shallow- and deep-water settings, thus allowing the reconstruction of their genetic and stratigraphic relationships.

In fact, contrary to the Apennines, Messinian successions preserved on Mediterranean continental margins are always reduced and incomplete, being more or less deeply cut by a subaerial erosional surface, developed in the time span during which, according to the popular *"deep desiccated basin"* model (Hsü et al., 1972), the Mediterranean basin almost completely dried up. The part of the story that is still missing, is recorded by those huge salt accumulations buried in the deepest Mediterranean basins, whose true nature and stratigraphy still wait to be fully unraveled.

The complete and expanded record of the Apennine will allow us to focus on several still open questions concerning the different evolutionary stages of the Messinian salinity crisis and, in particular, on a usually overlooked topic, i.e. the role of tectonics in controlling Messinian stratigraphic patterns.

Concluding these introductory notes, we hope the field trip participants will find it a stimulating chance for thorough discussion. For them, as well as for those who will use this guidebook to make the field trip by their own, we hope they will appreciate the strong character of this land, of its people and products, formed and developed through time, in a continuous interlacing of geology, culture, and history of science.

Messinian events, chronology, and modalities

In fact, it has long been recognized that the sedimentary record of Messinian events of the Apennine foredeep basin does not support the deep-desiccation model. No evidence for the desiccation has ever been found; which is usually explained by the particular paleoclimatic and structural context, that would have led to its premature isolation from the other Mediterranean basins, and to the persistence of a deep-water, non marine basin. For this reason the Apennine foredeep has always been considered an anomaly within the general picture and, consequently, often overlooked in the Messinian debate.

The comprehension of the different aspects related to the MSC is a long-lived issue in the scientific debate. Many important questions remain unanswered. The paleogeography and paleoclimatology of the Mediterranean area, the physical and chemical structure of the water column throughout the Messinian, and the possibly active role of biota during the crisis, are still poorly understood. The great advance in stratigraphic resolution, obtained in the last few years, after the adoption of astronomical calibrations and physical-stratigraphic concepts, has certainly improved our general knowledge and chances of understanding these phenomena. The

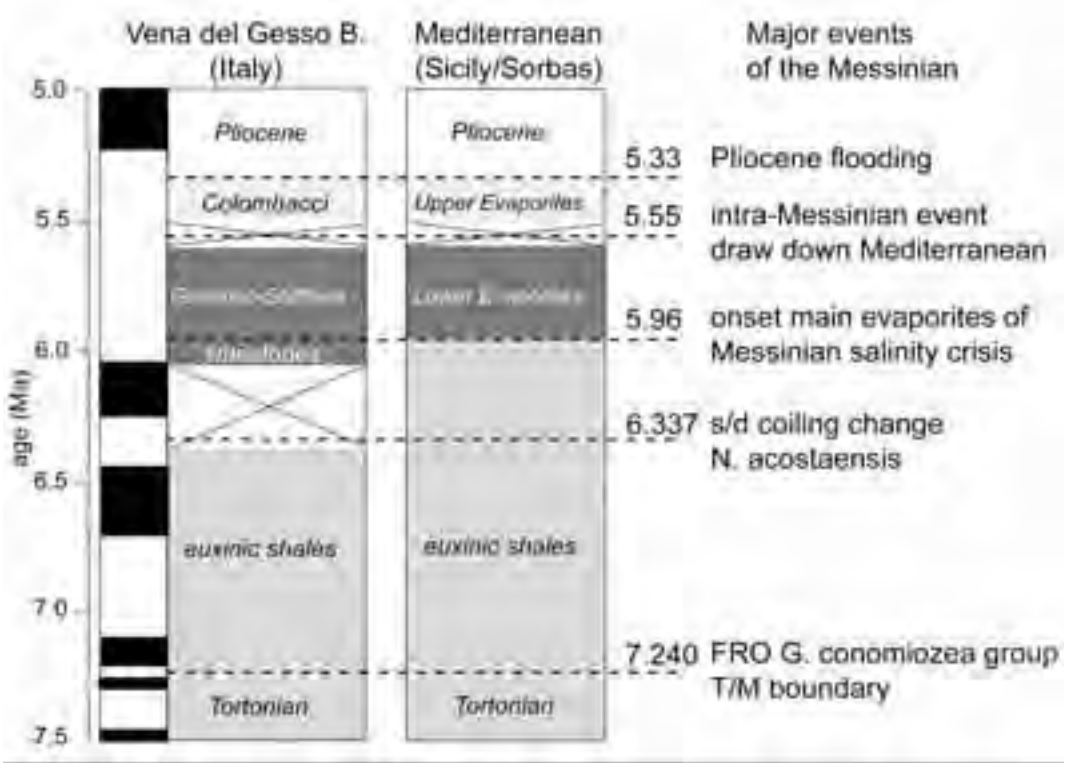

Figure 3 - Chronology of Messinian events according to Krijgsman et al. (1999a-b).

Messinian stage is now well time-constrained; the Messinian GSSP has been defined in the Oued Akrech section (Morocco), and an age of 7.251 Ma has been assigned to the Tortonian-Messinian boundary (Hilgen et al., 2000); the top of the Messinian corresponds to the Zanclean GSSP, defined in the Eraclea Minoa section (Sicily), with an age of 5.33 Ma (Van Couvering et al., 2000). Although differing views still exist, in recent years, a growing consensus has been reached about the chronology of Messinian events, as proposed by Krijgsman et al. (1999a-b; Fig. 3). This has been made possible by the well-developed cyclical arrangement of Messinian deposits. According to such a model, a classical three-fold subdivision of the Messinian stage can be envisaged: 1) pre-evaporitic (7.251-5.96 Ma), characterized by the common occurrence in deep-water settings of organic-rich, laminated deposits, which record sea-bottom low-oxygen conditions, related to a progressive reduction of water circulation within the Mediterranean; 2) Lower Evaporites (5.96-~5.61 Ma), the first episode of shallow-water evaporites precipitation in marginal basins; 3) Upper Evaporites, or post-evaporitic Lago Mare stage (~5.61-5.33 Ma), showing the widespread development of non-marine deposits with Mollusk, Ostracod, and Dinoflagellate assemblages of Paratethyan affinity (Lago Mare biofacies; Ruggieri, 1967; Iaccarino & Bossio, 1999). The end of the MSC is represented by the sudden, catastrophic return to fully marine conditions at the base of the Pliocene (Iaccarino et al., 1999).

Based on astronomic-controlled cyclostratigraphic considerations, the main Messinian events are considered to be synchronous throughout the Mediterranean area, pointing to strong external forcing, tectonic and/or climatic. The duration of the various Messinian 'phases' can thus be estimated: 1.2 My for the pre-evaporitic, 0.35 My for the evaporitic, and 0.35 My for the post-evaporitic phase. This age-model fits quite well with the two-step MSC proposed by Clauzon et al. (1996), which represents an updated version of the Hsü et al. (1972) deep-desiccated basin model. Such a model implies a diachronous deposition of evaporites across marginal and basinal settings at the boundary between the evaporitic and post-evaporitic stages. In marginal settings, this

boundary is represented by a subaerial erosional surface, deeply cutting the continental margins, and thought to have been developing during the acme of the MSC, when the Mediterranean sea-level dropped more than 1000 meters, and shallow-water evaporite precipitation was shifted towards the deepest parts. The astronomic polarity time scale (APTS) for the Neogene still shows indeed a gap lasting 90 kyr at the base of the post-evaporitic stage (Krijgsman et al., 1999a-b), related to the deep desiccation of the Mediterranean. The dramatic sea-level drop was also responsible for changing the drainage pattern in the peri-Mediterranean area, leading to the partial refill of desiccated basins with fresh to oligohaline waters of Paratethyan origin (Lago Mare stage). Despite the accurate and unifying chronology of Messinian events, which suggests a homogenous development, it has been recently proposed that the MSC evolved with distinct modalities across the different geotectonic settings involved (Sicily, Apennine foredeep, Andalusia, northwestern Mediterranean; Clauzon et al., 2001). According to this view, the different modalities can be summarized, and translated for simplicity, into two end-member successions: a **Mediterranean-type** and an **Apenninic-type**, the main difference being the non-desiccated character of the Apennine foredeep basin during the whole MSC.

The Apennine foredeep record of Messinian events

With respect to the supposed different Mediterranean and Apenninic modes of the MSC evolution, we now offer a different point of view to the discussion. The end-member successions basically – and very roughly - correspond to the record of distinct morphostructural settings: the Mediterranean-type to marginal, elevated areas, the Apennine type to basinal deeps.

The true "anomaly" of the Apennine foredeep is that, due to its geodynamic setting and post-Messinian evolution, both modalities actually occur and that the stratigraphic and genetic relationships between them can be clearly defined. In other words, all along the Apennine foredeep system, a true Mediterranean-type succession can be recognized in shallow, marginal sub-basins, while an Apennine-type succession developed in deeper ones. Based on a careful review of Messinian stratigraphy, carried out in the last ten years by several research groups, through the integration of surface and subsurface, data and the use of a physical stratigraphic approach (Gelati et al., 1987; Rossi et al., 2002; Bassetti et al., 1994; Bassetti, 2000; Roveri et al., 1998; Roveri et al., 2001; Roveri et al., 2003), a geologic and stratigraphic model for the Apennine foredeep Messinian deposits has been reconstructed. Such a model is summarized in Figures 4 and 5, and assumes the development of pre-evaporitic and evaporitic stages that are synchronous with, and with the same modalities as, the other Mediterranean basins. Primary evaporites were deposited only in shallow thrust-top basins whose formation dates back to the Late Tortonian, when the ensuing propagation of the Apennine compressive front led to the progressive fragmentation of a larger and deeper foredeep basin. The end of evaporite deposition is coincident with a paroxysmal acme of a regional tectonic phase, determining the uplift and emergence of the Apennine chain, and the concomitant migration of the foredeep depocenters toward the foreland. The intra-Messinian unconformity, a perfect equivalent of the erosional surface which cuts Lower Evaporites throughout the Mediterranean, is associated with an angular discordance, and hence it is strictly related to a regional tectonic uplift, leading to the dismantling and resedimentation of Lower

Figure 4 - Chronology of Messinian events in the Apennine foredeep. Modified from Roveri and Manzi (in press).

Evaporites in deep basins through large-scale mass-wasting and gravity flows in shelf and slope areas. By tracing down basin, the intra-Messinian unconformity is a problem solved, and its correlative conformity is placed at the base of the resedimented evaporites complex (Roveri et al., 1998, 2001). This unit accumulated in topographic lows during the subaerial exposure of uplifted basin margins, thus allowing us to bridge the last Messinian gap (Roveri & Manzi, in press). Based on its physical characteristics, a high-resolution stratigraphic framework for the post-evaporitic successions (discontinuities of different hierarchical rank, stacking pattern and cyclic sedimentary succession can be easily correlated to that developed in wedge-top basins through very distinctive physical elements. The distinction between the p-ev$_1$ and p-ev$_2$ unit is substantiated by the clear upward transition from high-efficiency to low-efficiency turbidite systems. Moreover, an ash layer of regional extent is an excellent key-bed in the p-ev$_1$ unit.

The first and second days of the field-trip will be spent in a marginal, Mediterranean-type context, the third and fourth days, in a Apenninic-type one. This will give the participants the chance to contrast and correlate the two stratigraphies and, consequently, to assess some basic Messinian features.

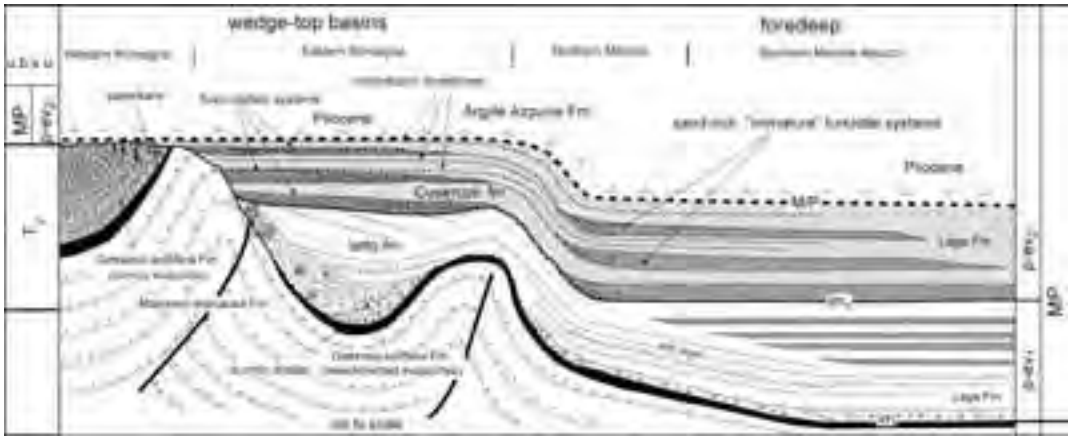

Figure 5 - The geologic-stratigraphic model for the Messinian deposits of the Apennine foredeep (Roveri et al., 2003).

organization of depositional system, key horizons), has been reconstructed. A second, younger regional unconformity splits the post-evaporitic Lago Mare deposits into two units; the lower one (p-ev$_1$), only occurring in structural depressions, is composed of resedimented evaporites at the base, overlain by a siliciclastic coarsening and shallowing-upward succession; the upper unit (p-ev$_2$), made up of coarser-grained deposits, has a general transgressive trend, and seals all the previously uplifted tectonic structures and generalized subsidence – and/or a base level rise – which preceded the Zanclean flooding.

The relatively small field trip area has the great advantage of being able to sumup all the elements of the larger-scale stratigraphic model. This area corresponds to a series of wedge-top basins (Fig. 5) which are characterized by different absolute paleobathymetry and subsidence rates. The two main foredeep Messinian depocenters are presently buried below the Po Plain, and crop out in the Southern Marche and Abruzzi (Laga Basin), and their

Regional geologic setting

The Romagna Apennines, extending from the Sillaro valley to the west, to the Marecchia valley to the east (Fig. 6), is part of the Northern Apennines, a ENE-verging arc, characterized by compression along the external front, and extension in the inner western part (i.e. the Tyrrhenian area).

The Apennine chain has been formed since the Late Eocene as a post-collisional fold and thrust belt, in the more general context of convergence between the African and Eurasian plates. The Romagna Apennine is characterized by an outcropping succession of Lower Miocene to Pleistocene siliciclastic deposits, overlying buried Mesozoic to Cenozoic carbonates. This sedimentary succession represents the infill of a foredeep basin system actively migrating to the northeast since the Oligocene (Ricci Lucchi, 1986), and formed above the Adria plate in what is defined the Umbria-Marche domain, the lowest structural unit of the Apennine orogenic wedge (for an updated

Volume n° 2 - from B16 to B33

Figure 6 - Simplified structural map of the Northern Apennines.

review of Apennine geology, see Vai and Martini, 2001).

To the west of the Sillaro valley, this unit is covered by the Ligurian nappe (Fig. 6), a chaotic complex of Jurassic to Eocene deep-marine sediments and ophiolithic slabs (Castellarin and Pini, 1989), formed as an accretionary wedge during the Late Cretaceous Alpine compressional phases and thrust over the Adria plate since the Oligocene (Kligfield, 1979; Boccaletti et al., 1990).

The uppermost structural unit of the Romagna Apennine consists of the Langhian to Messinian Marnoso-arenacea Fm, a turbiditic complex more than 3000 m thick (Ricci Lucchi, 1975, 1981), detached from its carbonate basement along a basal thrust, and showing a deformational style dominated by fault propagation folds (Capozzi et al., 1991). Seismic data show that the outermost front of the Apennine thrust belt lies in the subsurface of the Po Plain (Castellarin et al., 1986, Castellarin, 2001), where several ramp anticlines are buried by a thick succession of marine Plio-Pleistocene deposits. The Romagna Apenninic is split into two sectors (western and eastern) by the Forlì line (FL, Fig. 7), a complex fault zone oblique to the Apenninic trend. The two sectors defined by this feature have a different structural arrangement at the surface; the foothills of the western sector show a gentle N-NE dipping monocline of Messinian to Pleistocene deposits, resting above the Marnoso-arenacea Fm., while the same succession is deformed by several thrust-related anticlines with Apenninic trends in the eastern one. The Forlì line played a primary role in the geological evolution of the area, at least since the Late Tortonian (Ricci Lucchi, 1986; Roveri et al., 2002)

In a NW-SE cross-section, flattened at the Miocene/Pliocene boundary (Fig. 7), dramatic facies and thickness changes within the Messinian succession occur across structural highs related to the Forlì line. Such changes finally correspond to the two above-mentioned different Messinian stratigraphies, whose comparison and correlation is the main aim of the

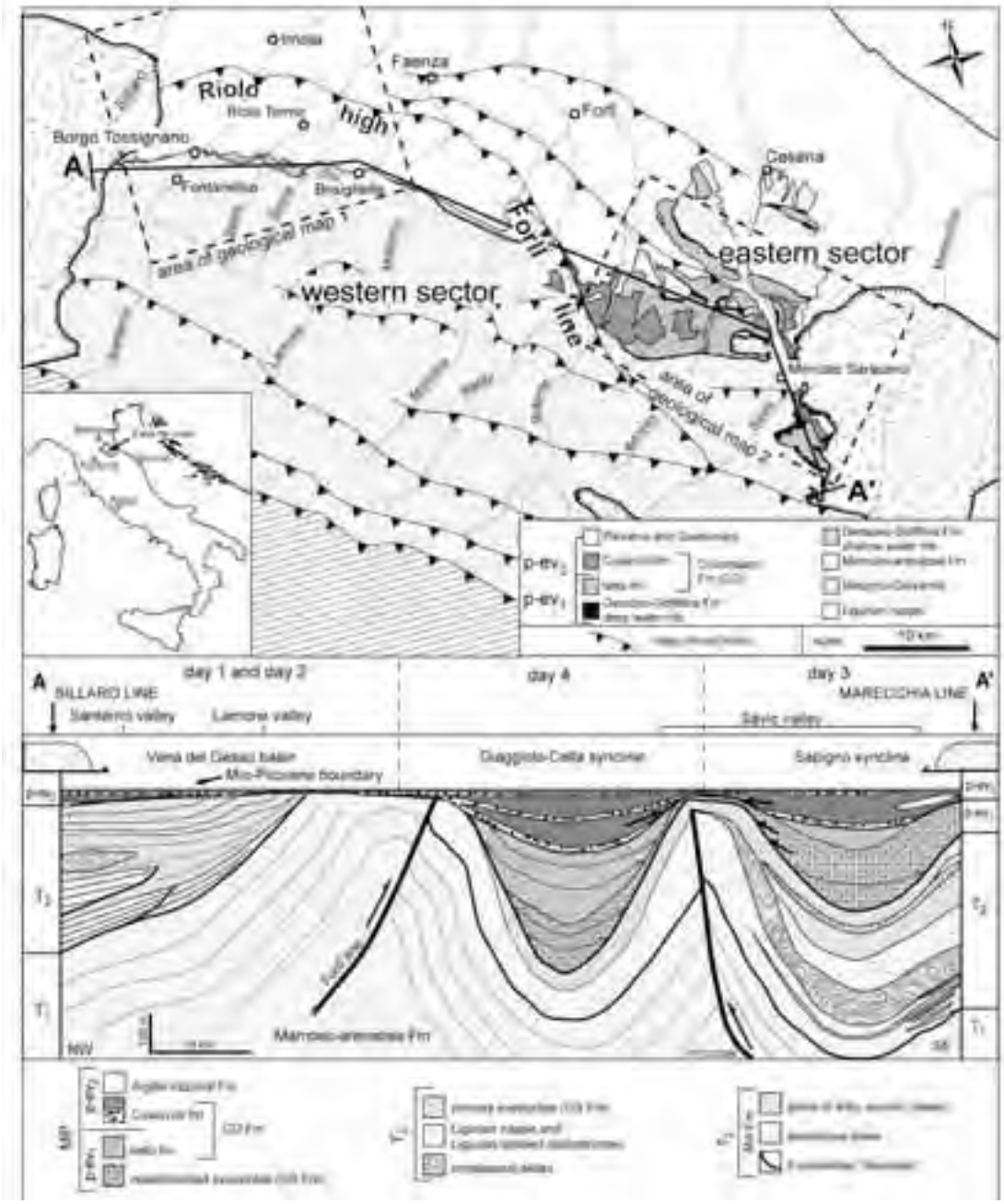

Figure 7 - Simplified geologic map (above) and cross-section (below) of the Romagna Apennines. The cross-section is flattened at the Miocene/Pliocene boundary to better illustrate the great facies and thickness changes characterizing the Messinian succession across main structural elements (modified from Roveri et al., 2003).

field trip.

The lithostratigraphy of the Langhian to Pliocene sedimentary succession of the Romagna Apennines consists of four formations (Vai, 1988; Fig. 8):

i) the ***Marnoso-arenacea Fm*** (MA, Langhian-Messinian), made up of deep-water siliciclastic

turbidites, derived from the Alps and, subordinately, from the central Apennines, is a huge clastic wedge, up to 3000 meters thick, filling a large foredeep basin elongated in a NW-SE direction, whose depocenter migrated towards the NE, following the propagation of the compressional front. Towards the top, thick and laterally-continuous turbiditic lobes are replaced by slope mudstones (*ghioli di letto*) which contain minor turbiditic sandstone and chaotic bodies; this is in turn overlain by a unit straddling the Tortonian-Messinian boundary, and made up of finely-interbedded organic and diatomite-rich laminites and mudstones, informally named *euxinic shales* (Upper Tortonian-Lower Messinian). Like the coeval Tripoli Fm in Sicily and Spain, such deposits show a well developed cyclical pattern, and record the paleoceanographic changes associated with the ensuing MSC.

The euxinic shales span a 1.5 My time

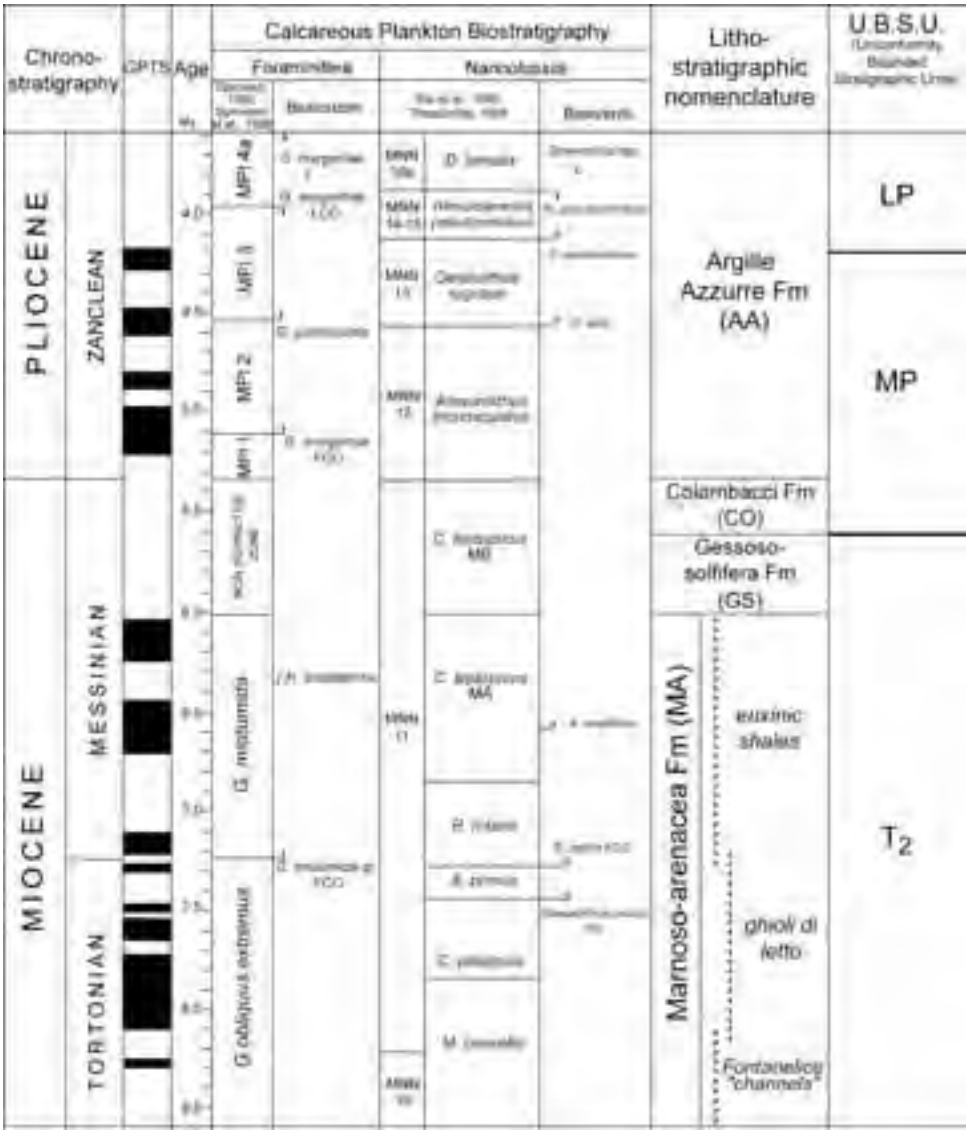

Figure 8 - Stratigraphic scheme of the Apennine foredeep Tortonian to early Pliocene time interval. Note that lithostratigraphy refers to marginal successions, i.e. those characterized by deposition of primary, shallow-water evaporites during the main evaporative event.

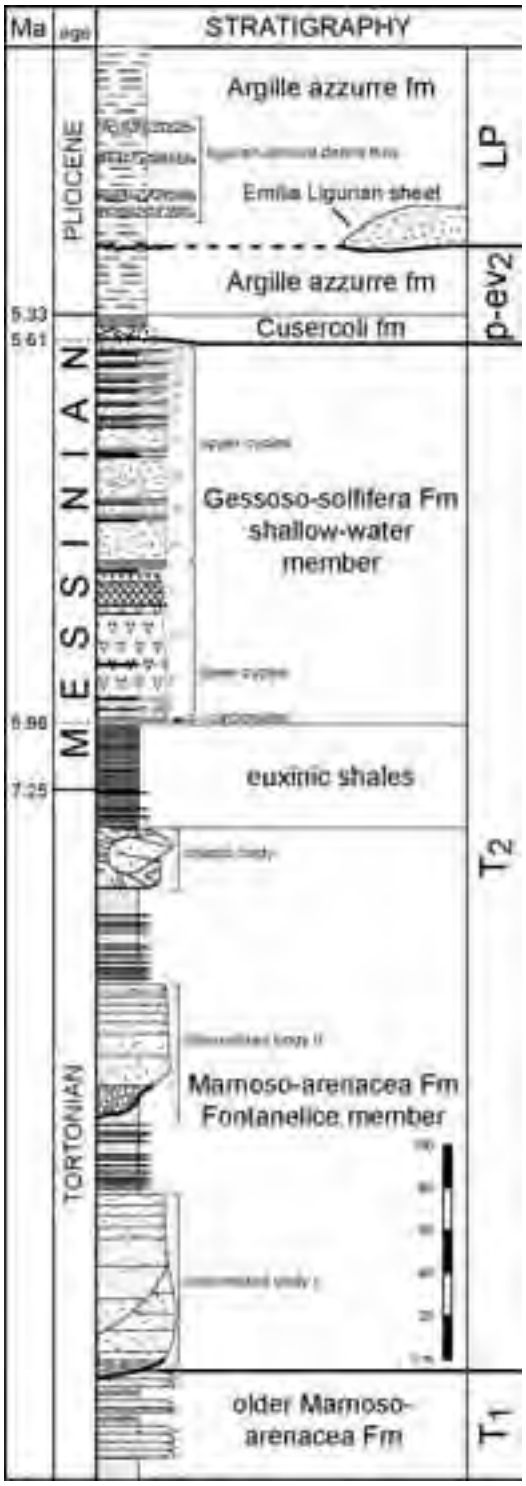

interval, characterized by well-defined bio- and magnetostratigraphic events; their calibration with astronomical cyclicity allowed a detailed chronostratigraphy to be established (Krijgsman et al., 1999a,b; Vai, 1997).

ii) the ***Gessoso-solfifera Fm*** (GS, Messinian), is made up of both primary and clastic, resedimented evaporites, with interbedded organic-rich shales, deposited during the evaporitic and post-evaporitic stages of the MSC;

iii) the ***Colombacci Fm*** (CO, Upper Messinian), consisting of mainly siliciclastic sediments derived from Apenninic sources, was deposited in both shallow and deep brackish or freshwater basins developed during the Lago Mare phase of the MSC. Based on a sharp vertical facies change, this unit has been subdivided by Roveri et al., (1998) into two informal units, the **Tetto fm.** (below), and the **Cusercoli fm.** (above). The Cusercoli fm is characterized in marginal basins by coarser-grained lithology and by the occurrence of thin lacustrine micritic limestone beds (*colombacci* limestones).

iv) the ***Argille Azzurre Fm*** (AA, Lower Pliocene), is made up of relatively deep marine mudstones deposited in a series of more or less connected wedge top basins locally encasing fan-delta conglomerates, and shelf to perched-basin turbiditic sandstone bodies, and small, isolated carbonate platforms deposits (***Spungone***).

From a physical-stratigraphic point of view, the Tortonian to early Pliocene succession has been subdivided into three large-scale synthems, separated by large-scale unconformities recording important phases of tectonic deformation of the Apennine orogenic wedge. From base to top, they are the T_2 (Tortonian-Messinian) synthem, the *MP* (Messinian-Pliocene), and *LP* (Lower Pliocene) synthems (Roveri et al., 1998; Roveri et al., 2001; Roveri et al., 2003). These large-scale units only slightly differ from those defined by Ricci Lucchi (1986) and can be further subdivided into lower rank U.B.S.U. delimited by minor unconformities and flooding surfaces (Roveri et al., 1998), still having a regional significance. The more reliable key events for long-distance correlations are the Tortonian/Messinian boundary (7.2 My), the Miocene/Pliocene boundary (5.33 My), and a widespread ash-layer within the post-evaporitic Lago Mare deposits, which holds a radiometric age of 5.5. My (Odin et al., 1997). Messinian deposits fall in the T_2 (pre- and evaporitic stage) and MP (post-

Figure 9 - Stratigraghy of the western secctor.

Volume n° 2 - from B16 to B33

Figure 10 - Panoramic view of the stratigraphic succession cropping our in the Santerno valley.

evaporitic stage) synthems. Hereafter, the successions developing in the western and eastern sectors will be described separately.

Western sector

The western area extends from the Sillaro valley to the west up to the Bidente valley to the east. These physiographic boundaries correspond to two important tectonic alignments, as previously reported. The Tortonian to Pliocene succession of this sector is particularly well exposed (Figs. 9, 10), along the Santerno valley, which will be visited during the first day of the field trip. The second day will be devoted to important details from outstanding outcrops along the Sintria and Lamone valleys.

T_2 synthem (Upper Tortonian-Messinian) - The base of the T_2 synthem corresponds to an abrupt facies change within the Marnoso-arenacea Fm. In previous stages, turbiditic deposits are characterized by tabular geometries and high lateral continuity, suggesting deposition by unconfined currents flowing parallel to the basin axis (i.e. in a NW-SE direction) in a nearly flat sea-bottom.

In the T_2 synthem, sandstone bodies are coarser-grained and show a lower lateral continuity; the abundance of basal scours, cut and fill, and water-escape structures, suggest deposition from flows strongly affected by topographic constriction (Mutti et al., 1999). This facies change has usually been related to a regional phase of tectonic uplift and basin narrowing (Ricci Lucchi, 1981, 1986).

In the western sector, this is well represented by the Fontanelice "channels", two turbiditic sandstone bodies confined within large-scale erosional depressions, and separated by a mudstone horizon (Ricci Lucchi, 1968, 1969, 1975, 1981).

The larger and thicker upper channelized body is encased in Upper Tortonian mudstones (*ghioli di letto*). In a section almost normal to the paleocurrents, the basal erosional surface deepens toward the SW, and a spectacular NE-wards onlap of sandstone fill can be observed. The sedimentary fill is composite, with basal conglomerate bars (pebble composition indicating an Alpine source; Ricci Lucchi, 1969), and at least two distinct sandstone bodies in the upper part. The upper Fontanelice system is overlain by a mudstone unit, with interbedded, smaller-size turbiditic sandstone bodies, forming an overall thinning-upward sequence. In the Santerno river section, the mudstone unit contains a slump body, up to 50 m thick, characterized by sandstone olistoliths, derived from minor turbiditic bodies. In turn, the mudstone unit is capped by a 40 m thick horizon of organic-rich *euxinic shales*. The euxinic shales, characterized by a well-developed lithologic cyclicity, have been studied in detail for bio-, magneto-, and cyclostratigraphic reconstructions in several sections (Monte del Casino, Monte Tondo, Monticino, Fig. 11; Vigliotti, 1988; Negri and Vigliotti, 1997; Krijgsman et al., 1999a; Vai, 1997). The topmost cycles are characterized by the development of thin carbonate layers.

The T_2 synthem is topped by the shallow-water evaporites of the Gessoso-solfifera Formation,

forming a continuous belt up to 150 m thick, from the Sillaro to the Lamone valleys. Gypsum deposits have a strong cyclical organization, as first recognized by Vai and Ricci Lucchi, (1977) which counted up to 16 small-scale, decametric-thick, shallowing-upward cycles, recording the progressive evaporation of shallow lagoons. These cycles have been interpreted more recently as controlled by periodic changes of orbital parameters (Vai, 1997; Krijgsman et al., 1999b).

The ideal complete cycle consists of the vertical superposition of 6 sedimentary facies (Fig. 12, 13, 14), five of them made up of gypsum and carbonates; it starts with basal organic-rich shales (facies 1), deposited in shallow lagoons below the wave base; these shales are overlain by gypsified limestone stromatolites (facies 2), massive autochthonous selenitic gypsum (facies 3), and well-stratified autochthonous and reworked selenitic gypsum (facies 4). The size of selenite crystals usually decreases upwards; this change is usually thought to be related to the progressive evaporative draw-down, and increasing salt concentration of the lagoon. The upper part of the modal cycles is characterized by nodular gypsum, acicular gypsum, gypsarenites (facies 5), and chaotic selenite breccia (facies 6). These deposits are interpreted as related to subaerial exposure and erosion at the end of an evaporative draw-down cycle, with strong gypsum reworking by waves or torrential streams action (Vai and Ricci Lucchi, 1977).

Progressive upward decrease in thickness and different facies distribution within individual cycles can be observed; upper cycles are thinner, and autochthonous evaporite facies are much less well-developed than the reworked clastic facies.

This suggests the superposition of an overall "regressive" trend on the smaller-scale, higher-frequency cyclicity. This trend provides the guideline for a precise cycle-by-cycle correlation throughout the Vena del Gesso basin, and further to the SE, in the Marecchia valley area (epi-Ligurian evaporites). For correlation purposes, the complete succession of 16 evaporite cycles has been subdivided into 2 thin "basal" cycles (facies 1 and 2 only), 3 thick "major" cycles (facies 5 missing), a very thick 6th cycle (complete sequence), and 10 thin "minor" cycles (complete sequences). The described longer-term

Figure 11 - Panoramic view of the late Tortonian-Messinian succession in the Santerno valley (stop 1.4). Note the chaotic horizon below the euxinic shales and the deformed gypsum unit on top.

Figure 12 - Facies 3 selenitic gypsum in a block of the Garisenda tower of Bologna.

Volume n° 2 - from B16 to B33

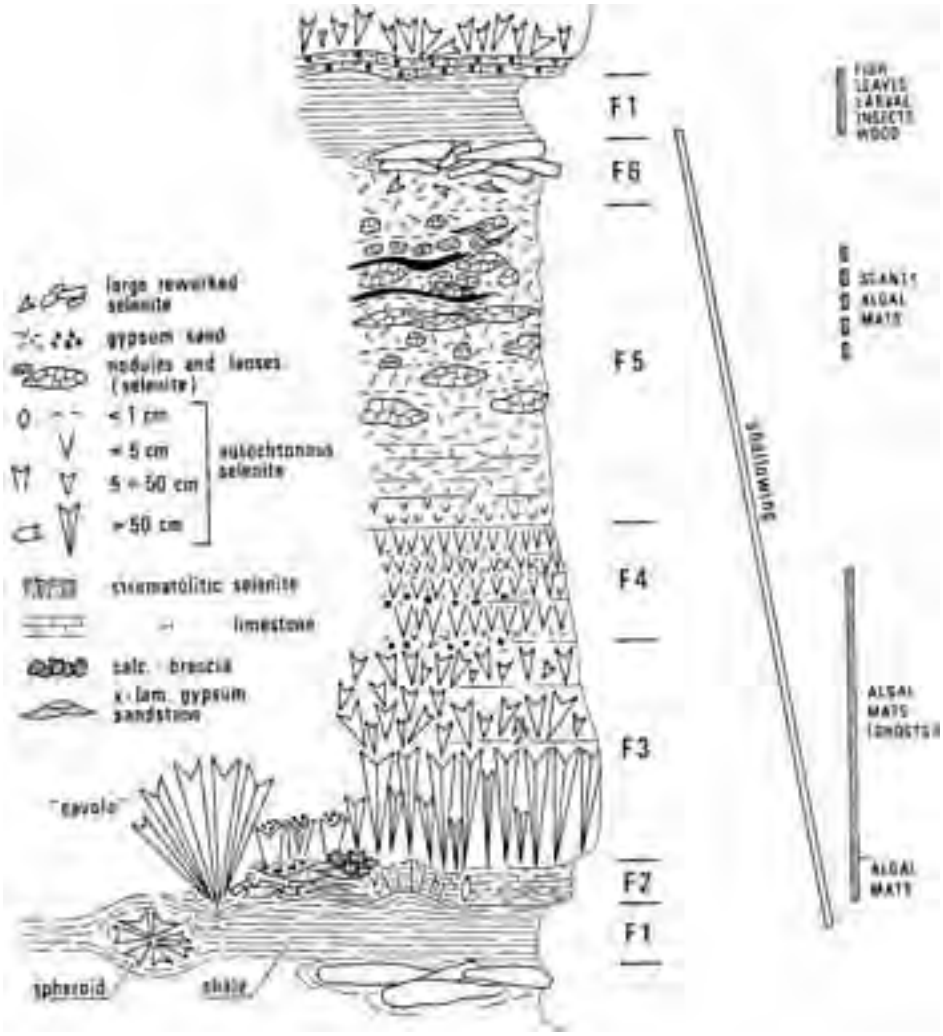

Figure 13 - The ideal depositional cycle of the Vena del Gesso evaporites (Vai and Ricci Lucchi, 1977)

trend culminates with a great erosional unconformity cutting the gypsum unit at its top, and marking the base of the overlying Messinian-Pliocene synthem (MP).

MP synthem (Messinian-Pliocene)

An angular unconformity is associated with the erosional surface (Vai, 1988), marking the T_2/MP boundary, clearly indicating its tectonic nature. This surface preserves spectacular evidence of subaerial exposure (karstic dykes, filled by continental deposits which are rich in mammal fauna, were found in the Monticino section, near Brisighella; Costa et al., 1986; De Giuli et al., 1988). The erosion associated with the MP unconformity deepens toward the southeastern end of this sector (Marzeno valley), where the evaporitic and pre-evaporitic Messinian deposits are completely missing.

Deposits of this synthem belonging to the Colombacci Fm and Argille Azzurre Fm, are very thin, and separated by the Miocene/Pliocene boundary. The uppermost Messinian Colombacci Fm consists mainly of gray to varicolored clays, containing an hypohaline faunal assemblage (*Melanopsis spp*., *Limnocardium spp*.). Small lenses of sandstone and pebbly sandstone, and calcareous conglomerate occur locally. In places, a white micritic layer is also found; locally named *colombaccio*, it gives its name to the formation itself. The Miocene/Pliocene boundary is

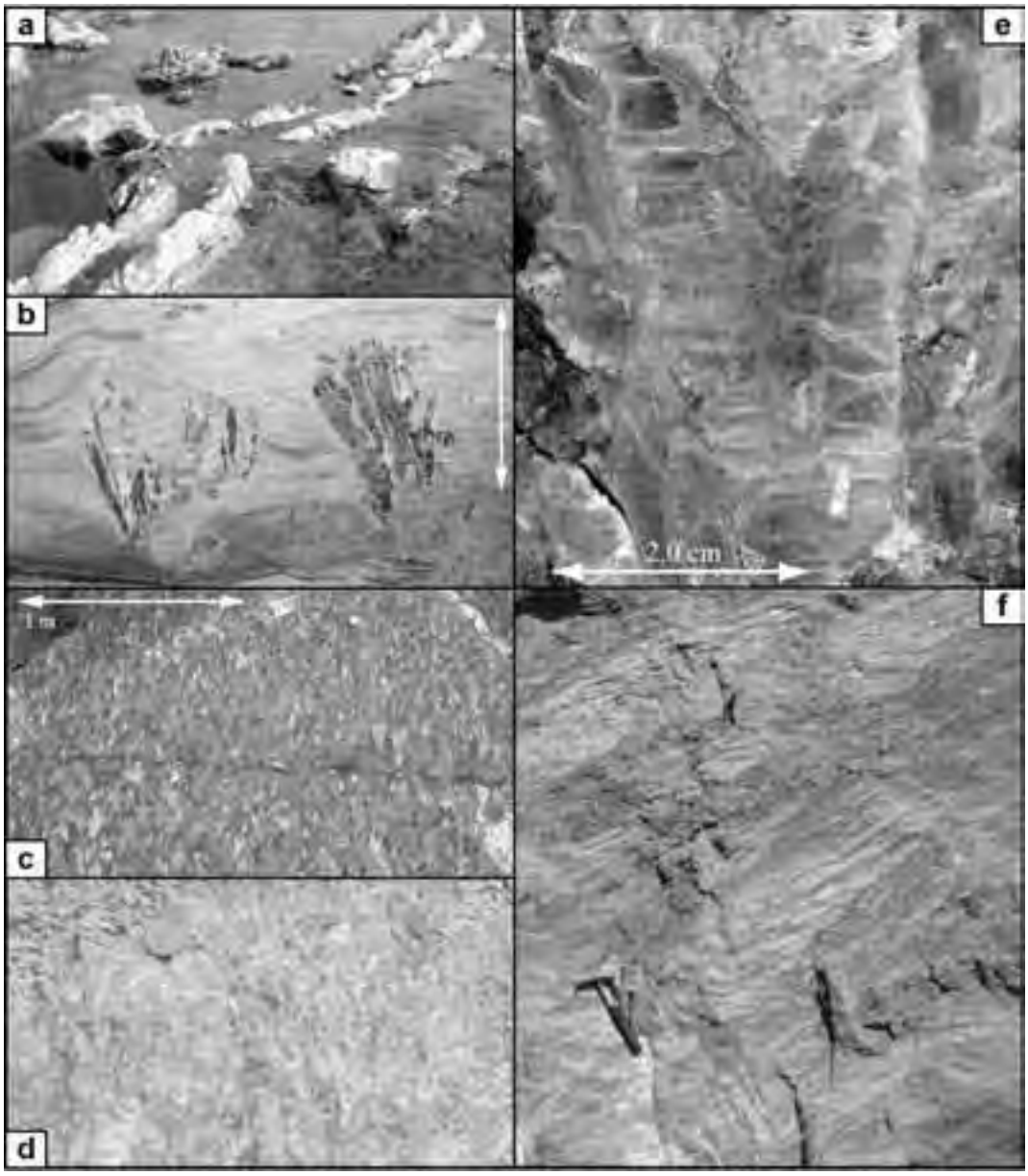

Figure 14 - Vena del Gesso evaporites. A) Santerno river bed. Slumped stromatolitic limestone (F2) and limestone breccia ("calcare di base") embedded in the topmost pre-evaporite mudstones; b) Rio Sgarba Quarry, Borgo Tossignano. GS, cycle II: euxinic shales (F1), and calc-gypsum laminites enclosing meter-sized "palisade"-type crystals of stromatolite-bearing gypsum (F2); c) Montebello Quarry, Marecchia Valley. GS, cycle III: upright and well-packed "swallow-tail" selenite crystals (F3). The evaporite growth is interrupted by an intra-cycle dissolution surface; d) Monte TondoQuarry, cycle VI, reworked selenite (facies F4); e). "Swallow-tail" selenite crystal (F3): an opaque stromatolite-bearing core is surrounded by a transparent diagenetic overgrowth;f) Monte Tondo Quarry, cycle VII, reworked small selenite crystals with nodules and lenses of whitish selenite.

Volume n° 2 - from B16 to B33

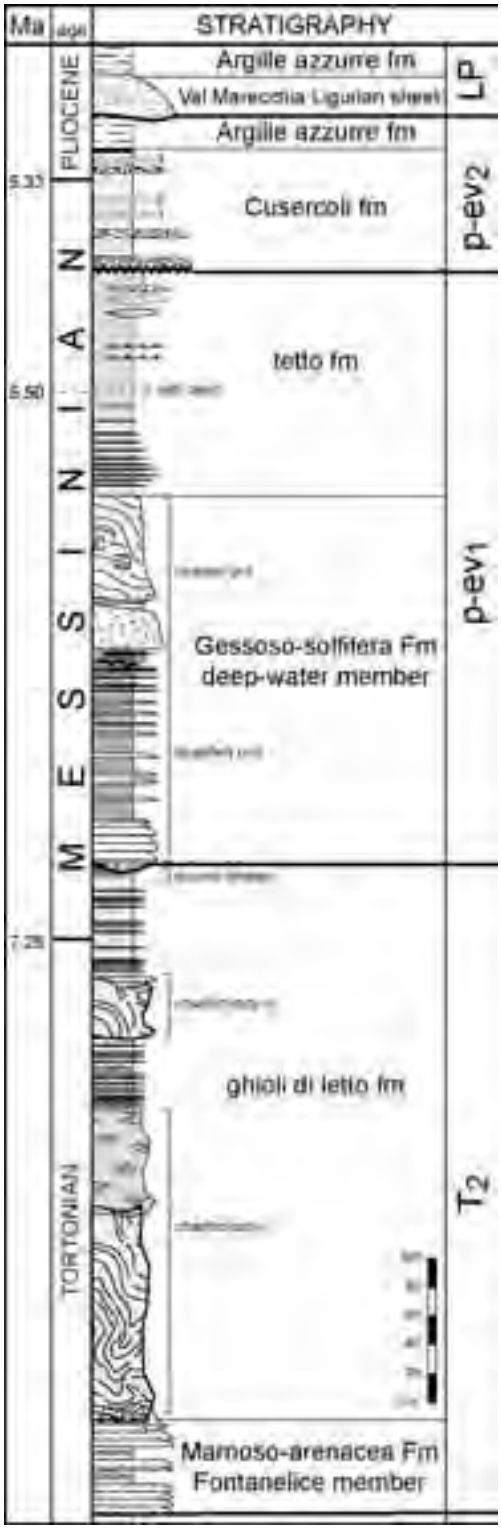

marked by a characteristic dark, organic-rich horizon, whose origin is still poorly understood. Through the boundary, the typically abrupt transition from non-marine to relatively deep-marine waters is observed; such a change is witnessed by the rich and diversified planktonic assemblages of the basal Pliocene.

Lower Pliocene deposits of this synthem consist of a thin unit (only 2 m thick in the Santerno section, according to Colalongo et al., 1982, and Cremonini et al., 1969) of deep-marine mudstones draping the whole area. Detailed biostratigraphic studies carried out in the Santerno and Monticino sections, show that a large hiatus is associated with the regional unconformity (LP) marking the top of the MP synthem. The LP unconformity occurs in the upper part of the Gilbert chron, and is related to the advance of the Apennine compressive front. This event is recorded in the Sillaro-Santerno area by the sudden appearance within deep marine clays of coarse, chaotic deposits (pebbly mudstones and debris flow), derived from the Ligurian units (Cremonini and Ricci Lucchi, 1982). The shallowness of the Lower Pliocene deposits of the MP synthem in this area is essentially related to the local strong erosion associated with the LP unconformity.

Deformation of primary evaporites

The gypsum unit of this sector is characterized by extensional and compressional deformations (Marabini and Vai, 1985), with rotated blocks and shallow thrust faults, partially affecting also the top of the underlying *euxinic shales*. Most of these deformations emanate from a detachment surface in the upper part of the *euxinic shales* (Marabini and Vai, 1985), and are sealed by MP deposits of the Colombacci Fm.

From W to E, the deformation shows different characteristics. To the west (Santerno-Sillaro sector), the gypsum unit, which is thinner and more discontinuous, shows both compressive and extensional deformations. Rotational listric faults affect the gypsum unit on the left bank of the Santerno river (see stop 1.2 Fig. 27), while further to the west (M. Penzola), shallow thrust faults are responsible for the vertical repetition of the lower gypsum cycles (stop 1.8). Traces of anhydritization (due to higher lithostatic loading during burial) and subsequent rehydration, have been observed from M. Penzola to the westernmost edge (Sillaro-Santerno valleys, Roveri et al., 2003).

Figure 15 - Stratigraphy of the eastern sector.

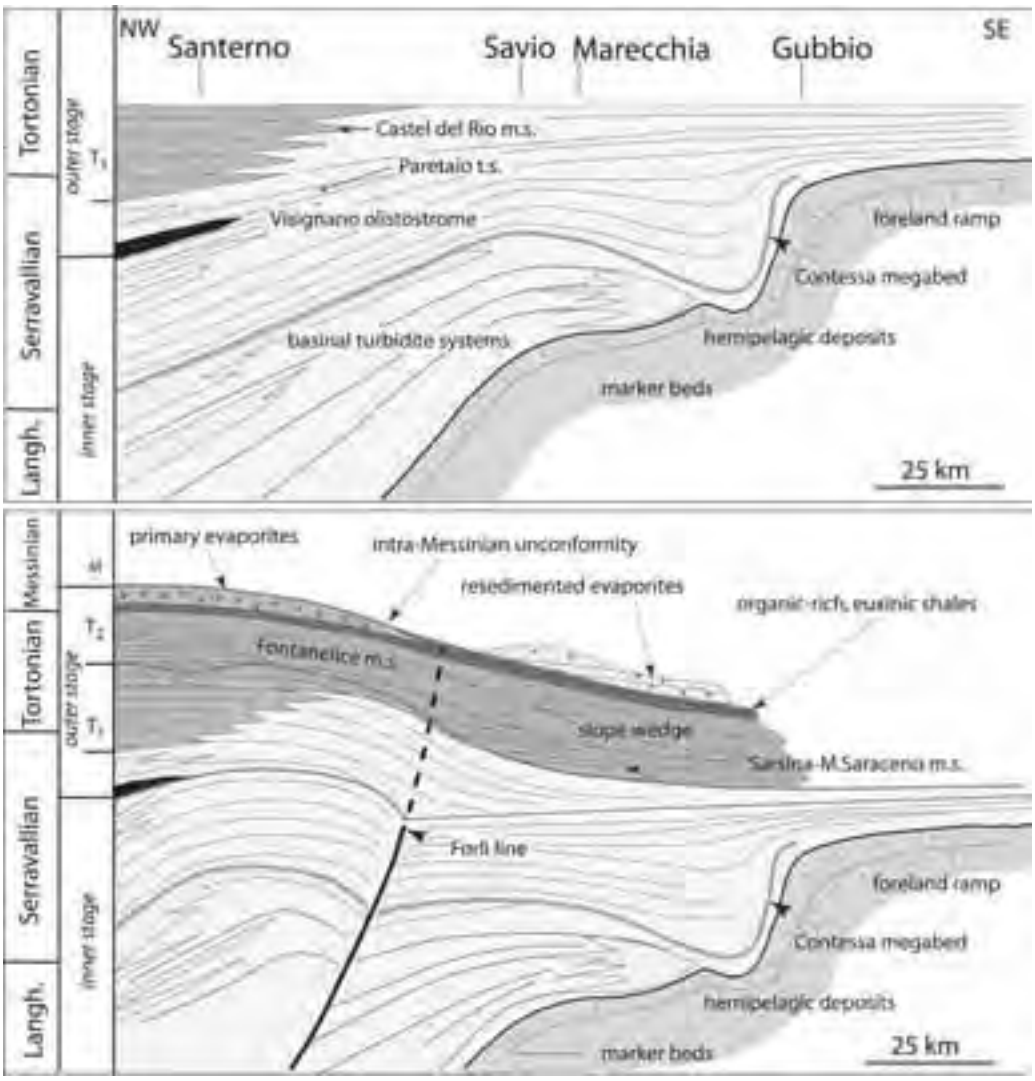

Figure 16 - Tortonian to late Messinian evolution of the Apennine foredeep basin (axial section) showing the longitudinal fragmentation due to the growth of the Forlì line - related structural high (Roveri et al., 2002)

To the east (Sintria valley), the deformation is more severe. Here the gypsum unit forms a complex imbricate structure made of three or more SW verging thrust sheets (Marabini and Vai, 1985; see Stop 2.2, Fig. 36).

Eastern sector

No obvious unconformities occur in this sector any where in the considered stratigraphic interval. The uppermost Marnoso-arenacea Fm. here consists (Fig. 15) of a thick pile of tabular turbiditic sandstone bodies, made up of thick-bedded, coarse to very coarse and pebbly sandstones, with frequent amalgamated beds and basal scours. Such deposits form the Savio turbidite system, a composite unit consisting of up to five sandstone bodies vertically arranged in a overall fining-upward sequence, with a maximum thickness of some 200 m, and cropping out discontinuously along the Savio valley. A direct genetic link with the channelized systems of the western sector (Fontanelice systems), has been recently suggested (Roveri et al., 2002; Roveri et al., 2003) on the basis of facies and regional geologic considerations.

As in the western sector, these sandstone bodies are

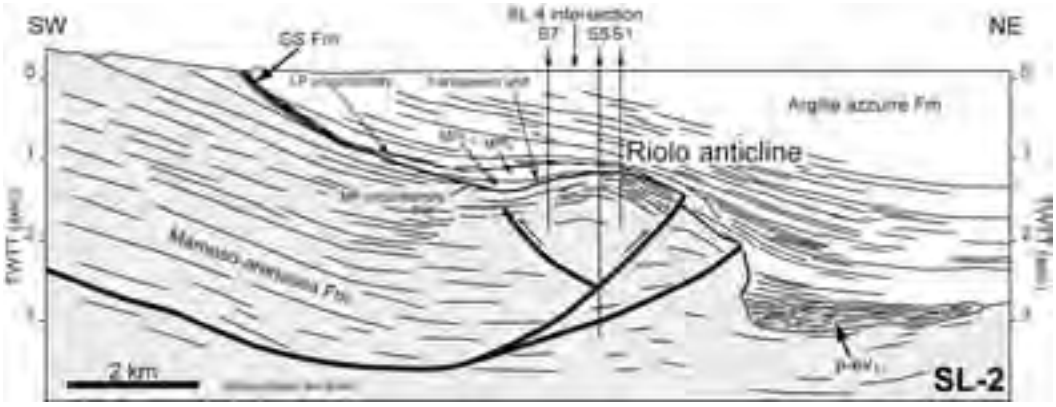

Figure 17 - Line drawing of a seismic profile showing the buried culmination of the Riolo anticline. See location in the geological map of Fig 24 (from Roveri et al., 2003).

overlain by a mudstone unit, here more developed, and containing two chaotic bodies separated by an undisturbed muddy horizon, 400 m thick. The chaotic bodies are made up of both intra- and extra-basinal deposits (Lucente et al., 2002); their thickness reaches some 300 m.

An organic-rich unit corresponding to the *euxinic shales* of the western area occurs above the chaotic horizon; here such a unit is thicker (100 m), and show a less evident lithologic cyclicity, due to the higher terrigenous content. As in the western sector, the Tortonian/Messinian boundary lies at the base of this unit, allowing reliable correlations.

The most striking difference with respect to the western sector is the total absence of primary, shallow-water evaporites. The Gessoso-solfifera Fm. consists here of a thick complex of resedimented evaporites, made up of well-stratified, thin-bedded gypsum turbidites, and huge olistostromes which contain large blocks of primary selenitic gypsum. These evaporites were deposited in relatively deep-waters, well below the wave-base, as suggested by the observed sedimentary structures (Parea and Ricci Lucchi, 1972; Ricci Lucchi, 1973; Roveri et al., 2001; Manzi, 2001). Interbedded mudstones have a moderate organic content, decreasing upwards. Neither traces of subaerial exposure, nor an obvious cyclical pattern, can be recognized.

Clastic gypsum deposits are overlain by a large thickness (up to 600 meters) of terrigenous non-marine deposits of the Colombacci Fm, in turn followed by Pliocene deep-marine deposits. The best outcrops of Upper Messinian and Lower Pliocene deposits occur in two large synclines (Giaggiolo-Cella and Sapigno synclines in Figs. 7, 15), possibly corresponding to local Messinian depocenters developed above the orogenic wedge. The basal Pliocene deposits have here the same facies characteristics as the western sector (epibathyal mudstones belonging to the Argille Azzurre Fm.) as well as the Miocene/Pliocene boundary, characterized by the typical black shale horizon.

Summarizing, the Messinian succession has an overall basinal character. In such a depositional context, a reliable stratigraphic framework can be based on the recognition of abrupt vertical facies changes, characterized by both compositional and/or grain-sizes changes in deep-water deposits. Such changes would correspond to large-scale reorganization of basin geometry and drainage patterns related to main tectonic events.

Using this approach, with the integration of bio- and magneto-stratigraphic data, the T_2 unconformity can be traced at the base of the Savio turbidite system. As for the MP unconformity, clearly developed in the western sector, Roveri et al. (1998, 2001) and Manzi (2001), suggested that it could be tracked into a correlative conformity at the base of the resedimented evaporitic complex of this area. According to this view, the Gessoso-solfifera Fm. would belong to the MP synthem, and a time equivalent of primary evaporites occurs within the local euxinic shales.

Preliminary bio-magneto-stratigraphic data (Manzi, 2001) pointed out the occurrence of a highly organic-rich, barren horizon, never observed in marginal, "Mediterranean-type" successions. This horizon would represent the deep-water counterpart of the primary evaporites.

The MP synthem can be subdivided into two units (p-ev_1 and p-ev_2, see Roveri et al., 2001; Fig. 4), separated

by a minor unconformity which marks important paleogeographic and structural changes.

The lower unit (p-ev$_1$) only occurs in structural depressions, and bridges the final Messinian gap (Krijgsman, 1999a,b). The p-ev$_1$ unit consists of a basal complex of resedimented evaporites, overlain by a thick, monotonous succession of finely laminated mudstones and siltstones, and containing minor turbiditic sandstone bodies and showing an overall coarsening-and shallowing-upward trend, related to the progressive and rapid basin infill (Tetto fm.); an ash layer, dated at ca. 5.5 My (Odin et al., 1997), represents an exceptional lithostratigraphic marker throughout the whole Apennine foredeep basin, allowing us to recognize the p-ev$_1$ unit across different sub-basins (Bassetti et al., 1994). Sedimentary facies and vertical trends, together with geometric characteristics (the cross-section triangular shape, and stratal convergence towards structural highs, reconstructed through surface and subsurface data), indicate the syntectonic nature of this unit.

The upper unit (p-ev$_2$), is tabular and thickens in structural depressions, but also overlies and seals all the previously uplifted and subaerially exposed areas. This unit consists of a cyclic alternation of coarse and fine-grained tabular lithosomes, arranged in a overall fining-upward trend. The basic cyclicity records the periodical, climatically controlled activation of fluvio-deltaic systems dominated by catastrophic floods (Roveri et al., 1998). 3 to 4 sedimentary cycles are normally observed in the upper unit; a similar, but less evident, cyclicity is observed in the upper part of the p-ev$_1$ unit. The overall fining-upward trend

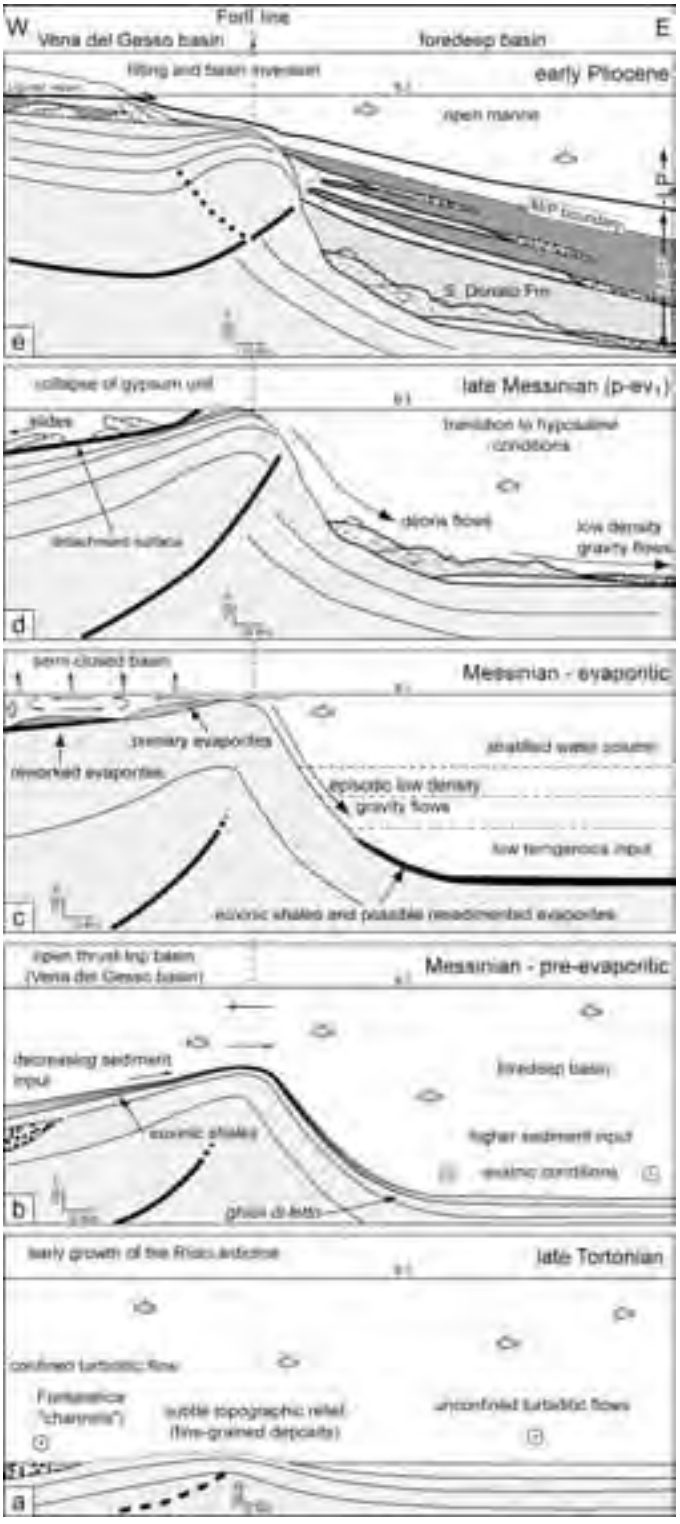

Figure 18 - Evolution of the Riolo anticline during the Upper Tortonian-Lower Pliocene time interval (from Roveri et al., 2003).

suggests a backstepping of fluvio-deltaic systems, possibly related to the progressive basin enlargement. Geological cross-sections clearly show the onlap of this unit against the Forlì structural high, and the progressive upward decrease of thickness and grain-size of the fluvio-deltaic sediments. Paleocurrents and facies changes (Manzi, 1997; Roveri et al., 1998) show that the entry points of fluvio-deltaic systems feeding the eastern Romagna basins (extensively outcropping in the Giaggiolo-Cella syncline – day 4 of the field trip), were located along the Forlì line. Coarse-grained bodies are regularly interbedded with muddy units containing three limestone horizons (*colombacci*). As in the western sector, the uppermost one lies just below the M/P boundary, here marked, as elsewhere in the Apennine foredeep, by a characteristic dark, organic-rich horizon.

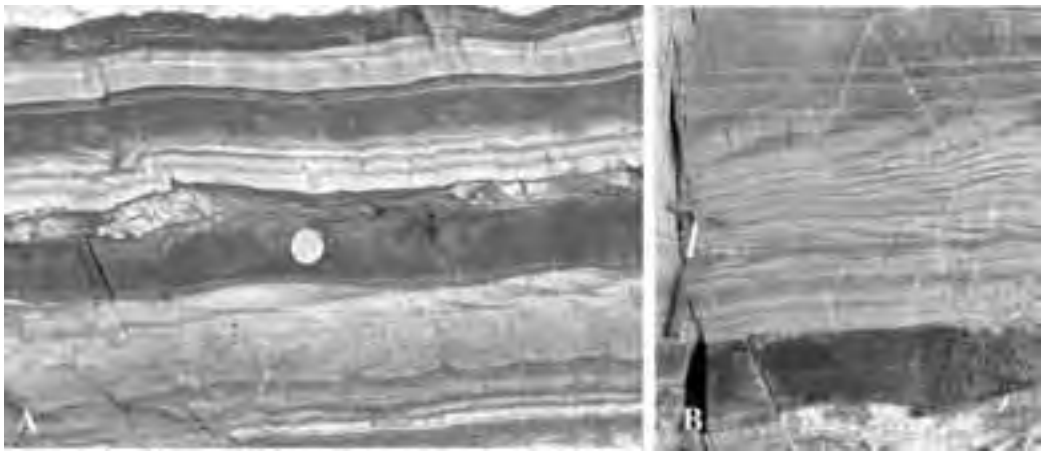

Figure 19 - Graded gypsarenite layers (Fanantello section, stop. 3.3). Each layer is composed by a light -dark couplet related to original grain-size. A) Note load structures at the base of thickest layer and long wavelength climbing ripples at the top of the coarser division. B) thick layer with two climbing ripple divisions showing opposite paleocurrents.

Messinian events and the tectonic evolution of the Apennine foredeep

The comparison and correlation of the western and eastern sectors of the Romagna Apennines (Fig. 7) allow us to reconstruct the sedimentary evolution of the Apennine foredeep basin during the Messinian. The most important feature that clearly arises from field data of this, as well as of the other sectors of the Apennine thrust belt, is the strong control of tectonically-derived topography on the areal distribution and vertical evolution of depositional systems. During the Messinian, an important uplift phase affected the Apennine thrust belt, leading to the closure and fragmentation of the Marnoso-arenacea foredeep basin, to its accretion to the orogenic wedge, and to the development of a new depocenter in a more external position, now buried under the Po Plain. This phase of tectonic deformation led to the emergence of the Apennine backbone, and to the development of an embryonic Apenninic drainage system, as witnessed by the abrupt change in sediment composition, and the dramatic increase of the sedimentation rate. The most impressive fact is the close time and genetic relationship that can be recognized between the tectonic history of the area ,and the main Messinian events. The Mediterranean-type Messinian succession of the western sector developed above, and was delimited by, an uplifting anticline related to the Forlì line (Riolo anticline in Figs. 7 and 16). Seismic data allowed Roveri et al. (2003) to trace this structure in the subsurface, and to reconstruct a single ENE verging arcuate structure plunging to the west, of which the FL represents the eastern lateral ramp (Fig. 17). The continuous uplift of this structure, starting from the Late Tortonian (Fig. 18), was responsible for the observed sedimentary evolution of the area. The first evidence of the growth of the Riolo anticline, was the creation of a small topographic relief elongated parallel to the basin axis, leading to the progressive narrowing of the Marnoso-arenacea basin with consequent lateral confinement of turbiditic flows running from the NW to the SE. The larger volume flows, accelerated by this lateral

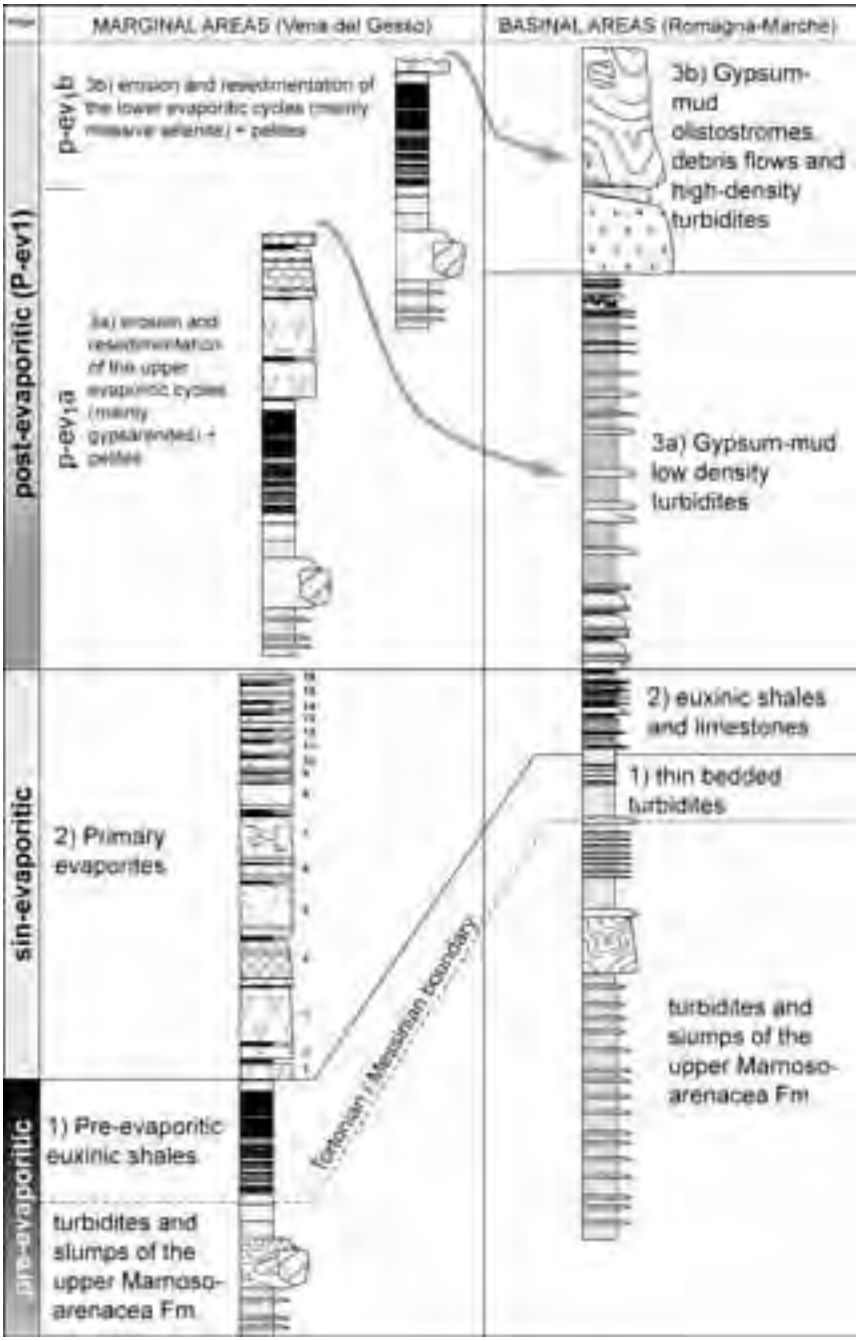

Figure 20 - Genetic and stratigraphic relationships between resedimented and primary evaporites (from Manzi, 2001).

Volume n° 2 - from B16 to B33

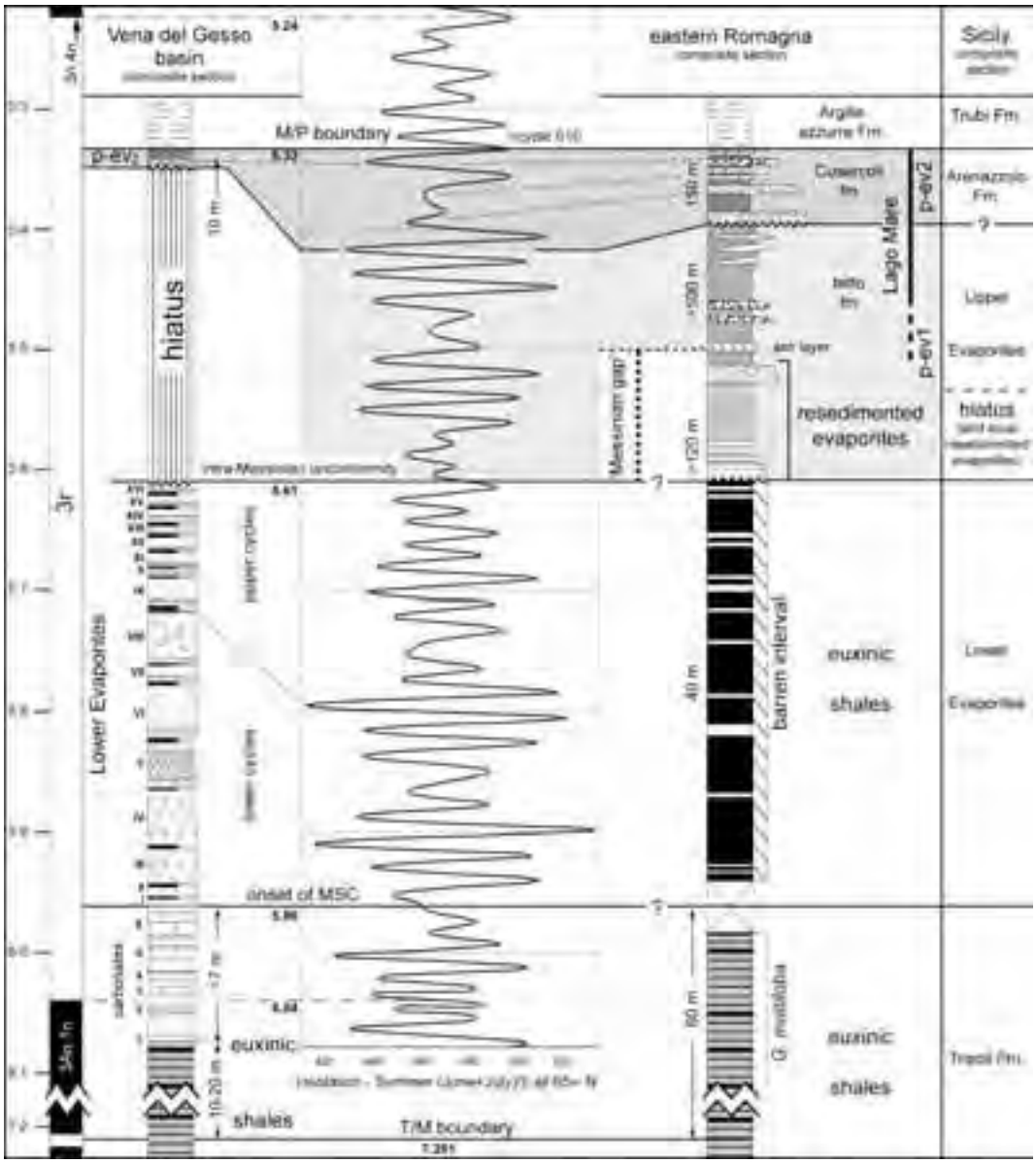

Figure 21 - Correlation of Messinian Apennine foredeep succession with astronomically forced insolation cyclicity. Post-evaporitic deposits show a well-developed cyclic pattern especially in the upper unit (p-ev$_2$).; p-ev$_1$ deposits, having a stronger syntectonic character, show a less-evident cyclicity, especially in the lower part

constriction, increased their erosional power, and cut large-scale erosional features (the Fontanelice "channels"); their sediment load was probably carried further down-basin to feed the Savio turbidite system. The thick sandstone beds of "channel" fills can be considered as lobes formed in a confined basin by smaller volume flows. The anticline growth, along the frontal and lateral ramp, split the foredeep into two different subbasins: an uplifting basin to the west, and a subsiding basin to the north and to the east. The former foredeep basin was gradually cut off from coarse-grained turbiditic sediment input, and a muddy slope developed in both sectors. This tectonically-active slope was characterized by strong

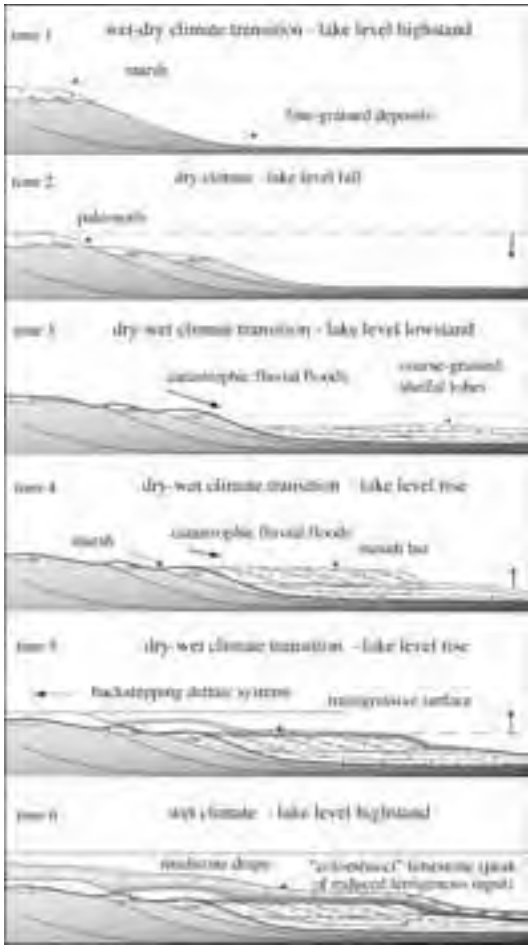

Figure 22 - Ideal evolution of uppermost Lago Mare cyclicity in the Apennine foredeep basins. Modified from Roveri et al. (1998).

instability, leading to huge sediment failures. The deeper and more subsiding character of the eastern sector is demonstrated by the higher thickness of the Tortonian to Lower Messinian succession, and by the higher terrigenous content of the local euxinic shales. Independent evidence for the uplift of the western sector during the Late Tortonian and Early Messinian comes from sediment rates and paleobathymetric reconstruction (Kouvenhowen et al., 1999; Van der Meulen et al., 1999); their combination suggests a sediment rate decrease, and a concurrent shallowing upward trend.

The decrease of sedimentation rate is essentially due to the suppression of the terrigenous component, related to the progressive cut-off of this uplifting area from turbidity currents. During the Messinian, the role of the Riolo anticline is clearly defined. Primary, shallow-water evaporites were deposited only in the western sector within a large, semiclosed wedge-top basin. The longer-term shallowing-upward trend, superposed on the small-scale gypsum cycles, suggests a gradual upward reduction in the amount of accommodation space created. The evaporites are cut by an erosion surface – the intra-Messinian unconformity – of inferred subaerial origin, that can be traced to the SE on the outcropping culmination of the structural high associated with the Forlì line lateral ramp, and to the NE above, the buried anticline crest, which has been revealed by seismic and well data. The unconformity is associated with an angular discordance, and was formed during a paroxysmal phase of tectonic activity. The time elapsed during erosion in marginal uplifting areas, is recorded in topographic depressions by a volume of sediment which corresponds to the lower post-evaporitic unit that occurs in the eastern sector. As a consequence, in the Apennine foredeep basin, a large-scale tectonic pulse stopped primary evaporite deposition, and caused the transition from a hypersaline to hyposaline basin. Deep-water settings never experienced desiccation, and evaporitic sediments were emplaced by gravity flows, forming a thick unit with tabular

Figure 23 - Isotopic composition of colombacci limestones showing the clear evolution toward the quasi-marine values field, suggesting higher water concentration or true incipient connection with ocean waters (from Bassetti et al., submitted).

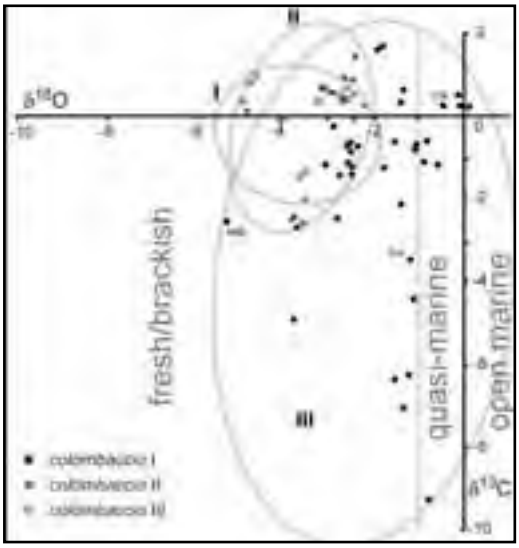

Volume n° 2 - from B16 to B33

geometry and onlap terminations against basin margins.

After the emergence, following the evaporitic phase, the FL structural high was sealed in the latest Messinian,; the Lago Mare deposits, resting above the intra-Messinian unconformity in the western sector, belong to the uppermost p-ev$_2$ unit, as indicated by the occurrence of the colombacci limestones. The basal Pliocene flooding occurred over an almost flat topography developed in a phase of slow and generalized subsidence and basin enlargement, following the intra-Messinian tectonic pulse. This phase lasted the whole Early Pliocene, during which fine-grained, deep-water sediments accumulated throughout the Apennine orogenic wedge. A new important tectonic event occurred at 4.2 My (LP unconformity), marking a significant propagation of the Apennine thrust front towards the Po plain area (Ricci Lucchi, 1986). During this phase, a generalized NE-ward tilting of the western sector led to the present-day structural setting, with the northern culmination of the Riolo anticline buried by a 1500 m thick Plio-Pleistocene cover.

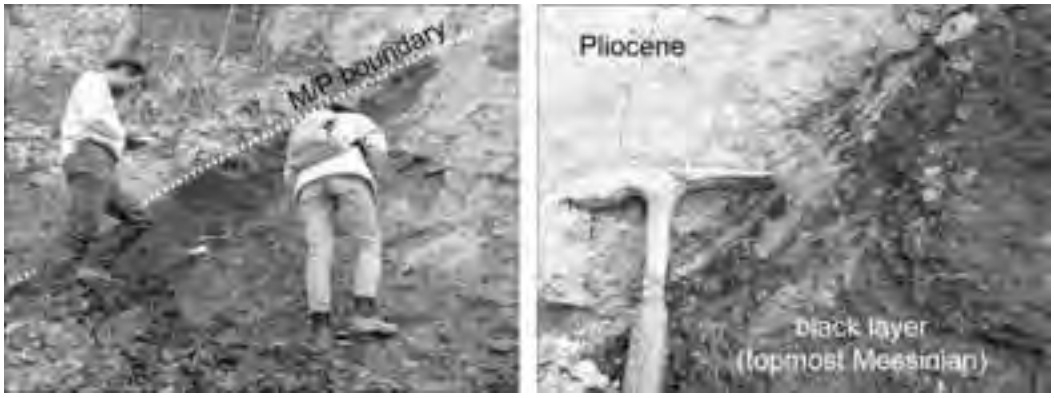

Figure 24 - The characteristic black layerunderlying the sharp transition to open and deep marine conditions at the Miocene/Pliocene boundary. Riccò section (western Emilia Apennines; from Roveri and Manzi, in press).

Hot Messinian topics

In this section, some of the "hottest" Messinian topics are briefly introduced. They derive from data and interpretations presented in this field trip, and should stimulate and focus the discussion around the larger scale implications of the Apennine foredeep Messinian record.

1 - The onset of the MSC

The onset of the evaporitic stage is commonly associated with a sea-level fall whose amplitude is not well-constrained (100 m according to Clauzon et al., 2001). The transition from euxinic shales to selenitic gypsum, observed in the Apennine foredeep marginal successions, is apparently abrupt. However, no reliable paleodepth indicators occur in the upper part of the pre-evaporitic deposits, due to low oxygen concentrations at the sea-bottom. Moreover, the stromatolitic limestones, marking the base of the evaporitic unit, do not necessarily imply a shallow-water origin (i.e. the photic zone). On the other hand, the Lower Evaporites are affected by severe post-depositional deformations, flattening out within the upper part of the euxinic shales, that are characterized by abundant shear planes. The commonly-envisaged purely tectonic origin of such deformations has been recently contested by Manzi (2001) and Roveri et al. (2003). Indeed, the reconstruction of the sedimentary and tectonic evolution of the western sector as essentially related to the uplift history of the Riolo anticline, also provide arguments for the Messinian development of a low-angle W-SW dipping paleoslope, corresponding to the southern, inner flank of the anticline. Renewed uplift during the intra-Messinian tectonic phase could have triggered large-scale gravity failures of the gypsum unit on a detachment surface within the euxinic shales, thus accounting for the observed SW verging thin-skinned deformation. According to the extent of translation along this paleoslope, gypsum is actually superposed to sediments deeper than those above its original substratum. A possible vertical displacement

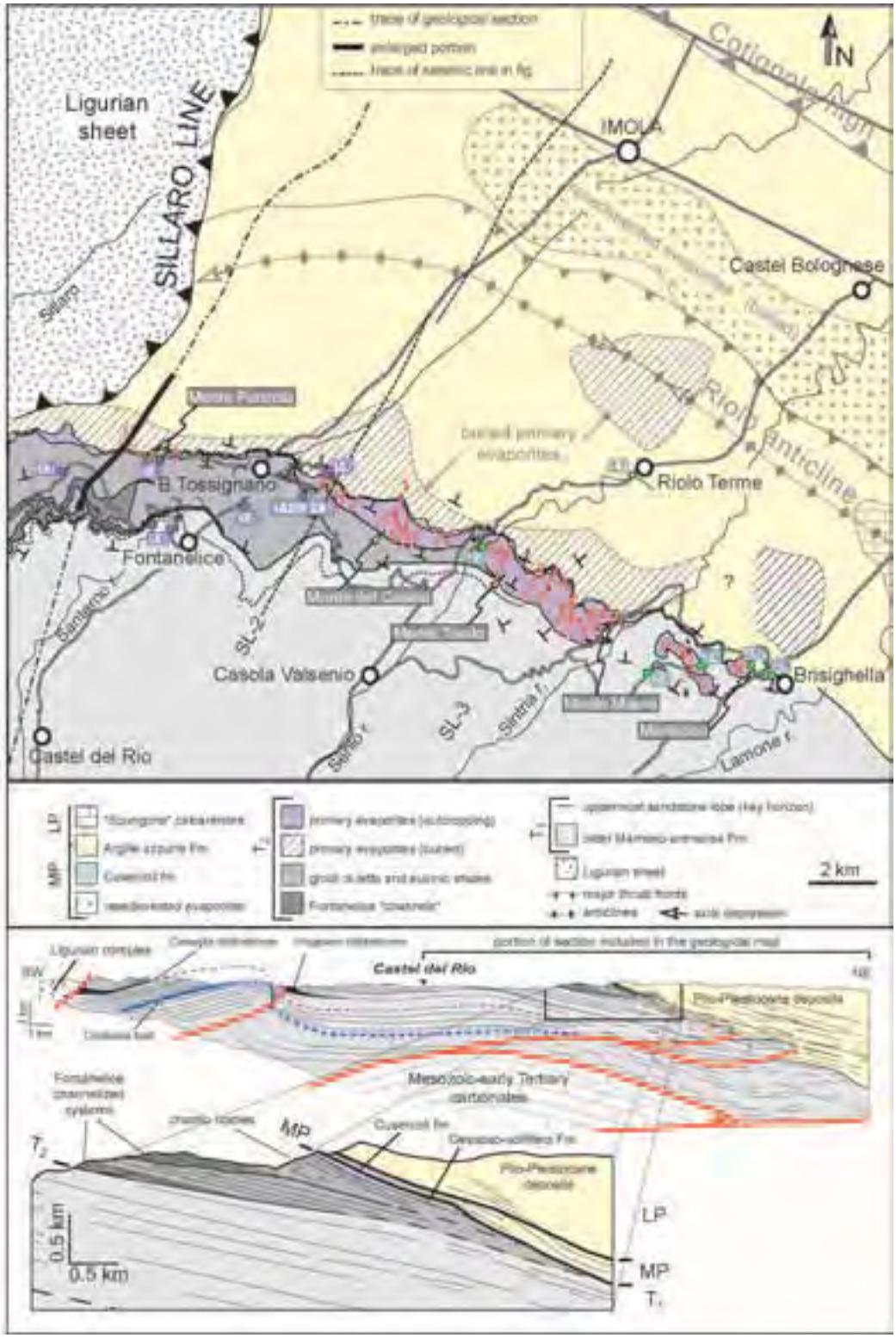

Figure 25 - Geological map of the western sector

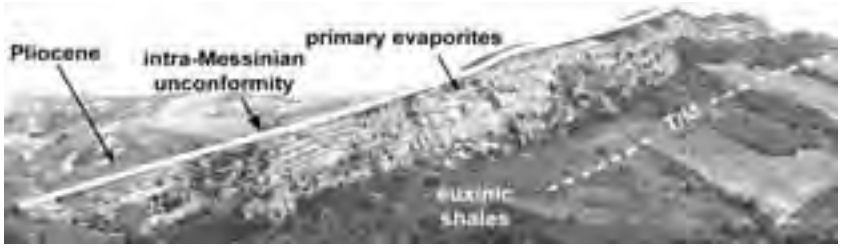

Figure 26 - Stop 1.3. The spectacular Lower Evaporites outcrop (Rio Sgarba sect.), looking eastward from Tossignano.

of 150-200 m has been calculated (Manzi, 2001). As a consequence, the "abrupt" vertical transition from euxinic shales to primary evaporites could be overestimated.

2 - Cyclicity and stacking patterns of Lower Evaporites

Actually, many differences from the above described ideal cycle of primary evaporites can be observed, especially concerning the regular superposition of facies, with decreasing size of selenite crystals (facies sequence 3-4-5) is concerned; in some cases, inverse facies trends or symmetrical rhythms (4-3-4) occur, and their significance has not been fully understood yet. Such anomalous facies sequences have been observed at the same stratigraphic level (i.e. in the same cycle) in other areas (Marecchia valley), suggesting external forcing factors on facies development.

The aggradational stacking pattern of the Lower Evaporites is a common feature across all the Mediterranean geodynamic settings, and necessarily implies a generalized subsidence or a sea-level rise. The latter hypothesis (Clauzon et al., 2001), would imply a larger water exchange with the Atlantic Ocean, as also supported by the evaporite isotopic composition (Flecker and Ellam, 1999). The vertical facies changes observed in the evaporitic cycles of the Apennine foredeep indicate that a longer-term shallowing-upward trend is superposed upon small-scale cycles. This indicates a gradual upward reduction in the rate of space creation, suggesting competition between sea-level rise and tectonic uplift; the latter was possibly heralding the strong intra-Messinian tectonic pulse.

3 - The tectonic vs. eustatic origin of the intra-Messinian unconformity

The transition between the Lower Evaporites, and the Upper Evaporites or Lago Mare stages of the MSC, is marked in all marginal basins of the Mediterranean area by the development of a large erosional surface (the intra-Messinian unconformity), associated with a hiatus of variable amplitude. The origin of this erosional surface is commonly related to an evaporative sea-level fall in excess of 1,000 meters, implying desiccation of the deepest Mediterranean basins. Such a catastrophic event led to the subaerial exposure of Mediterranean continental margins and to a huge fluvial rejuvenation with the incision of deep canyons in front of the largest rivers (for example, in front of the Nile, Rhone; Clauzon, 1973, 1982; Ryan, 1978; Ryan & Cita, 1978).

The attribution of the tectonically-enhanced nature of the intra-Messinian unconformity to a supra-regional deformational phase has been commonly rejected. However, in many basins which developed in different geodynamic settings (the Apennine foredeep, the Tyrrhenian basins, the Tertiary Piedmont Basin, Sicily, the Eastern Mediterranean, the Western Mediterranean), this erosional surface is clearly associated with an angular unconformity.

This suggests an important phase of structural reorganization all along the African-Eurasian collisional margin (Meulenkamp et al., 2000). Duggen et al., (2003) envisaged complex deep-crustal or mantle processes, occurring between 6.3 and 4.8 My, to explain the abrupt changes in magma composition of the Alboràn volcanic belt, and the large uplift (1 km) of the African-Iberian margin required to close the marine connections between the Atlantic and the Mediterranean. In the Apennine foredeep, this unconformity is associated with the most important deformational phase since the Early Miocene, as it marks the emersion of the Apennine chain. The consequences of such paleogeographic changes on climate have not been investigated yet.

4 - Resedimented evaporites: origin and significance

The term clastic evaporites was first used in the late 1960s-early 1970s to indicate some "gypsiferous sandstones" cropping out in the Laga basin (the

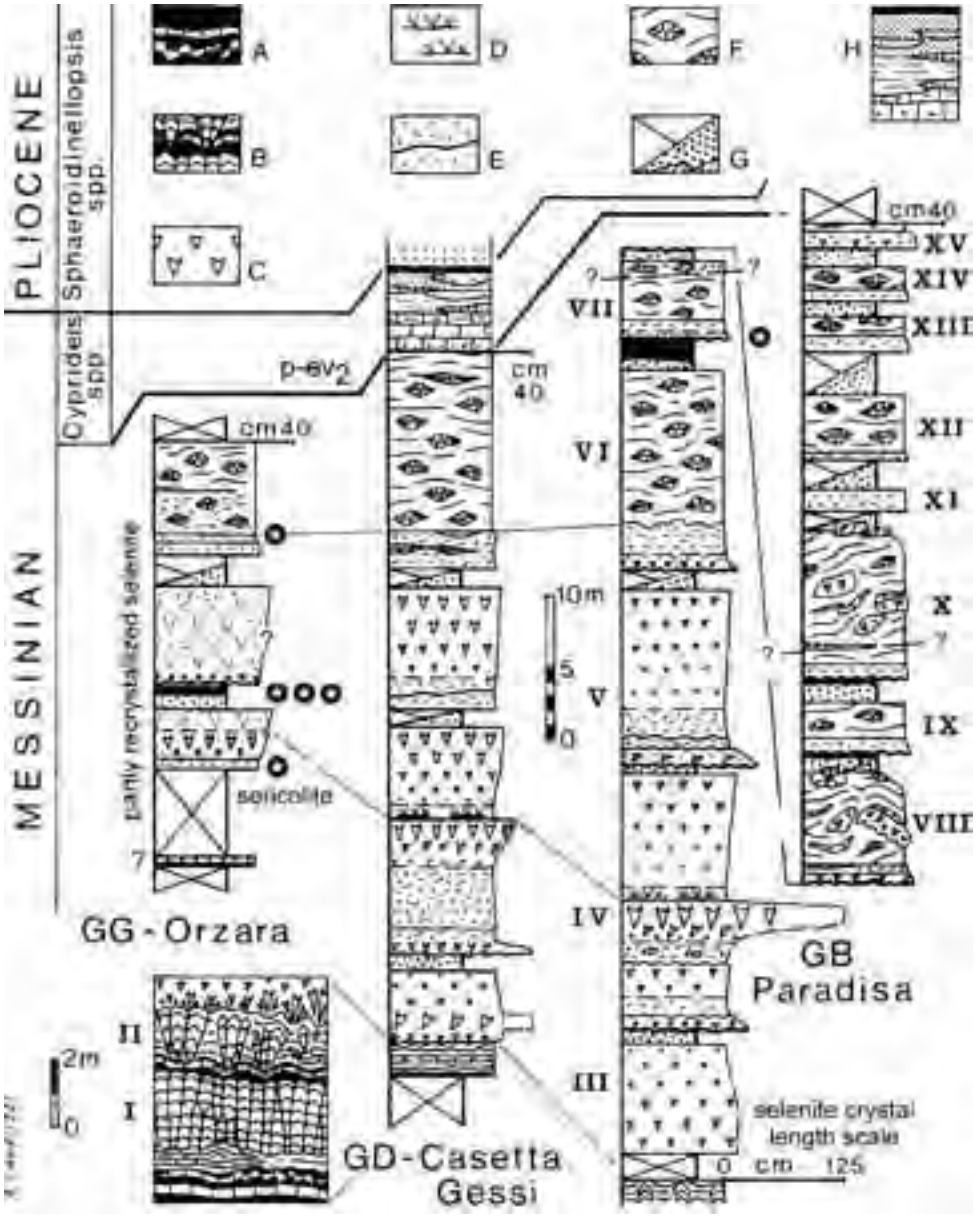

Figure 27 - Stratigraphic columns of the Vena del Gesso in the western side of the Santerno Valley (after Landuzzi, 1985): A= euxinic shales and stromatolitic limestones; B= euxinic shales, calc-gypsum laminites and gypsified stromatolites (facies 1-2); C= massive autochthonous selenite (facies 3); D= interbedded autochthonous and reworked selenite (facies 4); E= entirely reworked selenite (facies 4?); F= clastic, acicular and nodular gypsum (facies 5); G= chaotic gypsum in a clayey matrix (facies 6); H = post-evaporite deposits (see details in Figure28).

southern depocenter of the Messinian Apennine foredeep). These deposits were often associated with the "balatino gypsum", a well-laminated alternation of gypsum and bituminous shales, usually interpreted as a deep-water primary evaporitic facies. The occurrence within the "balatino gypsum" of sedimentary structures, interpretable as megaripples (Fanantello River, Schreiber, 1973; see stop 3.3; Fig. 19), was

Volume n° 2 - from B16 to B33

not adequately taken into consideration. Actually, due to the recognition of very indicative sedimentary structures (load casts, fluid-escape structures, bed gradation, cross-lamination, and tractions-plus-fallout structures), almost all the "balatino" gypsum facies of the Apennines has clearly to be re-interpreted as deposited from turbidity currents. The "balatino" facies is part of a wide spectrum of mass-flow deposits, ranging from olistostromes to low-density turbidity currents. As a matter of fact, this class of deposits should be dealt with as the siliciclastic gravity flow deposits are. However, due to the strong diagenetic effects typically undergone by evaporitic rocks, their study is a very difficult task.

One basic problem is the definition of original grain-size of clastic evaporites; in Manzi et al. (submitted), a siliciclastic-derived relationship between grain size and sedimentary structures is proposed in order to indirectly define this important parameter in diagenetically-transformed deposits.

On the basis of this approach, several facies and facies associations have been recognized. Their areal distribution is in good agreement with the hypothesis of the removal of primary evaporites which formed in shallow thrust-top basins through large submarine collapses and glides; and these collapses and glides are assumed to have been triggered by tectonic-induced gravitational instability, and were transformed down current into high and low-density turbidity currents. This is clearly evident when considering facies distribution along a NW-SE transect from the Forlì Line to the eastern Romagna and northern Marche basin. Of course, local tectonically-induced topography provides further complications to the general picture.

Figure 28 - Air photo of the Vena del Gesso in the western side of the Santerno Valley (M. Astorri). Normal faults and very small reverse faults offset the evaporite cycles, and are sealed by post-evaporite Messinian deposits, which mark a spectacular angular unconformity. The rotational offset of faulted blocks suggests gravity-driven normal faulting, gliding and thrusting on a shallow detachment level within the euxinic shales. Transport was to the S-SW.

Most of the evaporites of the Apennine foredeep are actually clastic deposits derived from the dismantling of primary, *in situ* evaporites, and resedimented through gravity processes into relatively deep waters, below the wave base (Parea and Ricci Lucchi, 1972; Ricci Lucchi, 1973; Manzi, 2001; Roveri et al., 2001; Manzi et al., submitted). Despite their common occurrence, they have been virtually ignored until recent times. Based on an integrated sedimentological, petrographic and geochemical study, Manzi et al. (submitted), have proposed a new facies classification, and a genetic model for resedimented evaporates, which implies a close similarity with siliciclastic turbidites. This sedimentological interpretation is strictly linked with the geodynamic model, which provides some constraints for the modalities of gypsum detritus production, and the definition of trigger mechanisms for the initiation of flow.

The general poor-to-absent terrigenous component in the resedimented evaporite unit could suggest a genesis from submarine collapses. Fluvial floods can be thus discarded, also considering the paleogeographic setting of the Messinian. Resedimented evaporites were accumulated at the very beginning of the intra-Messinian tectonic phase which led to the first emersion of the Apennine chain. A land area with a relatively well-developed fluvial drainage only formed at the end of this uplift phase, as witnessed by the composition of terrigenous sediments of the p-ev$_1$ and p-ev$_2$ units. This is also suggested by the vertical facies sequences observed in the resedimented evaporite unit; a clear bipartition very often occurs, with a lower part made up of well-stratified, fine-grained deposits, and an upper part made up of disorganized, very coarse clastites, dominated by slumping and olistostromes, often containing large blocks of lithified primary selenite.

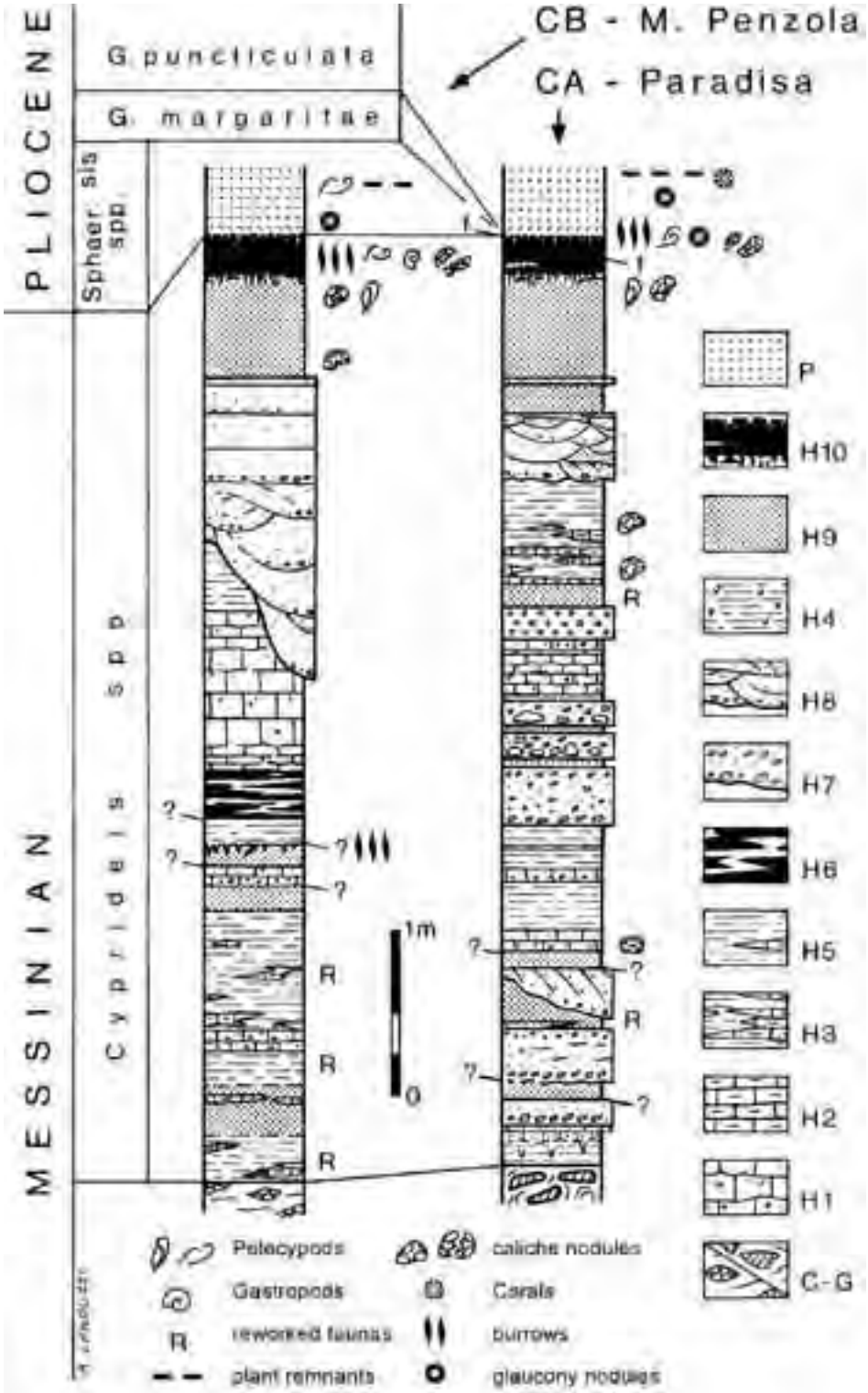

Figure 29 - Stratigraphic columns of the Colombacci fm (upper Messinian p-ev2 unit) in the western side of the Santerno Valley (after Landuzzi, 1985): C-G = GS facies 5-6 (see Figure 27); H1 = limestone breccia with gypsum moulds; H2 = fine-grained clastic limestone; H3 = "varve"-like silty clays with fine-grained limestone lenses; H4 = laminated silty clays; H5 = variegate green and yellow clays; H6 = variegate green and red clays; H7 = poorly sorted calcareous conglomerates in small channel bodies; H8 = festoon-bedded sandstones in small channel bodies; H9 = fossil-rich mudstones; H10 = dark organic-rich pebbly clays; P = Lower Pliocene marine clays (Argille Azzurre Fm).

Volume n° 2 - from B16 to B33

This vertical organization could well reflect a sort of "progradation" of the system related to the ongoing tectonic deformation; however, we believe that it rather records the progressive uplift and consequent exhumation and denudation of primary evaporitic units formed above or around structural highs (Fig. 20). According to this view, basal fine-grained resedimented evaporites could derive from the erosion of the thinner-bedded, mainly reworked, and unlithified uppermost cycles. The subsequent erosion of the early-cemented, thicker-bedded, and coarser-grained primary evaporites lower cycles could produce olistostromes and debris flows. As a consequence, a sort of "inverted stratigraphy" is recorded by the resedimented evaporitic complex, which could follow up with the muddy deposits of the p-ev1 unit deriving from the euxinic shales and underlying Upper Tortonian slope mudstones. Resedimented evaporites could be a common feature in other Messinian basins of the Mediterranean area. Their correct recognition would represent a fundamental step for a better comprehension of the Messinian paleogeography and environmental changes. Of course, the recognition of other subaqueously-deposited clastic evaporites, associated with the intra-Messinian unconformity, would put into discussion the true extent of the Mediterranean deep desiccation.

5 - Gypsum diagenetic transformation and origin of sulphur mineralization

The Gessoso-solfifera Fm. of the Romagna and Marche Apennine contains sulfur deposits that were mined from Roman times until the 1960s (Scicli, 1972). The sulfur mineralization consists of discontinuous, thin lenses, mostly restricted to the base of the evaporite formation, and particularly at the contact of the sulfate layers with the basal organic-rich shales (euxinic shales). In some areas (Perticara), the mineralization is also present in higher stratigraphic levels, in sulfate layers having particularly organic-rich shale interbeds. Sulfur-limestone layers appear to replace sulfate layers up to a few meters thick, but generally less than 1 m. The sulfur mean reach up to 40 %, but is generally around 12 %. The sulfur mineralization shows mostly nodular and breccia-veins textures, and less common ribbon and massive textures. Native sulfur is associated with calcite, celestite, barite, bitumen, and emissions of sulfuric acid and methane.

These characteristics indicate that elemental sulfur was formed by sulfate reduction. Characteristics and timing of sulfur formation are unknown, and detailed textural, petrographic, and geochemical studies are at their initial stage. One of the most significant aspects is that economically important sulfur concentrations are present only in the clastic sulfate evaporites of the Romagna-Marche area, which were transformed into anhydrite at burial diagenesis, and not in the unaffected autochthonous selenite of the Vena del Gesso Basin. This suggests that early synsedimentary formation was negligible, and that most sulfur originated through bacterial sulfate reduction, triggered by hydrocarbons, migrated from the associated organic-rich shales and marls. A thermochemical sulfate reduction origin for the sulfur can be excluded because the evaporite formation was buried at a relatively shallow depth (~ 500-1000 m). Most sulfur deposition possibly occurred through the oxidation of sulfuric acid by dissolved oxygen carried by groundwater during the rehydration of anhydrite.

6 - The closure of the 'Messinian gap', and the onset of the Lago Mare event

In Messinian Mediterranean successions, the common stratigraphic gap between 5.50 and ~5.60 Ma is usually associated with the desiccation of deeper basins (Krijgsman et al., 1999b; Fig. 3). This gap does not allow a full understanding of the most important Messinian events: that is, the switch from hypersaline to hyposaline waters leading to the Lago Mare stage. The causes, modality, and timing of such a dramatic paleogeographic change are obscure; the most commonly-accepted explanation is the capture of Paratethyan waters by a lowered Mediterranean base-level.

As stated above, in the Apennine foredeep, this gap only occurs above uplifted areas (e.g. the western sector of the Romagna Apennines); in deeper, subsiding basins, the record is continuous, and the hiatus was bridged by the lower part of the p-ev$_1$ unit, which is made up of resedimented evaporites, and by a thick pile of terrigenous, fine-grained sediments (Figs. 5, 21). This means that the Apennine successions have recorded such events, and for this reason, a detailed study of this interval is being carried out by a multidisciplinary research group. Preliminary observations and analysis carried out on a continuous core (Campea well, stop 4.1) have led to the recognition of the typical Lago Mare ostracod, and pollen and dynoflagellate assemblages immediately above the resedimented evaporite complex. This means that the typical Lago Mare hydrology was already established immediately after or during the deposition of the resedimented evaporite complex.

Cores have also pointed out the occurrence of well-defined organic-rich horizons, which are being studied to assess their paleoenvironmental meaning, and their potential as regional lithostratigraphic markers.

7 - High-frequency Milankovitch-type climatic cyclicity in the Lago Mare deposits

Like pre-evaporitic deposits and lower Evaporites, the Lago Mare successions show a fairly well-developed cyclic organization that can be used to establish a high-resolution stratigraphy, otherwise impossible to obtain in a non-marine unit encompassing a very short time span. According to Krijgsman et al. (1999a-b), the Lago Mare stage lasted more or less 270 Ky, 90 of them recorded by deep Mediterranean evaporites and by the basal p-ev$_1$ unit of the Apennine foredeep (Fig. 21). The bipartite character is an easily-recognizable, but usually overlooked, feature of the Lago Mare successions, not only in the Apennine foredeep, but also in many other basins (see for example the Upper Evaporites and Arenazzolo Fm. of Sicily). Only the upper part of the lower unit, locally characterized by the deposition of shallow-water, sabkha-like evaporites (Sicily), is there a well-developed cyclical lithological pattern.

In the Apennine foredeep basins, up to five cycles, defined on the basis of the regular alternation of coarse and fine-grained lithosomes, can be recognized above the ash layer, and can provide an independent, even if not particularly accurate, time calibration.

The upper p-ev$_2$ unit, which is widely recognized on a Mediterranean scale, is characterized by a well-developed, high-frequency cyclical pattern superimposed upon an overall transgressive trend. These two characteristics represent good criteria for high-resolution long-range correlations; 3 to 4 main cycles have been traced from shallow to deep-water successions of the Apennine foredeep (Roveri et al., 1998; Ricci Lucchi et al., 2002), 4 cycles have been recognized in the uppermost Messinian deposits at Cyprus (Rouchy et al., 2001), 3-4 cycles in the uppermost Messinian Nile Delta deposits (Abu-Madi Fm., Dalla et al., 1997), 4 cycles in the fluvio-deltaic deposits of the Tertiary Piedmont Basin (Ghibaudo et al., 1985); 3 to 4 cycles are reported from a thick terrigenous Lago Mare succession unconformably overlying the Lower Evaporites in the Corvillo basin (Sicily; Keogh and Butler, 1999). As a consequence, a total of 8/9 cycles can be recognized in the 180 ky interval between the ash-layer and the Miocene/Pliocene boundary.

This is consistent with a precessionally-driven climatic origin of small-scale sedimentary cycles, as occurred during the pre-evaporitic and evaporitic stages. By this way, the p-ev$_2$ unit would span a very short time interval of 60-80 Ky, and a tentative correlation of its small-scale sedimentary cycles with the insolation curve is shown in Fig. 21. According to Roveri et al. (1998), the basic lithological cyclicity given by the vertical repetition of sharp-based coarse-to-fine-grained couplets, observed in both shallow, marginal basins developed above the orogenic wedge, as well as in the foredeep depocenters, would reflect the periodic activation of catastrophic flood-dominated fluvial systems carrying coarse sediments into the Lago Mare during dry intervals, or at the transition between dry and wet periods (Fig. 22). During these phases (Fig. 5), small forestepping deltaic systems formed in shallow basins with low gradient shelves; in basins with reduced or steep shelves, fluvial floods could develop hyperpycnal flows which were able to carry their sediment load down-basin, forming small turbidite systems of "low-efficiency" (*sensu* Mutti et al., 1999). Water carried with sediments to the basin contributed to a rapid rise in the base-level and caused, together with a concomitant climate change towards wetter conditions, the de-activation of flood-dominated deltaic systems, and their landward migration. During wet phases, the base level reached its maximum, but sediment input was drastically lowered for both the reduction of the catchment area, and the possibly lower erosion rate which was due to the increased vegetation cover. In this phase only fine-grained, thinly-laminated mudstones accumulated in the basin. In some places, the rhythmic alternations of light and dark mudstone horizons give a typical banded aspect to the deposit, probably representing a distal lacustrine facies. Thin-bedded, finely-laminated limestone horizons ("colombacci") are usually found in the upper half of the cycles associated with mudstone deposits. According to Bassetti et al. (submitted - see topic 8), they derive from the inorganic precipitation of micrite-size crystals in a relatively deep-water environment which was possibly anoxic and related to permanent water mass stratification events during periods of lake level maxima, and associated peaks of reduced terrigenous input. However, the concomitant occurrence, in the same part of the cycles, of dark, organic-rich clay horizons, rich in specialized Mollusk assemblages (*Congerie*) and interpreted as palustrine deposits, suggests a far more complicated stratigraphic architecture and more complicated evolutionary trends, as tentatively illustrated in the model of Fig. 22. Palustrine horizons, found

Volume n° 2 - from B16 to B33

at different levels within mudstone units, are not compatible with a simple deepening upward cycle. According to their position within each cycle, the fine-grained lithosome could actually be subdivided into a lower transgressive, and an upper regressive unit, the latter topped by a subaerial erosional surface produced during base level fall in dry phases. In other words, a regressive hemicycle could be preserved in the uppermost part of the cycles. However, neither prograding coastal deposits, nor clear evidence of paleosoils, have been clearly recognized so far.

An exception is represented by the uppermost cycle (Roveri et al., unpublished data), where the dark layer marking the Miocene/Pliocene boundary, locally overlies an irregular surface with weak pedogenetic traces (Botteghino section in the Giaggiolo-Cella syncline).

However, the possibly very short time spans encompassed by subaerial exposure phases within each cycle, might not have been sufficient for paleosoil development; moreover, the erosion produced by catastrophic fluvial floods would have removed any trace. According to the model of Fig. 22, palustrine horizons could develop above the subaerial exposure surfaces during initial base-level rises; the *colombacci* limestones would represent a sort of condensed section marking the maximum retreat of clastic sediment sources. Detailed studies of these deposits is being carried out in order to understand better their organization and paleoenvironmental meaning; however, they appear to be analogous with the Lago Mare cycles from the topmost Messinian succession, which have been recently described in Cyprus (Rouchy et al., 2001).

8 - Origin of the colombacci limestones

As previously reported, the colombacci limestones are a typical lithofacies closely associated with the basinal mudstones of the p-ev$_2$ unit. They are abiotic, and formed as inorganic precipitates from the surface waters of the Lago Mare. According to Bassetti et al. (submitted), their precipitation required the periodic supersaturation of the epilimnion, possibly driven by climatically-induced events of lake-water stratification. This carbonate lithofacies is quite common in the Lago Mare deposits of the Mediterranean basins; their geochemical composition provides good elements to derive the hydrological structure of the basins and their degree of connection. As a general rule, isotopic compositions show negative ^{18}O values, indicating freshwater conditions, or at least a high degree of water dilution. The high-resolution stratigraphic model of the Apennine foredeep made it possible to compare isotopic compositions of colombacci limestones occurring in each cycle in different sub-basins, and hence to verify possible areal gradients and stratigraphic trends. The results (Fig. 23; Bassetti et al., submitted), show that the two lower horizons have homogenous, strongly negative isotopic values; the uppermost horizon has less negative values, almost falling in the "normal marine" range. This could either indicate a strong concentration due to evaporation in restricted basins or, on the contrary, a true connection with the ocean. The latter would be in good agreement with the aggradational stacking pattern of the p-ev$_2$ unit, suggesting a overall "transgressive" trend heralding the Zanclean flooding.

9 - Marine incursions during the Lago Mare stage?

Besides the above considerations based on the isotopic composition of limestone horizons, occasional marine incursions in the Lago Mare deposits have been reported from different Mediterranean basins, especially on the basis of nannoplancton assemblages (Blanc-Valleron et al., 1998; Pierre et al., 1998; Spezzaferri et al., 1998; Snel et al., 2001). Isotopic composition of the typical faunal associations (Keogh and Butler, 1999), suggest the possibility that during the final part of this stage, a large water body was present in the Mediterranean. As far as these notes were written, no clear indications of marine incursions have been found in the Apennine foredeep Lago Mare successions. However, the commonly observed foraminifera associations made up of small-size, dwarfed specimens need to be thoroughly investigated.

10 - The Mio/Pliocene boundary

The Mio/Pliocene boundary, marking the sudden return to fully marine conditions, is a synchronous event at a Mediterranean scale (Iaccarino et al., 1999). A peculiarly interesting feature is that the direct superposition of MPl1 deposits above rocks older than the uppermost Messinian, has never been reported. MPl1 sediments are always associated with Messinian Lago Mare deposits, as part of a longer-term transgressive sequence. This is particularly clear in the Apennine foredeep, where such a transition occurs in a phase of tectonic quiescence and generalized subsidence, that probably led to the almost complete submersion of the Apennine backbone, previously emerged with the intra-Messinian uplift. Significantly,

in successions deposited around topographic highs, and characterized by the permanent activation of fan-delta systems, the Miocene/Pliocene transition appears to be very gradual and such a boundary becomes very difficult to recognize (Roveri and Gennari, unpublished data). Elsewhere, a black, organic-rich layer always underlies the lowest deep-marine MPl1 sediments (Fig. 24). Its nature and significance are not clear, and its systematic study is currently being carried out. As previously reported (topic 7), in some cases, this organic-rich horizon seems to be associated with a slightly erosional surface and weak paleosoil traces.

According to the above-mentioned possible occurrence at the end of the Messinian of a large Mediterranean non-marine water body, and a higher degree of connection between the different sub-basins, the Miocene/Pliocene transition would be rather explained by a sudden hydrologic change associated with a bathymetric change of lower amplitude than usually thought. This would point to the Zanclean flooding being less catastrophic in character.

Field trip itinerary

Introduction to Days 1 and 2

These two days will be spent in an area between the Sillaro and the Lamone valleys (Fig 25). The Santerno Valley, that will be visited during day 1, surely offers one of the most continuous and spectacular Neogene sections of the Northern Apennines, and is particularly famous for the outcrops of the Miocene Marnoso-arenacea Fm, described in great detail in classical papers by Franco Ricci Lucchi and his co-workers in the late 1960s and 1970s. The local stratigraphic succession that can be observed spans in age from Lower Serravallian to Pliocene. The Marnoso-arenacea Formation is overlain by the Messinian evaporites which, in turn, are unconformably overlain by uppermost Messinian continental deposits and marine Pliocene-Pleistocene strata. The geology of the Santerno valley is relatively simple at the surface, where strata form a regular homoclinal, gently dipping to the northeast, i.e. down the valley. Moving upstream from Imola, we drop down into progressively older stratigraphic levels. A packet of vertical to slightly overturned strata interrupts this regular bedding attitude at Coniale; these beds represent the northern limb of the ramp anticline associated with the Mt. Castellaccio thrust, a tectonic feature elongate in a NW-SE direction, that can be traced as far as the Savio valley. In the Santerno valley, the core of the Coniale anticline is where the oldest stratigraphic level of the Marnoso-arenacea Fm is exposed. Further upstream, between S. Pellegrino and Firenzuola, the sand-rich Firenzuola system turbidites crop out in the southern flank of the Coniale anticline.

DAY 1

Stop 1.1:

The reception center of the Vena del Gesso Natural Park, Tossignano. Depending on time availability and weather conditions, this optional stop will be devoted to visiting a small museum exhibiting materials about nature, geology, mining activities, history, and country life in the unusual environment of the Vena del Gesso.

Stop 1.2:

Rocca di Tossignano. The ruins of the medieval castle on the hilltop are a wonderful place for a panoramic view over the Santerno valley and the Apennine foothills monocline (see cover photo and Fig. 26). From SW to NE, the geologist can visually explore up-section the following stratigraphic units, whose details will be dealt with in the next stops:

- Marnoso-arenacea Fm, Fontanelice member: coarse sandstone and conglomerate bodies, composed of multiple or individual “channel” fills.

- Marnoso-arenacea Fm., “ghioli di letto” unit: fine-grained, thin-bedded turbidites and marls in an overall thinning- and fining-upward trend.
- Marnoso-arenacea Fm, “euxinic shales” unit: marls embedding cyclic intercalations of bituminous clays. The Tortonian-Messinian boundary is situated about 60 m below the unit top.
- Gessoso-solfifera Fm: it is composed of up to 16 evaporite cycles, subdivided into 2 “basal” ones (not visible), 3 “major” ones (grey selenite), a very thick 6th one (grey selenite and white clastic gypsum), and up to 10 “minor” ones (mostly white clastic gypsum). All 16 cycles crop out only in the eastern side of the Santerno valley (Rio Sgarba quarry, stop 1.4). In the western valley side (Fig. 27), a maximum of 15 cycles is found in the old Paradisa quarry, while 7 cycles crop out at Mt. Penzola, and only 4 ones crop out at Orzara. Near the Santerno river bed, this W-ward reduction of the evaporite succession is clearly explained by a Upper Messinian angular unconformity (Fig. 27), while further to the W, a non-depositional hiatus is also possible. This alternative explanation would be

in agreement with the overall W-ward thinning of the individual evaporite cycles from the Senio valley to the Sillaro valley (Fig. 26).
- Colombacci fm: a hard-to-see horizon of continental Upper Messinian deposits (p-ev$_2$ sequence), which unconformably cover the Gessoso-solfifera Fm and the pre-evaporite shales. Thickness and facies of this fm are controlled by structural highs and lows of the evaporite unit (Fig. 28). For instance, conglomerates and sandstone pockets (facies H7-H8 in Fig. 29) are better represented within structural depressions.
- Argille Azzurre Fm: marine silty clays of Lower Pliocene age. Close to the western divide of the Santerno Valley, clays embed olistostromes and thick bodies of resedimented conglomerates, fed by epi-Ligurian fan-deltas. The well-stratified setting of all Pliocene units is clearly reflected in the landscape morphology (cover photo; Fig. 28).

Stop 1.3:

Tossignano, Resistance (II World War) Memorial Park. This panoramic view covers the GS from the Riva San Biagio cliff (Fig. 26), to the Rio Sgarba quarry. Basal, major, and minor cycles can be easily distinguished and correlated. Two slump horizons embedded in the 8th and 10th evaporite cycles can be used as additional marker beds. The provenance of those slumps is still unknown, but might be an important constraint to the evolution of the Riolo Terme high (Fig. 25). Evaporites are offset by Upper Messinian normal faults belonging to a *Graben* structure symmetrical to the bedding planes (Fig. 30). Perhaps those normal faults can be associated with gravity-failure structures, like those documented on the other side of the Santerno valley.
Topics: 2.

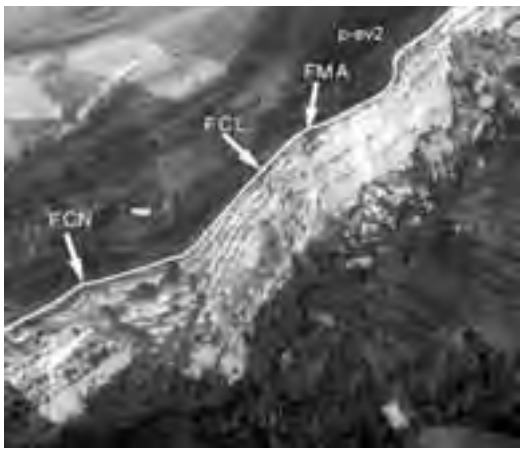

Figure 30 - Air photo of the Vena del Gesso in the eastern side of the Santerno Valley (M. Astorri). Longitudinal (FCN, FMA) and transverse (FCL) normal faults offset the evaporite cycles, and are sealed by post-evaporite Messinian deposits (p-ev2).

Stop 1.4:

Road Tossignano - Borgo Tossignano – Codrignano; deviations to the abandoned quarry in the Rio Sgarba valley, and to the old quarry at Paradisa, on the left bank of the Santerno river. Both sites were deeply investigated when the model of Vai and Ricci Lucchi (1973) was elaborated. The peculiar facies architecture of the modal cycle can be assessed in detail, starting from the 6th cycle, which is the first and thickest example of a complete facies sequence. Smaller scale discrepancies with the basic model represent an interesting subject for debate. For instance, the complex and anomalous crystal size variation in the 3rd, 4th and 5th cycle (Fig. 27), where reverse gradation, dissolution surfaces (Fig. 14 c), and reworked selenite intervals are common. These intra-cycle features, possibly related to brine dilution episodes, have the same impressive correlation potential as the entire modal cycles. Indeed, they can be traced throughout the para-autochthonous Vena del Gesso basin, and from it to the semi-allochthonous evaporite basin of the Marecchia-Conca area (Montebello, Gesso, Sassofeltrio). Another basin-scale problem is represented by the sharp and strongly irregular erosion surface which marks the onset of facies 5 in the 6th cycle. Some of the possible large-scale factors controlling evaporite deposition are summarized in the "hot Messinian topics" chapter.
Topics: 2, 7.

Stop 1.5:

Road Borgo Tossignano - Fontanelice, Molino Campola. A panoramic view from the Santerno river bed towards the western side of the valley allows the framing of a 50-60 m thick intraformational slump within the fine-grained closure facies of the MA (Fig. 31). The inferred slumping direction to the S-SW can be related to the Late Tortonian nucleation of the Riolo Terme high (Fig. 25).
Topics: 2.

Stop 1.6:

Road Fontanelice – Gesso. Other panoramic views illustrate the closure facies and the earliest deformation features of the MA clastic wedge. The uppermost "channel" body of the Fontanelice

member (Figs. 9, 10), the already described slump and the overall thinning- and fining-upward trend, are coherent indications of foredeep fragmentation and basin narrowing.
Topics: 1, 2.

Stop 1.7:

Pieve di Gesso and Sassatello valley. A panoramic view on the so-called "Sillaro line" portraits the synsedimentary overthrust of the Liguride nappe in Messinian times (Fig. 32). Olistostromes coming from the Liguride and epi-Ligurian units have been continuously forerunning the nappe advancement. Many of them were tectonically incorporated in the nappe itself, while others were embedded in the autochthon succession. An example of the second type is the Upper Messinian Sassatello olistostrome, enclosed in the para-autochthonous p-ev$_2$ unit. Its composition is characterized by Lower-Middle Miocene marls and typical Messinian carbonates, such as pre-evaporite and evaporite-derived limestones. A closer inspection of the olistostrome and the local Gessoso-solfifera Fm, gives us the opportunity to discuss the diagenetic transformations of primary evaporites.
Topics: 1, 2, 5.

Stop 1.8:

The "Mt. Penzola walk" We walk along the Santerno – Sellustra watershed from Mt. la Pieve to Mt. Penzola and Debolezza, then we go down to Casetta Gessi, and reach the nearest bridge on the Santerno River. (Fig. 28) The main subjects that are dealt with

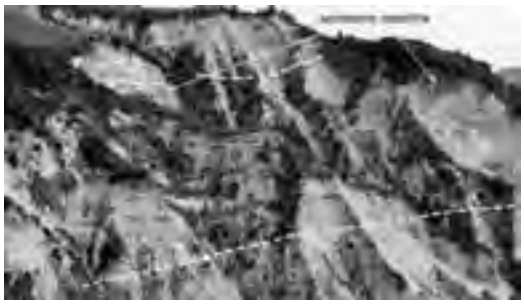

Figure 31 - Closure facies of the Marnoso-arenacea Fm in the western side of the Santerno Valley: two sandstone olistoliths mark a slump horizon in a fining-upward succession of thin-bedded turbidites. Local slumping transport was possibly to the S-SW.

are the Lower Pliocene clays and conglomerates, the angular unconformities in the post-evaporite p-ev$_2$ sequence, and the Late Messinian tectonics. The most attractive features of this itinerary are the M. Penzola thrust (Fig. 33), and a short but complete section of the Colombacci fm (Fig. 34, Fig. 29), featuring a very good outcrop of the Miocene/Pliocene boundary. Discussion is expected on the role of gravity vs. tectonics in the cortical deformation style of the evaporite unit.
Topics: 1, 2.

DAY 2

Stop 2.1:

Visit to the reception center of the Vena del Gesso Natural Park, Riolo Terme. This is another optional

Figure 32 - The Liguride nappe thrusting over the western Romagna para-autochthon: Messinian pre-evaporite (MA), evaporite(GS) and post-evaporite units are truncated atop by the overthrust surface, a gentle ramp dipping to the W. Olistostromes fed by Liguride and epi-Ligurian units occur both above and below the tectonic contact. Near Sassatello, a peculiar Messinian olistostrome is embedded in the p-ev2 unit of the para-autochthon.

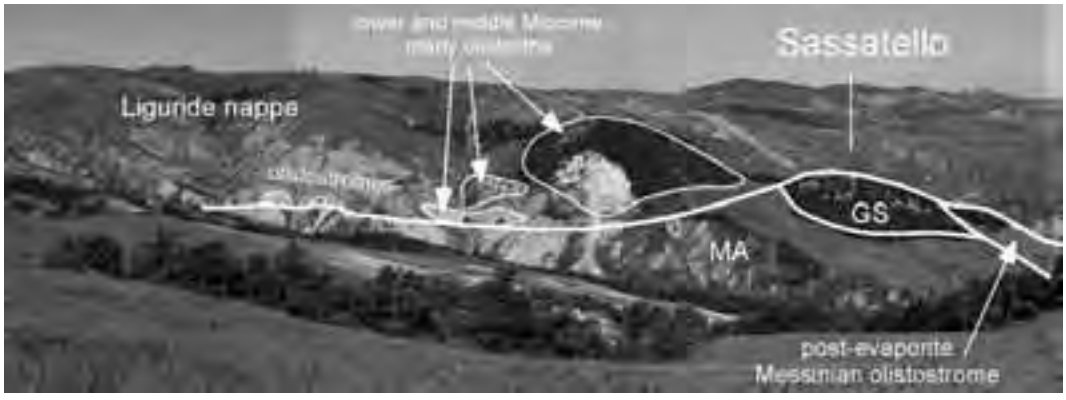

stop about the geological, ecological, historical and socio-economic importance of Vena del Gesso.

Stop 2.2:

Road Riolo Terme - Casola Valsenio, stop at Borgo Rivola: the Mt. Tondo quarry, and the adjoining Messinian outcrops. Monte Tondo and Monte del Casino are respectively situated on the eastern and western divide of the Senio valley. Actually, they are the two most important sampling sites for high-resolution cyclostratigraphy, magnetic calibration and astronomic dating of the main Messinian events in the Vena del Gesso basin. Discussion will mainly focus on the cyclicity of the pre-evaporite unit. If possible, participants will be driven to the site of the Mt. Tondo section, which straddles the Tortonian-Messinian boundary, and extends upwards to the GS base. The typical pre-evaporite Messinian is a dm-scale, dark-light alternation of thin-laminated bituminous shales (anoxic levels), non-laminated organic-rich clays (disoxic levels), and common marly clays (oxic levels).
Topics: 1, 2.

Stop 2.3:

Zattaglia - Brisighella road, near La Torretta. In a panoramic view over the western side of the Sintria Valley (Fig. 35), the most prominent tectonic feature is a well-developed imbricate stack of SW-verging Upper Messinian thrust-sheets, which involve the GS and the upper part of the pre-evaporite succession. In the neighborhood, no similar structure is found, neither in the MA, nor in the Argille Azzurre Fm. Indeed, back-thrusts are strictly confined to the evaporite unit. Another important characteristic of this peculiar

Figure 33 - Monte Penzola, western side of the Santerno Valley: a thin-skinned thrust carries the 2nd evaporite cycle over the 5th one. The N-NE vergency of the thrust is contrary to the S-SW transport of all the Vena del Gesso gravity structures. This anomaly might result either from complex accommodation of gliding blocks, or from "real" tectonic thrusting.

Figure 34 - Northern slope of Monte Penzola: an about 5 m thick Colombacci fm (see Figure 29) separates the GS (6th cycle, facies 5) from the lower Pliocene clays. The typical dark layer marking the Miocene/Pliocene boundary is slightly offset by normal faults.

imbricate stack is that not one of the thrust-sheets has "roots" in the valley-floor, as no gypsum crops out in the river bed. This anomalous setting creates big problems for any cross-section reconstruction, if interpreted as a purely tectonic feature. Things get simpler if we consider a progressive gravity-driven slope failure. In the upper parts of the slope, the evaporite unit is extended and dismembered by rotational normal faults, while in its lower parts, the faulted blocks keep gliding, and thrust over each other. This way, a stack of uprooted rock slices forms in the lower parts of the slope. Summarizing, from a merely structural point of view, the back-thrusts cropping out in the Sintria and Lamone valleys are likely to have been formed by gravitational failure and gliding. Other valid reasons are reviewed in the introduction of this Guide.
Topics: 1, 2.

Stop 2.4:

Carne' Natural Park and/or Tanaccia cave entrance. A short off-road walk gives the participants the opportunity to see recent karstic morphologies superimposed on Upper Messinian thrust-faults and sub-vertical gypsum strata.
Topics: 1, 2, 3.

Stop 2.5:

Brisighella: the Monticino Sanctuary and the adjoining gypsum quarry. Deformation and emersion of the evaporite unit in Late Messinian times are testified by an impressive angular unconformity between the Gessoso-solfifera Fm and the Colombacci Fm (Fig. 36). Subaerial erosion of gypsum is documented by karstic Neptunian dikes sealed by post-evaporite

Figure 35 Monte Mauro and the western side of the Sintria Valley, from the S: the SW-verging thin-skinned thrusts that involve the evaporite unit can be explained by gravity-driven block-gliding, on a shallow detachment level within the euxinic shale unit (MA). As in the Santerno Valley example (Figure 28), the initial effect of gliding was the development of SW-dipping normal faults dismembering the evaporite unit. During the subsequent gliding progression, the same faults were rotated and partly reactivated as thrusts (dashed lines).

Messinian deposits (p-ev$_2$). From 1985 to 1988, a very rich fauna of continental vertebrates was found in those paleo-karsts (Marabini & Vai, 1988). Panoramic and close views point out the present-day state of the quarry, which is being converted into an open-air geological museum.
Topics: 1, 2, 3, 10.

Stop 2.6:

Brisighella: participants will be offered a leisurely walk from the medieval castle to the Clock Tower, along faulted, vertical-bedded and karstified gypsum ridges.
Topics: 2.

Introduction to Day 3 and 4

In the Santerno section we examined a reduced, Mediterranean-type Messinian succession, developed above a structural high (Fig. 4). An abrupt facies and thickness change within the successions across the Forlì line ,that separates the marginal Vena del Gesso basin to the west, from the eastern Romagna basins, is the best evidence of the strong structural control on Messinian deposition (Fig.7).
In the Savio valley area, we will examine Messinian deposits cropping out in the Sapigno and Giaggiolo-Cella synclines (see geological map of Fig. 38), two wedge-top basins bounded to the west by the Forlì

Figure 36 - Monticino Quarry, Brisighella: the mining front represents the best possible exposure of the angular unconformity between the depositional sequences T2 and p-ev2. Some fractures sealed by the unconformity have been highlighted for their virtual relationship to the famous Vertebrate-bearing upper Messinian sedimentary dykes.
Figure 38 – Stop 3.1. Suggested along basin correlation of upper Tortonian deposits between the Santerno and Savio valleys (datum plane: ~ the Tortonian/Messinian boundary; From Roveri et al., 2002).

Volume n° 2 - from B16 to B33

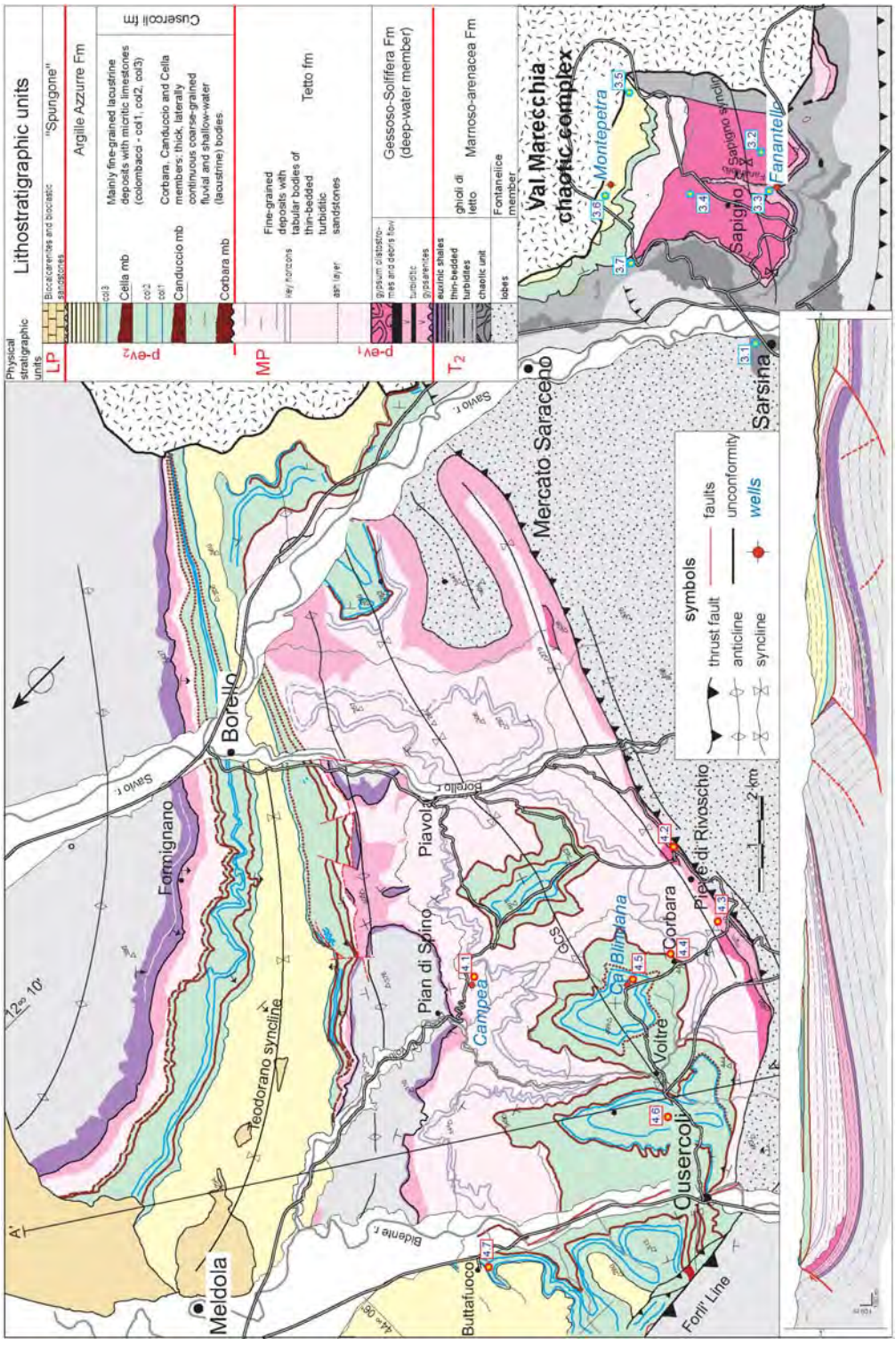

Figure 37 - Geological map of the eastern sector

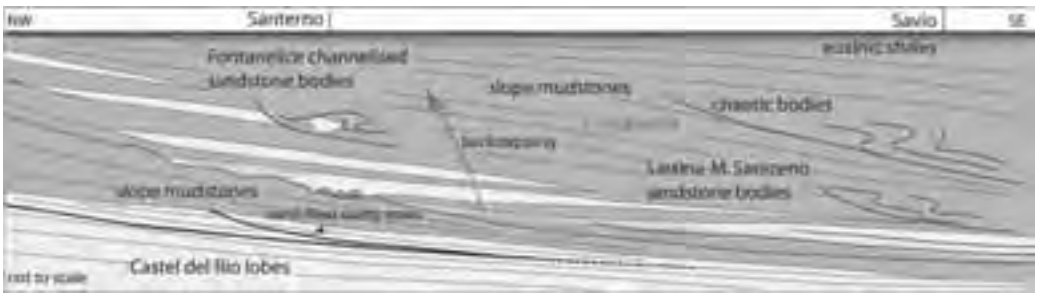

Figure 38 - Stop 3.1. Suggested along basin correlation of upper Tortonian deposits between the Santerno and Savio valleys (datum plane: ~ the Tortonian/Messinian boundary; From Roveri et al., 2002).

thrust, and filled up with more than 600 m of mainly post-evaporitic deposits. Shallow-water primary evaporites are lacking and are replaced by resedimented evaporites (turbiditic gypsarenites, olistostromes, olistoliths, and breccias made up of selenitic and alabastrine gypsum). Sedimentary features (graded beds with erosional bases, traction plus fallout structures, sole marks, load casts, climbing ripples, coarse-grained beds deposited by hyperconcentrated flows, debris flow, small to large-scale intraformational slumpings), show that these gypsum facies were deposited by gravity flows in a subaqueous setting. Siliciclastic deposits form the bulk of basin fill during the post-evaporitic stage. A very high sedimentation rate of more than 2mm/yr reflects the ongoing tectonic uplift and erosion of the Apennine chain following the intra-Messinian phase. Facies characteristics, paleoenvironmental meaning, and cyclic stacking pattern of uppermost Messinian deposits will be also dealt with during these two days.

DAY 3

Stop 3.1:

Savio valley, panoramic views along the National road to Mercato Saraceno. The Upper Tortonian-Lower Messinian succession of the Savio valley: correlation with the Santerno valley (Fig. 38).
Topics: 1, 4.

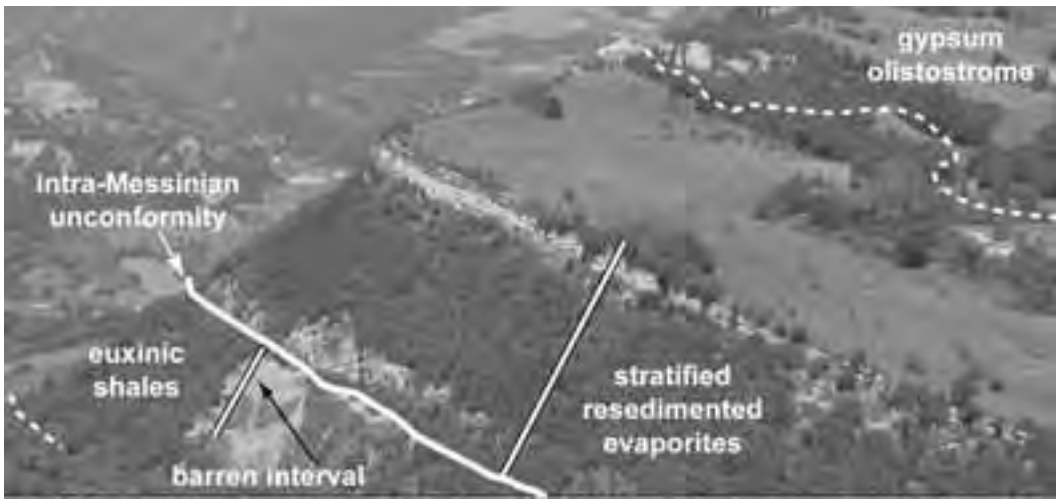

Figure 39 - Stop 3.2. Panoramic view looking west from Maiano of the Messinian succession of the Sapigno syncline. Note the clear bipartite character of the resedimented evaporite complex overlying the local euxinic shales, also well detectable from slope morphology: the tabular gypsarenitic bodies of the lower part are overlain through an irregular surface by a huge chaotic gypsum complex.

Stop 3.2:

Road Sarsina - S.Agata Feltria, deviation to Maiano. Panoramic view of the resedimented evaporites complex of the Fanantello section (Fig. 39). Body geometry and stacking pattern.
Topics: 3, 4.

Stop 3.3:

Road Sarsina-S.Agata Feltria: the Rio Fanantello section (1h walk along the 'Fanantello gorge'). The basal, stratified part of the resedimented evaporite complex crops out along the river bed, offering a spectacular chance for a close view of the facies characteristics of the *balatino* gypsum facies.
Topics: 4.

Stop 3.4:

Road Sapigno-Perticara. Panoramic view of the gypsum olistostrome, and of the post-evaporitic Lago Mare succession of the Sapigno syncline.
Topics: 4, 6.

Stop 3.5:

Perticara: visit to the local Mine Museum.
Topic: 5.

Stop 3.6:

Road Perticara-Montepetra. Panoramic views and core data (Montepetra well) of the uppermost post-evaporitic (Lago Mare) deposits, and the Miocene/Pliocene transition (Fig. 24).
Topics: 7. 8, 9, 10.

Stop 3.7: (optional)

Montepetra. Close inspection of the Montepetra "Lucina limestone", an Upper Tortonian-Lower Messinian deep-water chemioherm related to cold fluid seepage on the sea-floor. The Lucina limestones represent a classic topic for Apennine geology; their time and space distribution suggest a strong relationship with the structural evolution of the Apennine thrust belt.

DAY 4

Stop 4.1:

Road Piavola - Pian di Spino. Northern limb of the Giaggiolo-Cella syncline.
Panoramic and close-up views on general facies and the physical-stratigraphic characteristics of the basal post-evaporitic succession; the transition to hyposaline conditions - the 5.5 Ma ash layer - synsedimentary Messinian tectonics. Facies details of the p-ev$_1$ deposits in the cores of the Campea well.
Topics: 6.

Stop 4.2:

Road to Pieve di Rivoschio. Southern limb of the Giaggiolo-Cella syncline. Close view of an exceptionally thick gypsum layer (> 12 m) deposited by large-volume, high-density gravity flows. As with siliciclastic turbiditic beds, this gypsum layer has a lower coarser division with large-size mudstone clasts, eroded and incorporated within the flow head, and an upper, fine-grained laminated division, with possible evidence of flow rebound. Gypsum recrystallization makes it difficult to assess the original textures, but general facies characteristics are still easily recognizable.
Topics: 4.

Stop 4.3:

Road Pieve di Rivoschio – Voltre. Panoramic views of the post-evaporitic succession cropping out in the Giaggiolo-Cella syncline from its southern flank; general depositional characteristics, sedimentary trends, and stratigraphic architecture of the p-ev$_2$ unit (Cusercoli fm). This unit is made up of three backstepping, fluvio-deltaic coarse-grained bodies separated by lacustrine clays, characterized by thin, laterally-persistent limestone horizons (*colombacci limestones*).
Topics: 7.

Stop 4.4:

Road Pieve di Rivoschio - Voltre (close view) - Corbara. Flood-dominated, fluvio-deltaic systems of the p-ev$_2$ unit. Close-up view of the coarse-grained deposits forming the base of small-scale cycles (Fig. 40). They consist of tabular bodies made up of amalgamated massive sandstones and pebbly sandstones, with scoured erosional bases and clay chips (depositional lobe), passing down-current to hummocky, cross-stratified sandstones, and to thin-bedded, rippled sandstones; lobes are locally overlain by low-angle-inclined conglomerates forming sigmoidal bars. The facies sequence has a regressive character, and records the progradation in a shallow lacustrine basin of a small deltaic system dominated by catastrophic floods. Fine-grained deposits on top record the abandonment of the system due to a sudden decrease of flow volume.
Topics: *7*

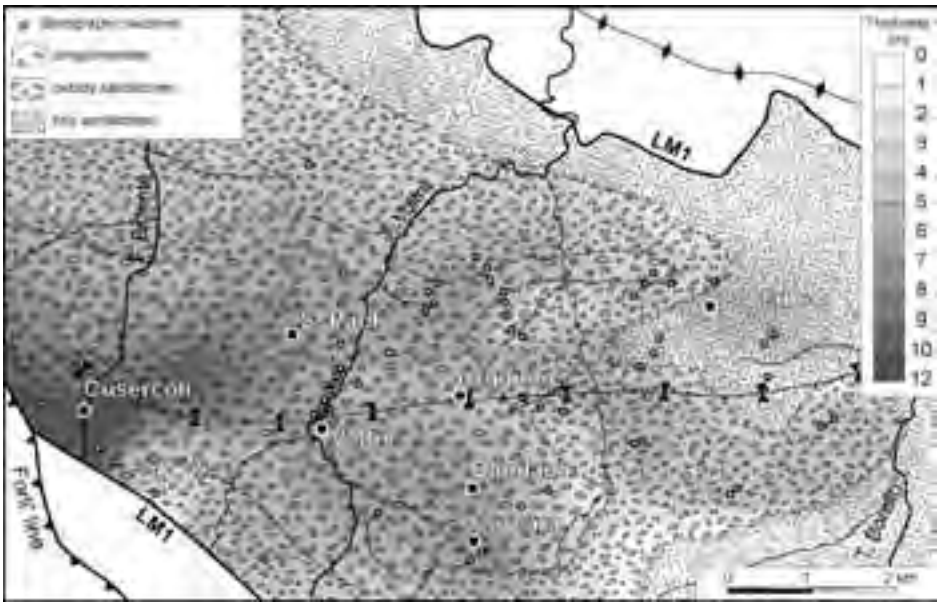

Figure 40 - Facies and thickness distribution of the lowermost corse-grained body of the Cusercoli fm (Corbara hzn)

Stop 4.5:

Road Voltre - Pian di Spino. Anatomy of the upper Lago Mare cycles from outcrop and core data (Cà Blindana well). The sedimentological and palaeoenvironmental meaning of fine grained deposits of the p-ev$_2$ unit. Facies characteristics and the origin of the "colombacci" limestones and of intervening black, organic-rich mudstones.
Topics: 7, 8, 9.

Stop 4.6:

Road Voltre - Cusercoli. Panoramic view, showing the clear stacking pattern of the uppermost Messinian deposits. Climatic vs. tectonic control of high-frequency cyclicity; the uppermost Messinian 'transgression' and the Pliocene marine flooding.
Topics: 7

Stop 4.7: (optional)

Road Cusercoli-Meldola, Bidente valley. Close-up view of the Miocene/Pliocene boundary in the Buttafuoco section.
Topics: 10.

Acknowledgments

The compilation of these notes wouldn't have been possible without the helpful work throughout the years of several students, that we gratefully acknowledge: L. Capece, R. Gennari, A. Laffranchi, F. Rizzini, and M. Castellari.
The authors are also indebted to G. Papani, S. Iaccarino, R. Flecker, C. Schreiber, W. Schlager, and E. Mutti, for their encouragement and helpful discussions about the different Messinian problems.

References cited

Bassetti M.A., Ricci Lucchi F., Roveri M., 1994. Physical stratigraphy of the Messinian post-evaporitic deposits in Central-southern Marche area (Appennines, Central Italy). Mem. Soc. Geol. It. 48, 275-288.

Bassetti M.A., 2000. Stratigraphy, sedimentology and paleogeography of upper Messinian ("Post-evaporitic") deposits in Marche area (Apennines, central Italy). Mem. Sci. Geol. 52/2, 319-349

Blanc-Valleron M.M., Rouchy J.M., Pierre C., Badaut-Trauth D., Schuler, 1998. Evidence of Messinian nonmarine deposition at Site 968 (Cyprus lower slope), Proceedings of the Ocean Drilling Program: Scientific Results, Volume 160, Pages 437-446

Boccaletti M., Calamita F., Deiana G., Gelati R., Massari F., Moratti G. and Ricci Lucchi F. 1990 Migrating foredeep-thrust belt system in northern Apenines and southern Alps. Palaeogeography, Palaeoclimatology, Palaeoecology 77, 3-14, Elsevier Science Publisher, Amsterdam.

Capozzi R., Landuzzi A., Negri A., Vai G.B., 1991. Stili deformativi ed evoluzione Tettonica della successione neogenica romagnola. Studi Geologici Camerti volume speciale (1991/1), pp. 36-278.

Castellarin A., Eva C., Giglia G, Vai G.B, with a contribute of Rabbi E., Pini G.A. and Crestana G. (1986) - Analisi strutturale del Fronte Appenninico Padano. Giornale di Geologia, 47 1/2, 47-75.

Castellarin A., 2001 .Alps-Appennines and Po Plain-frontal Appennines relations. In: Vai G.B. and Martini I.P., Eds, Anatomy of an orogen: the Apennines and adjacent Mediterranean basins. Kluwer Academic Publishers, Dordrecht-Boston-London, 177-196.

Castellarin A., Pini G.A. with the contribute of Borsetti A.M. and Rabbi E., 1989. L'arco del Sillaro: la messa in posto delle Argille Scagliose al margine appenninico padano (Appennino bolognese). Memorie della Società Geologica Italiana, 39, 127-142.

Clauzon G., 1973. The eustatic hypothesis and the pre-Pliocene cutting of the Rhone valley In Ryan W. B., Hsü K. J. Et al. Initial report of the Deep See Drilling Project. Washington XIII, 1251-1256.

Clauzon G., 1982. Le canyon messinien du Rhone: une preuve decisive du "desiccated deep-basin model" (Hsü, Cita et Ryan, 1973): Bulletin Societé Geologique de France 24, 597-610.

Clauzon G., Suc J.P., Gautier F., Berger A., Loutre M.F., 1996. Alternate interpretation of the Messinian salinity crisis: controversy resolved? Geology 24, 363-366.

Clauzon G., Rubino J.L., Casero P., 2001. Regional modalities of the Messinian salinity crisis in the framework of a two phases model. 2nd EEDEN Workshop, Sabadell 2001, Abstract Book, 17-18.

Colalongo M.L., Ricci Lucchi F., Guarnieri P, Mancini E., 1982. Il Plio-Pleistocene del Santerno (Appennino romagnolo), in Cremonini G., and Ricci Lucchi F., eds): Guida alla Geologia del margine appenninico padano. Guide Geologiche Regionali della Società Geologica Italiana: Bologna, Società geologica italiana, p. 161-166.

Costa G.P., Colalongo M.L., De Giuli C., Marabini S., Masini F., Torre D. and Vai G.B, 1986. Latest Messinian Vertebrate fauna Preserved in a Paleokarst-neptunian dike setting (Brisighella, Northern Apennines): Le grotte d'Italia, v. 12, p. 221-235.

Cremonini G., Elmi C., and Monesi A., 1969. Osservazioni geologiche e sedimentologiche su alcune sezioni plio-pleistoceniche dell'Appennino romagnolo: Giornale di Geologia, v. 35, p. 85-96.

Cremonini G., and Ricci Lucchi F., 1982. Guida alla Geologia del margine appenninico padano: Guide Geologiche Regionali, Società Geologica Italiana, 248 pp.

Dalla S., Harby H., Serazzi M., 1997. Hydrocarbon exploration in a complex incised valley fill: An example from the late Messinian Abu Madi Formation (Nile Delta Basin, Egypt). The Leading Edge, December 1997, 1819-1824.

De Giuli C., Masini F. and Torre D., 1988, The Mammal Fauna of the Monticino quarry, in De Giuli, C., and Vai, G.B. eds., Fossil Vertebrates in the Lamone valley, Romagna apennines, International Workshop: Continental Faunas at the Mio-Pliocene Boundary, Faenza, March 28-31, 1988, Guidebook, p. 65-69.

Duggen S., Hoernle K., Boogard P.v.d., Rupke L., Phipps Morgan J., 2003. Deep roots of the Messinian salinity crisis. Nature, 422, 602-606.

Flecker R., Ellam, R.M., 1999. Distinguishing climatic and tectonic signals in the sedimentary succession of marginal basins using Sr isotops: an example of Messinian salinity crisis, Eastern Mediterranean. Journal of the Geological Society, London, 156, 847-854.

Gelati R., Rogledi S., Rossi M., 1987. Significance of the Messinian unconformity-bounded sequences in the Apenninic margin of the Padan foreland basin, northern Italy (preliminary results). Mem. Soc. Geol. It. 39, 319-323.

Ghibaudo G., Clari P., and Perello M., 1985. Litostratigra fia,sedimentologia ed evoluzione Tettonico-sedimentaria dei depositi miocenici del margine sud-orientale del Bacino Terziario Ligure-Piemontese (Valli Borbera, Scrivia e Lemme): Bollettino della Società Geologica Italiana, v. 104, p. 349-397.

Hlgen F. J., Bissoli L., Iaccarino S., Krijgsman W., Meijer R., Negri A., Villa G., 2000. Integrated stratigraphy and astrochronology of the Messinian GSSP at Oued Akrech (Atlantic Morocco). Earth and Planetary Science Letters, 182, 237-251.

Hsü K.J., Ryan W.B.F., Cita M.B., 1972. Late Miocene desiccation of the Mediterranean. Nature, 242, 240-244.

Iaccarino S., M., Bossio A., 1999. Paleoenvironment of uppermost Messinian sequences in the western Mediterranean (sites 974, 975 and 978) In: Zahn R., Comas M.C. and Klaus A. (Eds.), Proceedings of the Ocean Drilling Program, Scientific Results 161, 529-540.

Iaccarino S., Papani G., 1980. Il Messiniano dell'Appennino Settentrionale dalla Val d'Arda alla Val Secchia: stratigrafia e rapporti con il substrato e il Pliocene. Vol. dedicato a S. Venzo, Univ. Studi di Parma, 15-46.

Iaccarino S., Castradori D., Cita M. B., Di Stefano E.,

Gaboardi S., McKenzie J.A., Spezzaferri S., Sprovieri R., 1999. The Miocene/Pliocene boundary and the significance of the earliest Pliocene flooding in the Mediterranean. Mem. Soc. Geol. It. 54, 109-131.

Keogh S. M. and Butler R.W.H., 1999. The Mediterranean water body in the late Messinian: interpreting the record from marginal basins on Sicily. Journal of the Geological Society, London, 156, 837-846.

Kligfield R., 1979. The Northern Apennines as a collisional orogen: American Journal of Science, v. 279, p. 676-691.

Kouwenhoven T.J., Seidenkrants M.S. and Van der Zwaan G.J., 1999. Deep-water changes: the near-synchronous disappearance of a group of benthic foraminifera from the Late Miocene Mediterranean: Palaeogeography, Palaeoclimatology, Palaeoecology, v. 152, p. 259-281.

Krijgsman W., Hilgen F. J., Marabini S., Vai G. B., 1999a. New paleomagnetic and cyclostratigraphic age constraints on the Messinian of the Northern Apennines (Vena del Gesso Basin, Italy) Mem. Soc. Geol. It. 54, 25-33

Krijgsman W., Hilgen F.J., Raffi I., Sierro F.J., Wilson D.S., 1999b. Chronology, causes and progression of the Messinian salinity crisis. Nature 400, 652-655.

Lucente C.C., Manzi V., Ricci Lucchi F. and Roveri M., 2002. Did the Ligurian Sheet cover the whole thrust belt in Tuscany and Romagna Appennines? Some evidence from gravity emplaced deposits: Memorie della Società Geologica Italiana, 1, 393-398.

Manzi V., 1997. Analisi di facies dei depositi messiniani post-evaporitici tra il Fiume Bidente ed il Fiume Savio: tra Corbara e Pieve di Rivoschio (Appennino romagnolo): unpublished Thesis, University of Bologna, 124 pp.

Manzi V., 2001. Stratigrafia fisica, analisi sedimentologica microscopica e caratterizzazione magnetostratigrafica dei depositi connessi all'evento evaporitico del Messiniano (Formazione Gessoso-solfifera l.s.). Ph.D. thesis Earth Science Department, Bologna University, Italy.

Marabini S., Vai G.B., 1985. Analisi di facies e macroTettonica della Vena del Gesso in Romagna. Bollettino della Società Geologica Italiana, v. 104, p. 21-42.

Marabini S. and Vai. G.B., 2003. Marsili's and Aldrovandi's early studies on the gypsum geology of the Apennines. In Vai and Cavazza eds., Fourth Centuries of the word Geology: Ulisse Aldrovandi 1603 in Bologna. Minerva Edizioni.

McKenzie J. A., 1999. From desert to deluge in the Mediterranean. Nature 400, 613-614.

Meulenkamp J.E., Sissingh W. et al., 2000. Late Tortonian. In: S. Crasquin (Ed.), Atlas PeriTethys, Palae×ogeographical maps – Explanatory notes. CCGM/CGMW, Paris, 195-201.

Mutti, E., Tinterri, R., Remacha, E., Mavilla, N., Angella, S. and Fava, L., 1999. An introduction to the analysis of ancient turbidite basins from an outcrop perspective: AAPG Continuing Education Course Note Series, #39,

Negri. A and Vigliotti L. 1997. Calcareous Nannofossil biostratigraphy and paleomagnetism of the Monte Tondo and Monte del Casino sections (Romagna Apennines, Italy) In (A. Montanari G.S. Odin and R. Coccioni, Eds): Miocene Stratigraphy - An Integrated Approach, Elsevier 478-491

Odin G.S., Montanari A., and Coccioni R., 1997. Chronostratigraphy of Miocene stages: a proposal for the definition of precise boundaries, in (Montanari A., Odin G. S., and. Coccioni R, eds): Miocene Stratigraphy - An Integrated Approach, Elsevier, p. 597-629.

Parea G.C., Ricci Lucchi F., 1972. Resedimented evaporites in the periadriatic trough (upper Miocene, Italy) Israel Journal of Earth-Sciences 21, 125-141.

Ricci Lucchi F., Bassetti M.A., Manzi V., Roveri M., 2002. Il Messiniano trent'anni dopo: eventi connessi alla crisi di salinità nell'avanfossa appenninica.Studi. Geologici Camerti 1, 127-142.

Ricci Lucchi F., 1973. Resedimented evaporites: indica×tors of slope instability and deep-basins conditions in Peri×adriatic Messinian (Apennines foredeep, Italy). Koninklijke Nederlandse Akademie Van Wetenshappen. Messinian Events in the Mediterranean. Geodynamics Scientific Re×port n° 7 on the colloquium held in Utrecht, March 2-4, 1973,142-149.

Ricci Lucchi F., 1968. Chanellized deposits in the middle Miocene flysch of Romagna (Italy). Giornale di Geologia, 36, 203-282.

Ricci Lucchi F., 1969. Recherches stratonomiques et sédimentologique sur le Flysch Miocéne de la Romagne (Formation Marnoso-arenacea). Proceedings of the 4th session, Committee on Mediterranean Neogene Stratigraphy, Giornale di Geologia, 36, 163-198.

Ricci Lucchi F., 1975. Depositional cycles in two turbidite formations of northern Apennines. Journal of Sedimentary Petrology, 45, 1-43.

Ricci Lucchi F., 1981. The Miocene Marnoso-arenacea turbidites, Romagna and Umbria Apennines. In: Ricci Lucchi F., Ed., Excursion Guidebook, 2nd European Regional Meeting of International Association of Sedimentologists, 231-303.

Ricci Lucchi F., 1986. The Oligocene to Recent foreland

Volume n° 2 - from B16 to B33

basins of the northern Apenines. Spec. Publs. Int. Ass. Sediment. 8, 105-139.

Riding R., Braga J. C., Martin J. M., 2000. Late Miocene Mediterranean desiccation: topography significance of the "Salinity Crisis" erosion surface on-land in southeast Spain: Reply Sedimentary Geology 133, 175-184.

Rossi M. Rogledi S. Barbacini G., Casadei D., Iaccarino S., Papani G., 2002. Tectono-stratigraphic architecture of the Messinian pigyback basino of the Northern Apennines: the Emilia folds in the Reggio-Modena area and comparison with the Lombardian and Romana sectors. Boll. Soc. Geol. It., 1, 437-477.

Rouchy J.M., Orszag-Sperber F., Blanc-Valleron M.M., Pierre C., Riviere M., Combourieu-Nebout N., Panayides I., 2001. Paleoenvironmental changes at the Messinian-Pliocene boundary in the eastern Mediterranean (southern Cyprus ba×sins): significance of the Messinian Lago-Mare. Sed. Geol., 145, 93-117.

Roveri M., Bassetti M.A., Ricci Lucchi F., 2001. The Medi×terranean Messinian salinity crisis: an Apennine foredeep per×spective. Sedimentary Geology 140, 201-214.

Roveri M., Manzi V., Bassetti M.A., Merini M., Ricci Lucchi F., 1998. Stratigraphy of the Messinian post-evaporitic stage in eastern-Romagna (northern Apennines, Italy). Gior×nale di Geologia 60, 119-142.

Roveri M., Ricci Lucchi F., Lucente C. C., Manzi V., Mutti E. 2002. Stratigraphy, facies and basin fill hystory of the Marnoso-arenacea Formation. In: Mutti E., Ricci Lucchi F., Roveri M. Eds. Revisiting turbidites of the Marnoso-arenacea Formation and their basin-margin equivalents: problems with classic models. 64th EAGE Conference and Exibition. Excursion Guidebook. Parma University and ENI – AGIP Division

Roveri M., Manzi V., Ricci Lucchi F., Rogledi S., 2003. Sedimentary and tectonic evolution of the Vena del Gesso basin (Northern Apennines, Italy): Implications for the onset of the Messinian salinity crisis. Geological Society of America Bulletin 115, 387-405.

Roveri M., Manzi V.. The Messinian salinity crisis: looking for a new paradygm? Palaeogeography, Palaeoclimatology, Palaeoecology. In press.

Ruggieri G., 1967. The Miocene and later evolution of the Mediterranean Sea. Systematics association pubblication no. 7, Aspects of the Tethyan biogeography. Editors Adams C.G. and Ager D.V., 283-290, Palermo.

Ryan W.B.F., Cita M. B., 1978. The nature and distribution of the Messininan erosional surface - indicators of a several-kilo×meters-deep Mediterranean in the Miocene. Marine Geology 27, 193-230.

Ryan W.B.F., 1978. Messinian badlands on the southeastern margin of the Mediterranean Sea. Marine Geology 27, 349-363.

Schreiber C.B., 1973. Survey of the physical features of the messinian chemical sediments Koninklijke Nederlandse Akademie Van Wetenshappen. Messinian Events in the Mediterranean. Geodynamics Scientific Report n° 7 on the colloquium held in Utrecht, March 2-4, 1973. 101-110

Scicli A., 1972. L'attività estrattiva e le risorse minerarie della regione Emilia Romagna. Artioli Editore, Modena, pp. 728.

Snel E., Marunteanu M., Meulenkamp J.E., 2001. Late Miocene-Early Pliocene marine connections between the Atlantic/Mediterranean and the Paratethys. 2nd EEDEN Workshop, Sabadell 2001, Abstract Book, 69.

Vai G.B., 1988. A field trip guide to the Romagna Apennine geology. The Lamone valley in De Giuli, C., and Vai, G.B. eds., Fossil Vertebrates in the Lamone valley, Romagna apennines, International Workshop: Continental Faunas at the Mio-Pliocene Boundary, Faenza, March 28-31, 1988, Guidebook, p. 7-37.

Vai G.B., 1997. Cyclostratigraphic estimate of the Messinian stage duration: *in* Montanari, A., Odin, G.S., and Coccioni, R., eds.,: Miocene Stratigraphy - An Integrated Approach: Amsterdam, Elsevier, p. 463-476.

Vai G.B. and Ricci Lucchi F., 1977. Algal crusts, autochthonous and clastic gypsum in a cannibalistic evaporite basin: a case history from the Messinian of Northern Apennines.: Sedimentology, v. 24, p. 211-244.

Vai G.B. and Martini I.P., 2001. Anatomy of an orogen: the Apennines and adjacent Mediterranean, Kluwer Academic Publishers, 632p.

Van der Meulen M.J., Meulenkamp J.E., Wortel M.J.R., 1999. Lateral shifts of Apenninic foredeep depocentres re×flecting detachment of subduced lithosphere. Earth and Planetary Science Letters 154, 230-219.

Vigliotti L., 1988. Magnetostratigraphy of the Monticino section 1987 (Faenza, Italy), in De Giuli, C., and Vai, G.B. eds., Fossil Vertebrates in the Lamone valley, Romagna apennines, International Workshop: Continental Faunas at the Mio-Pliocene Boundary, Faenza, March 28-31, 1988, Guidebook, p. 61-62.

Van Couvering J. A., Castratori D., Cita M. B., Hilgen F. J., and Rio D., 2000. The base of the Zanclean Stage and of Pliocene series. Episodes, 23 (3), 179-187

Back Cover:
field trip itinerary

32nd INTERNATIONAL GEOLOGICAL CONGRESS

FIELD TRIP MAP

Edited by APAT

Volume n° 2 - from B16 to B33

32nd INTERNATIONAL GEOLOGICAL CONGRESS

ULTRAHIGH AND HIGH PRESSURE ROCKS OF SAXONY

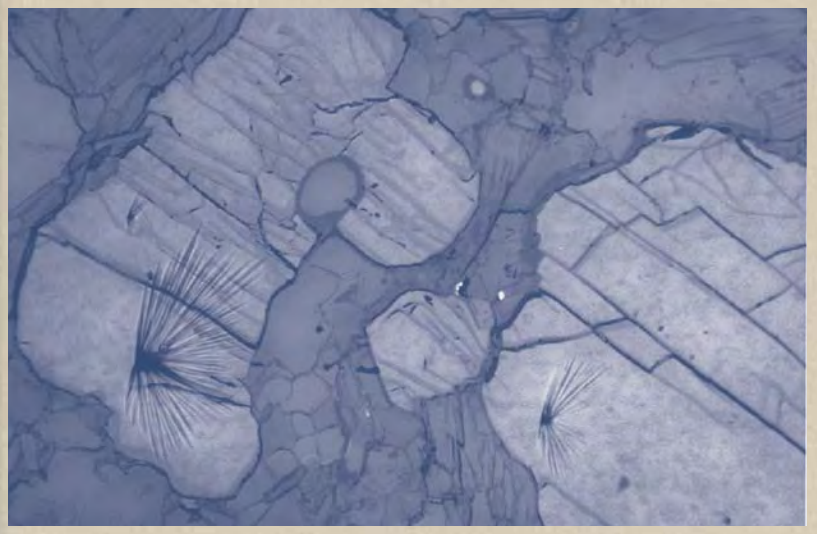

Leader: H.-J. Massonne

Associate Leader: H.-J. Bautsch

Field Trip Guide Book - B21

Florence - Italy
August 20-28, 2004

Pre-Congress **B21**

The scientific content of this guide is under the total responsibility of the Authors

Published by:
APAT – Italian Agency for the Environmental Protection and Technical Services - Via Vitaliano Brancati, 48 - 00144 Roma - Italy

Series Editors:
Luca Guerrieri, Irene Rischia and Leonello Serva (APAT, Roma)

English Desk-copy Editors:
Paul Mazza (Università di Firenze), Jessica Ann Thonn (Università di Firenze), Nathalie Marléne Adams (Università di Firenze), Miriam Friedman (Università di Firenze), Kate Eadie (Freelance indipendent professional)

Field Trip Committee:
Leonello Serva (APAT, Roma), Alessandro Michetti (Università dell'Insubria, Como), Giulio Pavia (Università di Torino), Raffaele Pignone (Servizio Geologico Regione Emilia-Romagna, Bologna) and Riccardo Polino (CNR, Torino)

Acknowledgments:
The 32nd IGC Organizing Committee is grateful to Roberto Pompili and Elisa Brustia (APAT, Roma) for their collaboration in editing.

Graphic project:
Full snc - Firenze

Layout and press:
Lito Terrazzi srl - Firenze

Volume n° 2 - from B16 to B33

32nd INTERNATIONAL GEOLOGICAL CONGRESS

ULTRAHIGH AND HIGH PRESSURE ROCKS OF SAXONY

AUTHORS:
H.-J. Massonne (Universität Stuttgart - Germany)
H.-J. Bautsch (Humboldt Universität - Germany)

Florence - Italy
August 20-28, 2004

Pre-Congress

B21

Front Cover:
Microdiamonds in garnets from quartzofeldspathic rock (saidenbachite), outcropping at the Saidenbach reservoir, Saxonian Erzgebirge, seen under reflected light. Striations around the diamonds allow to detect them easily. Image width is 3mm.

Leader: H.-J. Massonne
Associate Leader: H.-J. Bautsch

Introduction

Ultrahigh pressure (UHP) metamorphic rocks were first detected in the western Alps through the indicator mineral coesite (Chopin, 1984). Soon after this detection it turned out that UHP rocks are more widespread than expected after the first find. Coesite was also recognised in rocks of the Norwegian Caledonides, the Dabie Shan in China and orogenic regions elsewhere (Chopin, 2003). Evidence for UHP metamorphism, proven by both indicator minerals and mineral equilibria, has been reported only recently from the Variscan orogen in Europe. Typically, this orogen resulted from continent-continent collision in Phanerozoic times as the previously mentioned orogens with UHP rocks.

In portions of the Bohemian Massif, which is situated on the northwestern edge of the Variscan orogenic chain (Fig. 1), occurrences of eclogites and garnet peridotites were recognised more than a century ago and subsequent detailed mapping has revealed several hundred mostly small bodies spread over a very large area. Hints at UHP metamorphism came from specific mineral compositions (Al in orthopyroxene) and considerations of mineral equilibria, for instance, related to the Al-celadonite component in phengite. More recently, the indicator minerals coesite (Massonne, 2001) and microdiamond (Massonne, 1999) were detected in eclogites and quartzofeldspathic rocks, respectively, from the Erzgebirge. In addition, lamellae of garnet and clinopyroxene in clinopyroxenite from the nearby Granulitgebirge are interpreted as exsolution of former majoritic garnet (Massonne and Bautsch, 2002).

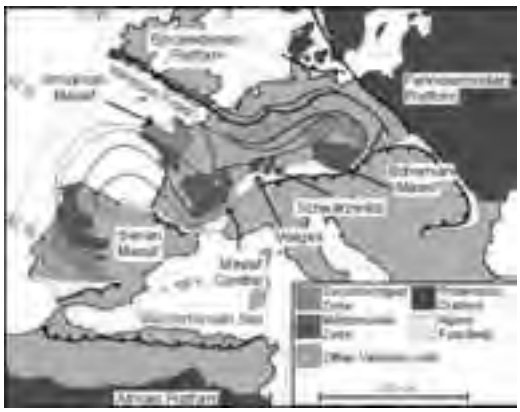

Figure 1 - Location of exposed basement areas of the Upper Palaeozoic Variscan orogen in Europe (Fig. 1 of O'Brien, 2000). These are subdivided in those belonging to the Saxothuringian Zone, Moldanubian Zone and other zones. Not shown are fragments of Variscan basement involved in the Cretaceous-Tertiary Alpine orogen.

The aim of our field trip is to present key occurrences of rocks formed at UHP and near-UHP conditions. These rocks are representative for high-pressure (HP) and UHP metamorphism in the Variscan orogen or at least in the Bohemian Massif. To gain detailed information on the regional geology we recommend having a look at the series of "Geologische Meßtischblätter". These maps with a 1: 25000 scale are distributed by "Sächsisches Landesamt für Umwelt und Geologie" at Dresden. In addition, explanatory text is available for each map. The following sheets cover the areas visited during our field trip: GK25 4943 Gehringswalde, GK25 4944 Waldheim, GK25 5042 Burgstädt, GK25 5043 Mittweida, GK25 5044 Frankenberg, GK25 5144 Flöha, GK25 5245 Lengefeld, GK25 5345 Zöblitz, and GK25 5543 Kurort Oberwiesenthal. Relevant overview maps with scale 1 : 200000 are GKÜ200 M33-VII Chemnitz, GKÜ200 M33-VIII Dresden, GKÜ200 M33-XIII Plauen, and GKÜ200 M33-XIV Annaberg-Buchholz.

Regional geology

It has become a common view that the Variscan orogen resulted from colliding continental plates. These were Gondwana and Laurentia-Baltica (or Laurussia). The latter were formed from originally separate plates during the Caledonian orogeny at the end of Early Palaeozoic times and, thus, shortly before the onset of Variscan events. It is assumed that after the end of the Caledonian orogeny (420-410 Ma) a single oceanic basin (Rheic ocean: e.g., Robardet et al., 1990; Tornquist Sea: Oliver et al., 1993) or two (e.g., Rheic ocean + Massif Central - Galician ocean, Matte, 1986; Rheic ocean + subsequently Palaeotethys, Stampfli et al., 2002) and more basins separated Gondwana and Laurentia-Baltica. The extension of the ocean(s) and the time of final closure is still a matter of debate (e.g., narrow: McKerrow et al., 2000; wide: Tait et al., 2000), which also includes the involvement of microplates, such as Armorica (see Tait et al., 1994: Armorican Terrane Assemblage), Avalonia (Murphy et al., 1999) or the Hun terrane (Stampfli, 1996), between Gondwana and Laurentia-Baltica. The many

Volume n° 2 - from B16 to B33

microplates were probably once contiguous to, or part of Gondwana (Tait et al., 2000; Hartz and Torsvik, 2002). In spite of the above uncertainties, the relative motion of Gondwana towards Laurentia-Baltica, implying the subduction of oceanic crust, is generally accepted. The subduction, also involving continental crust at a final stage, is assumed by many scientists to have been directed south or southeast (e.g., Franke and Stein, 2000) but the opposite direction is favoured by others (e.g., Matte, 1998). However, because of the bilateral symmetry of the structural elements of the Variscan orogen, two simultaneously active subduction zones with opposite directions, away from each other or even towards each other, were also taken into consideration by several geoscientists (e.g., Matte, 1986; Franke, 2000).

The basin of the Rheic ocean disappeared 340 Ma ago at the latest. However, attempts by some geoscientists to reconstruct the Variscan orogeny also consider a closure already about 400 Ma. Among such recent reconstructions, which also take into account the existence of HP and UHP rocks, is that by Matte (1998) proposing a process as suggested by the slab break-off model resulting in a relatively narrow mountain chain characterised by strongly thickened crust lasting for several tens of millions of years (Fig. 2). This also concerns the geodynamic model for the Variscan orogen presented by Massonne and O'Brien (2003) and Massonne (in press). However, these authors proposed underthrusting of one continental plate under the other to reach a Himalaya (+ Tibetan Plateau) type orogen by underplating during the course of several tens of millions of years (Fig. 3). After closure of the oceanic basin between Gondwana and Laurussia (called here: Rheic ocean) only small basins remained or were newly formed. In these, up to several km-thick sequences of Viséan and Upper Carboniferous sediments were deposited. Contemporaneously, large volumes of granitoid magmas intruded the Variscan crust.

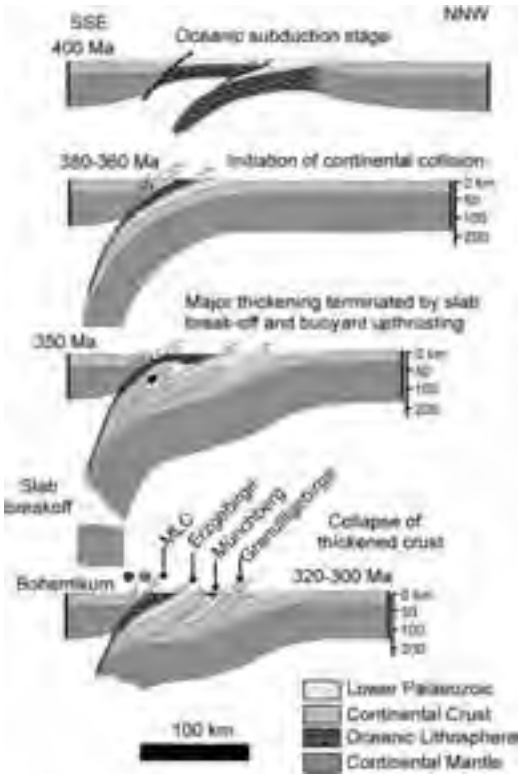

Figure 2 - The subduction-collision model by Matte (1998) redrawn by O'Brien (2000) for the northern Bohemian Massif.

The Bohemian Massif exposes the metamorphic core of the Variscan orogen at its eastern margin. It is a collage of several smaller basement areas differing in age and metamorphic evolution. These are termed Saxothuringian, Moldanubian, Tepla-Barrandian and in the east and northeast: Moravo-Silesian and Lugian = Sudetes (Fig. 4). Between the basement units, regions with Palaeozoic sediments exist that are predominantly only anchimetamorphic. Both sedimentary and metamorphic ages can be contemporaneous (e.g., Franke and Engel, 1986). Nappe tectonics (e.g., Schulmann et al., 1991) as well as major fault and shear zones (e.g., Krohe, 1996), which are widespread in the entire northern Variscan area, are responsible for the present collage-like aspect.

HP rocks in the Bohemian Massif, such as eclogites and garnet peridotites, are, in fact, abundant but are restricted to specific areas (dark in Fig. 4). As pointed out by Willner et al. (2000), the age data related to HP rocks are bimodal. Ages between 400 and 380 Ma, with up to 20 Ma younger cooling ages, were reported from the Münchberg Massif, the Góry Sowie (Owl Mountains) and the Tepla-Barrandian unit (Fig. 4). Clearly younger ages (345-340 Ma) were determined for HP rocks of the Granulitgebirge (Granulite Mountains), the Erzgebirge (Ore Mountains, Krušné hory in Czech), the Śnieżnik (Snowy Mountains) and the Gföhl unit. Cooling ages are on average only a few Ma younger. UHP rocks may occur in all units characterised by HP rocks but so far indicator minerals (see above) have only been found in the Erzgebirge.

Figure 3 - Collision of Gondwana and Laurussia presented by the position of these continental plates relative to each other in the Lower Devonian (left hand side), Lower Carboniferous and Upper Carboniferous (right hand side) according to Massonne (in press). The positions of the plates refer to palaeomagnetic data (see Tait et al., 2000). For orientation the current shapes of the continental plates, except portions overprinted by the Alpine orogeny (see Northern Africa), and other typical geographic shapes (Hudson Bay, Newfoundland, Great Britain, Black Sea) are shown. The estimated shapes of the continental plates at the corresponding times are displayed by dotted lines (northern margin of Africa refers to pre-Alpine times). Thick dashed lines mark orogenic zones (= thickened continental crust). Arrows point

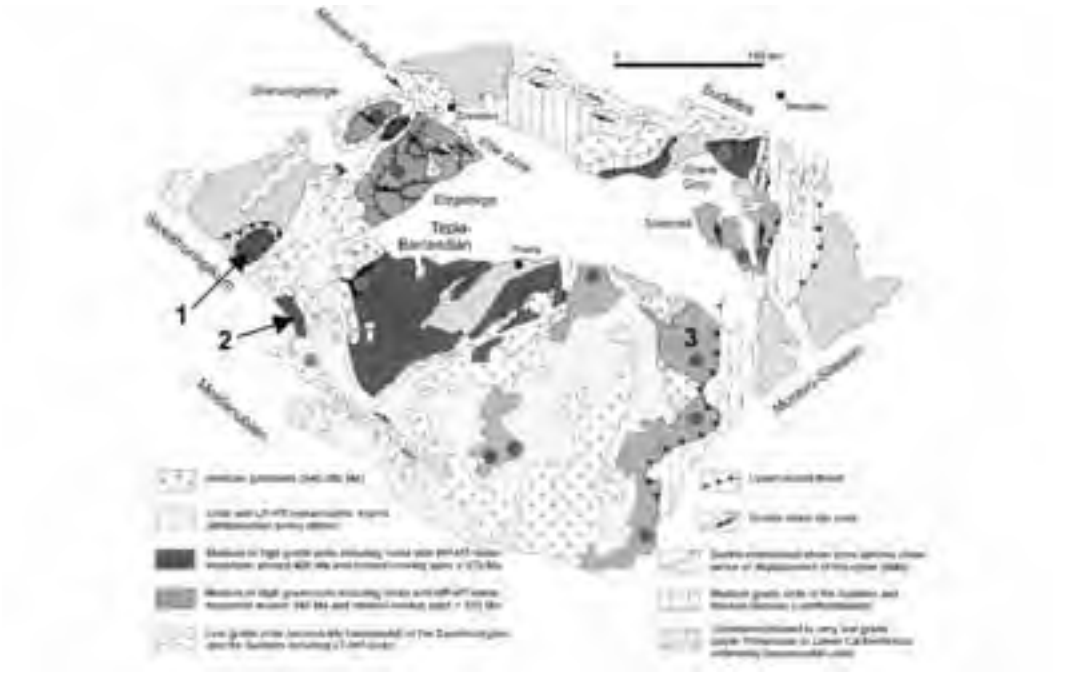

Figure 4 - Simplified geological map of the Bohemian Massif according to Willner et al. (2000). In addition to major units, specific areas are named (italics and 1 = Münchberg Massif, 2 = Zone of Erbendorf-Vohenstrauß, 3 = Gföhl Unit). Grey dots point to locations with HP rocks geochronologically dated.

Volume n° 2 - from B16 to B33

The crystalline complexes of both Granulitgebirge and Erzgebirge are anticlinal structures with ellipsoidal shape extending in WSW-ENE direction (Fig. 5). They are surrounded and, thus, covered by anchimetamorphic to low-grade metamorphic rocks. The outcropping rocks in the Granulitgebirge are either felsic and basic granulites with some ultrabasic bodies or younger granitoids (Fig. 5), whereas the rocks in the Erzgebirge are more variable in terms of metamorphic degree. Various suggestions exist to subdivide the metamorphic rocks. Here, we prefer the proposal by Willner et al. (2000) who suggested three major units for the medium to high-grade metamorphic rocks surrounded by a low-grade unit, the Phyllite Unit. Two of these three units, Mica-schist - Eclogite Unit (MEU) and Gneiss - Eclogite Unit (GEU), contain abundant eclogite lenses, whereas the Red and Grey Gneiss Unit does not contain any HP rocks. Detailed information on the P-T conditions of these units will be given in specific text portions related to corresponding rocks. This also refers to the Granulitgebirge. However, in general, it can be pointed out that the age of the HP metamorphism in both Granulitgebirge and Erzgebirge is close to 340 Ma (e.g. Massonne & O'Brien, 2003).

Figure 5 - Simplified geological map for the region of the Granulitgebirge (SGG) and the Erzgebirge (EZ) according to Blümel (1995). Vertically hatched - orthogneisses of the EZ, triangles - occurrences of larger eclogite bodies, crosses - granite bodies of Eibenstock, Bergen, and Schneeberg, swung dashes - phyllites surrounding the SGG, horizontally hatched - granitoid bodies in the SGG, black - serpentinite bodies. Abbreviations: FZ = Frankenberger Zwischengebirge, E.Z.R.F. = Erzgebirgssüdrand fault, D = Germany, CR = Czech Republic, CHEM = Chemnitz, DRE = Dresden, Fr. = Freiberg, O.W. = Oberwiesenthal, Rei. = Reitzenhain, Sa. = Sayda, W. = Waldheim.

Field itinerary

The field itinerary is subdivided into 4 portions according to the number of field trip days. The overview map at the back of the guide book shows the position of the various stops.

DAY 1

The route of the excursion starts in the city of Dresden towards the nearest access to Highway A4. Heading for Chemnitz on this highway, we leave it at exit 72 Frankenberg. After heading a few hundred metres towards Frankenberg, we turn right before reaching the inner town and cross the highway with an underpass. After about 1.5 km north, we see ahead the old "Fischerschänke" inn. Instead of following the road curving to the right, we turn left and stop at the parking area nearby.

Stop 1.1:

The target of this stop is to show a typical example for the border regions of the crystalline massifs. In order to demonstrate this, we walk northwest from the parking area along a hiking trail close to the eastern banks of the Zschopau river (Fig. 6). Before starting, we have a look at the cliffs of massive greenschists on the main road below "Sachsenburg" castle. After crossing the building area of the former "Schlossmühle" we can see slates outcropping on the right hand side. For the next 1.5 km, it is obvious that the metamorphic degree of the psammopelitic rocks, containing some basic intercalations, increase dramatically. Close to the granulites the slates have turned to micaschists and finally to migmatitic rocks containing cordierite. The first appearance of granulites is marked by cliffs along

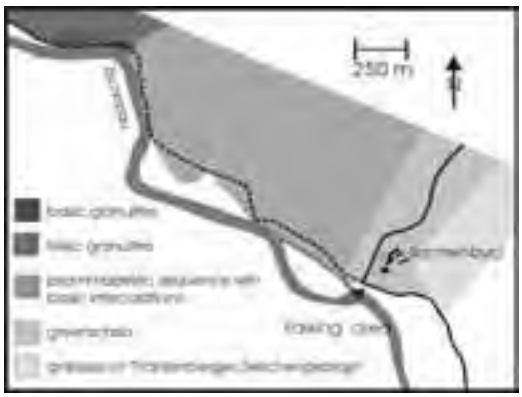

Figure 6 - Simplified geological map of the border zone at the south-eastern margin of the Granulitgebirge. The section shown is located in the Zschopau valley.

the hiking trail. These rocks are massive to platy and relatively fine-grained due to a mylonitic foliation. Felsic granulites are the dominant rock type there. They contain quartz, plagioclase, K-feldspar, minor garnet and kyanite. Biotite and amphibole seem to be retrograde phases of a medium temperature overprint. The intercalations and larger massive bodies of mafic

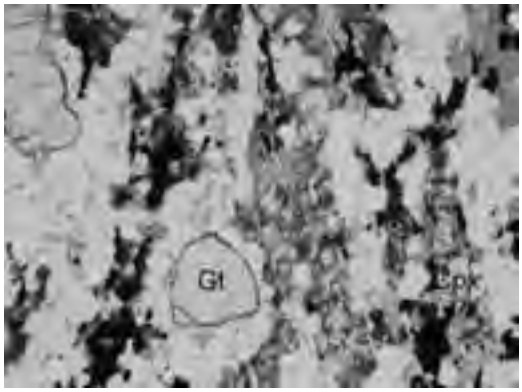

Figure 7 - Photomicrograph of basic granulite E301-3b. Plagioclase, amphibole, and ilmenite have formed at the expense of garnet (Gt), clinopyroxene (Cpx), and rutile. The latter phase is present as inclusion in garnet. Image width is 2 mm.

granulites are mainly formed from clinopyroxene, plagioclase, and garnet (Fig. 7). Minor constituents

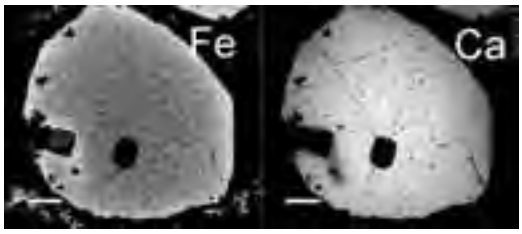

Figure 8 - Chemical zonation of garnet in basic granulite E301-3b. The grey code displays higher element concentrations by lighter tones. Scale bar represents 100 µm.

are orthopyroxene, rutile and quartz, which, however, can also be lacking. Amphibole, ilmenite and biotite are at least to some extent retrograde phases as in the felsic granulites. Orthoamphibole and chlorite can also occur as retrograde minerals.

Most minerals in the granulites are slightly zoned, thus, allowing estimations on the P-T evolution. For instance, garnet typically shows fairly homogeneously composed cores. Rims can be significantly poorer in Ca and Mg as well as richer in Fe (see Fig. 8 and Table 1). This chemical change follows the grain boundaries and is, thus, very likely due to a diffusional process at high temperatures. Clinopyroxene compositions tend to show decreasing jadeite contents towards the rim. For the granulites minimum P-T conditions were estimated to be 10 kbar and 800°C. It is not unlikely that the original

	Gt core	Gt rim	Cpx core	Cpx rim	Plag	Ilmenite	Amph	Amph	Biotite
	1321/12	1306/25	1306/15	1321/29	1319/5	1306/21	1320/19	1321/4	1320/3
SiO_2	38.76	37.78	50.43	51.60	60.05		44.19	40.53	35.63
TiO_2	0.16	0.08	0.43	0.25		51.93	1.96	2.70	3.32
Al_2O_3	21.38	20.92	3.35	2.12	26.21	0.07	9.97	14.51	14.19
Cr_2O_3	0.00	0.06	0.03	0.08		0.01	0.07	0.01	0.00
FeO	24.44	27.46	12.01	11.73	0.39	46.15	16.36	13.66	20.22
MnO	0.46	0.80	0.19	0.12		0.61	0.15	0.09	0.04
MgO	6.40	5.34	11.13	12.53		0.02	10.85	10.52	11.34
CaO	8.98	6.42	20.97	20.76	7.91	0.04	11.19	11.22	0.04
Na_2O			0.66	0.35	6.76		1.24	1.58	0.10
K_2O					0.29		0.92	2.20	8.89
Total	100.57	98.86	99.34	99.53	101.61	98.83	96.90	*97.13	*95.40
Si	5.947	5.980	1.917	1.950	2.637		6.570	6.067	5.535
Al^{IV}			0.083	0.050	1.356	0.002	1.430	1.933	2.465
Ti	0.018	0.010	0.012	0.007		0.997	0.220	0.304	0.388
Al^{VI}	3.866	3.902	0.067	0.044		0.002	0.316	0.627	0.132
Cr	0.000	0.008	0.001	0.002		0.000	0.008	0.001	0.000
Fe^{3+}	0.134	0.090	0.040	0.015	0.014		0.570	0.208	
Fe^{2+}	3.002	3.545	0.342	0.356		0.985	1.463	1.502	2.626
Mn	0.059	0.107	0.006	0.004		0.013	0.020	0.012	0.006
Mg	1.463	1.259	0.630	0.706		0.001	2.404	2.347	2.625
Ca	1.476	1.089	0.853	0.841	0.372	0.001	1.783	1.800	0.006
Na			0.049	0.025	0.575		0.357	0.458	0.029
K+Ba					0.016		0.174	0.426	1.861

*Table 1 - EMP analyses (in wt.%) of minerals from basic granulite E301-3b taken at the southeastern margin of the Granulitgebirge (Zschopau valley). *= total contains 0.11 wt.% (Amph) and 1.63 wt.% (Biotite) of BaO.*

Volume n° 2 - from B16 to B33

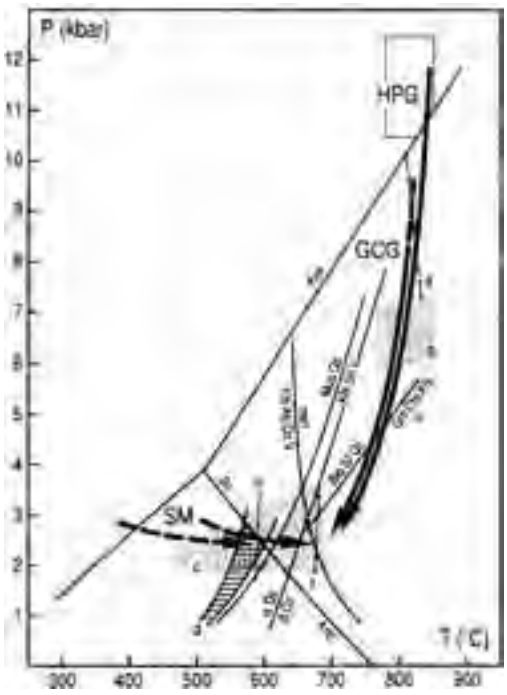

Figure 9 - P-T paths for the high pressure granulites (HPG) and the schist mantle (SM) of the Granulitgebirge according to Reinhardt and Kleemann (1994).

metamorphic conditions were significantly higher.

The retrograde alteration happened mainly during a strong pressure release at temperatures still above 700°C (see Fig. 9). On the contrary, the phyllite mantle as the hanging wall of the Granulitgebirge was drastically heated close to the contact to the granulites. This event occurred at depths of only 10 km (~ 3 kbar). According to strain indicators in the mantle rocks an extensional environment was suggested by Reinhardt and Kleemann (1994) as a cause for the final emplacement of a large fragment of lower crust, the Granulitgebirge, in such shallow crustal levels.

After returning to the parking area near the inn "Fischerschänke", we move back to Frankenberg. Again just before reaching the town, we turn left following route B169 heading for Hainichen and Döbeln. After about 11 km we cross Highway A4 and drive for an additional 4 km until reaching Greifendorf. Close to the centre of this village, we turn right to move along the banks of a brook for about 400 m. We stop at the road to then walk for about 150 m upwards to the entrance of an abandoned

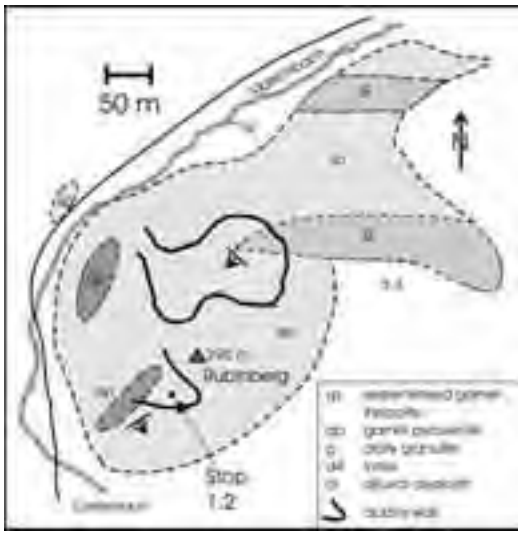

Figure 10 - Simplified geological map of the Rubinberg area, south-eastern Granulitgebirge.

quarry at Rubinberg hill (Fig. 10).

Stop 1.2:

The target of this stop is to show typical serpentinites of the Granulitgebirge, former garnet lherzolites, including pyroxenite bodies in these rocks. At the Rubinberg one can easily find serpentinites with relics of the mineral assemblage (Fig. 11) of a former lherzolite body that extends from the quarry of stop 1.2 to the northeast by about 3 km. From the partially conserved lherzolites one can reconstruct the fabric

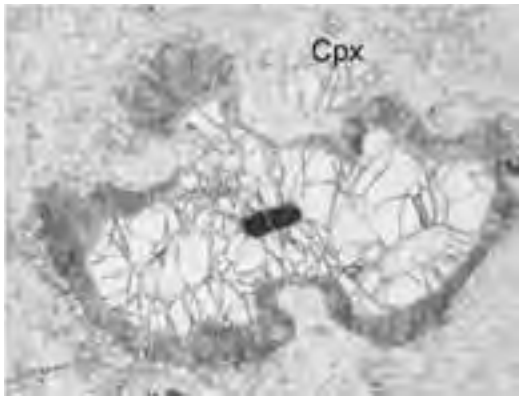

Figure 11 - Photomicrograph of a marginally altered garnet with decomposed inclusion minerals. The garnet is in serpentinised lherzolite GR99-1B. A larger relic of clinopyroxene (Cpx) is discernible nearby. Smaller relics of olivine and orthopyroxene are also present. Image width is 3.5 mm.

	Gt core 4-1B	Gt rim 1-1B	Cpx 16-1B	Cpx rim 29-1B	Opx 26-1B	Ol 18-1B
SiO_2	42.24	42.41	53.62	52.61	56.60	40.54
TiO_2	0.31	0.36	0.48	0.60	0.09	0.02
Al_2O_3	23.09	22.38	4.46	6.39	2.99	0.00
V_2O_3	0.03	0.04	0.06	0.08	0.01	0.00
Cr_2O_3	0.68	1.39	1.22	0.86	0.29	0.01
FeO	8.61	9.32	2.86	2.76	6.88	9.94
MnO	0.37	0.34	0.05	0.10	0.14	0.13
MgO	20.98	20.91	15.52	14.77	33.93	49.18
NiO			0.09	0.01	0.08	0.42
CaO	4.72	4.58	20.32	21.03	0.33	0.03
Na_2O	0.05	0.05	2.05	1.92	0.00	
K_2O			0.01	0.00	0.00	
Total	101.11	101.82	100.73	101.13	101.33	100.27
Si	5.889	5.909	1.929	1.886	1.932	0.992
Al^{IV}			0.071	0.114	0.069	0.000
Ti	0.033	0.038	0.013	0.016	0.002	0.000
Al^{VI}	3.795	3.676	0.118	0.157	0.052	
Cr	0.075	0.153	0.035	0.024	0.008	0.000
V	0.003	0.005	0.002	0.002	0.000	0.000
Fe^{3+}	0.127	0.167				0.016
Mg	4.360	4.344	0.832	0.789	1.726	1.793
Mn	0.044	0.040	0.002	0.003	0.004	0.003
Fe^{2+}	0.877	0.920	0.086	0.083	0.196	0.188
Ni			0.003	0.000	0.002	0.008
Ca	0.705	0.684	0.783	0.808	0.012	0.001
Na	0.014	0.013	0.143	0.134	0.000	
K			0.001	0.000		

Table 2 - EMP analyses (in wt.%) of minerals from serpentinised garnet lherzolite GR99-1B taken from the Rubinberg quarry, Granulitgebirge.

before serpentinisation. Garnets of several mm-size are in an equigranular matrix of significantly smaller clinopyroxene, orthopyroxene, and olivine. Together with the information on the chemical composition of the minerals (see Table 2) it is suggested that the relatively large, nearly homogeneous garnets belong to a pre-recrystallisation stage. Only the garnet rim adjusted chemically to the other silicates that were affected by deformation to recrystallise. In terms of relative pressure conditions, the chemical compositions are interpreted as follows. Garnet contains more Cr at the rim than in the extended core because of the breakdown of spinel as a result of pressure increase. Afterwards the matrix recrystallised. On the basis of geothermobarometry with garnet-clinopyroxene pairs as reported by Massonne and Bautsch (2002), P-T conditions close to 19 kbar and 1000°C can be derived for this stage. These data are compatible with the Al content in orthopyroxene associated with olivine and garnet. Subsequent pressure release is documented by increasing Al in clinopyroxene from core to rim.

Additional information on the P-T evolution

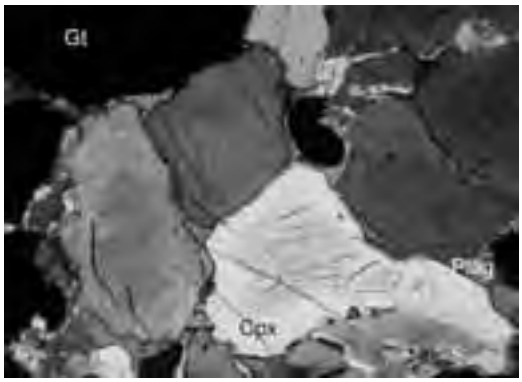

Figure 12 - Photomicrograph of an equigranular portion of sample GR99-1A rich in garnet (Gt) and clinopyroxene (Cpx). Plagioclase (Plag) and some amphibole occur along grain boundaries of garnet and pyroxene. Cpx contains numerous tiny inclusions of SiO_2 and alkalifeldspar all perfectly oriented. Image width is 1.5 mm.

comes from garnet-rich pyroxenite outcropping at the south-western wall of the quarry. This rock contains mainly mm-sized, equigranular garnet and clinopyroxene. However, rare cm-sized garnet can be detected as well. The large garnets are interpreted, similar to garnet in the lherzolite, as pre-recrystallisation mineral. Some plagioclase and rare amphibole have formed along grain boundaries mainly of clinopyroxene (Fig. 12). Small garnets seem to be also associated with plagioclase and amphibole. A process of partial melting is suggested also because of the irregular shape of garnet and the estimated temperature of about 1100°C for the rim compositions of garnet and clinopyroxene (Table 3). The corresponding pressure amounts to 22 kbar. Core compositions yielded somewhat higher temperatures at pressures of 26 kbar. At this stage the rock was an eclogite as the jadeite content in clinopyroxene was above 20 mol% (Table 3). In the clinopyroxene cores numerous, tiny and transparent rods could be detected (Fig. 12). Compositional investigations suggest SiO_2 and alkalifeldspar as exsolution of clinopyroxene. This phenomenon was assigned to UHP metamorphism, for instance, by Dobrzhinetskaya et al. (2002). Pressures as high as 30 kbar result at least from EMP analyses of clinopyroxene using a strongly defocused electron beam to obtain integral analyses of clinopyroxene and exsolution minerals (Table 3).

Returning to B169 at Greifendorf we move to the right but leaving the federal road almost immediately afterwards to go to Reichenbach and further on to Waldheim. In the centre of the town of Waldheim we

Volume n° 2 - from B16 to B33

	Gt core 42-1A	Gt small 53-1A	Cpx in Gt 43-1A	Cpx integr. 8N-1A	Cpx 59-1A	Plag 56-1A	Ilm 31-1A
SiO_2	39.95	39.90	49.63	51.49	49.15	60.88	
TiO_2	0.19	0.13	0.79	0.60	1.03	0.03	56.16
Al_2O_3	22.69	22.65	11.24	11.27	9.84	24.76	0.00
V_2O_3	0.05	0.03	0.14	0.10	0.13		1.11
Cr_2O_3	0.02	0.03	0.03	0.03	0.06	0.00	0.01
FeO	16.59	17.97	5.94	6.13	6.78	0.21	36.87
MnO	0.29	0.43	0.06	0.06	0.04	0.00	0.31
MgO	10.05	11.69	10.22	10.20	11.63	0.00	7.26
CaO	11.56	8.20	18.27	17.25	19.47	5.93	
Na_2O	0.05	0.03	3.46	3.46	1.97	8.51	
K_2O			0.00	0.02	0.02	0.26	
Total	101.45	101.07	99.78	100.61	100.12	100.58	101.73
Si	5.843	5.834	1.819	1.859	1.806	2.697	
Al^{IV}			0.181	0.141	0.194	1.293	
Ti	0.021	0.015	0.022	0.016	0.029	0.001	0.993
Al^{VI}	3.911	3.902	0.304	0.339	0.232		0.000
Cr	0.003	0.003	0.001	0.001	0.002	0.000	0.000
V	0.006	0.003	0.004	0.003	0.004		0.021
Fe^{3+}	0.081	0.091				0.008	0.013
Mg	2.191	2.547	0.558	0.549	0.637	0.000	0.255
Mn	0.036	0.053	0.002	0.002	0.001	0.000	0.006
Fe^{2+}	1.948	2.106	0.182	0.185	0.209		0.712
Ca	1.811	1.285	0.717	0.667	0.767	0.282	
Na	0.013	0.009	0.246	0.242	0.140	0.731	
K			0.000	0.001	0.001	0.015	

Table 3 - EMP analyses (in wt.%) of minerals (integr. = host + exsolution) from garnet pyroxenite (eclogite) GR99 -1A taken from the Rubinberg quarry, Granulitgebirge.

cross Zschopau river to turn left following the river to the south for some hundred metres. The main road then turns west heading for Reinsdorf. At the entrance of this village, an almost abandoned quarry is located on the right-hand side.

Stop 1.3:

Here another large serpentinite body of the Granulitgebirge was or still is quarried for macadam and to produce an artificial construction stone called "Terrazzo". However, the quarry seems to be used now to slowly fill up with construction debris and other trash. In contrast to the massive serpentinite of stop 1.2, the serpentinite body here is significantly layered due to a penetrative deformation event. This layering is concordant to the foliation of the surrounding felsic granulites. The ultrabasic body is as thick as 100 m outcropping over a larger area (Fig. 13). Pyroxenites occur as layers, 10 to 50 cm thick, or boudins parallel to the layering of the serpentinite. Veins and larger bodies of granitoids crosscut the ultrabasic rocks.

The serpentinite consists of about 60% orthochrysotile forming a mesh-like fabric. The meshes are oriented with an axial symmetry similar

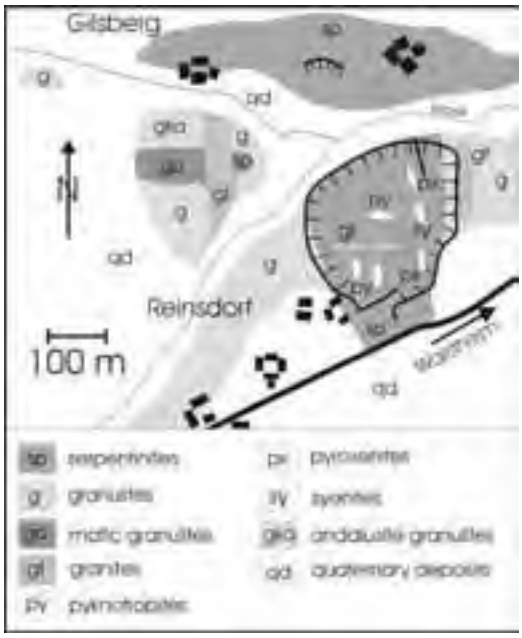

Figure 13 - Simplified geological map of an area east of the village of Reinsdorf, southeastern Granulitgebirge.

to the orientation of quartz c-axes in the nearby granulites. In addition to orthochrysotile, 20 to 30% lizardite occurs. Moreover, specific minerals such as carbonates appear close to the granitoids as a result of fluid-rock interaction. Originally, garnet was abundant but it is strongly altered. Nevertheless, pseudomorphs after garnet can be easily detected with the naked eye in many portions of the serpentinite body. However, very rare garnet up to 1 cm in size was found as well.

The pyroxenites can be subdivided into three groups. 1. Those consisting of garnet and clinopyroxene only; 2. clinopyroxenite with green spinel and garnet along the grain boundaries of coarse-grained clinopyroxene; 3. orthopyroxene-rich pyroxenite with some relics of megacrysts consisting now of thick lamellae of orthopyroxene and garnet. Type 1 pyroxenite can be collected along the eastern wall of the quarry whereas types 2 and 3 seem to have disappeared.

Portions of type 1 pyroxenite consist of parallel clinopyroxene (cpx) lamellae, which are fairly regularly spaced, as can be seen with the naked eye, and identically oriented since they display the same interference colour in a thin section under crossed nicols (Fig. 14A). X-ray studies by Reiche and Bautsch (1984) had confirmed this also for the garnet (gt) lamellae, which are topotaxially

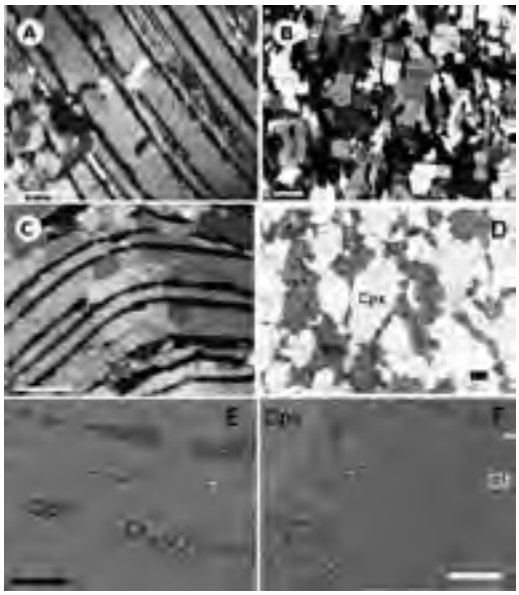

Figure 14 - Photomicrographs under crossed nicols (A-C) and under plain polarised light (D) as well as back scattered electron images (E,F) of pyroxenite types 1 (GR00-1: A-C) and 2 (PR 9457: D-F). Scale bars represent 1 mm (A-D) and 100 µm (E,F). The grey symplectites around spinel (Spi) in D have replaced garnet (Gt) at various stages as can be seen in F.

intergrown with clinopyroxene ((100)cpx//(110)gt and [001]cpx//[100]gt as well as (100)cpx//(100)gt and [001]cpx//[110]gt; Jekosch and Bautsch, 1991). As the lamellae can run parallel over cm, they were interpreted as former megacrysts (> 10 cm) with exsolution texture similar to those in pyroxenite type 3 (Reiche and Bautsch, 1985). The recrystallised fabric of equigranular garnet and clinopyroxene (Fig. 14B) close to the lamellae in pyroxenite type 1 is the result of deformation as we can see all kinds of transition from lamellar to equigranular fabric such as curved lamellae starting to recrystallise (Fig. 14C). Lamellar exsolution can also be observed in the mm-sized clinopyroxenes of type 2 pyroxenites. Here, formation of small garnet and more rarely spinel lamellae in clinopyroxene is obvious (Fig. 14E). But also the appearance of coarse grained garnet (and spinel?) along the grain boundaries of clinopyroxene is interpreted as reaction fabric (Fig. 14D). The orientation of clinopyroxene grains in pyroxenite types 1 and 2 is more or less isotropic whereas the recrystallised orthopyroxene grains in pyroxenite type 3, which frequently exhibit subgrain boundaries, are strongly oriented (Fig. 15). Finally, it is worthy of note that garnet can be replaced significantly

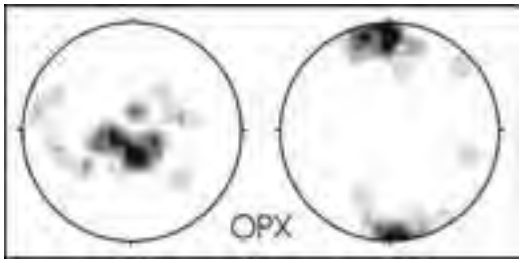

Figure 15 - Orientation of recrystallised orthopyroxene in type 3 pyroxenite (a-axes on the left, c-axes on the right hand side).

by various kinds of symplectites (Fig. 14F) often consisting of orthopyroxene and spinel but also of clinopyroxene, amphibole, potassic white mica and feldspars. The latter minerals are rather constituents of late alteration. Coarse-grained clinopyroxene is much rarer altered compared to garnet.

Electron microprobe analyses (Table 4) and element concentration maps (Figs. 16 and 17) show that garnet, clinopyroxene, and spinel in the clinopyroxenites are slightly non-homogeneously composed, thus, allowing to estimate various P-T conditions on the basis of the equilibria: (1) almandine (in gt) + 3 diopside (in cpx) = pyrope (in gt) + 3 hedenbergite (in cpx) and (2) 2 grossular (in gt) + pyrope (in gt) = 3 $CaAl_2SiO_6$ (in cpx) + 3 diopside (in cpx). For a sample of type 1 pyroxenite Massonne and Bautsch (2002) computed P-T data of about 25 kbar and 1000°C for an early stage due to formation of exsolution lamellae. Afterwards the mantle fragment was inserted into the lower portion of a thickened continental crust during the Variscan orogeny causing deformation and, thus, significant recrystallisation of the pyroxenite. This event was estimated to have happened close to 11

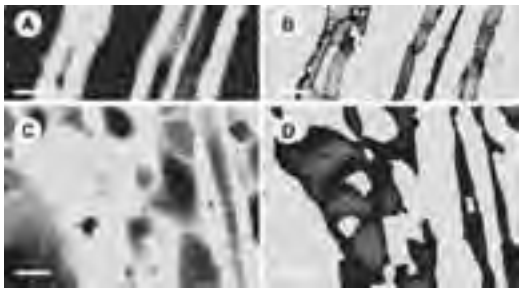

Figure 16 - Concentration maps of Al (left) and Ca (right hand side). A,B: Area (as in Fig. 14A) with lamellar microfabric of clinopyroxene and garnet (light in A and C). C,D: Strongly recrystallised area (as in Fig. 14B) close by. Lighter tones of the grey code refer to higher concentrations of the corresponding elements. Scale bars represent 200 µm.

Volume n° 2 - from B16 to B33

	PR 9457										GR 00-3			
	Gt1	Gt2	Gt3	Gt4	Cpx1	Cpx2	Cpx3	Cpx4	Spin1	Spin2	Gt1	Gt2	Cpx1	Cpx2
SiO_2	41.79	41.04	40.97	40.91	51.31	53.02	47.48	51.39	0.000	0.013	41.49	41.89	53.11	51.19
TiO_2	0.042	0.068	0.020	0.043	0.180	0.085	0.162	0.118	0.022	0.028	0.025	0.02	0.035	0.068
Al_2O_3	24.46	24.05	23.87	23.13	7.16	4.06	12.42	6.99	65.83	64.14	23.33	23.38	3.34	6.84
Cr_2O_3	0.184	0.180	0.208	0.472	0.087	0.063	0.068	0.085	2.25	1.74	0.295	0.295	0.171	0.212
V_2O_3	0.022	0.035	0.010	0.053	0.183	0.113	0.224	0.159	0.091	0.100	0.091	0.06	0.159	0.199
FeO	8.65	8.62	12.97	13.68	2.21	2.75	3.85	3.21	11.69	14.65	9.36	9.95	2.85	2.95
MnO	0.368	0.336	0.585	0.607	0.028	0.044	0.118	0.081	0.155	0.235	0.418	0.484	0.046	0.054
MgO	18.97	16.19	16.73	13.69	15.17	16.91	13.13	14.96	20.92	19.73	18.00	18.95	16.95	15.72
NiO				0.000				0.000	0.250	0.255	0.008	0.000	0.019	0.045
CaO	7.29	10.68	5.40	9.56	22.65	22.65	22.00	22.92	0.000	0.004	7.76	6.17	22.90	22.49
Na_2O	0.012	0.007	0.008	0.013	1.020	0.624	0.634	0.732			0.001	0.000	0.597	0.717
Total	101.80	101.22	100.78	102.07	99.99	100.28	100.02	100.62	100.99	100.91	100.78	101.19	100.18	100.47
Si	5.754	5.731	5.821	5.818	1.8591	1.9167	1.7308	1.8583	0.0000	0.0003	5.834	5.866	1.9185	1.843
Al^{IV}					0.1409	0.0833	0.2692	0.1417					0.0815	0.157
Ti	0.0043	0.0071	0.0021	0.0046	0.0049	0.0023	0.0044	0.0032	0.0004	0.0005	0.0026	0.0022	0.0010	0.0018
Al^{VI}	3.969	3.959	3.997	3.878	0.1649	0.0898	0.2645	0.1562	1.9276	1.9031	3.866	3.858	0.0610	0.1335
Cr	0.0200	0.0199	0.0234	0.0531	0.0052	0.0032	0.0065	0.0045	0.0442	0.0346	0.0328	0.0326	0.0049	0.006
V	0.0024	0.0039	0.0011	0.0060	0.0025	0.0018	0.0020	0.0025	0.0018	0.0020	0.0102	0.0068	0.0046	0.0057
Fe^{3+}	0.009	0.018	0.000	0.063					0.0255	0.0585	0.092	0.102	0.051	0.058
Fe^{2+}	0.987	0.989	1.541	1.564	0.0669	0.0831	0.1174	0.0970	0.2173	0.2500	1.010	1.062	0.035	0.031
Mn	0.0429	0.0397	0.0704	0.0731	0.0009	0.0013	0.0036	0.0025	0.0033	0.0050	0.0498	0.0574	0.0014	0.0016
Mg	3.892	3.370	3.544	2.902	0.8190	0.9110	0.7134	0.8063	0.7748	0.7406	3.770	3.956	0.9125	0.8435
Ni				0.0000				0.0000	0.0050	0.0052	0.0010	0.0000	0.0006	0.0013
Ca	1.076	1.598	0.822	1.457	0.8791	0.8773	0.8592	0.8881	0.0000	0.0001	1.168	0.926	0.8865	0.8675
Na	0.0024	0.0039	0.0011	0.0036	0.0717	0.0437	0.0448	0.0513			0.0002	0.0000	0.0420	0.0500

Gt1, Cpx1, Spin1 = core of coarse-grained garnet, clinopyroxene, and spinel, respectively; Gt2, Cpx2, Spin2 = corresponding rim compositions; Gt3, Gt4, Cpx3, Cpx4 = compositions of lamellae and blebs in coarse-grained Cpx.

Table 4 - EMP analyses (in wt.%) of minerals from pyroxenite types 1 (GR00-3) and 2 (PR 9457) in the serpentinite body at the village of Reinsdorf, Granulitgebirge.

kbar and 900°C. A more detailed P-T path could be derived from a type 2 pyroxenite (Massonne and Bautsch, 2003). This path (Fig. 18) shows a significant burial of the rock to depths of at least 100 km at temperatures above 1000°C during an early metamorphic stage. The subsequent exhumation path resembles that derived from type 1 pyroxenite. The late stage exhumation is compatible with the P-T path estimated for the granulites of the Granulitgebirge in general (see Fig. 9).

The bulk rock compositions of type 1 and 2 pyroxenites (Table 5) are not similar to those of common rocks such as gabbros. They rather reflect the composition of mono- to bimineralic layers as

Figure 17 - Concentration maps of Al and Ca of a section of sample PR 9457. The scale for the grey tones (increasing element concentrations towards the top) is on the right hand side. Scale bars represent 400 μm.

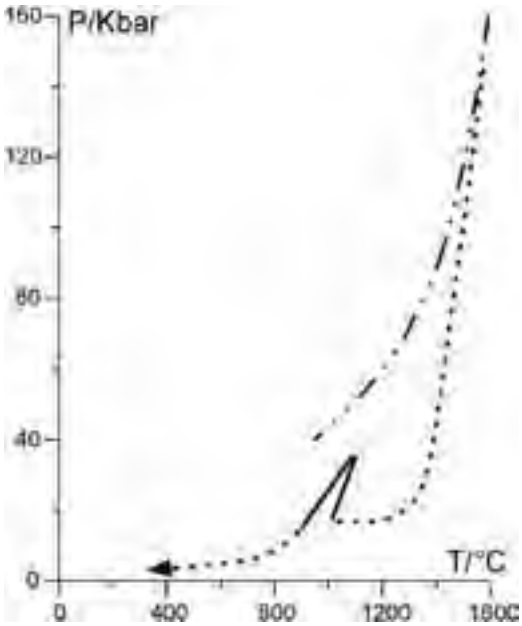

Figure 18 - P-T path (solid) derived for pyroxenites in the serpentinite body near the village of Reinsdorf, Granulitgebirge. The broken line of the path at UHP was inferred from geochemical studies (see text). The dashed-dotted curve represents the mantle geotherm.

Sample	PR9457	GR00-3L	GR00
Alteration in %	80	40	0
SiO_2 in wt.%	46.6	48.0	48.6
TiO_2	0.10	0.05	0.05
Al_2O_3	14.3	10.7	10.8
FeO	4.72	5.77	5.67
CaO	16.8	16.7	17.6
MgO	14.6	16.2	16.3
MnO	0.15	0.19	0.19
K_2O	0.38	0.20	0.00
Na_2O	0.28	0.48	0.50
P_2O_5	0.00	0.00	
H_2O_{tot}	0.59	0.45	
CO_2	0.26		
Sum	98.7	99.3	100.0
Li in ppm	84.5	31.8	22.5
Sc	91.5	112	112
V (XRF)	426	741	802
Cr (XRF)	1661	1247	1190
Ni	232	307	312
Cu	7.51	2.41	2.89
Zn	4.71	10.2	9.2
Ga	7.29	7.67	7.60
Rb	19.3	11.0	1.0
Sr	20.7	22.9	23.4
Y	11.0	8.92	9.3
Zr (XRF)	4	150	119
Nb	1.10	0.70	0.61
Sn	1.87		
Ba	45.8		< 20
Hf/Zr	b.d.l.	0.035	
Ta	1.44	0.70	0.55
Pb	0.04		
Th	b.d.l.	1.28	1.33
U	b.d.l.	0.89	0.90

Table 5 - XRF analyses of type 1 (GR00-3L) and type 2 (PR 9457) pyroxenites from the serpentinite body at the village of Reinsdorf, Granulitgebirge. The concentrations of most trace elements were determined by ICP-MS. GR00 shows values extrapolated to 0 % alteration using several analyses of similar rocks with various degrees of alteration. b.d.l.= below detection limit.

can be also inferred from the original megacryst nature at least of type 1 pyroxenites. On the basis of the REE patterns of the pyroxenites ($(Yb/Nd)_N$ > 10, Fig. 19), Massonne and Bautsch (2002, 2003) concluded that the pyroxenite layers originally consisted of majoritic garnets. For type 1 pyroxenite, such a garnet would have once contained about 50 mol% of $(Mg,Ca)_4Si_4O_{12}$ component. If this is true, the rock must have resided in the transition zone of the Earth's mantle (depths > 400 km). The uplift of the rock (for possible P-T path see Fig. 18) could have been facilitated by melts within a mantle plume. In the search for hints at such melts, boudins of quartz-free syenite, which are spatially related to the pyroxenites, were investigated (Massonne et al., 2002). However, the trace element pattern of the syenite showed no relation to ultrabasic rocks. It

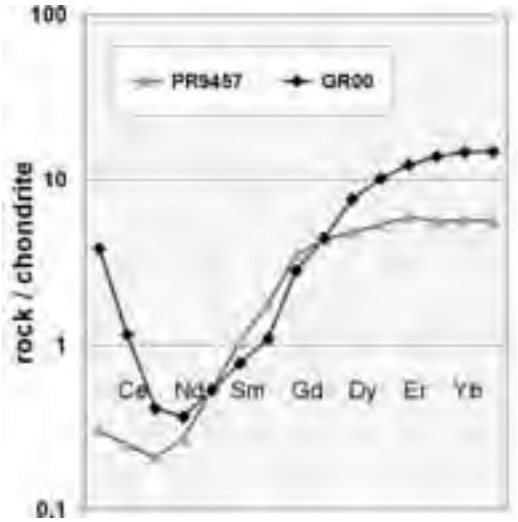

Figure 19 - REE pattern of clinopyroxenites occurring in the serpentinite body near the village of Reinsdorf, Granulitgebirge. The data were obtained by ICP-MS analyses and subsequently normalised to chondrite.

could be that the syenite was an ordinary felsic rock chemically altered by fluid-rock interactions with the serpentinite. This interpretation should hold true for the pyknotropites (see Fig. 13) which are former granitoids transformed to alkalifeldspar-rich rocks.

We return to Waldheim but stop soon after reaching the edge of town. We are now at the western banks of the Zschopau river. From here we walk southwards on a tourist trail along the river.

Stop 1.4: (optional)

Along the walk (see Fig. 20) cliffs appear on the right side of the tourist trail. Similarly, as seen during the walk of stop 1.1, we can discern felsic granulites as well as basic intercalations. It was about here where Rötzler and Romer (2001) discovered coarser grained metabasites and in them garnet with enclosed relics of omphacite. These authors used the original eclogitic nature of the rock to estimate early metamorphic P-T data. These were close to 1000°C and 22 kbar as also determined by Massonne and Bautsch (2002) for clinopyroxenites from the nearby village of Reinsdorf (see Fig. 18). Romer and Rötzler (2001) used the U-Pb system to determine the metamorphic event to 342 Ma. A very fast exhumation of the rock was deduced from almost identical U-Pb ages obtained from zircon, titanite, and apatite concentrates.

Volume n° 2 - from B16 to B33

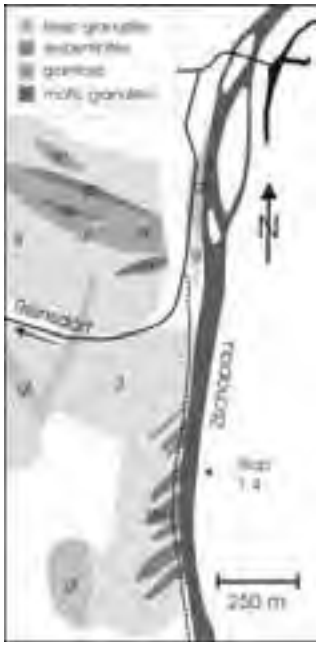

Figure 20 - Simplified geological map related to outcrops at the western banks of Zschopau river south of the town of Waldheim.

DAY 2

The route of the excursion continues from Waldheim to Hartha where we have access to federal road B175. We turn to the southwest heading for Rochlitz. Close to this town we change to federal road B107 heading for Chemnitz. After about 12 km, close to the entrance to Diethensdorf, we turn to the right passing this village by a relatively small road mostly going downhill. Just after crossing the Chemnitz river we turn at the road crossing to the right following the Chemnitz river valley to the northwest. After about a few hundred metres there are abundant parking lots on the left hand side and a large quarry, run by "Westsächsische Steinwerke", on the opposite side of the river.

Stop 2.1:

The target of this stop is to show again the typical felsic granulites of the Granulitgebirge but also ultrabasic and basic bodies in the felsic matrix. The extension of these bodies and their relation to the country rocks can be well investigated here because of the excellent exposure in the quarry (Fig. 21).

The felsic granulites consist mainly of quartz, plagioclase, K-feldspar, and some garnet. Relics of kyanite are discernible under the microscope (Fig. 22). More often, however, aggregates of sillimanite

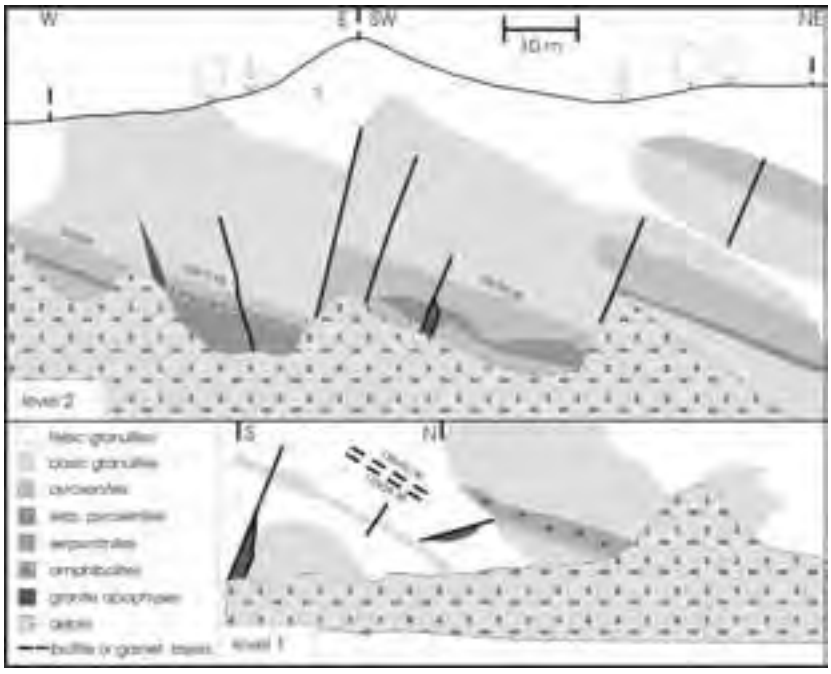

Figure 21 - Lithological relations seen at the walls of the large quarry in the Chemnitz valley close to the village of Diethensdorf, Granulitgebirge.

	Gt	Gt	Plag	Kf	Alkfs	Bt	Sill
	large core	small		small	with lamel.	small	
	2-8b	15-8b	13-8b	23-8c	25-8c	21-8c	19-8c
SiO_2	37.98	38.27	65.35	66.02	66.73	37.42	36.95
TiO_2	0.11	0.09	0.04	0.03	0.06	3.52	0.01
Al_2O_3	21.83	21.80	23.54	19.46	20.87	15.86	62.71
Cr_2O_3	0.01	0.03	0.00	0.01	0.01	0.05	0.00
FeO	29.16	30.76	0.09	0.03	0.01	13.58	0.56
MnO	0.50	0.61	0.00	0.00	0.03	0.01	0.01
MgO	6.71	8.16	0.00	0.01	0.00	14.59	0.02
CaO	4.23	1.02	3.90	0.05	1.10	0.00	0.01
Na_2O	0.00	0.00	8.39	1.01	4.77	0.19	0.01
K_2O			0.77	15.04	8.27	9.61	0.01
BaO			0.01	0.13	0.07	0.16	0.01
Total	100.53	100.77	102.09	101.79	101.92	94.98	100.32
Si	5.836	5.868	2.821	2.980	2.939	2.787	0.995
Al^{IV}			1.198	1.035	1.083	1.213	
Ti	0.013	0.010	0.001	0.001	0.002	0.197	0.000
Al^{VI}	3.954	3.940				0.179	1.990
Cr	0.002	0.004	0.000	0.000	0.000	0.003	0.000
Fe^{3+}	0.045	0.057	0.003	0.001	0.001		0.013
Mg	1.536	1.865	0.000	0.001	0.000	1.620	0.001
Fe^{2+}	3.703	3.889				0.846	
Mn	0.065	0.079	0.000	0.000	0.001	0.000	0.000
Ca	0.696	0.168	0.181	0.003	0.052	0.000	0.000
Na	0.000	0.000	0.702	0.088	0.407	0.027	0.001
K			0.042	0.866	0.465	0.913	
Ba			0.000	0.002	0.001	0.005	

Table 6 - EMP analyses (in wt.%) of minerals from the felsic granulite GR02-8c taken in the quarry at Diethensdorf, Granulitgebirge.

occur which have replaced kyanite. Biotite is probably a retrograde product only. Small portions of the rock contain mm-sized garnets being significantly larger than the ordinary garnets (Fig. 22). These portions seem to have been unaffected by the usual penetrative deformation that has led to fine-grained strongly foliated granulites. The composition of the extended cores of the large garnets differs significantly from that of their rims, which is nearly

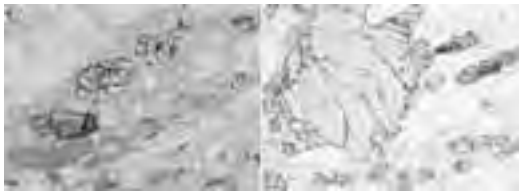

Figure 22 - Photomicrographs taken from felsic granulite sample GR02-8c (quarry close to Diethensdorf) under plain polarised light. Relics of kyanite (Ky) can be seen on the left hand side. Image width is 1.3 mm. On the right hand side, a large garnet (Gt) is discernible whereas garnets of common size in this rock are enriched in a layer below the big garnet. An aggregate of sillimanite (Sill) is a pseudomorph after kyanite. Image width is 2.5 mm.

	GR02-3c	GR02-7b	GR02-8b
SiO_2 in wt.%	43.97	43.59	40.28
TiO_2	1.29	1.34	0.46
Al_2O_3	16.30	16.82	10.35
Fe_2O_3	13.37	12.64	11.72
CaO	12.56	10.83	11.85
MgO	9.90	8.93	14.39
MnO	0.21	0.21	0.19
K_2O	0.10	0.45	0.01
Na_2O	1.47	1.89	0.66
P_2O_5	0.32	0.75	0.03
Sum	99.96	97.74	90.94
F	0.04	0.09	0.04
S	0.19	0.00	0.32
Cl	0.01	0.02	0.00
Sc in ppm	50	54	44
V	402	390	138
Cr	277	323	1418
Ni	113	113	1052
Cu	120	27	545
Zn	97	97	52
Ga	17	17	12
Rb	11	29	9
Sr	158	169	87
Y	24	39	26
Zr	58	93	208
Nb	9	13	0
Ba	210	134	3
La	13	27	7
Ce	50	65	23
Nd	16	40	8
Sm	5	7	3
Dy	5	7	3
Yb	3	5	12
Hf	4	4	3
Pb	4	9	1
Th	12	11	14
U	0	2	0

Table 7 - XRF analyses of garnet-rich pyroxenites from the Granulitgebirge.GR02-3c is from stop 1.2 (Rubinberg). GR02-7b was sampled close to stop 1.4 where railroad tracks are cut into the crystalline rocks a few hundred metres south of Waldheim station. GR02-8b is from the large quarry close to Diethensdorf (stop 2.1).

identical to the compositions of the small garnets (Table 6). Assuming 850°C and an anorthite activity of 0.2 in plagioclase (plag), the equilibrium: (3) grossular (in gt) + 2 kyanite + quartz = 3 anorthite (in plag) yields pressures as high as 17 kbar for the core composition of large garnets whereas pressures below 10 kbar result using the compositions of the small garnets.

The bulk compositions of garnet-rich pyroxenites associated with serpentinites were determined. Examples are given in Table 7. Whereas those from the Rubinberg quarry and from a body southwest of Waldheim (see Fig. 20) are, for instance, relatively rich in Ti, Al and light REE, the one in Table 7 from stop 2.1 is more similar to the garnet clinopyroxenites

Volume n° 2 - from B16 to B33

from the quarry at Reinsdorf. Relative high concentrations of Ni and Cu are here related to the presence of sulphides in the garnet pyroxenite.

We return to B107 passing Diethensdorf again. Then, we continue heading for Chemnitz but instead of passing the city of Chemnitz we take the alternative using Highway A4. We have access to A4 at the northern city limits heading for Dresden. After several km we leave the highway again at exit 72 Frankenberg. This time we are passing Frankenberg on its western side on B80 directed to Flöha. About 2 km after passing this town we turn left crossing Zschopau river in the village of Plaue. We continue heading for Augustusburg. If we want to go directly to stop 2.3 we have to turn left at a traffic light in the town, following the road sign to Leubsdorf, otherwise we keep going straight on for 150 m more. On the right-hand side there is a parking area for visitors.

Stop 2.2: (optional)

The famous castle of Augustusburg, erected by the Saxonian electors in only 4 years at the end of the 16th century, is settled on top of a remnant of a Permian rhyolitic lava flow. We recommend visiting a small abandoned quarry at the southeastern base of the castle hill by walking from the parking area about 200 m to the north (Fig. 23). The old quarry is somewhat hidden but close to the paved road leading to the castle. At the walls of the abandoned quarry the massive appearance of the reddish rhyolite can be

Figure 23 - Geological map showing the simplified relations of the Permian rhyolites to the crystalline basement around the town of Augustusburg, Saxonian Erzgebirge.

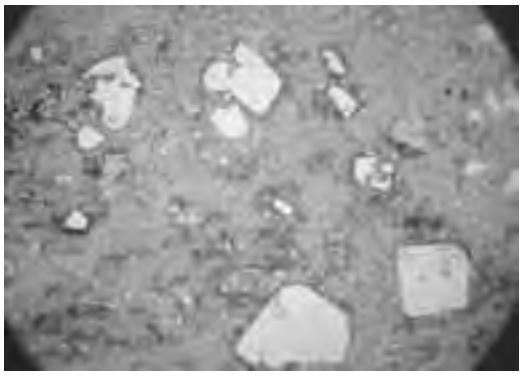

Figure 24 - Photomicrograph of a Permian rhyolite from Augustusburg containing phenocrysts of quartz and feldspars. Image width is 8.5 mm.

seen. The rock contains numerous quartz and feldspar phenocrysts (Fig. 24). A fluidal texture can also be easily recognised.

We return to the traffic light heading then towards Leubsdorf which we pass to follow the road to Eppendorf. Near the centre of this village we turn right into the road to Reifland then driving 1.6 km. A small road between houses appears on the left-hand side close to another road which turns to the right to Borstendorf.The road on the left leads us after 1.7 km to stop 2.3. We park ca. 50 m in front of another road our road leads to, because on the right-hand side there is a small abandoned quarry hidden in the forest.

Stop 2.3:

At this quarry we have a good exposure of massive eclogite belonging probably to a big lens or an assembly of several eclogite lenses (Fig. 25). In spite of the large eclogite bodies assumed to be below ground, further exposure of eclogite does not exist but abundant big blocks of eclogite can be found along the borders between fields and wood in the vicinity of stop 2.3. These blocks and the rocks in the quarry can contain fresh omphacite. However, this mineral can be completely altered to fine-grained symplectites of amphibole and plagioclase as well. Occasionally, omphacite + H_2O have reacted to form amphibole (Fig. 26) which could be as large as a few cm. This reaction still took place during the eclogite stage. The rare enrichment of potassic white mica might be also a reaction product of infiltrating H_2O when it contained potassium. Another interpretation of eclogitic layers rich in white mica is a pelitic protoliths originally present as thin strata within the basic rocks.

P-T conditions of the eclogite stage could be

Figure 25 - Simplified geological map of an area in the GEU of the Saxonian Erzgebirge, southeast of Eppendorf, with large eclogite bodies (grey) embedded in gneiss.

determined from phengite-bearing eclogite which contained quartz, common as a minor constituent of the eclogites, and kyanite as a rare accessory phase in the eclogites. Mineral equilibria of geobarometric importance are here those using components in phengite (phe) as, for instance: (4) pyrope (in gt) + 2 grossular (in gt) + 3 Al-Mg-celadonite (in phe) = 6 diopside (in cpx) + 3 muscovite (in phe) and (5) 2 kyanite + grossular (in gt) + 3 Al-Mg-celadonite (in phe) = 3 diopside (in cpx) + 3 muscovite (in phe) + 2 quartz/coesite. In addition, the equilibrium: (6) muscovite + 2 rutile = 2 quartz + Ti-muscovite (= $KAl_3SiTi_2O_{10}(OH)_2$) can be applied because rutile is omnipresent in the eclogites. In the absence of phengite, the equilibrium: (7) 3 diopside (in cpx)

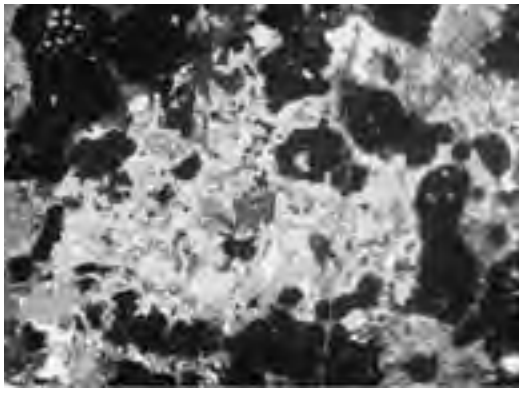

Figure 26 - Photomicrograph of an amphibole porphyroblast in eclogite sample Erz02-2 under crossed polarisers. The sample is from the quarry 2.5 km SE of the village of Eppendorf, Saxonian Erzgebirge. Image width is 4.5 mm.

	Gt		Omph		Phe	
	core	rim	core	rim	core	rim
	1109/09	1109/91	1109/80	1109/12	1109/33	1109/72
SiO_2	38.32	38.04	54.87	54.39	50.45	48.25
TiO_2	0.12	0.10	0.08	0.23	1.55	1.12
Al_2O_3	21.66	21.63	10.19	10.80	26.98	30.60
Cr_2O_3	0.01	0.04	0.00	0.03	0.02	0.01
FeO	21.07	20.96	4.63	4.25	1.28	1.29
MnO	0.38	0.43	0.00	0.07	0.00	0.00
MgO	5.65	6.13	8.81	9.03	4.01	2.71
CaO	13.12	11.85	15.21	15.76	0.00	0.00
BaO					0.18	0.11
Na_2O			5.40	5.33	0.47	0.83
K_2O					9.57	9.00
Total	100.33	99.19	99.36	99.88	94.51	93.93
Si	5.811	5.830	1.976	1.949	6.705	6.437
Al^{IV}			0.024	0.051	1.295	1.563
Ti	0.013	0.012	0.002	0.006	0.155	0.113
Al^{VI}	3.871	3.907	0.409	0.405	2.932	3.247
Cr	0.001	0.005	0.000	0.001	0.002	0.001
Fe^{3+}	0.128	0.088	0.000	0.003		
Fe^{2+}	2.544	2.598	0.139	0.125	0.142	0.144
Mn	0.049	0.056	0.000	0.002	0.000	0.000
Mg	1.277	1.400	0.473	0.483	0.795	0.539
Ca+Ba	2.131	1.946	0.587	0.605	0.010	0.006
Na			0.389	0.371	0.120	0.216
K					1.623	1.531

Table 8 - EMP analyses (in wt.%) of minerals from eclogite E174c taken from the large eclogite body SE of Eppendorf (stop 2.3), Saxonian Erzgebirge.

+ 2 kyanite = pyrope (in gt) + grossular (in gt) + 2 quartz/coesite could be also used for metamorphic pressure estimation. As the minerals are moderately chemically zoned (Table 8) a small portion of the P-T path for the eclogite could be deciphered. Due to the significant decrease of Si in phengite this path is related to exhumation at maximum temperatures around 800°C (Massonne, 1994). The path starts at UHP conditions of somewhat more than 30 kbar ending close to 20 kbar and 700°C. UHP conditions are required for the occurrence of K-cymrite ($KAlSi_3O_8 \cdot H_2O$). According to Massonne et al.

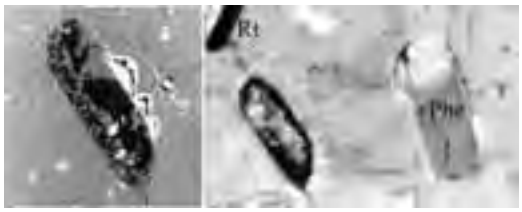

Figure 27 - Photomicrograph (right hand side) of inclusions (Rt = rutile, Phe = phengite) in omphacite of eclogite E174c (stop 2.3) under crossed polarisers. The inclusion (length about 140 µm) seen in the left corner at the bottom is also displayed as back-scattered electron image on the left hand side demonstrating the intergrowth of quartz and K-feldspar.

(2000), this mineral was enclosed in mineral cores mainly of omphacite but also in garnet. Now it is replaced by K-feldspar intergrown with quartz (Fig. 27). These pseudomorphs can be easily mistaken for those after coesite also because of cracks in the host mineral around the enclosed K-feldspar-quartz aggregate.

Results of geochemical analyses of eclogites from this locality and eclogite bodies nearby were reported by Massonne and Czambor (2003). These eclogites (SiO_2 = 48-52 wt.%, see Table 9) are characterised by $(Nb)_N$ = 5-36, $(Sr)_N$ = 5-17, Ta/Yb = 0.07-0.25, $(La/Sm)_N$ = 0.5-1.5, and $(Sm/Yb)_N$ < 1.8 (see Fig. 28). Massonne & Czambor (2003) referred these data to original MORBs. However, in addition to N-MORBs a trend to P-MORBs is discernible.

We take the road on the left heading for Großwaltersdorf. After passing this village we continue to Mittelsaida where we reach federal road B101. We turn left to drive ca. 19 km to the centre of Freiberg.

	1	2	3	4	5	6
SiO_2 in wt.%	49.76	49.93	51.58	51.25	49.50	50.29
TiO_2	1.88	2.06	1.32	1.54	1.92	1.67
Al_2O_3	15.78	15.60	16.47	16.14	14.80	16.70
FeO_{tot}	10.11	11.76	9.46	10.05	11.30	10.26
CaO	11.52	11.89	9.67	9.40	12.30	11.79
MgO	5.52	5.78	7.79	7.11	6.33	5.31
MnO	0.18	0.20	0.17	0.18	0.20	0.17
K_2O	0.09	0.09	0.13	0.38	0.23	0.40
Na_2O	2.78	2.39	2.52	2.62	2.32	2.48
P_2O_5	0.16	0.84	0.10	0.13	0.12	0.13
H_2O_{tot}	0.29	0.21	0.23	0.31	-	-
CO_2	0.16	0.12	0.05	0.15	-	-
Sum	98.23	100.87	99.49	99.26	99.02	99.20
Li in ppm	59.3	31.2	24.2	36.9	22.4	31.0
Sc	48.3	48.4	50.6	55.0	43.9	36.4
V (XRF)	326	365	225	236	353	336
Cr (XRF)	307	240	252	261	298	200
Ni	49.7	60.7	76.7	92.1	61.4	34.5
Cu (XRF)	80	57	16	26	69	89
Zn (XRF)	112	120	88	95	116	94
Ga	18.7	18.4	-	-	18.3	16.8
Rb	4.2	1.7	3.0	21.0	8.4	19.4
Sr	150	187	109	164	131	86
Y	60.1	59.0	24.2	24.5	39.7	31.8
Zr (XRF)	116	125	139	148	111	85
Nb	3.88	4.12	12.7	9.73	2.80	1.90
Sn	1.69	1.68	4.55	1.45	1.27	1.87
Ba (XRF)	56	31	71	61	42	274
Hf/Zr	0.043	0.054	0.028	0.034	0.032	0.040
Ta	1.17	0.74	1.01	0.76	0.34	0.26
Pb	3.33	2.10	4.35	2.37	1.59	1.45
Th	0.81	0.88	0.58	0.51	0.16	0.13
U	0.22	0.35	0.35	0.34	0.14	0.09

Table 9 - XRF and ICP-MS analyses of eclogites from the GEU of the Saxonian Erzgebirge. 1=Erz98-3 (at the village of Mittelsaida), 2=Erz98-4 (as 1), 3=KD39 (NE of the hamlet of Hutha), 4=KD59 (as 3), 5=E174c (stop 2.3), 6=E103c (1.2 km E of stop 2.3).

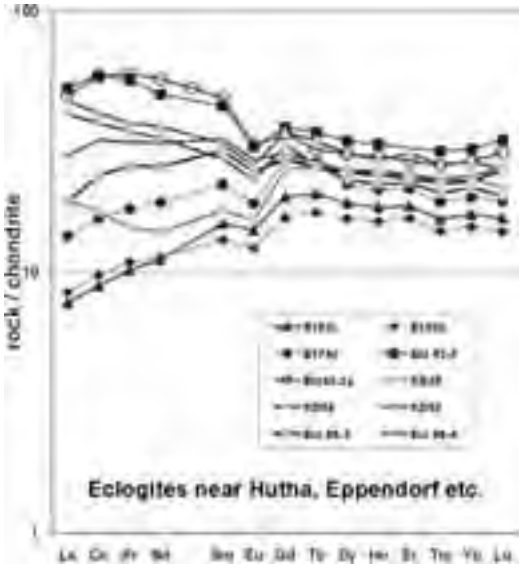

Figure 28 - REE patterns of eclogites in the northern to central portion of the GEU, Saxonian Erzgebirge. For localities see Table 9. The data were obtained by ICP-MS analyses and subsequently normalised to chondrite.

Stop 2.4:

At this stop we want to visit the mineralogical, petrological, and ore mineral collection of the Mining Academy at Freiberg. The museum is located in the town centre close to the dome erected in the 13th century. The Freiberg collections, founded in 1765, belong to the 10 oldest of currently more than 500 important geoscientific collections in the world. Especially the mineralogical collection is linked to famous names such as Werner, Mohs, Breithaupt, Weisbach, Kolbeck, and von Philipsborn. The exhibitions show a systematic mineral and rock collection, a regional collection of minerals and ore deposits of eastern Germany, specialities, for instance, related to precious stones and meteorites, and many more.

DAY 3

The route of the excursion continues from Freiberg to Annaberg-Buchholz. After about 23 km on B101 to the south we turn right at the entrance to the village of Forchheim heading for Lippersdorf. After 1.8 km we stop near the little bridge crossing the Saidenbach

brook. From here we have good access to the Saidenbach reservoir by walking on forest roads. As we want to visit first coesite-bearing eclogites at the northern shore of the reservoir (see Fig. 29), we take the trail on the north-western side of the brook. We walk for somewhat less than 2 km to reach the start of our tour along the shore of the reservoir provided that the water level is at least a few metres below maximum. However, this is usually so from July to September.

Stop 3.1A:

At this site we can easily find numerous blocks of eclogite along a 300 m section of the strand. Most of these blocks still contain fresh omphacite. The variety of eclogite here is surprising. Massive and foliated types exist as well as fine and coarser grained varieties. The eclogitic mineral assemblages are also variable. Rutile and quartz seem to be omnipresent. In a few cases, coesite could be detected in eclogite blocks from this locality (Massonne, 2001). However, it is only rarely preserved as inclusion in omphacite and garnet (Fig. 30) where it is then only partially transformed to quartz. Ba-rich potassic white micas with clearly decreasing Ba contents from core to rim were found in eclogite containing also cymrite but only as rare inclusion mineral (Table 10). Cl-rich apatite was reported by Massonne and Burchard (2000). This mineral, which is, untypical for apatite, significantly decomposed in the fresh eclogite, contained relative high amounts of Sr (> 4 wt.% SrO). Kyanite can be a rare constituent in eclogite blocks from this locality. Moreover, eclogites were found formed from conspicuous amounts of carbonate. Calcite, probably former aragonite, and dolomite can coexist in a single rock.

The bulk rock compositions of eclogites from stop 3.1A (Table 11) differ from those of MORBs. Instead of these rocks, magmatic protoliths related to oceanic islands, active continental margins or intraplate magmatism are conceivable. The REE patterns shown in Fig. 31 are compatible with such protoliths.

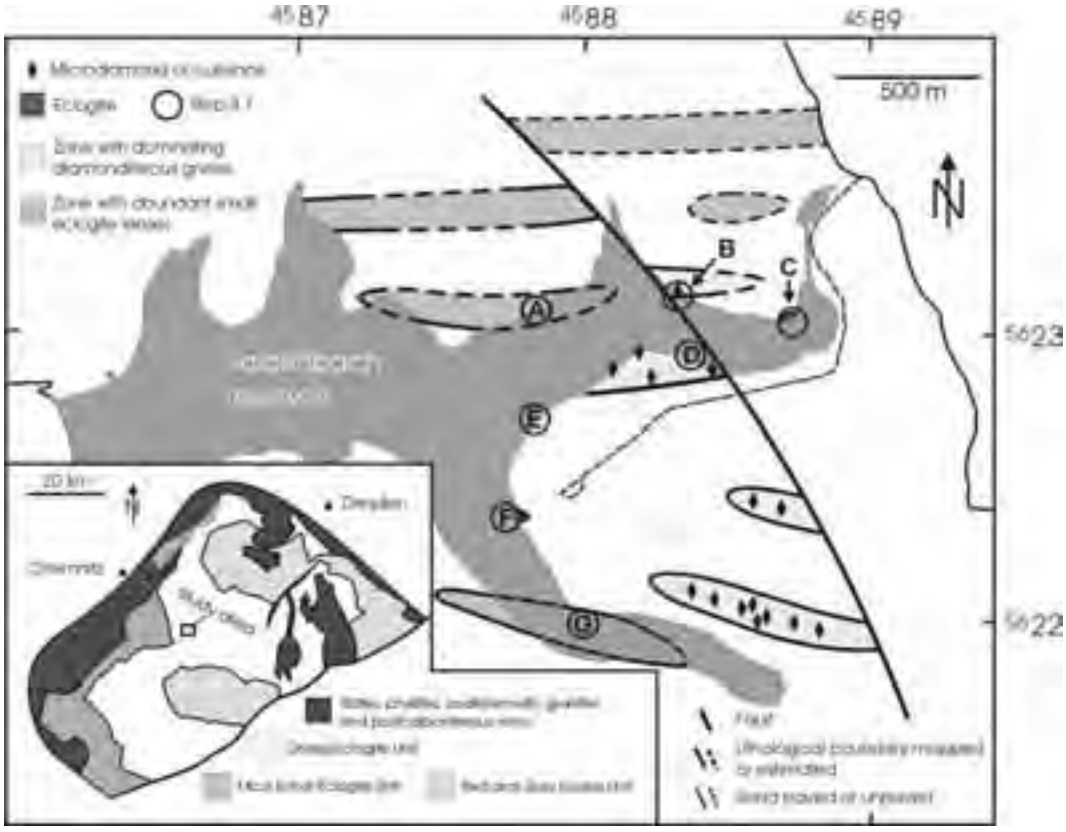

Figure 29 - Simplified geological map of the area around the Saidenbach reservoir. The map in the inlet shows the distribution of the GEU and MEU in the Saxonian Erzgebirge.

Volume n° 2 - from B16 to B33

Table 10 - EMP analyses (in wt.%) of minerals in coesite-bearing eclogitic rocks from the Saidenbach reservoir, Saxonian Erzgebirge. Most analyses were taken from Massonne and Burchard (2000) and Massonne (2001). Structural formulae were calculated as given in Table 12 and as follows: cymrite - 16 valencies, carbonates - 2 cations without C.

Mineral	garnet	garnet	calcite	dolomite	kyanite	omphacite	phengite	K,Ba-mica	cymrite
Sample	E99-24	E99-24	E99-24	E99-24	E99-24	E99-24	E99-24	E99-23	E99-23
SiO_2	38.67	38.64	0.21	0.10	36.54	54.27	48.23	37.40	31.54
TiO_2	0.14	0.12	0.00	0.04	0.09	0.26	2.29	8.42	0.17
Al_2O_3	22.85	23.12	0.08	0.05	63.40	13.89	27.02	30.11	24.62
Cr_2O_3	0.02	0.09	0.06	0.04	0.09	0.06	0.09		
FeO_{tot}	12.40	10.36	1.71	3.30	0.34	2.07	1.41	0.85	0.51
MnO	0.20	0.26	0.09	0.09	0.03	0.04	0.08		
MgO	10.45	11.00	7.49	19.23	0.05	8.09	3.33	2.72	0.17
CaO	14.54	11.05	48.42	32.83	0.03	13.86	0.11	0.06	0.05
Na_2O	0.09	0.06	0.07	0.02	0.00	6.17	0.31	0.61	0.12
K_2O	0.03	0.00	0.03	0.00	0.00		10.49	5.05	0.28
BaO	0.05	0.09	0.09	0.00	0.01		0.72	14.51	39.79
Cl								0.10	0.61
Total	99.60	99.67	58.24	55.69	99.62	99.31	92.13	99.84	97.86
Si	5.950	5.917	0.006	0.003	0.962	1.938	6.473	5.632	2.044
Ti	0.015	0.013	0.000	0.001	0.002	0.008	0.241	0.501	0.008
Al	3.915	3.981	0.003	0.001	2.024	0.583	4.419	5.344	1.881
Cr	0.002	0.010	0.002	0.001	0.002	0.002	0.010		
Fe	1.597	1.590	0.044	0.069	0.008	0.077	0.189	0.107	0.017
Mn	0.029	0.044	0.001	0.002	0.001	0.001	0.010		
Mg	2.394	2.393	0.342	0.858	0.002	0.429	0.690	0.611	0.016
Ca	2.269	1.721	1.589	1.069	0.001	0.535	0.020	0.010	0.004
Na	0.017	0.014	0.004	0.001	0.000	0.427	0.100	0.178	0.015
K	0.009	0.000	0.001	0.000			1.672	0.972	0.023
Ba			0.001	0.000			0.040	0.858	1.010
Cl								0.029	0.089

We

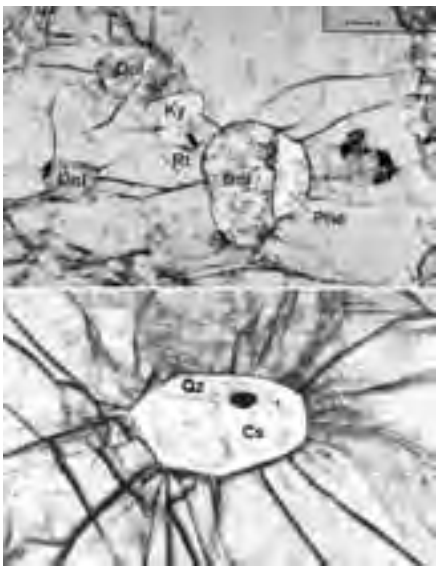

Figure 30 - Photomicrographs of inclusions (Dol= dolomite, Ky=kyanite, Phe=phengite, Rt=rutile) in garnet of eclogite sample E99-24 under plain polarised light. The sample is from stop 3.1A. Coesite (Cs) is surrounded by quartz (Qz). Image widths are 1.3 mm (at the top) and 0,65 mm (at the bottom).

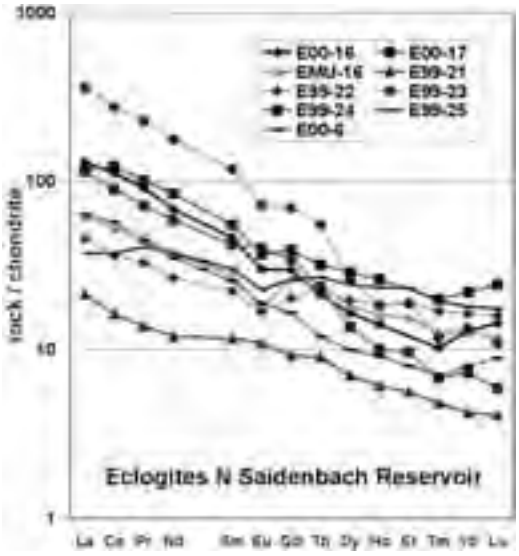

Figure 31 - REE patterns of eclogites from the northern shore of the Saidenbach reservoir (GEU, Saxonian Erzgebirge). The data were obtained by ICP-MS analyses and subsequently normalised to chondrite.

	E96-22	E96-23	E96-25	E00-6	E00-16	E00-17
SiO2 in wt.%	55.75	47.53	50.6	49.12	47.92	49.92
TiO2	1.89	0.89	3.37	1.22	1.06	3.07
Al2O3	15.80	17.83	15.28	16.55	16.66	16.23
FeOtot	6.94	7.28	12.33	7.97	9.37	12.44
CaO	7.44	10.08	8.34	12.84	10.41	8.28
MgO	4.24	8.76	4.28	6.42	7.54	4.03
MnO	0.14	0.11	0.20	0.14	0.15	0.20
K2O	1.54	0.86	0.78	0.41	0.41	0.51
Na2O	3.30	2.28	3.21	2.33	2.39	3.49
P2O5	0.15	0.22	0.79	0.15	0.16	0.64
H2Otot	0.82	0.36	0.57	0.25	0.23	0.22
CO2	0.12	0.34	0.10	0.25	0.41	0.11
Sum	99.60	96.23	99.89	99.55	97.33	99.34
Li in ppm	39.9	52.2	14.1	11.2	14.5	16.1
Sc	29.0	36.4	35.4	43.6	30.4	30.8
V (XRF)	214	158	317	227	193	317
Cr (XRF)	182	283	47	213	306	83
Ni	19.3	180	10.8	58.6	105	11.5
Cu (XRF)	22	79	37	81	81	30
Zn (XRF)	92	83	128	80	80	136
Ga	20.7	-	22.7	14.8	14.9	20.0
Rb	90.4	27.6	10.8	9.6	8.8	9.7
Sr	182	391	212	299	405	355
Y	29.9	18.8	37.1	19.7	25.5	55.0
Zr (XRF)	158	58	189	77	87	87
Nb	12.3	8.5	47.9	18.2	13.8	58.6
Sn	0.85	1.09	0.32	0.27	0.41	0.00
Ba (XRF)	606	2623	88	164	087	182
Hf/Zr	0.029	0.025	0.028	0.032	0.030	0.048
Ta	0.48	0.59	2.48	1.23	0.91	3.53
Pb	5.05	1.07	1.48	3.37	17.8	4.85
Th	0.97	1.92	0.17	0.48	5.43	3.83
U	0.27	4.41	0.64	0.89	1.29	0.60

Table 11 - XRF and ICP-MS analyses of eclogites from the northern shore of the Saidenbach reservoir, GEU of the Saxonian Erzgebirge.

move along the strand to the northeast. After crossing the issue of a little brook into the reservoir we walk for a few hundred metres to the southeast.

Stop 3.1B:

At this site we can recognise boulders differing from those of migmatitic gneisses ("Flammengneise") which appeared along the strand after we left the area with blocks of eclogites. These boulders consist of a non-foliated quartzofeldspathic rock with a homogeneous distribution of abundant mm-sized garnets. Muscovite forms a considerable portion of the matrix. Microdiamonds can be detected as inclusion in garnet and other phases (for details see stop 3.1D). Boulders of this rock, proposed to be named after the type locality saidenbachite (Massonne, 2003), occur very locally, so that this occurrence is interpreted as a lensoid body in the underground surrounded by migmatitic gneisses (see map of Fig. 29).

We continue to walk to the east for a few hundred metres and stop where the (former) Saidenbach brook changes direction.

Stop 3.1C:

At this corner, boulders of an eclogitic rock are concentrated. It seems to be that we can see here a real exposure of the rock. In contrast to the eclogites of stop 3.1A, this rock is homogeneous and non-foliated. Similar to the diamondiferous rock of stop 3.1B, mm-sized garnets are homogeneously distributed in the rock although the concentration of garnet is higher and the matrix is different compared to the rock of stop 3.1B. The matrix originally consisted mainly of phengite, quartz, and abundant omphacite. However the omphacite is entirely replaced by relatively coarse-grained symplectites of plagioclase and diopside-rich clinopyroxene or amphibole. Phengite is rarely completely but at least marginally substituted by biotite and plagioclase but also, probably during a late retrograde stage, by a fine-grained micaceous material. Microdiamonds could not be detected as inclusion mineral but omphacite rarely survived as inclusion in garnet (for more details see stop 3.1F).

We walk north to cross Saidenbach brook. Afterwards, we continue on the eastern strand heading south for several hundred metres and then to the west for several hundred metres more.

Stop 3.1D:

Again we meet with blocks of diamondiferous rocks seen before at stop 3.1B. Such blocks can be

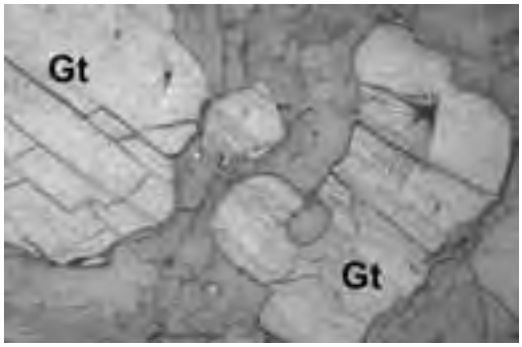

Figure 32 - Photomicrograph of microdiamonds enclosed in garnet (Gt) from quartzofeldspathic rock E97-3 seen under reflected light. Striations around the diamonds allow to detect them easily. Image width is 3 mm.

Mineral	garnet core	garnet core	garnet mediate	garnet rim	garnet incl. in zircon	jadeite incl. in zircon	kyanite	phengite core	phengite rim	phengite in garnet
Sample	[illegible]	E97-2	E97-2	E97-2	[illegible]	[illegible]	E97-3	E97-1	E97-1	[illegible]
SiO_2	[illegible]	[illegible]	[illegible]	[illegible]	[illegible]	[illegible]	[illegible]	[illegible]	[illegible]	[illegible]
TiO_2	[illegible]	[illegible]	[illegible]	[illegible]	[illegible]	[illegible]	[illegible]	[illegible]	[illegible]	[illegible]
Al_2O_3	[illegible]	[illegible]	[illegible]	[illegible]	[illegible]	[illegible]	[illegible]	[illegible]	[illegible]	[illegible]
Cr_2O_3	[illegible]	[illegible]	[illegible]	[illegible]	[illegible]	[illegible]	[illegible]	[illegible]	[illegible]	[illegible]
FeO_{tot}	[illegible]	[illegible]	[illegible]	[illegible]	[illegible]	[illegible]	[illegible]	[illegible]	[illegible]	[illegible]
MnO	[illegible]	[illegible]	[illegible]	[illegible]	[illegible]	[illegible]	[illegible]	[illegible]	[illegible]	[illegible]
MgO	[illegible]	[illegible]	[illegible]	[illegible]	[illegible]	[illegible]	[illegible]	[illegible]	[illegible]	[illegible]
CaO	[illegible]	[illegible]	[illegible]	[illegible]	[illegible]	[illegible]	[illegible]	[illegible]	[illegible]	[illegible]
Na_2O	[illegible]				[illegible]	[illegible]		[illegible]	[illegible]	[illegible]
K_2O	[illegible]				[illegible]	[illegible]		[illegible]	[illegible]	[illegible]
BaO								[illegible]	[illegible]	[illegible]
F								[illegible]	[illegible]	[illegible]
Total	[illegible]	[illegible]	[illegible]	[illegible]	[illegible]	[illegible]	[illegible]	[illegible]	[illegible]	[illegible]
Si	[illegible]	[illegible]	[illegible]	[illegible]	[illegible]	[illegible]	[illegible]	[illegible]	[illegible]	[illegible]
Ti	[illegible]	[illegible]	[illegible]	[illegible]	[illegible]	[illegible]	[illegible]	[illegible]	[illegible]	[illegible]
Al	[illegible]	[illegible]	[illegible]	[illegible]	[illegible]	[illegible]	[illegible]	[illegible]	[illegible]	[illegible]
Cr	[illegible]	[illegible]	[illegible]	[illegible]	[illegible]	[illegible]	[illegible]	[illegible]	[illegible]	[illegible]
Fe	[illegible]	[illegible]	[illegible]	[illegible]	[illegible]	[illegible]	[illegible]	[illegible]	[illegible]	[illegible]
Mn	[illegible]	[illegible]	[illegible]	[illegible]	[illegible]			[illegible]	[illegible]	[illegible]
Mg	[illegible]	[illegible]	[illegible]	[illegible]	[illegible]	[illegible]	[illegible]	[illegible]	[illegible]	[illegible]
Ca	[illegible]	[illegible]	[illegible]	[illegible]	[illegible]	[illegible]		[illegible]	[illegible]	[illegible]
Na	[illegible]				[illegible]	[illegible]		[illegible]	[illegible]	[illegible]
K								[illegible]	[illegible]	
Ba								[illegible]	[illegible]	
F								[illegible]	[illegible]	[illegible]

Table 12 - EMP analyses (in wt.%) of minerals in diamondiferous quartzofeldspathic rocks from the Saxonian Erzgebirge. The analyses were taken from Massonne (1999) as well as Massonne and Nasdala (2003). Structural formulae were calculated (as in previous and subsequent Tables) as follows: clinopyroxene (here: jadeite) - 4 cations, garnet - 10 six- and eightfold coordinated cations, kyanite - cation sum = 3, mica - 42 valencies without interlayer cations.

found for the next 500 metres continuing to walk westward. Thus, it is concluded that a larger body of diamondiferous quartzofeldspathic rock is subsurface. Detailed analytical studies of the mineral compositions (see Table 12) confirm that the microdiamonds (see Fig. 32) are enclosed in a specific compositional zone of garnet. This intermediate zone is characterized by low Ca concentrations (Fig. 33). Ca contents of the garnet core and the thin and irregular rim are higher. Micro-diamond inclusions in kyanite, which is, in general, a relic only as it is altered to white mica (Fig. 34), can occur in an intermediate zone as well. In the

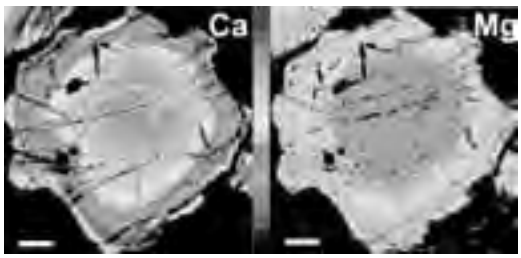

Figure 33 - Concentration maps of Ca and Mg of garnet in sample E97-2. The scale for the grey tones (increasing element concentrations towards the top) is in the middle. Scale bars represent 250 µm.

Figure 34 - Photomicrograph of a large kyanite from sample E97-3 seen under crossed nicols (Massonne, 2003). In the core of the crystal abundant small garnets are enclosed. Arrows point to microdiamonds. Image width is 4 mm.

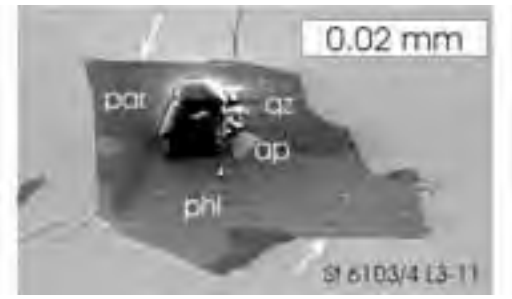

Figure 35 - SEM image of a polyphase diamond-bearing inclusion in garnet from quartzofeldspathic rock of the Saidenbach reservoir, central Saxonian Erzgebirge (Stöckhert et al., 2001). Arrows point to rational mica garnet interfaces. qz = quartz, par = paragonite, phl = phlogopite, ap = apatite.

kyanite core numerous small garnets are occasionally enclosed. Another interesting feature is the association of diverse minerals with diamond within a single inclusion in garnet (Fig. 35). Such minerals are quartz, feldspars, various micas, and occasionally apatite and rutile. Stöckhert et al. (2001) interpreted the polyphase inclusions as trapped siliceous fluid. In zircon, also containing microdiamonds (Nasdala and Massonne, 2000) in an intermediate growth zone, rare inclusions of garnet and jadeite were observed (Fig. 36). In addition, inclusions of phengite, quartz, and rutile occur in garnet cores. From these inclusion minerals, P-T conditions close to 18 kbar and 600°C were derived by geothermobarometry (Massonne and Nasdala, 2003). This result is almost identical to that by Willner et al. (1997) for gneisses in the vicinity of the saidenbachites. It was interpreted by Massonne and Nasdala (2003) as evidence for the location of the protolith of the saidenbachites at the base

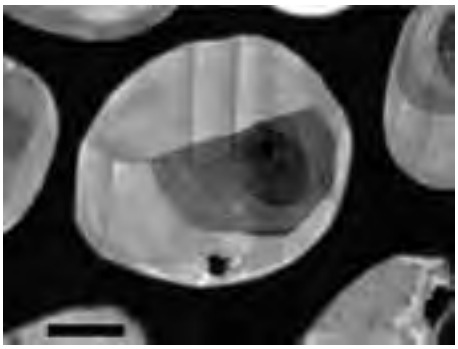

Figure 36 - Cathodoluminescence image of zircon from sample St6100. This mineral contains a jadeite inclusion (black) in the dark core zone. Microdiamond (black) appears in the lighter zone. Scale bar is 50 µm.

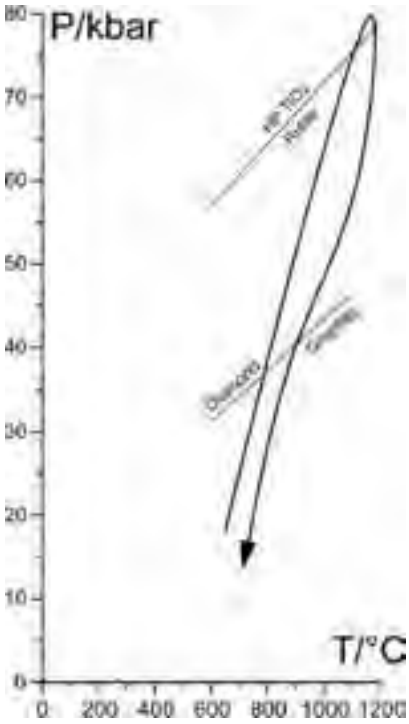

Figure 37 - P-T path derived for diamondiferous quartzofeldspathic rock from the Saidenbach reservoir, central Saxonian Erzgebirge. HP TiO_2 is TiO_2 with / -PbO_2 structure. The lower pressure limit of this phase was redetermined by Massonne et al. (2003).

of a thickened continental crust. Subsequently, the protolith was deeply subducted into the mantle to be heated to about 1200°C (Massonne, 2003). This caused considerable anatexis. The melts originated this way, still containing, for instance, garnet (cores), ascended from at least 200 km depth. Evidence for such depths is the appearance of a nanocrystal of HP TiO_2, which was found by Hwang et al. (2000) in a saidenbachite. During ascent, garnet and kyanite but also rutile, zircon, and diamond crystallised from the magma. Finally, the magma was emplaced in deep portions of thickened continental crust at P-T conditions of 15 to 18 kbar (55-60 km) and circa 750°C as determined by phengite geothermobarometry (Massonne, 1999). At this stage considerable quantities of muscovite were formed by a peritectic reaction from the remaining melt (Massonne, 2003). During the subsequent retrogression some biotite formed at the expense of muscovite. It is worthy of note that microstructural features were observed pointing to the formation of coesite, jadeitic pyroxene, and K-cymrite (Massonne,

	1	2	3	4	5	6
	E99-2a	E00-4	E98-7b	KD54	KD55	KD63
SiO2 in wt %	64.33	69.77	59.58	74.26	71.12	74.19
TiO2	0.79	0.61	1.04	0.29	0.42	0.30
Al2O3	18.03	15.04	21.56	14.19	14.64	13.29
Fe2O3	5.29	4.71	5.29	2.53	2.73	1.64
CaO	0.65	1.40	0.28	1.59	1.33	0.90
MgO	2.46	2.00	1.52	0.89	0.82	0.47
MnO	0.05	0.06	0.05	0.04	0.03	0.02
K2O	3.39	2.41	5.65	1.77	4.85	5.02
Na2O	2.51	3.23	0.37	4.29	2.92	2.51
P2O5	0.05	0.04	0.07	0.07	0.19	0.18
H2O+	1.30	0.56	2.89	0.53	0.56	0.62
CO2	0.09	0.08	0.04	0.03	0.04	0.05
Sum	99.21	99.99	99.31	100.46	99.62	99.79
Li in ppm	100.6	100.1	55.4	120.0	42.3	79.0
Sc	20.9	15.6	8.0	8*	7.2	4.9
V (XRF)	117	89	139	32	40	25
Cr (XRF)	77	94	114	1	11	0
Ni	45.4	29.1	23.1	8.66	8.45	5.01
Cu (XRF)	17	0	18	10	0	8
Zn (XRF)	104	67	22	11	41	30
Ga (XRF)	23	19	33	19	18	19
Rb (XRF)	135	103	338	73	170	252
Sr	112	102.4	12.8	27*	112.5	84.2
Y	13.8	14.6	10.2	65.9	45.1	49.0
Zr (XRF)	167	156	102	83	160	172
Nb	13.7	12.7	16.8	6.57	11.1	14.6
Sn	1.64	2.17	34.6	8.95	3.8	4.6
Ba (XRF)	415	297	699	142	657	430
HfO2	0.053	0.032	0.030		0.032	0.034
Ta	0.92	0.92	1.92	0.29	0.91	1.44
Pb	2.12	1.83	3.25	1.14	14.41	32.12
Th	2.44	6.38	4.58	0.54	12.80	16.84
U	1.23	1.82	4.30	0.10	0.77	5.42

Table 13 - XRF and ICP-MS analyses of quartzofeldspathic rocks from the GEU of the Saxonian Erzgebirge. 1,2 = diamondiferous rocks from the Saidenbach reservoir, 3 = rock without diamonds but with aspect similar to 1,2 taken northeast of the serpentinite body at Zöblitz, 4 = gneiss unusually rich in Na sampled SW of the village of Forchheim, 5,6 = ordinary gneisses taken close to diamondiferous rocks SW of Forchheim.

****=XRF data as an exception.***

2003; Massonne and Nasdala, 2003) during the ascent of the saidenbachitic magma.

The various metamorphic-magmatic stages were dated on zircons with a SHRIMP applying the U-Th-Pb-systems (Massonne et al., 2001). In addition, monazites were dated, which appear exclusively in the matrix of the saidenbachites and, thus, seem to be late stage minerals. The subsequent age data for ^{206}Pb and ^{238}U with 2$\hat{1}$ error were obtained: zircon core (dark in Fig. 36) - 336.1 ± 2.2 Ma, diamond-bearing zone (light in Fig. 36) - 336.0 ± 2.4 Ma, outer zone (very light but lacking in zircons of Fig. 36) - 329.9 ± 3.6 Ma, and monazite - 332.5 ± 3.8 Ma. Only very rare „magmatic" portions in zircon cores yielded ages as high as 396 Ma. The data of 336 Ma for the zircon cores are compatible with those around 340 Ma obtained by Kröner and Willner (1998) for gneisses of the GEU. Thus, the subsequent burial and exhumation process affecting the diamondiferous rocks took a few Ma or even less. The growth of the outermost layer of zircon and monazite formation happened some Ma after transport of the protoliths of the saidenbachites to maximum depth and also after inserting these rocks into the base of a still thickened continental crust.

Düffels and Massonne (2001) investigated the geochemical signatures of various quartzofeldspathic rocks from the GEU occurring between Saidenbach reservoir and the serpentinite body at Zöblitz (stop 3.2). Saidenbachites show clear differences from the surrounding country rocks (see, for instance, Cr, Ni, and Y of Table 13). This difference also concerns the REE patterns (Fig. 38) because all country gneisses have a very significant Eu anomaly. Thus, Düffels and Massonne (2001) disproved the idea that the saidenbachites are preserved portions of an UHP segment extending over many kilometres. It seems to be that saidenbachites and other UHP rocks form isolated bodies in rocks that had experienced, in fact, pressures as high as 20 kbar (Willner et al., 1997) but not more.

The recent investigation of the ^{13}C signature of microdiamonds in saidenbachite yielded $\delta^{13}C$(PDB)

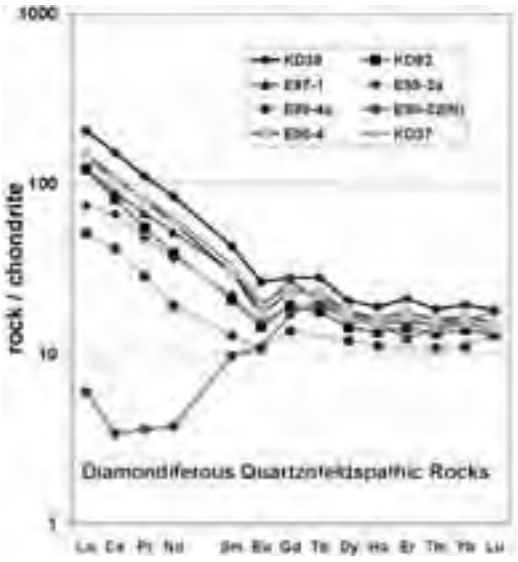

Figure 38 - REE patterns of saidenbachites from the GEU, Saxonian Erzgebirge. The data were obtained by ICP-MS analyses and subsequently normalised to chondrite. In sample E99-32(N) monazite is lacking, thus, explaining the exceptional pattern of the light REE.

values close to -30 ‰ (Massonne and Tu, 2003). This result is interpreted as an indication of an organic source of the carbon. Because bulk rock analyses of saidenbachites are very similar to those of clastic sediments (Table 13), organic material could have been already part of a sedimentary protolith. After sedimentation in Devonian times, according to the age of rare zircon cores with magmatic zonation features (Massonne et al., 2001), these rocks were deeply buried.

Stop 3.1E:

Already at the western end of the saidenbachite lens of stop 3.1D (see map of Fig. 29) but more obvious somewhat further to the southwest, blocks of quartzofeldspathic rocks appear containing cm-sized plagioclase crystals. The feldspar blastesis is interpreted as the result of an interaction of the country rocks at deep crustal levels with an alkali-rich fluid phase. The source of this phase could be the saidenbachites where it formed after the main crystallisation of the saidenbachitic magma.

Stop 3.1F:

Continuing along the strand for a few hundred metres further to the south we meet with outcropping eclogitic rocks that are virtually identical to that of stop 3.1C. Again the omphacite of the rock matrix was completely

	Gt	Omph	Phe	Gt	Phe	Phe	Phe
	core	foci	foci	rim	rim	core	rim
	1663/10	1665/4	1665/16	1665/24	1665/12	1771/13	1771/6
SiO2	38.80	54.75	51.10	38.66	48.05	50.21	50.56
TiO2	0.21	0.24	3.14	0.06	2.62	2.77	2.30
Al2O3	21.86	14.55	27.17	21.60	28.61	29.01	29.19
Cr2O3	0.00	0.00	0.09	0.06	0.03	0.00	0.01
FeO	19.65	4.58	1.72	21.96	2.36	3.15	2.60
MnO	0.37	0.02	0.04	0.33	0.00	0.01	0.01
MgO	6.60	6.95	4.09	7.94	2.74	3.35	3.21
CaO	12.63	12.57	0.01	8.60	0.00	0.00	0.00
BaO			0.09		0.19	0.25	0.20
Na2O		5.63	0.24		0.29	0.21	0.18
K2O			10.43		10.70	9.25	9.91
Total	99.93	99.42	98.57	99.53	95.61	98.13	97.73
Si	5.909	1.945	6.691	5.909	6.436	6.451	6.469
Al IV		0.055	1.409		1.562	1.549	1.532
Ti	0.025	0.026	0.308	0.010	0.264	0.267	0.221
Al VI	3.924	0.574	2.874	3.942	2.955	2.845	2.955
Cr	0.000	0.000	0.009	0.007	0.000	0.000	0.001
Fe2+	0.076	0.000		0.051			
Fe3+	2.319	0.121	0.184	2.754	0.264	0.333	0.278
Mn	0.047	0.001	0.005	0.009	0.000	0.001	0.001
Mg	1.673	0.368	0.777	1.785	0.549	0.641	0.611
Ca+Ba	2.061	0.479	0.015	1.392	0.012	0.015	0.016
Na		0.417	0.060		0.076	0.057	0.044
K			1.694		1.829	1.616	1.483

Table 14 - EMP analyses (in wt.%) of inclusion minerals in garnet from eclogite E42-1d as well as phengite from pegmatoid E42-1e (2 analyses on the right hand side). Both samples were taken from stop 3.1F.

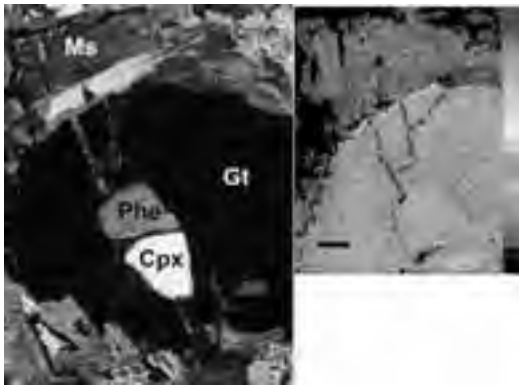

Figure 39 - Photomicrograph of a garnet (Gt) with inclusions of phengite (Phe) and omphacite (Cpx) from eclogite sample E42-1d seen under crossed polarisers. Outside garnet, muscovite (Ms) occurs. Concentration map of Mg with scale for the grey tones (increasing element concentrations towards the top) is on the right hand side. Scale bar represents 100 µm.

altered to symplectites but omphacite relics as well as phengite were found to be enclosed in garnet (Fig. 39).

Phengite geothermobarometry yielded P-T data above 30 kbar and 1000°C for the early metamorphic stage of the eclogite. In fact, no microdiamonds were found in the rock but UHP conditions or even a magmatic evolution similar to the saidenbachite cannot be excluded for this basic rock type.

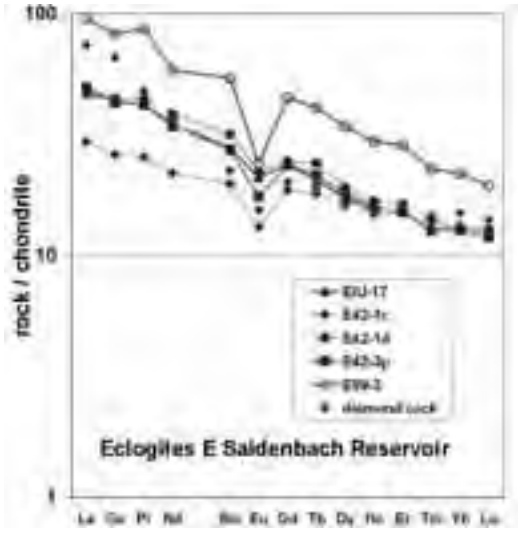

Figure 40 - REE patterns of eclogites from the eastern portion of the Saidenbach reservoir, GEU of the Saxonian Erzgebirge. The data were obtained by ICP-MS analyses and subsequently normalised to chondrite.

	E42-1c	E42-1d	E42/2	E42-3P	EU-17	E96-3
SiO2 in wt.%	50.54	51.17	50.13	54.83	51.67	52.13
TiO2	1.79	1.57	1.43	1.75	1.67	2.45
Al2O3	15.88	16.48	17.23	16.13	17.40	16.43
FeOtot	7.48	9.24	8.98	8.13	8.81	10.78
CaO	4.73	8.78	3.81	7.21	8.02	7.91
MgO	3.66	5.56	2.13	4.56	4.97	4.45
MnO	0.14	0.14	0.11	0.13	0.15	0.19
K2O	2.40	1.46	3.54	1.80	2.11	0.74
Na2O	3.31	3.63	3.18	3.40	3.08	3.37
P2O5	0.19	0.29	0.40	0.24	0.37	0.45
H2Otot	0.92	1.42	0.72	0.79	0.67	0.61
CO2	0.19	0.30	0.21	0.20	0.23	0.19
Sum	99.19	99.83	98.35	99.17	99.55	99.65
Li in ppm	31.0	21.1		34.4	13.9	29.6
Sc	22.8	27.5	17*	23.5	24.6	27.0
V (XRF)	181	207	104	203	214	261
Cr (XRF)	98	204	47	98	124	62
Ni	21.1	38.3	17*	25.3	25.1	22.4
Cu (XRF)	38	48	28	28	29	42
Zn (XRF)	85	93	68	93	88	129
Ga	17.6	19.6	22*	21.6	18.9	19.5
Rb	46.7	34.3	69*	34.7	41.4	27.9
Sr	366	198	271*	229	290	116
Y	26.4	25.1	36*	28.8	27.4	53.8
Zr (XRF)	206	171	442	190	202	139
Nb	30.5	23.7	21*	26.7	25.7	45.7
Sn	1.03	1.07		1.88	1.18	5.65
Ba (XRF)	260	145	1364	277	402	34
Hf/Zr	0.035	0.030		0.040	0.033	0.037
Ta	2.23	1.20		1.84	1.54	5.29
Pb	10.1	1.53		4.58	2.58	5.33
Th	0.97	0.31		1.73	0.38	2.45
U	0.73	0.17		0.68	0.16	1.61

Table 15 - XRF and ICP-MS analyses of eclogites from the eastern shore of the Saidenbach reservoir, GEU of the Saxonian Erzgebirge. *=XRF data as an exception.

The geochemical characteristics of the eclogites from the eastern portion of the Saidenbach reservoir (Table 15) were studied by Massonne and Czambor (2003). The rocks are basaltic to andesitic in composition. Similar to the eclogites from the northern shore, critical parameters are: $(Nb)_N > 20$, $(Sr)_N > 10$, $Ta/Yb > 0.14$, $(La/Sm)_N = 1.2 - 2$, and $(Sm/Yb)_N > 1.4$. A further typical feature is the clear negative Eu-anomaly in all investigated samples from the eastern portion of the reservoir (Fig. 40). Protoliths of these eclogites related to magmatic rocks, for instance, from oceanic island environments cannot be excluded but sedimentary protoliths (marls) are likely, although Sc, V, Cr, and Ni contents are relatively high (see Table 15).

An interesting rock at this site is a pegmatoid forming schlieren in the eclogite body rather than a vein. It contains cm-sized phengites which have also formed in the eclogite, as quartz and feldspars, by blastesis. The composition of the phengite is given in Table 14. Phengite geobarometry yielded pressures between 18 kbar for the phengite core and 15 kbar for the rim composition at 700-750°C.

From the eclogite outcrop we walk about 400 m to the southeast to another exposure of eclogitic rocks (Fig.41).

Figure 41 - Exposure of stop 3.1G at low water level of the Saidenbach reservoir.

Stop 3.1G:

At this site however, the eclogites occur instead as bands in less basic rocks occasionally even grading into garnet-rich quartzofeldspathic rocks containing relics of kyanite. In fact, phengites have replaced kyanite, but phengite itself can be strongly altered by biotite in garnet-rich layers (Fig. 42).

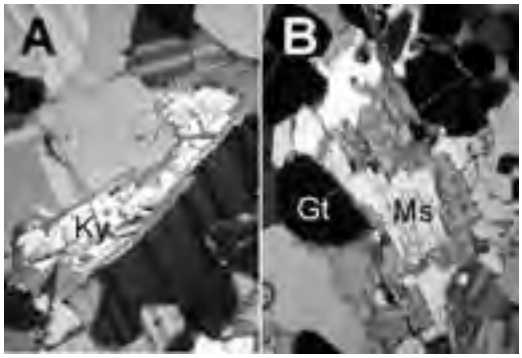

Figure 42 - Photomicrographs of objects in metapelitic sample E42/1b under crossed polarisers. A) Kyanite (Ky) relic marginally replaced by potassic white mica. Image width is 650 µm. B) Phengitic muscovite (Ms) marginally replaced by biotite. Gt = garnet. Image width is 850 µm.

From here on one could walk either back to the starting point at the road between Eppendorf and Lippersdorf or further to the east to reach after about 1.5 km the tourist parking area at the little castle of Forchheim, provided that a vehicle has been brought to this place. We practically cross the

federal road B101, heading uphill for Wernsdorf and then downhill to the Flöha valley. We cross the valley to move to Sorgau and then further to Zöblitz. Shortly after passing the town limit we must turn left to reach the entrance to the big serpentinite quarry after about 500 m. Here are parking lots on the right-hand side. The quarry is on the left-hand side (Fig. 43).

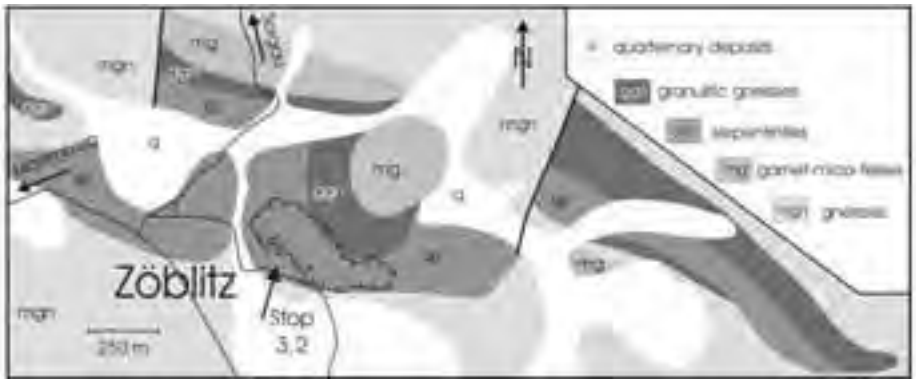

Figure 43 - Simplified geological map of the serpentinite body at the town of Zöblitz, GEU of the Saxonian Erzgebirge.

	Erz03-6d						18270			
	Gt		Opx	Cpx		Ol	Gt		Cpx	
	core	rim			rim		core	rim	core	rim
	1	6	15	20	36	40	14	140	35	139
SiO_2	43.31	42.26	57.80	54.77	54.39	40.91	39.81	40.35	53.64	51.10
TiO_2	0.68	0.63	0.14	0.41	0.44	0.02	0.57	0.25	0.49	1.03
Al_2O_3	21.52	21.83	0.96	3.72	3.47	0.00	21.97	22.72	5.45	9.61
V_2O_3	0.03	0.03	0.00	0.05	0.07	0.00	0.08	0.05	0.10	0.12
Cr_2O_3	1.60	1.87	0.14	0.92	0.85	0.00	0.01	0.03	0.32	0.04
FeO	9.00	10.08	6.49	2.91	2.59	10.15	14.72	15.91	4.79	3.50
MnO	0.33	0.41	0.11	0.07	0.06	0.09	0.27	0.30	0.02	0.00
MgO	21.31	20.42	34.96	15.52	15.69	49.14	9.19	10.35	13.25	12.93
NiO	0.00	0.00	0.00	0.01	0.02	0.37	0.00	0.00	0.00	0.00
CaO	4.20	4.47	0.39	19.81	20.49	0.00	14.81	11.48	20.16	20.40
Na_2O	0.08	0.08	0.08	2.53	2.19		0.05	0.05	2.74	2.39
K_2O				0.01	0.00		0.00	0.00	0.01	0.01
Total	101.52	101.91	101.27	100.83	100.24	100.70	101.61	101.50	100.67	100.13
Si	5.925	5.823	1.941	1.918	1.930	0.9870	5.655	5.818	1.851	1.704
AlIV			0.059	0.082	0.092				0.149	0.296
Ti	0.070	0.066	0.007	0.022	0.024	0.0003	0.060	0.028	0.026	0.056
AlVI	3.618	3.609	0.020	0.231	0.202	0.0000	3.799	3.927	0.312	0.442
Cr	0.177	0.169	0.008	0.052	0.048	0.0001	0.001	0.009	0.018	0.002
V	0.003	0.004	0.000	0.003	0.004	0.0001	0.009	0.006	0.006	0.007
Fe^{2+}	0.202	0.202				0.0044	0.191	0.061		
Mg	4.447	4.000	2.547	1.655	1.590	1.7659	2.009	2.262	1.416	1.397
Mn	0.039	0.048	0.006	0.004	0.004	0.0019	0.033	0.038	0.001	0.000
Fe^{2+}	0.853	0.979	0.370	0.188	0.153	0.2027	1.818	1.891	0.286	0.212
Ni	0.000	0.000	0.004	0.001	0.001	0.0072	0.000	0.000	0.000	0.000
Ca	0.840	0.672	0.026	0.001	0.001	0.0000	2.328	1.894	1.550	1.584
Na	0.022	0.021	0.011	0.350	0.305		0.014	0.008	0.382	0.335
K				0.001	0.000		0.000	0.000	0.001	0.001

Table 16 - EMP analyses (in wt.%) of minerals from serpentinised garnet lherzolite, Erz03-6d, and garnet-rich clinopyroxenite (eclogite), 18270, of the serpentinite body at the town of Zöblitz, Saxonian Erzgebirge.

Stop 3.2:

In past centuries serpentinite was quarried at Zöblitz as a rock for facing, for instance, the interior of churches and palaces. Nowadays, the main purpose of the still active quarry is to produce macadam. The serpentinite consists mainly of lizardite but clinochrysotile and antigorite are present as minor serpentine phases. In addition, aggregates of chlorite occur which are pseudomorphs after garnet. Occasionally, preserved portions of the original garnet lherzolite can be found. In such rocks garnet can form up to cm-sized crystals. As in the ultrabasic rock at Rubinberg (stop 1.2), the matrix consists of mm-sized equigranular olivine, clinopyroxene, orthopyroxene, and minor amphibole. In addition, the large extended garnet cores are chemically homogeneous. The observed fabric is interpreted as the result of recrystallisation because of deformation during the exhumation event. It started, according to the chemical composition of the matrix minerals (cores) and the garnet rim (Table 16) at P-T conditions of about 26 kbar and 1000°C applying the method reported by Massonne and Bautsch (2002). Virtually identical pressure results using the Al-content in orthopyroxene (opx) according to equilibrium (7): pyrope (in gt) = 3 $MgSiO_3$ (in opx) + Al_2O_3 (in opx). Schmädicke and Evans (1997) estimated higher pressure up to 33 kbar at temperatures somewhat below 1000°C for the garnet peridotite at Zöblitz.

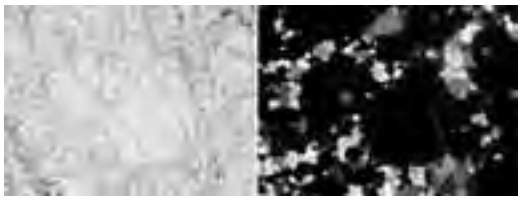

Figure 44 - Photomicrograph of garnets in clinopyroxenite (eclogite) sample 18270 under plain polarised light (left hand side) and seen under crossed polarisers (right). Image width is 4 mm.

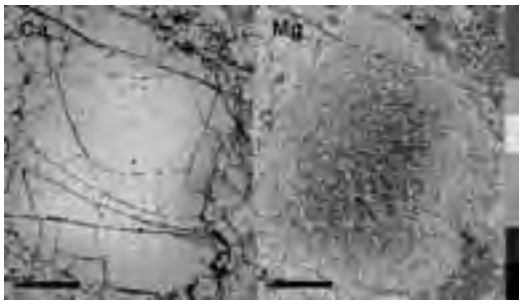

Figure 45 - Concentration maps of Ca and Mg in garnet, marginally recrystallised to garnet + clinopyroxene, in sample 18270. The scale for the grey tones shows increasing element concentrations towards the top. Scale bars represent 500 µm.

	Garnet Pyroxenites			Serpentinite
	E2b	18270	E00-7B	E3b
SiO2 in wt %	46.17	43.70	42.20	39.29
TiO2	0.45	1.00	1.30	0.08
Al2O3	14.79	16.10	17.88	2.04
FeO	8.11	12.51	12.64	7.04
CaO	8.16	12.40	13.60	0.68
MgO	17.72	10.70	8.39	37.99
MnO	0.21	0.23	0.21	0.11
K2O	0.06	0.01	0.46	0.00
Na2O	0.85	0.17	1.08	0.00
P2O5	0.02	0.04	0.08	0.00
H2Oto	1.41	1.52	1.27	11.63
CO2	0.08	0.16	0.15	0.31
Sum	99.00	97.54	99.23	99.11
Li in ppm	20.3	60.4	68.3	0.35
Sc	40.6	78.6	71.4	11.1
V (XRF)	220	402	485	51
Cr (XRF)	683	113	261	2501
Ni (XRF)	578	119	128	2350
Cu	88.2	12.5	50.5	18.6
Zn (XRF)	21	80	92	50
Ga	12.3	19.2	17.2	1.69
Rb	3.79	0.86	13.3	0.00
Sr	74.4	54.3	2.53	4.00
Y	13.1	22.7	25.8	1.77
Zr (XRF)	33	48	42	6
Nb	0.43	17.6	1.42	0.02
Sn	0.39	2.86	1.14	0.00
Ba	15.8	12.3	116	2.58
La	1.40	3.90	1.44	0.18
Ce	4.54	10.27	5.83	0.55
Pr	0.77	1.77	1.34	0.10
Nd	3.71	11.07	10.20	0.49
Sm	1.11	3.59	4.84	0.18
Eu	0.48	1.53	1.38	0.06
Gd	1.53	5.13	4.85	0.24
Tb	0.33	0.74	0.86	0.05
Dy	2.31	3.98	4.69	0.31
Ho	0.54	0.80	0.81	0.07
Er	1.71	2.57	2.02	0.21
Tm	0.29	0.31	0.33	0.03
Yb	1.57	2.31	2.42	0.20
Lu	0.25	0.31	0.34	0.03
Hf/Zr	0.033	0.032	0.050	0.026
Ta	1.26	1.33	0.10	0.00
Pb	0.42	2.86	37.1	1.71
Th	0.26	1.23	0.00	0.00
U	0.06	0.72	0.16	0.03

Table 17 - XRF and ICP-MS analyses of ultrabasic rocks from the serpentinite body at Zöblitz, GEU of the Saxonian Erzgebirge.

Within the peridotite body, layers of pyroxenite occur. These, when fresh, may consist mainly of clinopyroxene and garnet. Rutile is a common accessory phase. Some pyroxenites even show that up to cm-sized garnets have been marginally

transformed to smaller garnet crystals and equigranular clinopyroxene (Fig. 44). The remaining palaeocrysts are chemically zoned as shown in Fig. 45. Again, P-T conditions were determined on the basis of mineral analyses given in Table 16. For the rim composition, 16.6 kbar and 865°C were obtained. Core compositions gave much higher pressure of almost 39 kbar at 1100°C. Another possible indicator for such high or even higher pressure are abundant tiny, perfectly oriented ilmenite rods in some olivine cores of the preserved garnet lherzolite. Although no quantification in regard to the Earth's depth is possible yet, a similar exsolution feature, e.g. reported by Green et al. (1997) from the peridotite massif of Alpe Arami, was taken as a hint at UHP conditions. Summarizing the petrological information on the ultrabasic body at Zöblitz, it can be concluded that the exhumation history is virtually the same as for the ultrabasic rocks from the nearby Granulitgebirge.

Geochemical analyses of garnet pyroxenites from Zöblitz (Table 17) show that these rocks can vary significantly in composition. The garnet lherzolite (Table 17) is somewhat depleted in light REE.

From the serpentinite quarry we go to the centre of the town of Zöblitz to meet with federal road B171 heading to Marienberg and then on to Wolkenstein. After passing this town we reach federal road B101. From here it is as far as 9 km to the town of Annaberg-Buchholz.

DAY 4

The excursion continues from Annaberg-Buchholz via federal road B95 to the south reaching Hammerunterwiesenthal after 17 km. In the centre of this village we turn right heading uphill to Neudorf. Close to the Hammerunterwiesenthal exit a dirt road on the left leads to "Steinbruchbetriebe Richter".

Figure 46 - Simplified geological map of an area in the MEU of the Saxonian Erzgebirge close to the village of Hammerunterwiesenthal.

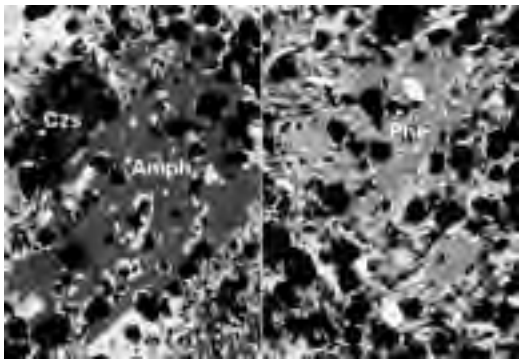

Figure 47 - Photomicrographs of porphyroblasts of amphibole (Amph), clinozoisite (Czs), and phengite (Phe) in eclogite 18333 (stop 4.1) under crossed polarisers. Image width is 900 µm each.

Here it is possible to talk to the owner of the eclogite quarry. This quarry, however, can be reached by taking the next dirt road to the left. This road ends at the eclogite quarry after about 1.3 km (Fig. 46).

Stop 4.1

At this stop we can visit what is left of a lens of homogeneous eclogite about 500 m long. In spite of the destruction of a formerly romantic site in the wood, as the Stümpelfelsen cliffs were considered, the relationships to the gneissic country rocks are well exposed now.

In fact, the eclogites at the Stümpelfelsen can be distinguished by lighter and darker varieties, but they are all massive and not as foliated as other eclogites in the vicinity. Another common aspect is produced by mm long, non-oriented amphibole crystals in a relatively fine-grained matrix consisting mainly of fresh omphacite and garnet (Fig. 47). A few larger single white mica flakes are also discernible with the naked eye in the common eclogite. In addition, several mm-sized amphiboles and oriented white mica flakes can be strongly enriched on mm thick planes often between eclogite and quartz segregations crosscutting the eclogite body. Also crosscutting are cracks, occasionally running parallel with dm spacings, along which late retrograde minerals, such as chlorite and actinolite, have formed. These caused a darker colouring in the mm range around the cracks.

In the light coloured variety the eclogitic mineral assemblage is characterised by garnet, omphacite, phengite, talc, amphibole, clinozoisite, quartz, rutile, and accessory phases. At a late stage (III) of metamorphism porphyroblasts of amphibole, clinozoisite, and phengite formed. Paragonite joined the assemblage even during a later stage

Mineral	Gt		Omph		Amph		Czs		Talc	Phe		Parag
Stage	Ib	II-IIIa	I-II	II-III	Ib	IIIa	Ib	IIIa	IIIa	Ib-II	IIIa	IIIb
SiO2 in wt.%	38.94	39.34	56.26	56.12	55.79	54.66	37.94	39.31	62.46	53.47	52.85	47.40
TiO2	0.11	0.08	0.04	0.06	0.05	0.13	0.14	0.12	0.02	0.23	0.28	0.07
Al2O3	21.75	22.06	9.15	10.57	3.13	5.69	29.03	31.11	0.43	28.90	28.20	39.41
Cr2O3	0.04	0.03	0.09	0.07	0.03	0.02	0.06	0.08	0.01	0.02	0.11	0.06
Fe2O3							6.15	3.33				
FeO	25.27	24.23	1.33	3.62	5.73	5.09			4.38	1.48	1.48	0.48
MnO	1.12	0.82	0.04	0.07	0.10	0.09	0.10	0.04	0.00	0.00	0.00	0.00
MgO	3.81	5.77	10.09	9.85	20.15	16.35	0.16	0.12	29.33	4.52	3.89	0.27
CaO	11.80	9.82	15.36	13.76	11.25	7.95	23.70	24.52		0.01	0.01	0.24
Na2O	0.02	0.04	5.62	6.65	1.48	3.09	0.00	0.04	0.09	0.53	0.64	6.83
K2O					0.07	0.12				10.34	9.53	0.99
BaO					0.00	0.00				0.24	0.19	0.00
Sum	102.06	102.19	99.98	99.79	98.79	95.60	97.12	98.68	96.72	97.73	96.94	95.83
Si	5.982	5.946	2.001	1.983	7.736	7.457	2.959	2.993	4.006	6.998	6.786	6.016
Ti	0.013	0.009	0.001	0.002	0.005	0.013	0.008	0.007	0.001	0.022	0.027	0.007
Al	3.938	3.929	0.384	0.443	0.502	1.097	2.668	2.791	0.033	4.668	4.299	5.885
Cr	0.005	0.003	0.003	0.002	0.003	0.003	0.004	0.005	0.001	0.002	0.011	0.007
Fe3+	0.056	0.067	0.000	0.024	0.331	0.313	0.361	0.191				
Fe2+	3.190	2.994	0.099	0.063	0.322	0.484			0.235	0.160	0.161	0.051
Mn	0.145	0.104	0.001	0.002	0.011	0.010	0.007	0.003	0.000	0.000	0.000	0.000
Mg	0.780	1.230	0.535	0.469	4.091	3.324	0.021	0.014	2.711	0.869	0.751	0.051
Ca	1.877	1.586	0.585	0.524	1.641	1.140	1.985	2.000	0.011	0.001	0.001	0.036
Na	0.007	0.013	0.391	0.459	0.390	1.046	0.000	0.006		0.132	0.212	1.690
K					0.012	0.021				1.702	1.572	0.161
Ba					0.000	0.000				0.012	0.011	0.000

Table 18 - EMP analyses (in wt.%) of minerals from eclogite 18333 sampled at the Stümpelfelsen cliff (stop 4.1), MEU of the Saxonian Erzgebirge. The data were taken from Massonne and Kopp (submitted).

(IIIb). The chemical zonation of the minerals are exemplary shown by Figs. 48 to 50 and Table 18. On the basis of this, various geothermobarometric methods were applied considering phengite and talc strongly. The constrained P-T path for the eclogite starts at about 480°C and 25 kbar (stage Ib in Fig. 51) followed by a significant temperature increase (stage II) at slightly increasing pressures. At the peak P-T conditions of 720°C and 27 kbar

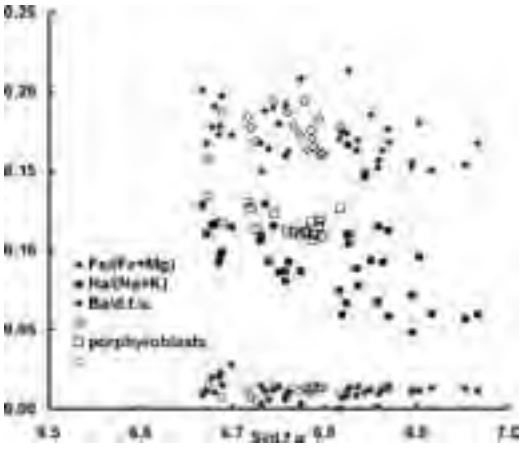

Figure 48 - Compositional variation of phengite as small grains of the matrix and as porphyroblasts in eclogite 18333 from the Stümpelfelsen cliff close to the village of Hammerunterwiesenthal.

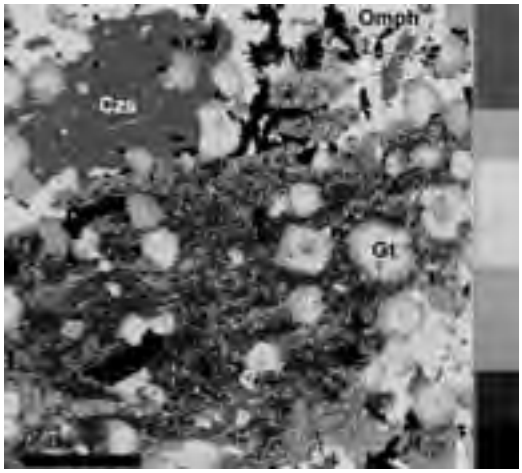

Figure 49 - Concentration map of Ca for a section of sample 18333 with an amphibole and clinozoisite (Czs) porphyroblast also shown on the left hand side of Fig. 47. Several grains enclosed in amphibole are garnet (Gt). Outside the porphyroblast is omphacite (Omph). The scale for the grey tones shows increasing element concentrations towards the top. Scale bar represents 250 µm.

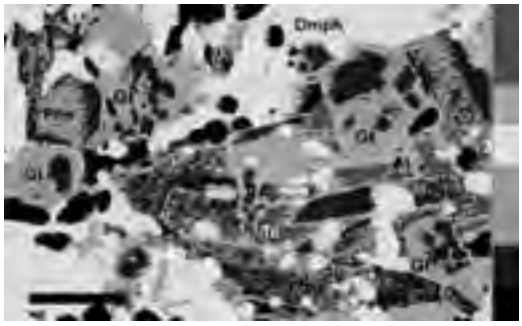

Figure 50 - Concentration map of Mg for a matrix section of eclogite sample 18333 from the Stümpelfelsen cliff close to the village of Hammerunterwiesenthal. Gt = garnet, Omph = omphacite, Phe = phengite, Tc = talc. The scale for the grey tones shows increasing element concentrations towards the top. Scale bar represents 100 µm.

	1	2	3	4	5	6
SiO_2 in wt.%	49.04	50.59	50.64	49.74	66.76	71.65
TiO_2	1.98	1.61	1.56	1.37	0.12	0.16
Al_2O_3	13.79	13.66	14.48	13.92	19.51	16.39
FeOtot	12.60	11.55	9.60	10.25	0.29	0.25
CaO	10.96	10.61	11.21	10.68	1.03	1.28
MgO	6.39	6.54	7.20	8.92	0.32	0.21
MnO	0.25	0.24	0.19	0.16	0.01	0.01
K_2O	0.01	0.90	0.21	0.25	0.64	5.48
Na_2O	2.17	2.66	2.89	2.99	10.65	5.75
P_2O_5	0.14	0.09	0.11	0.08	0.09	0.13
H2Otot	1.35	1.42	0.26	1.26	0.43	0.56
CO_2	0.01	0.03	0.11	0.33	0.17	0.08
Sum	98.90	99.89	98.65	97.96	100.20	99.96
Li in ppm	10.6	20.9	35.6	23.3		25.4
Sc	46.2	39.9	46.0	47.6	3*	0.50
V (XRF)	378	343	352	320	10	21
Cr (XRF)	214	183	239	287	21	0
Ni	62.1	56.5	46.3	52.5	1*	0.0
Cu (XRF)	36	52	17	17	<1	3
Zn (XRF)	112	130	128	87	6	9
Ga	14.0	14.2	14.0	15.2	15*	13.4
Rb	48.4	59.1	11.1	8.11	29*	94
Sr	72	54	159	88	49*	471
Y	49.4	43.0	45.2	44.7	18*	1.24
Zr (XRF)	102	81	90	74	52	95
Nb	1.92	2.03	3.09	1.72	9*	1.45
Sn	1.06	0.79	23.9	10.7		0.65
Ba (XRF)	47	170	22	29**	20	850
HfO2	0.045	0.040	0.049	0.052		0.029
Ta	0.21	0.20	0.27	0.16		0.0
Pb	6.91	2.95	9.73	4.38		31.51
Th	0.14	0.12	0.33	0.27		2.99
U	0.03	0.10	0.09	0.05		1.79

*Table 19 - XRF and ICP-MS analyses of eclogites from the MEU of the Saxonian Erzgebirge. 1 (E96-15b) and 2 (E96-15d) = stop 4.1, 3 (E22a) and 4 (E22c) = stop 4.3 Analyses 5 and 6 represent small volumes of rocks, either with pegmatoid or granitoid character, directly in contact to eclogites. 5 (Erz03-4) = stop 4.3, 6 (E42-1e) = stop 3.1F. *=XRF data as an exception.*

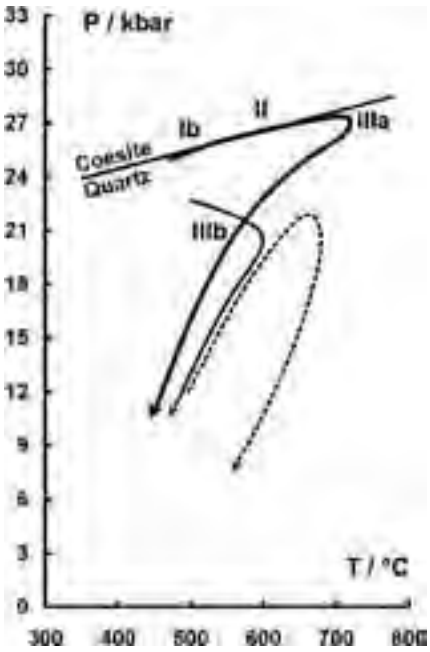

Figure 51 - P-T paths derived for low-temperature eclogites from the MEU of the Saxonian Erzgebirge. Bold: eclogite from stop 4.1. Roman numbers refer to metamorphic stages. Medium line: eclogite taken a few kilometres north of the town of Marienberg (Massonne, 1992). Dashed: eclogites of the MEU, in general, according to Schmädicke et al. (1992).

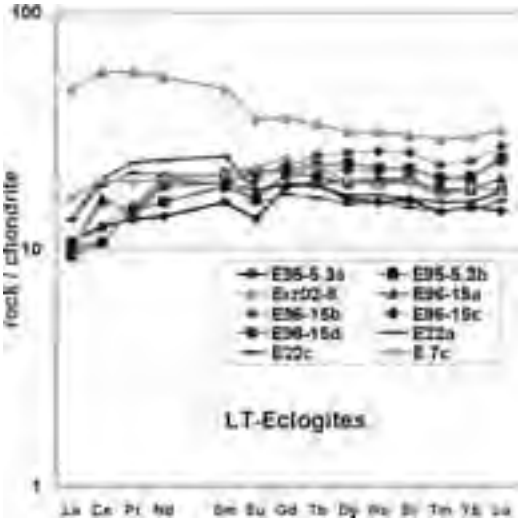

Figure 52 - REE patterns of eclogites from the western Erzgebirge´s crystalline massif. However, samples Erz02-8 and E7c were taken a few kilometres north and east, respectively, of the town of Marienberg. The data were obtained by ICP-MS analyses and subsequently normalised to chondrite.

porphyroblasts began to grow by invading hydrous fluids. Possibly the resulting density reduction caused buoyancy forces uplifting the eclogite. Subsequently, significant cooling occurred at still high pressures. Stage IIIb is characterised by P-T conditions around 520°C and 18 kbar at reduced water activities. This unusual late P-T history might explain the freshness of the eclogite including the preservation of chemical zonation on the micrometer scale.

The geochemical characteristics of eclogites from the MEU was investigated by Massonne and Czambor (2003). Among the analysed samples were those from the Stümpelfelsen cliff (Table 19). These eclogites could be assigned to former MORBs demonstrated, for instance, by the REE patterns of these rocks (Fig. 52).

In the quarry of stop 4.1 the typical country rocks are outcropping as well. These are quartz-rich gneisses, probably former greywackes, and mica schists occasionally with large garnets several mm in diameter. The latter rock type, which can also contain chloritoid, was studied by Rötzler et al. (1998). These authors estimated P-T conditions of 12 kbar and 525°C for the pressure climax as well as 8 kbar and 560°C for the subsequent temperature peak. These P-T data differ significantly from those derived for the eclogites. Willner et al. (2000, 2002) tried to explain this by a model involving rapid exhumation of high-pressure rocks from the root zone of a collisional orogen. Unfortunately, it is not clear yet, if the low-temperature eclogites of the western Erzgebirge were metamorphosed at the same time as those of the central Erzgebirge. Schmädicke et al. (1995) also determined ages as old as 355 Ma for the eclogites from the western Erzgebirge. If there is really a considerable time difference between metamorphism of (U)HP rocks from the western and central Erzgebirge, a single major event responsible for the exhumation of these rocks has to be called into question.

On the way back to the main road, we stop after about 1 km at the entrance to a larger, apparently abandoned quarry on the left-hand side (see Fig. 46).

Stop 4.2: (optional)

In this quarry we can see a good example for one of the many alkali-dominated subvolcanics which erupted in the Tertiary. In fact, this type of volcanism concentrated in the Eger-graben to the south, but there are quite a number of such stocks penetrating the crystalline massif of the Erzgebirge. Another reason to visit this quarry is a marble with some siliceous layers (Fig. 53) in the northern portion of the quarry. Such marbles form elongated bodies similar to those of the nearby eclogites. It is also obvious

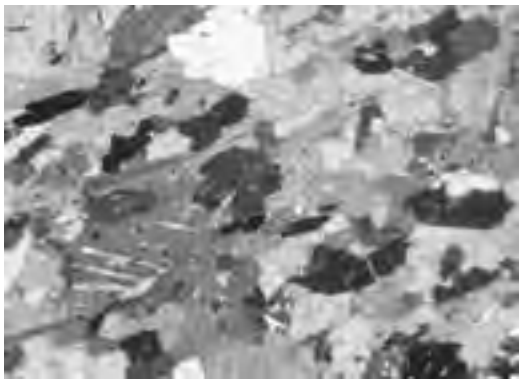

Figure 53 - Photomicrograph of a siliceous layer in marble from stop 4.2 seen under crossed polarisers. The silicates are amphibole and phlogopite. Image width is 4 mm

that both rock types marbles and eclogites are associated over a wide area, but a real contact between both does not exist. It is also not clear what the P-T conditions of the metamorphism of the marble were. The common mineral assemblage amphibole, clinopyroxene, and phlogopite with carbonates in particular does not allow to quantify pressure conditions.

After going back to the main road we turn left to reach the village of Neudorf after 4 km. Just after crossing the railroad track, we turn left heading for the forester´s house "Siebensäure". After 1.8 km, we pass this building to park our vehicle(s) on the left-hand side. As the road is closed to the public, we have to walk further to the west by about 600 m. Then we turn right into the forest. Already after some tens of metres cliffs occur which extend for a few hundred metres in a northwest direction.

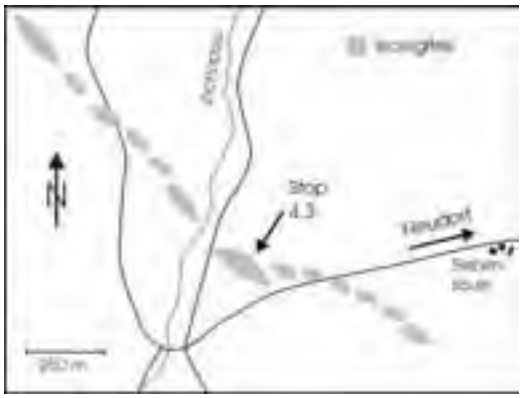

Figure 54 - Simplified geological map of an area in the MEU of the Saxonian Erzgebirge a few kilometres west of the village of Neudorf.

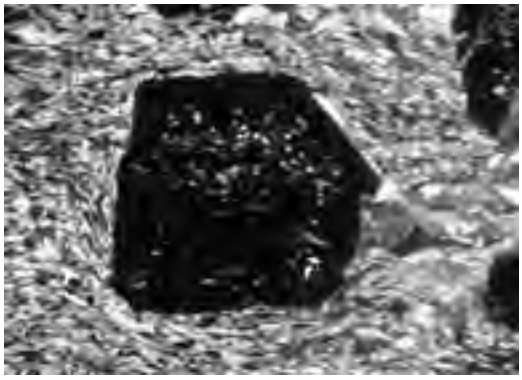

Figure 55 - Photomicrograph of a large garnet, seen under crossed polarisers, in a foliated matrix of sample E22h from stop 4.3. The matrix consists mainly of amphibole and clinozoisite. Image width is 4 mm.

At the end, another paved forest road appears.

Stop 4.3:

The cliffs in the forest consist of eclogites which form either a larger strongly elongated lens or, as shown on the map of Fig. 54, a number of smaller lenses. In fact, the eclogite of stop 4.3 is geochemically identical to that of stop 4.1 (see Table 19), but here it is, as typical for the western Erzgebirge, clearly

	Gt		Omph		Phe	
	core	rim	core	rim	core	rim
	98A/52	98B/85	98A/7	98B/22	98B/52	98B/25
SiO_2	37.88	38.87	55.14	56.68	53.67	52.66
TiO_2	0.12	0.03	0.04	0.02	0.22	0.27
Al_2O_3	21.14	21.91	6.66	10.13	26.75	28.62
Cr_2O_3	0.08	0.05	0.04	0.05	0.00	0.02
FeO	28.44	22.91	7.27	3.01	1.50	1.47
MnO	2.25	0.23	0.05	0.04	0.00	0.00
MgO	4.22	8.17	9.55	9.62	4.49	3.90
CaO	9.11	7.94	15.56	14.65	0.00	0.06
BaO					0.10	0.34
Na_2O	0.02	0.01	5.47	5.85	0.52	0.78
K_2O			0.02	0.03	11.04	10.61
Total	100.20	100.17	99.84	100.08	98.28	98.79
Si	5.925	5.916	1.992	2.001	6.919	6.751
Al IV			0.008	0.000	1.081	1.248
Ti	0.015	0.003	0.001	0.001	0.022	0.026
Al VI	3.898	3.921	0.276	0.421	2.983	3.110
Cr	0.000	0.000	0.001	0.001	0.000	0.002
Fe^{3+}	0.102	0.079	0.112	0.000		
Fe^{2+}	3.357	2.831	0.108	0.086	0.162	0.158
Mn	0.299	0.029	0.002	0.001	0.000	0.000
Mg	0.985	1.849	0.514	0.506	0.862	0.746
Ca+Ba	1.359	1.291	0.603	0.554	0.005	0.017
Na			0.383	0.428	0.131	0.188
K			0.001	0.001	1.815	1.737

Table 20 - EMP analyses (in wt.%) of minerals in eclogite E22h taken from stop 4.3.

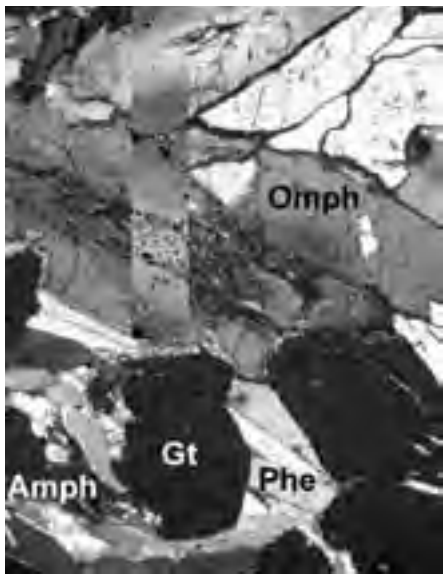

Figure 56 - Photomicrograph of a preserved portion of palaeocrysts in eclogite E22h seen under crossed polarisers. The superposed inlet is a concentration map showing rising Fe contents by increasingly lighter grey tones. Image width is 2.7 mm.

foliated. Occasionally, we can find in the cliffs of stop 4.3 a preserved fabric in the cm range, formed before deformation. In these preserved portions, mm-sized garnet and omphacite occur (Figs. 55 and 56). These minerals are strongly chemically zoned. From the core compositions of these minerals and a relatively coarse-grained phengite (see Table 20) about 24 kbar and 500°C were calculated for an early metamorphic stage. Rim compositions yielded 26 kbar and 650°C. The resulting P-T path resembles that obtained for eclogites from stop 4.1. Formation of amphibole and clinozoisite, from which the fine-grained foliated matrix mainly consists of, as well as deformation happened at the P-T climax and/or during the beginning of exhumation.

An interesting feature in the outcrop are granite-like segregations at the contact between eclogite and country rock. The composition of this granitoid is characterised by high Na_2O (> 10 wt.%, see Table 19) and, thus, high plagioclase contents. The same is true for similar segregations in the serpentinite body at Zöblitz and to some extent for the pegmatoid schlieren in eclogite of stop 3.1F (Table 19). However, no genesis model can be currently presented.

After going back to Neudorf, we take the road to the left and turn after a few hundred metres slightly to the left heading for Crottendorf and the village of Scheibenberg which we reach after 8 km. We

Figure 57 - Columns of nephelinite at Scheibenberg hill.

turn right into federal road B101, pass the village, and, at its exit, turn left heading for Zwönitz and further to Stollberg. Do not forget to have a look at the so-called "Orgelpfeifen" (Fig. 57) when leaving Scheibenberg. This natural monument consists of great vertical columns of nephelinite which intruded the Erzgebirge's crystalline massif during Tertiary times as well. The columns are still discernible although relatively far away.

After reaching Stollberg we turn north before entering the centre of the town. About 2 km north of Stollberg there is access to highway A72 heading for Chemnitz. At the northwestern edge of this city is the junction for highway A4 heading for Dresden. This city is reached after about 70 km.

Acknowledgements

Research in the Saxonian Erzgebirge, which contributed to a significant portion of this guide, was founded by Deutsche Forschungsgemeinschaft (project No. Ma1160/2 and Ma 1160/19). Thomas Theye and Andreas Brandelik supported our electron microprobe work, calculations of structural formulae, and preparation of some figures.

References

Blümel, P. (1995). V. Saxothuringian Basin C. Exotic metamorphic nappes 2. Metamorphic evolution. In "Pre-Permian geology of central and eastern Europe" (Dallmeyer, R.D., Franke, W. and Weber, K., Eds.), Springer Verlag, Berlin, 295-308.

Chopin, C. (1984). Coesite and pure pyrope in high grade blueschists of the Western Alps: a first record and some consequences. Contributions to Mineralogy and Petrology 86, 107-118.

Chopin, C. (2003). Ultrahigh pressure metamorphism: tracing continental crust into the mantle. Earth and Planetary Science Letters 212, 1-14.

Dobrzhinetskaya, L.F., Schweinehage, R., Massonne, H.-J. and Green, H.W. II (2002). Silica precipitates in omphacite from eclogite at Alpe Arami, Switzerland: Evidence of deep subduction. Journal of metamorphic Geology 20, 481-492.

Düffels, K. and Massonne, H.-J. (2001). Geochemical signatures of diamondiferous gneisses and their adjacent rocks from the Erzgebirge, Germany. Terra Nostra, 5/2001, 24-26.

Franke, W. (2000). The mid-European segment of the Variscides: tectonostratigraphic units, terrane boundaries and plate tectonic evolution. In "Orogenic Processes: Quantification and Modelling in the Variscan Belt" (Franke, W., Haak, V., Oncken, O. and Tanner, D., Eds.), Geological Society of London, Special Publication 179, 35-61.

Franke, W. and Engel, W. (1986): Synorogenic sedimentation in the Variscan belt of Europe. Bulletin Soc. geol. France 1986 II, 25-33.

Franke, W. and Stein, E. (2000). Exhumation of high-grade rocks in the Saxo-Thuringian Belt: geological constraints and geodynamic concepts. In "Orogenic Processes: Quantification and Modelling in the Variscan Belt" (Franke, W., Haak, V., Oncken, O. and Tanner, D., Eds.), Geological Society of London, Special Publication 179, 337-354.

Green, H.W. II, Dobrzhinetskaya, L., Riggs, E.M. and Jin, Z.-M. (1997). Alpe Arami: a peridotite massif from the Mantle Transition Zone? Tectonophysics 279, 1-21.

Hartz, E.H. and Torsvik, T.H. (2002). Baltica upside down: A new plate tectonic model for Rodinia and the Iapetus Ocean. Geology 30, 255-258.

Hwang, S.-L., Shen, P., Chu, H.-T. and Yui, T.-F. (2000). Nanometer-size α-PbO_2-type TiO_2 in garnet: a thermobarometer for ultrahigh-pressure metamorphism. Science 288, 321-324.

Jekosch, U. and Bautsch, H.-J. (1991). Orientierte Entmischungen in Pyroxenen. Zeitschrift für Kristallographie, Supplement, 4, 134.

Kröner, A. and Willner, A.P. (1998). Time of formation and peak of Variscan HP-HT metamorphism of quartz-feldspar rocks in the central Erzgebirge, Saxony, Germany. Contributions to Mineralogy and Petrology 132, 1-20.

Krohe, A. (1996). Variscan tectonics of central Europe: Postaccretionary intraplate deformation of weak continental lithosphere. Tectonics 15, 1364-1388.

Massonne, H.-J. (1992). Thermochemical determination of water activities relevant to eclogitic rocks. In "Water-rock interaction WRI-7" (Kharaka, Y.K. and Maest, A., Eds.), Proceedings of the 7th International Symposium, Park City, Utah, U.S.A., 2, 1523-1526.

Massonne, H.-J. (1994). P-T evolution of eclogite lenses in the crystalline complex of the Erzgebirge, Middle Europe: An example for high-pressure to ultrahigh-pressure metabasites incorporated into continental crust. First Workshop on UHP metamorphism and tectonics, Stanford University, Abstract Volume, A29-A32.

Massonne, H.-J. (1999). A new occurrence of microdiamonds in quartzofeldspathic rocks of the Saxonian Erzgebirge, Germany, and their metamorphic evolution. Proceedings of the 7th International Kimberlite Conference, Cape Town 1998, P.H. Nixon Volume, 533-539.

Massonne, H.-J. (2001). First find of coesite in the ultrahigh-pressure metamorphic region of the Central Erzgebirge, Germany. European Journal of Mineralogy 13, 565-570.

Massonne, H.-J. (2003). A comparison of the evolution of diamondiferous quartz-rich rocks from the Saxonian Erzgebirge and the Kokchetav Massif: are so-called diamondiferous gneisses magmatic rocks? Earth and Planetary Science Letters 216, 347-364.

Massonne, H.-J. (in press). Paläozoische Hochdruck- und Ultrahochdruck-Metamorphite in Mitteleuropa und ihre Beziehungen zur variszischen Orogenese. Zeitschrift für geologische Wissenschaften.

Massonne, H.-J. and Burchard, M. (2000). Exotic minerals in eclogites from the Central Erzgebirge – evidence for fluid-rock interaction at UH metamorphic pressures: Berichte der deutschen mineralogischen Gesellschaft, Beihefte zum European Journal of Mineralogy 12, No. 1, 122.

Massonne, H.-J., Dobrzhinetskaya, L. and Green, H.W. II, (2000). Quartz - K-feldspar intergrowths enclosed in eclogitic garnet and omphacite. Are they pseudomorphs after coesite? Extended Abstract, 31st International Geological Congress, Rio de Janeiro, Brazil: 4 pp. (on CD, search for Massone).

Massonne, H.-J., Nasdala, L. and Kennedy, A. (2001). U-Th-Pb dating of zircons and monazites from diamondiferous gneisses of the Saxonian Erzgebirge – implications for their UHP/HP evolution. 6th International Eclogite Conference, Niihama, Japan, Abstract Volume, 88.

Massonne, H.-J. and Bautsch, H.-J. (2002). An unusual garnet pyroxenite from the Granulitgebirge, Germany: origin in the transition zone (>400 km Earth's depths) or in a shallower upper mantle region? International Geology Reviews 44, 779-796.

Massonne, H.-J., Bautsch, H.-J., Kopp, J. and Theye, T. (2002). Enigmatic origin of syenite boudins in a serpentinite from the Variscan Granulitgebirge, Germany. 18th General Meeting of the International Mineralogical Association, Edinburgh 2002, Abstract Volume, 216.

Massonne, H.-J. and Bautsch, H.-J. (2003). P-T evolution of a spinel-garnet-bearing clinopyroxenite from the Granulitgebirge. Berichte der deutschen mineralogischen Gesellschaft, Beihefte zum European Journal of Mineralogy 15, No. 1, 127.

Massonne, H.-J., Burchard, M., Frost, D. and Theye, T. (2003). Thermodynamic properties of TiO_2 with / -PbO_2 structure based on HP experiments. Berichte der deutschen mineralogischen Gesellschaft, Beihefte zum European Journal of Mineralogy 15, No. 1, 128.

Massonne, H.-J. and Czambor, A. (2003). Protoliths of eclogites from the Variscan Erzgebirge. Norges geologiske undersøkelse Report 2003.055, Eclogite Field Symposium, Abstracts, 93-94.

Massonne, H.-J. and Nasdala, L. (2003). Characterization of an early metamorphic stage through inclusions in zircon of a diamondiferous quartzofeldspathic rock from the Erzgebirge, Germany. American Mineralogist 88, 883-889.

Massonne, H.-J. and O'Brien, P.J. (2003). The Bohemian Massif and the NW Himalaya. In "Ultrahigh Pressure Metamorphism" (Carswell, D.A. and Compagnoni, R., Eds.), EMU Notes in Mineralogy 5, 145-187.

Massonne, H.-J. and Tu, W. (2003). δ^{13}C-Signature of microdiamonds from the Saxonian Erzgebirge, Germany. Norges geologiske undersøkelse Report 2003.055, Eclogite Field Symposium, Abstracts, 91-92.

Massonne, H.-J. and Kopp, J. (submitted). A low-variance mineral assemblage with talc and phengite in an eclogite from the Saxonian Erzgebirge, Middle Europe, and its P-T evolution. Journal of Petrology.

Matte, P. (1986): Tectonics and plate tectonics model for the Variscan belt of Europe. Tectonophysics 126, 329-374.

Matte, P. (1998). Continental subduction and exhumation of HP rocks in Paleozoic orogenic belts: Uralides and Variscides. Geologiska Föreningens Stockholm Förhandlingar 120, 209-222.

McKerrow, W.S., Mac Niocaill, C., Ahlberg, P.E., Clayton, G., Cleal, C.J. and Eagar, R.M.C. (2000). The Late Palaeozoic relations between Gondwana and Laurussia. In „Orogenic Processes: Quantification and Modelling in the Variscan Belt" (Franke, W., Haak, V., Oncken, O. and Tanner, D., Eds.), Geological Society of London, Special Publication 179, 9-20.

Murphy, J.B., Keppie, J.D., Dostal, J. and Nance, R.D. (1999). Neoproterozoic - early Paleozoic evolution of Avalonia. In "Laurentia-Gondwana connections before Pangea" (Ramos, V.A. and Keppie, J.D., Eds.), Geological Society of America, Special Papers 336, 253-266.

Nasdala, L. and Massonne, H.-J. (2000).

Volume n° 2 - from B16 to B33

Microdiamonds from the Saxonian Erzgebirge, Germany: in situ micro-Raman characterisation. European Journal of Mineralogy 12, 495-498.

O'Brien, P.J. (2000). The fundamental Variscan problem: high-temperature metamorphism at different depths and high-pressure metamorphism at different temperatures. In "Orogenic Processes: Quantification and Modelling in the Variscan Belt" (Franke, W., Haak, V., Oncken, O. and Tanner, D., Eds.), Geological Society of London, Special Publication 179, 369-386.

Oliver, G.J.H., Corfu, F. and Krogh, T.E. (1993). U-Pb ages from SW Poland: evidence for a Caledonian suture zone between Baltica and Gondwana. Journal of the Geological Society of London 150, 355-369.

Reiche, M. and Bautsch, H.-J. (1984). Entmischungsstrukturen in Pyroxenen aus eklogitischen Gesteinen. Freiberger Forschungshefte C393, 19-33.

Reiche, M. and Bautsch, H.-J. (1985). Electron microscopical study of garnet exsolution in orthopyroxene. Physics and Chemistry of Minerals 12, 29-33.

Reinhardt, J. and Kleemann, U. (1994). Extensional unroofing of granulitic lower crust and related low-pressure, high-temperature metamorphism in the Saxonian Granulite Massif, Germany. Tectonophysics 238, 71-94.

Robardet, M., Paris, F. and Racheboeuf, P.R. (1990). Palaeogeographic evolution of southwestern Europe during Early Palaeozoic times. In "Paleozoic paleogeography and biogeography" (McKerrow, W.S. and Scotese, C.R., Eds.), Geological Society of London Memoirs 12, 411-419.

Romer, R.L. and Rötzler, J. (2001). P-T-t evolution of ultrahigh-temperature granulites from the Saxon Granulite Massif, Germany. Part II: Geochronology. Journal of Petrology 42, 2015-2032.

Rötzler, J. and Romer, R.L. (2001). P-T-t evolution of ultrahigh-temperature granulites from the Saxon Granulite Massif, Germany. Part I: Petrology. Journal of Petrology 42, 1995-2013.

Rötzler, K., Schumacher, R., Maresch, W.V. and Willner, A.P. (1998). Characterization and geodynamic implications of contrasting metamorphic evolution in juxtaposed high-pressure units of the Western Erzgebirge (Saxony, Germany). European Journal of Mineralogy 10, 261-280.

Schmädicke, E., Okrusch, M. and Schmidt, W. (1992). Eclogite-facies rocks in the saxonian Erzgebirge, Germany: high pressure metamorphism under contrasting P-T-conditions. Contributions to Mineralogy and Petrology 110, 226-241.

Schmädicke, E., Cosca, M.A. and Okrusch, M. (1995). Variscan Sm-Nd and Ar-Ar ages of eclogite facies rocks from the Erzgebirge, Bohemian Massif. Journal of Metamorphic Geology 13, 537-552.

Schmädicke, E. and Evans, B.W. (1997). Garnet-bearing ultramafic rocks from the Erzgebirge, and their relation to other settings in the Bohemian Massif. Contributions to Mineralogy and Petrology 127, 57-74.

Schulmann, K., Ledru, P., Autran, A., Melka, R., Lardeaux, J.M., Urban, M. and Lobkowicz, M. (1991). Evolution of nappes in the eastern margin of the Bohemian Massif: a kinematic interpretation. Geologische Rundschau 80, 73-92.

Stampfli, G. (1996). The intra-Alpine terrain: a palaeotethyan remnant in the Alpine Variscides. Eclogae Geol. Helvetiae 89, 12-42.

Stampfli, G.M., von Raumer, J. and Borel, G.D. (2002). Paleozoic evolution of pre-Variscan terranes: From Gondwana to the Variscan collision. In "Variscan-Appalachian Dynamics: The Building of the Late Paleozoic Basement" (Martínez Catalán, J.R., Hatcher, R.D. Jr., Arenas, R. and Díaz García, F., Eds.), Geological Society of America, Special Papers 364, 263-280.

Stöckhert, B., Duyster, J., Trepmann, C. & Massonne, H.-J. (2001): Microdiamond daughter crystals precipitated from supercritical COH silicate fluids included in garnet, Erzgebirge, Germany. Geology 29, 391-394.

Tait, J., Bachtadse, V. and Soffel, H.C. (1994). Silurian paleogeography of Armorica: new paleomagnetic data from Central Bohemia. Journal of Geophysical Research 99, 2897-2907.

Tait, J., Schätz, M., Bachtadse, V. and Soffel, H. (2000). Palaeomagnetism and Palaeozoic palaeogeography of Gondwana and European terranes. In "Orogenic Processes: Quantification and Modelling in the Variscan Belt" (Franke, W., Haak, V., Oncken, O. and Tanner, D., Eds.), Geological Society of London, Special Publication 179, 21-34.

Willner, A.P., Rötzler, K. and Maresch, W.V. (1997). Pressure-temperature and fluid evolution of quartzo-feldspathic metamorphic rocks with a relic high-pressure, granulite-facies history from the Central Erzgebirge (Saxony, Germany). Journal of Petrology 38, 307-336.

Willner, A.P., Krohe, A. and Maresch W.V. (2000). Interrelated P-T-t-d paths in the Variscan Erzgebirge dome (Saxony, Germany): Constraints on the rapid

Back Cover:
field trip itinerary

FIELD TRIP MAP

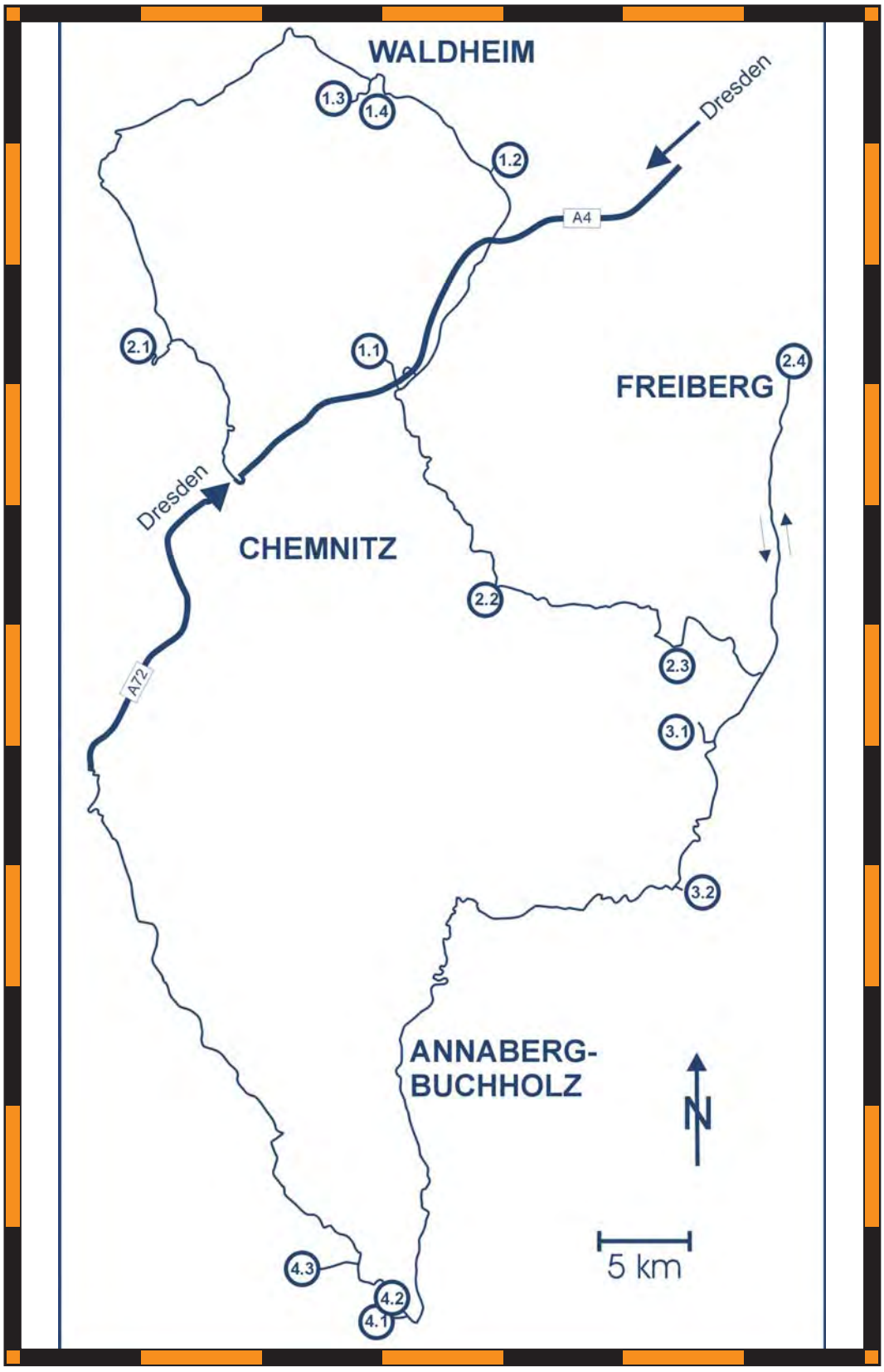

32nd INTERNATIONAL GEOLOGICAL CONGRESS

Edited by APAT

Volume n° 2 - from B16 to B33

32nd INTERNATIONAL GEOLOGICAL CONGRESS

PALEOZOIC OROGENIES IN THE FRENCH MASSIF CENTRAL A CROSS SECTION FROM BÉZIERS TO LYON

Leader: M. Faure

Associate Leaders: J.M. Lardeaux, P. Matte

Field Trip Guide Book - B22

Florence - Italy
August 20-28, 2004

Pre-Congress **B22**

The scientific content of this guide is under the total responsibility of the Authors

Published by:
APAT – Italian Agency for the Environmental Protection and Technical Services - Via Vitaliano Brancati, 48 - 00144 Roma - Italy

Series Editors:
Luca Guerrieri, Irene Rischia and Leonello Serva (APAT, Roma)

English Desk-copy Editors:
Paul Mazza (Università di Firenze), Jessica Ann Thonn (Università di Firenze), Nathalie Marléne Adams (Università di Firenze), Miriam Friedman (Università di Firenze), Kate Eadie (Freelance indipendent professional)

Field Trip Committee:
Leonello Serva (APAT, Roma), Alessandro Michetti (Università dell'Insubria, Como), Giulio Pavia (Università di Torino), Raffaele Pignone (Servizio Geologico Regione Emilia-Romagna, Bologna) and Riccardo Polino (CNR, Torino)

Acknowledgments:
The 32nd IGC Organizing Committee is grateful to Roberto Pompili and Elisa Brustia (APAT, Roma) for their collaboration in editing.

Graphic project:
Full snc - Firenze

Layout and press:
Lito Terrazzi srl - Firenze

Volume n° 2 - from B16 to B33

32nd INTERNATIONAL GEOLOGICAL CONGRESS

PALEOZOIC OROGENIES IN THE FRENCH MASSIF CENTRAL A CROSS SECTION FROM BÈZIERS TO LYON

AUTHORS:
M. Faure (University of Orléans - France)
P. Ledru (BRGM, Orléans - France)
J.M. Lardeaux (University of Nice - France)
P. Matte (CNRS, University of Montpellier - France)

Florence - Italy
August 20-28, 2004

Pre-Congress

B22

Front Cover:
View of gneiss-migmatite of the Montagne Noire axial zone (visited during D2) looking to the north. The village of Olargues is located in the micaschist envelope of the dome. The picture is taken from the northernmost part of the recumbent folds of the Montagne Noire southern side (visited during D1).

Leader: M. Faure
Associate Leaders: J.M. Lardeaux, P. Ledru, P. Matte

1. Introduction

The formation of the continental substratum of Medio-Europa occurred in Paleozoic times. The names of "Hercynian" or "Variscan" are used to deal with the geodynamic processes that took place from Cambrian to Carboniferous. It is now widely accepted that this Paleozoic Belt that crops out from Iberia to Bohemia (Fig. 1) results from a complex interplay of rifting, convergence and collision between three large continents, namely Laurentia, Baltica and Gondwana and several microcontinental stripes such as Avalonia or Armorica (Matte, 2001). Continental drifting and welding resulted in the opening and closure of several oceans such as Iapetus, Rheic and Medio-European. There is however a wide range of opinions concerning the location and width of these oceanic domains and the number, kinematics and timing of collisional processes (e. g. Autran and Cogné, 1980; Franke, 1989, 2000; Ledru et al., 1989; Matte, 1991; 2001; Faure et al., 1997).

The French Massif Central is one of the largest pieces of the Variscan Belt. The whole Massif Central provides a reference cross section throughout the north Gondwana margin deformed and metamorphozed during the Paleozoic. During the last two decades, and recently through the GéoFrance 3D program, developments made in the areas of geochronology, structural geology, metamorphic and magmatic petrology, allow us to draw a comprehensive structural map of the Massif Central and to discuss a possible scenario accounting for the Paleozoic tectono-thermal evolution.

This field trip presents representative lithological, structural, magmatic, metamorphic and geochronological data of the French Massif Central from unmetamorphozed kilometer-scale recumbent folds to UHP metamorphic rocks. Most of the controversial aspects of collisional orogens such as continental subduction and exhumation

Figure 1 - Location of the French Massif Central in the frame of the Paleozoic belt of Medio-Europa (Matte, 1991).

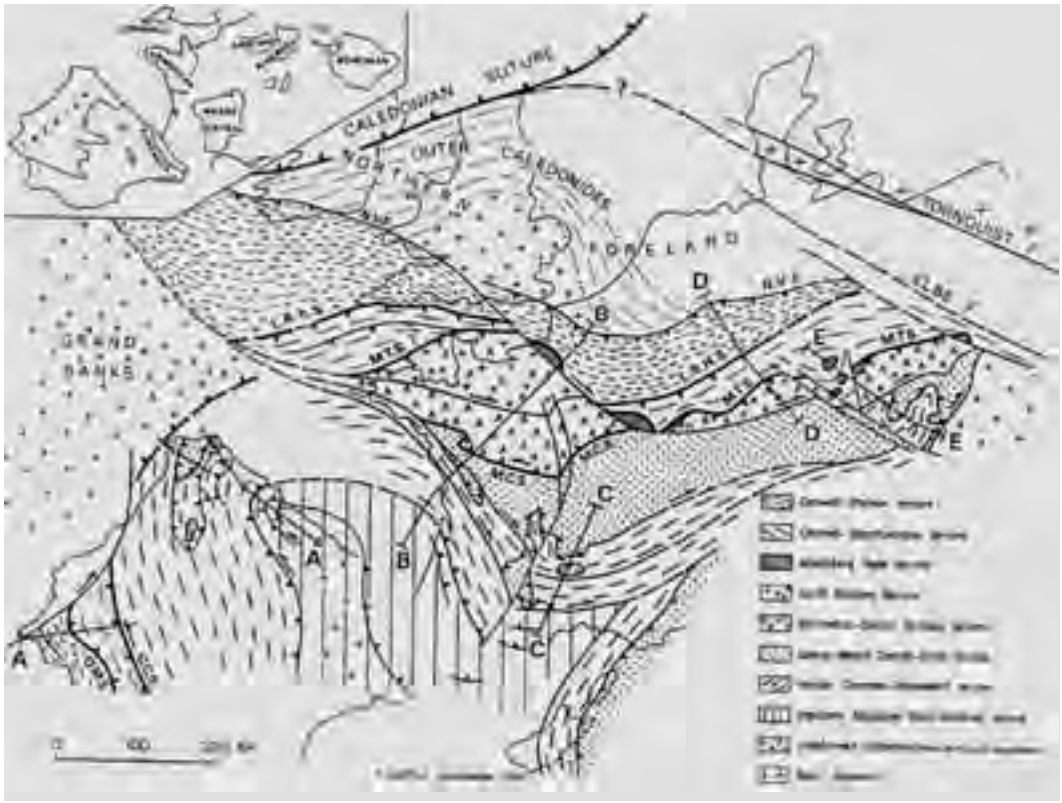

Volume n° 2 - from B16 to B33

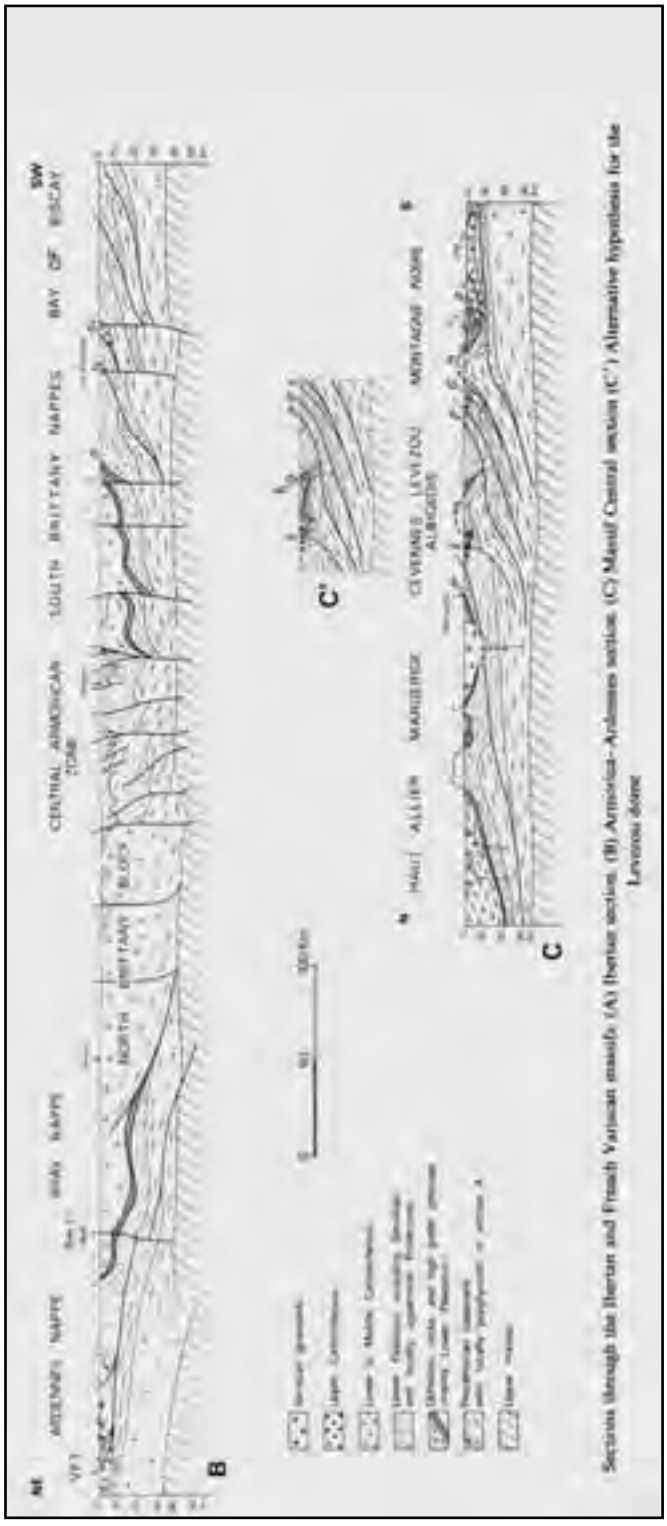

Figure 2 - Cross-sections from the Massif Armoricain to Ardenne (B) and through Massif Central (C). C' is an alternative section through the Lèvezou klippe (Matte, 1991).

of ultrametamorphic rocks, nappe kinematics, inverted metamorphism, syn- to post-orogenic extensional tectonics, crustal melting and tectonic setting of pluton emplacement will be addressed.

Field References

Topographic maps IGN 1/100 000: n°65 Béziers-Montpellier; n°58 Rodez-Mende; n°59 Privas-Alès; n°50 St-Etienne-Le Puy; n°51 Lyon-Grenoble.
Geologic maps BRGM 1/50 000: n°1014 St-Chinian; n°988 Bédarieux; n°862 Mende; n°863 Le Bleymard; n°839 Langogne; n°840 Burzet; n°792 Yssingeaux; n°745 St-Etienne; n°721 St-Symphorien-sur-Coise; n°697 Tarare.

2. Regional geological setting

2.1. A structural map of the French Massif Central.

It is now widely accepted that the structure of the French Massif Central is a stack of nappes (Ledru et al., 1989, 1994 Fig. 3). From top to bottom and also from south to north, six main tectonic units are distinguished.

i) The Southern Palaeozoic Fold and Thrust Belt involves a set of continental margin/platform series recording a more or less continuous sedimentation spanning from Early Cambrian to Early Carboniferous. The series is deformed within kilometer-scale recumbent folds well observed in the Montagne Noire area (Arthaud, 1970).

ii) The Para-autochthonous Unit that overthrusts the previous unit consists of a thick metapelite-metagrauwacke series (also called "Cévennes micaschists") with some quartzite beds and volcanic rocks. Although stratigraphic ages are lacking, a Neoproterozoic to Ordovician age is

Figure 3 - Structural map of the Massif Central (adapted from Ledru et al., 1989).

generally accepted.

iii) The Lower Gneiss Unit (LGU) is lithologically quite similar to the Para-autochthonous Unit. Early Cambrian and Early Ordovician alkaline granitoids, now transformed in augen orthogneiss, are also widespread. Both the Para-autochthonous Unit and Lower Gneiss Unit are interpreted as Proterozoic-Early Paleozoic remnants of the northern Gondwana margin that experienced crustal thinning and rifting in Ordovician times.

iv) The Upper Gneiss Unit (UGU) is made up of a bi-modal association called "leptynite-amphibolite" sequence which is a peculiar assemblage of mafic and felsic rocks. This unit experienced a higher metamorphic pressure under eclogite and HP granulite facies (ca. 20Kb). Ultra high-pressure metamorphism is reached locally near Lyon, coesite-eclogite facies rocks crop-out (Lardeaux et al., 2001). The protoliths of the UGU also include metasediments and granitoids. The upper part of the UGU consists of migmatites formed by the partial melting of pelitic and quartzo-feldspathic rocks within which amphibolite block are preserved as restites. Radiometric dates show that the magmatism occurred in Early Ordovician times (ca. 480 Ma) and the high-pressure metamorphism in Late Silurian (ca. 420-410 Ma, Pin and Lancelot, 1982; Ducrot et al., 1983). Due to the occurrence of rare metagabbros and serpentinized ultramafics, the UGU is considered by some authors as a remnant of an oceanic domain, the Medio-European Ocean, that opened in Early Paleozoic times during the rifting that led to the separation of Armorica from North Gondwana (e. g. Dubuisson et al., 1989; Matte, 1991). However, it is worth noting that the Upper Gneiss Unit is not a true ophiolitic sequence since oceanic sedimentary rocks such as radiolarites or siliceous shales are lacking and ultramafics or serpentinites are rare. A likely interpretation would be to consider that the UGU is a transitional crust between true continental and oceanic ones.

v) The Thiviers-Payzac Unit that crops out in the south Limousin, is the highest tectonic unit of the allochthonous stack in the French Massif Central. It is formed by Cambrian metagraywackes, rhyolites and quartzites intruded by Ordovician granite. Conversely to the underlying UGU, the Thiviers-Payzac Unit never experienced the high-pressure metamorphism. As revealed by seismic reflection line (Bitri et al., 1999), these relatively low grade rocks tectonically overly the UGU.

vi) In the NE Massif Central, near Lyon, the Brevenne Unit consists of mafic magmatic rocks (pyroclastites, pillow basalts, diabases, gabbros), serpentinized ultramafics, acidic volcanic rocks,

and siliceous sediments (radiolarites, siltites). The acidic rocks are dated of 366 ± 5 Ma (U/Pb method on zircon, Pin and Paquette, 1998). Petrology and geochemistry show that the Brevenne Unit and its extension in the Beaujolais area is a Middle Devonian oceanic sequence formed within an oceanic or a back-arc basin opened within the UGU (Sider and Ohnenstetter, 1986; Pin, 1990; Pin and Paquette, 1998). The Brevenne Unit records an early thrusting to the NW over the UGU followed by a NE-SW dextral strike-slip (Feybesse et al., 1988; Leloix et al., 1999). The precise age of the thrusting is unknown but since the metamorphic rocks are concealed below the Early Visean calcareous sandstone of the famous unconformity of Le Goujet (east of Lyon) an Early Carboniferous age is likely (see below).

2.2. The tectono-metamorphic evolution.

Structural information related to the high-pressure metamorphism and the prograde metamorphic evolution is poorly documented since these rocks are known only as relics. It is therefore quite difficult to draw a general view of this event. Moreover, three main synmetamorphic ductile events are recognized.

The earliest deformation found in the UGU, D1, is characterized by a NE-SW trending lineation with a top-to-the-SW shearing developed coevally with an intermediate pressure/intermediate temperature metamorphism and anatexis dated around 385-380 Ma (e. g. Floc'h, 1983; Quenardel and Rolin, 1984; Costa, 1992; Boutin and Montigny, 1993; Duthou et al., 1994; Roig and Faure, 2000; Figs. 4, 5). Since the D1 event is found in the migmatites that form the upper part of the UGU, it occurred during or at the end of the exhumation of the high-pressure metamorphic rocks. The radiometric dates comply with the Devonian stratigraphic age of the unmetamorphozed rocks (e. g. Villedé d'Ardin, Génis, Somme, Belfort

Figure 4 - Structural and geochronologic features related to the Late Silurian-Middle Devonian D1 event.

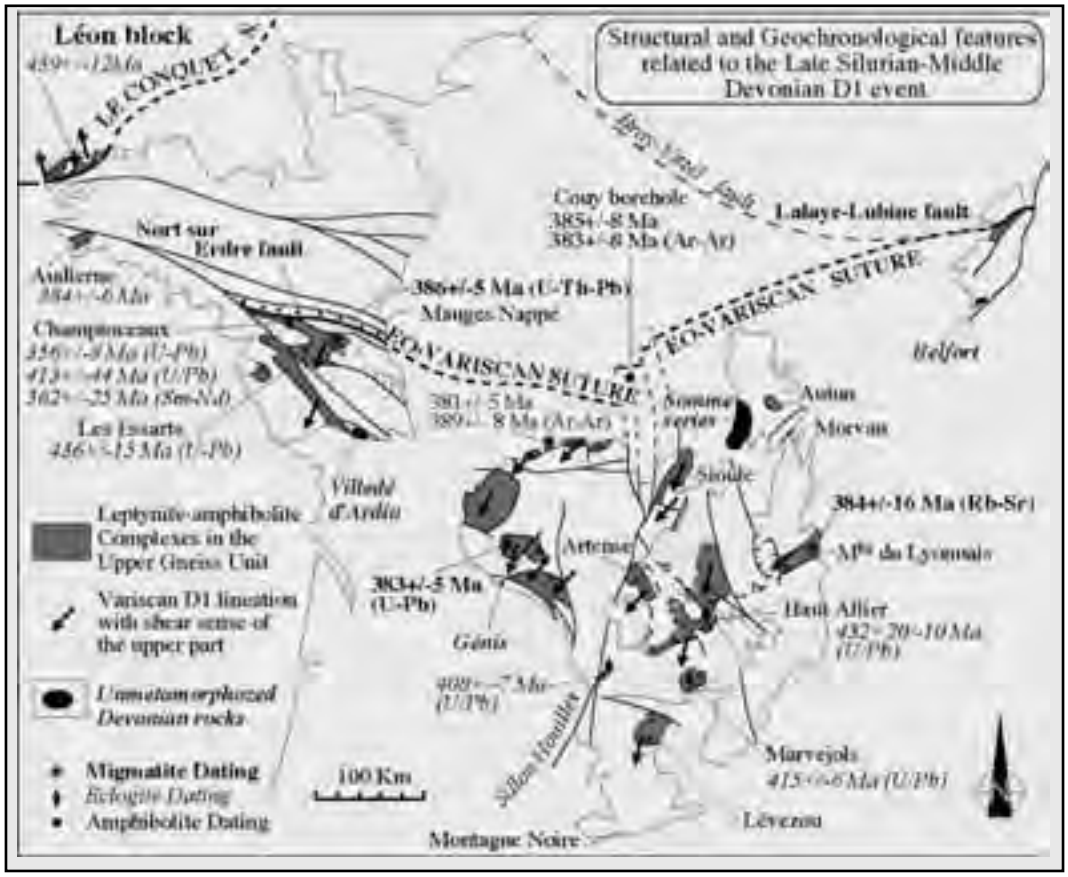

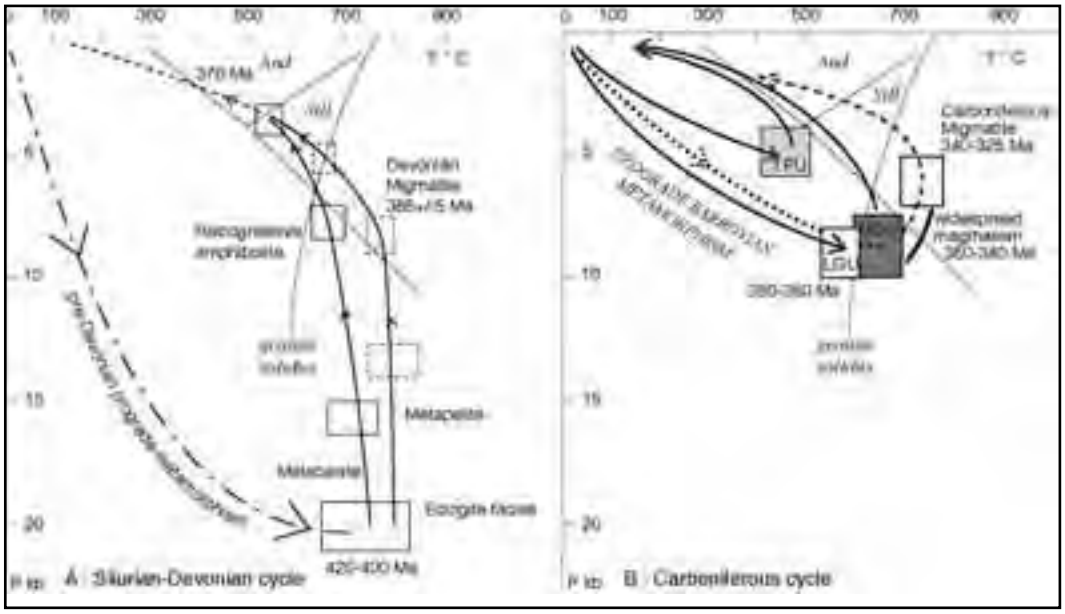

Figure 5 - P-T paths of the Silurian-Devonian and Carboniferous events for the different units.

areas, Fig. 4). Although a direct unconformity is never observed, field relationships suggest that D1 is older than Middle Devonian.

The second event, D2, is characterized by a NW-SE trending lineation coeval with a barrovian type metamorphism (Figs. 5, 6). $^{40}Ar/^{39}Ar$ dates on biotite, muscovite and amphibole range around 360-350 Ma. Most of the shear criteria developed along the NW-SE lineation indicate a top-to-the-NW shearing. In the Rouergue area, the Naucelle thrust is related to this event (Duguet and Faure, in press). The last increment of the ductile deformation in the metamorphic series is associated with the emplacement of peraluminous cordierite bearing granitoids such as the Guéret pluton that is the largest massif of this type. These granitoids exhibit magmatic to sub-solidus fabrics that comply with the synkinematic character of these plutons (e. g. Roig et al., 1998). A similar tectonic-metamorphic-magmatic pattern is also recognized in the south part of the Massif Armoricain. The closure of the Brevenne oceanic basins is chronologically and kinematically in agreement with the D2 event (Leloix et al., 1999). The geodynamic significance of the NW-SE lineation parallel to the belt is not clearly understood yet. Several hypotheses have been proposed (e. g. Burg et al., 1987; Bouchez and Jover, 1986; Mattauer et al., 1988) but none of them appears fully convincing. As discussed in section 2.4, this Early Carboniferous deformation is coeval with the closure of the Rheic Ocean and collision between Gondwana and Laurussia.

The third event, D3, is restricted to the southern part of the Massif Central. In the Para-autochthonous Unit of Cévennes-Albigeois, upper greenschist to amphibolite facies rocks are deformed by top-to-the-south ductile shearing along a submeridian lineation (Fig. 7). Available $^{40}Ar/^{39}Ar$ dates on the metamorphic minerals yield Visean ages around 340 Ma (Monié et al., 2000; Faure et al., 2001). This thrusting propagates southward in the Fold and Thrust Belt where kilometer-scale recumbent folds develop from Visean to Namurian. Although in the South Massif Central south-directed compressional regime lasts from Visean to Namurian (345 to 325Ma), conversely, in the northern part of the massif, the Late Visean (ca. 340 Ma) is a turning point in the tectonic evolution.

From Morvan to Limousin, the Late Visean time corresponds to the onset of syn-orogenic extension caracterized by a huge crustal melting. Structural studies indicate that the syn-orogenic extension is controled by a NW-SE maximum stretching direction (Fig. 7). The NW-SE spreading of the inner part of the Massif Central is also partly accommodated by ductile wrench faults well developed in Limousin (e. g. La Courtine or S. Limousin faults, Fig. 7) and in the Massif Armoricain. In the scale of the whole

Figure 6 - Structural, magmatic and geochronologic features related to the Late Devonian-Early Carboniferous D2 event (AMBP: Magnetic Anomaly of Paris Basin).

belt, the Late Visean to Namurian compression is also responsible for the development of north-directed thrusts in Ardenne and SE England.
The last ductile deformation events (ca. 320 Ma and younger ones) took place during the collapse of the belt. Since they are closely associated to magmatism, they will be considered in the next section.

2.3. A magmatic outline.
Like all the Variscan massifs, the Massif Central is also characterized by a voluminous magmatism mainly derived from crustal melting. Several generations of migmatites and granitoids are recognized (e. g. Duthou et al., 1984).

2.3.1. The pre-orogenic magmatism is not presented in detail here. The Early Ordovician bimodal magmatism, responsible for the formation of the leptynite-amphibolite complex in the UGU, and the Cambrian or Ordovician magmatic rocks are ductilely deformed, metamorphozed and included in the stack of nappes.

2.3.2. The Middle to Late Devonian calc-alkaline volcanic and volcaniclastic rocks that crop out in the Morvan area (called the Somme series) belong to a magmatic arc (Fig. 8; Pin et al., 1982; Delfour, 1989). In the south part of the Massif Armoricain, Eifelian-Givetian basaltic pillow lavas form the Meilleraie series. These rocks are interpreted as the aerial part of a magmatic arc. Moreover, mafic calk-alcaline rocks well known for a long time in the Limousin (Didier and Lameyre, 1971), are interpreted as the deep part of the same Devonian arc. Its geodynamic significance will be discussed in section 2.4.

2.3.3. The Tournaisian late-collisional magmatism is represented by the Guéret-type granites peraluminous plutons. Their magmatic fabric suggests that those plutons emplacement was controlled by the same strain field than the D2 deformation (Fig. 6) .

2.3.4. The Visean magmatism is well developed in the north and west part of the massif Central (Fig. 7). It consists in aerial products with lava flows, ignimbrites, pyroclastic deposits, called "Tufs anthacifères series", rhyolitic to dacitic dykes and hypovolcanic microgranites. Geochemistry indicates that crustal melting was triggered by heat imput from the mantle. Moreover, a mantle contribution as the source of magma is also likely (Pin and Duthou, 1990). The structural control of dyke intrusion complies with a NW-SE stretching related to the early stage of orogenic collapse. In the northern Cévennes, the Para-autochthonous Unit is underlain by migmatitic ortho- and paragneiss called " the Masméjean Unit " or pre-Velay migmatites (Faure et al., 2001). The anatexis is dated between 333 and 324 Ma by the Chemical U/Th/Pb method on monazite (Be Mezème, 2002). The migmatites and cordierite granites of the

Figure 7 - Structural and geochronologic features related to the Visean-Namurian D3 tectonics and Late Visean magmatism (AMBP: Magnetic Anomaly of Paris Basin).

Montagne Noire Axial Zone (cf D2 field itinerary in section 3) yield similar ages. In the present state of knowledge, this Late Visean event is still poorly studied. It is likely that other pre-Velay migmatites are not yet recognized also within the Velay dome.

2.3.5. The Namurian-Westphalian plutonism corresponds to the main period of magma production in the French Massif Central. It is well acknowledged (Didier and Lameyre, 1971) that this magmatism is represented by two types of granitoids, namely porphyritic monzogranites, such as the Margeride or Pont-de-Montvert-Borne plutons, and biotite-muscovite leucogranites such as the Brame or Millevache

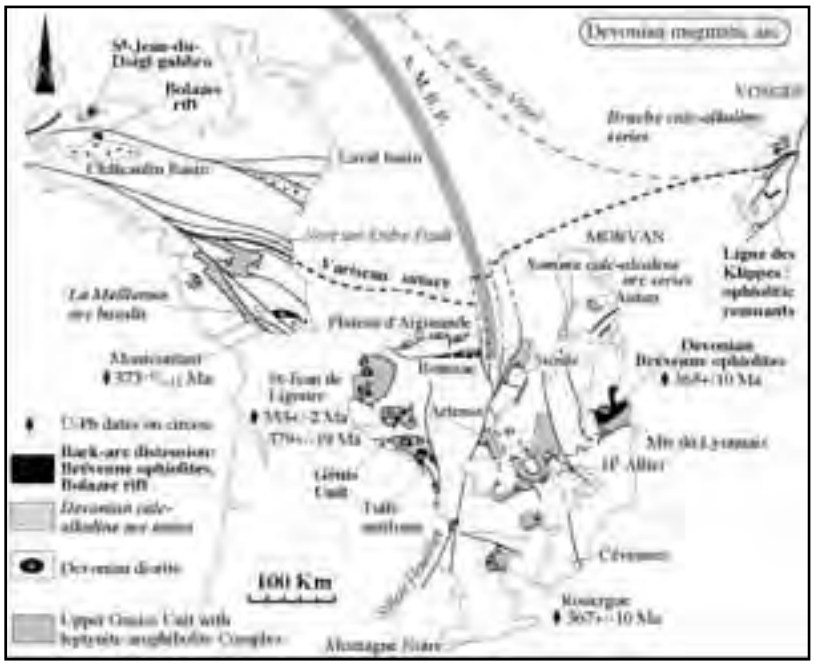

Figure 8 - Map showing the distribution of the Devonian plutons and volcanic rocks related to the magmatic arc and ophiolites (Brè venne, Ligne Klippes) interpreted as back arc basins (adapted from Faure et al., 1997).

Figure 9 - Distribution of the main granitic plutons coeval with the stretching lineation and kinematics related to theNamurian-Westphalian extensional tectonics. During this event, the pre-Visean GuÈret pluton behaves as a rigid body.

massifs (Fig. 9). Although both granite types crop out throughout the Massif Central, the former type is best represented in the central and southern parts of the massif and the later type is more abundant in the north and west parts. The two types were derived from different magmas, but field relationships and geochronology show that these two magmatic types emplaced coevally. Petro-structural and AMS studies of the Namuri-Westphalian plutons show that these bodies are characterized by a conspicuous NW-SE trending mineral, stretching and magnetic lineation. The same trend is also observed in biotite ans andalusite contact minerals in the pluton host rocks (Fig. 9). In the north Limousin, the Brame pluton is bounded to the west by the Nantiat ductile normal fault that also exhibits a NW-SE trending hot slickenline. A similar kinematics is also found along the Argentat ductile normal fault. This structural pattern is interpreted as the consequence of the syn-orogenic extensional tectonics of the Massif Central (Faure, 1995).

2.3.6. The Stephanian magmatism is represented by cordierite granite and migmatites of the Velay dome, and also by acidic tuf, ash layers and more rarely alkaline basalts interlayers with terrigeneous formations in the coal basins. The Velay dome is bounded to the north by a detachment fault, the Pilat ductile normal fault (Malavieille et al., 1990). Gneiss and micaschists belonging to the LGU that crop out north of the Pilat fault form the substratum of the Late Carboniferous St-Etienne basin.

2.4. A possible geodynamic scenario.

The above-presented data allow us to discuss a geodynamic evolution model. Presently, two scenari for the evolution of the French Massif Central are proposed. The first one emphasizes a continuous convergence between Gondwana and Laurussia from Silurian to Early Carboniferous (e. g. Matte, 1991, Lardeaux et al., 2001). The second one points out a polycyclic evolution (Pin, 1990; Faure et al., 1997). According to this model, an Early Paleozoic cycle, (Cambrian to Early Devonian), is related to the opening and closure of the Medio-European Ocean and correlatively drifting and rewelding of Armorica to Gondwana. A second orogenic cycle ranging from Middle Devonian to Carboniferous accounts for which the closure of the Rheic Ocean and the collision of Gondwana and Laurussia. Whatever the preferred model, the following stages are acknowledged.

2.4.1. The breaking of the north Gondwana margin.

From Cambrian to Early Silurian, the Massif Central belongs to the northern passive margin of Gondwana which extends from South America to China. From the study of Montagne Noire, the Cambrian-Ordovician corresponds to a terrigeneous environment, followed in Devonian by a carbonate platform. The lack of Late Ordovician and Silurian deposits is interpreted as the result of erosion on tilted blocks (Robardet et al., 1994). Evidence of an Ordovician rifting is also inferred from magmatism. In the Para-autochthonous Unit, alkaline mafic volcanics (sometimes with pillow lava), diabase dykes, gabbro intrude the grauwacke-pelite series (Pin and Marini, 1993). In LGU, the alkaline Ordovician granitoids also comply with continental rifting. It is worth noting that “pseudo-calc-alkaline” geochemistry of these granitoids is due to crustal contamination (Duthou et al., 1984; Pin and Duthou, 1990). In the UGU, crustal thinning due to continental rifting is coeval with the emplacement of the leptynite-amphibolite complexes. As a matter of

Figure 10 - Devonian geodynamic reconstruction (map and section) showing the closure of the Rheic Ocean by southward subduction below Gondwana and related microcontinents (from Faure et al., 1997).

fact, the Cambrian-Ordovician period is characterized by the formation of continental stripes, such as the Armorica microcontinent drifted from the north Gondwana margin. The question of the maximum width of the intervening Medio-European Ocean has not been not settled yet (see discussion in Robardet, 2003). A rough estimate suggests that this oceanic area was of limited extension (i. e. between 500 and 1000 km).

2.4.2. The closure of the Medio-European Ocean.
On the basis of available dates on the high-pressure metamorphism, the closure of the Medio-European Ocean started in Silurian. All authors accept a northward subduction of the Gondwana margin, however, structural constraints (i. e. kinematics coeval with the development of high-pressure assemblages) or geodynamic evidence (i. e. relics of a magmatic arc) are lacking. By Middle Devonian time, the Armorica microcontinent is rewelded to Gondwana. In NE Massif Central, (North of Lyon), undeformed and unmetamorphozed Givetian sedimentary rocks unconformably cover the migmatites and high pressure rocks (Delfour, 1989; Godard, 1990). Subduction of oceanic and continental rocks is followed by their exhumation in Early to Middle Devonian, around 390-385 Ma. The lack of large volumes of Devonian clastic rocks suggests that exhumation was tectonically assisted. Exhumation results in the extensive retrogression of the high-pressure rocks of the UGU and migmatisation of the pelitic parts.

2.4.3. Mid-Devonian magmatic arc-back arc system.
Frasnian-Fammenian calc-alkaline volcanism in the NE Massif Central and Vosges argue for subduction. In addition, the 380-370 Ma calc-alkaline diorite, tonalite, granodiorite plutons that crop out in NW Massif Central are interpreted as the deep part of this magmatic arc. However, in their present position, these plutons are rootless and tectonically included into the Hercynian nappes. Southward subduction of the Rheic Ocean is viewed as the cause of the calc-alcaline magmatism. At the same time, distension also occurred in the upper plate, giving rise to limited oceanic zones such as the Brévenne in the Massif Central or other areas in the Massif Armoricain and Vosges. Therefore, an arc-back arc pattern appears as the most likely geodynamic setting for Devonian times (Fig. 10). However a discussion of the Léon and microcontinents is beyond the scope of this presentation.

2.4.4. The closure of the Rheic Ocean and the Tournaisian collision.
Since the Late Fammenian, a complete closure of the Rheic Ocean led to a collision between the North European continent made by the assembly of Laurentia, Baltica and Avalonia during the Caledonian orogeny and Gondwana, including Armorica microcontinent rewelded to it. Intracontinental shortening follows the Lizard ophiolite obduction

Volume n° 2 - from B16 to B33

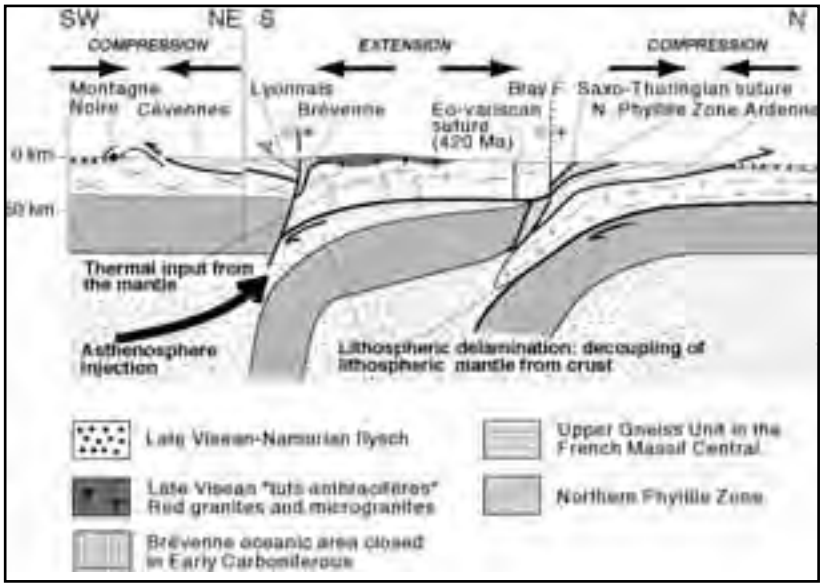

Figure 11 - Interpretative lithosphere scale cross section through the French Hercynian Belt in Late Visean. Mantle lithosphere delamination may account for the contrasted tectonic regimes (extensional and compressional), magmatism and heat flow in the central part of the belt (modified from Faure et al., 2002).

(which probably extends along the Magnetic Anomaly of Paris Basin). North-directed thrusts develop from the South of England to the Ardennes. In the northern Massif Central, the closure of the Brévenne oceanic area is characterized by top-to-the-NW shearing under upper greenschist-lower amphibolite facies in the mafic rocks. Top-to-the-NW ductile shearing coeval with middle temperature / middle pressure metamorphism, and dated around 360 Ma is also widespread in western and northern Massif Central. In the southern part of the Massif Central, southward shearing and recumbent folding develops with a progressively younging southward: ca. 345-340 Ma in the Para-autochthonous Unit to 330-325 Ma in the Fold and Thrust Belt.

2.4.5. Late Visean-Namurian syn-convergence extension.

As soon as Late Visean (ca 335 Ma), the northern Massif Central experienced crustal melting responsible for the "tufs anthracifères" acidic volcanism and related plutonism. The structural analysis of the Late Visean plutons and dykes emplacement is controlled by a NW-SE maximum stretching direction and argue for an incipient stage of syn-orogenic collapse in the inner part of the belt (Fig. 7). However, the southern and northern external zones of the Hercynian Belt, such as Montagne Noire and Ardenne respectively, are still under compression as shown by the development of kilometer-scale recumbent folds and thrusts.

In the Central and southern Massif Central, the thermal overprint is reponsible for migmatite and cordierite granite formation. The ca 330 Ma migmatites that crop out in the Montagne Noire Axial Zone and south of the late Carboniferous Velay massif belong to this event. However, in the present state of knowledge, the tectonic setting (namely extensional or compressional tectonic regime) is not settled yet. Decoupling of lithospheric mantle from crust, i. e. lithospheric delamination, is likely to play a significant role to account for the magmatism (Fig. 11).

From Namurian to Westphalian (ca 325-310 Ma), orogen parallel extension is well recorded by emplacement fabrics of leucogranites and granodiorites in the Massif Central (Fig. 9). In the Massif Armoricain, leucogranitic are also widespread. There, they are syn-kinematic plutons coeval with dextral wrenching (e. g. Berthé et al., 1978). However, it is worth noting that both in the Massif Armorican and Massif Central the wrench or extension controlled synkinematic plutons exhibit the same NW-SE maximum stretching direction. This tectonic stage corresponds also to the main metallogenetic epoch for mesothermal gold deposits.

2.4.6. Stephanian post-orogenic NNE-SSW extension

The last stage of the Hercynian orogeny in the French Massif Central corresponds to the collapse of the whole belt. Extensional regime is well recorded by the tectonic setting of intra-mountain Stephanian coal basins. Two structural types of basins are recognized : 1) half-graben bounded by pure normal faults or normal faults with a

Figure 12 - Massif Central map showing the Carboniferous extensional structures: coal basins, Velay granite-migmatite dome.

Figure 13 - Structural map of the Montagne Noire modified from Gèze (1949) and Arthaud (1970).

strike-slip component or 2) pull-apart controlled by wrench faults (Fig. 12). Among these intra-mountain basins, the St-Etienne coal basin is one of the most famous since it corresponds to the para-stratotype of the Stephanian stage. Nevertheless the structural control, either as a left-lateral pull apart or a half-graben is not settled yet (Mattauer and Matte, 1998). In the scale of the Massif Central, the deformation pattern of Stephanian extension is characterized by NE-SW stretching, NW-SE and vertical shortening. The amount of extension increases from west to east. NE-SW extension and correlatively coal basins are widespread in eastern Massif Central but are rare in western Massif Central and almost lacking in the Massif Armoricain. Several N-S to NNE-SSW trending wrench faults such as the Sillon Houiller and Argentat fault are interpreted as transfer faults that accommodate different amounts of extension. Magmatism and mid-crustal deformation associated to Late Carboniferous extension are less developed than during syn-convergence extension. The most spectacular structure is the 100 km diameter migmatitic-granitic Velay dome (Ledru et al., 2002). Heat imput from the mantle is responsible for high temperature granulitization of the lower crust (Pin and Vielzeuf, 1983).

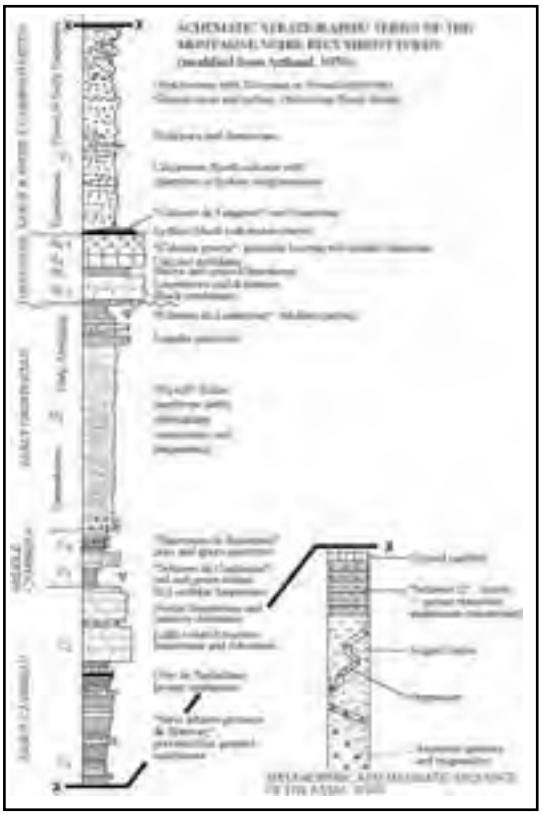

Figure 14 - Schematic stratigraphic column of the Paleozoic series found in the Montagne Noire southern side recumbent folds (adapted from Arthaud, 1970).

3. Field itinerary

DAY 1

Recumbent folding in the Montagne Noire Southern Side

Montpellier--> Béziers --> Cessenon D 136 to St-Nazaire de Ladarez

A. Geologic setting

Following Gèze (1949) and Arthaud (1970), the Montagne Noire area is classically divided from South to North, into a Southern Side, an Axial Zone and a Northern Side (Fig. 13). This last area is less studied than the previous two. The geology of the Axial Zone will be presented during D2. The Southern Side is worldwide famous for Paleozoic stratigraphy (Lower Cambrian,

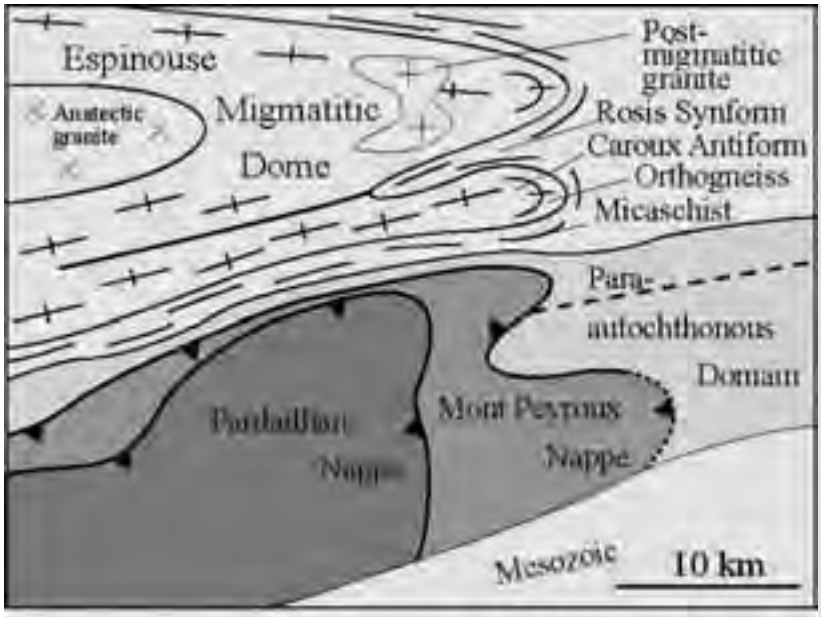

Figure 15 - Sketch of the main units observed in the eastern part of the Montagne Noire.

Lower Ordovician, Devonian, Carboniferous) and the development of kilometer-scale recumbent folds (or nappes). The stratigraphic column is schematically summarized in Fig. 14.

Five tectonic units are recognized in the southern side of the Montagne Noire, namely from top to bottom (Fig. 15):

i) The Pardailhan Nappe (or recumbent fold)

ii) The Mont Peyroux Nappe

iii) The Monts de Faugères Unit

iv) The Cabrières Unit

v) The Para-autochthonous domain

The Pardailhan Nappe consists of folded and overturned Cambrian to Devonian rocks. The Mont Peyroux Nappe includes Ordovician to Visean rocks. The Monts de Faugères Unit consists of several overturned folds of Devonian to Visean rocks. The Cabrières Unit is an olistostrome, with large-scale olistoliths of Carboniferous and Devonian limestones, Silurian volcanites and Ordovician turbidites are resedimented within a wild-flysch matrix corresponding to the foreland basin of the belt (Engel et al., 1980).

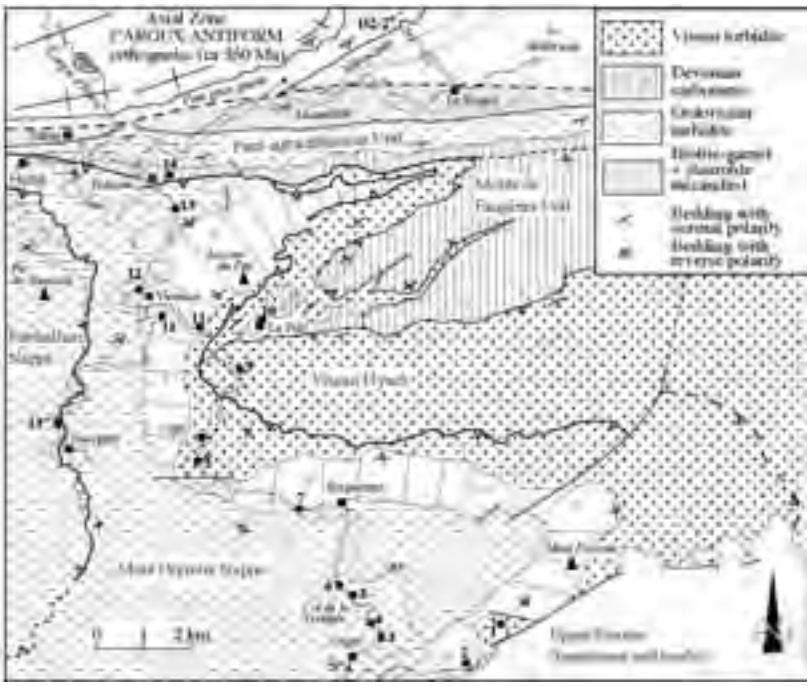

Figure 16 - D1 route map.

The Pardailhan Nappe exhibits a conspicuous axial planar cleavage, whereas in the Mont Peyroux Nappe, the transition between ductile deformation with axial planar cleavage folds and synsedimentary structures can be observed. On the basis

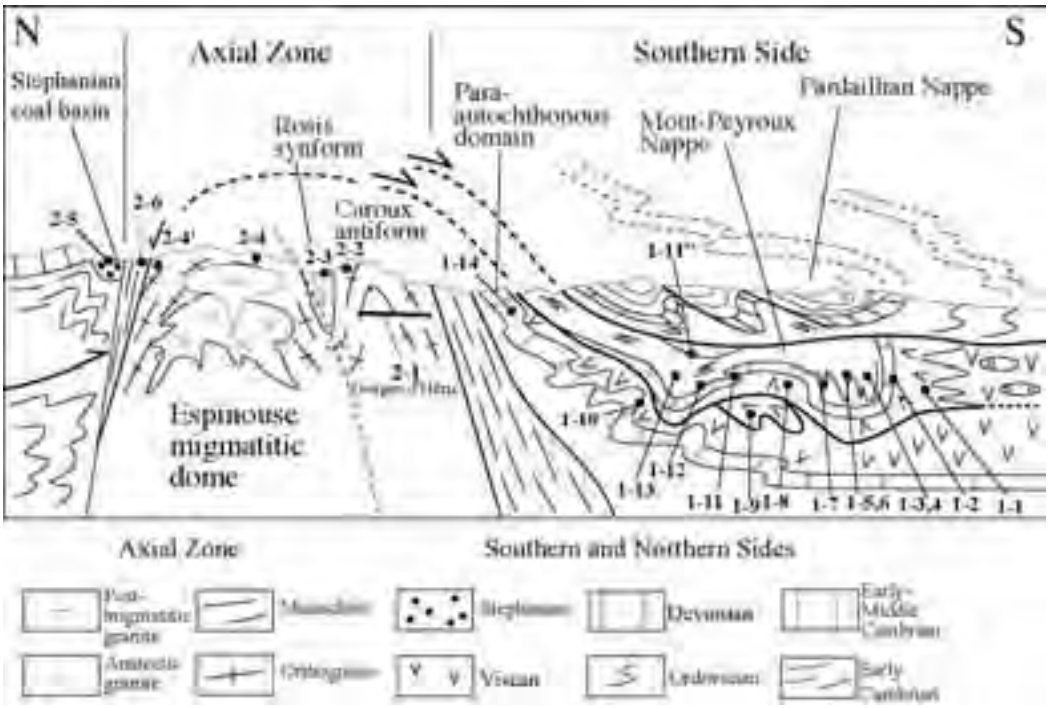

Figure 17 - Synthetic cross section of the Montagne Noire with location of the D1 and D2 stops.

of stratigraphy, those nappes were emplaced in Visean-Namurian times (around 330-325Ma).

The aim of this first day is to present the polyphase deformation of the Mont Peyroux recumbent fold through a South to North cross section along the Orb river (Fig. 16). There, the stratigraphic succession ranges from Early Ordovician (Tremadoc-Arenig) to Middle Carboniferous (Visean). Along this route, deformation and metamorphism increase from South to North, however most of the observed structures develop after recumbent folding during an upright deformation linked with the formation of the Axial Zone dome (cf. D2).

B. Stop description

The stops will show most of the lithological and structural aspects of the Mont Peyroux nappe and Para-autochthonous domain underneath (Figs. 16, 17).

Stop D1.1:

Visean flysch with limestone blocks.

The landscape shows Eocene limestone unconformably overlying at low angle Paleozoic rocks. The S. part of the section exposes Visean flysch with continuous sandstone beds dipping east (20E 60). The northern part that is folded and sheared exposes disrupted beds with sandstone lenses and limestone blocks. Devonian limestone overlying the Visean turbidite is seen on the other side of the valley and nearly 200m to the north of this stop.

Stop D1.2:

Coumiac quarry (protected area)
-Frasnian/Famennian boundary.

This old quarry was mined for red nodular limestone exported all over the world (e. g. the White House in Washington, or the Maison de la France in Rio de Janeiro). The vertical beds (N 30. 90) are Late Devonian (365 Ma) Goniatite limestone called “Griotte marble” (griotte is a type of cherry). This section has been chosen as the Global Stratotype Section for the Frasnian/Famennian boundary. This series corresponds to the “Famenian Biological Crisis” responsible for one of the most severe mass extinction in the Earth history (Kapper et al., 1993).

Stop D1.3:

Early Ordovician turbidite. NE of Lugné.

In the landscape, looking to the SE, the vertical cliffs are Early Devonian limestones continuous with those seen in the previous stop (D1-2) in the Coumiac quarry.

Sandstone-mudstone alternations lie subhorizontally, however graded bedding and load cast show that the sequence is upside down. Folds are apparently overturned to the north but correspond in reality to the inverted limb of the Mont Peyroux recumbent fold. This Early Ordovician turbidite is interpreted as deposited along the northern passive margin of Gondwana.

Stop D1.4:

Early Ordovician turbidite.

A few hundred meters from the previous stop.

The subvertical to north dipping upside down of the beds exhibits numerous load casts, ripple marks and bioturbation evidence (worm burrows). Locally Lingula shells can be abundant. Sandstones contain abundant floatted muscovite and heavy minerals. In this outcrop, like the previous one, cleavage is lacking.

Stop D1.5:

Panorama on Roquebrun synform and the Orb River. Col de la Vernède.

Below the road, the vineyards and Orb river are located in the Ordovician turbidites which form the core of the Roquebrun synform. Looking northward, above the Roquebrun village, the white cliffs are Devonian limestones. In the background, the hills with bushes are Visean flysch and in the distance, the last hills are made of Devonian limestone belonging to the Monts de Faugères Unit. To the West (left), the highest mountain is the Pic de Naudech made of inverted Cambrian rocks overlying inverted Ordovician turbidites belonging to the Pardailhan Nappe. Lastly, the farthest mountain to the NW is the Mt Caroux composed of orthogneiss belonging to the Axial Zone.

Along the other side of the road, the Ordovician turbidite is complexly folded. Superimposed folds are observed in the next stop.

Stop D1.6:

Superimposed folds in Ordovician turbidite. 200 m down to Roquebrun.

The Ordovician turbidite experienced two folding phases. Recumbent isoclinal folds (F1) are deformed by upright open folds (F2) with axes plunging 50° NW. F1 are related to the Mont Peyroux recumbent fold and F2 belong to the kilometer-scale upright folding responsible for the Roquebrun synform, Vieussan synform, and Axial Zone antiform (Fig. 17).

Stop D1.7:

Ordovician-Devonian contact. North of Roquebrun.

This stop shows the inverted stratigraphic contact between Ordovician detritals and Devonian carbonates in the northern limb of the Roquebrun synform. From south to north: Ordovician turbidite with top-to-the-S base (with load casts) dipping southward is underlain by Devonian calcareous sandstone, followed by limestone and dolomite. At the northern end of the outcrop, undeformed crinoid stems can be observed in the Devonian carbonates.

Stop D1.8:

Visean flysch. Chapelle St-Poncian, S. of Ceps.

Looking to the NW, the white rocks above the village of Ceps are inverted Devonian limestone, and to the W and SW, the vineyards are located in the Ordovician turbidite. The highest white cliff in the background (La Tour du Pin summit) is the northern extension of Devonian formations. Below the cliff and up to Ceps, the lowest parts of the mountains are made of Visean flysch, belonging to several tectonic units.

The outcrop exposes Visean mudstone-sandstone with limestone intercalations dipping south-westwards (S0-1: 130 SW 50). Contrasting with the Visean rocks observed at the first stop (point D1-1), here the Visean pelites are slightly metamorphosed (sericite) and exhibit a N70E trending crenulation lineation. Chevron folds and south-directed brittle shear zones with quartz veins deform S0-1. Along the road, Devonian rocks are not observed, a late fault separates the Visean and Devonian rocks.

Stop D1.9:

Monts de Faugères Unit. Large curve of Orb River below Chapelle St-Geminian.

Tournaisian (?)-Visean limestone and sericite metapelite present a westward (170W40) dipping foliation and a well marked mineral, stretching and crenulation lineation trending N 70E. Pressure-solution is the dominant deformation mechanism. S0-1 is also cut at high angle by west dipping tension

gashes filled by fibrous calcite.

Stop D1.10:

Para-autochthonous Domain. Le Pin and Le Lau anticlines.

Turning right to the road of Le Pin, we can observe the underlying Para-autochthonous Domain. North of Le Pin, this outcrop exposes the deepest part of the Orb section. From North to South, the upside down sequence consists of the Upper Devonian red nodular limestone (griotte marble) with goniatites (S0: 60NW60) with an inverted limb subhorizontal cleavage; Tournaisian radiolarian black cherts (lydiennes) and nodular limestones (calcaires de Faugères) and Visean flysch. North of this outcrop, the succession becomes normal from Devonian limestone to Visean flysch from bottom to top, respectively. This S-SE verging fold is called "Le Pin " anticline. Bedding-cleavage relationships with cleavage refraction in sandstone beds comply with the anticline geometry. A N70E composite lineation due to elongated nodules and goniatites, crenulation and intersection develops. Regionally, this para-autochthonous series is folded by two anticlines (Le Pin and le Lau folds) overturned to the South.

Back to the main road, the contact between the Para-autochthonous series and the Mont Peyroux nappe is marked by numerous quartz veins (no stop).

Stop D1.11:

Recumbent fold in Devonian limestone. Moulin de Graïs.

This famous outcrop (Color Plate 1, A) exposes a folded Late Devonian limestone (partly dolomitized). Bedding-cleavage relationships show a southward overturning. The horizontal part of the outcrop is the normal limb. To the south, radiolarian chert (Color Plate 1, B) and limestone are involved in isoclinal folds belonging to the same large-scale structure. It is worth noting that stretching lineation trends close to the fold axis and thus at high angle to the transport direction. In XZ section, pressure shadows indicate top-to-the-NE sense of shear.

Stop D1.11':

Optional. Landscape on the Vieussan antiform.

Turning left on D177, to Berlou, the large curve to the right provides a clear panorama of the northern limb of the Vieussan antiform, well marked in the Devonian limestones.

Stop D1.11»:

Basal thrust contact of the Pardailhan recumbent fold "Queue de cochon (pig's tail)".

Southward, the road goes through the Ordovician turbidite of the Mont Peyroux recumbent fold deformed both by isoclinal and upright folds. The contact between Ordovician turbidite belonging to the Mont Peyroux recumbent fold and the Devonian limestone boudins marking the basal thrust contact of the Pardailhan recumbent fold can be observed in the tight curve north of Escagnès. In spite of intense shearing, the limestone is weakly or undeformed. Back to Vieussan by the same road.

D1.12:

Ordovician/Devonian contact. N. of Vieussan.

Looking West, the hill slope shows several white masses corresponding to Devonian limestone boudins along the basal thrust contact of the Pardailhan recumbent fold (Fig. 18). The outrop exposes inverted stratigraphic contact between Ordovician turbidite to the left and Early Devonian sandstone to the right. Isoclinal folds with curved hinges can be observed in the Ordovician sandstone. The angular unconformity between Ordovician and Devonian formations, and the lack of Late Ordovician-Silurian rocks in most of the Montagne Noire southern side can be interpreted as a sedimentary consequence of a remote tectonic-metamorphic event that took place more to the north in the internal zone of the Belt. It is worth noting that sedimentology of eo-Devonian rocks indicates a northern source of the terrigeneous sediments. Detrital volcanic quartz grains, mica, garnet, zircon, rutile, tourmaline support a pre-Devonian metamorphic event occurring in the hinterland.

Stop D1.13:

Ordovician turbidite in the north part of the Mont Peyroux recumbent fold. N of Vieussan.

Looking to the north, the landscape presents the Axial Zone gneiss and the entrance of Gorges d'Heric visited on D2. The village of Tarassac is built on Devonian marbles (D1-14), the front view is Ordovician turbidite at the western pericline of the Vieussan antiform.

At the outcrop scale, the Ordovician rocks are black pelite and sandstone deformed by upright N80E trending folds (F2) and N50E isoclinal folds (F1). A few biotite grains can be observed in the vertical S2 foliation axial planar to F2.

Stop D1.14:

para-autochthonous Devonian marble. Tarassac, parking of VVP.

Muscovite bearing Devonian marble with pink calcite crystals corresponding to deformed crinoid stems exhibit a southward dip (70S60) and well marked subhorizontal mineral and stretching lineation. This marble is separated from the overlying Ordovician turbidite by a major thrust contact corresponding to the basal thrust surface of the Mont Peyroux recumbent fold. The Devonian marble and the underlying metapelites attributed to Ordovician (not seen here) are a normal sequence belonging to the Para-autochthounous Unit. $^{40}Ar/^{39}Ar$ date on muscovite gives 297 ± 3 Ma which is interpreted as the age of a Late Carboniferous gravity sliding event related to the formation of the Axial Zone (Maluski et al., 1991).

End of the 1st day. Overnight stay in Olargues

Figure 18 - Panoramic view of the contact between the Pardaillhan (top) and Mont-Peyroux nappe (bottom) marked by Devonian limestone boudins called " pig's tail ".

DAY 2

Migmatite dome of the Montagne Noire Axial Zone

A. Geological setting

The Montagne Noire Axial Zone remains one of the most controversial area in the geology of Massif Central (cf extensive references in Soula et al., 2001). The Late Visean-Early Namurian recumbent folds examined during D1 are overprinted by metamorphic and structural features related to a granite-migmatite gneiss dome developed in the Axial Zone (Figs. 13, 17). The foliation of micaschists and gneiss defines a NE-SW long axis elliptical dome whose western part is disturbed by the Eocene Mazamet thrust. Some authors argued that the Axial Zone metamorphic rocks correspond to the Precambrian basement of the Paleozoic series observed in the recumbent folds. In the present state of knowledge, there is no argument to support the existence of a Neo-Proterozoic (i. e. Cadomian) orogen in the Massif Central. Therefore, the reality of a Precambrian basement in the Montagne Noire Axial Zone is not supported by the data. The augen orthogneiss seen in the gorges d'Heric, are porphyritic granites intruding a Neo-Proterozoic to Paleozoic metasedimentary series of micaschists and gneiss and transformed into augen gneiss during Hercynian tectonics. Recent U/Pb dating supports an Early Paleozoic age for the magmatism. The presence of penninic style recumbent folds overturned to the north has also been assumed (Demange, 1975). Although possible, this interpretation cannot be demonstrated, mainly due to poor outcrop conditions.

The Axial Zone gneiss experienced a HT/LP type metamorphism up to partial melting giving rise to migmatites and anatectic cordierite granites (e. g. Laouzas granite). U/Pb dating on single grain zircon and monazite give a ca 330 age. Isograds of this HT/LP metamorphism define the same domal geometry as the foliation. Within the micaschist enveloppe, kyanite relics are locally found (K in Fig. 13). P-T paths for the gneiss core and metamorphic envelope have been proposed (e. g. Soula et al;, 2001; Fig. 19). It is worth noting that some amphibolites included in the gneiss are retrogressed eclogites (E in Fig. 13) with estimated pressure and temperature around 9 ± 2

Volume n° 2 - from B16 to B33

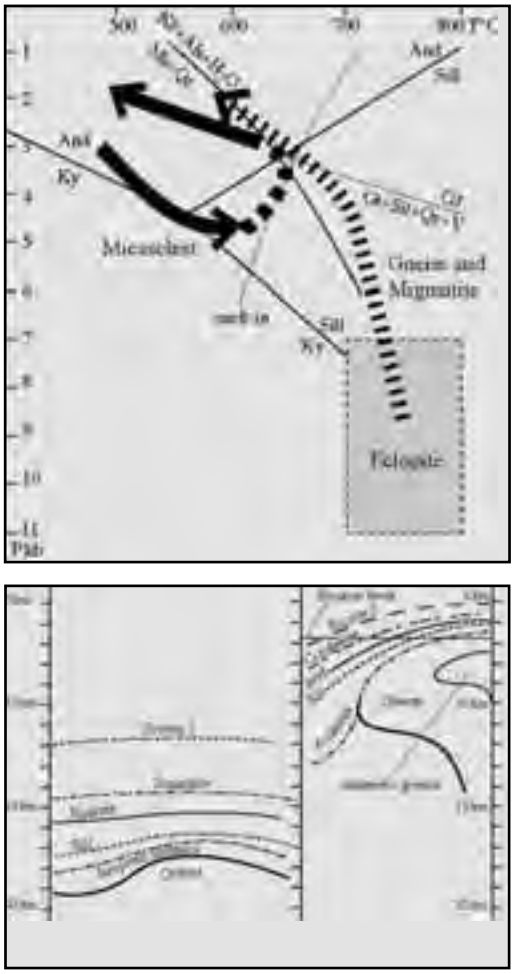

Figure 19 - P-T paths inferred for the Montagne Noire Axial Zone micaschist and migmatitic gneiss (modified from Soula et al., 2001 and Demange, 1985).

Figure 20 - Interpretation of the present-day geometry of the Montagne Noire Axial Zone. During upward doming of the migmatitic core, early isograds are deformed and new HT metamorphic minerals crystallize (from Soula et al., 2001).

kbar and 750 ± 50°C respectively (Demange, 1985). These high-pressure rocks suggest that the tectonic units situated under the recumbent fold were buried at ca 25-30 km depth. Although no radiometric date is available for the eclogites, a possible interpretation is that the high-pressure metamorphism and a part of the ductile deformation of the gneiss is related to compressional tectonics coeval with recumbent folding of the Paleozoic sedimentary sequence.

The Axial Zone is characterized by a conspicuous NE-SW trending stretching lineation which in the southern and northern sides overprints the recumbent folds (cf. stop D1-14). The kinematic analysis provides contrasted shear criteria. Around the dome northeastern and southwestern terminations, shearing is down dip, i. e. top-to-the-NE and SW respectively. However, along the subvertical dome long limbs, shear criteria are ambiguous, as seen along the famous section of "gorges d'Héric" visited in D2 morning.

The present shape of the isograds results from a combination of the tectonic and thermal structures due to the uplift of the migmatitic core (Fig. 20). However, the tectonic significance of the Montagne Noire doming remains disputed. Several interpretations are proposed, namely: i) NE-SW ductile wrench zone (Nicolas et al., 1977; Echtler et Malavieille, 1990); ii) NE-SW antiformal stack (Mattauer et al. 1996, Matte et al., 1998 ; iii) interference between migmatitic diapir and regional NE-SW shortening (Schuilling, 1960, Faure et Cotterau, 1988) ; iv) "metamorphic core complex" (Van den Driessche et Brun, 1991-92). A recent discussion of this problem can be found in Soula et al. (2001).

Although extensional tectonics plays an important role to account for the Late Carboniferous (Stephanian) tectonics (e. g. syntectonic infill of the Graissessac coal basin); the extensional gneiss dome hypothesis cannot account for the bulk structure of the Axial Zone. Indeed, the Vialais granite (Fig. 21) that crosscuts the migmatite foliation is dated by U/Pb on zircon and monazite at 327 ± 5 Ma (Matte et al., 1998).

B. Stop description (Fig. 21)

Stop D2.1:

Cross section of the Caroux Massif along the gorges d'Héric track, 1.5 km, an easy walk.

The morning is dedicated to the observation of the SE part of the Axial Zone, called "Caroux Massif". The Heric augen orthogneiss and paragneiss septa are the most common rock-types. Tourmaline-garnet pegmatitic dykes obliquely cut the foliation. At the entrance of the gorges d'Héric, most of the dykes dip southwards whereas near the top of the mountain, the dykes are flat lying.

After the second bridge, the foliation flattens but the lineation keeps the same N60-70E trend. Further north, the development of a NE-SW crenulation, strengthens

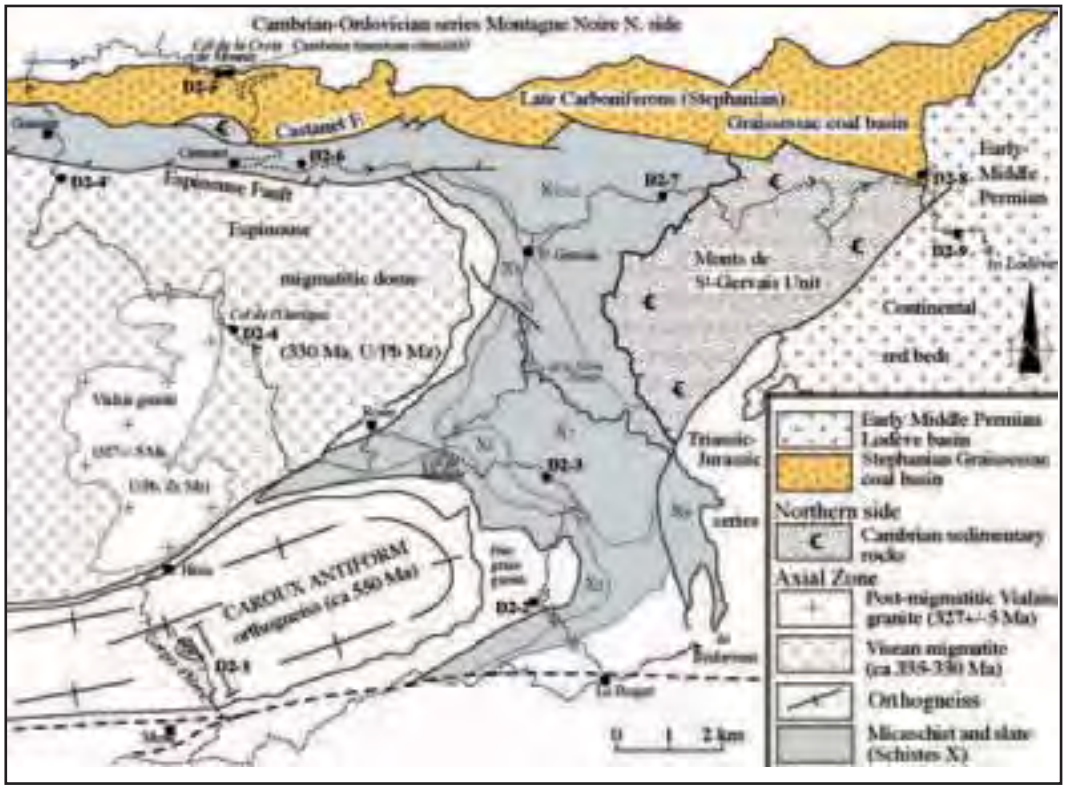

Figure 21 - D2 route map

the gneissic linear fabric. In the paragneiss, meter scale isoclinal folds are refolded by NE-SW trending upright folds.

Pegmatites dykes are also deformed by upright ptygmatitic folds and veins parallel to the fold axes are boudinated. Along the stream, amphibolite boulders (containing garnet locally) including retrogressed eclogites, boulders of migmatites and migmatized augen gneiss, sometimes containing sillimanite nodules are widespread. Outcrop of migmatite will not be visited along this route.

In spite of a clear stretching and mineral lineation, the sigma-type porphyroclast systems exhibit both dextral and sinistral asymmetry at the outcrop scale. The ambiguous sense of shear might be due to superimposed deformation (namely doming overprinted upon low angle shearing) or to strain partitioning with a significant component of pure shear (Color Plate 1, C) during doming.

The bulk structure of the Heric section is a gneiss antiform overturned to the north (Figs. 13, 17). The antiform hinge zone is parallel to upright folds in augen gneiss and meter to millimeter-scale crenulation.

Stop D2.2:

Augen gneiss and sheare pegmatite veins at the eastern part of the Caroux dome. Le Vernet .

From gorges d'Héric → east to Le Poujol → north (left) to Combes.

Fine grain augen gneiss (Sx 40SE 30) with a N70E trending stretching lineation at the eastern termination of the Caroux antiform. Sigmoidal K-feldspath indicates a down-dip, top-to-the East sense of shear. Pegmatite dykes cross cutting the foliation are also sheared to the East. Along the road next curves, many asymmetric pegmatite boudins can be observed within weathered gneiss (no stop).

Stop D2.3:

Biotite-Garnet-staurolite micaschists. Crossing of the road to Forêt des Ecrivains Combattants.

The gneiss-micaschist series experienced a high-

temperature and low-pressure metamorphism characterized by biotite, garnet, andalousite, staurolite tight isograds. The eastward dipping foliation (160E15) bears a composite crenulation, mineral and stretching lineation trending N70E along which top-to-the-E shear criteria develops. In thin section, quartz pressure shadows, helicitic garnet and staurolite, and shear bands indicate a top-to-the East shearing (Color Plate 1, D).

After the Col de Madale, the road runs within the Rosis synform which consists of crenulated and folded HT/LP micaschists between the Caroux antiform and the Espinouse dome.

Stop D2.4:

Migmatitic orthogneiss. Col de l'Ourtigas.

Partial melting develops at the expense of the Heric orthogneiss but MFK and gneissic fabric are still preserved. Migmatisation is dated at 330 Ma. After the pass, the road crosses the northern border of the Vialais granite, however due to poor exposure quality and parking difficulties, the excursion will not stop there.

Optional
Stop D2.4':

Sheared augen gneiss and migmatite.
S. of Ginestet.

The migmatitic orthogneiss experiences a ductile shearing, the NW-SE trending foliation dips 50NE and bears a N60E trending slickenline corresponding to the Espinouse normal fault. $^{40}Ar/^{39}Ar$ dates on muscovite and biotite indicate 297 ± 3 Ma (Maluski et al., 1991).

North of Ginestet, begins the Montagne Noire Northern Side. In spite of globally poor exposure quality, Early Cambrian carbonates can be observed on top of the mountains.

Stop D2.5:

Stephanian conglomerate. Falaise d'Orques.

At the pass of Croix de Mounis, the road enters into the Stephanian Graissessac coal basin. In the northern landscape, the Early Cambrian limestone cliffs are exposed.

The Late Carboniferous conglomerate contains cm to m size blocks of Early Cambrian sandstone and limestone. Along the road, a decameter-scale Cambrian limestone block that is probably an olistolith can be observed too. Stephanian beds dipping 110S10 unconformably cover the Paleozoic (Cambrian-Ordovician) sedimentary rocks of the Northern Side. Thus strictly speaking, the southern border fault of the Graissessac basin (Castanet fault) is reactivated after the deposition of the Stephanian rocks.

At the crossing with D22E road to Castanet-le-Haut, the landscape to the east shows the foliation of the Espinouse gneiss dome dipping north-eastward. The ductile dextral-normal Espinouse fault separates the Espinouse dome from the Stephanian Graissessac basin.

Stop D2.6:

Sheared rocks along the Espinouse fault.
N. of Nougayrols.

The Graissessac basin substratum (i. e. early Paleozoic rocks of the Northern Side) is sheared by the Espinouse fault. Quartz veins are well developed.

Stop D2.7:

Weakly metamorphosed schists. West of Castanet-le-Bas.

Weakly deformed and weakly metamorphosed greenish sandstone-pelite series correspond to the outermost part of the metamorphic rocks surrounding the Axial Zone. Centimeter- to meter-scale folds overturned to the SE can be observed at this outcrop.

East of Verenoux, the road goes through unmetamorphosed and undeformed greenish sandstone and pelite corresponding to the Early Cambrian (grès de Marcory). This Unit (called Monts de St-Gervais Unit) belongs to the Northern Side, and forms an extensional allochthon emplaced upon the Axial Zone micaschists. No stop.

Stop D2.8:

Stephanian massive sandstone and coal mesures. East of La Mouline.

The Late Carboniferous rocks belong to the Graissessac coal basin. They are fluviatile deposits dipping 120NE30 with coal intercalations. Decollement surfaces may develop along coal mesures. In the ancient open pit of the Graissessac mine (not visited) synsedimentary folds overturned to the South can be observed. These Late Carboniferous rocks are unconformably covered by Early Permian conglomerates, sandstones and pelites dipping 0E20, but unfortunately the contact cannot be observed there.

Stop D2.9:

Permian (Autunian) conglomerate.

West of La Tour-sur-Orb.
Continental conglomerates with quartz, sandstone pebbles.

Stop D2.10:

Permian extensional tectonics.
Mas d'Alary quarry.
In the ancient open pit formerly mined for uranium, continental red beds are cut by north dipping normal faults. Alike other early Permian basins in S. France (e. g. St-Affrique, Rodez), the Lodève basin is a half-graben bounded to its southern margin by normal faults.

End of the 2nd day. Drive to Millau (ca 60 km), overnight.

DAY 3

The stacking of Upper and Lower Gneiss Units and post-nappe crustal melting
Millau→ Highway to La Canourgue Exit n° 39

Leaving Millau to the North, the road crosses the Jurassic limestone plateau called Causse de Sauveterre. Near Séverac-le-Château, Toarcian black shales were mined for oil. The Jurassic sedimentary series observed along the road, is deformed by decameter to kilometer-scale wave-length upright folds and reverse faults. These structures are related to the Eocene compression due to the Pyrenean orogeny.

A. Geological setting

The Marvejols area (Fig. 22) is a famous place in the geology of the French Massif Central since it is one of the first places where Variscan syn-metamorphic nappe thrusting has been documented on the basis of geochronology, metamorphism and tectonics (Pin, 1979). The metamorphic inversion with HP rocks of the Upper Gneiss Unit upon the Lower Gneiss Unit was used as an argument for tectonic superposition (Fig. 23). The contact between the two units is a high temperature mylonitic zone (Faure et al., 1979). Moreover, radiometric dates document the tectonic

Figure 22 - D3 route map

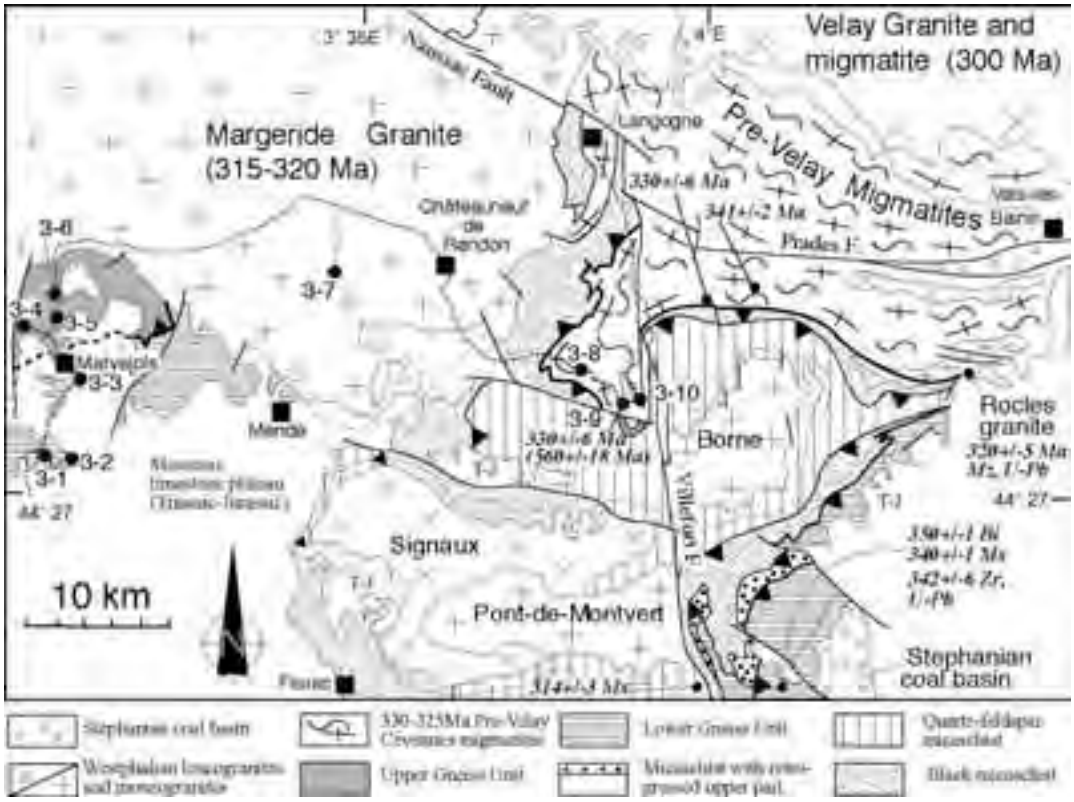

evolution of the area. The Lower Gneiss Unit, called locally the Lot Series, consists of a monotonous succession of metapelite and metagrauwacke intruded by various magmatic bodies:

1. Quartz-diorite orthogneiss is dated at 540 ± 12 Ma by U/Pb isotopic dilution method on zircon populations (Pin and Lancelot, 1978). This rock exhibits a well marked post-solidus planar and linear structure. 40Ar/39Ar dating on biotite gives 352 ± 1 Ma (Costa, 1989).
2. Pink K-feldspar orthogneiss of alkaline composition is not well dated due to inherited zircons. By comparison with the Mendic orthogneiss in the Montagne Noire northern side, an Early Cambrian age is generally accepted.
3. An acidic augen orthogneiss with mylonitic zones crops out immediately below the Upper Gneiss-Lower Gneiss Unit contact. An U/Pb age on zircon populations gives a lower intercept age of 346 ± 8 Ma (Pin, 1981). Due to its tectonic setting, and radiometric age this orthogneiss is interpreted as a synkinematic pluton coeval with the thrusting of the Upper Gneiss Unit. However, this conclusion does not comply with microstructural data and particularly with the NW-SE stretching lineation developed in the Lower Gneiss Unit (cf below). A preliminary chemical U/Th/Pb age of 370 ± 12 Ma is obtained on monazite (A. Joly unpublished data).
4. Other small gneiss masses are recognized in the Lower Gneiss Unit, some of them are considered as hypovolcanic granites or volcaniclastic metasediments (Pin, 1981).

As seen in the first stops of D3 day, the Lot Series of the Lower Gneiss Unit is characterized by a subhorizontal foliation and a conspicuous NW-SE trending mineral and stretching lineation. This ductile deformation is coeval with an intermediate temperature-intermediate pressure metamorphism. Biotite, garnet, staurolite, andalousite and muscovite are widespread in the metapelites. The Marvejols area is often taken as an example of the inverted metamorphism developed in the footwall of the Upper Gneiss Unit overthrust (Fig. 24). $^{40}Ar/^{39}Ar$ dates on biotite and muscovite from the Lot Series micaschist yields 351 ± 4 Ma and 342 ± 4 Ma respectively (Costa, 1989). The tectonic significance of the NW-SE trending stretching lineation which is widespread throughout the Massif

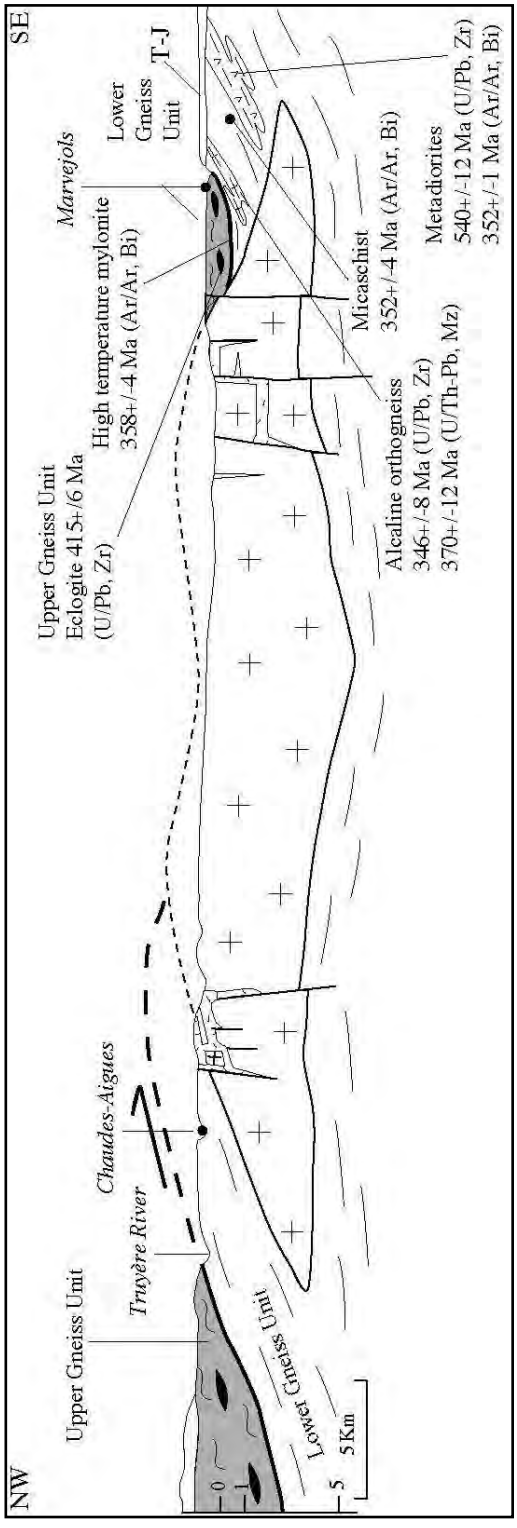

Figure 23 - General cross section from Marvejols to the Truyère area showing the tectonic superposition of the Upper Gneiss Unit upon the Lower Gneiss Unit and the shape of the Margeride pluton

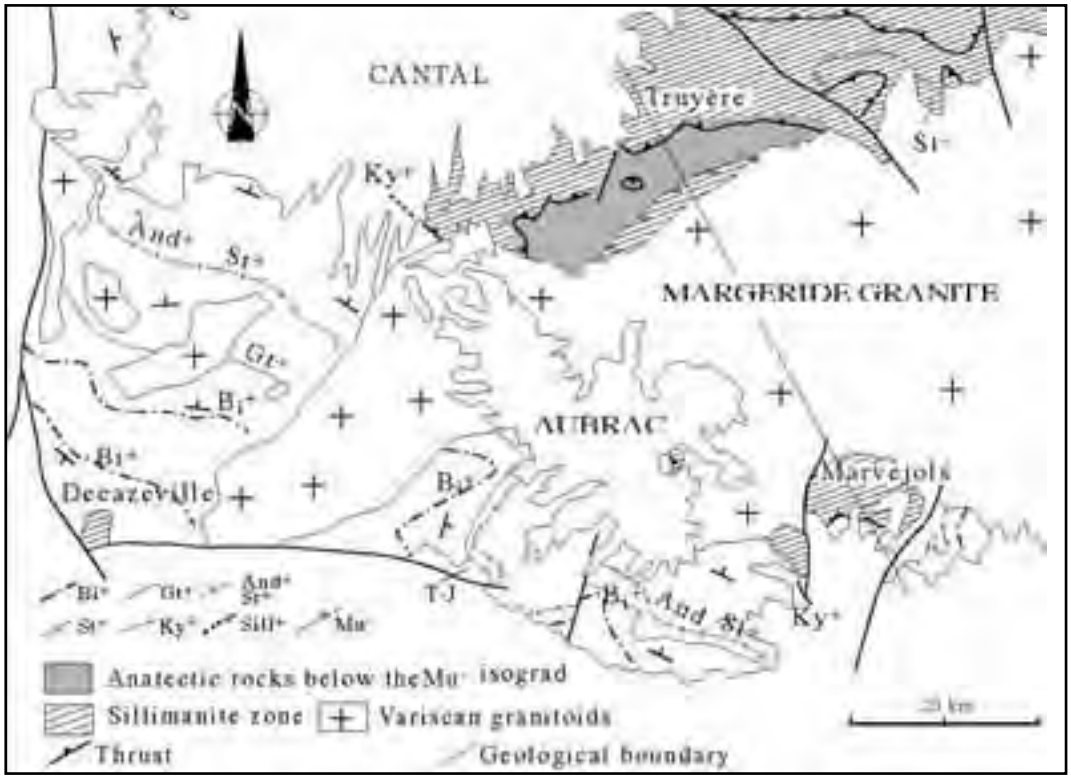

Figure 24 - Metamorphic map of the Lower Gneiss Unit around the west part of the Margeride pluton (Marvejols, Truyère, Châtaigneraie) showing the inverted metamorphism (adapted from Burg et al., 1984).

Central is not clearly settled yet.

The mylonitic zone at the base of the Upper Gneiss Unit is characterized by a N-S trending mineral and stretching lineation. In spite of intense recrystallization and post-kinematic annealing, top-to-the-south shearing can be observed. $^{40}Ar/^{39}Ar$ dating of synfolial biotite gives 358 ± 4 Ma interpreted as the age of thrusting. Moreover, a late muscovite developed upon the early foliation is dated at 340 ± 4 Ma (Costa, 1989).

In the Marvejols area, the Upper Gneiss Unit consists of a lower part called "leptynite-amphibolite" sequence and an upper part with migmatitic gneiss and micaschist. The leptynite-amphibolite sequence contains metamorphosed mafic rocks of magmatic or sedimentary origin such as metagabbro, metabasalt, amphibolite rare serpentinites and acidic rocks (i. e. leptynites) Meter to centimeter scale acidic-mafic alternations are probably of volcani-clastic origin. Several U/Pb ages on zircon populations are available (Pin and Lancelot, 1982). Namely, an amphibolite boudin is dated at 487 ± 6 Ma, and a coronitic metagabbro at 484 ± 7 Ma. An orthogneiss intrusive in the paragneiss gives 478 ± 6 Ma. These dates are interpreted as the evidence for an Ordovician magmatism related to the rifting of Armorica from Gondwana. Moreover, the 415 ± 6 Ma age of zircon populations from a high-pressure trondhjemite is considered as the age of melting coeval with eclogite facies metamorphism. Pressure and temperature constraints on this rock are 16 ± 4 kb and 800 ± 50°C respectively.

Upper and Lower Gneiss Units stacking was followed by huge crustal melting produced under distinct P-T conditions (Fig. 25). The second part of the D3 and the whole D4 days are devoted to the observation of some manifestations of the Middle to Late Carboniferous crustal melting. From older to younger, three stages are distinguished.

1. Pre-Velay Cévennes migmatites, dated between 333 to 324 Ma by chemical U/Th/Pb method on monazite (Be Mezème, 2002).
2. Namurian-Westphalian plutonism dated around

Volume n° 2 - from B16 to B33

320-315 Ma. This magmatism is characterized by porphyritic monzogranite (Margeride or Pont-de-Montvert-Borne plutons) and also by leucogranite (Signaux and Rocles plutons). Although distinct massifs derived from different magmas, field relationships show that these two magmatic types are coeval.

3. Velay migmatites and cordierite granite dated around 300Ma. This large massif will be examined during D4.

B. Stop description

Stop D3.1:

Cambrian quartz-diorite. N88, East of Pont des Ajustons, S. of Marvejols.

A fine-grained biotite-hornblende quartzdiorite originally intrudes micaschists (stop D3-2) belonging to the Lower Gneiss Unit. U/Pb dating on zircon populations gives a 540 ± 12 Ma age (Pin and Lancelot, 1978) for the emplacement of this pluton. $^{40}Ar/^{39}Ar$ dates on biotite provide a 352 ± 1 Ma age corresponding to the tectonic event (Costa, 1989). This well foliated and lineated rock experienced a NW-SE deformation.

Stop D3.2:

Lower Gneiss Unit of the Lot series.

The Lot series are composed of biotite-garnet ± staurolite micaschists originally intruded by porphyric granite and metadiorite. The flat lying foliation bears a conspicuous NW-SE mineral and stretching lineation, indicating a top to NW sense of shear (Color Plate 1, E). Biotite and muscovite $^{40}Ar/^{39}Ar$ ages are respectively 351 and 342 ± 4 Ma (Costa, 1989). In the background, Early Jurassic limestones unconformably overly the metamorphic rocks.

Stop D3.3:

Augen orthogneiss within the Lot series. Pont de Pessil.

The Lower Gneiss Unit includes augen orthogneiss with mylonitic fabric. In sections perpendicular to the foliation and parallel to the NW-SE lineation, asymmetric K-feldspar augen indicate a top-to-the-SE sense of shear. U/Pb date on zircon populations gives a lower intercept age of 346 ± 8 Ma (Pin, 1981). An U/Th/Pb chemical age on monazite gives 370 ± 12 Ma (Joly, unpublished data).

Stop D3.4:

Coronitic metagabbro belonging to the Upper Gneiss Unit. Le Croisier.

The Upper Gneiss Unit outcrops North of

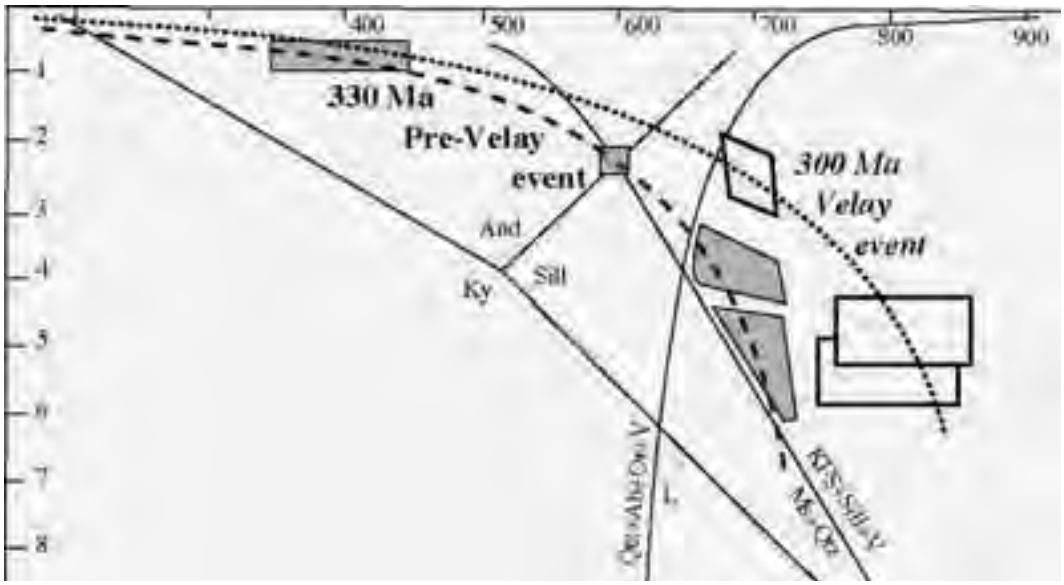

Figure 25 - P-T paths of pre-Velay and Velay events constructed from metamorphic rocks sampled in the south part of the Velay area (simplified from Montel et al., 1992).

Marvejols city. Metabasites, locally with mylonitic fabric, underwent the Eovariscan high-pressure metamorphism (Color Plate 1, F). However, due to the heterogeneity of deformation, magmatic textures are still preserved. This rock is dated by U/Pb method on zircon populations (upper intercept) at 484 ± 7 Ma (Pin and Lancelot, 1982).

Stop D3.5:

Leptynite-amphibolite complex
(Upper Gneiss Unit). Along the main road (N9).

This outcrop exposes a typical section of the "leptynite-amphibolite complex" made of alternations of mafic and acidic rocks considered as a volcaniclastic formation. The foliation exhibits meter to decameter-size amphibolite boudins (Color Plate 2, A). Zircon populations from an amphibolite give a U/Pb age of 487 ± 6 Ma age (upper intercept) interpreted as the rock formation age (Pin and Lancelot, 1982). The lower intercept at 340 ± 4 Ma is close to the thermal event (ca. 345-330 Ma) that overprints the tangential tectonics.

Stop D3.6:

Early Variscan migmatisation.
Gorges du Val d'Enfer.

The road runs from South to North in the leptynite-amphibolite complex which becomes migmatized northward. The migmatite is not dated here. By comparison with other places in the Massif Central, a ca 380 Ma age can be inferred.

Stop D3.7:

Middle Carboniferous Margeride pluton.
Truc de Fortunio.

Drive to St-Amans → Estables

The Margeride massif is one of the largest granitic plutons in the French Massif Central (3200 km^2). It consists mainly of a porphyritic monzogranite with large (up to 10cm) K-feldspar megacrysts. On the basis of biotite content, three facies, namely dark, intermediate and light facies, are distinguished

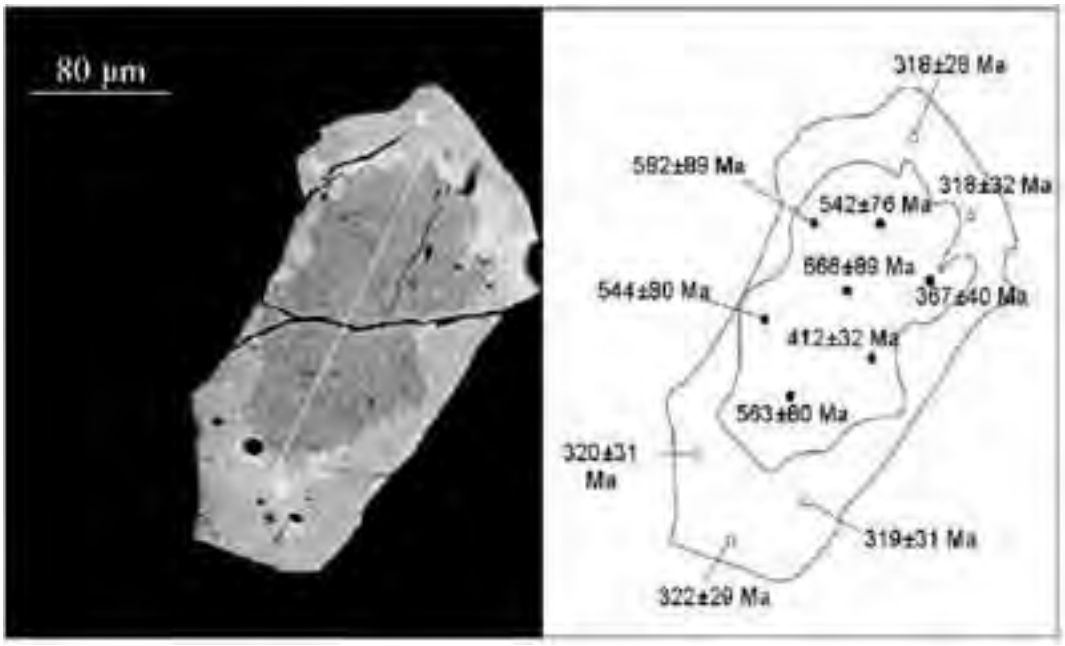

Figure 26 - Example of ponctual dating on monazite single grain by U/Th/Pb chemical method (Be Mezème et al., 2003).

(Couturier, 1977). Nevertheless, more than 80% of the massif is made of the intermediate facies. Moreover, muscovite-K-feldspar leucogranite intrude the monzogranite. Most of the leucogranites are meter-scale dykes, but east of the massif the Grandrieu leucogranite represents a kilometer-sized pluton. The monzogranite yields a Rb-Sr whole rock age of 323 ± 12 Ma (Couturier, 1977) and an isotopic

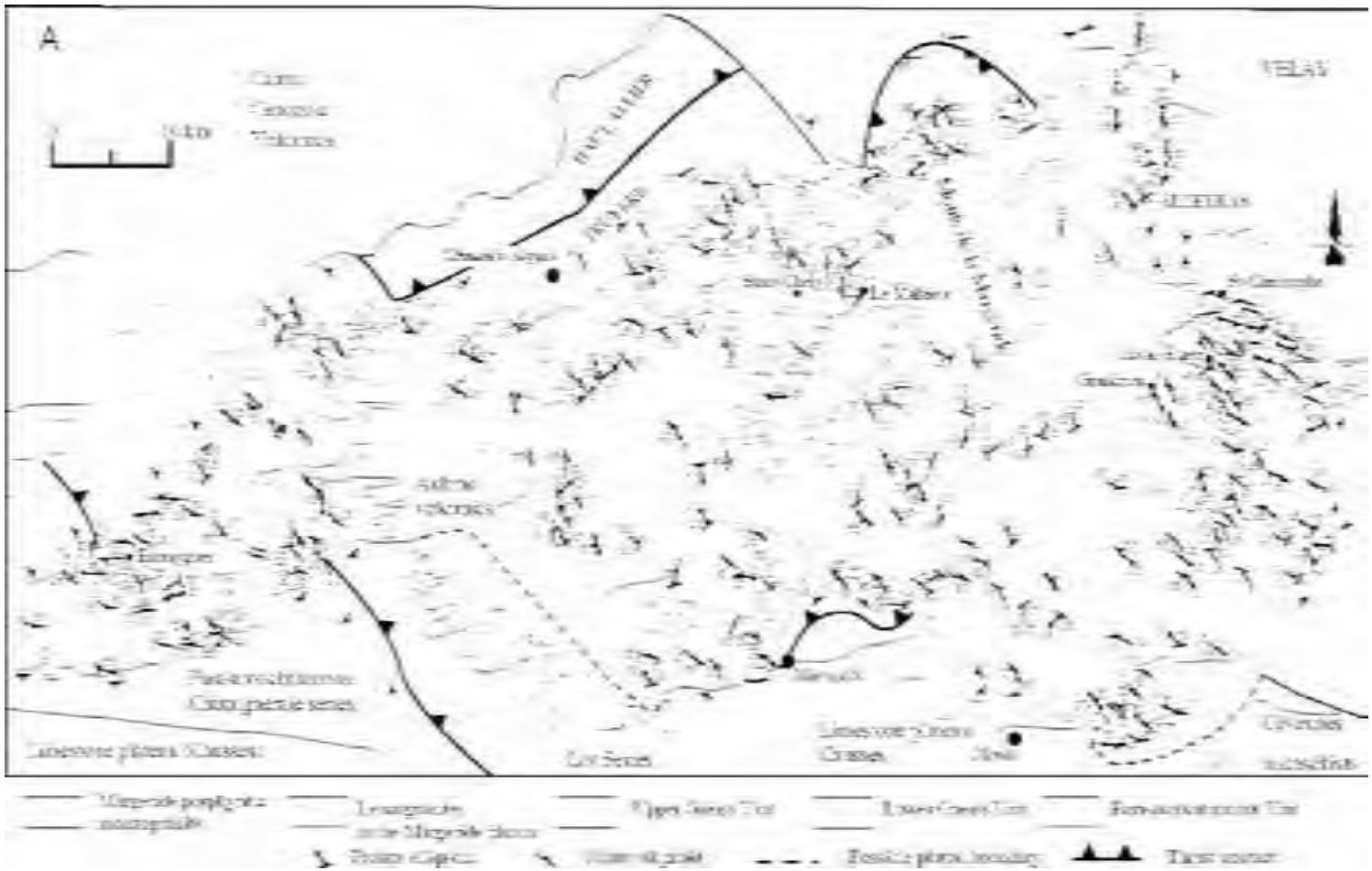

Figure 27 - A: Map of the planar and linear structures in the Margeride pluton inferred from AMS study (from J-Y. Talbot, unpublished).
B: Stereograms represent the magnetic lineation (K1) and the pole of foliation (K3).

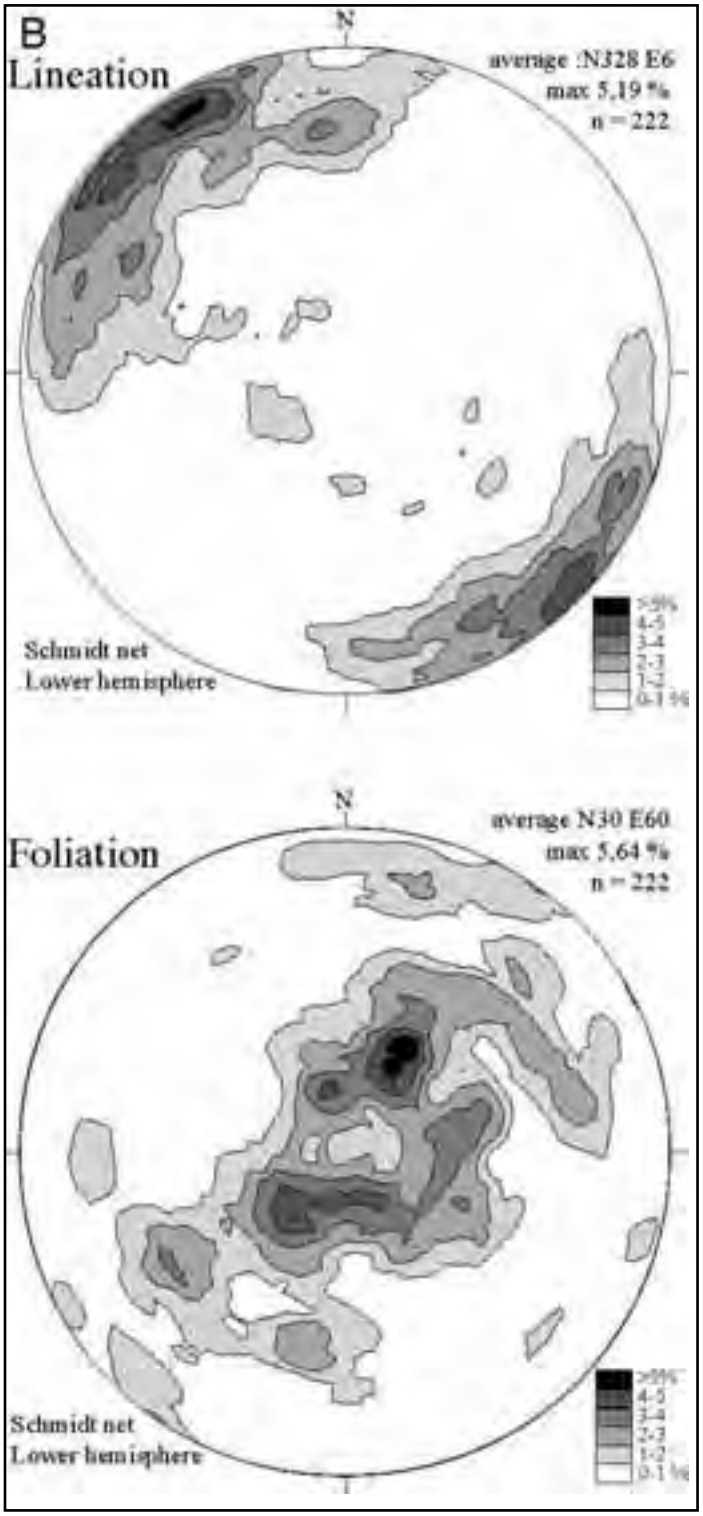

dilution U/Pb monazite age of 314 ± 3Ma (Pin, 1979); the Grandrieu leucrogranite is dated at 305 ± 4 Ma (U/Pb method, Lafont and Respaut, 1988). The Margeride pluton is a subhorizontal of 4 to 8 km thick (Fig. 23). Petrostructural and AMS studies (J-Y. Talbot, work in progress, Fig. 27) show a complex pattern of the foliation trajectories. Although the foliation trajectories do not show a consistent shape, at the scale of the whole pluton, the foliation presents a flat lying attitude. The lineation pattern exhibits a well-defined NW-SE trend. It is worth noting that such a trend is widespread throughout the whole Massif Central and corresponds to the maximum stretching direction of the Namurian-Westphalian syn-orogenic extension (Faure, 1985).

Stop D3.8:

Augen orthogneiss below the Para-autochthonous Unit.

Drive to Châteauneuf-de-Randon → Montbel → NE of Belvezet

SE of the Margeride pluton, the Cévennes area exposes the para-autochthonous Unit of the Massif Central. Below the unconformity of the Mesozoic sedimentary rocks, an augen orthogneiss and its host rocks crop out in a tectonic window below the Para-autochthonous Unit (Cévennes micaschists). The augen orthogneiss exhibits a subhorizontal foliation and NE-SW trending stretching lineation. The age of the granitic magmatism is not determined here but assumed to be Early Cambrian (ca 550 Ma) by comparison with other orthogneiss in the Massif Central. The chemical U/Th/Pb age of 560 ± 18 Ma in the core of monazites grains from migmatitic orthogneiss supports this interpretation (cf. Stop D3-9)

Stop D3.9:

A few kilometers eastward, biotite, garnet (± cordierite) paragneiss and quartz-micaschist correspond to the orthogneiss host rock.

Stop D3.10:

Migmatitic orthogneiss. Barrage de Puylaurent.

To the east, the orthogneiss experiences a partial melting giving rise to diatexites. Locally the orthogneiss fabric remains well preserved. A chemical U/Th/Pb dates on monazite give 560 ± 18 Ma and 324 ± 6 Ma for the grains core and rim respectively (Be Mezème, 2002, Cocherie et al., in press). The latter is interpreted as the age of migmatization.

Boudinaged dykes of leucogranites.

Pink granite dykes and leucogranite dykes intrude the metamorphic rocks. Muscovite dyke is dated by chemical U/Th/Pb method on monazite at 316 ± 5 Ma (Be Mezème et al., 2003; fig. 26).

In Prévenchères, turn to the north (left) to Langogne. The road follows the brittle left-lateral Villefort fault of Permian age. South of La Bastide-Puylaurent, the road is located in the Para-autochthonous Unit (Schistes des Cévennes). From La Bastide Puylaurent, to Langogne, the migmatitic orthogneiss crops out again along the Allier river.

End of the 3rd day. Overnight in Langogne

DAY 4

The Velay dome (French Massif Central): melt generation and granite emplacement during orogenic evolution

The generation of large granite-migmatite complexes by crustal melting during orogeny is a process still discussed in particular because of the deep, inaccessible location of their production sites (Clemens, 1990; Brown, 1994). Moreover, the development of a partially molten middle crust during collision tectonics implies a major change in the rheology of the thickened crust and largely control its behaviour during orogenic collapse (Vanderhaeghe and Teyssier, 2001). Thus, the Variscan belt which exposes numerous granitic intrusions and large migmatitic complexes is of great interest to study the role of partial melting during orogenic evolution (Brown and Dallmeyer, 1996; Gardien et al., 1997; Vanderhaeghe et al., 1999). The Velay migmatite-granite dome located in the SE Massif Central (Fig. 28, 29, 30) offers a unique opportunity to examine the thermal conditions required for widespread crustal anatexis and the consequences of the presence of the generation of a large volume of partially molten rocks on the evolution of the Variscan orogenic crust.

The aim of the fourth day is to illustrate the melt generation and granite emplacement of the Velay dome in connection with the tectonic evolution of the Variscan belt, by showing:

- incipient stages of melting in the Late Neoproterozoic pre-tectonic granite and metasediments on the southern margin;
- the cordierite-bearing granites and migmatites;
- the relation between granite emplacement, extensional tectonics and formation of the St Etienne Stephanian basin on the northern flank of the Velay dome.

A. Geological setting

The Velay dome (Fig. 28,29), about 100 km in diameter, is composed of peraluminous granites (about 70%) characterized by abundance of nodular and prismatic cordierite and by enclaves of gneisses (25%) and granites (5%) of various nature and size (Didier, 1973; Dupraz and Didier, 1988). Previous work in this area provided the following results and models

- Montel et al. (1992) describe two successive stages of anatexis, first under water-saturated conditions with biotite stable followed by melting under biotite dehydration conditions.
- Burg and Vanderhaeghe (1993) proposed that the amplification of the Velay dome cored by migmatites and granites reflects gravitational instabilities within a partially molten middle crust during late-orogenic extension.
- Lagarde et al. (1994) suggested that the deformation pattern of the Velay dome records southward lateral expansion of the granites below the detachment zone of the Pilat, one of the major normal faults developed during the collapse of the Variscan belt (Malavielle et al., 1990)
- Geochemical and petrological data published by Williamson et al. (1992), Montel et al. (1992) and Barbey et al. (1999), indicate that the Velay dome has followed a clockwise P-T-time evolution overprinted by a thermal peak due to the underplating of mafic magmas (Fig. 31).

Figure 28 - Simplified geologic map of the eastern margin of the Massif Central, Day 4 and Day 5 localities

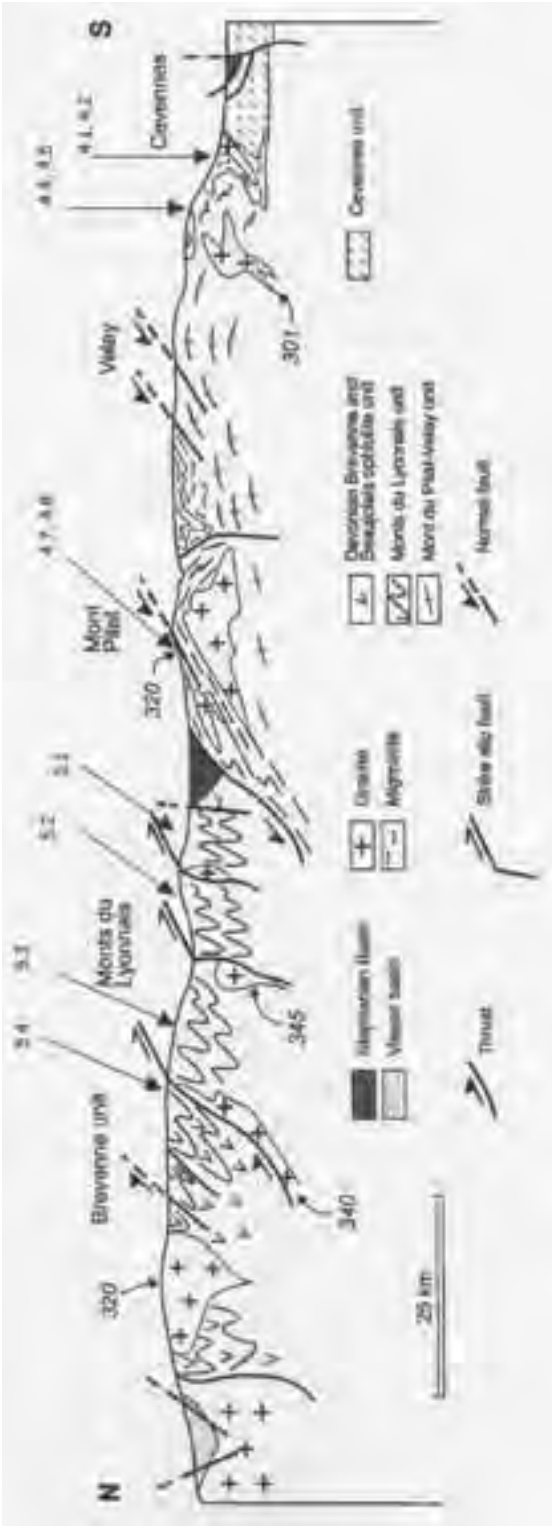

Figure 29 - Simplified cross section through the eastern margin of the Massif Central showing the main tectonic units and their structural relationships, Day 4 and Day 5 localities. Ages of some granites are indicated as specific geochronological markers.

According to Ledru et al., 2001, structural, petrologic and geochronological data indicate that the formation of the Velay migmatite-granite dome results from the conjunction of several phenomena.

- Partial melting of the thickened crust started at about 340 Ma, while thrusting in the hinterland of the Variscan belt was still active, and ended during collapse of the orogenic crust at ~300 Ma. Crustal anatexis responsible for the generation of the rocks forming the Velay dome hence lasted about 40 My.
- Partial melting took place within a dominantly metasedimentary crustal layer dominated by fertile pelitic compositions. Melting reactions evolved from the water-saturated granitic solidus to destabilization of hydrous minerals and indicate that melting started at the end of the prograde metamorphic path and ended during decompression associated with exhumation of the migmatite-granite dome.
- Thermal relaxation and increased radioactive heat production following crustal thickening likely caused a rise in temperature during the evolution of the Variscan orogenic crust. However, it is proposed that heat advection from mantle-derived magmas and also asthenospheric upwelling coeval with orogenic collapse have provided the extra heat source required to melt a large volume of the thickened crust and generate the migmatites and granites of the Velay dome.

The formation of the Velay dome, coeval with the activation of crustal-scale detachements, potentially corresponds to flow of a partially molten crustal layer in response to gravitational collapse.

Four main structural zones, that will be partially illustrated during this fourth day, are defined (Fig. 28, 30):

1. The host rocks. The Velay granite-migmatite dome is hosted by gneissic units stacked during the collision history of the Variscan belt (Ledru et al., 1994a, b):

- the Upper Gneiss Unit, that contains remnants of Early Paleozoic oceanic or marginal basins is presently in an upper geometric position, this unit

Figure 30 - Extension of Meso and Neovariscan metamorphism and foliation trends within the host rocks of the Velay migmatite-granite dome

Volume n° 2 - from B16 to B33

contains dismembered basic-ultrabasic complexes at its base overlain by gneisses derived from granites, microgranites, acid and basic volcanics, tuffs and grauwackes. Numerous eclogitic relics are preserved within basic layers marking an Eovariscan stage of lithospheric subduction (450-400 Ma). Structural and radiometric data show these rocks were exhumed from 90 km at 420-400 Ma to less than 30 km at 360-380 Ma while subduction was still active (Lardeaux et al., 2001).

- The north Gondwana continental margin is represented by (a) a Lower Gneiss Unit composed of metasediments derived from pelites and argilites, and augen orthogneiss (the "Arc de Fix") originating from peraluminous porphyric granite dated at 528 ± 9 Ma (Rb-Sr whole rock, R'Kha Chaham et al., 1990), and (b) a mainly sedimentary parautochthonous sequence. This margin underwent a general medium-pressure metamorphism attributed to the thrusting of the Upper Gneiss Unit which occurred during Devonian, prior to 350 Ma in the internal zone (Mesovariscan period). The Lower Gneiss Unit is intruded by syn tectonic granites precursor of the Velay dome emplaced between 335 - 315 Ma, including magnesio-potassic plutons, the so-called "vaugnerite". In the south (Fig. 2), the Cévennes micaschists are interpreted as the parautochthonous domain. Maximum P-T conditions during the metamorphic evolution are there estimated at 500 °C, 5 kbar, with the muscovite-chlorite-garnet parageneses being synchronous with southward thrusting and a thickening estimated at about 15 km (Arnaud and Burg, 1993; Arnaud, 1997). The closure of micas to Ar diffusion has been dated at 335-340 Ma ($^{40}Ar/^{39}Ar$, Caron et al., 1991).

2. The gneiss-migmatite zone, at the periphery and at the roof of the Velay dome. In the migmatites and in the gneissic hosts, the following melting reactions are identified (Fig. 31):

- The first melting stage developed under P-T conditions exceeding those for water-saturated quartz-feldspathic rocks, with biotite remaining stable: around 700 °C, 4 kbar within the metamorphic envelope, 5 kbar in the granitic core (M3 stage of Montel et al., 1992). The presence of corundum paragneiss enclaves confirms the initial presence of muscovite and the prograde character of this melting event (Aït Malek et al., 1995). A U-Pb monazite date indicates a minimum age of 314 ± 5 Ma (Mougeot et al., 1997). High-K magnesian monzodiorite, with mantellic affinity are also dated at 313 ± 3 and 314± 3 Ma (207Pb-206Pb and U-Pb respectively on zircon, Aït Malek, 1997). They contain peraluminous

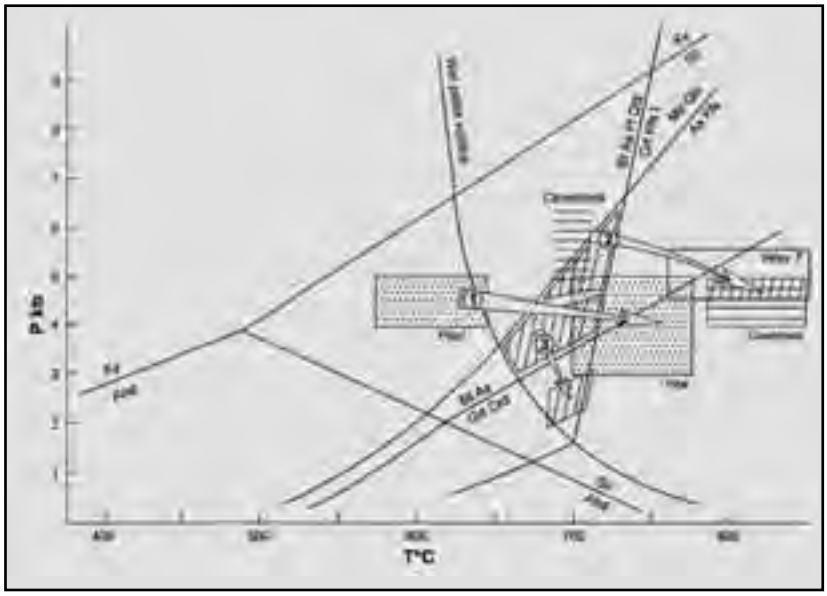

Figure 31 - Pressure-temperature evolution from the gneisses to the Velay granite
Mineral abbreviations: Ky = kyanite; Sil = sillimanite; And = andalusite; Cd = cordierite; Grt = garnet; Ms = muscovite; Qtz = quartz; Kfs = potassium feldspar; Pl = plagioclase; Bt = biotite; As = aluminium silicate; L = liquid. The transition from the M3 to the M4 metamorphic stage is indicated by arrows (1) in the Pilat micaschist (after Gardien et al., 1990), (2) in the migmatitic orthogneiss and granite in the southern part of the dome (oblique- and horizontal-ruled boxes, after Gardien et al., 1997, and Montel et al., 1992), (3) in the migmatitic part of the southern host rocks of the Velay granite (oblique-ruled boxes, after Montel et al., 1992)

xenoliths that record a first stage of isothermal decompression at 700-800 °C, 8-10 kb, consistent with a source located more than 30 km deep, followed by a stage at 5-6 kb (Montel, 1985). In view of the water-saturated conditions, it is unlikely that large quantities of granite (i.e. < 10-20%) were produced and extracted at this stage (Patiño Douce and Johnston, 1990).

- The second stage of melting is characterized by high-temperature metamorphism in the cordierite stability field, with biotite destabilized: 760-850 °C, 4.4-6.0 kbar (stage M4 of Montel et al., 1992). Leucosomes were dated at 298 ± 8 Ma based on Rb-Sr whole rock isochron (Caen-Vachette et al., 1982), and Rb-Sr whole rock-biotite isochrons yield ages between 305 and 276 Ma (Williamson et al., 1992). An age of 301 ± 5 Ma was obtained for the homogeneous parts of the granite using the U-Pb monazite method (Mougeot et al., 1997). Therefore, this second melting stage is considered to be generally synchronous with emplacement of the main cordierite-bearing granites. The volume of cordierite-bearing granites generated makes a case for massive partial melting at this stage, associated to destabilization of hydrous minerals.

3. The migmatite-granite domain. The various granites that appear in the Velay dome define a suite, with 3 main granite types distinguished according to age, structure, homogeneity, mineralogy and geochemistry:

- A heterogeneous banded biotite granite, found mainly on the western margin of the dome and locally on the southern and eastern margin. It corresponds to the first generated granite of the Velay suite. Foliation trajectories are in continuity with porphyric granites in the external rim of the dome suggesting continuity between these precursor granites and the development of the heterogeneous banded biotite granite.
- A main biotite-cordierite granite, in which several sub-types may be distinguished, in particular according to the cordierite habitus (Barbey et al., 1999).
  - a heterogeneous banded granite with abundant enclaves. Most of these enclaves represent incorporated and partly assimilated pieces of the Lower Gneiss unit and precursor plutons originating from the host rocks, although some enclaves with refractory composition or granulite facies metamorphism have a lower crustal origin (Vitel, 1985). Cordierite may be prismatic, cockade-type or mimetic overprinting previous biotite - sillimanite assemblages. Most of the heterogeneous granites indicate mixing between melts of lower-crustal origin and melts from the para- and ortho-derived host rock (Williamson et al., 1992).
  - a homogeneous leucocratic biotite-cordierite granite with mainly cockade-type cordierite. Its emplacement has been dated at 301 ± 5 Ma using the U-Pb method on monazite (Mougeot et al., 1997).
  - a homogeneous granite with biotite and prismatic cordierite as a primary ferromagnesian phase, with few enclaves. The heterogeneous and homogeneous granites with prismatic cordierite, with a high Sr content, have a mixed isotopic signature between the host rocks and a lower-crustal origin. The deep source is considered to be the melting of the lower mafic/felsic plutonic crust (Williamson et al., 1992).
  - a leucocratic granite with cockade-type cordierite, without enclaves. The cordierite-quartz aggregates posdate primary biotite bearing assemblages and probably prismatic cordierite.
- The late magmatic activity that includes:
  - homogeneous granite with K-feldspar porphyrocrysts and common prismatic cordierite, basic and micaceous inclusions (the Quatre Vios massif) (Fig. 10d). These granites are defined as late-migmatitic and are considered to originate from the melting of aluminous sediments at 4.5-5.5 kbar and 750-850 C, under water-undersaturated conditions and have a significant mafic component (Montel et al., 1986; Montel and Abdelghaffar, 1993). Ages at 274 ± 7 Ma (Rb/Sr whole rock, Caen Vachette et al., 1984) are considered to be partially reset during Permian or Mesozoic hydrothermal event.
  - Stephanian leucogranites, microgranite and aplite-pegmatite dykes, Permian rhyolites. Microgranite dykes have been dated at 306 ± 12 and 291 ± 9 Ma and a Permian hydrothermal event at 252 ± 11 and 257 ± 8 Ma (microprobe dating of monazite, Montel et al., 2002).

4. The Stephanian intracontinental basin of St-Etienne. This basin is formed along the hanging wall of the Mont Pilat extensional shear zone (Malavieille et al, 1990). The Mont Pilat unit, attributed to the lower gneissic unit at the scale of the French Massif Central

consists of aluminous micaschists, metapelites, orthogneisses and amphibolites. This unit has a gently north-dipping foliation plane bearing a north-south stretching lineation. Numerous leucogranitic pods outcrop more or less parallel to this main foliation plane and have been dated at 322 ± 9 Ma (Rb/Sr whole rock, Caen-Vachette et al., 1984). Shear criteria, observed at different scales, are compatible with a top-north extension dated between 322 and 290 Ma (39Ar/40Ar, Malavieille et al., 1990). This event was coeval with the progressive development of low pressure - high temperature metamorphic conditions (3- 5 Kbar and 700 - 780 °C, Gardien et al., 1997).

B. Stop description (Fig. 28, 29)

Stop D4.1:

Meyras, Road from Le Puy-en-Velay to Aubenas, N102, Road cut.

Stop D4.1 shows the incipient stage of melting within the orthogneiss of the Lower Gneissic Unit. An augen orthogneiss (the "Arc de Fix"), originating from peraluminous porphyric granite dated at 528 ± 9 Ma (Rb-Sr whole rock, R'Kha Chaham et al., 1990), constitutes an almost continuous rim around the Velay granite-migmatite dome. The melting is marked by the segregation of cordierite-free melts along the main inherited foliation and locally discordant cordierite-bearing granitic patches (Color Plate 2, B). Large phenocrists of K-feldspar attest of the porphyric type of the granite protolith while the foliation is marked by the elongation and crystallization of the quartzofeldspathic aggregates and biotite-rich melanosome. Magnesio-potassic dykes (the so-called "vaugnerite") are intrusive and boudinated within the orthogneiss.

The progressive development of the anatexis and textural evolution in the transition from subsolidus annealing to melting process has been studied in detail in this zone by Dallain et al. (1999). Anatexis first develops with the resorption of quartz along the existing foliation. The breakdown of muscovite is then accompanied by the growth of sillimanite. Quartz-plagioclase aggregates are replaced by assemblages that are in equilibrium with the granite eutectic point, although K-feldspar aggregates are preserved. The breakdown of biotite is responsible for the production of melt beyond 30-50 %, the value of the Rheological Critical Melt Percentage (Arzi, 1978). Leucosomes with cockade-type cordierite produced during this second melting stage tend to be discordant with the inherited structure. Structural orientations then become more varied as the leucosome proportion increases, with folds becoming abundant and randomly oriented.

Stop D4.2:

Pont de Bayzan, Road from Le Puy-en-Velay to Aubenas, N102, River banks of the Ardèche river.

Stop D4.1 shows the incipient stage of melting within paragneiss of the Lower Gneissic Unit. The metagranite observed at the stop 4.1. is originally intrusive in sediments (pelites and argillites, including refractory quatz-rich and calcic layers) The location of early melting is controlled by foliation anisotropy (Macaudière et al., 1992) and folding (Barraud et al., 2003).

Numerous resisters from refractory layers preserve microstructure developed during the pre-migmatitic tectonic evolution that resulted in a composite foliation (named regionally S2) and polyphased folding (Color Plate 2, C). The outcrop is characterized by open folds that play an active role in the segregation of anatectic melts: cordierite-free leucosomes accumulate in saddle reef and axial planes of the folding that is attributed to S3 (Barraud et al., 2003).

Stop D4.3:

Ucel, Road from Aubenas to Mezilhac, Road-cut.

Stop D4.3 shows the unconformity of the Mesozoic sandstone over altered granite and biotite-sillimanite migmatitic paragneiss. The exhumation of the Velay granite-migmatite dome occurred during the Stephanian as boulders of granites and gneisses are found in the conglomerates of the Stephanian basin in the North and Prades basin in the South. Apatites in granite and migmatites yield a U-Pb age at 289 ± 5 Ma that is interpreted as a cooling age during the uplift of the Vealy region (Mougeot et al., 1997). Finally, a regional unconformity is characterized at the base of the Trias sandstone and conglomerate. A recent and fresh road cut provides a spectacular illustration of this unconformity.

Stop D4.4:

Volane river, Road from Aubenas to Mezilhac, D578, Road-cut.

Stop D4.4 shows an hololeucocratic granite, with cockade-type cordierite, that represents one of the petrographic type of the Velay migmatite-granite dome (Color Plate 2, D). Detailed observation indicates that cordierite is formed at the expense of biotite, in the presence of a melt phase. Cordierite is formed from the early phase of melting to the end of the magmatic

evolution of the Velay granite. However some garnets are present in cordierite nodules, indicating that, in that area, melting started in the garnet stability field.

Stop D4.5:

Volane river, Road from Aubenas to Mezilhac, D578, Road-cut.

Stop D4.5 shows a late-migmatitic homogeneous granite and relations with migmatitic gneisses and heterogeneous cordierite-bearing granite. In the upper part of the outcrop, a late-migmatitic granite, the Quatre-Vios granite, is intruding the heterogeneous banded granite: it is a coarse grained peraluminous granite with prismatic cordierite and frequently oriented feldspar phenocrysts. It contains abundant mafic microgranular enclaves and surmicaceous enclaves including biotite, garnet, cordierite, sillimanite, hercynite, ilmenite and rare plagioclase. This unusual mineralogy (absence of quartz and potash feldspar) and the corresponding chemical composition indicate that these enclaves are restites. P-T conditions calculated from this mineralogy yielded water-undersaturated conditions estimated at 4.5-5.5 kbar and 750-850 C. The mafic microgranular (biotite+plagioclase) enclaves correspond to frozen blobs of mafic magma. Locally, another type of late-migmatitic fine-grained granite, with typical acicular biotite and devoid of enclaves, crosscuts the Quatre-Vios granite.

In the lower part of the outcrop, another dyke of late-migmatitic granite is intrusive within migmatitic orthogneiss in which the second stage of melting is well marked by the biotite breakdown that produces Fe-rich garnet and cordierite. This zone is itself enclosed within the heterogeneous banded granite that contains a lot of enclaves of migmatitic paragneiss.

Stop D4.6:

Mont Gerbier-de-Jonc, Road from Mezilhac to Le Puy-en-Velay, D378, Sight as seen from the road.

The Velay volcanism is made up of an eastern chain of Mio-Pliocene basaltic to phonolitic volcanoes and a western Plio-Quaternary basaltic plateau (Mergoil et al., 1993). The road to Le Puy-en-Velay shows nice sightseeing of this phonolitic chain that extends over more than 55 km with more than 180 points of extrusion, emplaced between 14 and 6 Ma.

The Mont Gerbier-de-Jonc is known as the spring of the Loire river. It is a phonolitic protrusion that displays a rough prismatic jointing.

Stop D4.7:

Moulin de Sezigneux, Road from St Chamond to Le Bessat, D2, Road cut.

The cordierite-andalusite-bearing micaschist of the Pilat Unit, seen at stop D4.7, displays extensional tectonics and HT-LP metamorphism within the Pilat series (Lower Gneissic Unit). This outcrop offers a good example of a low-pressure metamorphic unit, with micaschists and paragneisses intruded by syn-tectonic pegmatite dykes and pods. The main foliation plane is gently dipping to the North and shear criteria are well marked mainly around the pegmatitic pods indicating top to the North extensional tectonics. In the metamorphic rocks, the common mineralogy is: quartz + feldspars + biotite + andalusite and /or cordierite ± muscovite.

D4.8: Moulin de Sezigneux, Road from St Chamond to Le Bessat, D2, River banks.

Structure and metamorphism of the orthogneiss of the Lower Gneissic Unit are illustrated at stop D4.8. Ultramylonite and pseudotachylite textures are developed within the orthogneiss and S-C-C' structures indicate top to the North shear criteria compatible with extensional tectonics. Shear bands are underlined by syntectonic recrystallized biotites dated around 320-300 Ma ($^{40}Ar/^{39}Ar$). In the highly sheared parts of the outcrop ultramylonite bands and pseudotachylites are observable. The main foliation plane bears a north-south oriented stretching lineation. The metamorphic mineralogy is characterized by the association of quartz + feldspars + biotite + muscovite. Rare small-sized cordierites can also be observed.

End of the 4th day. Overnight stay in St Etienne

DAY 5

High to ultra-high pressure metamorphism and arc magmatism: records of subduction processes in the French Massif Central

The main goal of Day 5 is to present the geological and petrological records of subduction processes in the eastern Massif Central that preceeded the development of the Velay migmatite-granite dome illustrated during Day 4. These records are: remnants of high to ultra-high pressure metamorphism in both crustal and mantle-derived lithologies in the Mont du Lyonnais unit, a partially preserved back-arc derived ophiolitic sequence, the Brévenne unit.

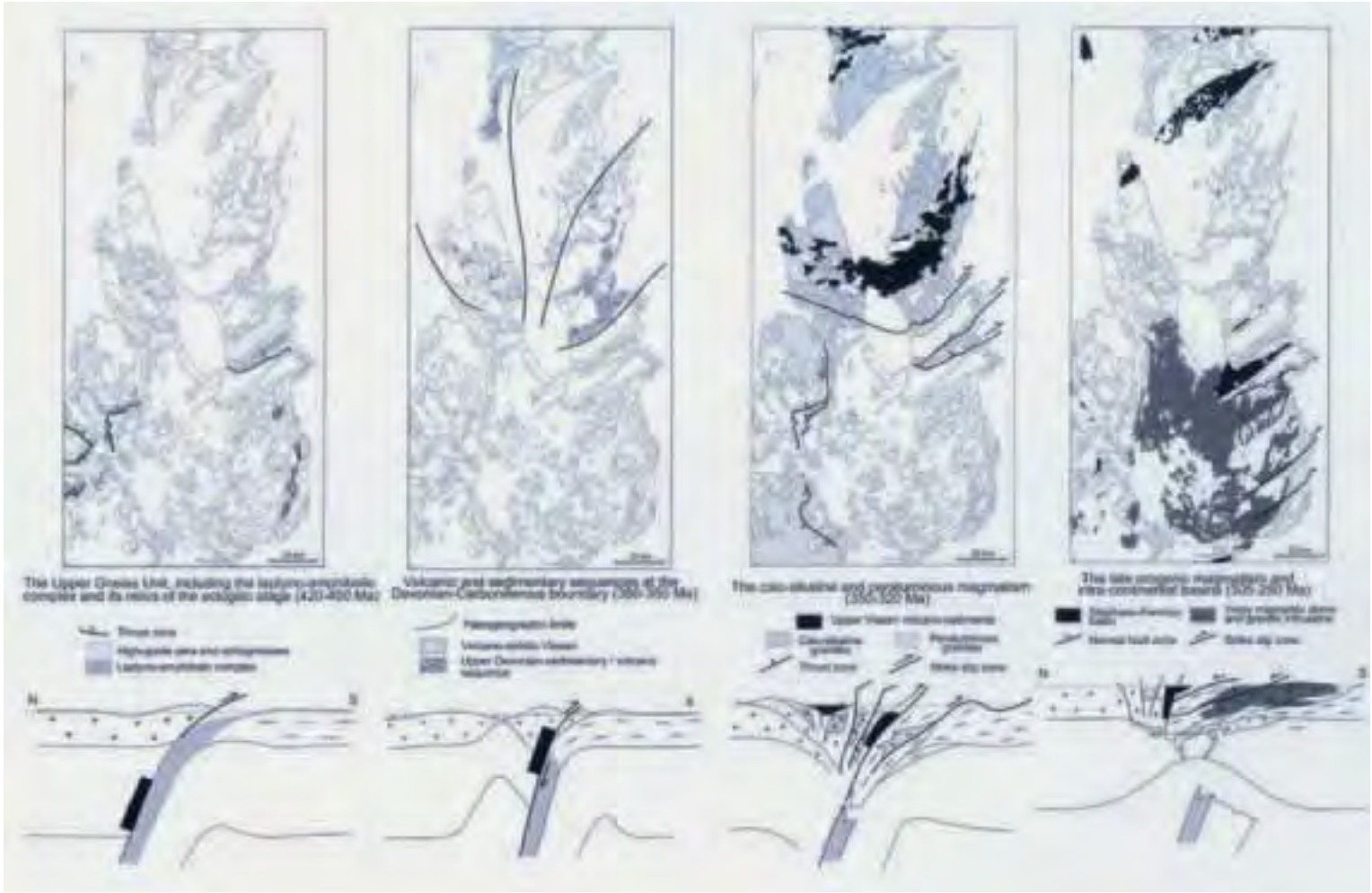

Figure 32 - Geological maps of the eastern margin of the Massif Central through time showing the progressive edification of the belt. The geodynamic cartoons show the possible position of the Monts du Lyonnais eclogites during the four critical periods illustrated (a to d).

A. Geological setting

1. Eclogites and garnet peridotite from The Monts du Lyonnais unit (Fig. 32a)

The Monts du Lyonnais unit belongs to the upper gneissic unit (Lardeaux, 1989; Ledru et al., 1994a). It comprises metasediments, orthogneisses (with protoliths of Ordovician age), leptynites (i.e. meta rhyolites), amphibolites and minor marbles. This unit also contains lenticular relics of either crustal (mafic and acid granulites, eclogites, Lasnier, 1968; Coffrant and Piboule,1971; Dufour,1985; Dufour et al.,1985; Lardeaux et al.,1989) or mantle origin (garnet and / or spinel bearing peridotites, Gardien et al., 1988, 1990). Eclogites outcrop, in close association with garnet-bearing peridotites, in the southernmost part of the Monts du Lyonnais unit. Eclogites and related garnet amphibolites also occur in a similar structural situation farther north (in the Morvan unit, Godard, 1990) and also southeast of the Monts du Lyonnais unit (in the Maclas-Tournon area, Gardien and Lardeaux, 1991). In the Monts du Lyonnais unit, three ductile strain patterns were distinguished (Lardeaux and Dufour, 1987; Feybesse et al., 1996) and related to high pressure and medium pressure metamorphic conditions:

- The relictual high-pressure structures
- A main deformation imprint, contemporaneous with amphibolite facies conditions, corresponds to a NW -SE crustal shortening with a finite NNE-SSW stretching direction (Fig. 32b)
- A deformation event developed under a transpressional regime dated between 335 and 350 Ma (Rb/Sr whole rock, Gay et al., 1981; $^{40}Ar/^{39}Ar$, Costa et al., 1993) which is correlated to the main deformation within the Brévenne ophiolite in relation with its overthrusting. (Fig. 32c)

With respect to this transpressive strain pattern, in the southern part of the Monts du Lyonnais unit, the eclogites outcrop exclusively in the strongly folded domains where they behave as rigid bodies in a deformed ductile matrix. We never found any eclogitic body within the shear zones.

2. The uppermost part of the magmatic arc: the Brévenne ophiolite (Fig. 32b)

The Devonian Brévenne ophiolitic unit consists of an association of metabasalts and metarhyolites together with intrusive intruded by trondhjemitic bodies (Peterlongo, 1970; Piboule et al., 1982,1983). The ophiolitic unit was initially emplaced in a submarine environment (Pin et al., 1982; Delfour et al., 1989). These intercalations are cut and overlain by intrusive gabbros and dolerites and by submarine basaltic lavas that, finally, are overlain by siltstones with pyroclastic intercalations (Milési et Lescuyer, 1989; Feybesse et al., 1996). A prograde greenschist to lower amphibolite facies metamorphism is recorded (Peterlongo, 1960; Fonteilles, 1968; Piboule et al., 1982; Feybesse et al., 1988). The Brévenne ophiolite underwent a polyphase deformation. An early event, well developed in the northern part of the unit, is characterized by a NW-SE stretching lineation with top to the NW shearing (Leloix et al., 1999). During the second event, the ophiolitic unit is overthrusting the Monts du Lyonnais along a dextral transpressional zone in which syntectonic granites emplaced between 340 and 350 Ma (Fig. 32c, Gay et al, 1981; Feybesse et al., 1988; Costa et al., 1993). Subsequently, monzonitic granites of Namurian- Westphalian age and a contact metamorphism aureole postdate this tectonics (Delfour, 1989).

3. The development of the Velay migmatite granite dome and the collapse of the orogen (Fig. 32b)

The tectonic evolution of the eastern Massif Central is achieved during Westphalian and Stephanian. The formation of the Velay dome, coeval with the activation of crustal-scale detachements, potentially corresponds to flow of a partially molten crustal layer in response to gravitational collapse.

B. Stop description (Fig. 28, 29)

Stop D5.1:

The Bois des Feuilles, Road from St Symphorien-sur-Coise to Rive de Gier, D2.

This outcrop consists of garnet bearing peridotites and eclogites occuring as boudins within garnet sillimanite paragneisses. The coesite-bearing eclogite occurs in the southern part of the Monts du Lyonnais unit, near St Joseph in the Bozançon valley (1/50.000 geological map " St Symphorien Sur Coise ", Feybesse et al., 1996) in association with "common" eclogites and serpentinites. In the whole area, eclogites are preserved in low-strain lenses (meter scale boudins) wrapped by amphibolites or amphibolite facies paragneisses. For practical reasons (difficult access), we shall observe only garnet-peridotites and "common eclogites".

Well-preserved peridotites occur as metric to decametric scale bodies within the paragneisses. In the less retrogressed samples, garnets in equilibrium with olivine, clinopyroxenes and orthopyroxenes can be observed. Frequently, garnets contain inclusions of spinels and pyroxenes, while in some samples

spinels are replaced by coronas of garnet. These microstructures indicate an evolution from spinel to garnet lherzolite facies during a prograde metamorphic P-T path involving a strong pressure increase associated to a moderate temperature increase (Gardien et al., 1990). In many samples, garnets are partly replaced by spinel and orthopyroxene while the porphyroclasts of olivine and pyroxenes are transformed into talc, amphibole, chlorite and serpentine. These mineralogical transformations document a retrograde evolution characterized first by a strong isothermal pressure decrease followed by both pressure and temperature decrease.

As a general rule, the eclogites from the Monts du Lyonnais unit are strongly retrogressed under granulite and amphibolite facies conditions, and in 80% of the cases, the mafic boudins are composed of garnet bearing amphibolites with relics of eclogitic minerals. Petrographically, three types of eclogite facies rocks can be distinguished:

- fine-grained dark-colored kyanite-free eclogites
- fine-grained light-colored, often kyanite-bearing eclogites
- coarse-grained meta-gabbros (with coronitic textures) only partly re-equilibrated under eclogite facies conditions.

As pointed out by various authors (Coffrant and Piboule, 1971; Coffrant, 1974; Blanc, 1981; Piboule and Briand, 1985), dark-coloured eclogites are iron and titanium rich (Fe0 + Fe_2O_3 near 13 % and TiO_2 > 2%), Al-poor metabasalts (Al_2O_3 near 13-15 %), while light-coloured eclogites have higher aluminium contents (Al_2O_3 near 17-20 %), and higher average magnesium values but lower titanium contents (TiO_2 < 1,3 %). Detailed geochemical investigations (Blanc, 1981; Piboule and Briand, 1985) have shown that these eclogites can be regarded as the variably

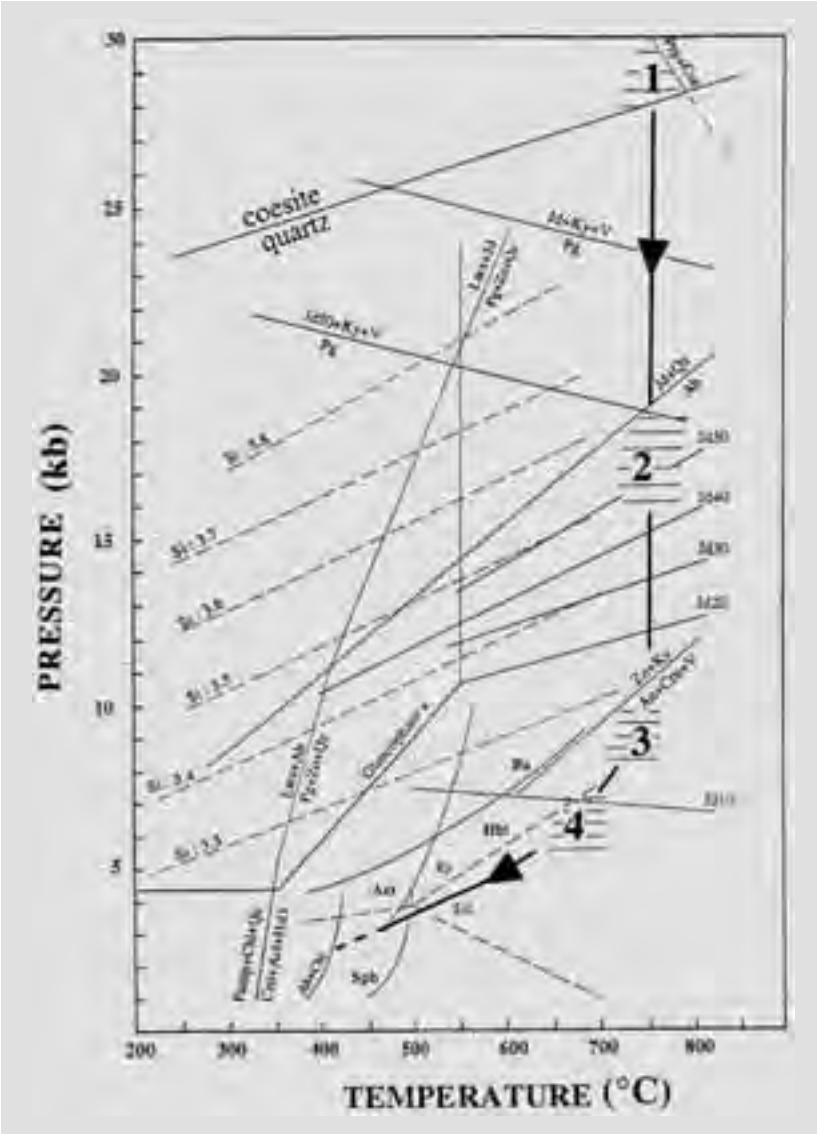

Figure 33 - P-T path of the Monts du Lyonnais coesite-bearing eclogite (see detailed legend of the reactions in Lardeaux et al., 2001).

fractionated members of a volcanic tholeiitic suite.

In the less retrogressed samples, the following mineral assemblages, representing the relicts of eclogite facies metamorphism, are recognized in the dark (1-2) and light (3-4) eclogites from the Monts du Lyonnais (Fig. 33):

- Garnet - omphacite - quartz - zoisite - rutile - apatite - sulfides,
- Garnet - omphacite - quartz - zoisite - colourless amphibole - rutile - sulfides,
- Garnet - omphacite - quartz (or coesite) - zoisite - kyanite - colorless amphibole - rutile,
- Garnet - omphacite - quartz - zoisite - kyanite - phengite - rutile.

Coesite and quartz pseudomorphs after coesite were exclusively detected as inclusions in two garnet grains within one sample of kyanite-bearing eclogite (Color Plate 2, E, F). SiO2 polymorphs were distinguished optically, i.e. coesite was first positively identified relative to quartz by its higher refractive index, and then confirmed by Raman spectroscopy, by observation of the characteristics Raman lines 177, 271, 521 cm-1. Only two coesite grains are preserved as relics and, generally, coesite is otherwise completely transformed into polycrystalline radial quartz (palisade texture) or into polygonal quartz surrounded by radiating cracks. The extremely rare preservation of coesite in the Monts du Lyonnais eclogites is clearly the result of the high temperature conditions (near 750°C, see details in Dufour et al., 1985 and Mercier et al., 1991) reached during decompression as well as the consequence of fluid influx (hydration) during retrogression. Indeed, the kinetics of the coesite ---> quartz transformation are strongly temperature and fluid dependent (Gillet et al., 1984; Van der Molen and Van Roermund, 1986; Hacker and Peacock, 1995; Liou and Zhang, 1996) and consequently in the studied area, coesite has been almost entirely transformed into quartz.

Stop D5.2:

St-André-la-Côte, Road from St-André-en-Haut to Mornant.

Migmatites and granulitic rocks outcrop in the northern part of the Monts du Lyonnais. Near St-André-la-Côte village, mafic and acid granulite facies rocks are well exposed. In mafic granulites the following metamorphic assemblages are described (Dufour, 1985; Dufour et al., 1985):

- Garnet + plagioclase + orthopyroxene + ilmenite,
- Garnet + plagioclase + amphibole + ilmenite,
- Clinopyroxene + orthopyroxene + plagioclase ± amphibole + ilmenite,
- Garnet + clinopyroxene + othopyroxene + plagioclase ± amphibole + ilmenite.

In acid granulites (Dufour, 1982; Lardeaux et al., 1989), the common mineralogy consists of quartz + plagioclase + K-feldspar + garnet + sillimanite ± spinel ± biotite. Kornerupine - bearing granulites have been also locally recognized in this outcrop (Lardeaux et al., 1989).

In this northern part of the Mont du Lyonnais unit, the metamorphic imprint is typical for Intermediate Pressure granulite facies and there is no trace of eclogitic high-pressure facies metamorphism.

Stop D5.3:

The Yzeron quarry, Road from Ste-Foy-l'Argentière to Craponne, D489.

Stop D5.3 shows the migmatitic orthogneisses from the northern Monts du Lyonnais. These rocks are metamorphosed and strongly foliated under amphibolite facies conditions. Their typical mineralogy is an association of quartz + plagioclase + K-feldspar + biotite ± sillimanite. Muscovite and chlorite are developed during retrogression. In the Yzeron quarry, superposed fold systems have been described in relation with progressive deformation under amphibolite and greenschist facies metamorphic conditions. The main foliation observed in the orthogneisses is folded and / or reworked in the ductile strike-slip shear zones related to the development of a regional scale transpressive regime.

The northern Monts du Lyonnais area, with intermediate–pressure granulite and amphibolite facies metamorphic rocks can be interpreted as remnants of the upper overriding continental crust on which the magmatic arc and the Brévenne back-arc were emplaced. In this model, the southern part of the Monts du Lyonnais unit corresponds to a subduction complex (remnant of subduction channel) located on the top of the lower plate (i.e. Pilat – Velay units).

Stop D5.4:

Brévenne valley, road cut: bimodal magmatic sequence.

Stop D5.4 shows different lithologies, like metabasalts, metarhyolites, metapyroclastites and metasediments, typical for the Brévenne ophiolitic unit. All the lithologies are metamorphosed under greenschist facies conditions. In mafic lithologies, the common mineralogy corresponds to an association of

plagioclase + actinolite + chlorite + sphene ± calcite ± quartz.
The different lithologies are also deformed and involved into a regional scale fold system with sub-vertical axial planes. These folds are related to the regional transpressive regime which affects also the Monts du Lyonnais unit at around 350 – 340 Ma.
Recent geochemical investigations support the origin of the Brévenne ophiolitic sequence, during Devonian, in a back-arc basin developed upon the upper plate of a subduction system.

End of the 5th day in Lyon (airport and railway station)

Acknowledgements

O. Monod is thanked for his review of the first draft of this guidebook. Mrs S. Matrat and D. Quiniou provided a great help during the final stages for preparing this guidebook.

References cited

Arzi, A.A. (1978). Critical phenomena in the rheology of partially melted rocks. *Tectonophysics* 44, 173-184.
Ait Malek, H. (1997). Pétrologie, Géochimie et géochronologie U/Pb d'associations acide-basiques: exemples du SE du Velay (Massif central français) et de l'anti-Atlas occidental (Maroc). Thèse doctorat de l'INPL, Univ. Nancy, 297 pp.
Ait Malek, H., Gasquet, D., Marignac, C. and Bertrand, J.M. (1995). Des xénolites à corindon dans une vaugnérite de l'Ardèche (Massif central français) : implications pour le métamorphisme ardéchois. *C. R. Acad. Sci. Paris* 321, 959-966.
Arnaud, F. (1997). Analyse structurale et thermo-barométrique d'un système de chevauchements varisque : les Cévennes centrales (Massif Central français). Microstructures et mécanismes de déformation dans les zones de cisaillement schisteuses. Thèse 3ème cycle, Institut National Polytechnique de Lorraine, Documents du BRGM, 286, 351 pp.
Arnaud, F. and Burg, J.P. (1993). Microstructures des mylonites schisteuses: cartographie des chevauchements varisques dans les Cévennes et détermination de leur cinématique. *C. R. Acad. Sci. Paris* 317, 1441-1447.
Arthaud, F. (1970). Etude tectonique et microtectonique comparée de deux domaines hercyniens : les nappes de la Montagne Noire (France) et l'anticlinorium de l'Iglesiente (Sardaigne). Thèse d'Etat, Univ. Montpellier, France, 175pp.
Arthaud F. and Matte P. (1977) - Late Paleozoic strike slip faulting in southern Europe and northern Africa: result of right lateral shear zone between Appalachians and the Urals. *Geol. Soc. Am. Bull*. 88, p. 1305 -1320.
Autran, A. and Cogné, J. (1980). La zone interne de l'orogenèse varisque dans l'Ouest de la France et sa place dans le développement de la chaîne hercynienne. (J. Cogné J. and M. Slansky M. Eds.), Géologie de l'Europe du Précambrien aux bassins sédimentaires post-hercyniens, 26ème Cong. Géol. Int., Coll. C6, Paris 1980. *Ann. Soc. géol. Nord*, Lille XCIX, 90-111.
Barbey, P., Marignac, C., Montel, J.M., Macaudière, J., Gasquet, D. and Jabbori, J. (1999). Cordierite growth texture and the conditions of genesis and emplacement of crustal granitic magmas: the Velay granite complex (Massif Central, France*). J. Petrology* 40, 1425-1441.
Barraud, J., Gardien, V., Allemand, P. and Grandjean, P. (2003). Analog models of melt-flow in folding migmatites. *J. Struct. Geol*. in press.
Be Mezème, E. (2002). Application de la méthode de datation à la microsonde électronique de monazite de migmatites et de granitoïdes tardi-hercyniens du Massif Central français. Master thesis, Univ. Orléans, 40 pp.
Bernard-Griffiths, J., Cantagrel J.M. and Duthou J.L. (1977) - Radiometric evidence for an Acadian tectono-metamorphic event in western Massif Central français. *Contrib*. *Mineral. Petrol*. 61, 199-212.
Berthé, D., Choukroune, P and Jegouzo, P. (1978). Orthogneiss mylonite and non coaxial deformation of granite: the exemple of the South armorican shear zone. *J. Struc. Geol.* 1, 31-42.
Bitri, A., Truffert, C., Bellot, J.P., Bouchot, V., Ledru, P., Milési, J.P. and Roig J.Y. (1999) - Imagerie des paléochamps hydrothermaux As-Sb d'échelle crustale et des pièges associés dans la chaîne varisque : sismique réflexion verticale (GéoFrance 3D : Massif central français). *C. R. Acad. Sci. Paris* 329, 771-777.
Blanc, D. (1981). Les roches basiques et ultrabasiques des monts du Lyonnais. Etude pétrographique, minéralogique et géochimique. Thèse Doctorat 3ème cycle, Univ. Lyon 1, 152 p.
Bouchez, J.L., and Jover, O. (1986). Le Massif Central : un chevauchement de type himalayen vers l'ouest-nord-ouest. *C. R. Acad. Sci. Paris* 302, 675-680.
Boutin, R. and Montigny, R. (1993). Datation

39Ar/40Ar des amphibolites du complexe leptyno-amphibolique du plateau d'Aigurande : collision varisque à 390 Ma dans le Nord-Ouest du Massif central français. *C. R. Acad. Sci. Paris* 316, 1391-1398.

Brown, M. (1994). The generation, segregation, ascent and emplacement of granite magma: the migmatite-to-crustally-derived granite connection in thickened orogens. *Earth Science Reviews* 36, 83-130.

Brown, M. and Dallmeyer, R.D. (1996). Rapid Variscan exhumation and the role of magma in core complex formation: southern Brittany metamorphic belt. *J. metamorphic Geol*. 14, 361-379

Burg, J.P., Leyreloup, A., Marchand, J. and Matte, P. (1984). Inverted metamorphic zonation and large-scale thrusting in the Variscan belt: an example in the French Massif Central. *In:* " Variscan tectonics of the North-Atlantic region " (D.H.W. Hutton, and D. J. Sanderson,, Ed.),. pp. 47-61, Spec. Publ. Geol. Soc. London, 14,.

Burg, J.P. Bale, P., Brun, J.P. and Girardeau, J. (1987). Stretching lineation and transport direction in the Ibero-Armorican arc during the siluro-devonian collision. *Geodinamica Acta* 1, 71-87.

Burg J.P., Brun, J.P. and Van Den Driessche, J. (1991) - Le Sillon Houiller du Massif central français : faille de transfert pendant l'amincissement crustal de la chaîne varisque. *C. R. Acad. Sci. Paris* 311, II, 147-152.

Burg, J.P. and Vanderhaeghe, O. (1993). Structures and way-up criteria in migmatites, with application to the Velay dome (French Massif central). *J. Struct. Geol.* 15, 1293-1301.

Burg, J.P., Van Den Driessche, J. and Brun, J.P. (1994). Syn- to post-thickening extension: mode and consequences. *C. R. Acad. Sci. Paris* 319, 1019-1032.

Caen Vachette, M., Couturié, J.P. and Didier, J. (1982). Age radiométrique des granites anatectiques et tardimigmatitique du Velay (Massif Central français). *C. R. Acad. Sci. Paris* 294, 135-138.

Caen Vachette, M., Gay, M., Peterlongo, J.M., Pitiot, P. and Vitel, G. (1984). Age radiométrique du granite syntectonique du gouffre d'Enfer et du métamorphisme hercynien dans la série de basse pression du Pilat (Massif Central Français). *C. R. Acad. Sci. Paris* 299, 1201-1204.

Caron, C., Lancelot, J.R., and Maluski, H. (1991). A paired 40Ar-39Ar and U-Pb radiometric analysis applied to the variscan Cévennes, french Massif central. EUG Strasbourg, *Terra abstracts* 3, 205.

Clemens, J.D. (1990). The granulite-granite connexion. *In:* "Granulites and Crustal Evolution" (D. Vielzeuf and Ph. Vidal, Eds.), Kluwer Acad. Publ., pp. 25-36.

Coffrant, D. (1974). Les éclogites et les roches basiques et ultrabasiques associées du massif de Sauviat-sur-Vige, Masssif central français. *Bulletin de la Société Française de Minéralogie Cristallographie* 97, 70-78

Coffrant, D. and Piboule, M. (1971). Les éclogites et les roches associées des massifs basiques de Saint-Joseph (Monts du Lyonnais, Massif Central français). *Bull. Soc. Géol. Fr.* 7, XIII, 283-291

Couturier, J.P. (1969). Le massif granitique de la Margeride. Thèse d'Etat, Univ. Clermont-Ferrand, France, 190 pp.

Costa, S. (1989). Age radiometrique $^{39}Ar/^{40}Ar$ du métamorphisme des séries du Lot et du charriage du groupe leptyno-amphibolique de Mavejols. *C. R. Acad. Sci. Paris* 309, 561-567.

Costa S. (1992). East-West diachronism of the collisional stage in the French Massif Central: implications for the european variscan orogen. *Geodinamica Acta* 5, 51-68.

Costa, S., Maluski, H. and Lardeaux, J.M. (1993). 40Ar-39Ar chronology of Variscan tectono-metamorphic events in an exhumed crustal nappe: the Monts du Lyonnais complex (Massif Central, France). *Chem. Geol.* 105, 339-359.

Dallain, C., Schulmann, K. and Ledru, P. (1999). Textural evolution in the transition from subsolidus annealing to melting process, Velay dome, French Massif Central. *J. Metamorphic Geol*. 17, 61-74.

Delfour, J. (1989). Données lithostratigraphiques et géochimiques sur le Dévono-Dinantien de la partie sud du faisceau du Morvan (nord-est du Massif Central français). *Géologie de la France* 4, 49-77.

Demange, M. (1975). Style pennique de la zone axiale de la Montagne Noire entre Saint-Pons et Murat-sur-Vèbre (Massif Central). *Bull. BRGM* 2, 91-139.

Demange, M. (1985). The eclogite facies rocks of the Montagne Noire, France. *Chemical Geol.* 50, 173-188.

Didier, J. (1973). Granites and their enclaves. The bearing of enclaves on the origin of granites, 2, Developments in *Petrology Series*, Amsterdam, Elsevier, 3, 37-56.

Didier, J. and Lameyre, J. (1971). Les roches granitiques du Massif central. *In*: Symposium J. Jung : "Géologie, géomorphologie et structure profonde du Massif central français", pp. 17-32,

Clermont-Ferrand, Plein Air Service.

Dubuisson, G., Mercier, J.C.C., Girardeau, J. and Frison, J.Y. (1989). Evidence for a lost ocean in Variscan terranes of the western Massif Central, France. *Nature* 337, 23, 729-732.

Ducrot, J., Lancelot, J.R. and Marchand, J. (1983). Datation U-Pb sur zircons de l'éclogite de la Borie (Haut-Allier, France) et conséquences sur l'évolution anté-hercynienne de l'Europe Occidentale. *Earth Planet. Sci. Lett.* 18, 97-113.

Dufour, E. (1982). Pétrologie et géochimie des formations orthométamorphiques acides des Monts du Lyonnais (Massif Central français). Thèse Doctorat de 3ème cycle, Univ. Lyon 1, 241 p.

Dufour, E. (1985). Granulite facies metamorphisme and retrogressive evolution of the Monts du Lyonnais metabasites (Massif Central France) *Lithos* 18, 97-113

Dufour, E., Lardeaux, J.M. and Coffrant, D. (1985). Eclogites and granulites inthe Monts du Lyonnais area: an eo-Hercynian plurifacial metamorphic evolution. *C. R. Acad. Sci, Paris* 300, 141-144

Dupraz, J. and Didier, J. (1988). Le complexe anatectique du Velay (Massif Central français) : structure d'ensemble et évolution géologique. *Géologie de la France* 4, 73-87.

Duthou, J.L, Cantagrel, J.M., Didier, J. and Vialette, Y. (1984). Paleozoïc granitoïds from the French Massif Central: age and origin studied by 87Rb/87Sr system. *Phys. Earth Planet. Int.* 35, 131-144.

Duthou, J-L., Chenevoy, M. and Gay M. (1994). Age Rb/Sr Dévonien moyen des migmatites à cordiérite du Lyonnais (Massif Central français). *C. R. Acad. Sci. Paris.* 319, 791-796.

Echtler, H. and Malavieille, J. (1990). Extensional tectonics, basement uplift and Stephano-Permian collapse basin in a Late Variscan metamorphic core complex (Montagne Noire, Southern Massif Central). *Tectonophysics* 177, 125-138.

Engel, W., Feist, R. and Franke, W. (1980). Le Carbonifère anté-stéphanien de la Montagne Noire : rapports entre mise en place des nappes et sédimentation. *Bull. BRGM* 2, 341-389.

Faure, M. (1995). Late orogenic carboniferous extensions in the Variscan French Massif Central. *Tectonics* 14, 132-153.

Faure, M., Pin, C. and Mailhé, D. (1979). Les roches mylonitiques associées au charriage du groupe leptyno-amphibolique sur les schistes du Lot dans la région de Marvejols (Lozère). *C. R. Acad. Sci. Paris* 288, 167-170.

Faure, M. and Cotterau, N. (1988). Données cinématiques sur la mise en place du dôme migmatitique carbonifère moyen de la zone axiale de la Montagne Noire (Massif Central, France). *C. R. Acad. Sci. Paris* 307, Il, 1787-1794.

Faure, M., Leloix, C. and Roig, J.Y. (1997). L'évolution polycyclique de la chaîne hercynienne. *Bull. Soc. Geol. France* 168, 695-705.

Faure, M., Monié, P., Maluski, H., Pin, C. and Leloix, C. (2001). Late Visean thermal event in the northern part of the French Massif Central. New $^{40}Ar/^{39}Ar$ and Rb-Sr isotopic constraints on the Hercynian syn-orogenic extension. *Int. J. Geol* 91, 53-75.

Feist, R. and Galtier, J. (1985). Découverte de flores d'âge namurien probable dans le flysch à olistolithes de Cabrières (Hérault). Implications sur la durée de la sédimentation synorogénique dans la Montagne Noire (France Méridionale), *C. R. Acad. Sci. Paris* 300, 207-212.

Feybesse, J.L., Lardeaux, J.M., Johan, V., Tegyey, M., Dufour, E., Lemiere, B. and Delfour, J. (1988). La série de la Brévenne (Massif Central Français): une unité dévonienne charriée sur le complexe métamorphique des Monts du Lyonnais à la fin de la collision varisque. *C. R. Acad. Sci. Paris* 307, 991-996.

Feybesse, J.L., Lardeaux, J.M., Tegyey, M., Kerrien, Y., Lemiere, B., Mercier, F., Peterlongo, J.M. and Thieblemont, D. (1996). Carte géologique de France (1/50000), feuille St Symphorien-sur-Coise (721). BRGM Orléans.

Floc'h, J-P. (1983). La série métamorphique du Limousin central. Thèse d'Etat, Univ. Limoges, France, 445pp.

Fonteilles, M. (1968). Contribution à l'nanalyse du processus de spilitisation. Etude comparée des séries volcaniques paléozoïques de la Bruche (Vosges) et de la Brévenne (Massif Central français). *Bull. BRGM* 2, (3), 1-54

Franke, W. (1989). Tectonostratigraphic units in the Variscan belt of central Europe. *In* " Terranes in the circum-Atlantic Paleozoic orogens " (R.D. Dallmeyer Ed.), pp. 67-90. Special paper, Geological Society of America, 230.

Franke,W. (2000). The mid-European segment of the Variscides: tectonostratigraphic units, terrane boundaries and plate tectonic evolution, in Orogenic Processes. *In* " Quantification and Modelling in the Variscan Belt "(W. Franke, V. Haak, O. Oncken, D. Tanner, Eds.) pp. 35-61. Special Publications, 179, Geological Society of London.

Gardien, V., Lardeaux, J.M. and Misseri, M. (1988). Les péridotites des Monts du Lyonnais (Massif Central français) : témoins privilégiés d'une subduction de lithosphère paléozoique. *C. R. Acad. Sci. Paris* 307, 1967-1972.

Gardien, V. (1990). Reliques de grenat et de staurotide dans la série métamorphique de basse pression du Mont Pilat (Massif Central français): témoins d'une évolution tectonométamorphique polyphasée. *C. R. Acad. Sci. Paris* 310, 233-240.

Gardien, V., Tegyey, M., Lardeaux, J.M., Misseri, M. and Dufour, E. (1990). Crustal-mantle relationships in the french Variscan chain: the example of the Southern Monts du Lyonnais unit (eastern French Massif Central*). Journ. Metam. Geol.* 8, 477-492.

Gardien, V. and Lardeaux, J.M. (1991). Découvertes d'éclogites dans la synforme de Maclas: extension de l'Unité Supérieure des Gneiss à l'Est du massif central. *C. R. Acad. Sci. Paris* 312, 61-68.

Gardien, V., Lardeaux, J.M., Ledru, P., Allemand, P. and Guillot, S. (1997). Metamorphism during late orogenic extension: insights from the French Variscan belt. *Bull. Soc. Géol. Fr*. 168, 271-286.

Gèze, B. (1949). Etude Géologique de la Montagne Noire et des Cévennes Méridionales*. Mem. Soc. Géol. France* 24, 215.

Gay, M., Peterlongo, J.M. and Caen-Vachette, M. (1981). Age radiométrique des granites en massifs allongés et en feuillets minces syn-tectoniques dans les Monts du Lyonnais (Massif Central français*). C. R. Acad. Sci. Paris* 293, 993-996.

Gillet, P., Ingrin, J. and Chopin, C. (1984). Coesite in subducted continental crust: *P-T* history deduced from an elastic model. *Earth Planet. Sci. Lett.* 70, 426-436

Godard, G. (1990). Découverte d'éclogites, de péridotites à spinelle et d'amphibolite à anorthite, spinelle et corindon dans le Morvan. *C. R. Acad. Sci. Paris* 310, 227-232.

Hacker, B.R. and Peacock, S.M. (1995). Creation, preservation, and exhumation of UHPM rocks. *In:* "Ultra-high-Pressure Metamorphism". (Coleman, Wang, Eds.), Cambridge University Press, Cambridge, pp. 159-181

Lagarde, J.L., Dallain, C., Ledru, P. and Courrioux, G. (1994). Deformation localization with laterally expanding anatectic granites: Hercynian granites of the Velay, French Massif Central. *J. Struct. Geol*. 16, 839-852.

Lardeaux, J.M. (1989). Les formations métamorphiques des Monts du Lyonnais *Bull. Soc. Géol. Fr.* 4, 688-690

Lardeaux, J.M. and Dufour, E. (1987). Champs de déformation superposés dans la chaîne varisque. Exemple de la zone nord des Monts du Lyonnais (Massif Central français). *C. R. Acad. Sci. Paris* 305, 61-64.

Lardeaux, J.M., Reynard, B. and Dufour, E. (1989). Granulites à kornérupine et décompression post-orogénique des Monts du Lyonnais. *C. R. Acad. Sci. Paris* II 308, 1443-1449

Lardeaux, J.M., Ledru, P., Daniel, I. and Duchène, S. (2001). The variscan French Massif Central - a new addition to the ultra-high pressure metamorphic «club»: exhumation processes and geodynamic consequences. *Tectonophysics* 323, 143-167.

Lasnier, B. (1968a). Découverte de roches éclogitiques dans le groupe leptyno-amphibolique des Monts du Lyonnais. *Bull. Soc. Géol. Fr.* 7, 179-185

Ledru, P., Lardeaux, J.M., Santallier, D., Autran, A., Quenardel, J-M., Floc'h, J-P., Lerouge, G., Maillet, N., Marchand, J. and Ploquin, A. (1989). Où sont les nappes dans le Massif Central français ? *Bull. Soc. Géol. France* 8, 605-618.

Ledru, P., Autran, A. and Santallier, D. (1994a). Lithostratigraphy of Variscan terranes in the French Massif Central. A basic for paleogeographical reconstruction. *In:* "Pre-Mesozoic geology in France and related areas", (J. D. Keppie, Ed.). pp. 276-288. Springer Verlag.

Ledru, P., Costa, S. and Echtler, H. (1994b). Structure. *In*: "Pre-Mesozoic geology in France and related areas", (J. D. Keppie, Ed.). pp. 305-323, Springer Verlag.

Ledru, P., Courrioux, G., Dallain, C., Lardeaux, J.M., Montel, J.M., Vanderhaeghe, O., and Vitel, G. (2001). The Velay dome (French Massif Central): melt generation and granite emplacement during orogenic evolution. *Tectonophysics* 332, 207-237.

Leloix, C., Faure, M. and Feybesse, J.L. (1999). Hercynian polyphase tectonics in north-east French Massif Central : the closure of the Brévenne Devonian-Dinantian rift. *Int. J. Earth. Sci.* 88, 409-421.

Liou, J.G. and Zaang, R.Y. (1996). Occurrences of intergranular coesite in ultrahigh-P rocks from the Sulu region, eastern China: implications of lack of fluid during exhumation. *Am. Mineralogist* 81, 1217-1221

Macaudière, J., Barbey, P., Jabbori, J. and Marignac, C. (1992). Le stade initial de fusion dans le développement des dômes anatectiques : le dôme du Velay (Massif Central français*). C. R. Acad. Sci. Paris* 315, 1761-1767.

Volume n° 2 - from B16 to B33

Malavieille, J., Guihot, P., Costa, S., Lardeaux, J.M., and Gardien, V. (1990). Collapse of the thickened Variscan crust in the French Massif Central: Mont Pilat extensional shear zone and St Etienne upper Carboniferous basin. *Tectonophysics* 177, 139-149.

Mattauer, M., Brunel, M. and Matte, P. (1988). Failles normales ductiles et grands chevauchements : une nouvelle analogie entre l'Himalaya et la chaîne hercynienne du Massif français. *C. R. Acad. Sci. Paris* 306, 671-676.

Mattauer, M., Laurent P. and Matte P. (1996). Plissements hercyniens synschisteux post-nappe et étirement subhorizontal dans le versant Sud de la Montagne Noire. *C. R. Acad. Sci. Paris.* 322, 309-315.

Mattauer, M. and Matte, P. (1998). Le bassin stéphanien de St-Etienne ne résulte pas d'une extension tardi-hercynienne généralisée : c'est un bassin pull-apart en relation avec un décrochement dextre. *Geodinamica Acta* 11, 23-31.

Matte, P. (1991). Tectonics and plate tectonics model for the variscan belt of Europe. *Tectonophysics* 126, 329-374.

Matte, P. (2001). The Variscan collage and orogeny (480-290 Ma) and the tectonic definition of the Armorica microplate : a review. *Terra Nova* 13, 122-1128.

Matte, P., Lancelot, J-R. and Mattauer, M. (1998). La zone axiale hercynienne de la Montagne Noire n'est pas un " metamorphic core complex "extensif mais un anticlinal post-nappe à cœur anatectique. *Geodinamica Acta* 11, 13-22.

Maluski, H., Costa, S. and Echler H. (1991). Late Variscan tectonic evolution by thinning of an earlier thickened crust. An $^{40}Ar/^{39}Ar$ study of the Montagne Noire, southern Massif central, France. *Lithos* 26, 287-304.

Mercier, L., Lardeaux, J.M. and Davy, P. (1991). On the tectonic significance of the retromorphic P-T paths of the french Massif Central eclogites. *Tectonics* 10, 131-140.

Milési, J.P. and Lescuyer J.L. (1989). The Chessy Zn-Cu-Ba massive sulphide deposit and the Devonian Brévenne volcano-sedimentary belt (eastern Massif Central, France). Project: identification of diagnostic markers of high-grade massive sulphide deposits of of their enriched zones in France and in Portugal. CEE contrat MA IM-0030-F(D). Rapp. BRGM 89 DAM 010 DEX (final report)

Mergoil, J., Boivin, P., Blès, J.L., Cantagrel, J.M. and Turland M. (1993). Le Velay. Son volcanisme et les formations associées, notice de la carte à 1/100000. *Géologie de la France* 3, 3-96.

Monié, P., Respaut, J.-P., Brichaud, S., Bouchot, V., Faure, M. and Roig, J.-Y. (2000). $^{40}Ar/^{39}Ar$ and U-Pb geochronology applied to Au-W-Sb metallogenesis in the Cévennes and Châtaigneraie districts (Southern Massif Central, France). *In*: "Orogenic gold deposits in Europe", (V. Bouchot, Ed.), pp. 77-79. Document BRGM 297, Bureau de Recherches Géologiques et Minières, Orléans.

Montel, J.M., 1985. Xénolithes peralumineux dans les dolérites du Peyron, en Velay (Massif Central français). Indications sur l'évolution de la croute profonde tardihercynienne. *C. R. Acad. Sci. Paris* 301, 615-620.

Montel, J.M., Weber, C., Barbey, P. and Pichavant, M. (1986). Thermobarométrie du domaine anatectique du Velay (Massif Central français) et conditions de genèse des granites tardi-migmatitiques. *C. R. Acad. Sci. Paris* 302, 647-652.

Montel, J.M. and Abdelghaffar, R. (1993). Les granites tardi-migmatitiques du Velay (Massif Central): principales caractéristiques pétrographiques et géochimiques. *Géologie de la France* 1, 15-28.

Montel, J.M., Bouloton, J., Veschambre, M., Pellier, C. and Ceret, K. (2002). Age des microgranites du Velay (Massif Central Français). *Géologie de la France* 1, 15-20.

Montel, J.M., Marignac, C., Barbey, P. and Pichavant, M. (1992). Thermobarometry and granite genesis : the Hercynian low-P, high-T Velay anantectic dome (French Massif Central). *J. Metam. Geol.* 10, 1-15.

Mougeot, R., Respaut, J.P., Ledru, P. and Marignac, C. (1997). U-Pb chronology on accessory minerals of the Velay anatectic dome (French Massif Central). *Eur. J. Mineral*. 9, 141-156.

Nicolas, A., Bouchez, J-L. Blaise, J. and Poirier, J-P. (1977). Geological aspects of deformation in continental shear zones. *Tectonophysics* 42, 55-73.

Patiño Douce, A.E. and Johnston, A.D. (1990). Phase equilibria and melt productivity in the pelitic system: implications for the origin of peraluminous granitoids and aluminous granulites. *Contrib*. *Mineral. Petrol*. 107, 202-218.

Peterlongo, J.M. (1960). Les terrains cristallins des monts du Lyonnais (Massif Central français). *Ann. Fac. Sci.* Univ. Clermont-Ferrand 4, (1), 187

Peterlongo, J.M. (1970). Pillows-lavas à bordure variolitique et matrice basique dans la série métamorphique de la Brévenne (Rhône, Massif Central Français). *C. R. Acad. Sci. Paris* 2, 190-194

Piboule, M., Briand, B. and Beurrier, M. (1982). Géochimie de quelques granites albitiques dévoniens de l'Est du Massif Central (France). *Neues Jb. Miner. Abh.,* 143, 279-308.

Piboule, M., Beurrier, M., Briand, B. and Lacroix, P. (1983). Les trondhjemites de Chindo et de St-Veran et le magmatisme kératophyrique associé. Pétrologie et cadre géostructural de ce magmatisme Dévono-Dinantien. *Géologie de la France* I, 2, (1-2), 55-72

Piboule, M. and Briand, B. (1985). Geochemistry of eclogites and associated rocks of the southeastern area of the French Massif Central: origin of the protoliths. *Chem. Geol.* 50, 189-199

Pin, C. (1979). Géochronologie U-Pb et microtectonique des séries métamorphiques anté-stéphaniennes de l'Aubrac et de la région de Marvejols (Massif Central). Thèse 3° cycle, Univ. Montpellier, France, 220pp.

Pin, C. (1981). Old inherited zircons in two synkinematic variscan granitoids: the "granite du Pinet" and the "orthogneiss de Marvejols" (southern French Massif Central). *N. Jb. Miner. Abh*. 142, 27-48.

Pin, C. (1990). Variscan oceans: ages, origins and geodynamic implications inferred from geochemical and radiometric data. *Tectonophysics* 177, 215-227.

Pin, C. and Lancelot, J. (1978). Un exemple de magmatisme cambrien dans le Massif Central : les métadiorites quartzites intrusives dans la série du Lot. *Bull. Soc. Géol. France* 7, 203-208.

Pin, C. and Lancelot, J. (1982). U-Pb dating of an early paleozoïc bimodal magmatism in the French Massif Central and of its further metamorphic evolution. *Contrib. Mineral Petrol,* 79, 1-12.

Pin, C., Dupuy, C. and Peterlongo, JM. (1982). Répartition des terres rares dans les roches volcaniques basiques dévono-dinantiennes du nord-est du Massif central. *Bull. Soc. Géol. Fr.* 7, 669-676.

Pin, C. and Vielzeuf, D. (1983). Granulites and related rocks in Variscan median Europe: a dualistic interpretation. *Tectonophysics* 93, 47-74.

Pin, C. and Duthou, J.L. (1990). Sources of Hercynian granitoids from the French Massif Central: inferences from Nd isotopes and consequences for crustal evolution. *Chemical Geology* 83, 281-296.

Pin, C. and Marini, F. (1993). Early Ordovician continental break-up in Variscan Europe: Nd-SR isotope and trace element evidence for bimodal igneous associations of the southern Massif Central, France. *Lithos* 29, 177-196.

Pin, C and Paquette, JL (1998). A mantle-derived bimodal suite in the Hercynian Belt: Nd isotope and trace element evidence for a subduction-related rift origin of the Late Devonian Brévenne metavolcanics, Massif Central (France). *Contrib Mineral Petrol* 129, 222-238.

Quénardel, J.M. and Rolin, P. (1984). Paleozoic evolution of the Plateau d'Aigurande (N-W. Massif Central, France). *In* "Variscan tectonics of the North Atlantic region" (D. Hutton and D. Sanderson, Eds.), pp. 63-77, Geol. Soc. London Spec. pub, 14.

R'Kha Chaham, K., Couturié, J.P., Duthou, J.L., Fernandez, A. and Vitel, G. (1990). L'orthogneiss oeillé de l'Arc de Fix : un nouveau témoin d'âge cambrien d'un magmatisme hyper alumineux dans le Massif Central français. *C. R. Acad. Sci. Paris* 311, 845-850.

Robardet, M., Verniers, J., Feist R. and Paris, F. (1994). Le Paléozoïque anté-varisque de France, contexte paléogéographique et géodynamique. *Géol. de la France* 3, 3-31.

Robardet, M. (2003). The Armorica 'microplate': fact or fiction? Critical review of the concept and contradictory palaeobiogeographical data. *Palaeogeography, Palaeoclimatology, Palaeoecology* 195, 125-148.

Roig, J-Y. and Faure M. (2000). La tectonique cisaillante polyphasée du Sud-Limousin (Massif Central français) et son interprétation dans un modèle d'évolution polycyclique de la chaîne hercynienne. *Bull. Soc. Géol. Fr.* 171, 295-307.

Roig, J-Y., Faure, M. and Truffert, C. (1998). Folding and granite emplacement inferred from structural, strain, TEM, and gravimetric analyses: the case study of the Tulle antiform, SW French Massif Central. *J. Struct. Geol.* 20, 1169-1189.

Sider, J-M. and Ohnenstetter, M. (1986). Field and petrological evidence forfor the development for an ensialic marginal basin related to the Hercynian orogeny in the Massif Central, France. *Geol. Rundschau* 75, 421-443.

Soula, J.C., Debat, P., Brusset, S., Bessière, G., Christophoul, F. and Déramond, J. (2001). Thrust related, diapiric and extensional doming in a frontal orogenic wedge: example of the Montagne Noire, southern French Hercynian Belt. *J. Struct. Geol.* 23, 1677-1699.

Van den Driessche J. and Brun, J-P. (1991-92). Tectonic evolution of the Montagne Noire (French Massif Central): a model of extensional gneiss dome. *Geodinamica Acta* 5, 85-99.

Vanderhaeghe, O., Burg, J.P. and Teyssier, C. (1999).

Exhumation of migmatites in two collapsed orogens: Canadian Cordillera and French Variscides. *In:* "Exhumation processses: normal faulting, ductile flow and erosion" U. Ring, M.T. Brandon, G.S. Lister and S.D. Willett (Eds.) 181-204, *Geological Society, London*, Special Publications, 154,

Vanderhaeghe, O. and Teyssier, C. (2001). Partial melting and flow of orogens. *Tectonophysics* 342, 451-472.

Van der Molen, I. and Van Roermund, H.L.M. (1986) The pressure path of soild inclusions in minerals: the retention of coesite inclusions during uplift. *Lithos* 19, 317-324

Vitel, G. (1985). La transition faciès granulite faciès amphibolite dans les enclaves basiques du Velay. *C. R. Acad. Sci. Paris* 300, 407-412.

Williamson, B.J., Downes, H. and Thirlwall, M.F. (1992). The relationship between crustal magmatic underplating and granite genesis: an example from the Velay granite complex, Massif Central, France. *Trans. Royal Soc. Edinburgh*, *Earth Sciences* 83, 235-245.

Back Cover:
field trip itinerary

FIELD TRIP MAP

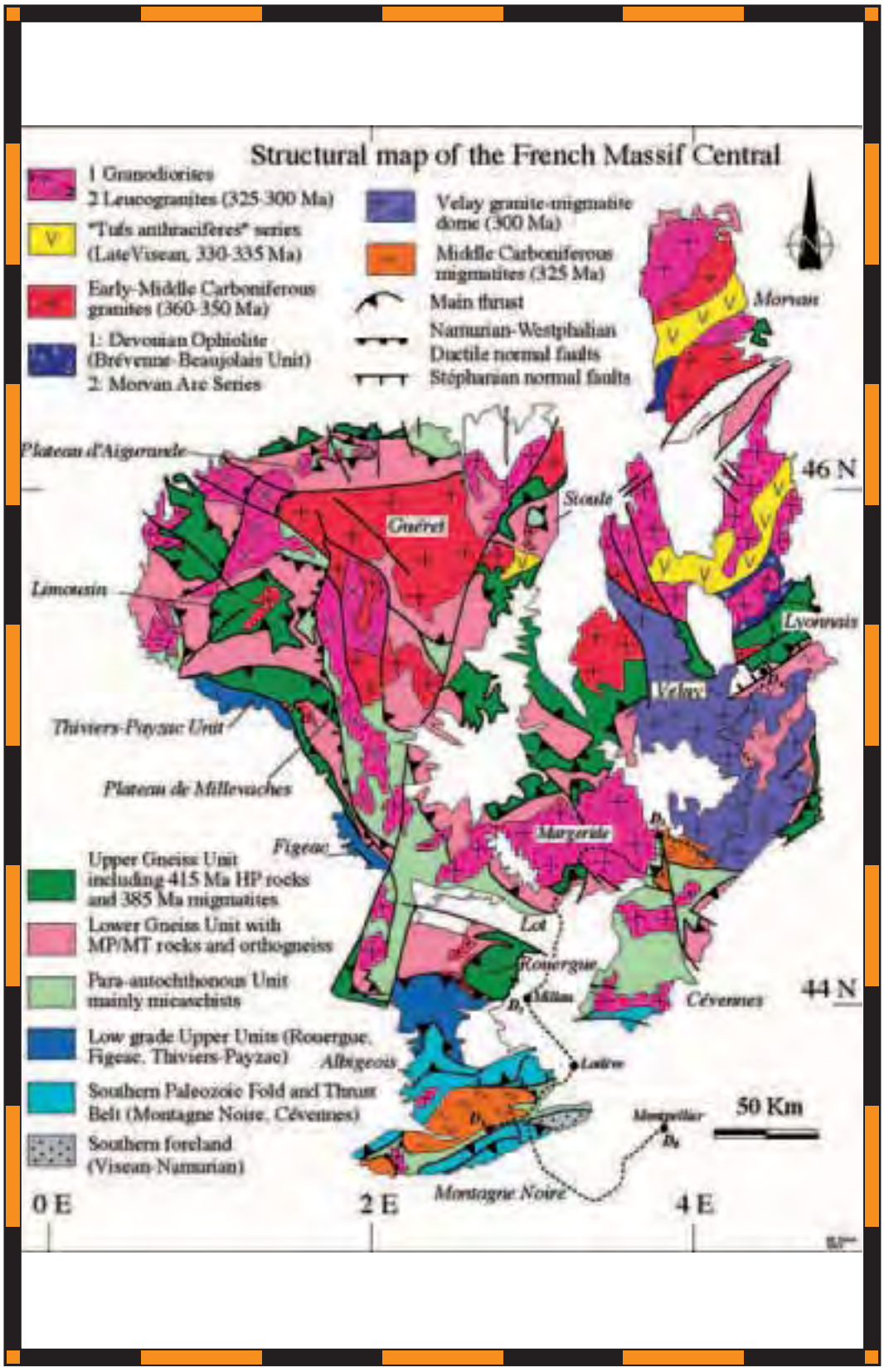

Edited by APAT